Politechnika Wrocławska

FIELD OF SCIENCE: ENGINEERING AND TECHNICAL SCIENCE

DISCIPLINE OF SCIENCE: CIVIL ENGINEERING, GEODESY AND TRANSPORT

DOCTORAL DISSERTATION

Optimization of Network Tied-Arch Bridges with Metaheuristic and Gradient-Based Algorithms

Mgr inż. Adrian Błonka

Supervisor:
Prof. dr hab. inż. Wojciech Glabisz

Assistant supervisor:
Dr inż. Ryszard Hołubowski

Keywords: network arch bridges, genetic algorithms, evolutionary structural optimization, gradient based algorithms, cost-oriented optimization, in-plane geometrically nonlinear buckling, multi-variant angular divergence model

WROCŁAW 2025

Dedication

I wish to extend my sincere gratitude to my family and close ones for their steadfast emotional support and motivation, which have been of immeasurable value throughout the course of my doctoral studies.

I am equally indebted to my supervisor and co-supervisor for their invaluable scholarly guidance, constructive advice, and continuous support. Their profound expertise and dedicated mentorship have been instrumental in bringing this dissertation to completion.

Contents

1 General

1.1 Nomenclature

@KEY	-	Method in SOFiSTiK to refer in Teddy to results database
AESO	-	Additive Evolutionary Structural Optimization
AI	-	Artificial Intelligence
Animator	-	SOFiSTiK's animated results visualizer
APA	-	All Parameters Applied
BESO	-	Bi-directional Evolutionary Structural Optimization
BIWAP	-	Manually added best individual with all remained parameters
BIWNP	-	Manually added best individual with hangers' topology but without the original remaining parameters
CARSM	-	Constant Angle to Radius Slope Model
CDB	-	SOFiSTiK's computed database
CS	-	Cross Section
CSM	-	Constant Slope Model
CSMP	-	Construction Stage Modeling Process
DE	-	Differential Evolution
DRL	-	Deep Reinforcement Learning
EA	-	Evolutionary Algorithm
ESO	-	Evolutionary Structural Optimization
FDL	-	Factor Delta L (from SOFiSTiK manual)
FEA	-	Finite Element Analysis
FEM	-	Finite Element Modeling
FLS	-	Fatigue Limit State
GA	-	Genetic Algorithm
GF	-	Goal or Objective Function
GH	-	Rhinoceros Grasshopper
GNA	-	Geometrically Nonlinear elastic Analysis
GNIA	-	Geometrically Nonlinear elastic Analysis with Imperfections
GM	-	General Method for lateral and lateral torsional buckling of structural components
GMNIA	-	Geometrically and Materially Nonlinear Analysis with Imperfections
Grasshopper	-	graphical programming environment
GSS	-	Gradient Step Size
LBA	-	Linear Elastic Bifurcation Analysis
LM71	-	railway load model
ML	-	Machine Learning
NAB	-	Network Arch Bridge
NBA	-	Nonlinear elastic Buckling Analysis
NN	-	Neural Network
NPA	-	No Parameters Applied
PDF	-	Probability Density Function
PLC	-	Primary Loadcase
PSO	-	Particle Swarm Optimization

PUSH	-	post-critical analysis in SOFiSTiK
QUAD	-	Shell element in SOFiSTiK software
Rhinoceros	-	Geometry generation software
SLS	-	Serviceability Limit State
SOFiSTiK	-	Finite Element Analysis software
SPS	-	SOFiSTiK's hidden solver (without program window)
Teddy	-	SOFiSTiK's code compilation environment
TH2	-	2nd order theory
TH3	-	3rd order theory
TH3b	-	3rd order theory for all elements except beam elements Analysed in 2nd order theory
TS	-	Tandem Load
UDL	-	Uniformly Distributed Load
UGLI	-	Unique Global and Local Imperfection
ULS	-	Ultimate Limit State
ULTI	-	Load incremental procedure in SOFiSTiK running until unstable Solution is achievement
V-CSM	-	Variant-Constant Slope Model
Wingraf	-	SOFiSTiK's detailed results visualizer
WPS	-	SOFiSTiK's visible solver (with program window)

1.2 Symbols

α_{cr}	-	critical load factor
$\alpha_{cr,ip}$	-	critical load factor for in-plane buckling
$\alpha_{cr,op}$	-	critical load factor for out-of-plane buckling
χ	-	buckling factor
χ_{LT}	-	lateral torsional buckling factor
χ_{ip}	-	in-plane buckling factor
χ_{op}	-	out-of-plane buckling factor
$\alpha_{ult,ip,k}$	-	the minimum load amplifier of the design loads to reach the characteristic resistance of the most critical cross section of the structural component considering its in-plane behaviour without taking lateral or lateral torsional buckling into account however accounting for all effects due to in-plane geometrical deformation and imperfections, global and local, where relevant
$\alpha_{ult,p,k}$	-	the minimum load amplifier of the design loads to reach the characteristic resistance of the most critical cross section of the structural component considering its in-plane behaviour without taking lateral or lateral torsional buckling into account as well as all effects due to in-plane geometrical deformation and imperfections, global and local, where relevant
$\alpha_{ult,s,k}$	-	the minimum force amplifier for the axial force configuration N_{Ed} in arch to reach the characteristic resistance N_{Rk} of the most axially stressed, cross section without considering in-plane imperfection
η_{init}	-	imperfection shape
$\eta_{cr,ip}$	-	buckling shape
$N_{cr,ip}$	-	in-plane critical force
$N_{cr,op}$	-	out-of-plane critical force
η	-	utilization

1.3 Naming convention

stage	-	contains initial and final part in the first attempt of the optimization algorithm; The first part includes ESO method and the second part includes both ESO and GA methods
phase	-	part of ESO method in both stages in the first attempt of the optimization algorithm; Divided into three parts, called 0, 1 and 2
step	-	a pair contains one each of both ESO and GA methods in the final stage in the first attempt of the optimization algorithm
critical point	-	the unstable point on a critical path with geometrically nonlinear analysis
bifurcation point	-	the unstable point on a critical path within linear elastic bifurcation analysis where at least two load-deflection paths cross and are mathematically valid

2 Introduction

2.1 Description of Network Arch bridges

The network arch bridges are tied-arch bridges with network hangers' arrangement, in which each hanger cross other hangers at least twice [113]. The first concept was developed by Nielsen in his patent in 1926 [107], where hangers crossed once. He continued his research in PhD dissertation [68]. It was then improved by Per Tveit starting from his Master's thesis in 1955 [106], who continued to develop this concept in his PhD thesis from 1964 [103] and for the rest of his carrier and propagated this new type of arch bridges. He conducted lectures in over 50 countries around the world [114]. He published many technical reports [100, 102, 113], conference materials [107, 116, 109, 111, 112] and articles [108, 105, 104]. All these Tveit's researches and developments will be referred collectively by this manuscript [115], where this knowledge is included and partially repeated collectively in all articles. Tveit updates this manuscript with new information. The collection of knowledge from Tveit and other authors about network arches is included in manuscript [117]. Individual breakthrough discoveries from these and other authors will be cited separately.

There are three most popular network hangers' arrangements [75]. The first one is Constant Slope Model (CSM) [115], which has constant slope inclination of the hangers along the span length, Fig. 2.1a. The second is Variant-Constant Slope Model (V-CSM) [115], where the slope inclination is changing along the bridge, but the difference of hangers' inclinations is constant, Fig. 2.1b. It is a more general definition than CSM. The last is Constant Angle to Radius Slope Model (CARSM) or radial hangers' arrangement [87], which is constructed by making hangers inclined by a constant angle to the uniformly distributed lines on the arch perpendicular to the circular arch curvature, Fig. 2.1c.

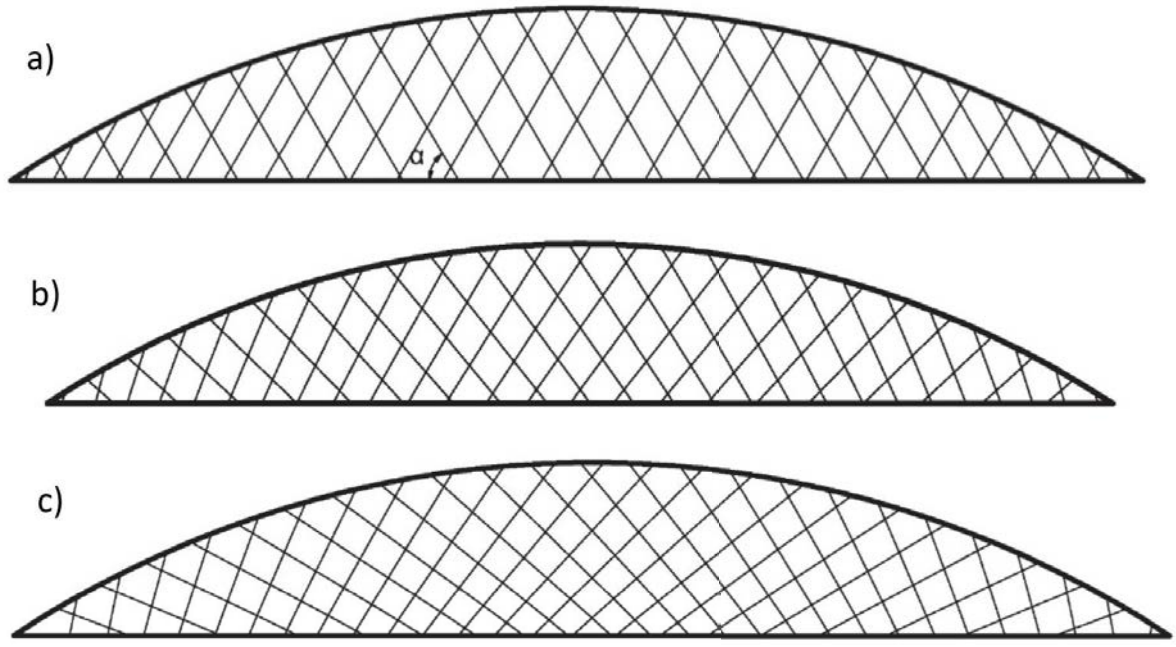

Figure 2.1 Arrangement considered in [75] with (a) constant slope model (CSM), (b) variant-constant slope model (V-CSM) and (c) constant angle to radius slope model (CARSM) or radial hangers' arrangement

The tied-arch bridges are arch bridges with tie-deck integrated with the arch and carrying the entire horizontal forces from the arch. Therefore, arches are compressed, and ties are under tension. Since the internal forces are self-balanced in tied-arch bridges, the abutments are smaller than for arch bridges, where the abutments have to take the entire horizontal force [115]. Due to tension forces in the tie, it can be made of post-tensioned concrete slab [115], steel grid or composite steel and reinforced concrete deck [42]. In case of steel section presence, the most common are hollow sections for span length above 100 m [115]. The arches can be made of steel profiles, preferable universal column UC [115] or HD section, but also hollow circular [64] or rectangular sections [42]. The arches are mostly braced with each other for carrying wind loads and improving buckling properties [115].

The arches can be inclined inwards [115, 64]. The recent studies utilized also concrete arches [120], arches inclined outwards [120], non-braced arches [120], arches made of glulam [72], aluminium [139] and double network arches combined [83]. Arches can be shaped as a part of ellipse, mixture of circular parts with different radius or simply circular arch [115, 19]. The recent studies proved, that non-symmetrical arches are equally economic as symmetrical [129]. The arch elevation is usually equal to 14-17% of the span length [115]. The hangers can be made of structural steel or cable steel with the circular section [115]. The recent studies utilized carbon-based hangers [92, 63] and diverged hangers' arrangement [72]. The relaxation of the hangers was one of the most important obstacles, that Tveit faced during his initial research [103]. The relaxation of the hangers causes problems with hangers' fatigue and arches' increased localized bending moments [115]. The well-defined hangers' arrangement have this problem solved [115]. The manual adjustment of hangers near ends are required in order to reduce locally increased bending moments [115].

The network arrangement of the hangers causes low bending moment amplitudes in the arch and the tie, which increases the material and cost efficiency, making this type of arch bridges slender and the most economic [115]. A good example is Brandanger bridge, Fig. 2.2 [115]. The dominant internal force in the arch is normal force, therefore the arch can be made slenderer than in classic arch bridges with vertical hangers' arrangements [115]. The shear forces in the arches are compensated by the hangers, which act as a web analogue in the steel girder sections [115]. Since the material efficiency of the structure is high, the overall weight is low, which makes network arches easy to install even in one piece [115].

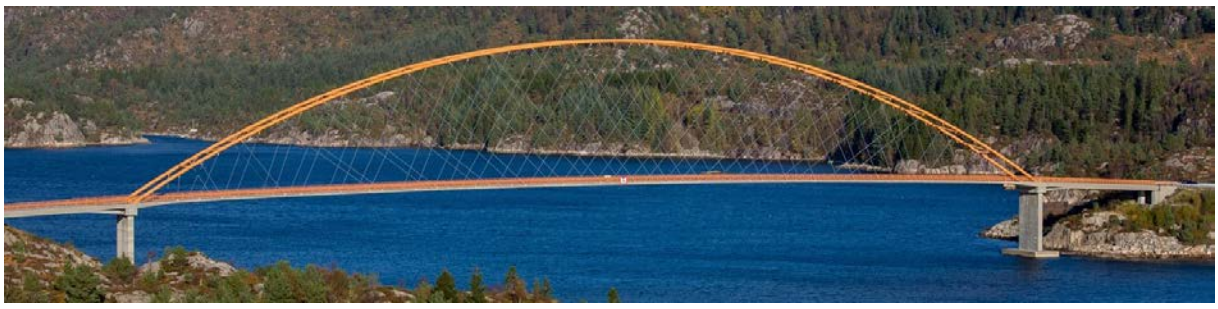

Figure 2.2 Illustrations of the Brandanger bridge [142]

The network arch bridges are used for pedestrian, road and railway traffics purposes [115] [19]. Their effective span length is between 80 and 170 m [115], but bridges with 55 m [139] and 380 m [143] also exist, covering great part of middle span bridges. Due to their much greater stiffness than in vertical hangers' arrangement [115], they can be slender and robust even for railway traffic, which is more restricted in deformations criteria than for other traffic loads [115]. They are also suitable for seismically active regions, as confirmed by bridges built

in Japan [115].

The improvements in terms of internal forces distribution in the arch and the tie in the already well-defined arrangements progressed in early 2000s. The optimal number of hangers divided by the span length expressed in meters was obtained as constant value of maximum 0.48 [87] for span length of 100 m. Other research tested different arrangements and set this value for span lengths less and 100 and up to 250 m [97]. After thousands of iterative calculations, the radial arrangement was considered the most optimal in terms of internal forces distribution for 100-150 m of span length [75]. For span lengths outside these limits, the V-CSM was governing or was equally well [75]. The angular characteristics of hangers' inclinations were confirmed similar by independent researches. Author in [97] iteratively calculated and compared tied-arch bridge with constant inclination arrangement (CSM), uniformly increasing inclination angle arrangement (V-CSM), uniformly decreasing inclination angle arrangement, radial arrangement (CARSM) and constant distances between the hanger connection points in the middle of the lower chord arrangement. The uniformly increasing inclination angle and radial arrangements were the most favourable in terms of internal force distribution. Author in [75] calculated and compared constant inclination arrangement (CSM), uniformly increasing inclination angle arrangement (V-CSM) and radial arrangement (CARSM). The most optimal arrangements were V-CSM and radial but their dominance varied from number of hangers and span length. Authors in [97, 75] provided optimal shaping of each favourable arrangement in terms of internal force distribution. The iterative approaches had their limits due to vast number of predefined geometries to calculate, counted in thousands [97, 75]. Authors started to improve arrangements and geometrical properties of well-known arrangements. The utilized optimization techniques were among others pattern search optimization [6], multi-step optimization process [13], gradient algorithms based on sparse nonlinear optimizer [13], simulated annealing [7], evolutionary operation [2, 40], particular swarm optimization [7], genetic algorithm [94]. The researches used mass minimization [7], volume minimization [13] or internal forces minimization objective function [93]. The network arrangements showed well properties in reducing bending moments in the arch and the tie, but the smaller their number, the greater these amplitudes got [93]. The genetic optimization algorithms allowed to search through custom made hangers' arrangement [94]. So called sparse system provided lower objective function value oriented around informing internal forces in the arch and the tie than radial arrangement showing a room for improvement with smaller number of hangers [93]. The recent studies utilized cost as a objective function component [2, 40] but used the same material properties in the process, which means that price for each material was constant in the optimization process. One article was found, which considered various steel grades with different prices [52], but for tied-arched with vertical hangers, not network hangers' arrangement.

All of the mentioned aspects make network tied-arch bridges a good candidates for the economic, aesthetic and easy to construct structures that can be used for variety of span lengths and all traffic loads even in demanding, seismic regions [115].

2.2 Motivation

The network arrangement in tied-arch bridges [115, 117] was proven to be more optimal in terms of material usage and internal forces distribution than other types of hangers' arrangements. The leading arrangement so far was radial arrangement for majority of cases alternated by V-CSM arrangement [75, 97]. At the same time, even though progress was made in network arrangements, the most optimal solution in terms of material or internal forces minimization remained unknown due to the complexity and nonlinearity of these structures [115, 117]. The

requirement of a manual modification near end suggested [87, 83], that there was still room for improvement near the ends. The sparse hangers' system showed [93], that the network arrangements started to result in greater internal forces' amplitudes than custom made arrangement if the number of hangers was limited and arrangement principles were not restricted to known solutions. Therefore, there is room for improvement at least of hangers' arrangement in sparse system. Authors in papers [4, 35] showed the importance of including geometrical nonlinearity in the out-of-plane buckling analysis, since the linear approach led to capacity overestimation. According to author's best knowledge, the existing literature did not provide a systematic methodology for determining the influence of geometrically nonlinear in-plane buckling on the capacity of the arch.

The optimizations done so far were based on iterative calculations of predefined geometries [75, 97] or optimized with modern optimization algorithms with among others genetic algorithms [93] and particle swarm optimization [6] as the most popular metaheuristic approaches. The iterative approaches [75, 97] could not investigate more than were predefined and were time-consuming. Metaheuristic-based methods often involved simplifications in geometry and calculation procedures. None of them included geometrically nonlinear buckling analysis, and in some cases, buckling analysis was omitted entirely [6]. They focused on changing the geometry of the bridge, sections' properties, hangers' quantity and their arrangement but within the already known and well described arrangements. Two publication was found, which additionally defined cost-oriented objective function, but unit cost for material remained the same, since material did not change [2, 40]. The cost-oriented objective function with different price for varying steel grade was observed in tied-arch bridge optimization, but with vertical hangers [52]. In other optimization processes the geometry of the structure and cross sections of the arch and the tie were kept constant, while the hanger cross sections and any distribution of hangers were allowed to vary [94, 93]. This made it possible to check custom-made arrangements, but for one predefined number of hangers for a single optimization process. The objective functions were mostly based on relevant values of internal forces or mass of the structure [6, 75, 97]. All found articles within network arch optimization had predefined steel and/or concrete strength during the optimization process, since it did not affect the mass or redistribution of internal forces, and so did not affect objective function value. Authors in [6] noticed, that limited optimization process leads to situation, where obtained parameters reflecting optimal solutions are scattered and less restricted process should allow to solve this problem.

After conducting a literature study, author noticed rooms for improvements:

- There was no optimization algorithm that optimized the structure including geometry, cross sections, material properties and allowed to have any hangers' arrangement with changing number of hangers at the same time in the optimization process. The goal function would focus on cost reduction, which would allow for including material properties as a variable, since capacity of material is positively correlated with its cost. Such an approach was considered more general and would allow for exploring solutions not discovered so far. Introducing the option of any hangers' arrangement would allow for the creation of a more general optimization algorithm, although at the cost of increased complexity. The objective function based on material and assembly cost would help in exploring more possibilities in geometry shaping than using only one steel grade and/or concrete class,
- Researches in network arches optimization did not utilize buckling analysis that would include the in-plane geometrically nonlinear behaviour of hangers. Author wanted to investigate this impact in relevance to linear elastic bifurcation and include the more accu-

rate nonlinear approach in the optimization algorithm for correct capacity determination of the arches.

Another motivating factor was related to the market demand for increasingly sustainable and cost-effective structures. The network arches were considered the most optimal in terms of cost for the middle range of span lengths, which covered a great portion of the designed bridges. At the same time, this type of arch bridge was not that commonly used and was met with resistance from person in charge of accepting this as a solution according to authors' experience from [86]. Considering the fact that there was still room for improvement and low acceptance in the industry, the author was motivated to:

- Investigate new possibilities and contribute to the popularization of this type of bridges,
- Establish an optimization algorithm that could be reused by other engineers. Having this in mind, the pipeline was intended to be developed in a way where the FEA software could be replaced by other and the external code could be coded in other, more suitable to user preferences script language, but the principles would remain the same.

The aim of this dissertation was to improve and implement these components into the optimization algorithm. At the same time, author wanted to make own pipeline of optimization in order to have more control of the optimization process. The first developed optimization algorithm was too restricted by external Grasshopper (GH) plug-in, but the lessons were learned, and the second developed version had every aspect custom-made as desired and provided the desired results.

2.3 Objective of the dissertation

The primary objective of this thesis was to define an original optimization algorithm (O) capable of achieving greater cost reductions in network-like tied-arch bridges than those attainable with conventional, well-established network arrangements. Additionally in this dissertation, the author aimed to demonstrate the following results (R) and actions (A):

- (R1) The possibility of having any hangers' arrangement at the same time with geometry, cross section, material capacity modifications and any number of hangers in the optimization process defined with cost-oriented objective function allows to obtain more cost-efficient solutions than the known and well-defined network arch arrangements,
- (R2) In the cost-oriented optimal solution, the regions near the ends have different hangers' arrangements in comparison to hangers' arrangements in the middle part of the span length. The transition between these regions is smooth,
- (R3) The critical form of the arch in a network arch bridge in geometrically nonlinear buckling analysis is a multi-periodic sinusoidal wave, similar to the buckling mode of a beam continuously supported on springs and results in lower critical load factor and lower buckling resistance than in linear elastic bifurcation analysis,
- (R4) The network-like arrangement of hangers is the most cost and mechanical-efficient type of arrangement in tied-arch bridges,
- (A) Determination of the price, weight and geometrical properties guidelines of optimal bridges in terms of cost minimization for varying span lengths and deck widths.

2.4 Scope of work

Section 3 presented the review of optimization methods for global optimization process of structures, the types of arch bridges and development of network arch bridges, including their improvements progression, as well as global optimization approaches developed exclusively for network arch bridges. The section included design principles and comparisons to other types of bridges in terms of material efficiency.

In section 4, the investigation of geometrically nonlinear buckling analysis on the in-plane capacity of the arch in network arch bridges was conducted. It included presentations of various approaches from Eurocodes and literature to the in-plane instability problem, the tests on simplified cases of the used software in terms of assessing the correctness of its calculations, as well as tests on the network arch bridge with changing parameters of pretension force, post-tension force, elevation and single or double rapture of hangers. The results were compared with the literature's simplified approaches and linear elastic bifurcation analysis results in terms of arch's section capacity and relevant conclusions were formulated.

In section 5, the first optimization approach was described in principles and tested. It included genetic algorithms combined in a loop with simplified evolutionary structural optimization. The optimization was divided into two stages, which were subdivided into phases. Each next phase and stage were characterized by increasing detail of the calculations and design method as the number of hangers gradually declined. The final results were not achieved, since the tests of the established algorithm showed geometrical instabilities within SOFiSTiK during analysis, cross-software integration issues between Grasshopper and external Python code, undesired excessive hangers sagging, limitations of GA included in Galapagos module, increased complexity of concrete section design and ESO limitations. The projected time consumption was also not acceptable. Therefore, the conclusions were formulated.

Section 6 included the improvements concluded from the 1st optimization algorithm attempt. It introduced several simplifications, among others, load application, reduction of the structure to a plane model, replacement concrete by structural steel elements. The optimization algorithm was based on the custom-made genetic algorithm coded in Python without any external optimization-oriented extensions, with integrated possibility of mixing and changing number of hangers in the process as well as integrated custom-made gradient descent algorithm. The new approach was tested and improved by implementing modifications to the optimization algorithm. The algorithm was tested on the existing structures with successful cost reduction in each case. The long simulation was conducted for various span lengths and deck widths, and the optimal results were achieved and integrated. The analysis of the results was done in terms of finding universal principles in shaping network arch bridges, as well as new type of hangers' arrangement named Multi-Variant Angular Divergence Model (MVADM) was established and tested against optimal CARSM arrangements. The conclusions were formulated and the field of improvements of the new arrangement, as well as further research plans, were presented.

In section 7 the conclusions from the conducted researches were presented, which included: (1) the results description of the in-plane geometrically nonlinear analysis in the network arch bridges in comparison with the analytical solutions and linear elastic bifurcation analysis results, (2) the lessons learned from the first optimization algorithm, (3) the suggested improvements learned from the first optimization algorithm that were implemented into the second optimization algorithm, (4) the cost- and weight-oriented optimal results comparison with the literature guidelines and real structures, (5) shaping guidelines description according to obtains cost-oriented optimal results, (6) description of the authored MVADM and comparison with CARSM.

The section 8 the plans on further researches were presented, including: (1) investigation

of concrete tie in the optimization process, (2) separate determination of in- and out-of-plane critical load factors with geometrical nonlinearity, (3) including higher structural steel grades in the optimization process, (4) determination of missing cost-oriented optimal parameters of MVADM arrangement, (5) modification of GF formula by combining the two-step optimization process into a single-step procedure, (6) determination of imperfection shape and amplitude value of the arch in network arch bridges including geometrical nonlinearity.

3 Literature review

3.1 Optimization algorithms

In Annex A, for the reader's convenience, same optimization methods were discussed in more details. More details about optimization techniques used in network arch bridges are presented in Sec. 3.2.2.

In civil engineering, one of the most commonly used root and solution searching algorithms are bisection, false position, fixed-point, Newton-Raphson and secant [15]. They are mainly used in convergence problems in structural optimization. For instance, the bisection method can be used in solving for parameters in frequent equations for vibration modes [41], in shape-finding of cables in suspension bridges [122], finding instability bifurcation point [65]; the false position method is found in solving nonlinear equations in structural mechanics [30]; the Newton-Raphson method is used in cables' form-finding in suspension bridges [77] or in finding numerical solution of a reinforced concrete beam [90]; the secant method can be used in cables iterative force determination process for hangers in suspension bridges [57]. These methods are mainly used in the local problems, as the aforementioned form-findings or section optimization, due to their fast convergence, but their utilization is limited mainly to the local problem solving, not the global optimization approaches, which are much more complex. One of the restrictions are the continuous function and in case of Newton-Raphson method also continuous first derivative, which are considered as disadvantages in case of unknown function characteristics [15]. The starting points of these methods have to be chosen close the searched root, otherwise the method might not converge [15]. Nevertheless, they can be utilized in the optimization subprocesses in the global optimization approach, such as iterative determination of sagging effect in cables provided in finite element analysis (FEA) software.

The next type of algorithms is minimum/maximum search. As the contrary to the root search algorithms, the exact value to search for is unknown, but the goal is to obtain the most extreme possible value of the unknown function [15]. One of the most common examples in structural optimization is gradient-based method [125]. The gradient-based methods are considered as a conventional procedure at the initial stage of optimization [15]. They are simple in application, but come with couple of drawbacks, such as converging to local optima, inefficiency and difficulty in implementation in complex problems, the requirement for problem continuity, and method-specific limitations that make them unsuitable for all scenarios [15]. However, they reach local extreme value fast and guarantee local convergence, but they are highly depended on the starting point and the quantity of the local convex regions [15]. The unknown function can be multidimensional, which makes them applicable in the optimization tasks with many variables. The algorithm does not guarantee reaching the global extreme value [15]. Nevertheless, gradient-based algorithms are still used for example, among others, in cable-stayed bridge optimization [60], suspension bridges optimization of cable geometry determination [99], obtaining "the deflection influence line of the bridge dynamic test structure and the overall vibration frequency of the structure" [119], "optimizing a vehicle's suspension characteristics for

ride comfort" [99], in the shape global optimization of the structure [74]. Other gradient-based methods are machine learning and artificial neural network [25].

Authors in paper [25] describe applications, advantages and challenges regarding supervised machine learning (SML), unsupervised machine learning (UML) and reinforcement machine learning (RML). These methods are used well in fields like real-time stress prediction, reducing computational effort in nonlinear stress analysis, formulating material stiffness matrix, predicting damage, optimizing the manufacture process, automatic mesh generation and others [25]. These fields are great support to reduce the computational time, which in complex structural optimization plays a key role [25]. Nevertheless, using the available software, these improvements can only be made by the suppliers, not engineers, the users. Machine learning requires great data set, which is hard to achieve with long time demand for the calculation of a single model in civil engineering [25].

Therefore, the metaheuristic methods get more attention as an intermediate approach between gradient-based and machine learning methods (ML) [125]. Hybrid methods that combine machine learning and metaheuristics are also present in the literature [16]. The most commonly mentioned in bridge optimization [125] are ant colony optimization (ACO), genetic algorithm (GA), tabu search, artificial bee colony (ABC), particle swarm optimization (PSO). Recently, the hybrid algorithm was developed [17, 14] enhancing the traditional metaheuristic algorithms. One of the examples is combining harmony search algorithm with particular swarm optimization [17], integrating gradient-based algorithm with particular swarm optimization [14].

The metaheuristic approaches are a more sophisticated approaches of a random search optimization method [15, 39]. They do not require continuity of the problem function, which makes them flexible in application, more than gradient approaches. They are suitable for large problems with many local optima [15]. Metaheuristic algorithms still require a lot of computations power and have to be adopted to the specific problem by adopting their parameters [125]. The random component and the initial higher exploration make metaheuristic algorithms less vulnerable being stuck in local optimum [125]. Nevertheless, the global optimum is not guaranteed [1]. They are characterized by exploration and exploitation [1]. Exploration takes place at the beginning and allows to reduce the chance of exploring only local optimum region [1]. Overtime, the algorithm starts to be more concentrated on the best solution and exploit this promising region near it [1]. These methods are recently popular not only in bridge optimization, but specifically in network arch bridges. For instance, authors in [94, 93] use GA in their optimization. In [7, 6] the GA and PSO are used and concluded, that the efficiency of these two algorithms is comparable. The evolutionary operation (EVOP) is included in [40, 2]. The hybrid methods are also presents, for instance combined evolutionary algorithm with pattern search [6], sparse nonlinear optimizer (SNOPT) with quadratic programming (QP) solver [13], combined PSO with simulated annealing [7].

From the comparisons presented in [1], the fastest metaheuristic algorithms on 30 tested functions are DE, PSO and GA respectively. The GA reaches global optimum faster for smooth functions and functions with noise [1]. According to author's own experience from Master thesis [11], the first property of reaching fast the optimum in smooth goal function is suitable for section optimization and worked faster than PSO algorithm. According to [115], the bending moments in network arch bridges are desired to be low. That makes these bridges more sensitive to hangers' position change than vertical hangers' arrangement, where the bending moments are greater by an order of magnitude or higher. Since GAs are suitable for noise functions as well [62], it makes them suitable for their optimization.

3.2 Arch bridges review

3.2.1 Types of arch bridges

Arch bridges used to be utilized even by ancient Romans [10]. The arches were made out of stones and were based on the compression force, since stone blocks or later brick work better under compression [10]. As time passed, the new materials of reinforced concrete and steel were developed, which opened doors for greater spans and more economic solutions, but the main principles remained the same. The significant compression force from the arch is handled by the soil at the end of the arch [156]. The greater the arch is and the less inclined it gets, the greater the horizontal force that needs to be transferred to the ground [156]. The horizontal force can be greater than the vertical component if arch's elevation is low enough, requiring greater foundations and/or more robust soil [156]. This type of bridges is especially valuable in mountain regions, where rock is shallow and bedrock's greater than soil capacity is utilized in order to withstand horizontal force from an arch [156]. Otherwise, bigger foundations are required, which might be an argument against this type of bridge in terms of cost efficiency of the project in regions without sufficient soil conditions from author's experience.

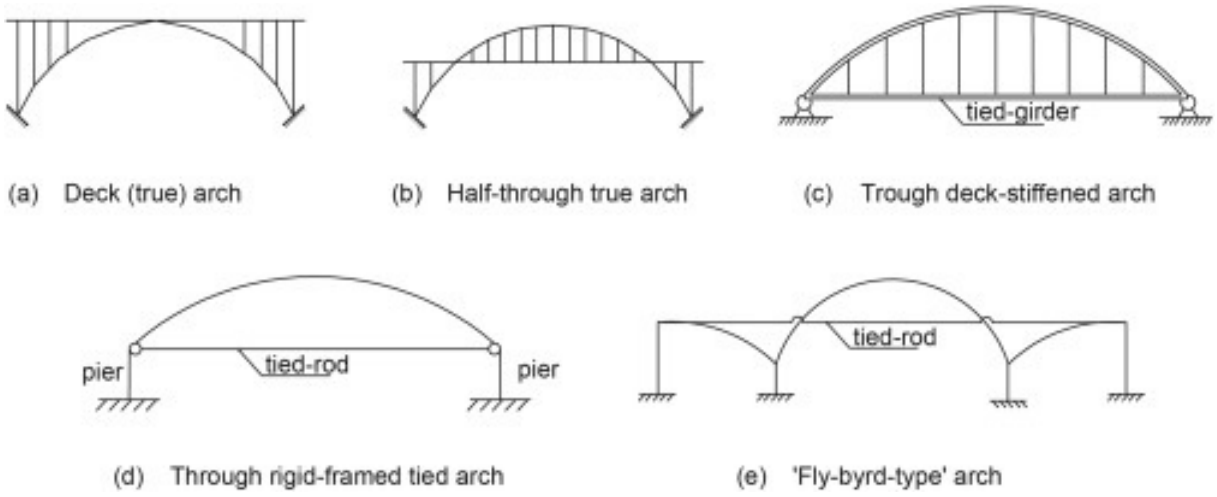

Figure 3.1 Types of arch bridges [138]

Among many types of arch bridges, the most principle are presented in Fig. 3.1 [138]. The deck arch bridge, Fig. 3.1a, is the oldest type of arch bridge. The live loads are applied on the deck above the arch, which can be filled with solid material, as ancient stone bridges, or with vertical ties as in modern bridges. The oldest type of modern arch bridge is The Ironbridge from 1779 [155], Fig. 3.2. The next type is half-through arch, Fig. 3.1b, where the deck is located approximately in the middle of the height of the arch. It requires introduction of both compressed and tensioned vertical ties connecting the deck with the arch. Nevertheless, the horizontal forces are still significant in the foundations. The simplified version is tied-arch bridge, Fig. 3.1c, where the deck is located under the arch and the vertical ties are under tension. The deck acts as a tie taking the entire horizontal force and making the bridge self-balanced in a static schema of freely supported beam. Thanks to that, the foundations can be much smaller taking mainly vertical components, which makes it more cost-efficient and accessible in places with worse soil conditions. The last types are through framed-tied-arch bridge, Fig. 3.1d, and fly-byrd-type arch bridge, Fig. 3.1e, which are a variant of half-through arch and tied-arch bridges.

Figure 3.2 The Ironbridge [155]

Figure 3.3 The Windsor Railway tied-arch bridge [159]

The first known example of tied-arch bridge is Windsor Railway Bridge from 1849 [159], which is still in operational, Fig. 3.3. The arch and the tie are connected by truss-like structure in between [159]. The truss-like structure was later replaced by more efficient and slender hangers and their arrangement developed over time. The most common topologies of hangers are vertical, fan, Nielsen and network, Fig. 3.4 [138].

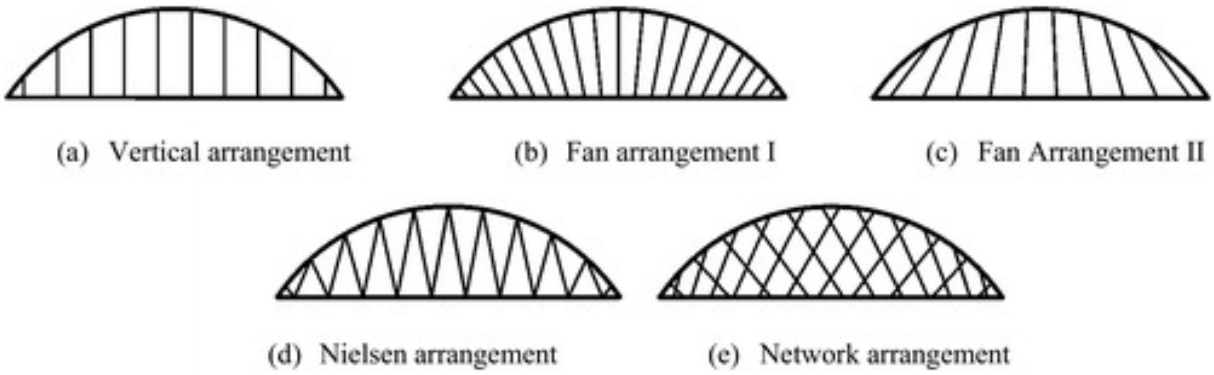

Figure 3.4 Types of hangers' topology in tied-arch bridges [138]

The vertical, Fig. 3.4a, and fan hangers, Fig. 3.4b and c, can be considered as the same type, since the differences in stresses distribution are negligible [20]. They are characterized by the simplest topology among arch bridges. The arch used to be made of steel beams or trusses for larger spans and the tie used to be made of steel grid, boxes, composite or post-tensioned concrete elements [115]. Their common use in the past, made them well described in EN 1993-2 in terms of buckling analysis and requirements [134]. Since the bending moments are the dominant internal forces in both the arch and the tie, the cross sections of arches used to be hollow, to make them more stocky [115].

The hangers' topology concept, that resulted in more stiff structure and improved internal forces distribution in arch and tie, was patented by Nielsen in 1926 [107], Fig. 3.5a. He continued research in his PhD thesis [68]. In the contrary to vertical hangers' arrangement, the hangers crossed with each other maximum once, which helped in better distribution of loads between the arch and the tie by even an order of magnitude [18]. However, Nielsen had never utilized his patent [107] and his design from 1928 in Sweden contained inclined hangers similar to his patent, but without crossing with each other, Fig. 3.5b [107]. It was called Nielsen hangers' arrangement, Fig. 3.4d. The solutions to both the arch and the tie are similar to the tied-arch bridges with vertical hangers. According to authors [18] in case of significant unsymmetrical live load, the relaxation in hangers causes the arch and the tie in Nielsen arrangement to act similarly to vertical hangers' arrangement.

a) Nielsen patent 1926

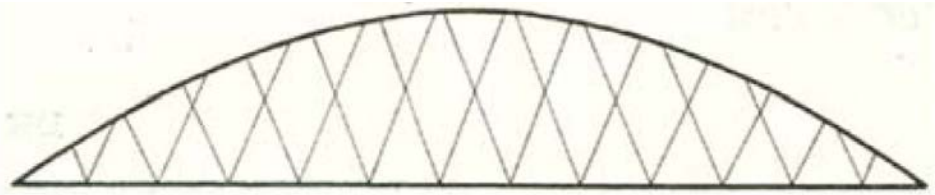

b) Nielsen design in 1928

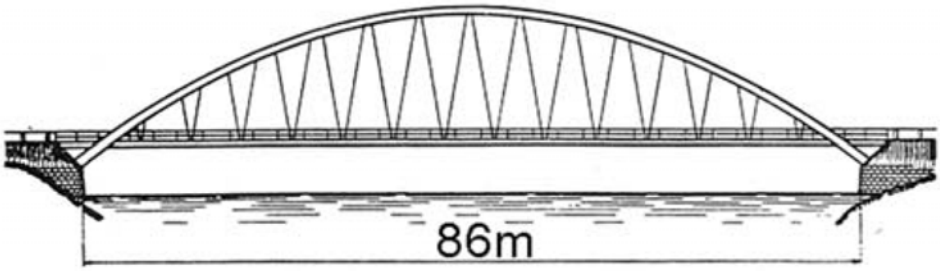

Figure 3.5 Nielsen patent from 1926 (a) and Nielsen's design from 1928 (b). The patent has never been utilized by Nielsen [107]

The last type is network arch bridge, Fig. 3.4e, so called NAB, where the hangers cross between each other at least twice [115], and it is considered as the most optimal hangers' arrangement type in tied-arch bridges [115]. This type of hangers' topology was suggested by Tveit in his graduation thesis from 1955 [106] and continued in his PhD thesis from 1959 [103], as presented in Fig. 3.6, and was not widely recognized at the beginning. The Riesa bridge, Fig. 3.7, with similar topology, but compressed truss system, which Tveit mentioned in his graduation thesis from 1955 [106], did not gain much attention despite improved mechanical properties in

comparison to traditional vertical hangers' arrangement. The network arrangement makes the arch and the tie even stiffer comparing to the Nielsen arrangement, which reduces the bending moments and deflections severely, even by two orders of magnitude, comparing to the standard vertical hangers' topology as presented in Fig. 3.8 [86]. Author of [18] made independent comparison of vertical and network arrangement and went into the same conclusion published in [86]. Because of much lower bending moments in both the arch and the tie, the cross sections can be slenderer than so far [115, 117]. Tveit proposed cross section of universal column UC [115, 117] for the arch, since it has great cross section area and is slender with lower bending capacity since it is not needed that much as in vertical hangers' arrangement. Furthermore, the UC cross section requires less welding than box sections, it is easier to manufacture by bending the element with desired curvature according to authors' experience in [45, 126]. Because of the great thickness of the flanges reaching 140 mm, the steel grade needs to be reduced [132], but nowadays there are technological procedures to keep the steel grade much less affected by wall thickness effects, like HISTAL [137]. In the welded joint between two elements with HD or US cross section, the shear capacity is reduced, but since the shear forces in the arch are relatively low, lower capacity is not an issue [127]. Nevertheless, the first network arch bridge (NAB) designed by Tveit in 1963 in Steinkjer does not have HD nor UC section, but closed triangular box [113], Fig. 3.9 and Fig. 3.10.

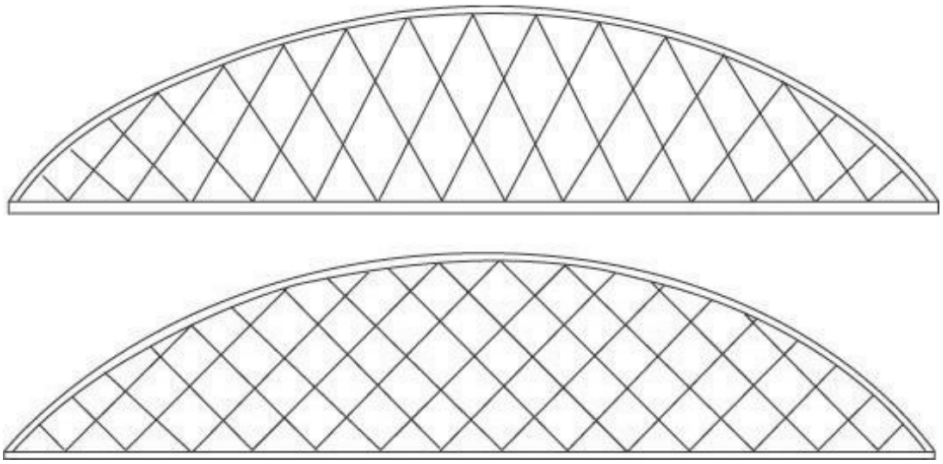

Figure 3.6 The original network arrangement proposed by Tveit in his Master thesis from 1955 [106]

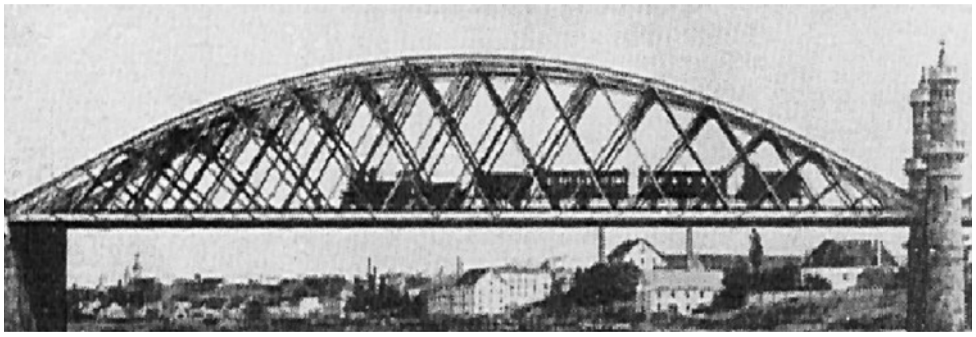

Figure 3.7 The Riesa arch bridge over the Elbe built in 1877/78 [117]

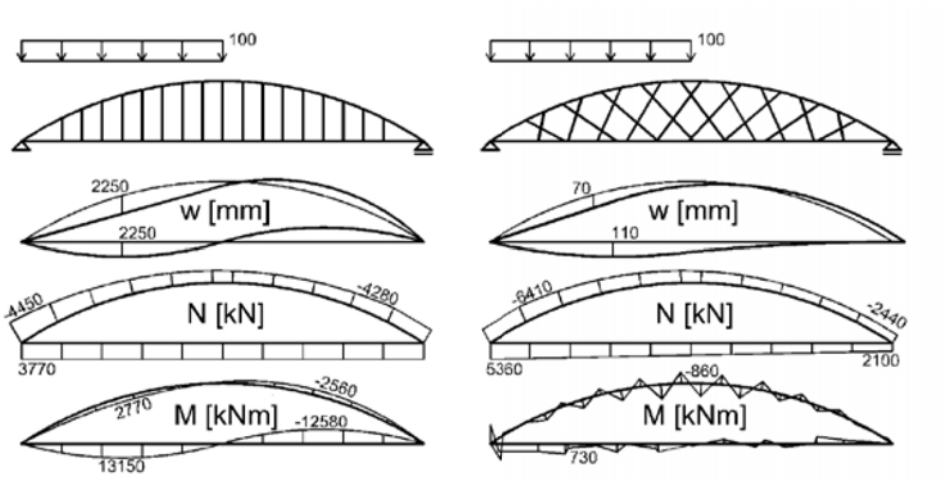

Figure 3.8 Difference in displacements *w*, normal forces *N*, bending moments *M* in arch bridges with vertical (left) and network (right) hangers' arrangements [129]

Figure 3.9 The bridge in Steinkjer designed by Tveit and opened in 1963 [107]

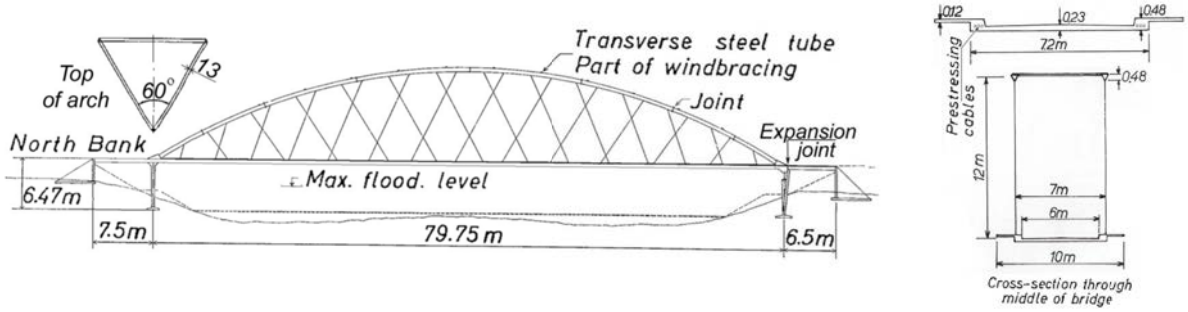

Figure 3.10 The technical drawings of the bridge in Steinkjer designed by Tveit and opened in 1963 [107]

When it comes to the tie, the reduced bending moments allow a reduction in height and shift focus from lateral into axial-oriented section properties [115, 117]. Tveit proposed a tie made of post-tensioned concrete slab with edge beams at the line determined by the hangers' plane [115,

117]. This is applicable for the distance between hangers' planes lower than 20 m [115, 117]. For the distance between arches greater than 10 m, the transverse post-tension force should be applied. Smooth distribution of internal forces in the tie makes uneven distribution of hangers' anchorages in the tie acceptable [115, 117]. However, hangers' anchorages along the arch are recommended to be evenly distributed [115, 117]. The example of the cross section for the arch and the tie are presented in Fig. 3.11 [115].

Figure 3.11 The example of proposed type of sections for the arch, UC section, and the tie, post-tensioned concrete slab [115]

In order to prevent from hangers' sagging effect and correct imperfection caused during assembly, forces in hangers are adjustable [115]. Since the adjustment of one hanger has an impact on nearby hangers due to relatively low stiffness of the deck, hangers used to be adjusted in multiple rounds [115]. In Hangar bridge hangers did not require adjustment of internal forces [139]. No sagging effect of hangers' is important for internal force distribution between the arch and the tie, which provides lower amplitude of bending moments and allows for slender arch and tie [115]. Tveit determined the necessary slope of hangers [113] for reasonable height to span length ratio in the NAB. Hangers' inclination is dependent from ratio of live load to dead load and load length to span length. In general, the greater the height-to-span length ratio is, the greater hangers inclination. Secondly the greater the live-to-dead load ratio and load-to-span length ratio, the lower the inclination can be. The exception to these trends is a concentrated load with low live-to-dead load ratio value.

Due to low weight of NAB, the transport and assembly are cheaper since smaller cranes are needed [115]. The exposed steel surface is low, which requires less corrosion protection [115]. Because of the low weight, high strength, self-balanced static schema and vulnerability to uneven settlements, these bridges are suitable for earthquake zones, which justifies their popularity in Japan [158, 115]. The network arch bridges are suitable to both road and railway loads, even the high-speed railway, due to their low deflection at the ends and higher stiffness than the other types of hangers' arrangement [115, 18]. Lastly, but significantly, they are less dominant in the landscape due to their slender structure [115] and possibility to asymmetric but still aesthetic and economical shaping, making them less repeatable and more flexible in design [129]. The economical estimations result in about 40% cost reduction and 70% steel weight reduction comparing to other solutions [115, 117]. They are also applicable in wide range of span length. One of the shortest span lengths of network arch bridges is found in Luznice, measuring 40 m, which was investigated in the Master's thesis in terms of optimal hangers' arrangement and arch shape [69]. On the contrary, the longest NAB, Bugrinsky Bridge, has 380 m of span length [26].

3.2.2 Optimization approaches to network arch bridges

According to the literature [115, 117] hangers' network arrangement is more economic and sustainable comparing to other hangers' arrangements in tied-arch bridges. Authors in the article [37] compared steel weight for various types of railway and road bridges. Tveit updated the diagram with addition of network arch bridges at the IABSE congress in Vienna in 1980 [109]. The weight of steel part in relevance to the span length presented in Fig. 3.12a [115] shows, that network arch bridges include less structural steel weight per area of bridge among other types of bridges in range between 80 and 300 m. More detailed distribution of steel weight in network arch bridges from the article [75] is presented in Fig. 3.12b, where steel in the arch is the most dynamically increasing and dominant component of the total weight of steel in network arch bridges.

a) Weight of steel in various types of bridges depending on the span length [115]

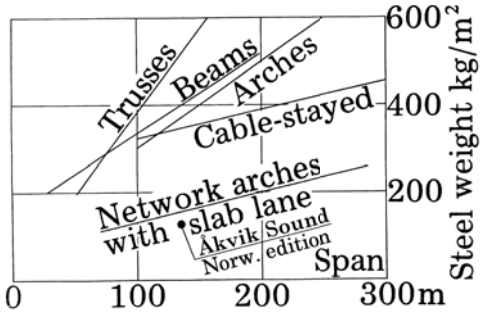

b) Weight of steel for different components in network arch bridges [75]

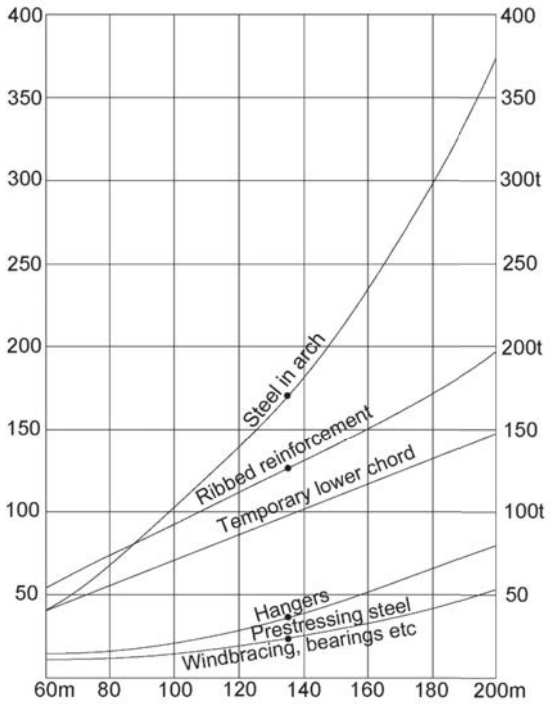

Figure 3.12 The weight of steel (a) in various types of bridges in relevance to span length and (b) different components in network arch bridges [115, 75]

Since Tveit's first publications about network arch bridges, many improvements have been made in order to make this solution even more economical. The investigations were done mainly in terms of tie and arch geometry, arches shaping and hangers' arrangement, which are considered as the most complex part [115, 117].

The recommended slab thickness in relevance to the distance between arches was investigated in the graduation thesis [98], Fig. 3.13. It is applicable for road bridges with an arch distance lower than 15 m. The concrete class used to be in range C40/50 to C60/75. For greater distances or heavier loads with wider deck, the composite sections are in use. As an example of wider deck, the Troja bridge in Prague [42, 43] has 4 lanes of road and two lanes for trams with steel-concrete composite tie of 29.5 m width, Fig. 3.14.

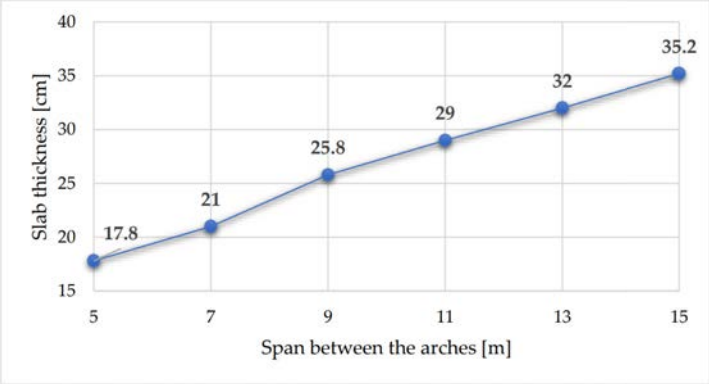

Figure 3.13 The slab thickness in network arch bridges with post-tensioned concrete tie and universal column as an arch [98]

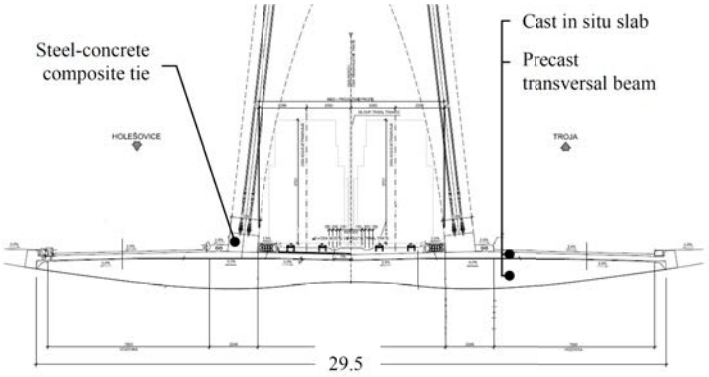

Figure 3.14 The cross section of the deck of Troja bridge as an example of wider decks in network arch bridges [42]

When the arch is made out of steel, the curvature of the arch is suggested to be constant [115, 117]. Further improvements show, that if the arch has different curvature radius at the ends of the arch, the portal frame is shorter, which improves the distribution of the forces and making bending moments smaller caused by reduce size of portal frame [115, 117]. These recommendations changed over time from 0.8, Fig. 3.15a [101] to 0.5, Fig. 3.15b [107] of the main radius near the arch ends. The similar effect to double radius arch curvature can be achieved by elliptical shape [96]. The optimal arch rise in terms of reduction of material weight and internal forces distribution, varies from 14% to 17% [86]. This inclination is considered more aesthetic than higher inclinations due to high slenderness [117], which allows to interrupt less with surrounding [117].

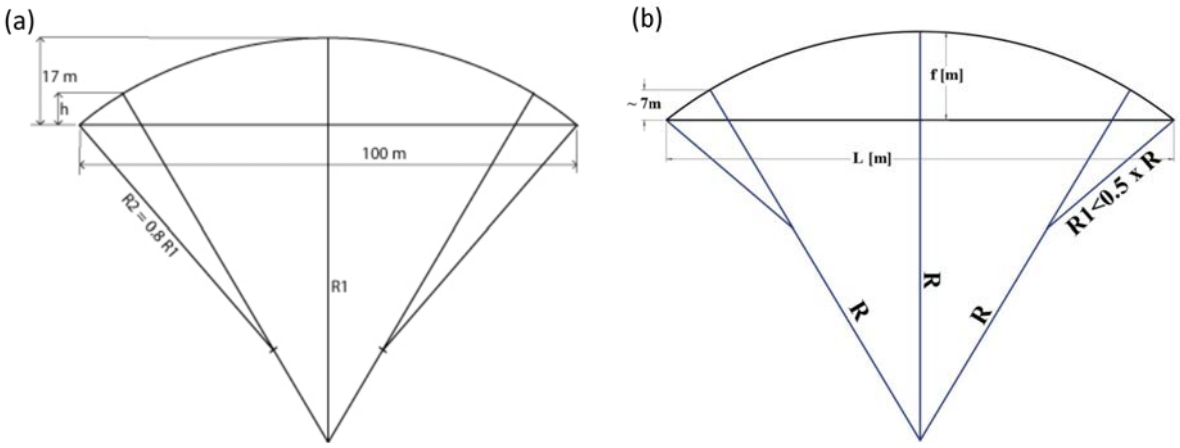

Figure 3.15 The recommendation of the arch's geometry based on the first solution (a) and modified so far (b) [101, 107]

The asymmetric shape of the arch in network arch bridges was also investigated in [129]. The additional skewness and asymmetry in the arch geometry do not cause much difference comparing to the symmetrical solution [129]. The examples of arch shaping with asymmetry is presented in Fig. 3.16 and Fig. 3.17 [129]. This characteristic provides opportunity for more creative shaping in terms of better aesthetic looking and less repeatable solutions as well as better in adoption to the surrounding terrain with addition of skewness [129].

a) Shaping principles of asymmetric network arch bridges with two different radius R1 and R2 for the first and the second asymmetric part of the span length

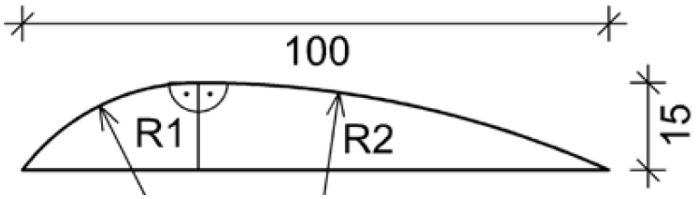

b) Schematic network arch bridges with asymmetric and skewed arches

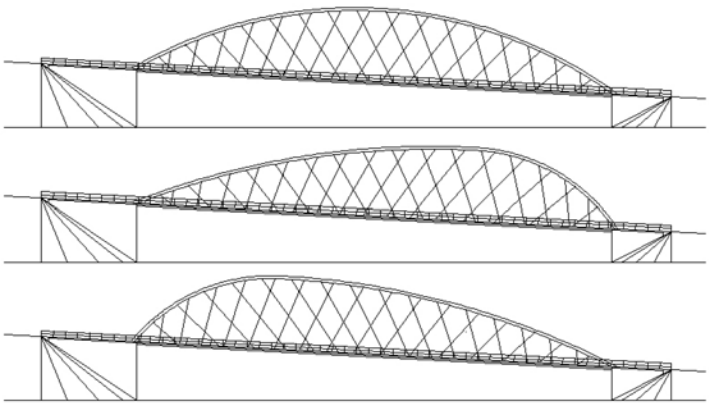

Figure 3.16 Illustrations of (a) shaping principles and (b) schematic network arch bridges with asymmetric and skewed arches [129]

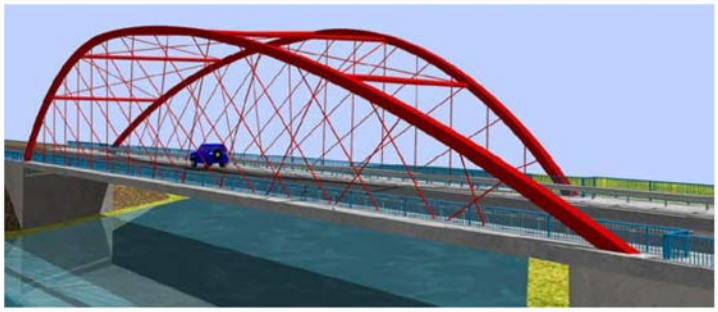

Figure 3.17 Visualization of both skewed and asymmetric network arch bridges [129]

One of arches' cross section types in network arch bridges are heavy duty steel sections of HD or UC with plate thickness reaching 140 mm. The example can be found in Cracow's network arch railway bridges [89], Fig. 3.18. This cross section in the arch seems suitable for the spans up to around 150 m [102]. For greater span lengths or heavier loads, the rectangular or circular shaped boxes are in use. The example of rectangular hollow cross section is the longest network arch bridge, the Bugrinsky bridge [26], Fig. 3.19, with the span length of 380 m. The example of circular hollow cross section is the slenderest network arch bridge, the Brandanger bridge [107], Fig. 3.20, with the span length of 220 m and slenderness of 198. The steel grade of arches in network arch bridges used to be with high strength [115], like S460. Arches' material capacity can be greater with keeping high slenderness and stiffness of a bridge at the same time [115].

Figure 3.18 Illustrations of network arch bridge with HD arch section [146]

Figure 3.19 Illustrations of network arch bridge with rectangular arch section [143]

Figure 3.20 Illustrations of network arch bridge with circular arch section [142]

The stability of the arch is commonly considered linear by using FEA software [18]. Alternatively, the approach of simplifying arch and hangers' system by a simply supported beam on the uniform spring support is proposed in [85], which is also a linear-based approach. Other papers [13, 8] use the methods included in the Eurocodes for arch bridges [134], which do not cover the network, but vertical hangers' arrangements. Two recent papers [4, 35] show the importance of including geometrical nonlinearity in the out-of-plane buckling analysis, since the linear approach leads to capacity overestimation. The capacity reduction due to geometrically nonlinear analysis was mainly caused by the geometrical and mechanical properties of the bracing system, arrangement of the hangers (vertical and network were investigated), height of the portal frame, out-of-plane moment of inertia of the arch ribs and inwards inclination of the arches [4, 35]. **According to author's best knowledge, no research was found, that investigated geometrically nonlinear in-plane buckling in network arch bridges.**

The inclination of the arches pointing inwards results in increased capacity for buckling in-plane [18]. At the same time, the closer the arches are towards each other, the smaller the bracing system gets and so weights less [18]. The hangers' arrangement does not have much affection to the buckling of the arch in out-of-plane direction, which is mainly provided by the stiffness of the arch and bracing system [18]. Hangers contribute in in-plane instability of the arches [18]. In arches inclined inwards, the impact of hangers' arrangement is not significant on the buckling and mainly affects the internal forces distribution in the arch, since arches inclined inwards have the first buckling form corresponding with the out-of-plane form [18]. The critical normal force calculated for arches with inwards inclination of 79^o used to be between 10 to 50% greater comparing to vertical hangers' arrangement [18]. The author [18] pointed, that the procedure from EN 1993-2 can be used only in case of lack of bracing between arches or when the bracing is very stiff. Otherwise, different methods have to be investigated. The examples of arches inclined inwards in network arch bridges are presented in Fig. 3.21a and Fig. 3.21b.

There are also examples of arches inclined outwards, as Sixth Street Viaduct presented in Fig. 3.21c. It includes concrete arches inclined 9^o outwards and cast in place [123]. The reason why the concrete arches are not that popular, is their weight during transport or a need to cast on the construction site or a need for greater crane for placing [19, 123]. The concrete has its advantage when it comes to its damping under seismic, which is a case in Los Angeles region [120]. The arches are not braced, and greater stiffness of the concrete section helps in out-of-plane buckling comparing to much slender steel arches [19].

The development of material in network arches is not limited to concrete and steel but also extends to timber/glulam material [19, 9]. The first network arch made of the glulam arch with at the same time the longest span length of 88.2 m is presented in Fig. 3.22. One of the recent research projects in this topic is included in the PhD [72], where author introduced new network arch arrangement consists of modified radial arrangement into two focal points instead of one aligned with the center of the arch, Fig. 3.23. This provided more control over hangers'

anchorage position on the tie. The second improvement in [72] was diverging hangers from the plane of the arch, Fig. 3.24a, into two symmetrical planes, Fig. 3.24b. This improvement allows to involve hangers in stabilizing the arch in out-of-plane buckling form [72], where in non-diverged scenario, the hangers' contribution in out-of-plane form is negligible [18].

a) Troja bridge in Prague [157]

b) Palma del Rio bridge [150]

c) Sixth Street Viaduct [153]

Figure 3.21 Illustrations of inclined (a), (b) inwards and (c) outwards network arch bridges

Figure 3.22 The Steien bridge [154], the first network arch bridge made of timber [72]

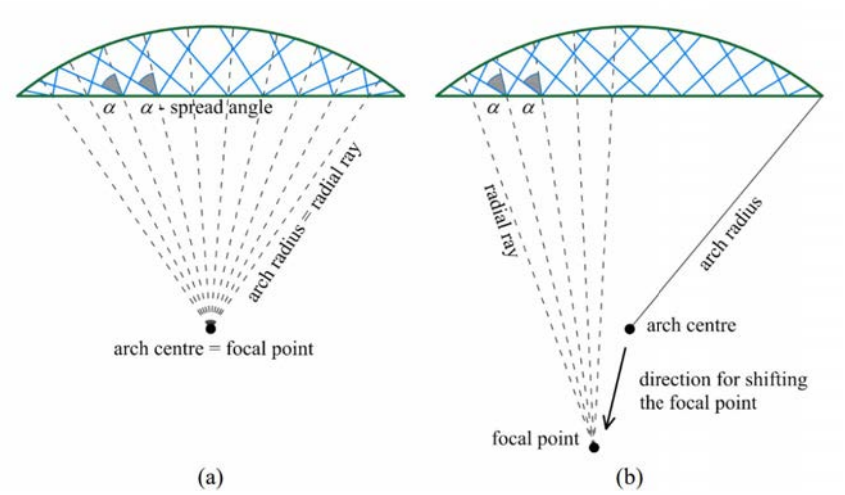

Figure 3.23 The classic radial arrangement of hangers (a) in comparison with the modified radial arrangement (b) included in [72]

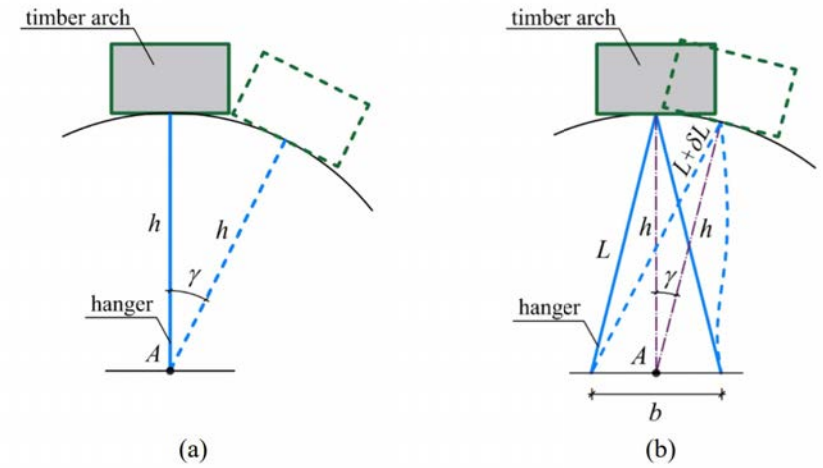

Figure 3.24 The classic single plane hangers placement (a) and diverged (b) [72]

In the article [56] the concept of half-through network arch bridge with coarse aggregate ultra-high-performance concrete (CA-UHPC) with steel tube in the arch is investigated, Fig. 3.25. The total span length is 470 m. The deck was proposed as composite steel and reinforced concrete section. The arch is made of internal hollow steel circular section connected by dowels with the outer CA-UHPC, making the entire section a composite. This type of section was first introduced to network arch bridge [56]. The arch column, which are under compression, are extended also above the deck close to the arch intersection with the tie in order to reduce the bending moments in the arch in this region [56], Fig. 3.25. The bracing between the arch is optimized using multi-material bi-directional evolutionary structural optimization (MBESO) method according to [58, 59, 31]. Topology optimization is also used in the spherical bearings, reducing steel use and improving structural efficiency, Fig. 3.25.

The innovative solution is compared with the truss half-through arch bridge with vertical hangers. The proposed solution reduces the CO_2 emission by about 16% compared to the truss arch. The costs of both bridges are almost the same, with 1% advantage for the concept. The NAB is also compared visually with the truss bridge, and by an aesthetic point of view, the NAB is less disturbing the surrounding, Fig. 3.26, proving Tveit's words about more aesthetic

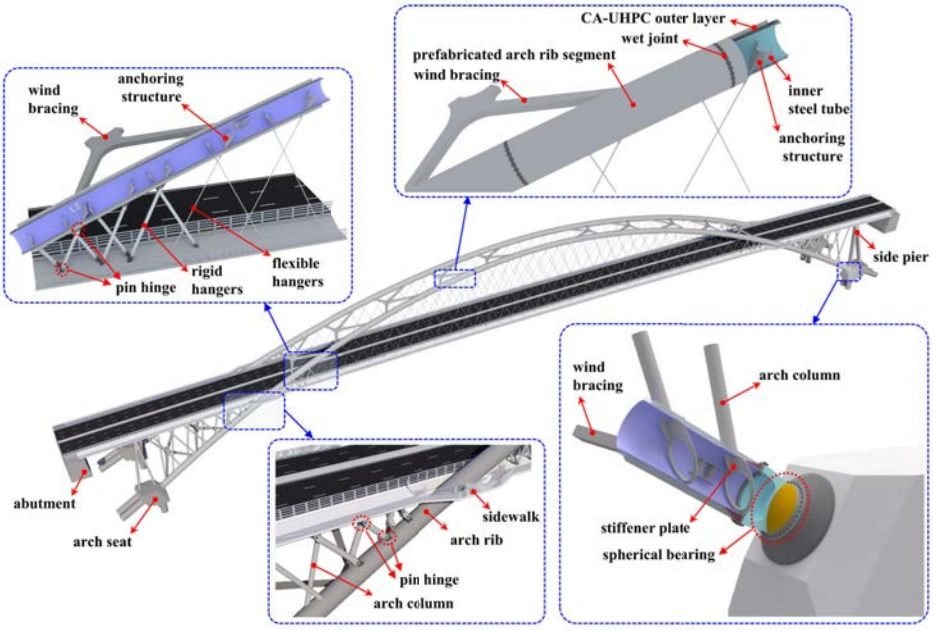

Figure 3.25 The concept of half-through network arch bridge with CA-UHPC called the Fengjie 2nd Yangtze River Bridge [56]

properties over the other type of arch bridges [115]. The used optimization method and different materials help reducing total costs of the structure by 1%, which is not much in this case, but the total CO_2 emission is reduced by 16.5% which is considered significant [56].

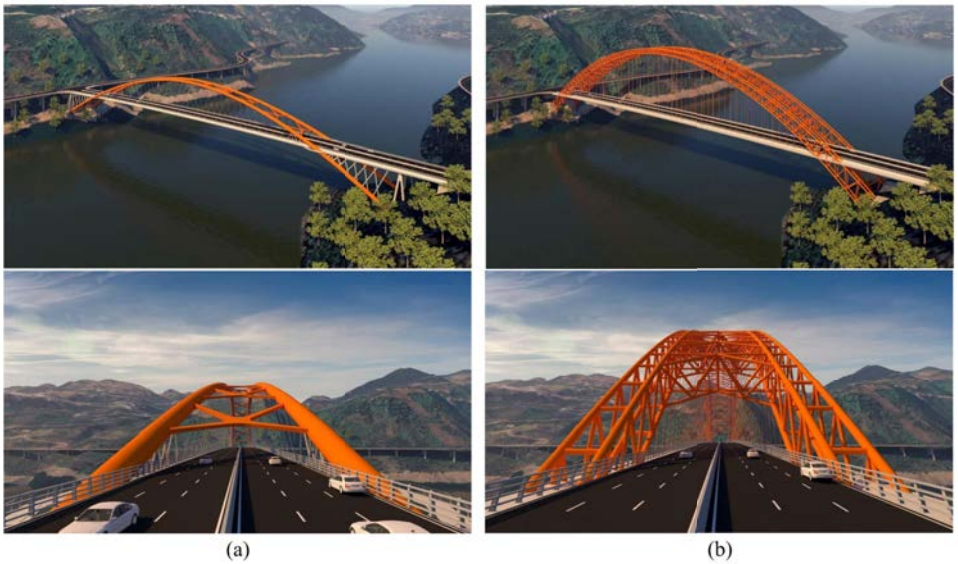

Figure 3.26 The comparison of (a) CA-UHPC-steel tube composite half-through network arch bridge with (b) truss arch bridge with vertical hangers' arrangement [56]

In network arch bridge over the Odra River at the border between Germany and Poland, the carbon fiber reinforced polymer (CFRP) was used in hangers [92, 63]. Because of CFRP material high performance in both strength and fatigue, their cross section is reduced to one quarter of the alternative steel solution [92]. The positive side effect of reduced diameter is less disturbed of the structure to surrounding, Fig. 3.27. The research shows [63], that these hangers

provides 67% lesser carbon footprint than the standard steel hangers. Moreover, the total mass of the carbon system is 51.9 tons, and the standard steel system would be 1050 tons, which is a significant reduction [63].

Figure 3.27 The NAB over Odra river made wih CFRP hangers [63]

The distribution of the internal forces between the arch and the tie, as well as total required material weight, are significantly dependent on hangers' arrangement. In [98, 102] authors suggested the arrangement of equally spaced hangers' anchorages in the middle of the tie and gradually decreasing towards one end and increasing into an opposite end, Fig. 3.28a. The solution is then mirrored symmetrically. An example of bridge constructed with these principles is Great Colonnade Way bridge [152].

The next type of arrangement is constant slope inclination, where hangers are inclined at a constant angle, Fig. 3.28b, also called Constant Slope Model (CSM) [75]. The solution is then also mirrored symmetrically. Author noticed its description in [75] but the origin of this arrangement was not found, however the principles presented in Nielsen's PhD [68] and Tveit's Master thesis [106] are similar to constant slope inclination model. Nielsen-Lohse bridge is an example of this arrangement usage [149].

Another type of hangers' arrangement is a constant increase of the hangers' inclination along the deck proposed in [110], called Variant-Constant Slope Model (V-CSM) as well [75]. The two required parameters are the initial inclination angle of the first hanger and angular inclination difference between two nearest hangers, Fig. 3.28c. The solution is then also mirrored symmetrically. The arrangement can be considered as more general version of constant slope inclination angle. An example of this arrangement is River Irwell bridge [151].

One of the latest arrangements of the hangers is Constant Angle to Radius Slope Model (CARSM) [75] proposed in [87, 86], Fig. 3.28d. The idea is based on the fact, that the loads acting perpendicularly to the arch's tangent should cause mainly compression axial force and low bending moment [87]. The fan arrangement fulfils these principles, but traffic loads in bridge are not stationary and do not act uniformly along the entire span length [87]. In case of asymmetric traffic loads on the tie, the bending moments increase severely in fan arrangement [87]. When each hanger is split into pair symmetrically to arch radius, Fig. 3.29a, and the divergence point is lowered from the arch, the load distribution from the tie to the arch becomes more even for unsymmetrical loads [87]. Adding more hangers improves force distribution [87]. The hangers used to be equally spaced in the arch [87]. The divergence angle can be different, Fig. 3.29b, and its optimal value in terms of forces distribution is investigated in later researches [75, 97]. The hangers need to be adjusted at the end of the bridge where the distance between the arch and the tie is going to zero, Fig. 3.29c. The local radial arrangement used to be applied in these regions and the hangers' arrangement is changed iterative [83, 87, 86] in order to reduce the excessive bending moments close to the supports.

a) Ellipse-based hangers' node spacing [98, 102]

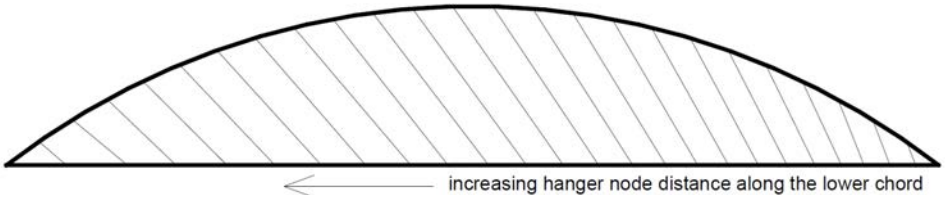

b) Constant slope inclination [75]

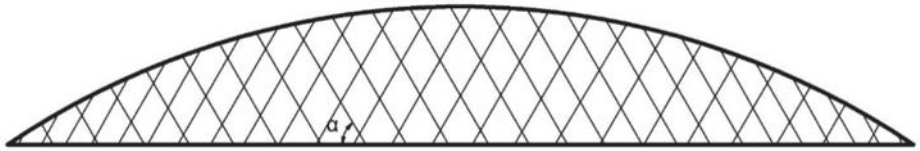

c) Variant-constant slope inclination [110]

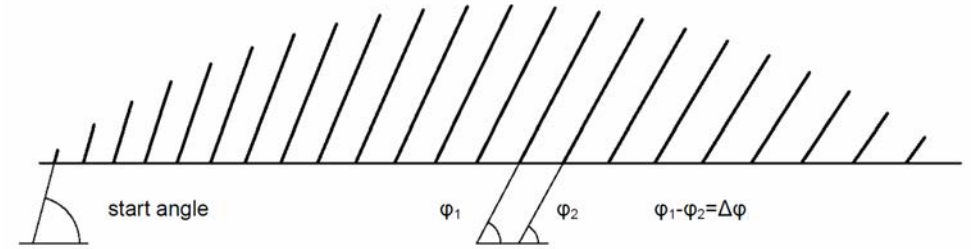

d) Constant angle to radius slope model [87]

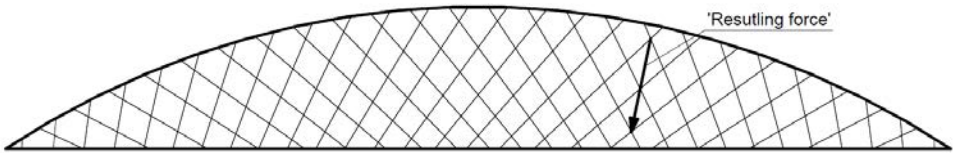

Figure 3.28 Schematic illustration of hangers' arrangement in (a) ellipse-based hangers' node spacing, (b) constant slope inclination, (c) slope arranged variant and (d) radial arrangement [98, 102, 75, 110, 87]

The CARSM arrangement was compared with hangers' arrangement in Åkviksound bridge with V-CSM arrangement designed by Tveit [87] and deeply analysed in [98]. The cross sections and geometry, except the hangers' arrangement, remained the same [87]. The CARSM arrangement provided 2% decrease in axial force in the arch, 21% decrease in hangers forces and 19% reduction in bending moments [87]. Deflection was reduced with the similar order of magnitude [87]. Similar improvements were achieved, when loads were applied uniformly on the entire span length and about half of span length [87].

Authors in [87] also stated, that the number of hangers for 100 m span length railway bridge in relation to the span length expressed in meters should not exceed 0.48.

a) Radial arrangement principles

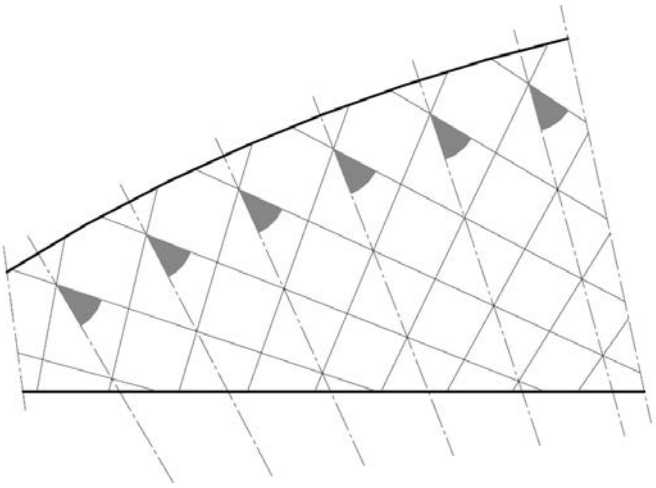

b) Examples with different divergence angle

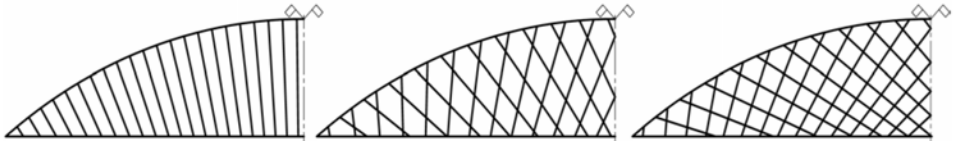

c) Examples with hangers adjustment close to the support

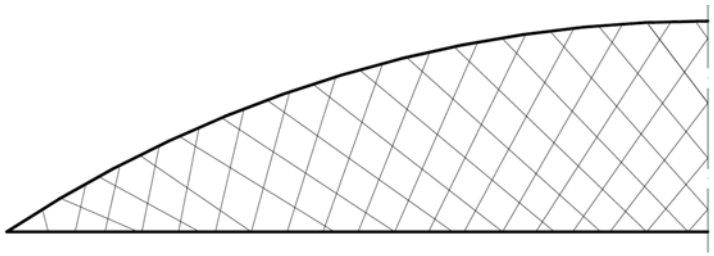

Figure 3.29 Schematic illustration of hangers' arrangement in radial arrangement with (a) marking divergence angle to the symmetrical lines, (b) examples of radial-like arrangement, 25^o and 41^o and (c) hangers angle adjustment close to the support [87, 83]

In the article [75] an investigation of different span length and network hangers' arrangement are conducted for various number of hangers' arrangements and both for road and railway traffic loads. The three arrangements are considered. The CSM with the slope angle between 45 and 75^o, he V-CSM with a starting angle of 30^o and angular change between 0.5 and 3^o, and the CARSM with hangers' divergence angle between 30 and 50^o [75]. The optimization criterion is based on minimization of bending moments in structural elements. The solution that provides lower bending moments, is considered more optimal [75]. The arrangements are presented in Fig. 3.30 [75]. The results are presented in Tab. 3.1 for the type of arrangement and number of hangers, and in Fig. 3.31 for the optimal angle parameter of hangers [75].

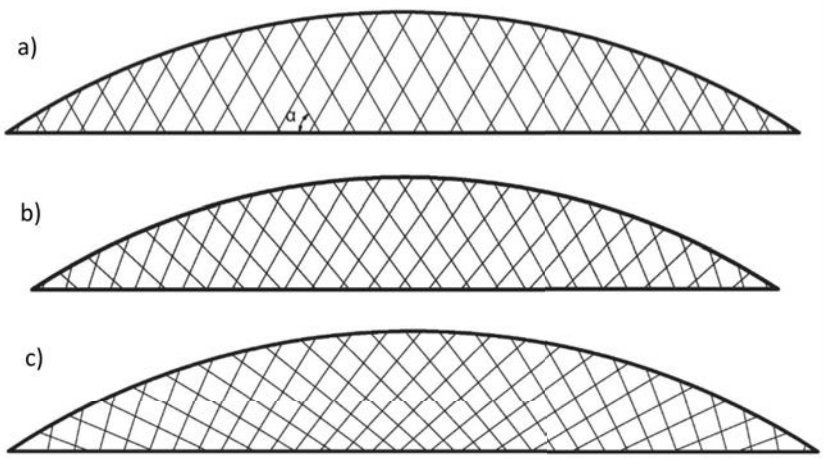

Figure 3.30 Arrangement considered in [75] with (a) constant slope model CSM, (b) variant-constant slope model V-CSM and (c) constant angle to radius slope model CARSM

From the obtained results, the CARSM provides the best performance for majority of spans length and number of hangers [75], Tab. 3.1. It is the most suitable for span length from about 100 m in road bridges and from 70 m for railway bridges. The greater the traffic load is, the wider the range of CARSM usage is over other arrangements. The second-best arrangement is V-CSM, which is superior in road bridges with span length lower than 100 m and railway bridges with span length below 80 m and below 36 hangers. The V-CSM is then alternative to CARSM for spans length greater than 170 m and at least 36 number of hangers for road bridges and from 160 m in span length for railway bridges with at least 36 number of hangers. The general trend is, that the lower the number of hangers and span length or the greater the span length and number of hangers, the better performance is achieved from the V-CSM than from the CARSM. For the remaining cases the CARSM is superior to V-CSM. The CSM arrangement is not more optimal than any of these two arrangements for any span length and number of hangers. Nevertheless, author [75] determines the optimal constant angle for CSM varying between 40 and 80^o and increasing over the number of hangers, Fig. 3.31. On the contrary, the divergence angle in the CARSM varies between 30 and 45^o. This angle decreases for smaller span lengths over the increasing number of hangers, and opposite for greater span lengths, Fig. 3.31.

Table 3.1 Optimal hangers' arrangement for (a) road and (b) railway bridges depending on the number of hangers and span length CARSM [75]

a) Optimal hangers' arrangement for road bridges

Span lenght [m] vs. Hanger number	18	24	36	48	60
60	V-CSM	V-CSM	V-CSM	V-CSM	V-CSM
70	V-CSM	V-CSM	V-CSM	V-CSM	V-CSM
80	V-CSM	V-CSM	V-CSM	V-CSM	V-CSM
90	V-CSM	V-CSM	V-CSM	V-CSM	V-CSM
100	V-CSM	V-CSM	CARSM	CARSM	CARSM
110	V-CSM	CARSM	CARSM	CARSM	CARSM
120	CARSM	CARSM	CARSM	CARSM	CARSM
130	CARSM	CARSM	CARSM	CARSM	CARSM
140	CARSM	CARSM	CARSM	CARSM	CARSM
150	CARSM	CARSM	CARSM	CARSM	CARSM
160	CARSM	CARSM	CARSM	CARSM	CARSM
170	CARSM	CARSM	CARSM	CARSM	V-CSM
180	CARSM	CARSM	CARSM	V-CSM	V-CSM
190	CARSM	CARSM	CARSM	V-CSM	V-CSM
200	CARSM	CARSM	V-CSM	V-CSM	CARSM/V-CSM

b) Optimal hangers' arrangement for railway bridges

Span lenght [m] vs. Hanger number	18	24	36	48	60
60	V-CSM	V-CSM	V-CSM	CARSM	CARSM
70	V-CSM	V-CSM	CARSM	CARSM	CARSM
80	V-CSM	CARSM	CARSM	CARSM	CARSM
90	CARSM	CARSM	CARSM	CARSM	CARSM
100	CARSM	CARSM	CARSM	CARSM	CARSM
110	CARSM	CARSM	CARSM	CARSM	CARSM
120	CARSM	CARSM	CARSM	CARSM	CARSM
130	CARSM	CARSM	CARSM	CARSM	CARSM
140	CARSM	CARSM	CARSM	CARSM	CARSM
150	CARSM	CARSM	CARSM	CARSM	CARSM
160	CARSM	CARSM	CARSM	CARSM	CARSM
170	CARSM	CARSM	CARSM	CARSM	CARSM/V-CSM
180	CARSM	CARSM	CARSM	CARSM/V-CSM	CARSM/V-CSM
190	CARSM	CARSM	CARSM	CARSM/V-CSM	CARSM/V-CSM
200	CARSM	CARSM	CARSM/V-CSM	CARSM/V-CSM	CARSM/V-CSM

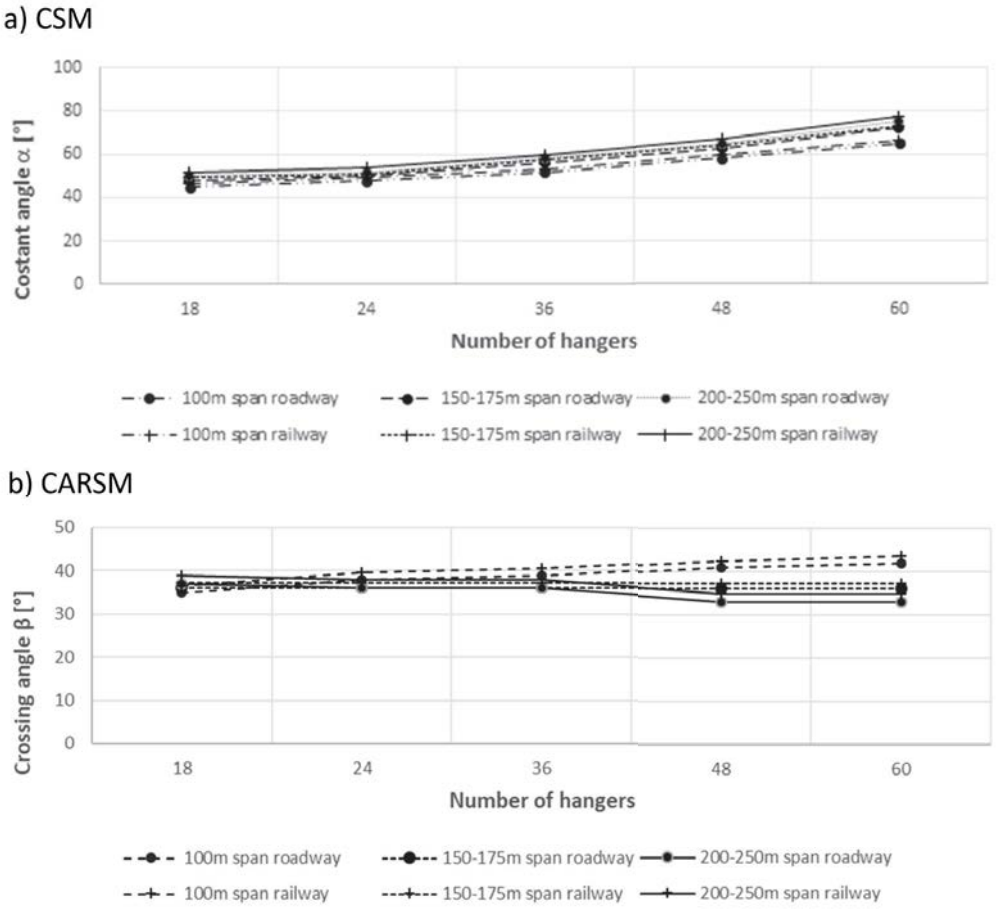

Figure 3.31 Optimal hangers angle for (a) CSM and (b) CARSM arrangements [75]

The next research is conducted by Teich in [97], where 5 arrangements are investigated. Among them, author [97] presents 3 the most promising arrangements showed in Fig. 3.32. Network 2 stands for V-CSM, network 4 stands for CARSM and network 5 stands for constant hangers spacing in the middle determined from elliptical principles. Author in [97] investigates as well CSM and hangers' arrangement with backward inclination, but both provide worse result than networks 2, 4 and 5. The optimal angle parameters for the two most optimal arrangements, the network 4 and 2 respectively, are presented in Tab. 3.2, Tab. 3.3 and Tab. 3.4.

The results from Teich [97] showed, that in terms of objective function of making normal forces uniform, the best arrangement is CARSM in the vast majority of cases, followed by V-CSM as the second best, Fig. 3.32. The most optimal number of hangers oscillated from 30-44 for the span lengths lower than 100 m, up to 42-52 for span length of 250 m [97], Tab. 3.2. The average ratio of number of hangers to the length of the span expressed in meter is 0.41, 0.29, 0.23 and 0.19 for 100, 150, 200 and 250 m respectively [97], Tab. 3.2. The decreasing trend of this ratio over the span length is observed. With that optimal ranges of the number of hangers, the CARSM optimal divergence angle is 39.5, 36, 34 and 33^o for the 100, 150, 200 and 250 m of span length respectively, Tab. 3.4. The V-CSM has the optimal initial angle of 40, 32.5, 20 and 17.5^o in average and optimal angle inclination of 2.75, 2.88, 2.88 and 2.25^o in average for the 24, 36, 48 and 60 number of hangers respectively, Tab. 3.3.

Table 3.2 The parameters of the most optimal hangers' arrangement for constant hangers spacing in the middle determined from elliptical principles [97]

Span length in m	< 100	100	150	200	250
Number of hangers	30-44	36-46	38-48	40-50	42-52

Span	24 Hangers		36 Hangers		48 Hangers		60 Hangers	
< 100 m	Network 2 or Network 4							
100 m	**1. Network 4**	**100**	**1. Network 4**	**100**	**1. Network 4**	**100**	**1. Network 2**	**100**
	2. Network 5	88,4	2. Network 2	94,1	2. Network 2	98,6	2. Network 4	99,3
	3. Network 2	83,1	3. Network 5	89,9	3. Network 5	87,5	3. Network 5	80,4
125 m	**1. Network 4**	**100**	**1. Network 4**	**100**	**1. Network 2**	**100**	**1. Network 2**	**100**
	2. Network 5	88,2	2. Network 2	94,3	2. Network 4	99,9	2. Network 4	97,9
	3. Network 2	83,2	3. Network 5	93,7	3. Network 5	96,9	3. Network 5	84,3
150 m	**1. Network 4**	**100**	**1. Network 4**	**100**	**1. Network 4**	**100**	**1. Network 4**	**100**
	2. Network 5	85,8	2. Network 2	94,2	2. Network 2	99,6	2. Network 2	99,7
	3. Network 2	80,3	3. Network 5	91,1	3. Network 5	93,2	3. Network 5	82,8
175 m	**1. Network 4**	**100**	**1. Network 4**	**100**	**1. Network 2**	**100**	**1. Network 2**	**100**
	2. Network 5	86,1	2. Network 2	94,7	2. Network 4	97,6	2. Network 4	99,6
	3. Network 2	80,8	3. Network 5	90,7	3. Network 5	89,2	3. Network 5	78,1
200 m	**1. Network 4**	**100**	**1. Network 4**	**100**	**1. Network 4**	**100**	**1. Network 4**	**100**
	2. Network 5	84,4	2. Network 2	93,2	2. Network 2	99,2	2. Network 2	97,6
	3. Network 2	78,1	3. Network 5	88,5	3. Network 5	88,5	3. Network 5	80,3
225 m	**1. Network 4**	**100**	**1. Network 4**	**100**	**1. Network 2**	**100**	**1. Network 4**	**100**
	2. Network 5	82,4	2. Network 2	93,2	2. Network 4	98,9	2. Network 2	99,3
	3. Network 2	75,8	3. Network 5	88,0	3. Network 5	86,8	3. Network 5	76,4
250 m	**1. Network 4**	**100**	**1. Network 4**	**100**	**1. Network 4**	**100**	**1. Network 4**	**100**
	2. Network 5	75,6	2. Network 2	93,0	2. Network 2	99,2	2. Network 2	98,1
	3. Network 2	66,2	3. Network 5	87,4	3. Network 5	87,1	3. Network 5	81,1

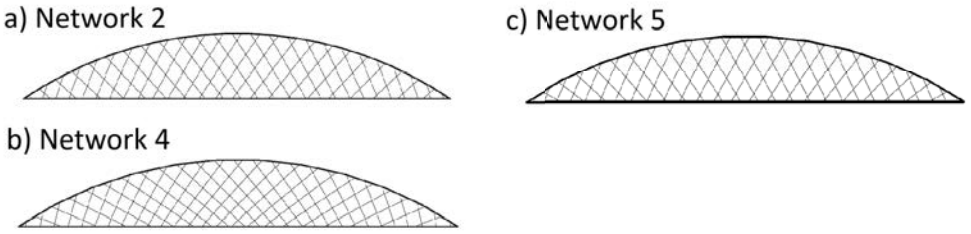

Figure 3.32 Optimal hangers' arrangement according to [97] with the hangers' arrangement of (a) V-CSM, (b) CARSM and (c) constant hangers spacing in the middle determined from elliptical principles

Table 3.3 The parameters of the most optimal hangers' arrangement for network 2 [97], where α_1 is the initial hanger's inclination and $\Delta\alpha$ is a constant angular inclination difference between two following hangers

Number of hangers	optimal value range	also provide favorable results
24	35° ≤ α1 ≤ 45° 2,5° ≤ Δα ≤ 3,0°	optimal α1 in combination with smaller Δα (1,5°-2,5°) larger α1 (50°) in combination with smaller Δα (1,5°-2,5°)
36	30° ≤ α1 ≤ 35° 2,75° ≤ Δα ≤ 3,00°	optimal α1 in combination with smaller Δα (2,00°-2,75°) larger α1 (40°-45°) in combination with smaller Δα (1,5°-2,5°)
48	15° ≤ α1 ≤ 25° 2,75° ≤ Δα ≤ 3,00°	optimal α1 in combination with smaller Δα (2,00°-2,75°) larger α1 (30°-40°) in combination with smaller Δα (1,5°-2,5°)
60	15° ≤ α1 ≤ 20° 2,0° ≤ Δα ≤ 2,5°	larger α1 (25°-30°) in combination with smaller Δα (1,5°-2,0°) larger α1 (25°-30°) in combination with optimal Δα

Table 3.4 The angular parameters of the most optimal hangers' arrangement for network 4 [97]

	24 Hangers	36 Hangers	48 Hangers	60 Hangers
100 m	39°	39°	40°	42°
125 m	36°	36°	39°	39°
150 m	36°	36°	36°	36°
175 m	36°	33°	36°	36°
200 m	36°	36°	33°	33°
225 m	36°	33°	33°	33°
250 m	36°	36°	33°	33°

In the review paper [125], authors provided a comprehensive summary of historical trends in bridge optimization. The optimization in bridges started to get more attentions in recent 15 years [125], Fig. 3.33a. Authors [125] distinguished four main subjects in optimization covered by these publications. The first one was cost optimization, which stood for the cost minimization by reducing structural volume [125]. The second was structural performance, which stood for improving the properties of the bridge [125]. A good example could be shape optimization due to vortex shedding effect, the buckling vulnerability, seismic vulnerability. The third subject was environmental impact [125], which referred to among others the CO_2 emission reduction, water usage reduction, influence reduction on flora and fauna. The last subject was multi-objective optimization, which took at least two usually mutually exclusive optimization criteria [125]. The criteria are usually not described by the same indicators, for example cost optimization is driven by volume of the structure, and environmental optimization is driven by the CO_2 emission and these two values are incomparable due to their different units.

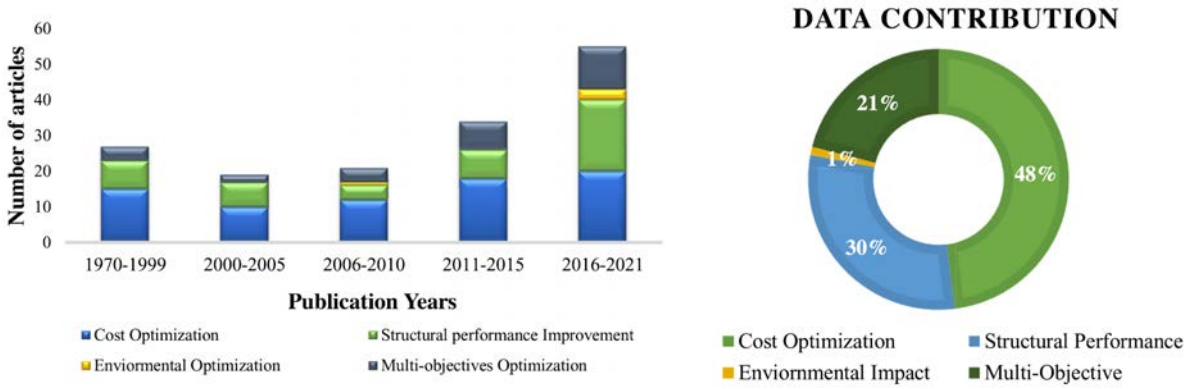

(a) The number of publication with separation to the subjects

(b) The percentage distribution of the subjects

Figure 3.33 The presentation of (a) the number of publications in bridge optimization and (b) the percentage distribution of the subjects [125]

The data in Fig. 3.33a showed growing attention to structural and multi-objective optimizations from 2010 in proportion to all subjects [125]. Cost optimization has received a greater number of publications, but its contribution has decreased since 2010 [125]. Among the various optimization objectives, environmental impact has received the least attention over the years [125]. The total distribution of cost optimization, structural performance, environmental impact and multi-objective optimization was 48, 30, 1 and 21% respectively, so despite losing attention in recent years, the cost optimization was the most popular optimization subject, Fig. 3.33b [125]. This phenomenon is reasonable, since the lower costs of the structure mostly means less material and less environmental impact, so even though it is a single-objective problem, it contributes to improving other objectives.

The authors [125] noticed, that the top three continents with the greatest number of articles have been published from Asia, then North America and Europe respectively. In less developed countries, the cost and structural optimization were the most popular subjects [125]. In more developed countries these subjects were still dominant, but the environmental impact started to attract more attention [125]. Multi-objective optimization was less popular than structural optimization [125].

When it comes to optimization in network arch bridges, many approaches has been noticed, which vary in their complexity. The first one is the calculation of thousands of discrete numbers of geometries for a specific type of hangers' arrangement and arch elevation [75, 97, 87]. The cross sections and materials are the same in the optimization process. The objective function is based on the internal forces distribution improvement or weight minimization. This approach provides detailed investigation of the discrete domain, helping deeply understand the trends and finding global extreme, best solutions for a given optimization criterion. However, they require great computation time to evaluate thousands of geometries, even with simplifications. Another drawback is limitation to the search domain itself, since predefined arrangements with discrete change of angle and/or spacing of hangers do not allow to investigate other topology or modify the arrangement locally.

The next approach in optimization of network arch bridge was the implementation of metaheuristic algorithms. Authors in [94, 93] used genetic algorithms to optimize hangers' arrangement without restraints in hangers' distribution in terms of minimization of internal forces amplitudes. Authors in [7, 6] utilized genetic algorithms and particular swarm optimization in determining the optimal parameters of the network bridge with CARSM arrangement in terms of mass reduction. In [40, 2] authors optimized V-CSM arrangement for cost minimization objective function using evolutionary operations (EVOP). Even though the cost was considered, the material remained the same, but assembly costs were included. The literature also implemented hybrid methods of metaheuristic and gradient based approaches. In [6] authors combined evolutionary algorithm with pattern search. In [13] authors used sparse nonlinear optimizer (SNOPT) with quadratic programming (QP) solver. Paper [7] combined PSO with simulated annealing. The partition of the optimization procedure into several steps allowed to reduce the time consumption and complexity of the calculations [13].

The presented results from [97, 75] provide optimal shaping of hangers' arrangements and help in determining, which arrangement is optimal in given conditions. These results are determined by heavy loads of road and railway traffic loads. For lighter pedestrian loads, the number of hangers is not required as high to carry these loads. However, maintaining the well-defined arrangement principles with sparse hangers' distribution causes a significant increase of internal forces in both arch and tie [93], especially when the number of hangers passes around 16–20, as shown in Fig. 3.34.

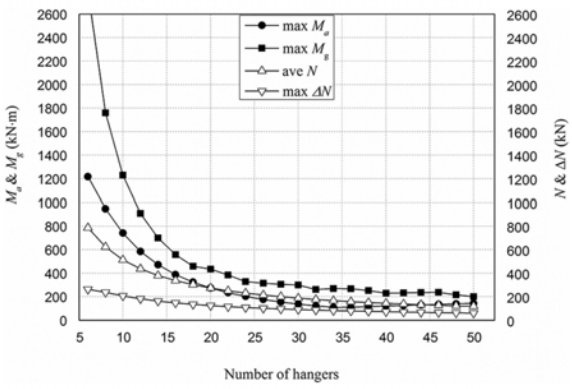

(a) Number of hangers influence to internal forces for V-CSM [93]

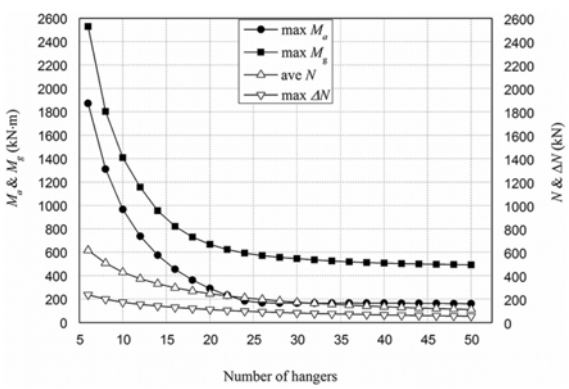

(b) Number of hangers influence to internal forces for CARSM [93]

Figure 3.34 The impact of the number of hangers to the internal forces in arch and tie in (a) V-CSM and (b) CARSM arrangement [93]. Max M_a is the maximum absolute bending moment in the arch, Max M_g is the maximum absolute bending moment in the tie, ave N is the average axial force of the hangers and maximum ΔN is the maximum variation of axial force in hangers

Authors in [93] explored the possibility of considering custom made hangers' arrangements using genetic algorithms in order to obtain smaller internal forces than in CARSM and V-CSM arrangements for sparse hangers' system. They chose 12 hangers and internal forces from well-defined arrangements as reference in the objective function [93]. If the objective function's value was smaller than 1.0, the arrangement improved internal forces distribution [93]. Hangers had 10 anchorage points for the first half of the arch and the tie, which resulted in 19 anchorage points for both arch and tie, since the solution had to be symmetrical. The position of the hangers were a part of genetic algorithm's chromosome definition. The chromosome coding was presented in Fig. 3.35.

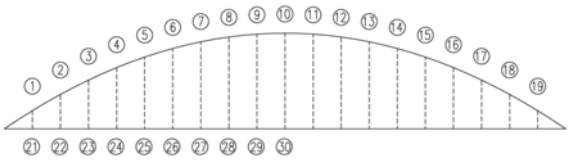

(a) The encoding principles [93]

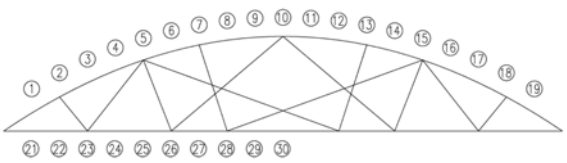

(b) The example of hangers' arrangement [93]

Figure 3.35 The principles of (a) the hangers anchorage encoding in the arch and the tie and (b) the example of hangers' arrangement [93]

Authors [93] utilized ANSYS FEA software with the optimization procedure coded in MATLAB environment. The sections were not changed in the optimization process as well as geometry of the arch [93]. The hangers were simplified to link elements and were considered geometrically nonlinear [93]. The remaining elements were made of beam elements [93]. The objective function was defined in Eq. (3.1) [93].

$$F = \left(\frac{\max M_a}{\max M_{a,12}} + \frac{\max M_t}{\max M_{t,12}} + \frac{aveN}{aveN_{12}} + \frac{\max \Delta N}{\max \Delta N_{12}} \right) /4 \tag{3.1}$$

where $\max M_{a,12}$, $\max M_{t,12}$, $aveN_{12}$ and $\max \Delta N_{12}$ were maximum bending moment in the arch and tie, average normal force in hangers and maximum difference of normal force in hang-

ers for the reference network arrangement of 12 hangers and were constant during the optimization process. Symbols without "12" in subscript applied to varying resultant geometries in the optimization process.

The obtained results were a combination of different arrangements' types, mostly network system in the middle part and vertical arrangement near the ends [93], Tab. 3.5a. The improvement reached up to 19.4% [93]. **This clearly showed the potential of optimization in sparse hangers' systems and suggested, that the custom-made arrangements could provide better performance in internal forces distribution and resulted in more cost-efficient solutions.**

Authors from [93] made earlier the article [94] with similar approach, but this time they compared the results to Nielsen arrangement. As expected, their algorithm provided better results in terms of force distribution [94]. The results for this optimization approach were presented in Tab. 3.5b and were different from the results in Tab. 3.5a, even though the optimization algorithm remained unchanged. **Therefore, the hangers' arrangement could be flexibly shaped to meet aesthetic preferences with equal performance** [93, 94].

Table 3.5 The optimal arrangement of hangers in sparse system according to [94, 93]

Scheme	Objective Function	Chromosome Coding	Arrangement Diagram
①	F= 0.806	{9 6 8 4 2 7 27 28 30 24 22 25}	
②	F= 0.831	{10 5 2 4 8 7 26 29 22 24 29 26}	
③	F= 0.849	{ 7 9 2 5 4 8 30 27 22 27 24 25}	
④	F= 0.859	{7 5 4 2 9 8 26 28 23 23 28 30}	
⑤	F= 0.864	{8 10 2 4 6 7 29 28 22 24 28 26}	
⑥	F= 0.888	{9 8 4 7 6 2 27 30 23 25 28 25}	

(a) The sparse optimal hangers' arrangement for pedestrian bridge according to [93]

Scheme	Objective Function	Chromosome Coding	Arrangement Diagram
①	f=0.682	{10 2 3 6 5 8 26 24 23 22 29 27}	
②	f=0.685	{ 7 5 5 10 9 3 6 9 2 6 10 4}	
③	f=0.709	{ 7 3 5 1 9 7 10 4 4 3 7 3}	
④	f=0.714	{ 3 11 5 8 5 7 3 8 8 6 3 10}	
⑤	f=0.733	{ 2 8 9 4 9 6 5 9 5 4 10 7}	
⑥	f=0.742	{ 4 13 10 3 6 8 3 9 7 6 9 6}	

(b) The sparse optimal hangers' arrangement for pedestrian bridge according to [94]

The noticeable difference was the applied loads. The total self-weight in [93] was 1235 kN, the other permanent loads 18.8 kN/m, which results in 3115 kN in total. The variable load was equal to 3.5 kPa. On the contrary, the total self-weight in [94] was 5381.6 kN, which was 72.8% more. The variable load was 4.0 kPa, so 14.2% more. The span length remained the same in both cases. In the first case [93], for the deck width of 4.0 m, the total variable load was 1400 kN and in the second scenario [94] 1600 kN. The permanent-to-variable loads ratios were 2.23 and 3.36 respectively.

Moreover, author concluded, that **the value of the applied loads and the ratio between variable and permanent loads had an impact on the optimal solution**, which varied significantly for the best obtained results.

In Fig. 3.36 the percentage reduction of four objective function's components in comparison to reference V-CSM arrangement. The most optimal solution did not reduce bending moment the most among six best performing solutions. Since the arch's cross section used to be slender in network arch arrangement, reduction of bending moments in the arch should lead to the greatest improvement of the structure. However, the second-best performing geometry reduced

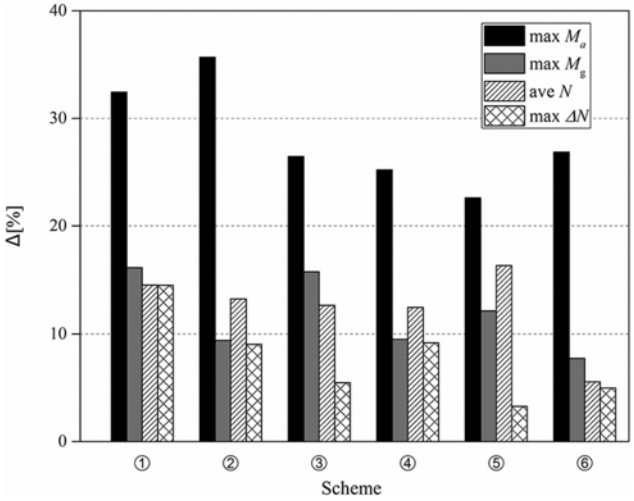

Figure 3.36 The objective function component value reduction in comparison to the reference V-CSM geometry [93]

bending moment the most, but remained parameters were improved less than in the first best solution. Moreover, the difference between the first and the sixth best solution, Fig. 3.5a, was vertical or network-like arrangement respectively, but the objective function value differed by 10% caused mainly by change of parameters referring to hangers.

Author suspected, that **the bending moments reduction should lead to greater improvement in terms of material efficiency than reduction of normal forces in hangers, and therefore different weight approach should be utilized. Alternatively, the cost-driven objective function implementation would solve this issue, since cost of each structural element (arch, tie, hangers) would be a reflection of importance itself.**

In [6] authors optimized network arch pedestrian bridges with V-CSM arrangements in terms of mass reduction. They considered span lengths from 18 to 54 m, dead loads from 13 kN/m to 39 kN/m, live load equal to 13 kN/m [6]. The span lengths were low from network arch perspective, especially arch bridge with 18 m. The results were compared against under-deck cable-stayed bridges [6]. Authors used genetic algorithms with pattern search [6]. The variable parameters were number of hangers, hangers' arrangement, arch elevation, ratio of ellipse radii, arch and tie sections [6]. The constants were span length, material, loads, maximum allowed deflection, lower and upper radius dimension of hangers and available profiles [6].

During the analysis, authors [6] noticed, that the algorithm provided several results with close mass value, but with great difference in the number of hangers, Fig. 3.37. Authors [6] mentioned, that they had to repeat calculations multiple times, since every time, the results were different, which they considered as a property of metaheuristic methods. This feature allowed to obtain multiple equally optimized solutions [6], so engineers could choose the most suitable for their needs. The comparison results to under-deck cable-stayed bridges are presented in Tab. 3.6.

Thanks to combined EA and pattern search algorithm, the resulting network arch bridges were still superior even at low span length [6]. The optimal shape of the arch was elliptical [6]. The simplification of the arch from elliptical to circular resulted in loss in the total mass up to 12% for longer spans and heavier loads [6]. The optimal arch rise to span length ratio was between 0.20 and 0.23 [6], which was higher than usual for network arrangements [86]. The starting angle was greater than 90^o and ended at 25-50^o range [6]. The remaining optimal parameters were more scattered [6]. To obtain more precise results, the global optimization

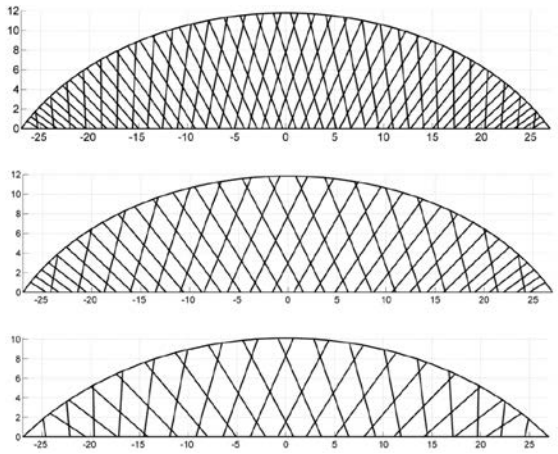

Figure 3.37 The best arrangements with similar masses [6]

Span m	Load case	Mass of network arch bridge kg	Mass of under-deck stayed bridge kg
18	L1	**482.2**	569.4
	L2	**602.7**	788.1
	L3	**786.5**	985.1
30	L1	1677.4	**1527.4**
	L2	**1982.9**	2164.8
	L3	**2355.6**	2746.6
42	L1	3233.0	**2943.4**
	L2	**4105.1**	4292.7
	L3	**4683.1**	5582.0
54	L1	5102.5	**5064.8**
	L2	**6773.2**	6966.8
	L3	**8234.3**	9002.5

Table 3.6 Mass comparison of optimal network arch bridges and under-deck stayed bridges [6]

program should be implemented [6]. One of these dispersed parameters was the ratio of the bending stiffness of the arch to the bending stiffness of the tie, which varied between 2.1 and 7.4 [6]. Since authors pipeline included independent mesh pre-processing, linear analysis in FEA software, post-processing and EA optimization algorithm, each of these steps could be substituted according to users' needs [6].

From these results, author thought, that **the objective function-based on cost would allow to avoid the situation with having equally optimal solutions with drastically different number of hangers**. Practically, the solution with smaller number of hangers, but with equal mass as other solutions with greater number of hangers, would be cheaper considering cost of transportation and assembly and would require more time to construct. The objective function should include then the assembly costs of each hanger.

Authors [6] continued their research in paper [8]. Instead of V-CSM arrangement [6], the CARSM arrangement was optimized in arch pedestrian bridges as well [8]. The evolutionary algorithms were used in the optimization process. The genetic algorithms, particle swarm optimization and simulated annealing demonstrated similar results [8]. Authors defined hangers' arrangement with angular divergence of hangers in pair to the radial line α and angular distribution of the radial line β along the arch [8]. Four scenarios were examined, ranging from fully constrained, where both angles were constant, to fully flexible, where both angles were variable, and including intermediate cases with one angle fixed and the other variable. [8]. The angular parameters visualization was presented in Fig. 3.38 [8]. The symmetrical and three asymmetrical load cases from variable loads were considered. During the analyses, the out-of-plane buckling was not considered for simplification [8]. The cables were simplified as truss elements, not as cable elements [8]. Authors claimed [8], that the nonlinear static analysis was used, which increased the bending moment in the arch and the tie, but nonlinearity was not present in the buckling analyses [8]. The steel grade was assumed as S355 for all the elements [8]. The objective function was mass-oriented [8]. The variables in the optimization process were: rise of the arch, number of hangers, angular parameters, height and width of hollow cross sections of the arch and the tie and the radius of hangers' cross sections.

Authors noticed, that the algorithm preferred greater number of hangers with smaller diameters [8]. Therefore, the cases with bounded diameter of hangers were considered [8]. The results of optimal results in terms of mass reduction were presented in Fig. 3.39 [8]. All of

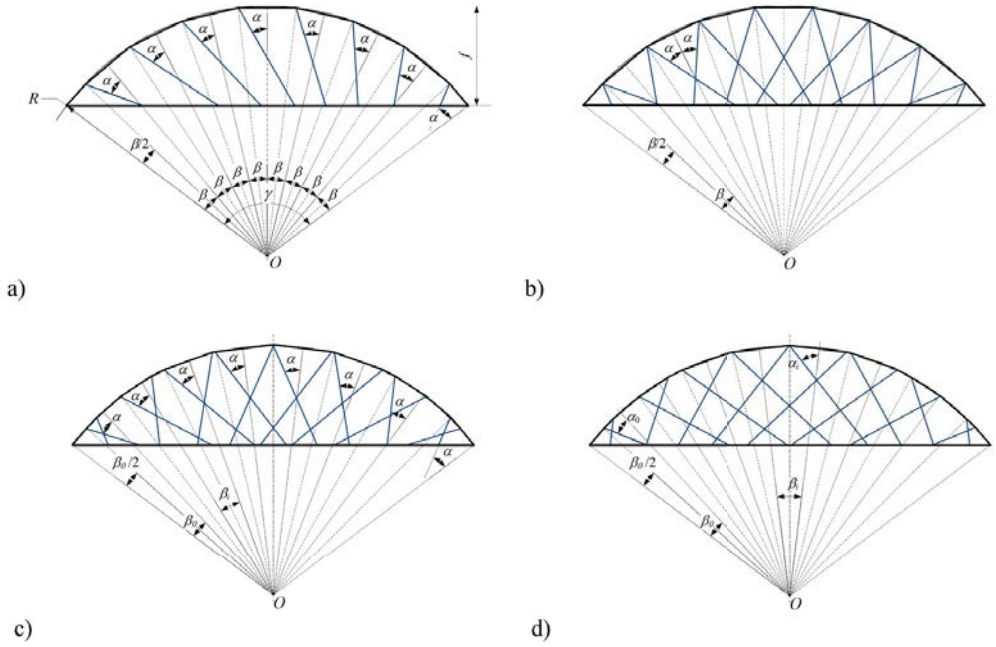

Figure 3.38 The definition of hangers' arrangements with constant (a) (b) and variable (c) (d) angular parameters [8]

the four scenarios regarding angular parameters resulted in the same total mass of the bridge until reaching rise ratio of about 0.22. After that, the most restrained case resulted in a rapid growth of total mass. The less restrained angles were, the more total mass reduced its value. The minimum total mass was achieved for both variable angles at rise ratio of about 0.3 [8].

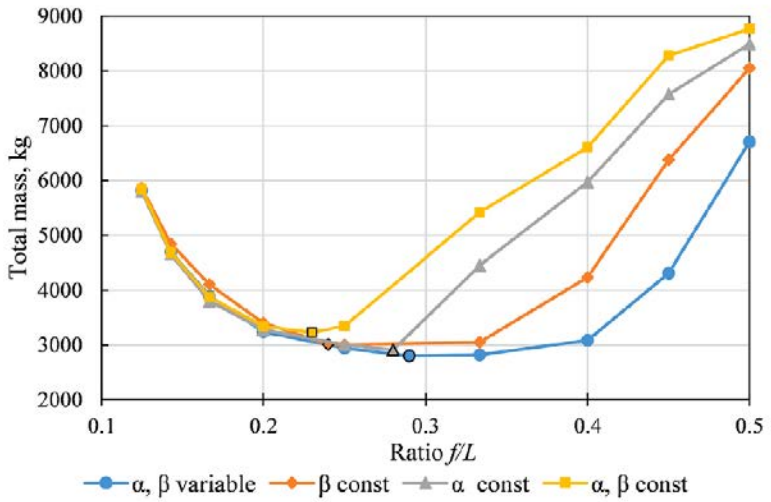

Figure 3.39 The optimal mass of the entire structure for four different angular cases as a function of the arch rise ratio [8]

The lowest mass was achieved for the unbounded diameter of the hangers, but as authors [8] claimed, this total number of hangers was large and equal to 70 hangers. From the practical point of view, the hangers' diameter was bounded [8]. The greater the lower limitation was, the greater the total optimal mass got [8], Fig. 3.40a. Between 20 and 28 mm of hanger's diameter, the total optimal mass of the arch and the tie remained almost unchanged for all four angular

scenarios [8], Fig. 3.40b and c. Then their mass started to increase for lower restriction of 40 mm [8], Fig. 3.40d.

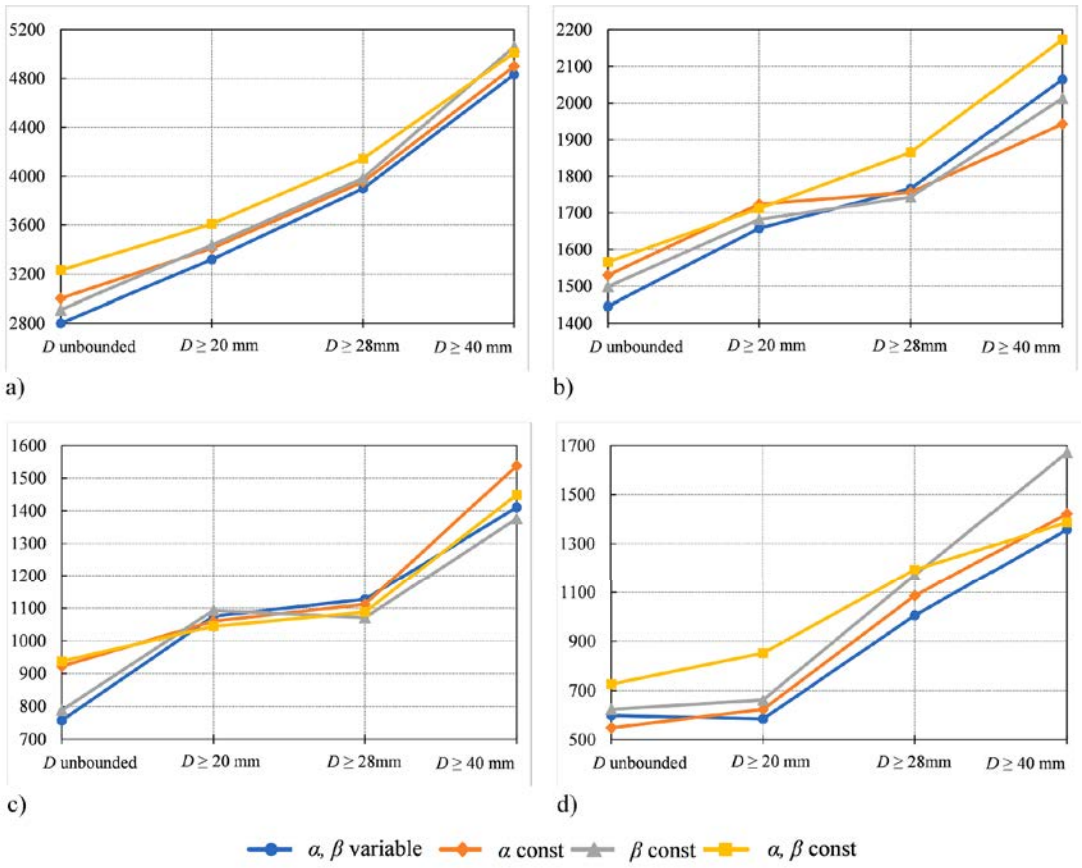

Figure 3.40 The impact of hangers diameter to the mass expressed in kilograms of the (a) entire bridge, (b) arch, (c) tie and (d) hangers [8]

According to authors [8], the optimal value of the arch rise ratio for pedestrian bridges was between 0.22 and 0.30. The diameter of the hangers should be small with number of hangers greater than 50 in the optimal solutions [8]. The optimal angular divergence of the hangers to the radial line should be between 28 and 35^o [8]. The arch should be 2-2.5 times stiffer in bending than the tie in the optimal solution [8]. In the optimal solution, approximately 30% of the total mass is allocated to the tie, 40–50% to the arch, and the remainder to the hangers [8]. Authors [8] continued their research and provided more alternative optimal solutions and their parameters with more detailed results in [7].

Author concluded, that **providing more flexibility for the variables led to more optimal solutions**. At the same time, **low restrain for hangers led to the most optimal but impractical solution due to great number of hangers in the mass-based objective function**. Author suspected, that cost-based objective function with added constant cost of hangers' installation would automatically solve this issue.

In the article [13], a three-step optimization method was proposed. The first step included optimization of hangers' post-tension forces under the self-weight in order to keep the tie straight [13]. The initial section of the arch and the tie were estimated in this step. The rectangular hollow sections made of structural steel S420 were used for the arch and the tie cross sections, whereas hangers were made of prestressed steel. The arch geometry was considered to be parabolic, and the height-to-span length ratios for medium and long span lengths of 50 m and 180 m were considered as 0.17 and 0.167 respectively. The cables were prevented from

sagging by increase of the post-tension force in them. If the force was too high, more material would be added.

In the second step [13], the live load was applied and the bridge was designed for the ULS, SLS and FLS criteria. The arch, tie and hangers were optimized in this step. The stress and deformations criteria were checked. The material contribution was reduced in an iterative procedure, by reducing the cross section areas. Hangers were allowed to have different cross section areas.

In the third step [13], the algorithm compared the results from the latest step to the current one. If the difference in post-tension forces in cables, cross section properties of the arch, tie and cables were significant, the allowed step of the change was refined. If the change was small, the algorithm stopped and assumed a reach of convergence. Author in [13] used word *girder* when describing the tie. While discussing the results from this paper [13], the word *tie* and *girder* were used interchangeably.

The article [13] optimized CSM and vertical hangers' arrangement, called NAB and VHAB respectively in [13]. The objective function was based on the arch and the tie volume minimization. Hangers' constant inclination angle was equal to 60^o with even spacing of 5.00 m. Bridges with 50 m and 180 m of span lengths were considered. For bridges with 50 m of span length, the permanent nonstructural loads were assumed as 80 kN/m and 50 kN/m. The live loads included point load of 1200 kN and uniform load of 42 kN/m. Live loads were applied in multiple positions in order to find the critical load positions. For bridges with 180 m of span length, the permanent nonstructural loads were assumed as 170 kN/m and 50 kN/m. The live loads included point load of 2000 kN and uniform load of 69 kN/m. The design approach of the buckling analysis was considered according to Method II, EN 1993-1-1 Annex D [132].

The optimization was done with gradient algorithm based on SNOPT method, where the gradient of objective function and constraints was conducted by using numerical differentiation [13]. The SNOPT used a sequential quadratic programming algorithm, where the objective function was considered as a quadratic polynomial and constraints as linear [13]. The optimal solution was achieved by conjugate-gradient QP solver [13]. The article [13] utilized similar approach as article [6], where the optimization process was controlled by the external optimization solver programmed in MatLab. Even though the principal limit states of ULS, SLS and FLS were checked, authors [13] made simplifications, among which the most distinguished was modelling hangers as truss elements but with sagging and buckling analysis based on Method II, EN 1993-1-1 Annex D [132].

The optimization results for network arrangement with 50 m of span length wre presented in Fig. 3.41a. The tie-to-arch cross section areas ratio stabilized at 0.86 [13], and the tie-to-arch inertial moments ratio stabilized at 1.11 [13]. It meant, that the tie had smaller cross section area, but greater inertial moment. The total normalized weight of arch and tie stabilized at about 0.12 [13], and arch had greater participation in the total mass than the tie. The hangers mass participated was the lowest and stabilized at about 0.015 [13]. The cross section area of hangers was not constant in the optimal result, but it decreased towards ends towards opposite direction to hangers' skewness [13], Fig. 3.41b.

The results for the 180 m span length for network and vertical hangers' arrangements were presented in Fig. 3.41c and 3.41d respectively [13]. In the network arrangement, the area ratio stabilized at 0.3, the inertial moments ratio at 0.5. Both arch and tie were utilized for almost 100% with tie being utilized slightly more. The area and moment inertia ratios for 180 m of span length changed noticeably comparing to results for 50 m of span length. This time, the tie had both smaller cross section area and inertial moment than the arch.

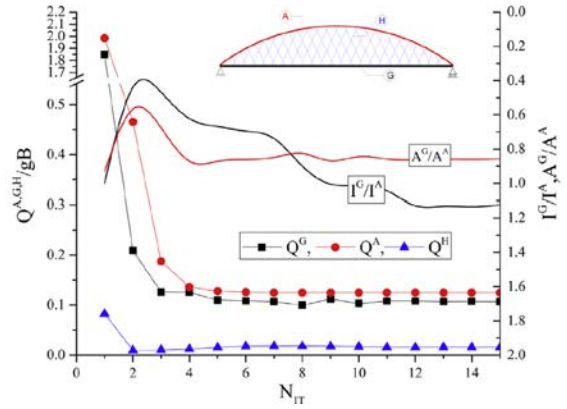

(a) Normalized material steel quantities (Q) involved in the Arch (A), Girder (G) and Hangers(H), normalized ratios between cross-section areas (A^G/A^A) and inertial moments (I^G/I^A) as a function of the number of iterations (N_{IT}) for Network arrangement with 50 m of span length [13]

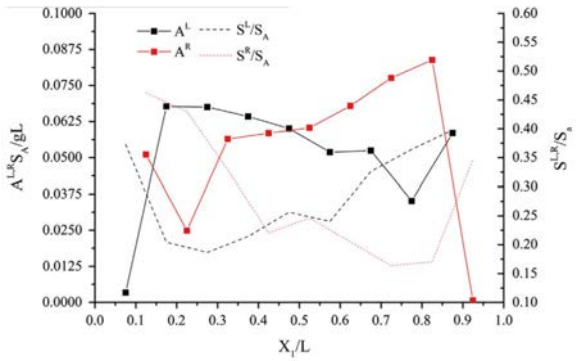

(b) Distribution of the cross-section areas of the hangers and the stresses under Dead Load as a function of the normalized girder position (X_1/L) for Network arrangement with 50 m of span length [13]

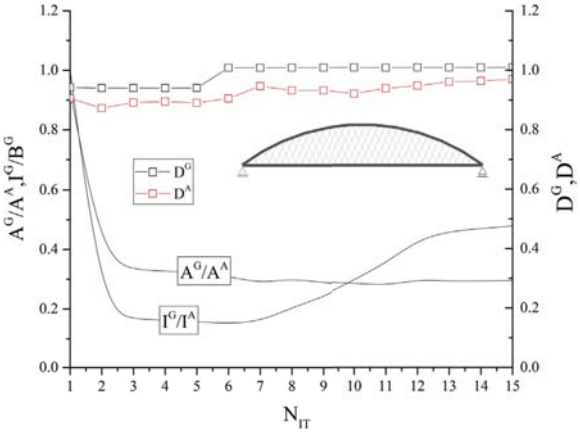

(c) Normalized ratios between cross-section areas (A^G/A^A) and inertial moments (I^G/I^A), worst values of the design criteria in the arch (D^A) and girder (D^G) as a function of the number of iterations (N_{IT}) in Network arrangement with 180 m of span length [13]

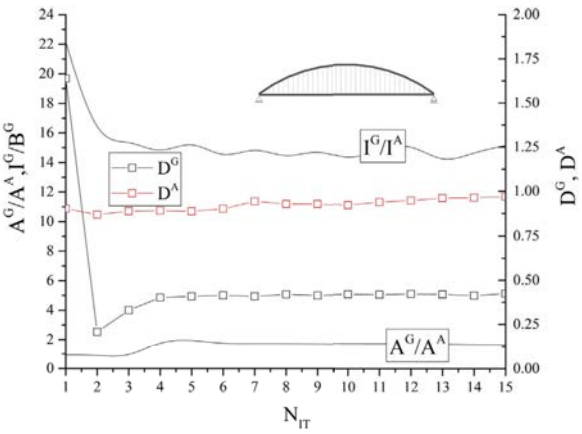

(d) Normalized ratios between cross-section areas (A^G/A^A) and inertial moments (I^G/I^A), worst values of the design criteria in the arch (D^A) and girder (D^G) as a function of the number of iterations (N_{IT}) in vertical hangers' arrangement with 180 m of span length [13]

Figure 3.41 Selected results from [13] for span length of 50 m and 180 m with network and vertical hangers' arrangements

In the vertical arrangement, the optimal area ratio stabilized at 1.0, the inertial moment ratio at 16.0 [13], Fig. 3.41d. The utilization reached almost 100% in the arch and about 40% for the tie, which showed that the network arrangement utilized material more efficiently since both utilizations were almost equal to 100% [13]. About 32 times greater inertial moment ratio in vertical hangers' arrangement than in network arrangement proved that the network bridges were govern by axial forces, not bending moments. This was also reflected in the absolute values in Tab. 3.7, where inertial moment of the tie in VHAB was an order of magnitude greater than in NAB [13]. Even though the arch in NAB experienced less bending moment than in VHAB, the optimal inertial moment was greater about 4 times in NAB than in VHAB with similar cross section area [13], which was counter intuitive. The greatest saving in favour for

NAB was obtained in the tie, which optimal cross section area was reduced almost 5 times comparing to VHAB [13]. The post-tension force in hangers ranged from 320 to 350 kN in the middle of span length in NAB, and from 360 to 390 kN in VHAB [13], indicating comparable magnitudes.

Table 3.7 The optimal sections properties in VHAB and NAB [13]

Scheme	Girder			Arch		
	A^G [m^2]	I_z^G [m^4]	I_y^G [m^4]	A^A [m^2]	I_z^A [m^4]	I_y^A [m^4]
VHAB	0.438	0.373	0.251	0.257	0.0277	0.115
NAB	0.088	0.052	0.036	0.2866	0.115	0.0225

Author suspected, that **the optimal hangers' arrangement should not be defined with the same principles along the entire bridge length** by considering the fact of reduced hangers cross section area toward the opposite direction of skewness as a possibility. **The relevant properties of the arch and the tie were suspected to not be constant over the changing span length and/or applied loads** based on the changed area and inertial moment ratios between 50 and 180 m of span length. **The multi-step algorithm provided fast converging results.**

In the article [2], authors optimized V-CSM hangers' arrangement in road arch bridges and compared the results with vertical hangers' arrangement. The evolutionary optimization method was used [2]. Authors [2] used this method later also in the minimum cost design of a two span continuous post-tensioned concrete I-girder bridge structure [79]. The objective function was cost-oriented, but the material and, as a result, unit costs remained constant during the optimization process [2]. The cost minimization was focused on the arch and hangers, not the tie [2]. Authors included the installation costs and material costs [2]. The bridges were loaded and designed according to AASHTO [136] and AISC [135] codes [2]. The optimization process was coded in FORTRAN and C++ and calculations of internal forces were done in ANSYS FEA software [2]. The bridge model was in 3D. The arch was made of rectangular reinforced concrete section, tie was made of reinforced concrete slab and hangers were made of wire steel [2]. The arches were braced by reinforced concrete beams [2]. Cables were modelled as link elements [2]. The optimization parameters were: number of hangers, angular parameters of V-CSM arrangement, height and width of arch cross section, cross section area of hangers and rise of the arch [2]. The bridges had 100 m of span length and 10 m of deck width [2]. The arch had circular shape [2]. Reinforcement optimization was included in the optimization process [2]. The most optimal hangers' arrangement was presented in Fig. 3.42.

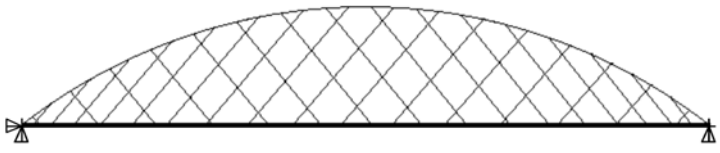

Figure 3.42 The most optimal hangers' arrangement [2]

The most optimal network arrangement reduced the total cost of reinforcement in the arch by 79% comparing to the vertical hangers' arrangement [2]. Even though, the V-CSM arrangement was defined with possibility of having constant inclination change between near hangers, the optimal solution had this angular constant difference equal to 0.027^0 or -0.029^0 [2], which was negligible and practically it turned into CSM arrangement. The initial angles in the optimal

solution were equal to 40^0 or 31^0 [2]. The optimal number of hangers was 32 [2]. The arch elevation in the optimal solution was 0.17 [2]. The optimal network arrangement reduced total cost of hangers, concrete and reinforcement in the arch by almost 50% comparing to optimal vertical hangers' arrangement's results [2], whereas the cost of reinforcement steel in the arch was reduced by 79% [2].

The authors of [2] extended their research in [40], where a similar analysis was carried out using the same optimization approach. However, the arches with both circular and parabolic geometries were considered [40]. The optimal shape of the arches and angular inclination of the hangers were presented in Fig. 3.43.

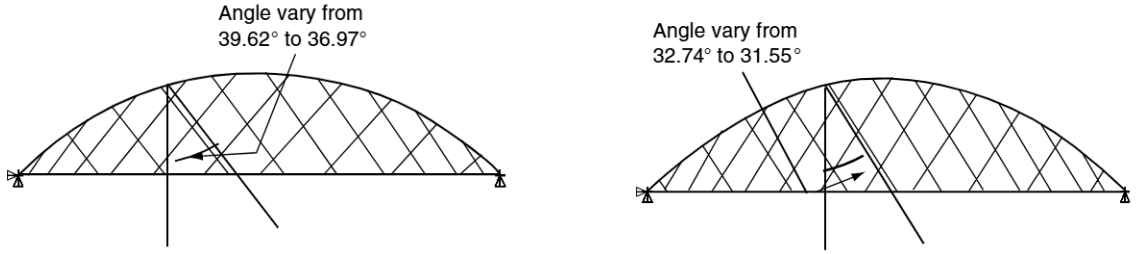

(a) The optimal design shape and angles for circular arch [40]

(b) The optimal design shape and angles for parabolic arch [40]

Figure 3.43 The optimal shaped network arch bridges with (a) circular and (b) parabolic geometry [40]

The optimal hangers' inclination was almost constant for parabolic arches with a value of 32^o, and for circular arches it varied from 36 to 39^o [40]. The optimal parabolic arch with network arrangement was about 10% cheaper in terms of total cost of the hangers and the arch comparing to the optimal circular arch with network arrangement [40]. The optimal circular arches required less hangers than the optimal parabolic arch [40]. The arch rise in the optimal bridge with circular arch was 0.21, whereas for the optimal bridge with parabolic arch the arch rise was 0.24. The optimal circular arch was characterized by reduced arch rise in comparison to optimal parabolic arch [40].

Author noticed, that the arch rise in the optimal results from [40, 8], where the metaheuristic optimization algorithms were used, exceeded the recommended optimal arch rise from literature [115, 117], which did not utilize the modern optimization algorithms. Therefore, it was concluded, that **the metaheuristic optimization approaches went beyond the standard ranges with material or cost-oriented objective function**. The cost-oriented objective function [40] did not provide as dense optimal hangers' arrangements as mentioned in [8] with mass-oriented objective function. Therefore, was concluded, that **the cost-oriented optimization led to more practical solutions.** The metaheuristic optimization results demonstrated that parabolic arches achieved greater cost minimization compared to circular arches [40], revealing more flexibility in arch shaping than the standard configurations [115, 117], where circular, double circular, or elliptical arches were considered the most optimal.

3.3 Conclusions

After the literature review, the conclusions were the following:

- Repeat of calculations in metaheuristic optimization methods provided more certainty of the obtained results [7],
- The optimization process division into steps allowed to reduce complexity of the optimization process [13],
- Simplifications of calculations and model were preferable in order to reduce time consumption [6, 7, 94, 93, 75, 97, 2],
- Less restrained global optimization algorithm should provide less scattered values of optimized parameters [6],
- GA were as efficient as PSO [7], were suitable for sparse hangers' systems [94, 93] and provided similar optimal results with comparable performance [8],
- There was a room for improvement in sparse system in comparison to well-defined hangers' arrangements [94, 93],
- Cost-oriented objective function [40] resulted in practical number of hangers in the optimal solution comparing to mass-oriented objective function [8],
- The metaheuristic driven optimization algorithms demonstrated, that the optimal solutions in terms of mass [8] or cost [40] minimization could exceed the standard ranges of arch rise or arch shaping from literature [115, 117], where iterative, predefined geometries were considered in searching for the optimal shaping,
- The iterative calculations over the predefined set of geometries were limited to investigating the influence of various predefined hangers' arrangements on the distribution of internal forces, the minimization of which was the objective function [75, 97]. That limited the spectrum of possible solutions,
- The metaheuristic-based optimization extended the variable parameters by cross sections, arch elevation and type of the arch. At the same time, the objective function changed to mass or cost minimization criterion [2, 13, 8],
- The metaheuristic-based optimization gave a possibility to investigate custom, not predefined hangers' arrangements but kept the other parameters constant [94, 93],
- No paper was found in network arch bridge optimization, which included the following: (i) varying cross section of the arch, tie and hangers, (ii) varying arch rise, (iii) cost-based objective function with (iv) varying material properties of the structural elements, (v) changing topology of hangers, (vi) changing number of hangers, all at the same time. More generally defined global optimization algorithm should lead to more predictable results [8],
- Hangers' arrangements of V-CSM and CARSM were considered the leading types of arrangements in terms of the internal forces' distribution [75, 97],
- Literature did not mention geometrically nonlinear buckling analysis in the optimization process of network arch bridges,
- The stability of the arch was not mentioned in the optimization of the network arch bridges or was simplified to methods presented in Eurocodes [132, 134, 13, 8, 6].

4 Geometrical instability

4.1 Problem description

In the design of the network arch bridges the LBA is mainly conducted. It was commonly solved using FEA software [18]. The linear elastic bifurcation analysis might have been accurate for the vertical hangers' topology, because the buckling form for this type of topology was the same as for an arch without any hangers from the imperfection form point of view [73], Fig. 4.1a and Fig. 4.1b [134]. The only difference was in the in-plane buckling length factor β - the more vertical hangers are in the bridge, the lower the in-plane buckling length factor β is and the higher the in-plane critical normal force $N_{cr,ip}$ is, Eq. (4.1) [134]. The out-of-plane critical normal force $N_{cr,op}$, Eq. (4.2) [134], based on the graphs in Fig. 4.1c and Fig. 4.1d [134]. These critical forces are proportionally depended from the bending stiffness in-plane EI_{ip} and out-of-plane EI_{op} of the arch respectively. Authors in [8] used Method II from EN 1993-2 [132] in the design of network arch bridge during the optimization process, which was a simplification.

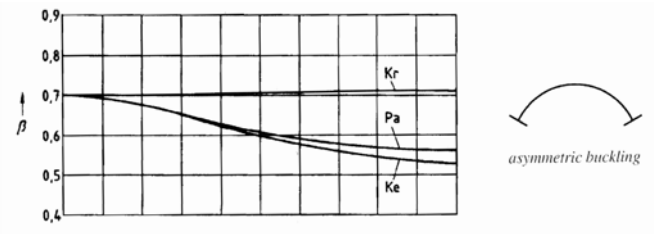

(a) In-plane buckling length factor β for arches for *f/l* > 0.1 [134]

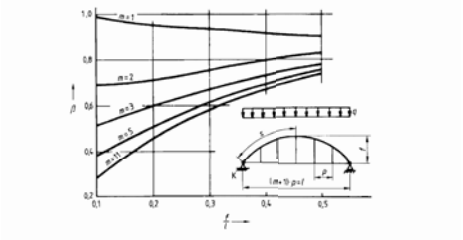

(b) In-plane buckling length factor β for arches with vertical hangers for *f/l* > 0.1 [134]

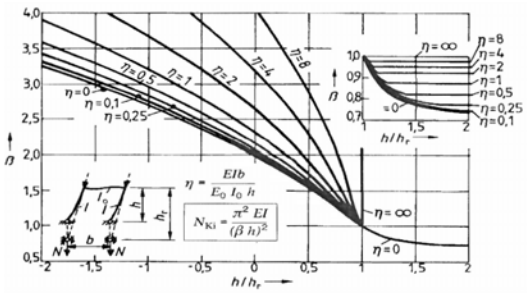

(c) Out-of-plane buckling length factor β for hinged arches [134]

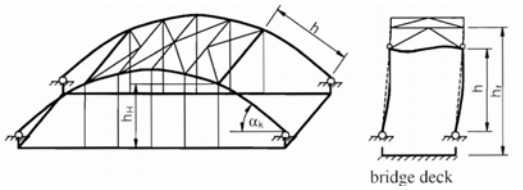

(d) Out-of-plane buckling form and heights description [134]

Figure 4.1 The length factor for arch bridges [134]

$$N_{cr,ip} = \left(\frac{\pi}{\beta s}\right)^2 EI_{ip} \tag{4.1}$$

$$N_{cr,op} = \left(\frac{\pi}{\beta l}\right)^2 EI_{op} \tag{4.2}$$

Unfortunately, Eurocodes [132, 134] did not provide information about the buckling force determination for arch bridges with topology different than vertical hangers. In paper [85] author proposed an approach to determined the critical force in the network arch bridges. The

arch with hangers was simplified by a buckling of compressed beam supported by line spring support along the entire length of the beam, which reflected the stiffness of hangers, Eq. (4.3)-(4.5) [85].

$$N_{cr,ip,hanger} = \min \left(\left[\left(\frac{n\pi}{\alpha_0} \right)^2 - 1 \right] \frac{EI_{ip}}{R^2} + \frac{\frac{EA_p n_p R}{2f\alpha_0} \sin^3 \alpha}{\left(\frac{n\pi}{\alpha_0} \right)^2 - 1} \right) \tag{4.3}$$

$$R = \frac{f^2 + s^2/4}{2f} \tag{4.4}$$

$$\alpha_0 = \arcsin \left(\frac{s}{2R} \right) \tag{4.5}$$

Where:

$N_{cr,ip,hanger}$	-	in-plane buckling force for arch with hangers,
n	-	number of waves,
EI_{ip}	-	in-plane bending stiffness of a beam or arch,
f	-	height of an arch,
EA_p	-	axial stiffness of a hanger,
s	-	span of an arch,
α	-	angle between arch and hanger,
n_p	-	number of hangers.

The number of wave n had to be determined iteratively in order to obtain the lowest critical force value according to Eq. (4.3) [85]. The presented approach did not provide a solution to out-of-plane critical force for the network arch bridges.

The sophisticated method from EN 1993-2 [134] was the physical implementation of an imperfection for the arch. The imperfections were described for arch without hanger and for arch with vertical hangers, Tab. 4.1.

Table 4.1 shape and amplitudes of imperfections in buckling of arches [134]

	1	2	3			
		shape of imperfection (sinus or parabola)	e_0 according to classification of cross section to buckling curve			
			a	b	c	d
1		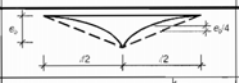	$\frac{s}{300}$	$\frac{s}{250}$	$\frac{s}{200}$	$\frac{s}{150}$
2	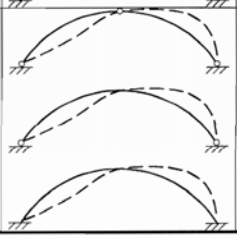	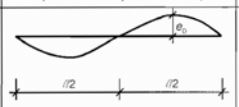	$\frac{\ell}{600}$	$\frac{\ell}{500}$	$\frac{\ell}{400}$	$\frac{\ell}{300}$

(a) Shape and amplitudes of imperfections for in-plane buckling of arches [134]

	shape of imperfection (sinus or parabola)	e_0 according to classification of cross section to buckling curve			
		a	b	c	d
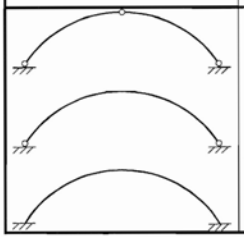	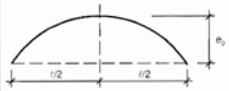	$\ell \le 20$ m	$\frac{\ell}{300}$	$\frac{\ell}{250}$	$\frac{\ell}{200}$	$\frac{\ell}{150}$
		$\ell > 20$ m $\ell_1 = \sqrt{20\,\ell[\text{m}]}$	$\frac{\ell_1}{300}$	$\frac{\ell_1}{250}$	$\frac{\ell_1}{200}$	$\frac{\ell_1}{150}$

(b) Shape and amplitudes of imperfections for out-of-plane buckling of arches [134]

Authors in [4, 35] investigated the influence of the geometrically nonlinear out-of-plane buckling of the network arch bridges. They concluded, that the linear elastic bifurcation analysis led to overestimation of the structural capacity [4, 35]. Moreover, the stiffness of the wind bracing system, height of the portal frame, type of hangers' arrangement, out-of-plane moment of inertia of the arch ribs and inwards inclination of the arches had great influence on the out-of-plane buckling capacity of the arch [4, 35].

In order to implement the imperfection shape of the arches in the network arch bridges, author considered the usage of unique global and local imperfection (UGLI) method provided in EN 1993-1-1 [132]. The method was based on scaling the buckling form of an arch η_{cr} by the imperfection magnitude e_0, Eq. (4.6)-(4.8) [132]. The method was similar to the imperfection instruction for arches, Tab. 4.1, but the shape and the amplitude of an imperfection should have been determined from the analysis instead from the code predefined imperfection amplitudes and shapes.

$$\eta_{init} = e_0 \frac{N_{cr}}{EI\,|\eta''_{cr}|_{max}} \eta_{cr} \tag{4.6}$$

$$e_0 = \alpha\left(\overline{\lambda} - 0.2\right)\frac{M_{Rk}}{N_{Rk}} \cdot \frac{1 - \chi\overline{\lambda}^2/\gamma_{M1}}{1 - \chi\overline{\lambda}^2} \tag{4.7}$$

$$\overline{\lambda} = \sqrt{\frac{\alpha_{ult,k}}{\alpha_{cr}}} \tag{4.8}$$

Where:

α	-	is the imperfection factor for the relevant buckling curve,
χ	-	is the reduction factor for the relevant buckling curve depending on the relevant cross-section,
$\alpha_{ult,k}$	-	is the minimum force amplifier for the axial force configuration N_{Ed} in members to reach the characteristic resistance N_{Rk} of the most axially stressed cross section without taking buckling into account,
α_{cr}	-	is the minimum force amplifier for the axial force configuration N_{Ed} in members to reach the elastic critical buckling load,
M_{Rk}	-	is the characteristic moments resistance of the critical cross section, e.g. $M_{el,Rk}$ or $M_{pl,Rk}$ as relevant,
N_{Rk}	-	is the characteristic resistance to normal force of the critical cross section, i.e. $N_{pl,Rk}$,
N_{cr}	-	is the critical normal force at the critical cross section,
$EI\|\eta''_{cr}\|_{max}$	-	is the bending moment due to η_{cr} at the critical cross section,
η_{cr}	-	is the shape of elastic critical buckling mode,
$\overline{\lambda}$	-	is the relative slenderness of the structure,
γ_{M1}	-	is the partial factor for resistance of members to instability assessed by member checks.

The UGLI method was promising, but to consider the geometrically nonlinear behaviour of hanger, a linear elastic bifurcation analysis (LBA) should not have been taken into consideration. It might have affect on both the shape of the buckling form and the value of critical load factor. In order to utilize the UGLI method suitable for arch bridges' utilization determination with custom hangers' arrangement that might appear in the optimization process, firstly the tests of SOFiSTiK FEA software were done in terms of investigating if geometrically nonlinear buckling analysis acted properly. Then the influence of geometrical nonlinear buckling analysis in network arch bridges was investigated and compared to the linear elastic bifurcation analysis results.

4.2 Tests

The results in this chapter were based partially on the results made for the need of preparation for the article [12].

Three tests were proposed. The first, Misses truss, checked if SOFiSTiK managed to achieve limit or critical point if it was lower than the first bifurcation point with TH3 analysis. The results were compared with analytical solutions. In the second test with arch under bending load, the critical buckling mode from the geometrically nonlinear analysis was compared with

that from the LBA. The last test with arch under compressive load, checked if TH2 and TH3 analysis acted adequately to represented theories. The second and the third test were related to the arch buckling phenomenon for both bending and compressing, which were two the most significant forces applied on the arch in NAB.

4.2.1 Mises truss

The Misses truss was well-known as an example of a snap through phenomenon [44, 29, 24, 70]. It was a phenomenon, where slight increase of applied load caused sudden and significant displacements of the structure. The equilibrium path representing applied force as a function of displacement decreased after reaching local extremum called critical limit point. This decrease continues until reaching the next limit point from which the applied load started to increase again. The path between critical limit points was unstable. In real life scenario, the applied load would not decrease to follow the critical path, but it would keep rising. It caused the phenomenon of skipping the unstable part and jump directly from limit point to post-snapping point causing significant displacement with negligible increase of applied load. That's why such phenomenon was always sudden. To determine the equilibrium path with the noticed decrease of applied load value, the displacement load was applied and the support reaction were considered as applied load value on the graph. In the Mises truss, the bifurcation point was usually higher than the first limit point, which rose the need of conducting nonlinear buckling analysis.

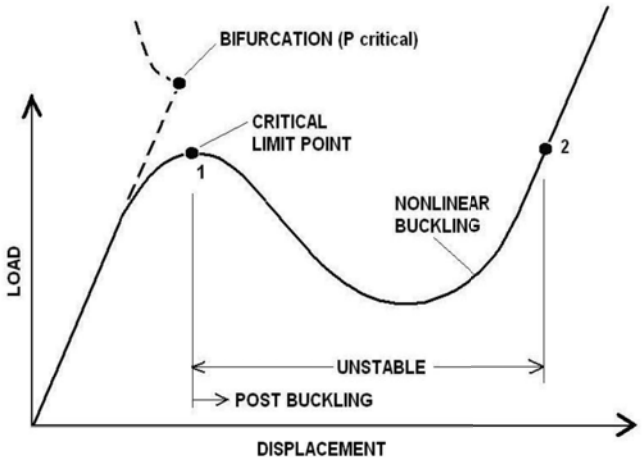

Figure 4.2 Example of equilibrium path of Mises truss phenomenon [3]

In order to check the software's capabilities related to geometrically nonlinear analysis, the Mises truss was modelled as a symmetrical beam structure with a shape of double slope roof and 10% inclination. Supports and the top point were hinged. The span length L was set to 2.0 m and the height h was 0.1 m to match 10% of inclination. Cross section was assumed as IPE 100 and material as steel S355, Fig. 4.3.

First of all, the analytic solution was determined. For this reason, the correlation between applied force and vertical displacement including axial stiffness of the beams was determined by author from static equations and presented in Eq. (4.9).

$$P(x) = 2EA\left(1 - \sqrt{\frac{(L/2)^2 + (h-x)^2}{(L/2)^2 + h^2}}\right) \cdot \frac{h-x}{\sqrt{(L/2)^2 + (h-x)^2}} \tag{4.9}$$

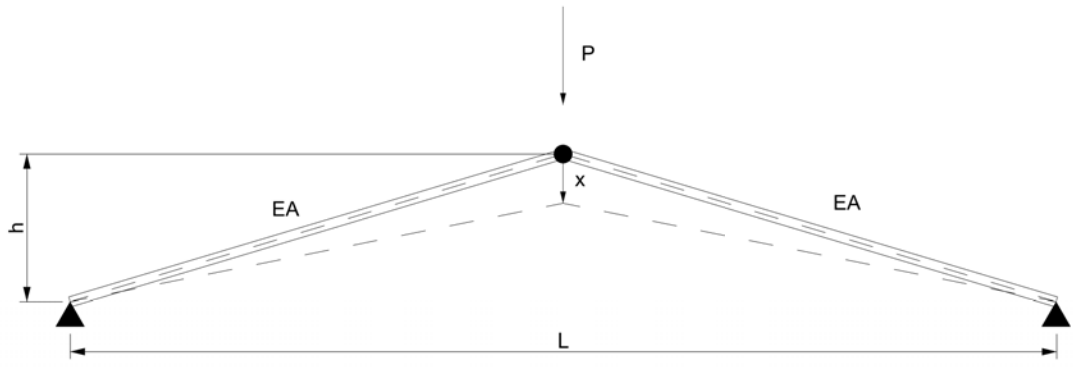

Figure 4.3 The von Mises truss schema

According Eq. (4.9), the first limit point should occur for 0.042 m of displacement of the middle point. The second limit point should occur with 0.158 m of the displacement of the middle point. The force at the limit points had an applied of 82.5 kN. After the second limit point, the force should start increasing and reach the stable part of the equilibrium path for 0.216 m of the displacement of the middle point and continue increasing indefinitely. The equilibrium path should cross the neutral axis for 0.100 m of displacement of the middle point, which matched the intuition, since both beams would be horizontal and therefore no vertical reaction on the supports could be expected. The analytical equilibrium path was presented in Fig. 4.4.

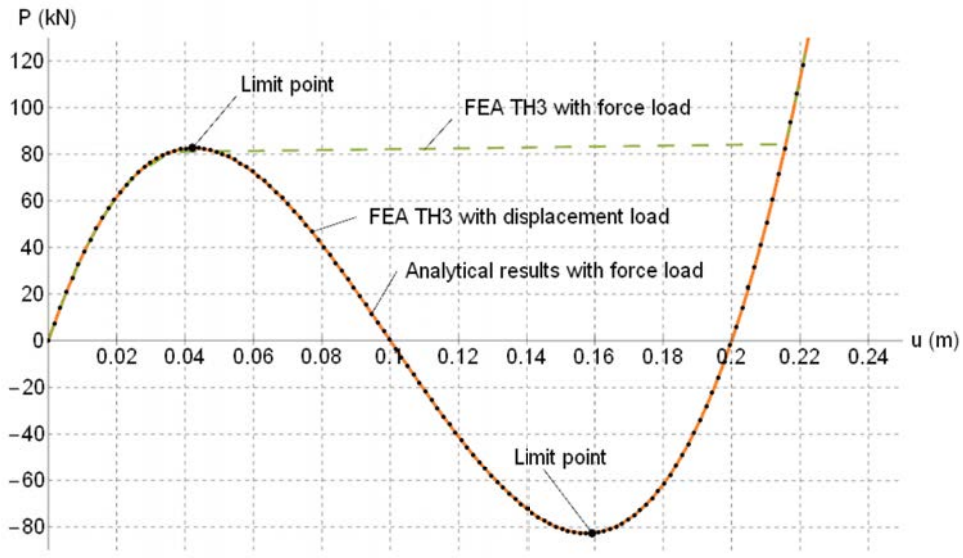

Figure 4.4 Mises critical path for nonlinear buckling analysis - analytic solution (dotted), FEA displacement solution (orange dashed) and FEA force solution (green dashed) [12]

For the comparison, the linear critical load was determined. The initial force in a single beam was equalize with the critical force of a single beam, which resulted in establishing the formula by author of the linear critical load P_{cr} for a single beam in the Mises truss, Eq. (4.10).

$$P_{cr} = \frac{2\pi^2 E I_y}{((L/2)^2 + h^2)\sqrt{1 + (L/2h)^2}} \tag{4.10}$$

Substitution of the values from the structural model into Eq. (4.10) resulted in P_{cr}=698 kN, which was significantly greater than nonlinear critical force P_{ncr}=82.5 kN. This result was expected in the Mises truss, which underlined the importance of including geometrical nonlinearity in buckling analysis for structures vulnerable to this phenomenon.

The second attempt was the FEA analysis, where two loads were considered: the 1 kN force and 1 mm displacement, Fig. 4.5a.

The first analysis contained linear bifurcation for an external point load of 1 kN. The first buckling form whad a bow shape of a single beam with a critical force equal to 698 kN, which corresponded with the analytic solution for hinged compressed beam, Eq. (4.10), Fig. 4.5b. This value was much higher than 82.5 kN of nonlinear critical load achieved from analytic solution for nonlinear buckling analysis.

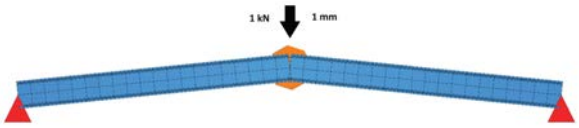

(a) The Mises truss model in SOFiSTiK [12]

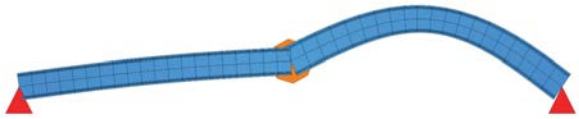

(b) 1^{st} linear elastic bifurcation form - P_{cr} = 698 kN [12]

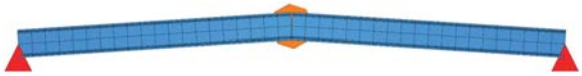

(c) Pre snap-through deformation - limit point for P = 82.5 kN and u = 0.042 m [12]

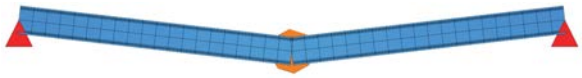

(d) Post snap-through deformation - P = 82.5 kN and u = 0.216 m [12]

Figure 4.5 The Mises truss model visualization (a) with instability forms: (b) linear elastic bifurcation form, (c) limit point deformation and (d) deformation after snap through [12]

The second analysis based on the step load factor increase, so called ULTI procedure in SOFiSTiK [61], of 1 kN force. In this procedure, the stiffness matrix was updated after each step of load increment. The geometrical nonlinear analysis was implemented as TH3 approach in SOFiSTiK, so called the theory of large displacements. If the task parameters were set correctly with enough size of load step increment, the snap through phenomenon could be observed, Fig. 4.5c and 4.5d. The force and corresponded displacement of the center point matched the analytical equilibrium path, except the unstable part, where the force should have decreased to follow the equilibrium path, Fig. 4.4. The force decrease was not possible in incremental ULTI method. For this reasons the 1 mm displacement load was applied with incremental ULTI procedure. From each displacement step, the sum of vertical components from both supports were treated as an equivalent of the applied force *P* from the force analysis. Since the solutions from each displacement step analysis were convergent, the full equilibrium path was reached as in the analytic solution, Fig. 4.4.

The tests confirmed that the SOFiSTiK software was capable of performing bifurcation analysis and allowing identifying critical points on the equilibrium path.

4.2.2 Arch loaded by vertical load

This example was meant to check stability behaviour of an arch with vertical load. The arch was modelled in SOFiSTiK with a span length of 120 m and elevation of 12 m, Fig. 4.6. The cross section was assumed as profile HD 400x990, prismatic along the whole arch length. The arch was divided into 400 elements. Both supports were hinged. The task was solved in 2D. The uniform load of 1.0 kN/m was applied along the whole arch length as shown in Fig. 4.6.

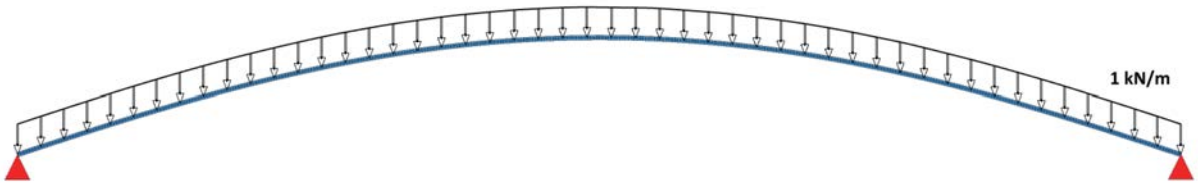

Figure 4.6 Bended arch SOFiSTiK model with applied load [12]

First of all, the LBA was conducted. The shape was a single period sinusoidal curve as expected, Fig. 4.7. This shape were described in [134], Tab. 4.1a in row 2. Buckling form did not include the bow imperfection.

In the second analysis, the TH3 analysis with ULTI procedure was conducted. The result was the deformation in the critical point, represented by the red curve in Fig. 4.7. After that, the post-critical analysis was conducted with PUSH procedure in SOFiSTiK with TH3 analysis. The program started the process from the critical point. In order to show only the displacements progression after the critical point, the deformations in the critical point were subtracted from the deformations after the critical point, which was represented by the dashed curves in Fig. 4.7. The results from LBA were scaled to almost match the deformations of the 20 pushes results.

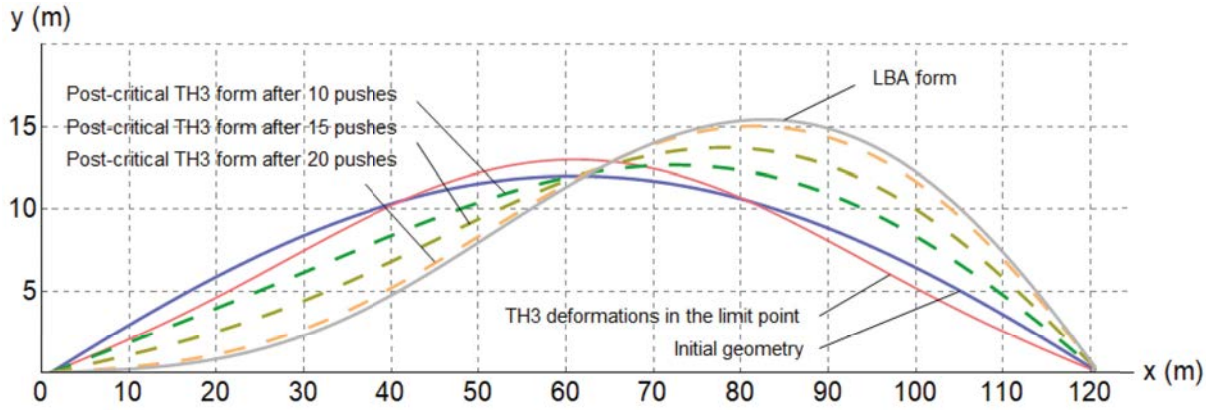

Figure 4.7 Scaled deformation forms from buckling and TH3 analysis [12]

The more push steps were proceeded, the more shape matched the buckling form. It was especially visible for the position of the inflection point. For the case of 10 pushes, this point was almost in the center of the arch, but for the case of 20 pushes, it almost matched the inflection point from the LBA form. Scaling of the graphs did not affect the position of this point, since its displacement was always 0 from the arch perspective.

In this case, the TH3 analysis provided the same results as LBA, in terms of both critical load factor and shape.

4.2.3 Arch loaded by horizontal load

The last test was meant to check stability behaviour of an arch with horizontal compression force. The arch was modelled in SOFiSTiK with two length spans of 40 m and 100 m. For each one of them elevations of L/300, L/200, L/100, L/30, L/20 and L/10 were analysed, resulting in 12 cases. The cross section was assumed as IPE 100, prismatic along the whole span length. The arch was divided into 400 elements. Both supports were hinged, but the right one was horizontally movable. The results were presented for 40 m span with elevation of L/300.

a) Arch with the lowest elevation of 1/300 [12]

b) Arch with the highest elevation of 1/10 [12]

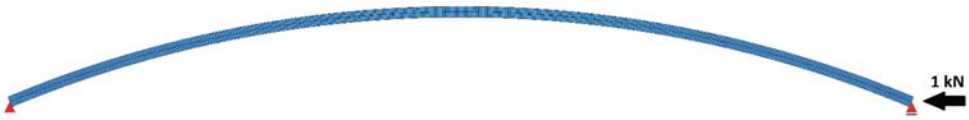

Figure 4.8 Compressed arch SOFiSTiK model with applied load for (a) the lowest elevation and (b) the highest elevation [12]

First of all the LBA was conducted with results of linear critical load factor of 33. The results from these analyses should be a horizontal asymptote for TH2 analysis. For this purposes, the ULTI procedure from SOFiSTiK was implemented but this time with TH2. The equilibrium path approached asymptotically the resultant critical load factor from LBA, Fig. 4.9. The path behaved as expected.

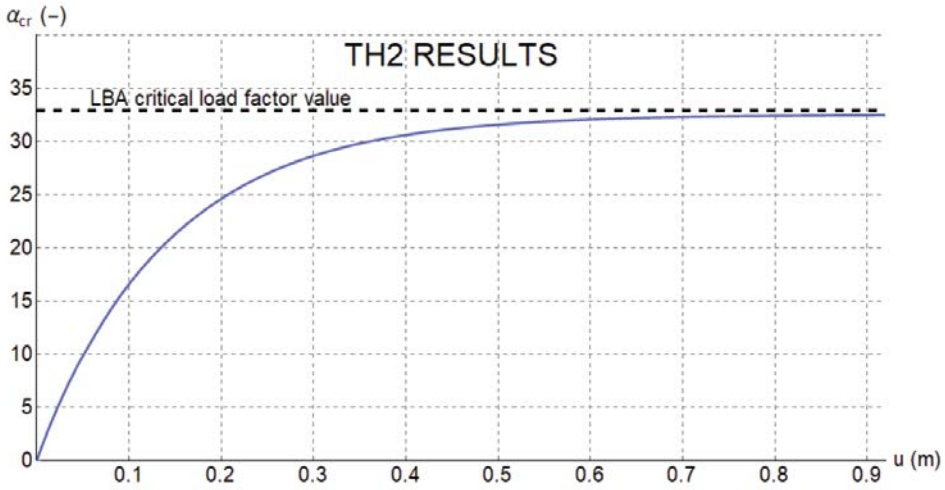

Figure 4.9 Arch center point equilibrium path for TH2 analysis with asymptotic critical load factor from LBA - 40 m long arch with a 1/300 elevation [12]

In the second attempt, the TH3 analysis was conducted also with ULTI procedure. According to theory, the equilibrium path was expected to pass through the LBA critical load factor.

The equilibrium path of the displacements at the center point of the arch passed through the critical load factor value determined by LBA, Fig. 4.10a red point. The displacement for this factor were significantly greater than the deformations from the analysed TH2, Fig. 4.10b. Generally TH2 analyses should have resulted in infinitive displacement before approaching critical

a) Arch center point equilibrium path for TH3 analysis [12]

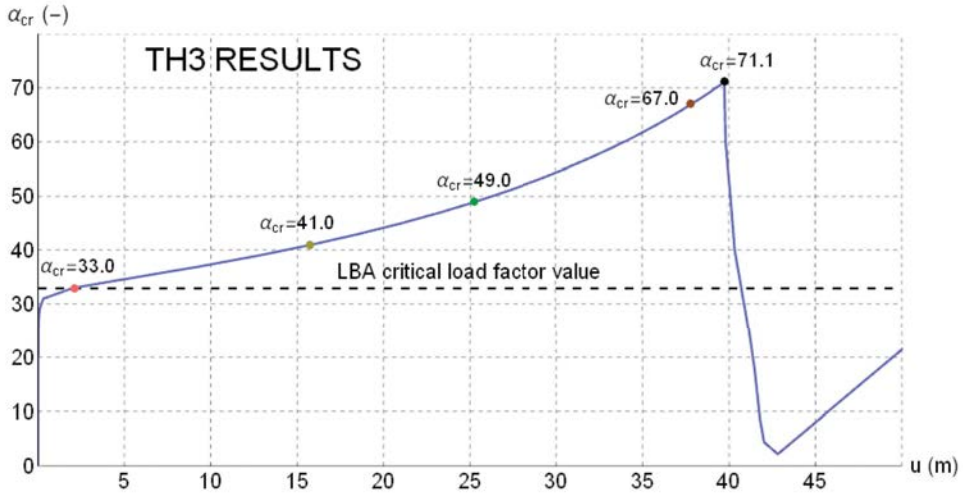

b) Arch sample deformations for TH3 analysis [12]

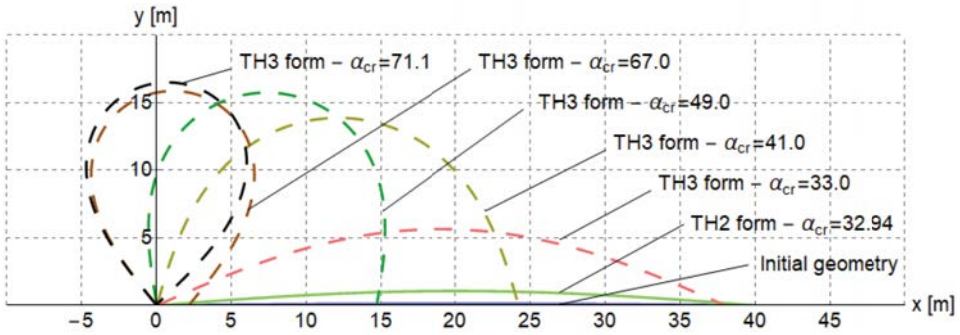

Figure 4.10 Results of TH3 analysis of (a) equilibrium path and (b) sample deformations - 40 m long column with a 1/300 elevation [12]

load factor, but the analyses was always limited to limited number of steps, which explained small deformations from TH2 analysis on this graph. Nevertheless, displacement from TH3 analysis at the level of LBA critical load factor should be finite, and it was. The values on the equilibrium path increased then nonlinearly and the deformations started to turn from bow shape to reversed U-like shape represented by purple, green and brown colors in Fig. 4.10a and b. When the critical point was achieved, the equilibrium path rapidly declined. The displacement graph reached a water-drop-like shape, where the column started to overlap with each other, represented by black color in Fig. 4.10a and b. This phenomenon happened for critical load factor equal 71.1, which was more than twice as high as the critical load factor from LBA.

In this case the TH2 analysis provided the same results as LBA, in terms of both the shape and critical load factor value. The TH3 analysis provided higher critical load factor value and different shape. From engineering point of view, the typical LBA was enough when designing the structure.

The SOFiSTiK software could be utilized in the next stages of this study for conducting more advanced analyses, as it enabled both the correct achievement of results from LBA and the correct identification of limit and critical point and post-critical unstable states for arch structures loaded with both lateral and compressive loads, as well as in low inclined structures.

4.3 Investigation in Network Arch Bridges

The results in this chapter were based partially on the results made for the need of preparation for the article [12].

After investigating the possible types of analyses in SOFiSTiK, including LBA, TH2, TH3 and pre-critical and post-critical states for a simple cases, it was decided to research the impact of the geometrically nonlinear buckling analysis in NAB comparing to the LBA. Four tests were done for these reasons. The first investigated the impact of change of post-tension and pretension force in tie and hangers respectively. The second investigated the impact of elevation change of the arch. The third and the forth tested the impact of a single and double rapture of hangers.

The model was based on the Cracow railway NAB over the Vistula river [126, 45, 89]. Since the in-plane instabilities were investigated, the model was prepared in 3D with prevention of out-of-plane buckling phenomenon by an addition of supports perpendicular to the NAB plane in every anchorage of hangers. The static scheme of the NAB was a freely supported beam. The bridge had unusual solution of the skewback, Fig. 4.11 [12]. The skewbacks were a composite solutions with widen cross section from the arch, allowing for smooth force transition from the arch to the supports. The arch was made of rolled HD 400 x 1299 and steel S460 HISTAL, which was the first of its kind for railway bridges. The span length was 116 m and elevation of 17.4 m. The change of arch cross section started 12 m from the supports. This change of height happened linearly to 1520 mm. The skewbacks were 1.20 m thick and made of concrete C55/67, Fig. 4.13. The tie was a post-tensioned deck with dimensions of 600 x 7000 mm, corresponding to approximately half of the deck width. The tie material was concrete C55/67. Hangers were distributed radially, with spacing along the arch ranging from 1.3 to 2.7 m, which resulted in a variation of the inclination angle from 30° to 75°, Fig. 4.12 [12]. There were 44 hangers in total. Hangers cross section was a circular shape with 87 mm in diameter and S460 as steel material. The arch and tie were modeled as beam elements, the skewbacks as shell elements and hangers as cable elements for lack of bending capacity considerations.

Figure 4.11 Photos of NAB in Cracow [12]

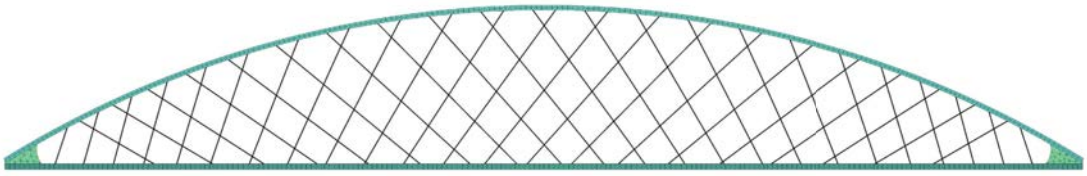

Figure 4.12 Side view of NAB SOFiSTiK model [12]

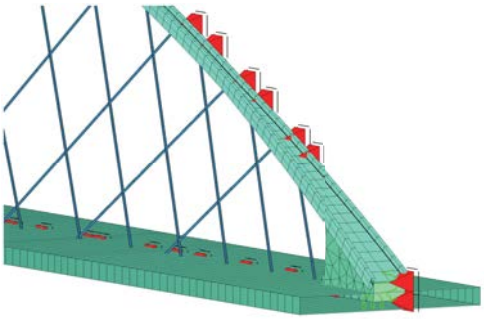

Figure 4.13 Skewback view in NAB SOFiSTiK model [12]

Since the NAB was a railway bridge, it was decided to apply load similar to the most decisive LM71 railway load model, according to [131], Fig. 4.14. The point loads were distributed along the length of their presents resulting in 250 kN / 1.6 m = 156.25 kN ≈ 160 kN. This value was around twice as high as the remaining uniformly distributed part of the LM71 load model equal to 80 kN/m. Based on this fact, the uniformly distributed load was always applied on the span length and the remaining 80 kN/m from the point load range was treated as a moving load along the span length with a load length of 6.4 m. The moving load was considered in 9 positions, starting from the beginning of the bridge and ending in the middle, Fig. 4.15 [12]. Application of the load on the second half was not needed since the hangers' topology and support conditions were symmetrical. Self-weight was always considered in the researches. Post-tensioned and tension forces were considered depending on the conducted analysis.

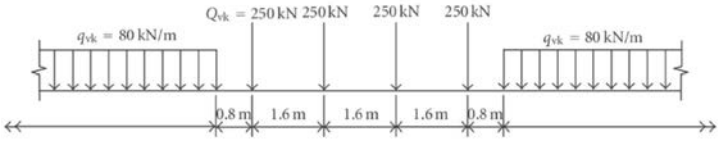

Figure 4.14 Load model of LM71 according to EC [131, 12]

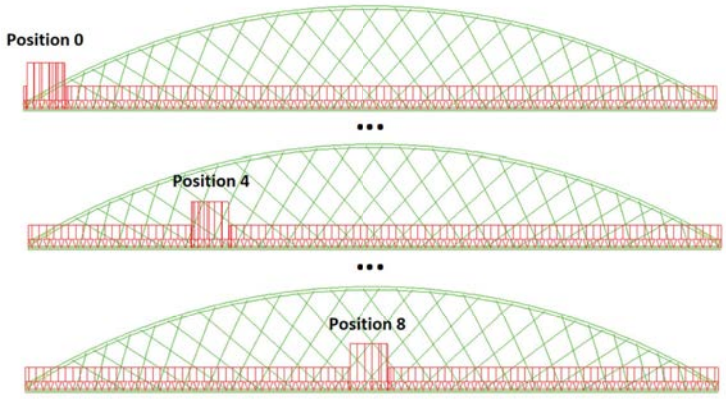

Figure 4.15 Simplified moving part of LM71 load [12]

4.3.1 Post-tension and pretension

In the first analysis, the impacts of post-tension force in the tie and pretension in hangers were investigated. The test contained LBA and geometrically nonlinear buckling analysis

made with ULTI procedure until reaching the maximum load factor, where the convergence was achievable. Each step in the ULTI procedure was considered converged for a considered load factor, if the residual forces were smaller than 0.001 of the maximum force in the given finite element between two following iterations. Moreover, ULTI procedure determined the load factor with the 0.5% precision. After ULTI procedure, the PUSH procedure was used for obtaining deformations after the last converged step from ULTI procedure, so called critical point. These deformations were reduced by deformations from the critical point achieved in the ULTI procedure resulting in just critical deformations, but with geometrical nonlinearity of the hangers, as it was done in Sec. 4.2.2. This time the analysis was done with TH3B type, which was a TH2 for beam elements and TH3 for cables [61]. Thanks to that, the sagging effect in hangers was included in the stiffness matrix and the arch would not have exceeded the bifurcation point. This methods mixture made the comparison of both linear and nonlinear buckling related to sagging effects of hangers without potential critical point exceeding the bifurcation point value of critical load factor. Nevertheless, the solution reached the critical point, but it was always below than the one from the LBA.

Three values of post-tension force and pretension force were checked. The post-tension forces were 10 MN, 15 MN and 20 MN, corresponding with low, medium and high post-tension force. The pretension forces were 1 kN, 500 kN and 1000 kN, corresponding with small, medium and high pretension. The reference case was analysed, where no post-tension and pretension forces were applied. In the first step, the critical load factors from linear and nonlinear analyses, $\alpha_{cr,LBA}$ and $\alpha_{cr,ULTI}$ respectively, were compared by a nonlinear-to-linear critical load factor ratio, Fig. 4.17 [12]. The range of all obtained critical load factors was presented in Fig. 4.16 [12].

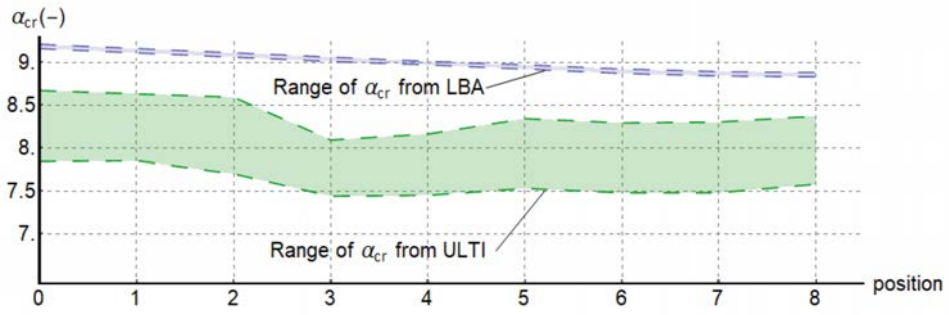

Figure 4.16 Range of all critical load factors from both LBA and ULTI procedure [12]

The range of linear critical load factor remained almost the same for every vehicle position with the value of about 9.0. The nonlinear critical load factor had much more diversified range of values depending which tension and stress values were considered. The range took the values between 7.5 and 8.6. For the 3rd position, the values of nonlinear critical load factor got the lowest among all positions. In general, the point load position generated the highest bending moment is about 20-25% of the total arch length, corresponding with 2.40-3.25 position on the arch, and the 3rd position obtained from the results fits this range.

The results in Fig. 4.17 [12] were split into four ranges related to value of pretension force in hangers, since the post-tension force in the tie had negligible affect on the values of nonlinear-to-linear critical load factor ratios. The greater the tension force was, the smaller the ratio became. For the lowest tension force, the ratio reached value up to 95%, the middle 90% and the highest 86.5%. The significant decline was again spotted for the 3rd position as in Fig. 4.16 [12]. It dropped the values for lowest, medium and highest tension force to 90%, 85% and 82.5% respectively.

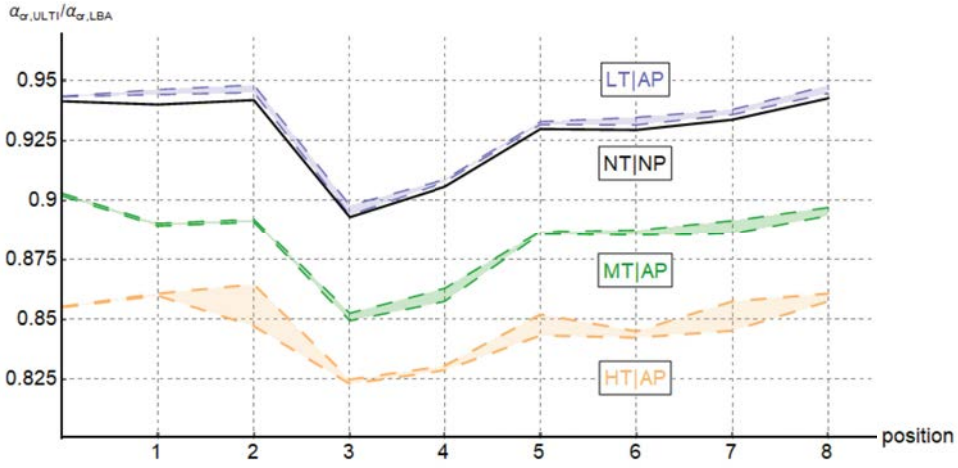

Figure 4.17 Resultant ranges of critical load factor ratios. NT – no pretension, LT – low pretension (1 kN), MT – middle pretension (500 kN), HT – high pretension (1000 kN), NP – no post-tension force, AP – all post-tension force cases (10 MN, 15 MN, 20 MN) [12]

In Fig. 4.18 the ratios of normal force capacity obtained from nonlinear buckling analysis to that from linear elastic bifurcation analysis were compared with various imperfection factors α. The investigation showed, that the LBA resulted in maximum 5.5% of divergence for high-tension and 2.5% of divergence for low-tension scenario in comparison to the nonlinear results. The section of rolled I or welded box sections were expected to be characterized by maximum imperfection factor related to the "c" curve in z-z direction, EN 1993-1-1 [132], clause 6.3.1.2, Tab. 6.2. In that case, the difference changed to 4.5% for higher-tension force and less than 2.0% for low-tension case. The divergence of up to 5% sound reasonably high to not neglect it in the design process.

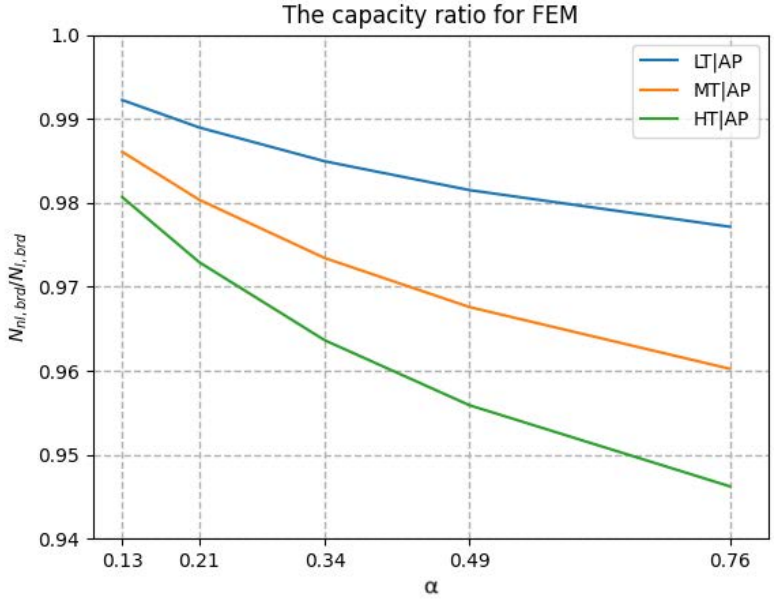

Figure 4.18 The ratio of normal force capacity obtained from nonlinear buckling analysis to that from linear elastic bifurcation analysis, as a function of imperfection factor

Additionally, the results were compared with the analytic Schanack formula, Eq. (4.3)-(4.5) [85]. Since the arch section had h/b ratio greater than 1.2 and the flange thickness was also above 100 mm, the EN 1993-1-1 [132] could not cover this type of section in terms of buckling curve, therefore the ArcelorMittal producer's documentation [91] was used, Tab. 4.2 [91].

Table 4.2 The suggested buckling curves for the I-profiles proportions [91] not included in the basic EN 1993-1-1 [132]

Cross-section	Limits		Buckling about axis	Buckling curve S235 S275 S355 S420	Buckling curve S460 S500
Rolled I-sections 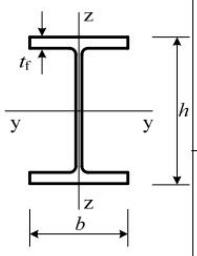	$h/b > 1.2$	$t_f \leq 40$ mm	y-y z-z	a b	a_0 a_0
		$40 < t_f \leq 100$ mm	y-y z-z	b c	a a
		$t_f > 100$ mm	y-y z-z	b c	a b
	$h/b \leq 1.2$	$t_f \leq 100$ mm	y-y z-z	b c	a a
		$t_f > 100$ mm	y-y z-z	d d	c c

The arch buckled around z-z axis, which corresponded to "b" buckling curve for steel S460 according to [91]. The Schanack formula was iterated as long as the minimum critical force value was achieved. That corresponded to 8 waves buckling form, and resulted in 54.5 MN of design normal force capacity including buckling and 170.7 MN of critical force, Tab. 4.3. The results from nonlinear buckling were conducted for all three values of tension forces in the cables. For simplification, the maximum normal force was taken from each position as a reference design normal force in the arch and the critical load factor was an average from each vehicle position. In the linear elastic bifurcation, the design normal force was taken as an average from the three nonlinear maximum design normal forces in the arch, since the differences were negligible between them. The critical load factor was taken as the average of each three tension forces in cables calculated for each vehicle position, Tab. 4.4.

The critical force for linear elastic bifurcation was 188.5 MN and for the three tension forces, starting from smallest to the greatest, the results were 175.2 MN, 166.1 MN and 159.1 MN respectively. The critical force decreased the more, the more tension in hangers was. Similar trend was observed in the design buckling resistance, which was for linear elastic bifurcation 55.7 MN and for nonlinear buckling 54.8 MN, 54.2 MN and 53.7 MN respectively.

The design buckling resistance of nonlinear results was lower between 1.5% and 3.6% comparing to the linear elastic bifurcation results. The same trend was in critical force with values between 7.1% and 15.6% lower compared to the linear elastic bifurcation results. When comparing to the Schanack's formula, the design buckling resistance for LBA was greater by 2.1%, and for nonlinear buckling results varied, showing values up to 0.6% higher or up to 1.6% lower respectively. The similar trend was observed in the critical force, where for the linear elastic bifurcation the critical force was 10.4% greater than the result obtained form the formula, and between 2.6% greater and 6.8% lower for the nonlinear results respectively. In general, the greater the tension force in cables was, the greater the divergence to the linear elastic bifurcation was. However, the formula-based solution resulted almost in the middle between low and medium tension force results for nonlinear buckling, underestimating for the low tension force

and overestimating for the medium tension force. Similar trend was observed in the critical buckling force. In general linear elastic bifurcation overestimates the results in relevance to the formula and nonlinear buckling results.

Table 4.3 The calculations of the critical force and design normal force capacity including buckling according to Schanack formula Eq. (4.3) [85]

Schanack formula capacity calculations			
number of waves	n	8	-
arch span	s	116	m
height of an arch	f	17.4	m
coefficient	R	105.4	m
coefficient	α_0	0.583	-
bending moment of inertia z-z	I_z	0.00254	m^4
Young modulus	E	210	GPa
bending stiffness z-z	EI_z	534261	kNm^2
number of hangers	n_p	44	-
hanger diameter	d_p	0.087	m
hanger area	A_p	0.00594	m^2
angle between arch and hangers	α	0.942	-
critical force	N_{cr}	**170722**	kN
slenderness	λ	0.660	-
buckling curve index	curve	b	-
imperfection factor	α	0.34	-
coefficient	ϕ	0.796	-
buckling coefficient	χ	0.806	-
safety factor	γ_{M1}	1.1	-
design buckling resistance	N_{brd}	**54532**	kN

Table 4.4 The calculations of the critical force, design normal force capacity including buckling for the linear and nonlinear buckling analysis with the comparisons including the Schanack formula results Eq. (4.3) [85]

		linear buckling	nonlinear NT|AP	nonlinear MT|AP	nonlinear HT|AP	
section area	A	0.1655	0.1655	0.1655	0.1655	m^2
yield sterngth	f_y	450	450	450	450	MPa
characteristic normal force capacity	N_{rk}	74462	74462	74462	74462	kN
design normal force in arch	N_{ed}	21008	20988	21012	21025	kN
critical load factor	a_{cr}	8.97	8.35	7.91	7.57	-
critical normal foce	N_{cr}	**188542**	**175201**	**166140**	**159111**	kN
relative slenderness	λ	0.628	0.652	0.669	0.684	-
buckling curve index	curve	b	b	b	b	-
imperfection factor	α	0.34	0.34	0.34	0.34	-
coefficient	ϕ	0.770	0.789	0.804	0.816	-
buckling coefficient	χ	0.823	0.810	0.801	0.793	-
safety factor	γ_{M1}	1.1	1.1	1.1	1.1	-
design buckling resistance	N_{brd}	**55679**	**54841**	**54199**	**53654**	kN
ratio of nonlinear to linear design buckling resistance	$N_{nl,brd}/N_{l,brd}$	**1.000**	**0.985**	**0.973**	**0.964**	-
ratio of FEM to formula solution	$N_{brd}/N_{formula,brd}$	**1.021**	**1.006**	**0.994**	**0.984**	-
ratio of nonlinear to linear critical force	$N_{nl,cr}/N_{l,cr}$	**1.000**	**0.929**	**0.881**	**0.844**	-
ratio of FEM to formula solution	$N_{cr}/N_{formula,cr}$	**1.104**	**1.026**	**0.973**	**0.932**	-

The results were prepared for other imperfection factors α in comparison to formula-based solution Eq. (4.3) [85] and presented in Fig. 4.19. The maximum divergence of the formula-based results from the nonlinear buckling results was up to about 2.5%, which was smaller than the divergence to the linear elastic bifurcation equal to maximum 3.3%. For the imperfection factor related to the "c" buckling curve, the low tension divergence was 0.6% and for high tension 2.0%. Surprisingly, the linear elastic bifurcation capacity provided overestimation in relevance to the formula-based solution by up to 3.3% for all cases and 2.5% for the imperfection factor related to the "c" buckling curve. The low and medium tension force results were almost symmetrical to the reference formula-based results.

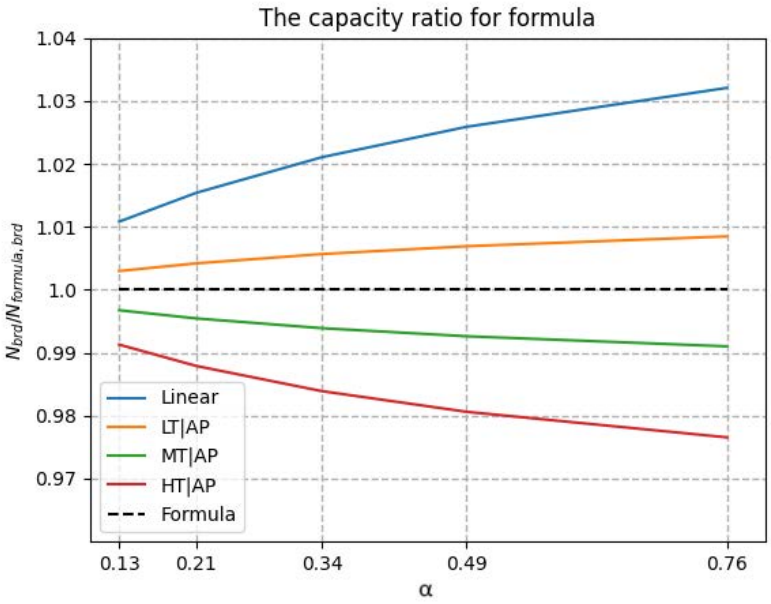

Figure 4.19 The ratio of normal force capacity obtained from nonlinear buckling analysis and linear elastic bifurcation analysis to that determined from the formula, as a function of imperfection factor

The formula-based solution was closer to the nonlinear buckling results than the linear elastic bifurcation results, which made it more accurate estimation in the preliminary design than LBA from the software.

In the article [85], the maximum divergence in critical buckling force was stated to be up to 6.6% in comparison to the LBA results. The obtained results for imperfection coefficient related with the "b" buckling curve showed the divergence up to 10.4% for linear elastic bifurcation on the safe side, which was significantly greater than stated in [85], Tab. 4.4. On the hand, the divergence to the nonlinear buckling was up to 6.8% on the unsafe side, which was much closer to the statement in [85], Tab. 4.4. From the capacity point of view for all imperfection factors, the difference was up to 3.3% for the linear elastic bifurcation results on the safe side and up to 2.5% for the nonlinear buckling results on the unsafe side, Fig. 4.19. The formula-based solution provided lower critical force and buckling resistance values than the LBA and was closer to the actual, nonlinear solutions.

It was worth to mention, that these divergence included only the effect of tension force in hangers. Others aspects were not included in this comparison. The FEM-based analysis had an advantage over the formula solution in providing the solution for any hangers' arrangement or geometry of the arch. Therefore, the suggested nonlinear buckling analysis provided good convergence to the analytic solution and expanded it usability to other aspects as varying tension

force in hangers, making it more universal in case of non-standard hangers' arrangements.

For the middle vehicle position, the linear elastic bifurcation form had deformations concentrated in the center part of the arch with amplitude declining to 0 in the point of 25% of span length, which resulted in lack of imperfection for around 50% of the arch's length, Fig. 4.20a. This was in contrary to the imperfection shape included in EN 1993-2, Annex D, for arches and arches with vertical hangers, where a single period sinusoidal imperfection shape covered the whole arch's length. In the nonlinear critical form, obtained after 50 pushes, the multiperiodic sinusoidal shape occurred along the whole arch's length and the amplitude looked the same for every wave, Fig. 4.20c. The multiperiodic shape matched the principles of critical force determination according to Shanack formula, Eq. (4.3). The form was slightly down even though the deformations from the pre-critical state were subtracted, Fig. 4.20b.

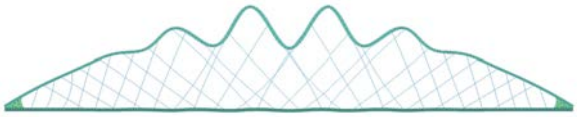

(a) Linear elastic bifurcation form [12]

(b) Nonlinear precritical buckling form [12]

(c) Nonlinear critical buckling form after 50 pushes reduced by deformations from the critical point [12]

Figure 4.20 Bridge deformations from (a) linear elastic bifurcation analysis, (b) critical point and (c) post-critical analysis after 50 pushes [12]

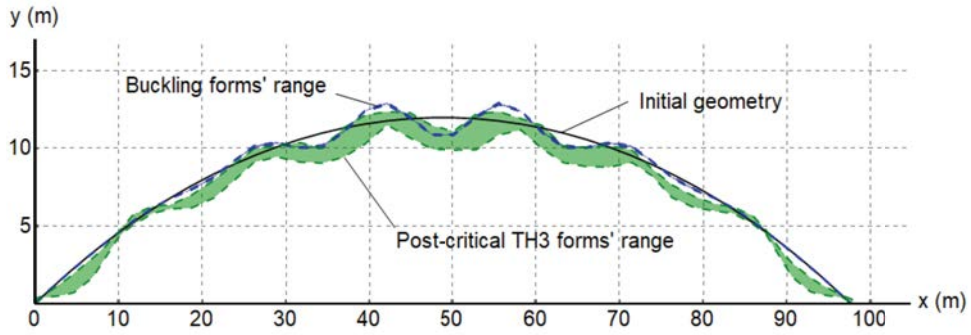

Figure 4.21 Shape spectra for linear and nonlinear buckling analysis from every vehicle position for arch between skewbacks [12]

The deformations of the arch between skewbacks from every vehicle position were presented in Fig. 4.21. The deformation from linear elastic bifurcation and nonlinear buckling analyses were scaled in regards to the extreme deformation value. The shape spectrum for LBA was very narrow and it might have been assumed, that the position of vehicle had not affected the shape of imperfection form scaled with the same factor for the visualization purposes. **On the other hand, the shape spectrum for nonlinear buckling analysis varied noticeably and the shape kept its multi-periodic sinusoidal trend, similar to the analytical formula, Eq. (4.3)-(4.5) [85]**. Both forms ranges had corresponding extreme values of the waves in the center part of the arch. The linear elastic bifurcation spectrum had a mean value in place of non-deformed arch, but the nonlinear buckling spectrum had noticeably lowered mean deformation in comparison to the non-deformed arch. This phenomenon looked similar to the bow

imperfection included in EN 1993-2 [134], Fig. 4.1a in row 1. This aspect was not present in linear elastic bifurcation form.

The geometrically nonlinear buckling analysis of the network arch bridge resulted in expected multi-periodic sinusoidal critical form of the arch, which matched the expectations from the Schanack's formula solution but conducted in FEA software. Since the geometrically nonlinear buckling analysis matched the expectations in tests Sec. 4.2 and in comparison to the Schanack's formula, it was considered enough, that **the nonlinear buckling analysis could be considered as an generalized extension to analytic formula**. **The geometrical nonlinear approach could enable a more accurate determination of the arch's capacity, accounting for custom hangers' arrangements and other factors not captured by the analytical formula.**

4.3.2 Elevation

In the next test, the arch's elevation impact on nonlinear-to-linear critical load factor ratio was investigated. The LBA was conducted to obtain α_{cr}, and TH3b analysis was conducted with ULTI procedure in SOFiSTiK until reaching the critical point. The process was repeated for every vehicle position. The ratio trend was presented in Fig. 4.22 for 0.12, 0.14, 0.15, 0.16 and 0.18 L elevation ratios. The pretension forces in hangers were not included. The difference for the most extreme elevations was 0.01 at maximum, which allowed to conclude low influence of the elevation for nonlinear-to-linear critical load factor ratio within reasonable range of arch rise values. The ratio took values between 0.89 for position 3 up to 0.95 for position 8. It resulted in 5-11% reduction of critical load factor due to geometrical nonlinearity. The maximum reduction occurred for the position 3, which was caused by the same reasons as in post-tension/pretension test. The shape spectra for both linear and nonlinear analyses were also comparable to those in Sec. 4.3.1, which meant, that **the nonlinear buckling analysis had more influence to the capacity reduction than the arch elevation change itself.**

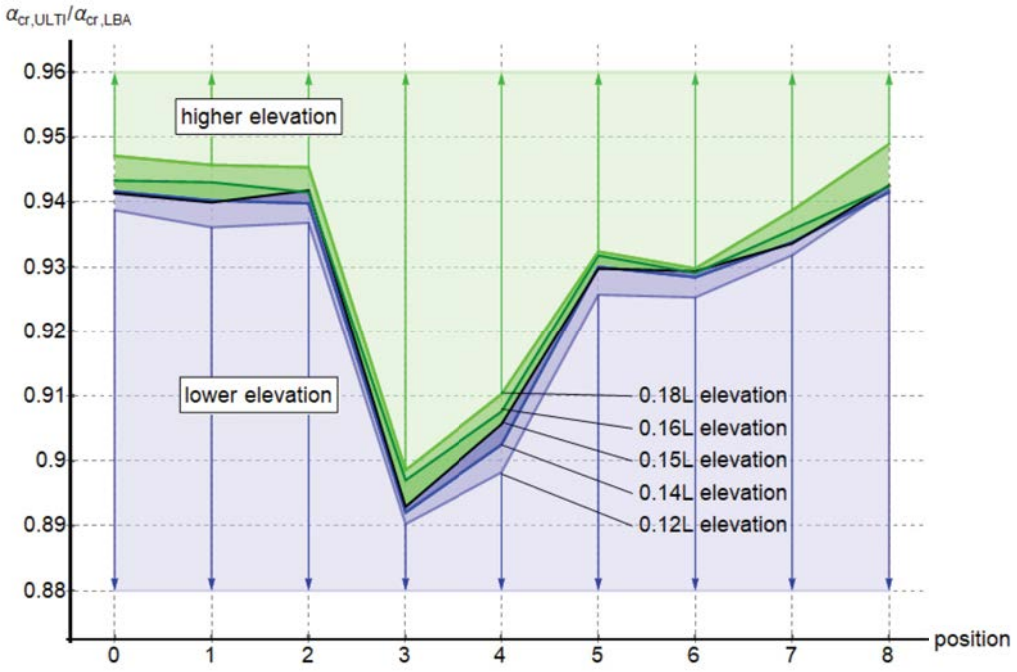

Figure 4.22 Nonlinear-to-linear critical load factor ratio graph in regard to elevation influence [12]

4.3.3 Single rapture

In this test, the affection of rapture of a single hanger on the nonlinear-to-linear critical load factor ratio was investigated. The task was divided into analysing left and right skewed hangers. The hangers were numbered starting from left to right, Fig. 4.23. As it used to be, the LBA and TH3b until reaching critical point analysis with ULTI procedure were considered. The vehicle moved from left to the center in 9 positions. The pretension forces in hangers were not included.

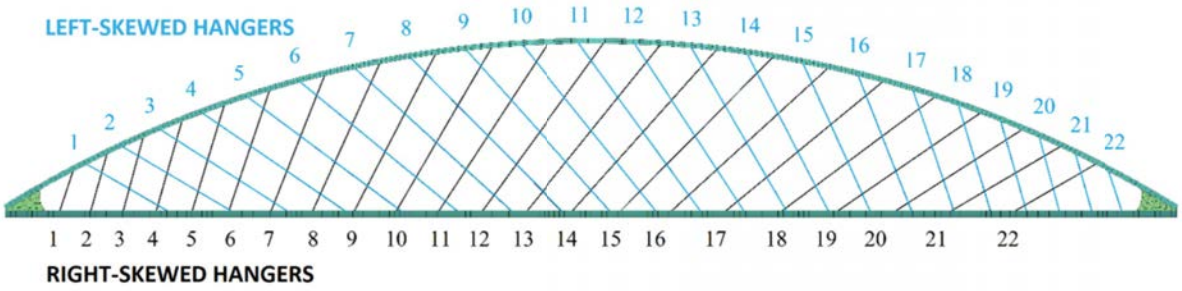

Figure 4.23 Numeration of hangers' rapture [12]

The ratio values differed between 0.6 and 0.9. The spectra shapes for left and right skewed hangers were symmetrical to each other in relevance to the center of the bridge. The left-skewed hangers had high value fluctuations from 0.6 to 0.9 for the first 5 rapture hangers and then stabilized in range between 0.7 to 0.825 for hangers rapture in 8 to 15 range. After that, value started to increase and reached value in 0.85 to 0.90 range. The opposite trend was observed in right skewed hangers. The highest value fluctuations corresponded with the vehicle position around the worst position for arch, which was about 20-25% of the span length. The fluctuation of the left skewed hanger in range of 1 to 5 hanger number were wider than the one for right skewed hangers in range of 18 to 22 hanger number. The reason of this phenomenon was the vehicle movement from left to the bridge center, which caused wider range of forces since the force was closer to the rapture hangers.

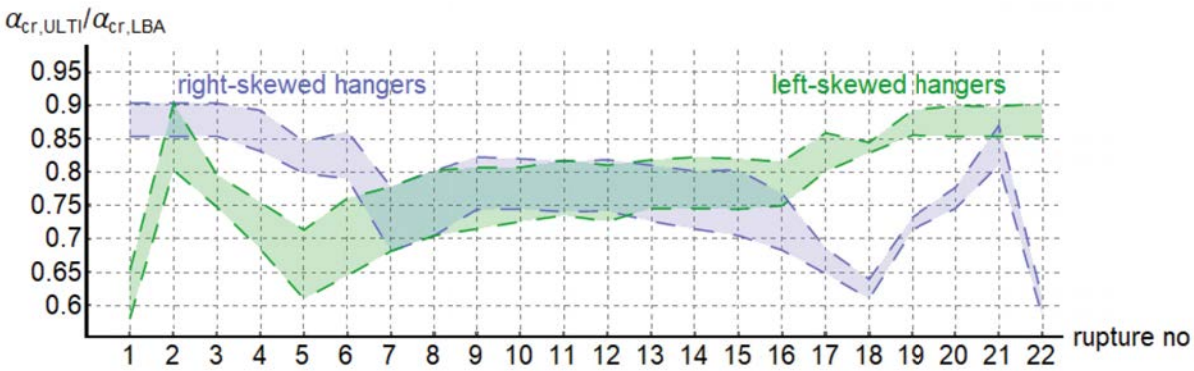

Figure 4.24 Nonlinear-to-linear critical load factor ratio spectra for every vehicle position and for both skewness directions [12]

The critical load factor was up to 40% lower from nonlinear buckling analysis than from the linear elastic bifurcation analysis. This difference was not negligible and showed sever overestimation of the arch's capacity in the accidental case. The analytic formula, Eq. (4.3)-(4.5) [85], would not be able to include this effect.

4.3.4 Double rapture

In the final test, the affection of rapture of a double hanger on the nonlinear-to-linear critical load factor ratio was investigated. The hangers were numbered starting from left to right, Fig. 4.25. The pairs of the two nearest hangers' anchorage points number on the tie were determined. The numbers in the bracket corresponded with the rapture hangers' anchorage point number on the arch. It resulted in 35 pairs. As it used to be, the LBA and TH3b until reaching critical point analysis with ULTI procedure were considered. The vehicle moved from left to the center in 9 positions. The rapture in the middle were marked as (14,8) rapture coordinates in Fig. 4.25 and Fig. 4.26 [12]. The pretension forces in hangers were not included.

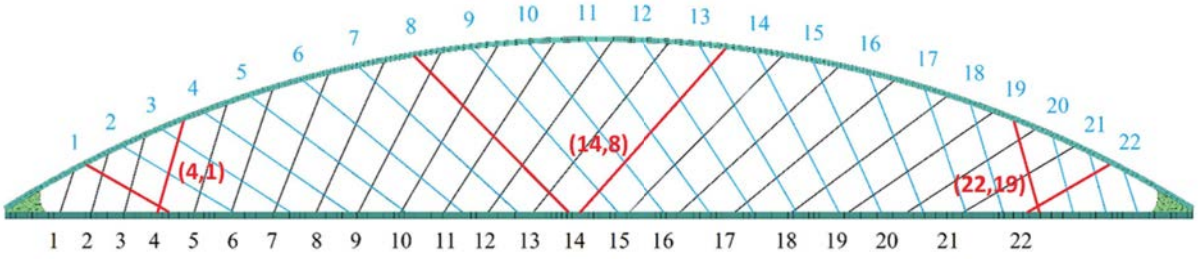

Figure 4.25 Numeration of hangers' rapture [12]

The ratio fluctuations occurred in the most extreme 7 hangers pairs within 0.725 to 0.90 range of values. Then it started stabilizing slowly changing values from 0.8 to 0.75 in average in the middle of span length. The average value of 0.75 in the middle of span length corresponded with the 0.75-0.80 range of values from the single rapture case also in the middle of the span length, Fig. 4.24. The range of fluctuated values was smaller in the double rapture case than in a single one. The ratio values got more narrow in the second half of the graph, since the vehicle moved until the center point and its influence on the right side hanger pairs was less concentrated than on the left side. Nevertheless, the graph remained symmetrical along the middle rapture pair.

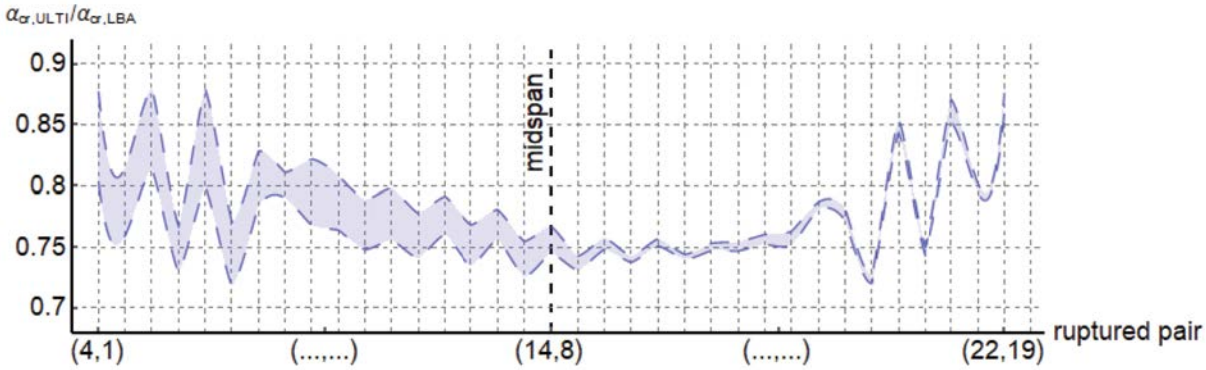

Figure 4.26 Nonlinear-to-linear critical load factor ratio spectra for every vehicle position and for both skewness directions [12]

The difference between nonlinear and linear critical load factor was up to 28%, which was much smaller than for a single rapture case. Nevertheless, this difference was not negligible and linear elastic bifurcation analysis severely overestimated the arch's capacity in this accidental case. The analytic formula, Eq. (4.3)-(4.5) [85], would not be able to include this effect.

4.3.5 Combined influence on the buckling coefficient

Author decided to compare the nonlinear critical buckling coefficients with the linear buckling coefficients including all the investigated influences. The buckling coefficient were determined assuming the same $\alpha_{ult,k}$ value in $\overline{\lambda}$ value determination according to Eq. (4.8) [132]. The imperfection factor α referred to b buckling curve, since it represented the considered cross section of HD 400 x 1299 and steel HISTAL S460. The reference χ values were determined for the slenderness in range of 0.20 to 1.00, black curve in Fig. 4.27a and 4.27b. Then the α_{cr} were modified to include the nonlinear effects and other investigated influences. Author modified the relative slenderness formula $\overline{\lambda}$ from Eq. (4.8) [132] that included the reductions due to geometrically nonlinear effects, which was presented in Eq. (4.11).

$$\overline{\lambda}(\alpha_{red}) = \sqrt{\frac{\alpha_{ult,k}}{\alpha_{red}\alpha_{cr,ip}}} = \overline{\lambda}_{ref}\sqrt{\frac{1}{\alpha_{red}}} \tag{4.11}$$

where $\overline{\lambda}_{ref}$ was the reference relative slenderness assumed from 0.20 to 1.00, α_{red} was the reduction coefficient of the linear critical load factor due to geometrically nonlinear effects and $\overline{\lambda}(\alpha_{red})$ was the applied relative slenderness during buckling coefficient χ determination. For the linear elastic bifurcation results, the α_{red} value was always equal to 1.00, since linear elastic bifurcation was not affected by geometrically nonlinear effects.

The first approach included the post-tension force, hangers' pretension and elevation impacts (STE) and the second included additionally the rapture of a hanger (STER), Fig. 4.27. The analysis was done for the worst and center vehicle position. The α_{cr} for the first approach included 0.825 reduction for the 3rd position from the post-tension/pretension impact and additional 0.99 reduction from the elevation influence, resulting in $\alpha_{cr,nonlinear} = 0.8168\alpha_{cr,linear}$. For this modified critical load factor, the buckling factor was determined, orange curves in Fig. 4.27a and 4.27b. The α_{cr} for the second approach additionally included the rapture impact of 0.60, but because the general impact of the nonlinear behaviour of hangers was already included in the post-tension/pretension influence, only the additional high tension in hangers had to be included. For the worst vehicle position in the low-pretension forces in hangers the reduction coefficient was 0.900, Fig. 4.17. Therefore, in order to exclude the nonlinear influence of the hanger's rapture results, the STE reduction coefficient was to be divided by 0.900, resulting finally in $\alpha_{cr,nonlinear} = 0.825/0.900 \cdot 0.99 \cdot 0.60\alpha_{cr,linear} = 0.5445\alpha_{cr,linear}$. For this modified critical load factor, the buckling factor was determined, green curves in Fig. 4.27a and 4.27b. The reference curve represented the critical load factor determined from the linear elastic bifurcation analysis, blue curves in Fig. 4.27a and 4.27b.

The greater the relative slenderness was, the greater the divergence of buckling factors values from the reference buckling factor curve was, Fig. 4.27c and 4.27d. More divergence was present for the worst vehicle position. In the state without accidental hangers rapture, so called normal case scenario, the reduction of buckling coefficient varied between about 10% for the highest considered slenderness of 1.0 and about 1.0% for the lowest considered slenderness of 0.20. Almost the same trend was present both in the worst and the middle position of the vehicle. According to author's experience, the relative slenderness in NAB laid in range from around 0.4 to 0.6, which corresponded with the nonlinear buckling coefficient reduction of about 2% to 4% comparing to the linear buckling coefficient. **These capacity reduction were considered not negligible and in-plane geometrically nonlinear analysis should be included in the analysis in order to prevent capacity overestimation of the arch.**

In the rapture case, the differences were much greater. For the worst vehicle position, the decrease of buckling coefficient ratio was almost 35% for the highest relative slenderness and

almost 2.5% for the lowest considered slenderness. For the middle position these reductions changed to 22.5% and 2.0% respectively. For the expected relative slenderness values between 0.4 and 0.6, the reductions were about 7-15% for the worst vehicle position and about 4-9% for the middle vehicle position. **These reductions were about 2 to 4 times greater than for the normal design case scenarios. These reductions showed the importance of including in-plane geometrically nonlinear analysis in the design of network arch bridges in order to not overestimate the capacity of the arch sections.**

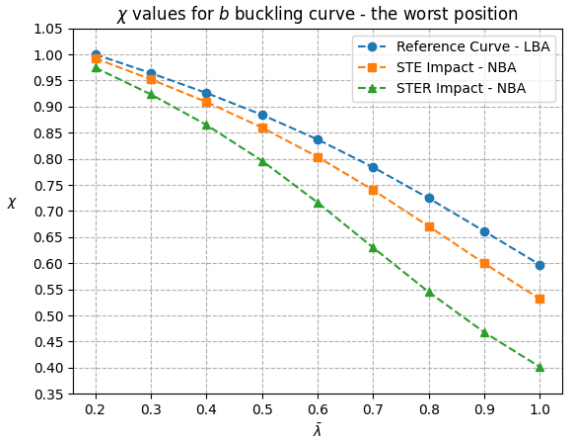

(a) Buckling coefficient curves for "b" imperfection factor as a function of relative slenderness for the worst-case vehicle position

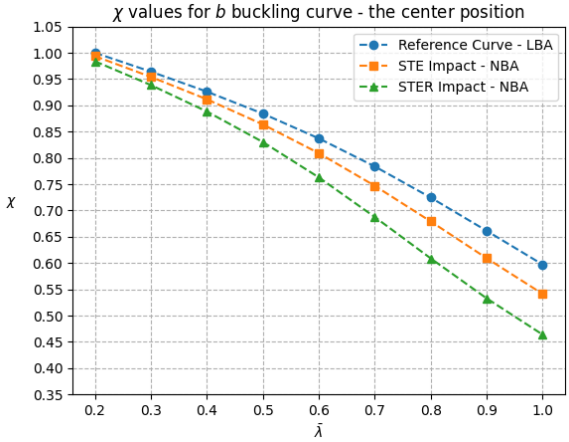

(b) Buckling coefficient curves for "b" imperfection factor as a function of relative slenderness for the center vehicle position

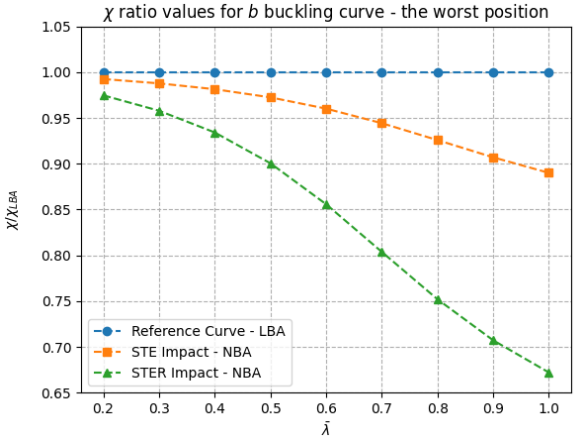

(c) Curves of the ratio between the nonlinear and linear buckling coefficients for "b" imperfection factor as a function of relative slenderness for the worst-case vehicle position

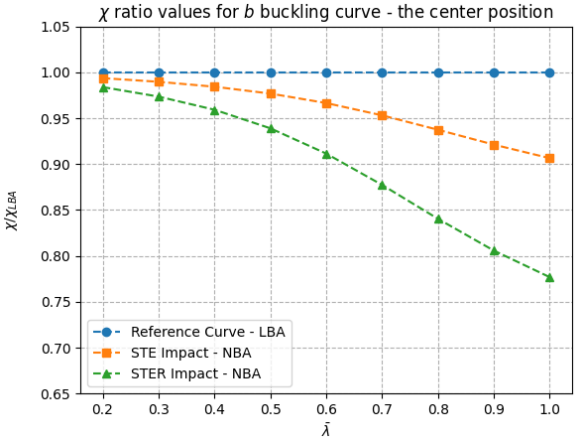

(d) Curves of the ratio between the nonlinear and linear buckling coefficients for "b" imperfection factor as a function of relative slenderness for the center vehicle position

Figure 4.27 The geometrically linear and nonlinear results of the buckling coefficient for "b" imperfection factor as a function of relative slenderness for (a, c) the worst-case and (b, d) center vehicle positions with (a, b) absolute values and (c, d) values related to the linear buckling coefficient

The same analysis was done for all 5 imperfection coefficients α and presented in Fig. 4.28a and Fig. 4.28b for both the worst and the middle positions respectively. The reference constant line with ratio value of 1 represented the results from the linear elastic bifurcation analysis, black lines in Fig. 4.28. The greatest divergence in value in STER scenario occurred for relative slenderness of about 0.6, where values spread between 0.80 and 0.92 for the worst vehicle

position and between 0.87 and 0.95 for the middle vehicle position, green curves in Fig. 4.28. It meant, that for the expected relative slenderness value between 0.4 and 0.6, the greatest the influence of the imperfection factor was in comparison of the nonlinear-to-linear buckling coefficient ratios. For the STE scenario, the divergence was almost the same for the worst and the middle vehicle positions and covered in total the range from about 0.94 to 0.98, orange curves in Fig. 4.28. Surprisingly, for relative slenderness of about 0.9, the reduction due to nonlinearity started to be worse for "a_0" buckling curve instead of "d" in STER scenario. This phenomenon did not happen in STE scenario and reaching this relative slenderness value was considered unlikely in network arch bridges.

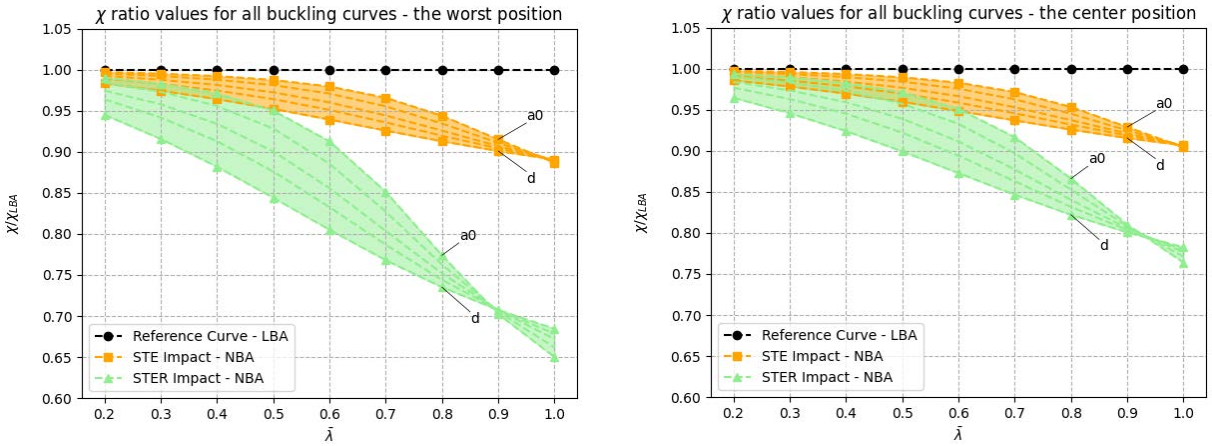

(a) Curves of the ratio between the nonlinear and linear buckling coefficients for all imperfection factors as a function of relative slenderness for the worst-case vehicle position

(b) Curves of the ratio between the nonlinear and linear buckling coefficients for all imperfection factors as a function of relative slenderness for the center vehicle position

Figure 4.28 The geometrically linear and nonlinear results of the buckling coefficient for all imperfection factors as a function of relative slenderness for (a) the worst-case and (b) the center vehicle positions with values related to the linear buckling coefficient

The conclusion regarding the impact of hangers geometrical behaviour was that the in-plane buckling coefficient should have been reduced in average by about 4% for normal state (STE) and 9-14% for hangers rapture state (STER). This reductions were not negligible from the design perspective. Considering negligible imperfection in the distance of 20-25% span length from the skewbacks in the linear elastic bifurcation form, which on the contrary was present in the nonlinear buckling form, Fig. 4.21 [12], this reduction might be even greater than presented, if the application of imperfection instead of simplified buckling coefficient method was utilized.

4.4 Conclusions

After investigation in this chapter, author concluded:

- The nonlinear buckling analysis resulted in multi-periodic sinusoidal critical form with similar value of the maximum amplitude distributed along the entire length of the arch, which matched the expectation based on the analytic formula for network arch bridges, Eq. (4.3)-(4.5) [85],
- The critical buckling form from nonlinear analysis included bow-like imperfection, which was not present in the linear elastic bifurcation form and was considered as an analogue of the bow imperfection from EN 1993-2 [134],
- The combined bow-like and sinusoidal imperfections were included simultaneously in the nonlinear buckling form,
- The analytical formula for network arch bridges matched the nonlinear critical load factor results between low and medium pretension forces,
- The nonlinear buckling analysis conducted in the considered commercial FEA software could be used with success for accurate buckling resistance determination as an extension of analytical formula to more general geometry definition of network arch bridges with custom hangers' arrangement,
- The influence on the nonlinear-to-linear critical load factor ratio of the arch elevation change was negligible within the reasonable range,
- The expected reduction of linear buckling coefficient due to influence of geometrical nonlinearity was about 4% for normal design scenario and about 9-14% for cable loss scenario for the reasonable range of arch relative slenderness and imperfection factor for rolled sections. For welded I-sections these values increased to 5% and 10-15% in average. These reductions were not negligible,
- The accidental case of cable loss resulted in sever difference of up to 40% between nonlinear and linear critical load factors, which was not negligible,
- The investigation showed the importance of conducting geometrically nonlinear analysis for the purposes of arches buckling resistance determination, since the linear elastic bifurcation results provided significant overestimation of arches capacity,
- The accurate capacity determination from the geometrical nonlinear analysis was considered crucial for the need of optimization algorithm, since the overestimated results from the linear elastic bifurcation analysis would lead to unrealistic solutions.

5 Optimization algorithm - 1st attempt

Originally, the one version of optimization algorithm was planned, but because of the issues that happened during this process, it was decided to start with a new algorithm from the beginning based on the experience from the approach number 1. It would have been more time-consuming to continue with the already existing script and adopt it to new approach and fix errors, than starting over again and fix the noticed problems. These issues were described in Sec. 5.3 as well as during the description in the Sec. 5.2. Nevertheless, author decided to present the first approach and took conclusions from that, which was helpful in developing new method based on the issues and disadvantages made in the first approach, as an integrated part of the development of the optimization algorithm. The description presented the intended pipeline, but all the steps were not utilized completely.

5.1 Description

5.1.1 Software

The calculations of the bridge were conducted in SOFiSTiK FEA software. Software provided internal forces, displacements and buckling factors. The geometry definition, data procedure and genetic optimization were conducted in Grasshopper (GH) by graphical script, internal ironPython script, SOFiSTiK input language script and SOFiSTiK computed database (CDB) language script. The evolutionary structural optimization (ESO), control of the optimization process and data migration were defined in the external Python script. Finally, the interpolation process was supposed to be defined by external Python script.

The SOFiSTiK software was chosen as a popular design tool in the bridge industry, widely used in Europe. The software allowed to code the entire design task, including material and sections, geometry, load cases and analysis definitions. Moreover, there were two ways of exporting results from the computed database. The first was written in the same code as the design task definition, in SOFiSTiK input language with SOFiSTiK CDB language script prompt. The second was a direct reference by application programming interface (API) in popular programming languages, for instance Python, C++, C#. That potentially provided the possibility of adoption to other languages depending on the user's preferences.

The RhinoCeros with Grasshopper extension was used as a popular parametric tool in geometry definition and data manipulation. It allowed programming in ironPython, exporting and importing data to and from external files, analysing the geometry and creating it parametrically, visualizing the results. Furthermore, SOFiSTiK and other engineering software offered extensions for GH that provided the direct export of data to the related software. The mix of different software was available within the same script. In case of using software other than presented, the user could replace the export definition with the desired software components if available. The library of components for other users was also available.

The Python coding language was chosen, because of its current popularity, easiness to start, great optimization tools spectra and one of the supported languages with access to SOFiSTiK CDB by API. Python 3 was applied as a more advanced version than Python 2, making it more universal in the future.

5.1.2 Geometry

The initial geometry of the bridge was based on the Cracow's NAB presented in Sec. 4. The bridge analytical model was defined in GH with an export to SOFiSTiK, where all calculations were proceeded. The model was done in 3D, Fig. 5.1.

a) The side view

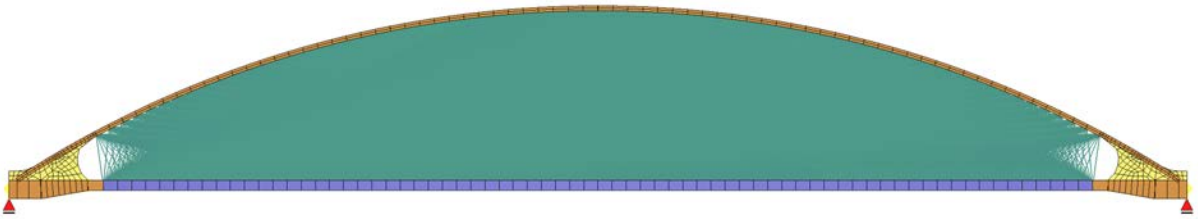

b) The front view

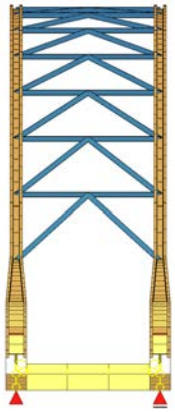

c) The top view

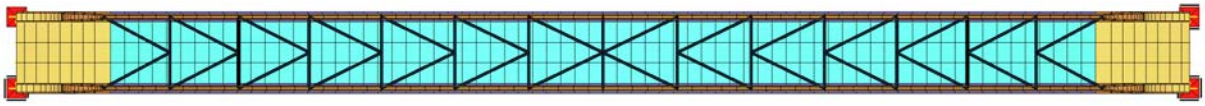

d) The perspective view of the support zone

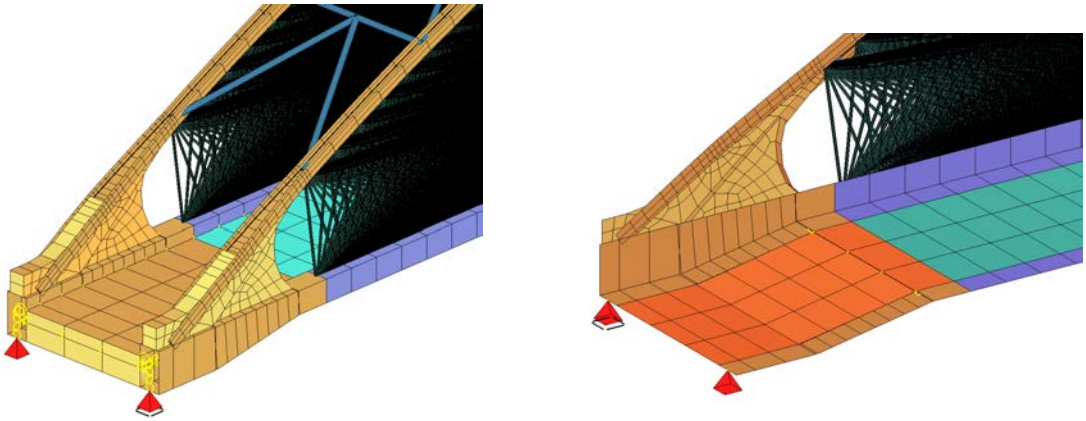

Figure 5.1 The model in the initial stage of the algorithm. The side view, the front view, the top view and the detail views on the support regions respectively.

The cross section of the steel arch was assumed as HD 400 x 1299 for the start, Fig. 5.2, Fig. 5.3 and Fig. 5.1. The cross section was rotated in the way where flanges were oriented vertically. The cross section remained constant after the first 8.5 m distance from the support point. Then changed linearly between 4.5 m and 8.5 m distance from standard HD profile to the modified one. The modified cross section was based on the HD profile, where the two halves were cut in the middle of the web's height and then separated, which resulted in total height increase. The section started to be composite in this zone. The volume underneath the web and between the cut was filled with concrete resulting in the composite cross section. After reaching maximum separation, the cross section remained constant. Additionally, the volume between arch and tie was finished with concrete in smooth radial shape in the support zone, so called support stiffener. This filling started when the linear cross section interpolation began. The purpose of the concrete filling was to increase buckling resistance of the steel arch at the end zones of the bridge. Because of the traffic limitation and height of the portal frame, the support parts were vulnerable to the out-of-plane buckling.

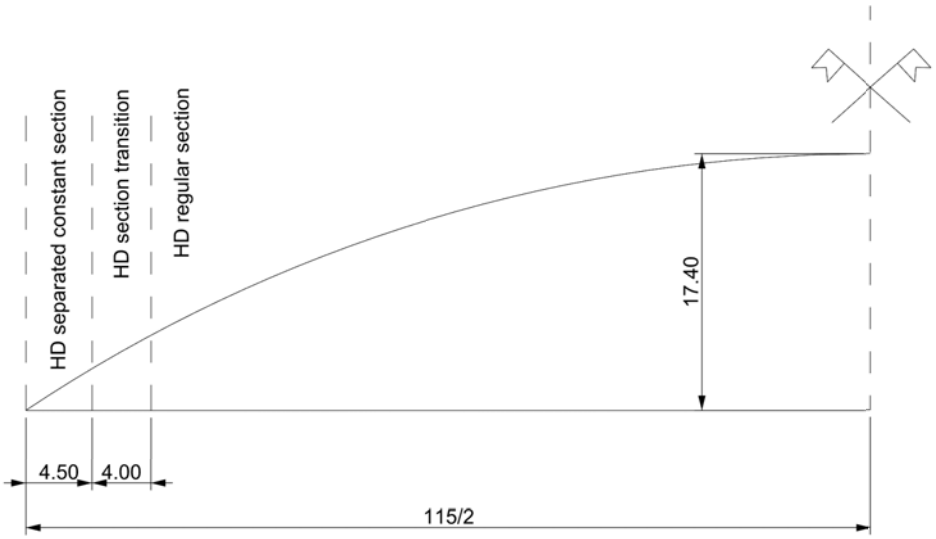

Figure 5.2 The arch HD section transition description

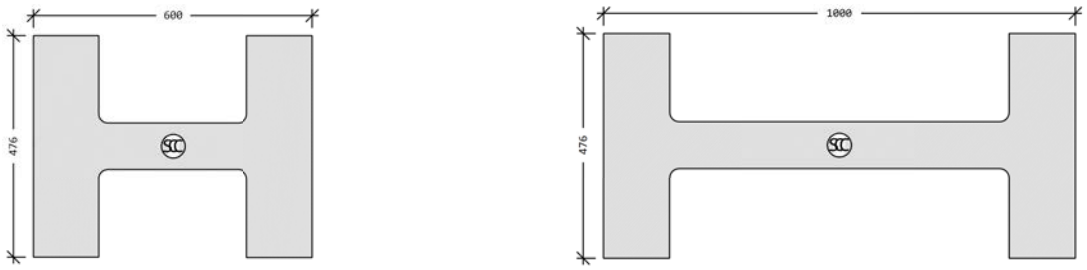

(a) The middle part

(b) The support part

Figure 5.3 The HD sections of the arch

The deck was modelled by both beam and shell (quad) elements made of reinforced concrete, Fig. 5.4, Fig. 5.5 and Fig. 5.1. The shell elements had constant thickness of 0.500 m starting from 7.7 m distance from the supports toward the center. Then the shell elements changed the thickness from 0.500 m to 1.300 m in a distance from the support between 3.1 m to 7.7 m and for the last 3.1 m remained its 1.3 m thickness. The shell elements in the thickest part

and in the transition-zone were defined as two elements in the same plane. It allowed to define the hole shell-based deck on the same plane along the entire bridge's length. The shell elements in the middle part were offset with alignment to the bottom edge. Tendons were not modelled in shell elements. The side part of the deck was modelled as rectangular beam elements. All post tension force was defined symmetrically in beam elements. The side beams were 1.0 m by 1.0 m rectangular sections and their placement resulted in being 0.500 m above the top edge of the shell elements. At the supports, the section got higher as the plate got thicker and the section had 1.8 m by 1.0 m dimensions.

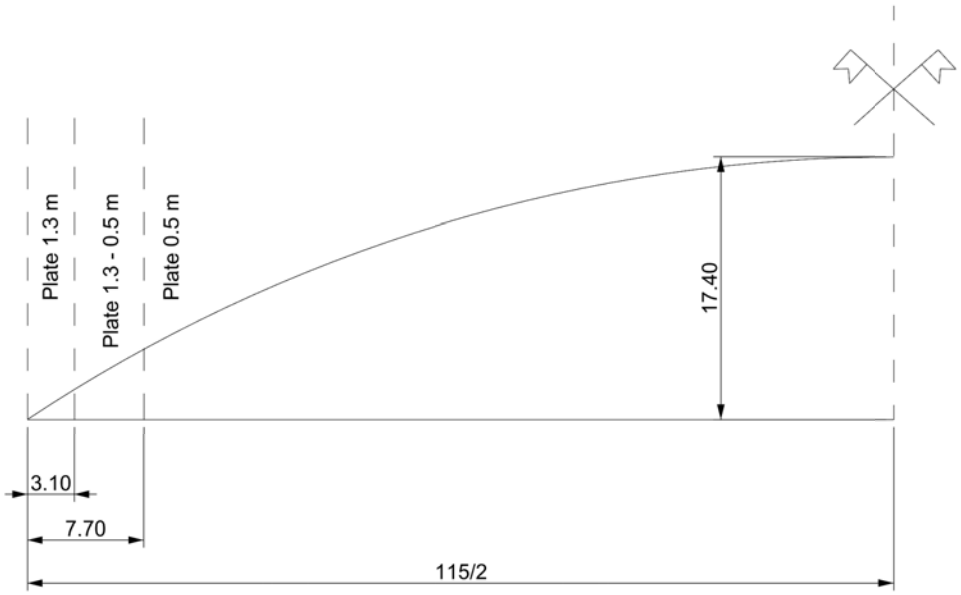

Figure 5.4 The tie plate section transition description

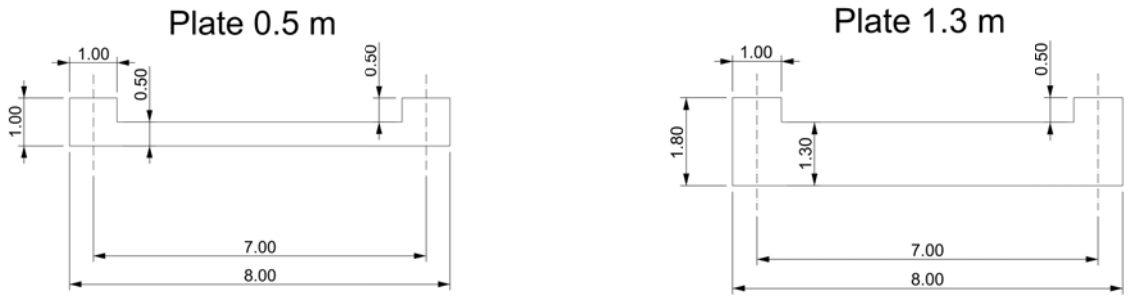

(a) The middle part

(b) The support part

Figure 5.5 The deck sections of the tie

The hangers were modelled as steel solid circular section of 100 mm in diameter, Fig. 5.1 and Fig. 5.8. The arch and the tie were divided into seventy-one points each. Every point from the arch was connected with every point from the tie by hangers. The spacing between points was even. The example of the connections from point No. 0, 17 and 35 was presented in Fig. 5.6. The detail example of the hangers' anchorages to the arch and the tie was presented in Fig. 5.7. The hangers were distributed within the arch's regular HD section length. The hangers were modelled as cable elements, so they only carried normal tension forces when a geometrically nonlinear analysis was used, and the sagging effect was then included as well. In case of geometrically linear analysis, the cables acted in both tension and compression.

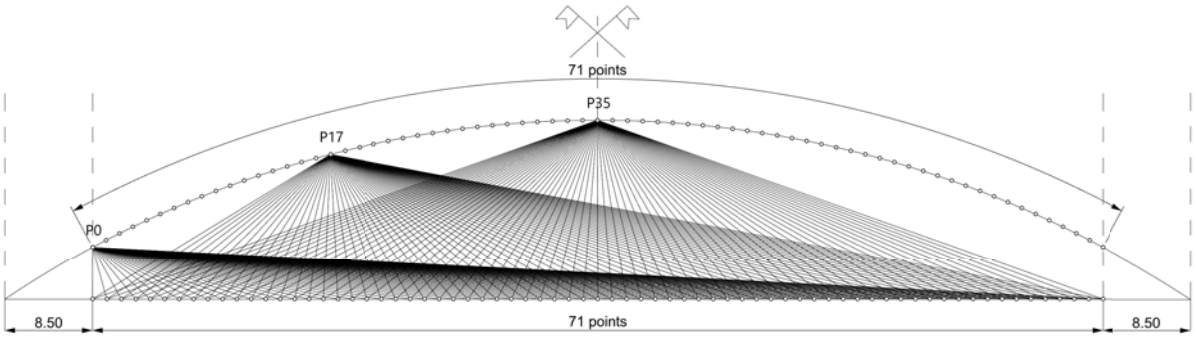

Figure 5.6 The hangers initial arrangement description

a) The detail example of hangers anchorage on the arch

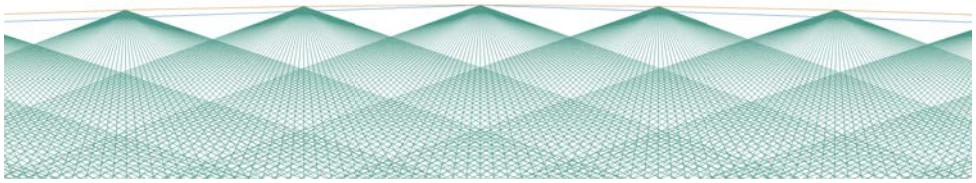

b) The detail example of hangers anchorage on the tie

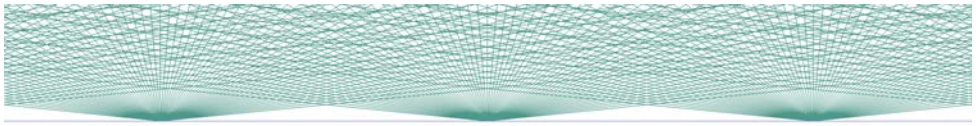

Figure 5.7 The hangers initial arrangement detail description

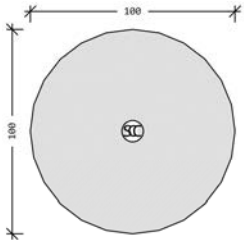

Figure 5.8 The hangers cross section

The wind bracing was modelled as steel hollow circular cross sections with the outer diameter of 260 mm and wall thickness of 40 mm, Fig. 5.10. The spacing between bracings was even and equal to five times the spacing of the hangers' anchorage points along the arch, Fig. 5.9. The bracing's topology remained the same along the arch and was made in the K-type system, which proved to provide the greatest out-of-plane critical load factor [35]. Diagonal and horizontal bracing's cross sections were considered separately. Connections between bracing and steel arch as well as the connections within bracing were fixed. The bracing was described within the arch's regular HD section length.

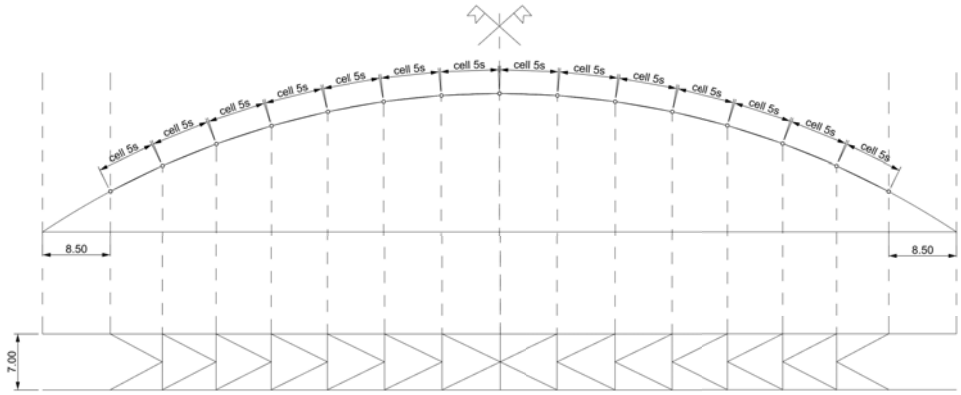

Figure 5.9 The bracing cell arrangement, where *s* means spacing between hangers arch anchorage

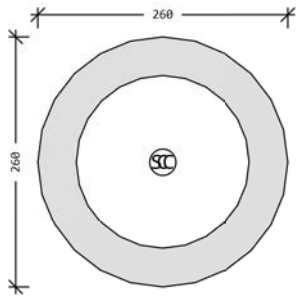

Figure 5.10 The bracing cross section

There were no overlapping elements in the model to avoid doubling of the stiffness. That was why:

- The bracing started at steel arch cross section inner flange's edge and were connected to the arch by fully fixed kinematic constraints. The same came to the tie side beams,
- The side concrete beam center was connected to the deck shell elements' edge by fully fixed kinematic constraints,
- The concrete ends above the tie were connected to the edge beams by fully fixed kinematic constraints,
- The supports were modelled at the bottom edge of the support beam,
- The skewbacks' vertical shell elements were connected from the side beams' top edge to the center line of them.

All the finite elements, except concrete filling between steel arches and concrete tie's edge beams, were meshed parametrically to keep control of the quality of meshing and to make results more comparable and repeatable. Moreover, it was useful for controlling the number of finite elements in the system, which had an impact on calculation time.

5.1.3 Loads

In the analysis, self-weight was automatically included in the calculations. The tie's post-tension force and the equipment loads remained the same in the optimization process. The

traffic load was a variable moving load along the bridge. The pretension force in the hangers was optional and varied in the optimization process including lack of pretension force in hangers.

In order to make the design more general and unrelated to the national Annex across Eurocodes, the design was mainly focused on permanent and the traffic loads. The other variable loads, including wind and thermal actions, depended on the location, so the same solution might not be applicable or non-optimal in other locations within European countries. Because of that, the thermal load was not considered in the analysis. Furthermore, the static schema was the freely supported beam and temperature would have a negligible effect on the structure. The wind load was omitted, since the dominant load was the traffic load and literature also used to focus mainly on the variable traffic loads in the optimization process [6, 7, 13, 93, 94, 97, 75].

The traffic load was based on load model LM1 defined in EN 1991-2 [131]. The uniformly distributed load (UDL) was applied on the total span length. For simplification, the maximum value of 9.0 kPa was applied on all the lanes, even if the accessible bridge width for traffic was 7.0 m. The weight of equipment, asphalt and other additional covers were set to 3.0 kPa and included as a part of the UDL, resulting in 12.0 kPa in total, Fig. B.1a in Annex B. The tandem load (TS) was distributed evenly at the width of the bridge as load from the contour of the vehicle distributed evenly on the vehicle contour, resulting in 600 kN / (3.0 m x 2.2 m) = 90.9 kPa. Consequently, the heaviest tandem load was applied on all the lanes regardless of the bridge width, which was an assumption on the safe side. Only vertical component was considered, no horizontal forces from the traffic loads. The load was considered as moving load along the entire length of the bridge, Fig. B.1b-d in Annex B. The number of positions depended on the conducted optimization step.

The pretension force in the hangers was set to be initially maximum of 300 kN and proportional to the hanger's length since the stiffness of the hanger $K_{cable,eff}$ is proportional to the inverse of the length, Eq. (5.10).

After consultation with the engineers involved in the network arch bridges project, the decision was made of not including the post-tension force of the tie in the analysis. The tie had been post-tensioned before the arch was fully constructed, which meant that the arch did not experience the effect of the applied force in the final stage. It was only applicable to the tie, which had an impact on the internal force in the tie and the curvature caused by the applied force. The assumption in the calculations was that the tie was completely flat when opened and the cross section of the tie was sufficient enough. The post-tension force could have been included if the construction stage modelling process (CSMP) was used in the calculations, but it would require more calculation time. Since the optimization algorithm was already time consuming, the decision of not including the post-tension force in the design was made.

Post-tension force also required to be changed according to the hangers' topology. If the hangers' topology was sparser in one and denser in another part of the bridge, the cables position in the concrete cross sections would need to be adopted in order to compensate for the change of the bending moments along the tie. This would have been another complex consequence of including post-tension force in the tie and would elongate the time consumption of the optimization algorithm due to influence on the hangers' internal forces. Therefore, the cross section of the tie was not a variable part of the optimization process, but assumed constant within considered optimization process. Similar approach was found in [2, 40].

5.1.4 Design and combinations

The design criteria were limited to ultimate limit state (ULS) and serviceability limit state (SLS). The fatigue limit state (FLS) was not considered since the fatigue resistance of steel may

increase in the future by, for instance, structural rearrangement of steel crystals [53] or thermal treatment [50]. Furthermore, fatigue used to be significant in railway bridges, not road bridges. The fatigue design category depends on the shaping of connections and the method of welding. Also, according to national Annexes, the safety factors may differ a lot. For instance, the default maximum safety factor according to basic EN 1993-1-9 [133] is γ_{Mf}=1.35, whereas according to the Norwegian Annex, it is γ_{Mf}=2.00. This difference is significant. Moreover, one of the latest NAB in Trondheim (Norway), the Hangar bridge, was the first network arch bridge made of aluminium, which has much lower fatigue design category than steel [38] and proved, that the fatigue resistance could be achieved high enough even with much lower fatigue design category and higher safety factors. Considering all these aspects, it was found reasonable to simplify the design principles and did not include the FLS in the analysis.

In general, the ULS criteria included in-plane geometrically nonlinear buckling analysis, in-plane imperfections according to EN 1993-1-1 [132], clause 5.3.2(11), determined by UGLI procedure from SOFiSTiK and out-of-plane LBA. For the design purposes of steel part, the general method (GM) for lateral and lateral torsional buckling of structural components was used according to EN 1993-1-1 [132], clause 6.3.4, described by:

$$\frac{\chi_{op}\alpha_{ult,ip,k}}{\gamma_{M1}} \geq 1.0 \tag{5.1}$$

$$\alpha_{ult,ip,k} = \frac{f_{yk}}{|\sigma_{ip,Ed}|_{max}} \tag{5.2}$$

$$\chi_{op} = \min\left(\chi_{L,op}, \chi_{LT}, \chi_{T}\right) \tag{5.3}$$

To determine χ_{op}, the LBA was conducted but only the out-of-plane form was considered, which meant lateral out-of-plane buckling form $\chi_{L,op}$, out-of-plane lateral-torsional buckling form χ_{LT} and torsional buckling form χ_{T} were searched for, Eq. (5.3).

Since the algorithm took the first critical load factor from the linear elastic bifurcation analysis and there was no guaranty of obtaining the first buckling form as out-of-plane form, the solution was found, which required calculations of in-plane and out-of-plane LBA. To make sure that the first form in the in-plane bifurcation analysis was oriented in the plane of the arch, the springs were added to the arch preventing movement in out-of-plane direction. This support was not considered in the LBA's primary loadcase (PLC) to get correct force distribution in the arch and not get any forces in the temporary supporting spring elements. These spring elements were only added during LBA. In the second approach, the springs were removed from the system, resulting in a loss of restraint against out-of-plane buckling. The first form in terms of critical load factor, which was different from the forms in the in-plane buckling analysis, was considered as the first out-of-plane buckling form.

In the papers [35, 4], the out-of-plane geometrically nonlinear buckling analysis led to lower critical load factors than the linear elastic bifurcation analysis. Authors in [35, 4] also stated, that the great influence to this difference was the portal frame size and stiffness, bracing system stiffness, hangers' arrangement, out-of-plane moment of inertia of the arch ribs and inclination of the arches. The presented approach of determination of the out-of-plane critical load factor was not applicable for geometrical nonlinearity. Alternatively, the arch's movement in-plane direction could be restricted during buckling analysis by adding perpendicularly defined spring supports in-plane of the arch for each arch's node. This support would not be considered in the

primary loadcase (PLC) to get correct force distribution in the arch and not get any forces in the temporary supporting spring elements. These spring elements would be only added during LBA. However, the alternative approach would not be applicable nonlinearly either. The reason was that using in-plane springs to prevent in-plane buckling and enforce only out-of-plane deformation would cause forces to develop in the artificially added spring elements during the iterative load increase process of a nonlinear buckling analysis from ULTI procedure. This, in turn, would lead to a divergence from the correct results. Author was unable to develop method, that would solve this issue in the optimization process, where any hangers' arrangement could occur. Therefore, the simplified approach of LBA for the sake of out-of-plane critical load factor was kept in the optimization process with author's will to solve this issue as a continuation of this dissertation. Nevertheless, in order to provide the greatest possible critical load factor in out-of-plane buckling, the stiff skewbacks and K-type bracing system were utilized, according to conclusions from [35, 4].

When it comes to $\alpha_{ult,ip,k}$, the in-plane imperfection had to be considered. Since the rules for arch bridges in EN 1993-2 [134] were only defined for arches with vertical hangers, the more general method, so called UGLI according to EN 1993-1-1 [132], was used, described by:

$$\eta_{init} = e_0 \frac{N_{cr,ip}}{EI \left|\eta''_{cr,ip}\right|_{max}} \eta_{cr,ip} = k_{cr} \eta_{cr,ip} \tag{5.4}$$

$$e_0 = \alpha \left(\overline{\lambda}_{ip} - 0.2\right) \frac{M_{Rk}}{N_{Rk}} \cdot \frac{1 - \chi_{ip} \overline{\lambda}_{ip}^2 / \gamma_{M1}}{1 - \chi_{ip} \overline{\lambda}_{ip}^2} \tag{5.5}$$

$$\overline{\lambda}_{ip} = \sqrt{\frac{\alpha_{ult,s,k}}{\alpha_{cr,ip}}} \tag{5.6}$$

The critical in-plane form $\eta_{cr,ip}$ was obtained considering geometrical nonlinear behaviour of hangers. To achieve that, firstly the analysis was conducted with ULTI method in SOFiSTiK for 3^{rd} order theory (TH3). The method allowed to reach critical point. The load multiplication factor at this point was represented by a nonlinear critical buckling factor $\alpha_{cr,ip}$. Secondly, a post-critical analysis was conducted by PUSH method in SOFiSTiK with TH3. The number of post-critical steps was set to 20 and was arbitrary. The results from the last PUSH step were reduced by the results from the critical point achieved at the end of ULTI procedure. As a result, the nonlinear buckling results were obtained, including deformations, rotations and bending moments in the arch. To reduce the numerical error in determining the maximum second derivative of the displacement graph $\left|\eta''_{cr,ip}\right|_{max}$, the first derivative of the rotation graph could be chosen. However, the best option would be direct import of the critical bending moment M_{cr}, which directly expresses the denominator in the Eq. (5.4), the $EI \left|\eta''_{cr,ip}\right|_{max}$. This would neglect the interpolation errors from the two previously proposed approaches. The approach of directly taking M_{cr} from the obtained results was adopted at the end. The representative cross section was the one with the greatest critical bending moment. Since the normal force in the arch is almost uniform along the arch and the bending moments have major influence on the varying utilization of the arch along its length, it was acceptable to consider the maximum critical bending moment as a simplification.

The minimum force amplifier to reach characteristic yield strength of steel in non-imperfect state $\alpha_{ult,s,k}$ was determined based on the normal stresses caused by axial force for the most

critical cross section. That allowed to determine λ_{ip}, χ_{ip}, N_{Rk}, M_{Rk}, e_0 and as a result k_{cr}, except the imperfection factor α since it was depended by the cross section properties. After obtaining the scaling factor of the critical form k_{cr}, the critical form was scaled resulting in the initial imperfection form η_{init}. The calculations were conducted once again with TH3 but this time for the imperfect geometry.

The minimum stresses amplifier $\alpha_{ult,ip,k}$ was determined as a ratio of characteristic yield strength f_{yk} and the resultant stress $|\sigma_{ip,Ed}|_{max}$, so called von Mises stresses, for already imperfect in-plane geometry of the arches, Eq. (5.2), which differentiated it from $\alpha_{ult,s,k}$, which is a *simplified* version without imperfection and was based on the normal force amplification. Since the elements were designed in the elastic range and 4^{th} was prevented, the simplification of stresses ratio was acceptable. Safety coefficient γ_{M1} was always set to 1.1 as default value for bridges.

The tie remained unaffected by imperfections and kept its original geometry. The same came to hangers. The results from the elements located at the very ends of the bridge, where the support stiffeners began, were excluded from the analysis to avoid the influence of local stress peaks. These regions could be shaped more freely than the rest of the bridge, so any necessary local strengthening could be implemented at minimal cost compared to modifying other parts of the structure. Such modifications would not impact on the overall design or global performance of the bridge. The assumption was that the skewbacks were shaped in such a way that they did not cause higher utilization of the arch and tie within their region compared to the areas outside the skewbacks. Simultaneously, the perpendicular post tension force in the shell elements was not modeled in these regions.

The default design rules in EN 1990 [130] were used to make the solutions as universal as possible, as described in Sec. 5.1.3. The default material coefficient for steel in bridges were used according to EN 1993-2 [134], clause 6.1.

The load coefficients γ in ULS and SLS were the same and equal to 1.0, for simplification. In order to consider the variable deflection component of the combined loads, the deflection from the self-weight load case was subtracted from the combinations' loadcases. It was needed because of the geometrical nonlinear analysis. The maximum tie's deflection was the only considered SLS design criterion. The ULS design was limited to the aforementioned general method with prevention of 4^{th} in the section of the arch. The bracings system and concrete elements were not optimized in the process. The local checks of hangers' anchorages, bracings connections and bearings support zones were not considered. The localized design criteria were considered solvable with low affection to the global costs.

5.1.5 Custom components

SOFiSTiK provided components in GH allowed to define geometry and line load. For the time of preparation of this dissertation, these components did not allow to define post-tension force load in tie, pretension force in hangers, all needed types of analysis, data export and data import and results visualization. Therefore, **the needed import and export components had to be scripted by author**. Load and analysis definitions were scripted inside GH by SOFiSTiK input language. Data import and export were scripted inside GH by SOFiSTiK CDB language. Results visualization was defined in GH using output from import/export components. The components visualizations and their detailed explanations were included in the Annex B, Fig. B.2. Author also presented the components in two videos [141, 140].

5.1.6 Parameters

The parameters of the optimization task were divided into constant and variable. The constants were unchangeable, Tab. 5.2, and the variables were changeable in the optimization process, Tab. 5.1. The optimization algorithm was responsible for providing the most optimal solution in terms of cost minimization for a given constant boundary condition by changing the variables. The process was repeated for other sets of constants. The obtained discrete database of optimal solutions was supposed to be interpolated in order to transform the discrete solutions domain into continuous.

For the steel grades between S235 and S355 and between S355 and S460, the prices were interpolated linearly. The relevant steel price was 18,000 PLN/ton for steel S355 and prices of S235 and S460 were respectively smaller and greater by 2500 PLN/ton. The price of steel S355 was based on the price catalogue in Poland [144] including labour and transportation costs and author's experience from the Norwegian market. The prices for steel S235 and S460 were assumed according to authors experience.

It was worth to mention, that the price of structural steel S355 varied a lot during the preparation of this PhD, starting from 10,700 PLN/ton in 2020 and ending with 19,800 PLN/ton at the end of 2024 [144]. The assembly cost per hanger's side was assumed from author's experience, which included pretension of hangers, but transport and other assembly costs were already included in the steel price.

Table 5.1 Variables in the optimization algorithm

	Variables	Range
Bridge	height	0.14-0.20*L*
Arch	steel grade	S235 - S460
	cross section	HD type
Hangers	diameter [mm]	30-100
	pretension force [kN]	0-300
	steel grade	S235 - S460
	quantity	10-100
	position on the arch	middle part
	position on the tie	middle part

Table 5.2 Constants in the optimization algorithm

	Constants	Range
Bridge	span length *L* [m]	100-250
	curvature type	circular
	width axially [m]	7-13
Tie	section height [m]	0.5-1.5
	concrete class	C50/60
Load	number of positions	21
	type of variable load	LM1
	values [kN/kPa]	600/12
Design	criteria	ULS & SLS
	analysis	GNA & GNIA
Cost	steel price [PLN/ton]	S235 - 15,500 S355 - 18,000 S460 - 20,500
	hangers assembly [PLN/hanger/side]	5000

5.1.7 Goal function

The goal function GF contained two aspects, cost C, utilization level η and punishment component p, expressed by Eq. (5.7):

$$\min_{v} GF(cv, v, \eta, p) = \begin{cases} C(cv, v) & \text{if } \eta \leq 1.0 \\ C(cv, v) + \eta \cdot p & \text{if } \eta > 1.0 \end{cases} \tag{5.7}$$

where *C* was the total cost expressed in PLN, η was the maximum utilization, *cv* were the constant values from Tab. 5.2, *v* were the variable values from Tab. 5.1 and *p* was a punishment component set to 10^8 PLN.

The goal function aims to minimize its cost value by changing variable values. The cost C included both the cost of material of steel elements and the assembly and transportation costs, according to Tab. 5.2. The cost of material was calculated considering weight of the steel elements and their price per ton. Each hanger had additional assembly cost included in *C* value, according to Tab. 5.2. The goal function based on cost was considered more general than approaches based on mass minimization [7], volume minimization [13] or internal forces minimization objective functions [93] presented in literature. The reason was, that it allowed to include changing material properties during the optimization process and impact of this property change was reflected by the cost of material and affected the goal function. Reducing restraints in the optimization process was considered positive and allowed to investigate more possibilities [8]. **Adding changing material as a variable parameter in the optimization process was considered as restraints, reducing factor not present in the optimization of network arch bridges from literature**. The addition of assembly cost value for each hanger was intended to avoid the situation, where algorithm would consider two structures with the same mass but with various numbers of hangers equally optimal in terms of cost minimization. **For the same total mass, it was preferable to have less hangers with greater diameter rather than more hangers with smaller diameter due to difference in the amount of installations, as it was presented in Fig. 3.37 [6]. Based the objective function on the costs and adding hangers' assembly cost should solve this problem and favour more practical and cheaper solutions without any restriction to the diameter or number of hangers in the optimization process, which was unique in the optimization of network arch bridge**. Author found several articles [2, 40] that used cost as a part of goal function in the optimization of network arch bridges, but the material properties did not change in the optimization process, which made this parameter constant. **The proposed changing material properties during the optimization process of network arch bridges was a unique part of this thesis according to author's best knowledge.**

This formulation of the goal function was present in the article [52], where tied-arch bridges with vertical hangers were optimized. The goal function was restricted to not exceed the capacity of the structure. The intention behind the added to cost C punishment of $\eta \cdot p$ was to provide a punishment component in case of exceeding capacity. The value was set high enough to overcome the potential cost range of the bridge under 100% of utilization. This value was a strong signal for the optimization algorithm to avoid development of the solutions above the capacity of the structure. Therefore, this value could be greater than suggested, since it would provide the same effect. At the same time, the utilization η was used as a factor for the additional price step value of *p* in order to gratitude the structures above their capacity with lower punishment value and guide algorithm to be more likely to remove more utilized bridges than less utilized. The lower the cost of the structure was, the better the objective function value was perceived. Since the objective function under the structure's capacity was based on the cost and no gratification of having lower utilization was included, it was expected from the algorithm to keep structure as much utilized as possible, since that would result in lower material consumption, but it was not required by its definition. By utilization, author meant exceeding any of ULS and SLS criteria implemented into the algorithm.

The penalization in the objective function could be solved in other ways. In [7] authors multiplied the material weight by a factor of 2 if any of the capacity or relaxation restrictions was exceeded. Authors in [93] added constant penalization component to the goal function if the elements capacity or deflections were exceeded. The component was great enough for the algorithm to always consider the punished individuals less favourable than not punished. The objective function was based on relative internal force minimization in the arch, the tie and the

hangers. The researches from [94] formulated the objective function as a sum minimization of the vertical deflections of the points on the tie. The penalization component was not present, but the cross sections of the bridge were not optimized. Authors focused on changing hangers' arrangements with the constant number of hangers in the process. In [13] authors introduced constrains to the ultimate limit state of the arch and the tie.

The presented researches showed, that application of penalization in the goal function was a common practise for unconstrained optimization problems.

In general, steel with lower capacity have lower price per kilogram than more expensive. This parameter might change depending on the supplier. According to author's experience, some suppliers produce steel S235 and S355 for the same price. In general, it is expected, that smaller steel grades will be less and less common in the future due to their lower properties. At the same time, the steel price changed significantly during the preparation of this dissertation, what was mentioned in Sec. 5.1.6, which would affect the properties of the optimal solution in terms of costs minimization. Nevertheless, for generalization, the three most common steel grades were used with linear approximation for steel grades between them.

Author was aware, that the prices could vary from: location, order size, moment in time and other factors. These variables affect the optimal solutions in terms of cost minimization. It would be preferable to investigate the influence of varying steel prices, but considering the fact of time demanding calculations of the optimization process, it was decided to keep it for further researches.

The formulation of the goal function was improved in the further part of this dissertation based on the conducted tests in the second approach of the optimization algorithm.

5.1.8 Optimization model

According to the literature approaches, the most used optimization methods [1] were DE, PSO and GA, where PSO and GA were the most common metaheuristic methods used in the optimization of network arch bridges, Sec. 3.2.2. The conclusions presented in Sec. 3.3 and Sec. 3.1, as well as author's own experience from Master thesis [11], the GA was chosen as an optimization algorithm. On the contrary, the ESO-based algorithms were not found in the optimization of network arch bridges, but were used in civil engineering in general. Therefore, it was decided to investigate the possibility of implementing step optimization, where different approaches were used. As a result, **the optimization algorithm based on both GA and ESO methods was investigated, which was authored concept in the optimization process of network arch bridges**. The principles were to take advantage of both methods and neglect their disadvantages if possible. **The utilization of ESO in the optimization process of network arch bridges was unique**, even though the utilized ESO was a simplified version of ESO known from literature [95, 34, 78, 128].

General description It was decided to use two optimization methods: ESO and GA. The purpose of ESO method was to optimize the structure by hangers' quantity **reduction** with hard-kill method, Fig. 5.11. On the other hand, the GA was responsible for structure optimization by **modification** of cross section dimensions, arch's height, tension force in hangers and hangers' top and bottom anchorage points position along the arch and the tie, Fig. 5.11. The task was divided into two stages.

The first stage, so called initial stage or stage 1, included only ESO method and was designed to initially limit the substantial number of hangers to small enough for considering TH3 effects in a reasonable period. The idea was to automate the process of initial reduction of hangers by

the algorithm itself so the whole optimization task would have been then less vulnerable to the initial hangers' topology defined by the user. The initial selection would then depend on the applied loads and details of the analysis set by the user. The simplification of the analysis was required at this stage, since implementing full TH3 analysis with imperfection would be very time demanding with number of hangers counted in thousands, while in typical structures this number was closer to hundred and less. To reduce the time consumption of the initial phase, the ESO method was divided into three phases, so called phase 0, 1 and 2. Every next phase got more and more detailed in calculation and the final phase 2 did not include any simplification when it came to considered analysis and was used in the second, more detailed stage.

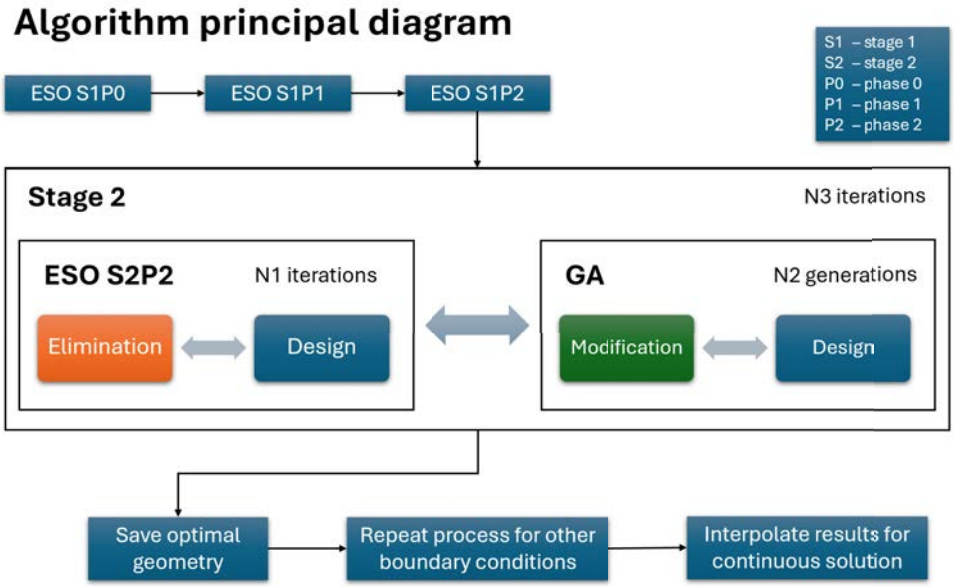

Figure 5.11 The general principles of the optimization algorithm

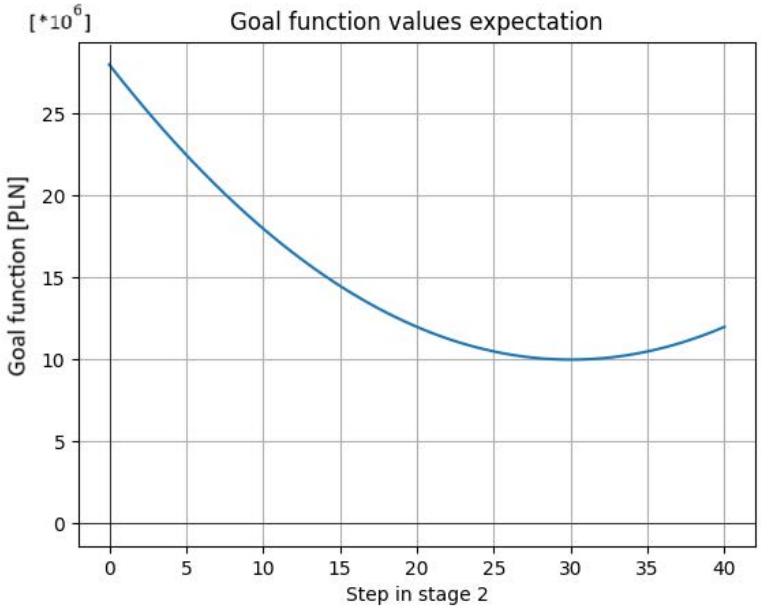

Figure 5.12 Expected goal function graph

In the second stage, so called detailed stage or stage 2, both ESO and GA methods were

proceeded one after another in a loop. When GA finished its part of changing the parameters of the geometry, the ESO method started its part by reducing slightly number of hangers. The output of GA was the input for ESO, and out of ESO was an input for GA. The pair of actions, which included GA and ESO, was called step. The process ended when the next five consecutive steps had the same goal function value. This indicated no progression of the optimization algorithm and pointed out the potential local extremum, Fig. 5.12.

In the first stage, the mechanical properties of the arch, tie and hangers were set to the maximum possible. It referred to setting the maximum steel grade, concrete class and maximum cross section size of arch, tie and hangers. This made sure that the cross-section resistance was not exceeded at any point before stage 2 was reached. If the algorithm succeeded, these initial assumption might be changed.

Hangers elimination algorithm The ESO method was used with hard-kill approach in the initial and final stage, and it was utilized in three phases. Every next phase was more detailed than the previous one with more detailed analysis and the criteria for removal of hangers from the system. **The ESO was an author coded script in an external Python environment with support of Rhinoceros 7 and Grasshopper 1 without any external optimization-oriented libraries and components.**

In the **initial phase 0**, hangers were connected between each node in the arch with each node in the tie, as described in Fig. 5.1a, Fig. 5.6 and Fig. 5.7. Since the number of nodes for each side was 71, it resulted in $71 \cdot 71 \cdot 2 = 10,082$ hanger on both sides. Even though hangers seemed to intersect with each other, the connection in the crossing points was not permitted in meshing, so each hanger acted individually. For simplification, hangers were modelled as single-meshed elements only in this phase.

There was no pretension force applied in hangers at this state. Self-weight and road layers were considered. The only variable load was the movable traffic load. The static analysis was simplified to linear analysis. The algorithm created separate folders varied by the position of the movable variable load, so there were the same number of geometries to analyse as the number of the traffic load positions. The results from each position of the traffic load were exported and only the forces in hangers were analysed. The hangers could have been compressed at this preliminary phase, but it was acceptable since the purpose of this phase was not the detailed design, but initial reduction of number of hangers. The algorithm chose twenty of the most utilized hangers from each position of the traffic load. The number of traffic positions was 93. The vehicle started from the end of the skewbacks' curve part, since its impact on the hangers' internal force was much smaller if the vehicle was not applied directly where the hangers were modelled, Fig. 5.13. These twenty hangers from each position were then saved and the initially reduced topology of hangers was saved and used as an input in the next phase 1.

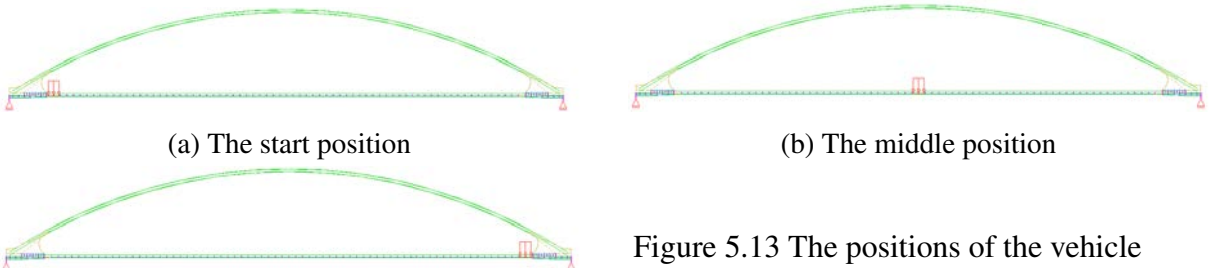

(a) The start position

(b) The middle position

(c) The end position

Figure 5.13 The positions of the vehicle in the initial phase

In the simplified phase, so called **phase 1**, the geometry was taken from phase 0 but the

hangers were divided into several cable elements. The load application was the same as in phase 0. The number of geometries was the same as the number of traffic load positions. The TH3 analysis was carried out, so hangers' sagging and geometrically nonlinear behaviour of the structure were included. The geometrically nonlinear buckling analysis was conducted using ULTI method in SOFiSTiK. This procedure was carried out for each geometry separately, so the nonlinear critical load factor was individually obtained from every traffic load position. The utilization of the arch and hangers was considered. The number of hangers removed from the system in a single iteration was set to five by default. The algorithm stopped until it reached one hundred hangers or 80% of utilization in any designed element.

The only simplification made in the phase 1 comparing to phase 2 was the lack of UGLI method applied in the design process, which required to define in-plane imperfection of the arch needed in the GM. Based on the research about the stability of NAB in Sec. 4 and the article [12], the nonlinear critical load factor $\alpha_{cr,ip}$ was assumed to be equal to 90% of the linear critical load factor. Then, the LBA was carried out, the obtained linear critical load factor $\alpha_{cr,ip}$ was reduced by 10% and the in-plane buckling factor χ_{ip} was determined. Author decided, for the simplification purposes at this phase, that the $\alpha_{ult,ip,k}$ factor in the GM formulation, Eq. (5.1), could be decomposed into minimum stress amplifier $\alpha_{ult,p,k}$ for the *perfect* geometry and in-plane buckling coefficient χ_{ip} that would cover the amplification of the stress from $\alpha_{ult,p,k}$ due to in-plane geometrically nonlinear analysis with imperfection. This modification applied to Eq. (5.1) could be expressed by equation:

$$\frac{\chi_{op}\chi_{ip}\alpha_{ult,p,k}}{\gamma_{M1}} \geq 1.0 \tag{5.8}$$

where the $\alpha_{ult,p,k}$ coefficient was defined the same as $\alpha_{ult,ip,k}$, Eq. (5.2), except it did not contain influence of in-plane imperfection, and was determined for *perfect* geometry without geometrically nonlinear stresses amplification. Nevertheless, $\alpha_{ult,p,k}$ included the sagging effects of hangers since stresses in *perfect* geometry were defined from TH3 analysis. In general, approach with implementation of imperfection with geometrically nonlinear analysis is considered the most accurate [67, 66] and substitution by buckling factor is on a conservative side, which was acceptable for the assumed simplification.

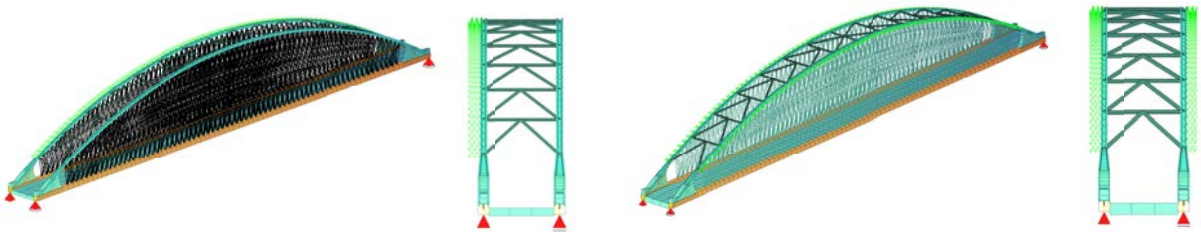

(a) The springs on one arch (b) The springs on both arches

Figure 5.14 The NAB with one or two arches with springs

Since the algorithm took the first critical load factor from the linear elastic bifurcation analysis for the determination of the buckling coefficient, it was found reasonable to divide the in-plane and out-of-plane buckling into two separate analyses. To make sure that the first form in the in-plane bifurcation analysis was oriented in the plane of the arch, the springs were added to the arch preventing movement in out-of-plane direction. Both a single arch and both arches with springs were investigated, Fig. 5.14. In the second approach, the springs were removed

from the system, which allowed for the out-of-plane buckling to occur. The first form, which was different from the forms in the in-plane buckling analysis, was considered as the first out-of-plane buckling form. Thanks to that, the in-plane and out-of-plane critical load factors would be determined.

The geometry of the skewbacks changed between phase 0 and 1. The reason behind it was the convergence problem in geometrical nonlinear analysis in phase 2. The problem was with two shell elements defined in the same plane, which occurred in the support zones, Fig. 5.15a. The reason behind this error in convergence was unknown. To fix this problem, the geometry for phase 1 and 2 was modified in comparison to phase 0. The deck had the same thickness in the middle part and was made thicker on the support zones, Fig. 5.15b. The side beams had the same section for the entire length of the bridge. Since the plate was defined in the same plane, the step in plate thickness was visible and unrealistic structurally. Nevertheless, it was accepted, since the calculations were simplified, and this issue was oriented locally.

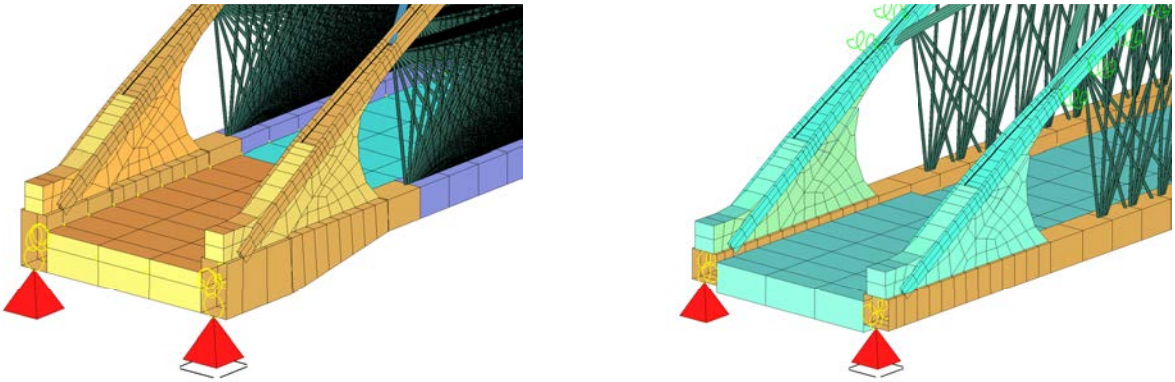

(a) The support zone in phase 0

(b) The support zone in phase 1 and 2

Figure 5.15 The comparison of the support zones between phase 0 and phase 1 and 2

In the **phase 2**, the analysis was not simplified as in phase 1. The proper GM was utilized with UGLI method to determine the geometrical nonlinear imperfection form with a usage of the ULTI and then the PUSH procedures. After the imperfection application, the geometrical nonlinear analysis was conducted to determine section utilization with included secondary effects in-plane of the arch. At the end the out-of-plane buckling coefficient was obtained as a result of LBA. It meant that each model had to be calculated twice for each traffic load position, once for non-imperfect and once for imperfect geometries, which doubled the time needed to calculate a single iteration. The number of hangers removed from the system in a single iteration was set to two by default. The algorithm stopped until it reached sixty hangers or 80% of utilization in any designed element. The same geometry principles were used in phase 2 as in phase 1.

In the investigation of the in-plane imperfection form, the springs limiting the movement in out-of-plane direction were used with the same principles as in in-plane buckling in phase 1. After the definition of the in-plane imperfection form, the out-of-plane buckling was investigated after removal of the springs. The first form that had different critical load factor than in in-plane form, was considered as the first out-of-plane form.

Geometry modification algorithm The geometry modification was controlled by genetic algorithm from the already provided tool in the Grasshopper from Rhinoceros named Galapagos. The detailed information about the algorithm was presented on website [82] and the shorter description was included in Annex B, Sec. B.3.

5.1.9 Process execution

The whole pipeline was intended to be fully automated and not require any user's actions during the optimization process. It was applicable for both stages. The execution was more Python-oriented in stage 1, and more GH-oriented in stage 2. **The entire script in Python and GH was made by author except using one already-made component from Galapagos for genetic algorithm optimization.**

STAGE 1 In the first stage, the optimization process was defined in the external Python code. The geometry was defined in two Rhinoceros files. The first approach was utilized for the ESO phase 0, and second for phase 1 and 2.

Evolutionary Structural Opimization - phase 0. The GH code in phase 0 defined the initial geometry, loads, calculations and exported results. All points on the arch in the initial geometry were connected with each point on the tie, except the points in the concrete web endings. The loads included permanent and variable components. The permanent load was represented by the UDL and the cover weight load as one loadcase number 100. The movable load was defined as the heaviest TS vehicle distributed onto its projected area and applied on the allowed traffic width. Self-weight was included automatically. Since the length of this load was 2.0 m and the distance between concrete web endings was 94.0 m, the total number of tandem positions resulted in ninety-three with a step size of 1.0 m.

The loadcase range was defined between 1000 and 1092. The loads were applied in the construction stage modelling process in SOFiSTiK (CSMP). The first construction stage included self-weight of the structure. In the second construction stage the remaining permanent loads were applied. After that, the movable loads were applied step by step but separately, so one step at the same time. The construction stage method allowed to consider self-weight and other permanent loads' influence on the stress distribution as a primary loadcases. The previous step of the movable load had no effects on the next step of movable load, which was called short-term-load stage in CSMP's nomenclature. The loads and analysis were defined in SOFiSTiK input language. The CABLE component was introduced, Annex B, which coded the export procedure of normal forces from all individual cables from each construction stage. When GH script finished defining loadcases, analysis and export, the data was exported into SOFiSTiK *dat* file. Grasshopper exported as well a *txt* file with information for the external Python code about finalization of all intended procedures. Then Python script ran calculations in SOFiSTiK by WPS, which was terminated with CMD commands. The results export, defined in SOFiSTiK CDB language, saved all needed data in *dat* files. In the last step, SOFiSTiK created a *txt* file with information for Python, that the export had been finished. Python then imported cable forces listed by CABLE component and chose twenty of the most utilized cables for each movable load step. The number and position of chosen cables were saved in data exchange format between GH files for the next step. Then Python executed a batch file with written instructions to terminate Rhinoceros, because for an unknown reason, termination of Rhinoceros from Python's sub processes or by CMD commands execution did not work. In the final part, Python code created folders for the new step with data about geometry, hangers' arrangement from the previous step and copied Rhinoceros and GH files included other version of algorithm needed for geometry generation, data procedure, export and import for the phases 1 and 2.

Evolutionary Structural Optimization - phase 1 & 2. First, Python opened Rhinoceros with GH and waited until GH exported file with the information that the file had been finished loading. Since GH file functioned as an extension to Rhinoceros, the execution of the GH file by the external Python code resulted in launching Rhinoceros first and then GH. Because GH

could not be opened before Rhino, Python considered finishing opening Rhinoceros as a final of GH file execution. Since it was not possible to monitor the execution of the GH's components, the GH's script exported a file with any information after the end of the script's execution. It allowed to determine, if the GH finished compilation.

In phase 1 and 2 the geometry was generated based on the information about the selected hangers from the previous stage. Then GH defined loads, their application, data export/import and analysis. Unmovable loads contained UDL with self-weight. The movable load based on TS was defined and executed in a similar way as in phase 0. Number of vehicle positions was limited to 21, since this was considered accurate enough for the stage 1 to get both different types of buckling forms and the extreme internal force envelope for the arch, tie and hangers, according to the research done in [12]. Data import and export was extended into CABLE, BEAM and QUAD import/export components, Annex B. They were applicable to the cables, arch and tie, excluding skewbacks and bracing system. The imported data was proceeded in GH for the design purposes based on GM approach. The analysis included TH3 calculations and the LBA for all traffic load positions. Buckling and GM design were the parts where phase 1 and 2 varied.

In the **ESO phase 1**, the simplified GM approach with LBA was defined as enough considering substantial number of hangers and its time consumption to analyse. The schematic diagram of the process was presented in Fig. 5.16.

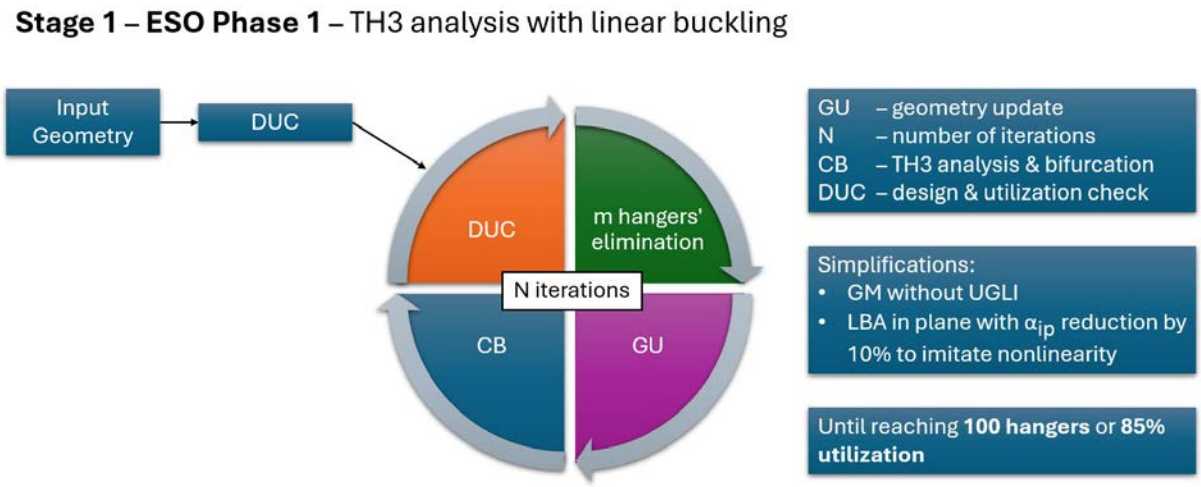

Figure 5.16 ESO Phase 1 diagram in Stage 1

First, the loadcase permanent loads and one moveable vehicle position at a time was defined and calculated with TH3 analysis. Then, the results from this loadcase were used as a primary loadcase for the LBA excluding the initial deformation of the structure. Two buckling analyses were defined. The first one investigated in-plane buckling phenomena by an addition of perpendicular springs to arch's plane preventing out-of-plane movement in buckling form. The second one checked out-of-plane buckling by removing all the springs and comparing the in-plane and out-of-plane critical load factors with each other. The first critical load factor in the unrestrained by springs critical load factors set of values that varied from the in-plane critical load factors set, was considered as the first out-of-plane critical load factor. The in-plane critical load factor was reduced by 10% in order to get closer in value to the nonlinear critical load factor according to investigation in [12]. With all of these procedures' definitions done, GH created folders in a loop with executable files, each for different vehicle positions. Then in the same loop, all the files were executed in WPS by internal Python code with CMD commands. After execution,

SOFiSTiK exported files with information about the critical load factor values and all needed data for cable, beam and shell elements as well as the file with information about calculations finalization. This file refreshed the export/import components in GH. Components' results and critical load factors were used in the simplified GM described in Sec. 5.1.8, Eq. (5.8). The utilization of the arch and hangers were determined for each finite element and the extreme values were exported to the text files for each vehicle position. Then GH chose five of the less utilized hangers per side from all the positions and excluded them from the hangers list for the next step. After finishing, Python code closed Rhinoceros by batch executable file, checked the utilization, created new folder for the next step. If the utilization exceeded 85% or the number of hangers was less than one hundred, phase 1 finished and switched into phase 2 part of the optimization algorithm. If not, the same routine was repeated with phase 1 principles. The hangers' arrangement was intended to be symmetrical. If the chosen five of the least utilized hangers matched from both halves of the bridge, the algorithm would remove less than 10 hangers in total. Both arches had the same arrangement of hangers as well.

In the **ESO phase 2**, the LBA was conducted in order to find out-of-plane critical load factor and in-plane buckling form, but the geometrically nonlinear buckling analysis in-plane was conducted in order to obtain the accurate nonlinear critical load factor. The physical imperfection of the arch was the most significant difference from phase 1. The schematic diagram of the process was presented in Fig. 5.17.

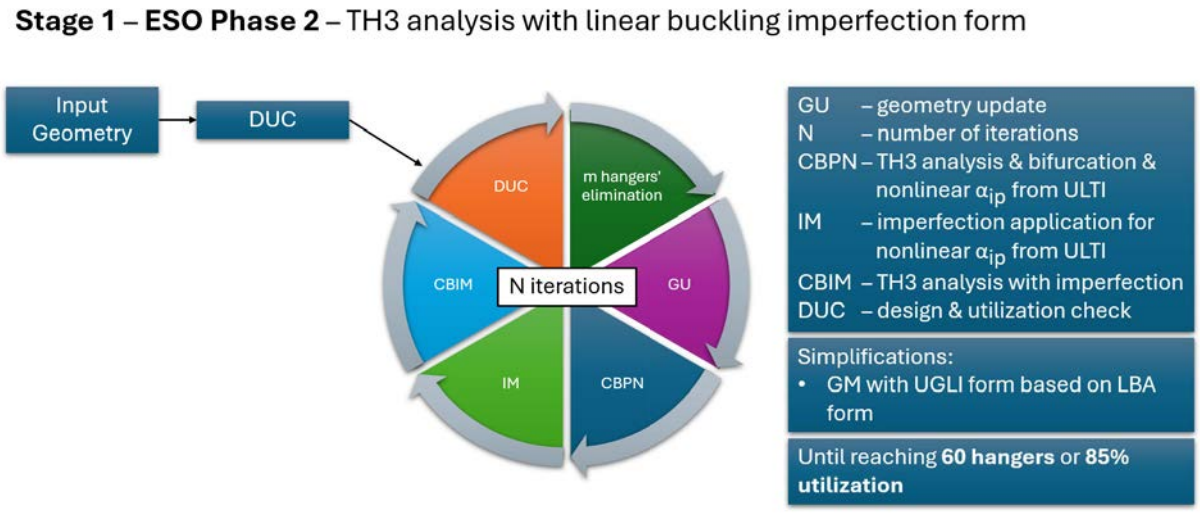

Figure 5.17 ESO Phase 2 diagram in Stage 1

The definition of load cases and vehicle positions as well as method of out-of-plane critical load factor determination were done the same as in phase 1. The GM method was used, Eq. (5.1), with UGLI procedure, Eq. (5.4)-(5.6), but the in-plane imperfection form was obtained from LBA with nonlinear critical load factor determination from ULTI procedure. The simplified linear imperfection approach was considered due to still high number of hangers and similarity of the linear and nonlinear buckling form in the middle of the arch for most of the vehicle positions, as investigated in Fig. 4.21.

After GH finished the loop of SOFiSTiK calculation and imported the internal forces and displacements for beam, cable and shell elements as well as nonlinear critical load factor and linear elastic bifurcation in-plane form displacements, the UGLI procedure was executed within GH. Starting from e_0, Eq. (5.5)-(5.6):

- γ_{M1} was taken as 1.1,

- M_{Rk} and N_{Rk} were the same for any arch cross section, since the arch is prismatic between endings. The properties were defined for in-plane buckling,
- α was taken according to CS properties for in-plane buckling case,
- $\alpha_{cr,ip}$ was taken from ULTI as nonlinear critical load factor of in-plane buckling form,
- $\alpha_{ult,s,k}$ was determined based on N_{Rk} to N_{Ed} ratio for the cross section, where the buckling shape second derivative had the maximum value. In the original definition in [132], this ratio should be the minimum one along the considered element, but at the same time the second derivative should be the maximum one along the same element. It might have happened, that these two demands did not happen for the same cross section. Since the normal force in the arch does not vary as much as bending moments and remains relatively constant in comparison to the bending moments in the network arch bridges, it was decided to determine $\alpha_{ult,s,k}$ for the CS, where the second derivative was maximum,
- λ_{ip} and χ_{ip} were determined based on CS properties and $\alpha_{ult,s,k}$ and $\alpha_{cr,ip}$ values.

After that, the scaling coefficient k_{cr} was obtained, Eq. (5.4). The maximum second derivative $\left|\eta''_{cr,ip}\right|_{max}$ value was established by firstly the import of the rotation results from SOFiSTiK and preparation of the rotation interpolation graph for the in-plane buckling form. Secondly the tangent vector to this graph was determined for denser division than the arch points spacing, since the interpolated graph offered this possibility. The extreme tangent vector inclination was interpreted as the maximum second derivative of the displacement graph since the rotation was already the first derivative and tangent vector differentiate it further to the second order derivative. This approach was considered more accurate than conducting second derivative on the displacement graph twice, where divergences were already present in the first derivative of the displacements, Fig. 5.18-5.20.

Figure 5.18 The example of in-plane buckling form

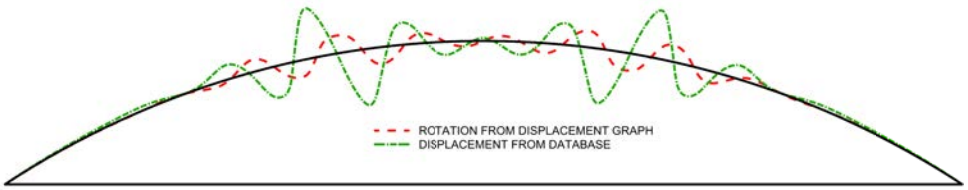

Figure 5.19 The comparison between displacement obtained from the database and rotation angle determined from the tangent vector in the displacement graph - graphs scaled evenly

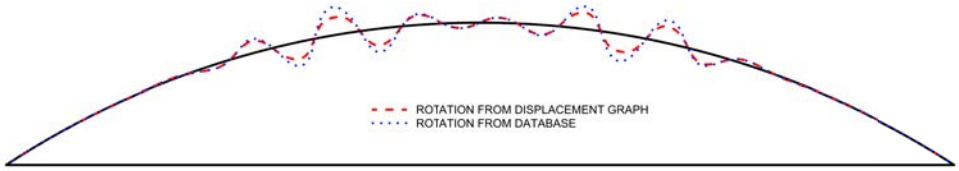

Figure 5.20 The comparison between rotation angle obtained from the database and determined from the tangent vector in the displacement graph - graphs scaled evenly

Since in the Eq. (5.4), the denominator included the critical bending moment component $EI\left|\eta''_{cr,ip}\right|_{max}$, the bending moments could be imported directly from the linear elastic bifurcation or nonlinear buckling form, which would provide greater accuracy results without a need of data manipulation by derivative operation on the discrete, interpolated results. The comparison of the critical bending moment diagram obtained from displacement, rotation and directly imported from database, as well as the graph of the critical bending moments in SOFiSTiK were presented in Fig. 5.21 and Fig. 5.22.

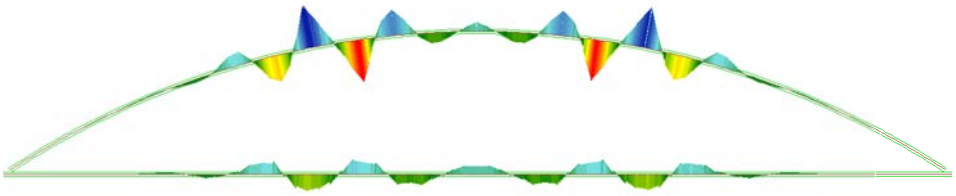

Figure 5.21 The critical bending moments diagram in SOFiSTiK

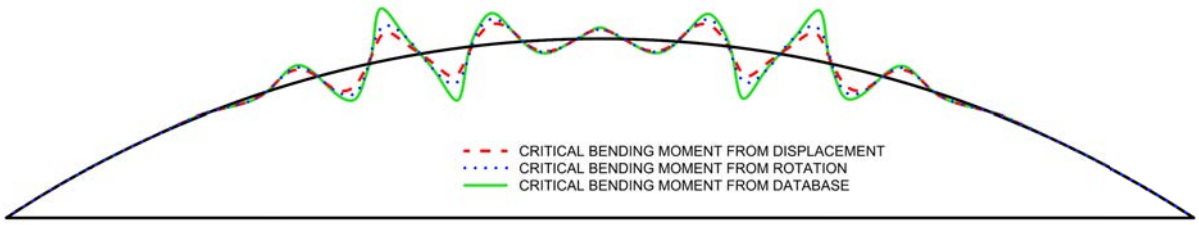

Figure 5.22 The comparison between critical bending moment obtained from (red) displacement, (blue) rotation and (green) bending moments imported directly from the database

The comparison of the results, presented in the Fig. 5.22, from these three different methods of the M_{cr} value determination showed, that the maximum value of $EI\left|\eta''_{cr,ip}\right|_{max}$ for twice-differentiated displacements was equal to 53.2% of the accurate critical bending moment value and equal to 66.5% for once differentiated rotations. This clearly showed that, for coarser mesh configurations, direct export of the critical bending moments was preferable, as scaling the imperfection shape using a value nearly half of the accurate one would lead to overly optimistic utilization determination of arch cross-sections.

At the end, the imperfect form in-plane η_{init} was obtained, Eq. (5.4). The nodes in the arch were moved according to this imperfection, but hangers' tie anchorage and tie remained the same. This caused negligible change of hangers' inclination, since the top nodes were imperfect and bottom remained perfect. However, this approach was considered acceptable, as the imperfection shape was intended to reflect the worst-case imperfection likely to occur in actual manufacturing and construction processes. After that, the new geometry and calculations tasks were exported to SOFiSTiK with the definition of TH3 analysis, as geometrically nonlinear

elastic analysis with included imperfections (GNIA). The plastic deformation of the arch was not allowed. After exporting all new SOFiSTiK definitions to new folders, GH exported information files, so that external Python code got the signal to execute all new tasks with WPS. The last calculated SOFiSTiK file contained the export of information file, informing GH script, that the process had been finished, which refreshed the import/export components for the arch, hangers and tie. Then GH determined the utilization of hangers as in phase 1. The utilization of the arch was done with GM but this time without the simplification made in phase 1. The χ_{op} was calculated based on the $\alpha_{cr,op}$ obtained in the first round of calculations in phase 2, so before the imperfection determination. The $\alpha_{ult,ip,k}$ was established by finding the minimum ratio of the characteristic steel yield strength to the maximum resultant stresses along the arch obtained from the TH3 GNIA. The utilization of all considered elements were checked for each vehicle position. Each vehicle position had unique in-plane imperfection form, in-plane nonlinear critical load factor, out-of-plane linear elastic critical load factor and utilization.

GH exported the results, and the list excluded two of the least utilized hangers. After this signal, the external Python code imported all this information and closed Rhino by the commands defined in the batch file. Then new folders were created, and a new Rhinoceros file was copied into them with other files containing information about hangers' topology. The process was then repeated. If the number of hangers was less than sixty and utilization was higher than 85%, the algorithm entered stage 2. In general, ESO phase 2 was more than twice more time consuming as ESO phase 1.

Stage 2 The stage 2 included repeatable steps of ESO and GA, Fig. 5.23. The step started with GA, which optimized the structure by **modification** of the geometry, cross sections, hangers' positions and steel grade. After that, ESO optimized the structure by **elimination** of the least utilized hangers. This process continued with limited number of hangers after every step.

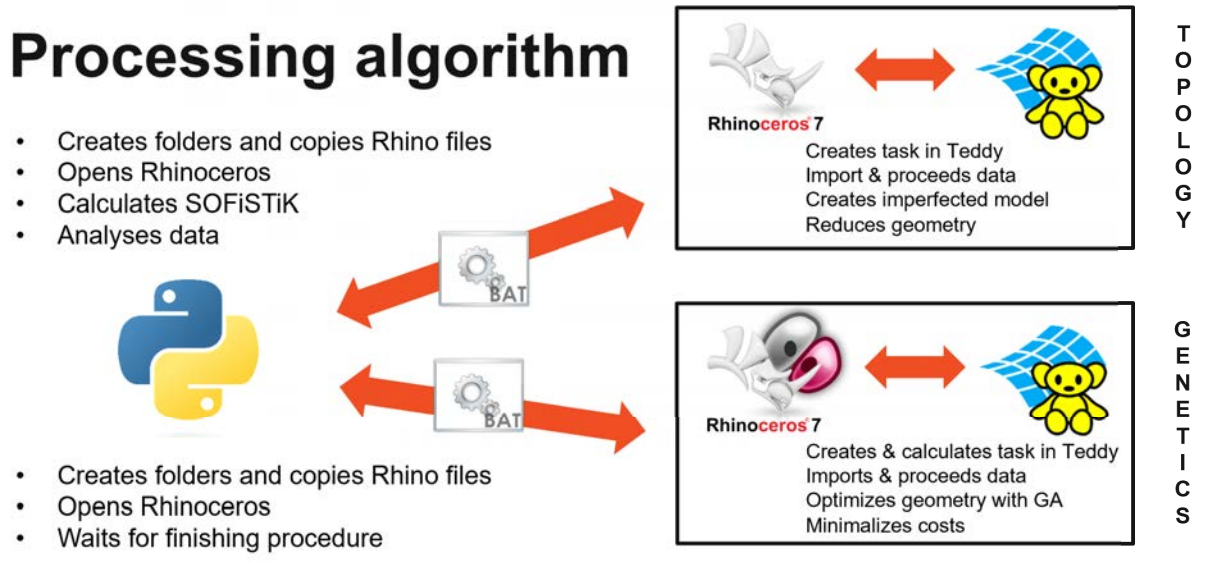

Figure 5.23 Stage 2 diagram

Genetic Algorithm. The external Python code's rule was limited to two steps. Python created a folder where Rhinoceros file was copied. Then it opened Rhinoceros file and waited until the GA optimization process was finished, since it was defined in GH, not in Python. The remaining tasks were defined and controlled by GH. The schematic diagram of the process was presented in Fig. 5.24.

Genetic optimization was managed by Galapagos component in GH. Unfortunately, for the moment of implementing this solution (February 2021), the component could not run externally, so users had to trigger this component every time the GA-step was in use. This was considered a big disadvantage, since the general idea was to let the process run without user's intervention. However, the option of manually triggering this component was added. The second disadvantage was lack of control or limited control over used methods inside Galapagos. It referred to population generation, selection, coupling, coalescence and mutation.

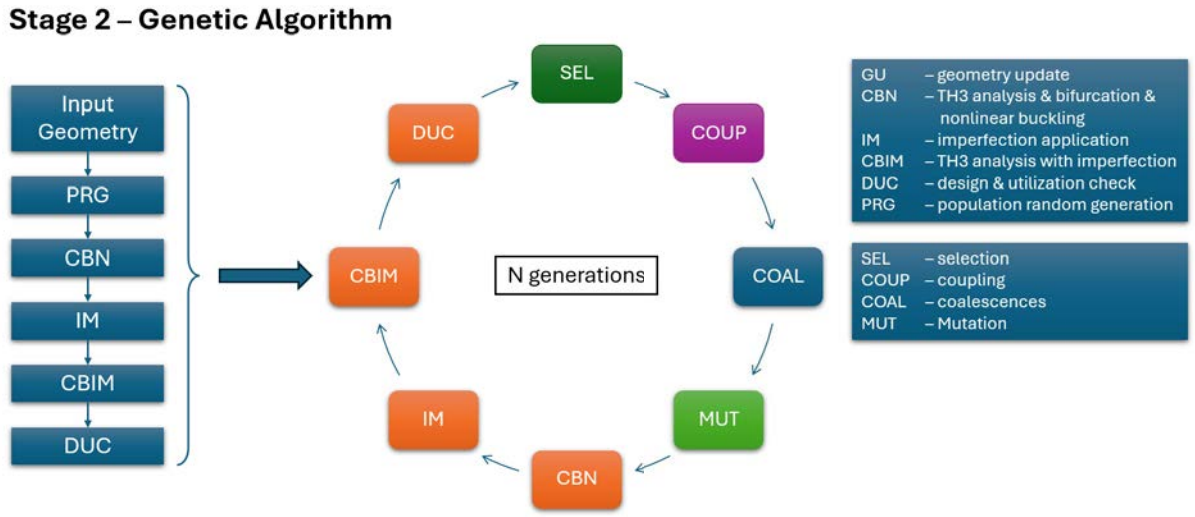

Figure 5.24 GA diagram in Stage 2

Grasshopper file firstly imported geometry data from the previous step of stage 1 if it was the first step in stage 2. Then it used this data to define geometry, including arches' elevation, cross sections' properties and steel grade. Loads were in the next step and their division was the same as in phase 2 of stage 1. The analysis definition included: (1) GNA based on TH3 of combined loads, (2) nonlinear buckling analysis managed by GNA based on TH3 and utilized by ULTI procedure until reaching critical point, (3) post-critical analysis managed by GNA based on TH3 and utilized by PUSH procedure until reaching twenty steps by default and (4) out-of-plane critical load factor determination. The (1) analysis was for determining forces and stresses in non-imperfected structure needed for the determination of the imperfection according to UGLI method. The (2) analysis was for obtaining nonlinear critical load factor and precritical deformations. The (3) analysis was for obtaining post-critical deformations including precritical deformations. Subtracting (2) deformations from (3) deformations resulted in critical deformations including geometrical nonlinear behaviour of the structure, especially hangers. The (4) LBA was for obtaining out-of-plane critical load factor by restrained and unrestrained procedure presented in phase 2 of stage 1.

When the definition was completed for all vehicles positions, folders were created and files with all needed definitions were allocated into these folders. Files included export definition results as well as an information file interpreted by GH as a signal that calculations were finished and allowed to refresh export/import components. Grasshopper executed SOFiSTiK files by

internal Python code with CMD commands. After finishing calculations, GH imported data needed for the GM. Firstly, UGLI method was applied in an analogous way as in phase 2 in stage 1, but this time the imperfection form was obtained from nonlinear buckling form, not from linear one as earlier. After determining scaled imperfection form according to UGLI, the new SOFiSTiK task was defined with TH3 GNIA for the purpose of determining $\alpha_{ult,ip,k}$. Before that, the out-of-plane critical load factor was determined on the perfect geometry for the sake of χ_{op} determination. After determination of $\alpha_{ult,ip,k}$ and χ_{op}, the GM condition was checked, Eq. (5.1).

The last step was to summarize the costs of all elements in the bridge. This sum as well as utilization were then used in the goal function, Eq. (5.7). The goal function had to be minimized. The lower the value of this function was, the better the structure was considered.

After this procedure, the user had to run Galapagos manually in each step, which was predicted to be required approximately every second day with the default setting. The settings for each step were kept the same and were presented in Fig. 5.25.

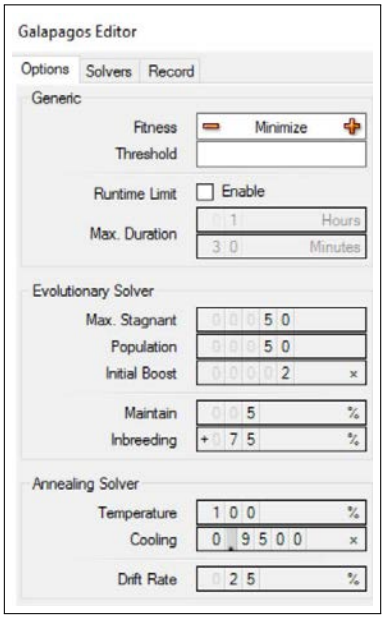

Figure 5.25 Galapagos options

The following options were chosen:

- fitness - minimum - following goal function definition,
- threshold - no value was specified, since the lower, the better and the global minimum was unknown,
- runtime limit - not specified, since Galapagos did not considered the time needed for SOFiSTiK calculations so the process was stopped manually,
- max stagnant - due to time consumption it was set to 20 as minimum accepted by the solver,
- population - also 20 as the minimum allowed value and high time consumption,
- initial boost - it was set to 2 as recommended,
- maintain - 5%,
- inbreeding - 75%.

Galapagos iterative procedure was cancelled manually, when the number of populations i was greater than fifty and if the there was no change of the goal function value G for the five consecutive populations, Eq. (5.9). The maximum utilization u_{max} was allowed to be maximum 90%, so the next following ESO would still have capacity left for its optimization part.

$$G_i = G_{final} \text{ if } \begin{cases} i \geq 50, \\ G_{i+5} = G_i, \\ u_{max} \leq 90\%. \end{cases} \tag{5.9}$$

After finishing the GA optimization process, the GH exported geometry, utilization, material and hangers' topology data to external files of the most optimal geometry. Rhinoceros was then closed manually, which was the signal for external Python code, that the process was finished and the data from the exported files were then proceeded.

Evolutionary Structural Optimization. On the contrary to GA, involvement of external Python code in the optimization process was greater. Firstly, the folder was created with the

Rhinoceros and data files copied into it. Then Rhinoceros file was launched. GH imported data from the previous GA calculations, including geometry, cross sections' properties and materials' grade and classes. The loads were defined in the same way as in GA. The analysis definition included: (1) GNA based on TH3 of combined loads, (2) nonlinear buckling analysis managed by GNA based on TH3 and utilized by ULTI procedure until reaching critical point, (3) post-critical analysis managed by GNA based on TH3 and utilized by PUSH procedure until reaching twenty steps and (4) out-of-plane critical load factor determination. The process of managing these procedures was the same as in GA. After determination of $\alpha_{ult,ip,k}$ and χ_{op}, the GM condition was checked, Eq. (5.1). The schematic diagram of the process was presented in Fig. 5.26.

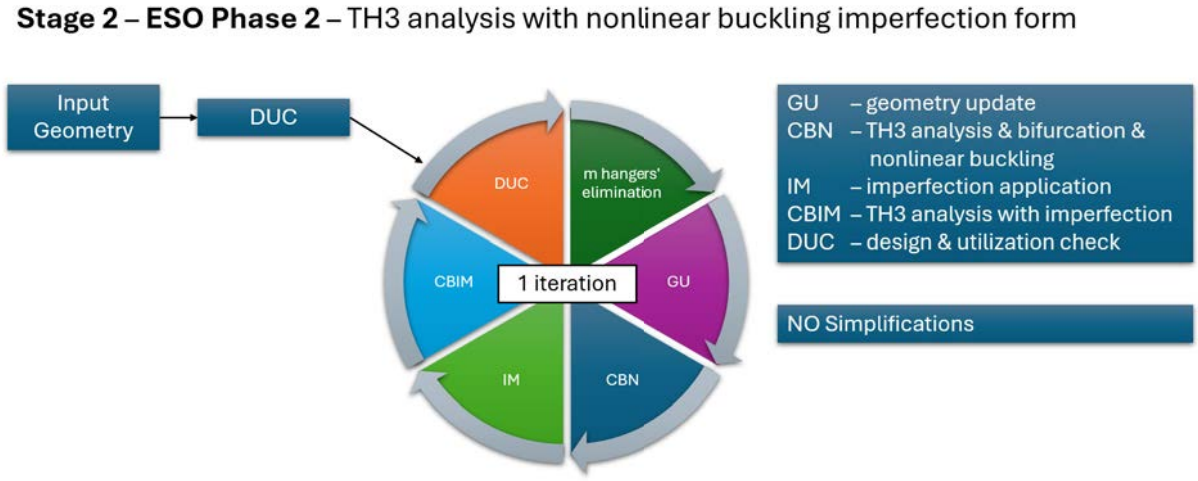

Figure 5.26 ESO Phase 2 diagram in Stage 2

After this process, GH exported data files with information about utilization of each hanger and the file with information about finishing all procedures in GH. External Python code imported the utilization data and closed GH by batch's commands. This process was repeated for every vehicle position and the minimum utilization among all hangers from every vehicle position was determined and the least utilized hanger was deleted from the system. Since the arrangement of hangers was always symmetrical, the actual number of deleted hangers was two per each arch. This new hangers' arrangement was exported into file and was imported by GH in the following GA optimization.

GA-ESO loop. The GA and ESO operated in a loop in stage 2. ESO was responsible of optimization by elimination of the hanger elements from the model. GA was responsible of optimization by geometry adoption to the new number of hangers obtained from the previous ESO method. The general principles of the optimization algorithm were presented in Fig. 5.11.

According to the studies presented in [94, 93], a reduction in the number of hangers led to less optimal internal force distribution in the arch when using a regular network hangers' arrangement. On the contrary, a custom sparse hangers' topology resulted in better structural performance, which should support cost reduction progression. It was expected, that when the number of hangers was too low, the bending moments in the arch would increase enough, that any arrangement of hangers would not manage to reduce the utilization of the arch and so the cost of the structure. The very extreme case would be the situation with only one hanger. According to those principles, it was expected to be an extreme value of the goal function in the elimination and adoption process of looped ESO and GA. The principal graph was presented in Fig. 5.12.

The minimum goal function value was considered as the result of the optimization process for the given boundary conditions. External Python code was intended to finish the optimization process after 5 steps of no improvement of the goal function value. The process was intended to be repeated many times, and the discrete results were intended to be interpolated to make the results continuous and allow for prediction of optimal solutions for the boundary conditions, which were not considered. This would be applicable to the optimal geometry prediction for the intermediate span lengths and tie widths.

5.1.10 Interpolation of discrete results

The interpolation was managed after the optimization process. The variables, after which the interpolation was made, were bridge length and bridge width. The bridge width had an implication of an increase of load applied on the tie, changing the proportion between self-weight and variable loads.

The optimization process had to be managed for different width and length values, both as discrete values. The results between the discrete solutions were then interpolated. Since the number of variables was intended to be two, the interpolation could be defined deterministically. More advanced methods, such as neural networks (NN) were not needed, and Hermite interpolation method was intended to be used. The interpolation would concern the hangers' inclination distribution, number of hangers, cross sections' properties, arches' elevation, pre-tension forces value and materials' grades and classes.

5.2 Results

5.2.1 ESO - stage 1/phase 0

The comparison of the results between the initial geometry and the end of the ESO phase 0 process were presented in Fig. 5.27.

a) Initial topology

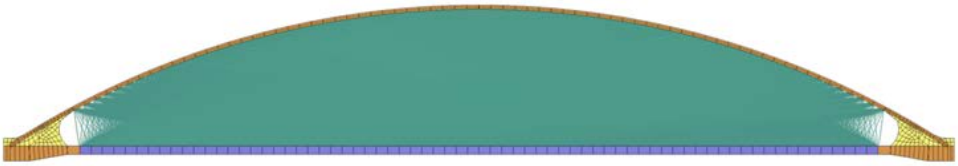

b) Initially optimized topology

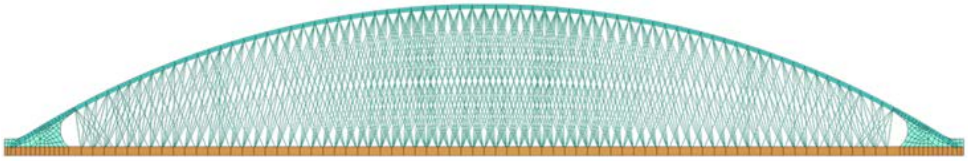

Figure 5.27 Graphical representation of initial state (a) and the resultant hangers' topology after the phase 0 optimization (b)

The number of hangers per side was $71 \cdot 71 = 5041$, but after the optimization process, this number decreased to 444. The mean inclination angle of the hangers to the tie was 73.9^o with the standard deviation on 6.58^o. The hangers' inclination angle was presented in Fig. 5.28. Majority

of the results were in the 65-85^o range. According to [75], the optimal angle for the CSM arrangement was between 62^o and 70^o, with the assumption of the maximum considered number of hangers of 60 and span length between 100 m and 150 m, Fig. 3.31a. The results obtained from the initial analysis were close to this range. For the best sparse hangers' arrangement optimization obtained in [93, 94], the average angle was 68.5^o, which was also close to the determined value in the preliminary stage, Tab. 3.5. These results were considered promising for the later optimization procedure.

Each vehicle position took around 5 minutes to execute with the linear analysis. Considering ninety-three vehicle positions, it took 465 minutes to calculate. This time consumption showed the need for simplification in the preliminary stages of the optimization algorithm.

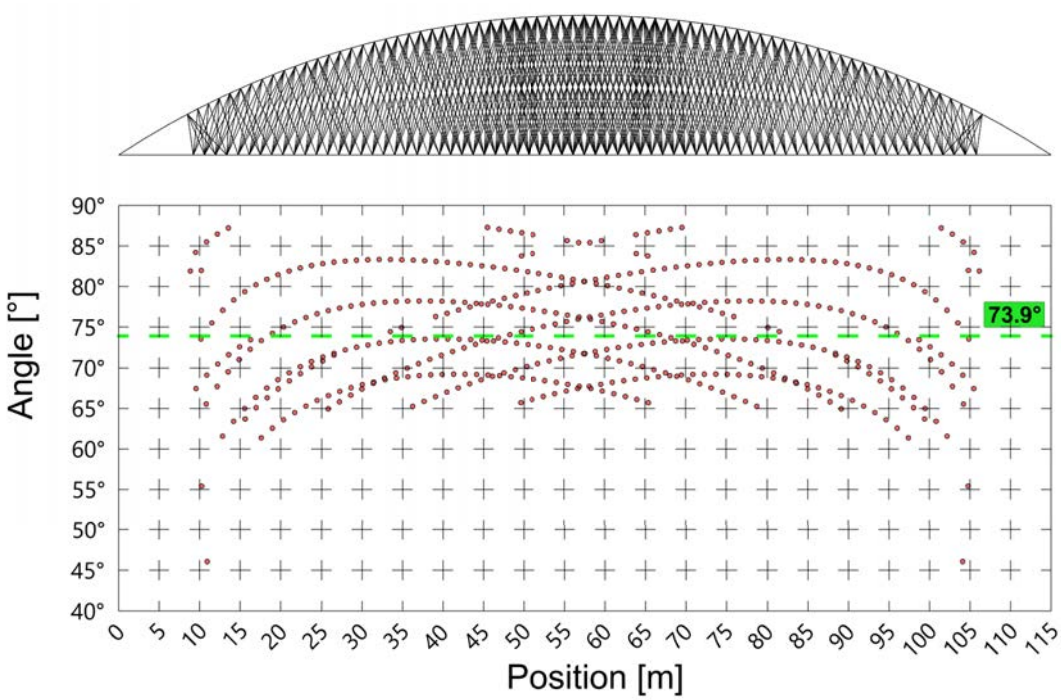

Figure 5.28 Graphical representation of the hangers inclination angle along the bridge as a results of the phase 0 optimization

5.2.2 ESO - stage 1/phase 1

The algorithm managed to reduce the number of hangers from 444 to 100 within 87 iterations. The results were presented in Fig. 5.29.

The mean inclination angle of the hangers to the tie was reduced from 73.9^o to 67.2^o with the standard deviation reduced from 6.58^o to 4.36^o, with the greatest hangers' inclination near the ends. The hangers' inclination angle was presented in Fig. 5.30.

In ESO stage 1, phase 1, the buckling analysis started to be utilized. The first issue was noticed about the buckling form. The first two buckling forms were the bracing forms both in the situation with and without springs, Fig. 5.31 and Fig. 5.32.

a) Initial topology in phase 1

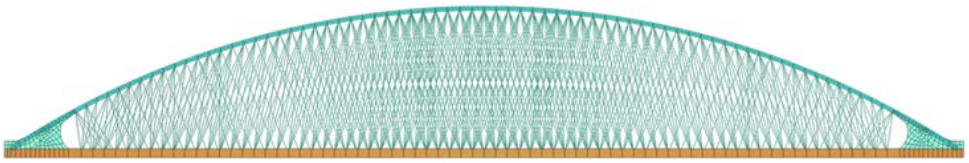

b) The end result in the phase 1

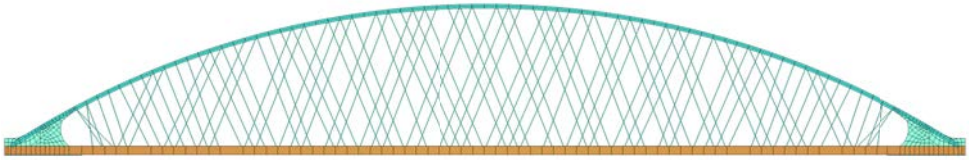

Figure 5.29 Graphical representation of initial state in phase 1 (a) and the resultant hangers' topology at the end of the phase 1 optimization (b)

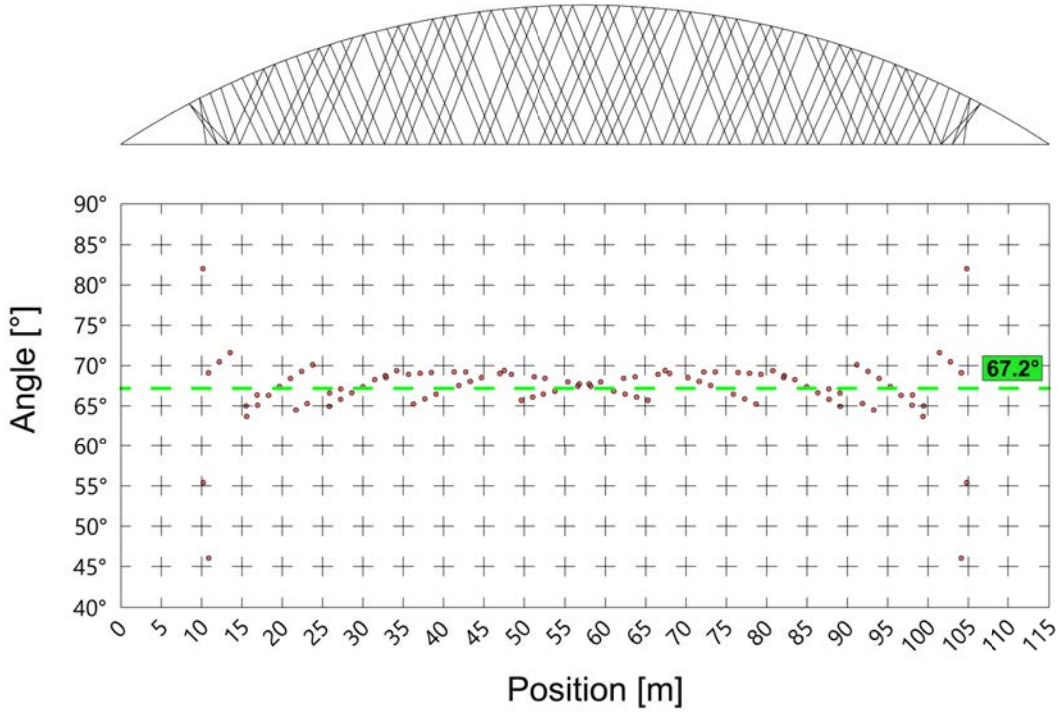

Figure 5.30 Graphical representation of the hangers inclination angle along the bridge as a results of the phase 1 optimization

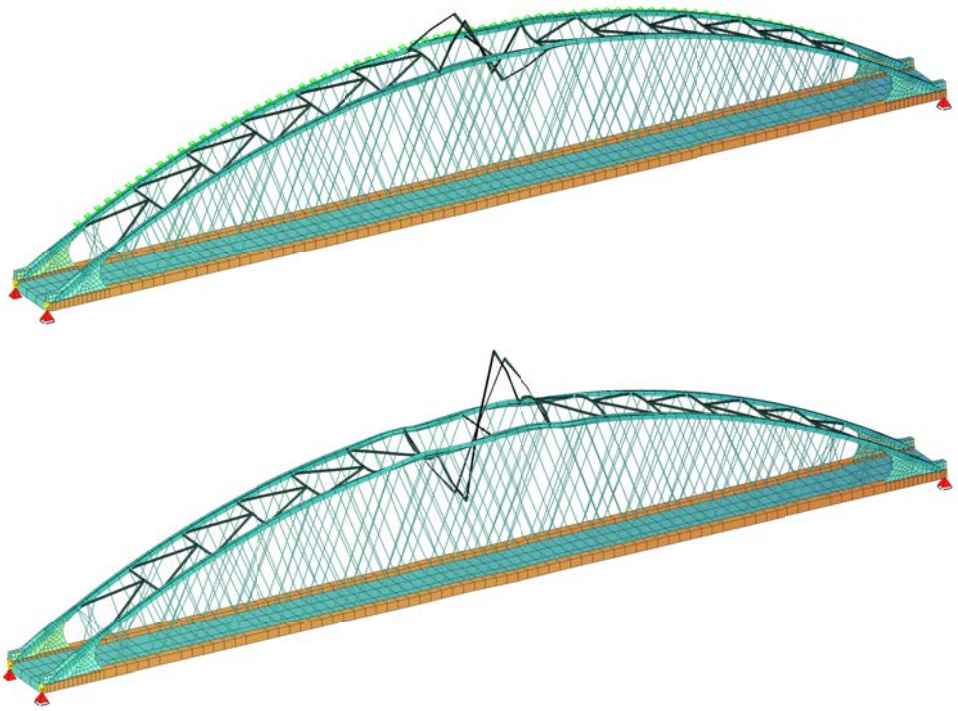

Figure 5.31 The first buckling forms - bracing - situation with and without springs on one side - in both cases $\alpha_{cr} = 15.47$

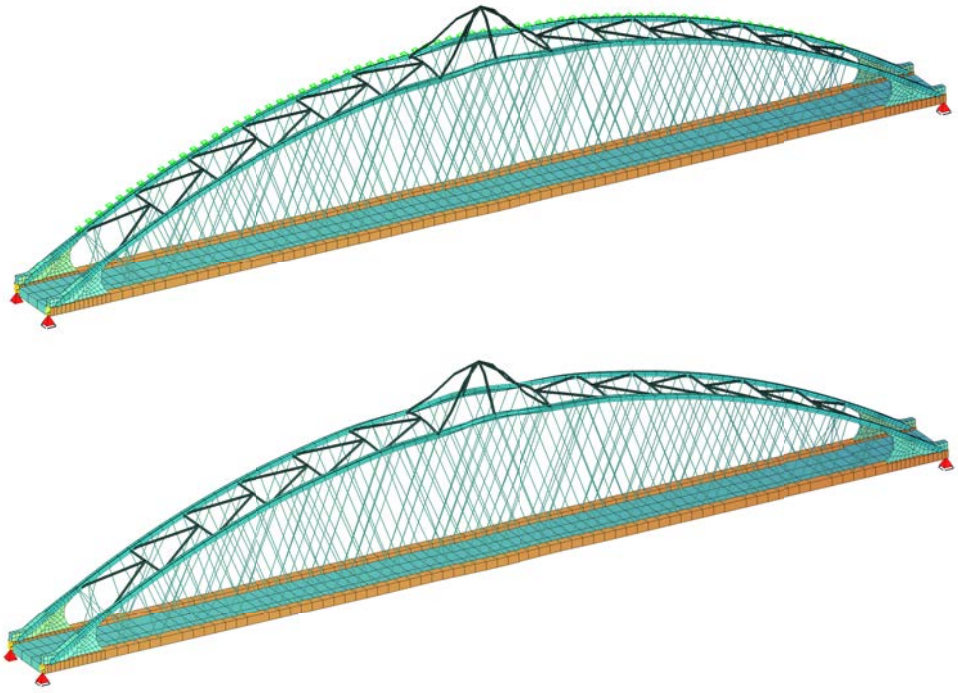

Figure 5.32 The second buckling forms - bracing - situation with ($\alpha_{cr} = 18.74$) and without ($\alpha_{cr} = 18.71$) springs on one side

Most of the results were in the 65-70^o range reflecting algorithm's preferences in more horizontally inclined hangers than the ones from ESO phase 0. **Referring to [75], the hangers' arrangement was obtained entirely within the optimal angle range for optimal CSM arrangement**. In relevance to the sparse hangers' arrangement obtained in [93, 94], the average

inclination angle of the obtained results so far differed by 1.3^o from the optimal average angle, but the arrangement was still too dense for this comparison. These results narrowed the deviation compared to the ESO phase 0 results and converged closer to the optimal results from the literature.

Firstly, the calculations were conducted for the case without pretension of hangers, since the number of hangers was still high enough, which would have significant effect on the utilization of the arch.

At this stage, the algorithm took the first buckling form with spring restraints as the first in-plane buckling form of the arch. In the situation without springs for out-of-plane critical load factor determination, the first form was considered, that represented the critical load factor different from the critical load factors' set in the situation with springs. **In this scenario, the first in-plane and out-of-plane forms were the bracing forms, since the second form differed by just 0.03**. It happened even though the bracing beams were modelled as single elements to force software to artificially increase the critical load factor for the bracing, which was hoped to allow avoiding the first forms to be bracing-related. **In terms of the design, this approach was conservative, since lower critical load factor was taken for the calculations of the χ_{ip} and χ_{op}, but in the next stage, this phenomenon was not desired, since it was not arch-buckling-oriented form and would underestimate the capacity of the arch.** This could be solved by increasing the stiffness of the bracing system by, for instance, increasing its diameter of the circular hollow cross section. Then the first form would be more likely to happen for the arch. On the contrary, bracing's purpose is mainly to increase out-of-plane stability of the arch and carry the wind loads applied on the arch. If the stiffness of the bracing was increased too much, its contribution in carrying part of the normal forces from the arch would increase, which was not desired. Therefore, increase of bracing system's stiffness was not considered, which would lead to a potential scenario of arches' capacity underestimation due to lowered critical load factor, if the bracing was present in the first buckling form.

In the situation with springs on one side, the first buckling form, which was not related to bracing, was the out-of-plane buckling form of the unrestrained arch, Fig. 5.33. This phenomenon was expected to happen and the solution of using the spring elements on both sides was evaluated. The first two buckling forms were again related to the bracing, but the previous out-of-plane buckling form of one arch was prevented and the first in-plane buckling form of both arches occurred, Fig. 5.35. The in-plane buckling of both arches matched the form and critical load factor value for the situation with springs on one side only, Fig. 5.34. The in-plane buckling of both arches with spring restrain on one arch occurred after the out-of-plane buckling of a single arch. The approach of using springs on both sides was considered as the correct method for LBA and NBA, since undesired out-of-plane buckling form of the arch was prevented and the in-plane critical load factors matched for both restrained on one side and on both sides.

The investigation of the internal forces of the first buckling forms related to bracing showed, that even though the springs were modelled in arches' every node with great spring stiffness of 100 GN/m each, the arch experienced non-negligible bending moment in out-of-plane direction represented by the perpendicular bending moments and torsional moments, Fig. 5.36. The magnitude of the out-of-plane related internal forces was smaller than the one for the in-plane bending moment, but they were not considered negligible. The reason behind it should not be sparse enough spacing of the spring elements, because the out-of-plane bending diagram did not have chainsaw-like pattern between the nodes and it was smooth with the pick value in the very top of the arch. The same came to the torsional moment, which was almost constant between the bracing nodes along the arch.

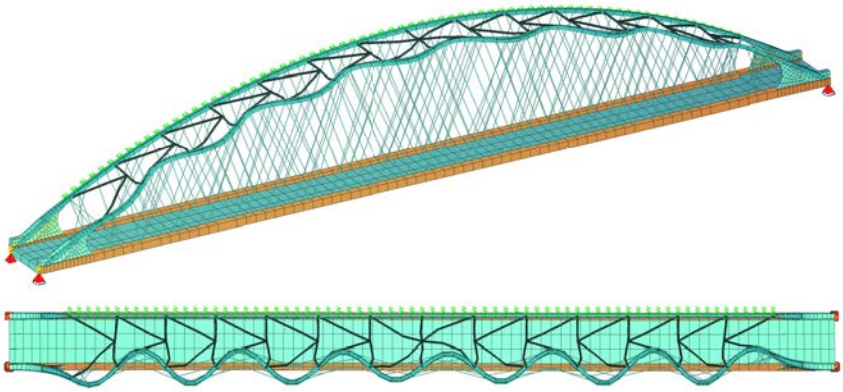

Figure 5.33 The first arches' buckling form in the situation with springs on one side ($\alpha_{cr} = 20.40$)

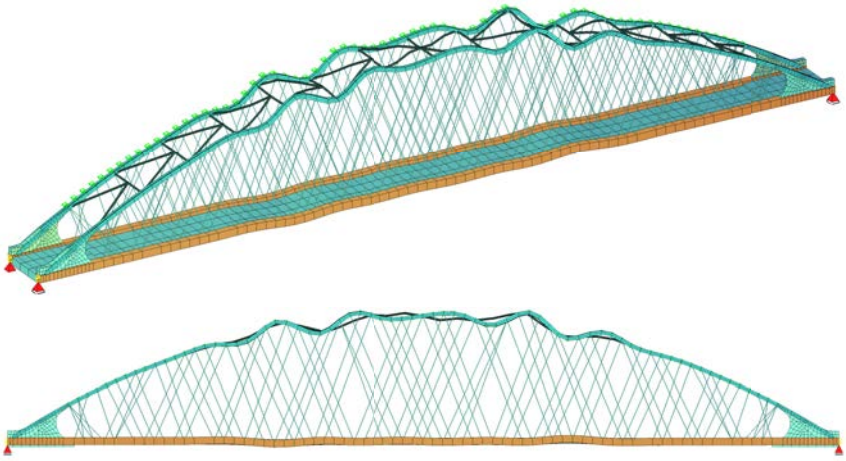

Figure 5.34 The first arches' in-plane buckling form in the situation with springs on one side ($\alpha_{cr} = 25.61$)

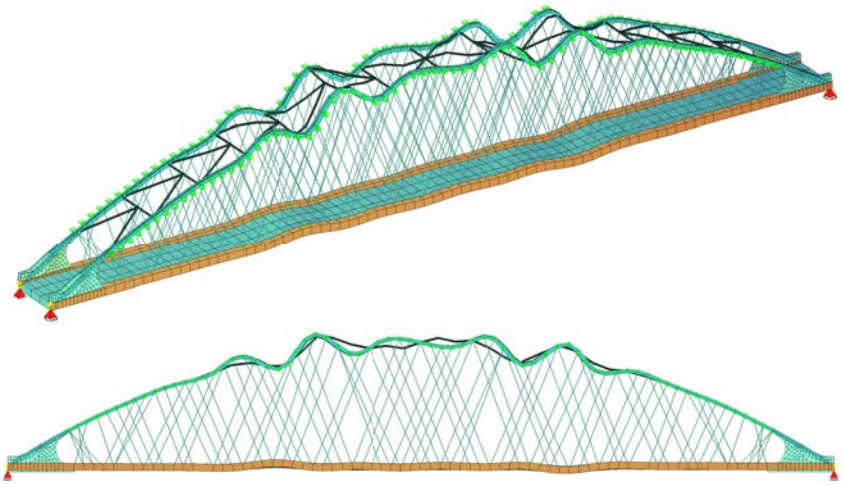

Figure 5.35 The first arches' buckling form in the situation with springs on both sides ($\alpha_{cr} = 25.61$)

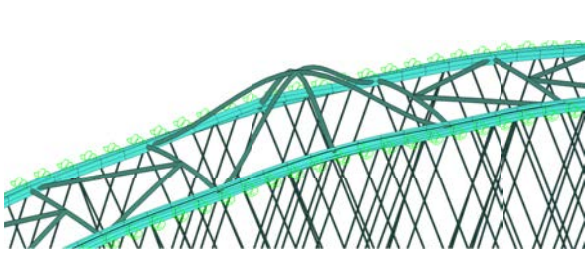

(a) Buckling form

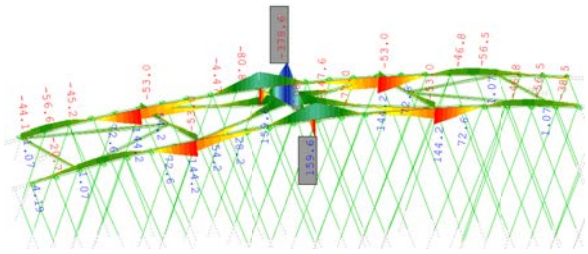

(b) In-plane bending moments

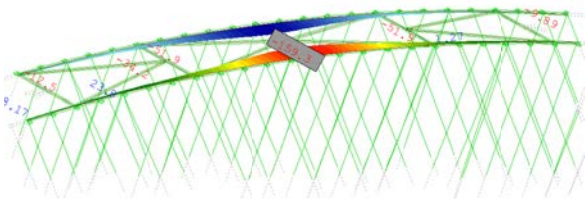

(c) Out-of-plane bending moments

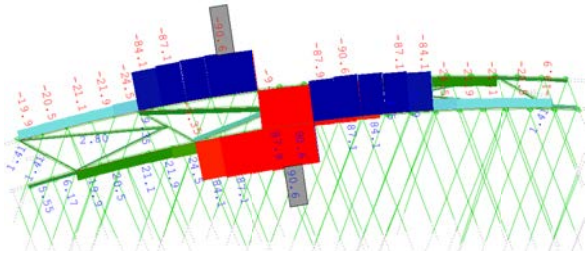

(d) Torsional moments

Figure 5.36 The detail zoom on (a) the second bracing buckling form with results of the (b) bending moments in-plane, (c) bending moments out-of-plane and (d) torsional moments

The arch in Fig. 5.36a experienced torsion as well, which was more visible than the out-of-plane lateral movement. This movement was caused by the lateral buckling of the bracing, but the torsional moment in the arch suggested that the torsional form might occur before the in-plane lateral form. If so, the algorithm would take the torsional critical load factor as the in-plane buckling phenomena, and would omit this form for the out-of-plane buckling coefficient determination, which would result in considering twice the out-of-plane buckling form instead of once in- and once out-of-plane. Again, the approach was conservative from the design point of view, but it was undesired to happen in next stage. **This particular case in Fig. 5.36 was driven by the lateral buckling of the bracing and was not considered as the arch buckling, but as the potential torsional form, that could happen before the in-plane lateral buckling form. Author did not find a solution to prevent this phenomenon for the geometrical nonlinear buckling analysis**. The rotational springs matching the local tangent vector on the arch for each anchorage point of the hangers could be a solution in LBA, since these springs were added after the PLC was determined and would prevent the twist of the arch. This solution would not work for nonlinear buckling analysis, since the springs had to be present in the model from the beginning of the iterative load amplitude increase in the ULTI procedure. This would lead to situation, where the artificially added spring would carry part of the external load and as a result, disturb the internal forces' distribution in the arch making results unrealistic.

5.2.3 ESO - stage 1/phase 2 and stage 2

Since ESO stage 1/phase 2 was similar to ESO stage 1/phase 1, the buckling forms and critical load factors issues were expected to be the same and so the conclusions as well. Since it might be a case also in stage 2 and that ESO stage 1/phase 2 was a simplified version of ESO stage 2, it was decided to investigate first the ESO stage 2, where the nonlinear buckling analysis was fully used, since that would participially cover potential issues also in the simplified version. The output from ESO stage 1/phase 1 was taken as a reference. The hangers' arrangement was considered in two cases. The first one was found in the same way as the solution from ESO stage 1/phase 1. The second was restricted to having possible hangers' anchorage points

offset by one from the end of the arch and tie in comparison to the non-restricted arrangement in ESO stage 1/phase 1. These two arrangements' investigation was a part of a different boundary conditions investigation. The comparison of the stage 1/phase 0 results between the offset and non-offset, as well as the results of the stage 1/phase 1 procedure, were presented in Fig. 5.37.

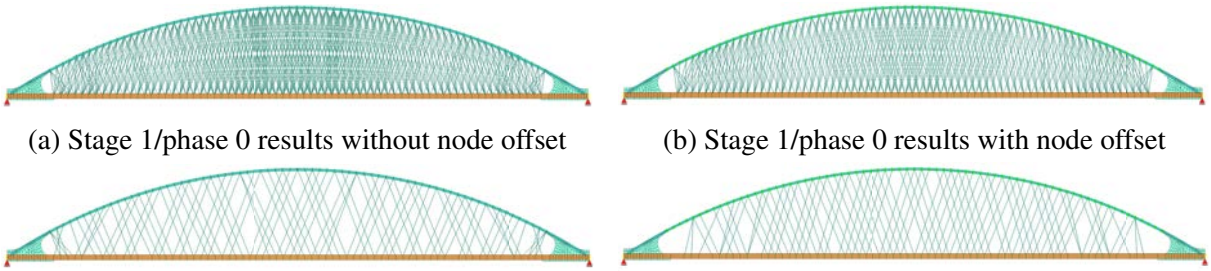

(a) Stage 1/phase 0 results without node offset

(b) Stage 1/phase 0 results with node offset

(c) Stage 1/phase 1 results without node offset

(d) Stage 1/phase 1 results with node offset

Figure 5.37 The results of the ESO phase 0 and phase 1 results

a) The critical point deformation - scaled 5 times - load factor 16.12

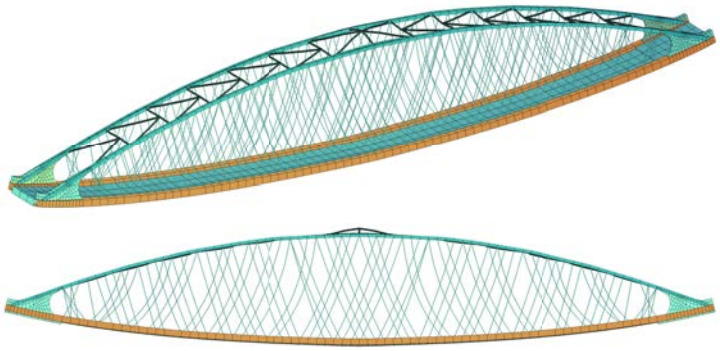

b) The 20 post-critical pushes after the critical point deformation - real scale

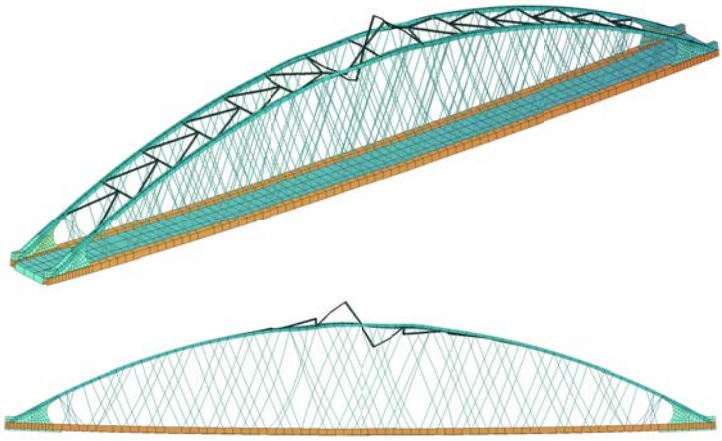

Figure 5.38 The results of the geometrical nonlinear analysis of non-offset geometry with (a) critical point and (b) post-critical deformations. The springs and supports were hidden

The algorithm preferred to offset even more than one node, while in the non-offset case the last nodes were still used as an anchorage. The nonlinear buckling analysis of the non-offset hangers' arrangement resulted in the critical load factor of 16.12, which diverged by about 4%

from the LBA critical load factor of 15.47. The buckling form was also middle-bracing-oriented as in the LBA, Fig. 5.38, but in NBA the form was asymmetrical and in LBA symmetric.

The results presented in the Fig. 5.38 were conducted for the parameter FDL equal to 0.05. This parameter, named by SOFiSTiK as Factor Delta L, stood for a fraction of the last ULTI displacements [61]. In this case, the software tried to reach 5% of the last ULTI displacement in every PUSH step. The method was presented in Fig. 5.39. In the example, the ULTI procedure equilibrium path was marked green. After that PUSH procedure was used twice, once, marked red, with FDL=0.3, which meant, that the intended displacement in each PUSH step was intended to reach 30% of the displacement obtained from the last ULTI step [61]. The second, marked yellow, was conducted with FDL=0.4, so each step was then equal to 40% of the displacement obtained from the last ULTI step [61]. SOFiSTiK did not guarantee reach of the displacement in each step [61]. Each step in the ULTI and PUSH procedures was considered converged for a considered load factor, if the residual forces were smaller than 0.001 of the maximum force in the given finite element between two following iterations.

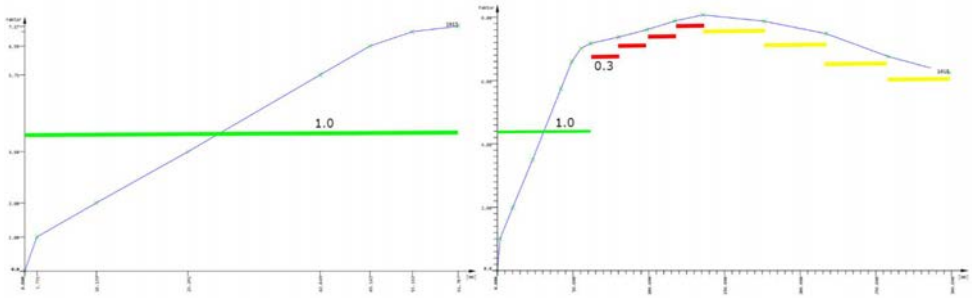

Figure 5.39 The example of equilibrium path [61]. The green mark represents the normalized displacements at the end of ULTI procedure. The red marks represent the FDL=0.3 of the total length of the green mark after ULTI procedure [61]. The yellow marks represent the FDL=0.4 of the total length of the green mark after the last PUSH step [61].

It was decided to investigate the sensitivity of the calculations against the FDL parameter. The tests were conducted for the FDL=0.5, 0.1 and 0.05 and the forms were presented in Fig. 5.40. All the calculations were made to reach the same final displacement. The time needed for each of these FDL settings was about 5, 35 and 140 minutes respectively. In general, during the PUSH analysis, the convergence was usually not reached in every iteration step. According to SOFiSTiK's manual this fact was acceptable since the obtained states were not stable by the definition of the post-critical analysis [61]. This phenomenon was also observed in von Mises truss investigation, Fig. 4.4. When the force load was applied, the residual forces increased and the load factor dropped in the process, but if the iteration step was chosen right, the *jump* to the stable part of the equilibrium path was achieved, Fig. 4.4. If the force load was changed to the displacement load, the equilibrium was reached since the force was a consequence of the increase displacement, not the opposite, Fig. 4.4. This approach was considered in the NAB, but the right approach was not found, and the force iterative process remained.

The form for FDL=0.5 was caused by the arch's instability, Fig. 5.40a and 5.40b, not the top bracing's as presented for FDL=0.05 and FDL=0.1 results, Fig. 5.40c-5.40f. **The form was locally asymmetric and the arch near skewbacks twisted, which was considered as torsional form caused by normal force**, Fig.5.40b. Therefore, this form should be classified as an out-of-plane form even though the springs restrain to both arches was used. From the global point of view, the form was similar to the multi-period sinusoidal wave obtained in Fig. 4.21, which was expected, Fig. 5.40a.

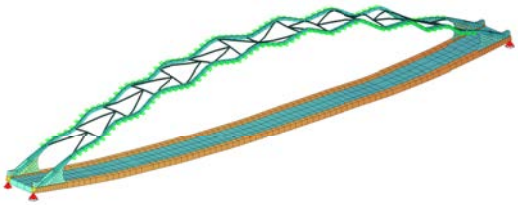

(a) The post-critical form for FDL=0.5

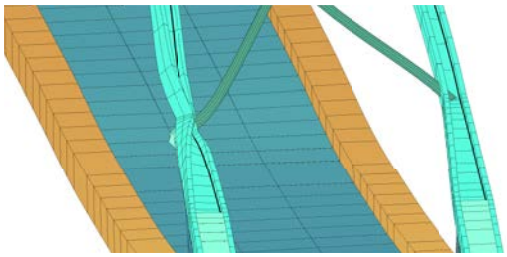

(b) The detail view of the arches near skewbacks

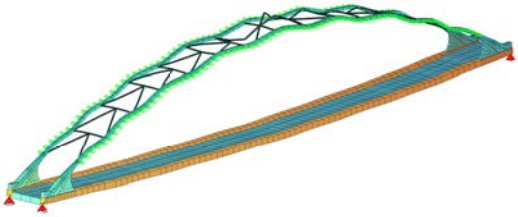

(c) The post-critical form for FDL=0.1

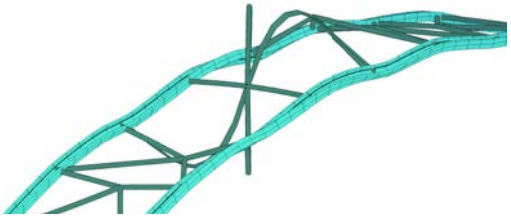

(d) The detail view of the arches in the middle

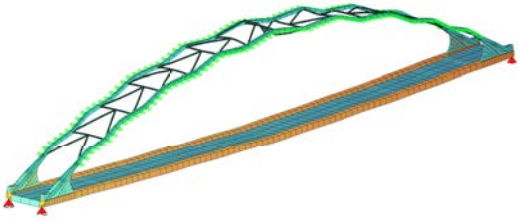

(e) The post-critical form for FDL=0.05

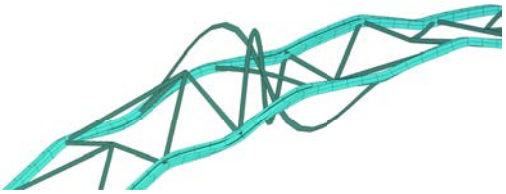

(f) The detail view of the arches in the middle

Figure 5.40 The post-critical global form without hangers for FDL=0.5 (a), FDL=0.1 (c), FDL=0.05 (e) and detailed view of the deformations (b), (d), (f). The hangers group was hidden as well as springs in the detailed view

The results for the FDL=0.1 and FDL=0.05 matched locally the shape of the buckling form from the LBA, which was oriented around the bracing and the arch twisted mainly in the middle section, Fig. 5.40d and Fig. 5.40f. However, from the global perspective, the multi-period sinusoidal waves were also obtained, Fig. 5.40c and Fig. 5.40e, which was not present in the LBA results as expected.

The NBA forms looked similar graphically, so more detailed comparison of in-plane displacements and rotations were done, Fig. 5.41. The LBA displacements were symmetrical and concentrated around the middle part of the arch, similarly to the results presented in Fig. 4.20. The form corresponding with FDL=0.5 was irregular with divergence visible closer to skewbacks. The lower the FDL value was, the more regular the form was. The LBA form was both symmetrical and regular. The NBA forms experienced bow-like imperfection, which did not happen in LBA form. The NBA displacement forms looked different enough from each other, especially in the middle and on the right side of the arch. The form for FDL=0.05 looked the most correct form to consider as an imperfection form, since it was the most regular and symmetrical as expected, but it required the most time among all considered FDL values.

When it came to the rotational forms, the LBA provided symmetrical and regular forms as it was done for the displacements. The differences between the NBA forms were more visible than the displacements. The results for the FDL=0.5 provided irregular form with significantly greater amplitude of the rotation near the right skewbacks compared to other rotations of the arch for this form. The result for the FDL=0.1 looked the most similar to the LBA results among the analysed cases and was the most symmetrical among all NBA results, but the rotations on the left half were greater than the ones on the right. The smallest step of FDL=0.05 looked similar

to the FDL=0.1 results, but the form had lower amplitude of rotation for the same multiplication factor. The maximum amplitude of rotation for the FDL=0.05 happened on the right half of the bridge, but for FDL=0.10 it happened on the left side, so the form was counter symmetrical. No convergence to symmetrical shape was noticed in NBA and forms varied from each other more than for the displacements, which were considered converging. The FDL=0.5 results outstand drastically from other NBA results.

a) The displacements comparison

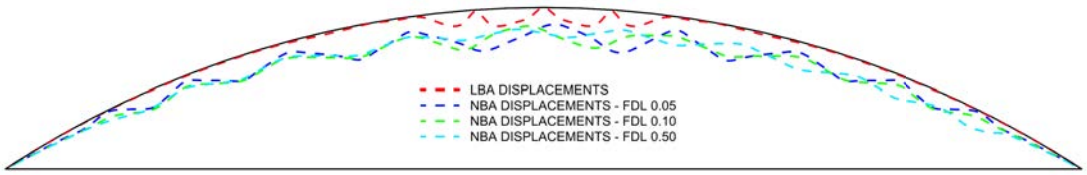

b) The rotations comparison

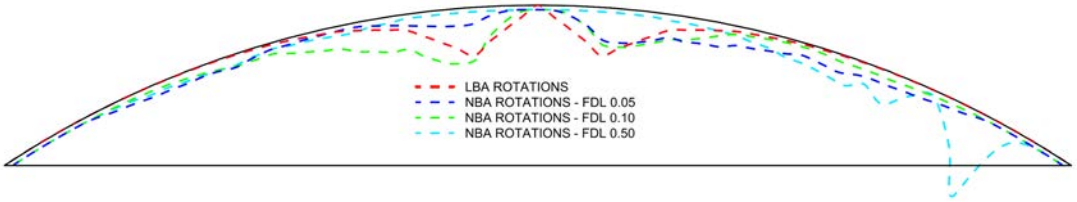

Figure 5.41 The comparison of the (a) displacements and (b) rotations from the critical forms between the LBA and NBA with FDL parameter equal to 0.05, 0.10 and 0.50. The NBA results were scaled with the same factor. The LBA results were presented for reference.

The load factor in a function of iteration number (FIN) paths for the NBA were investigated and presented in Fig. 5.42. The FIN approach was not exactly the equilibrium path, which reflects applied force in a function of displacement. This simplified approach was considered more general for the sake of determining the moment, when the critical and post-critical points occurred. The value differences of the critical points for these three approaches were caused by initialization of PUSH procedure not from the last ULTI iteration, but from the second to last. It was caused by instability in the last ULTI procedure and SOFiSTiK did not allow PUSH calculations to continue from the unstable loadcase. This principle was not always applicable, and the PUSH procedure could start from the last ULTI iteration, but for generalization, the second to last was assumed. The path for FDL=0.50 did not have the post-critical point, but other FDL did. The last buckling form was taken from the last PUSH iteration, but ideally the first point on the FIN path after reaching again the FIN path should be considered. Due to limitations in SOFiSTiK, which did not allow to use of decreasing load factors in the PUSH analysis when loads were applied as forces rather than displacements, it was not possible to determine whether the FIN path was described with a *snap-through* or *snap-back* phenomenon, but this information was not needed in this analysis. The FIN path for FDL=0.05 and 0.10 after about iteration number 130 got again positive load factor value but the path was linear for both. This linear trend was suspicious to author considering nonlinear shape of the FIN path before the critical point and also in the tests done in Sec. 4. After reaching the maximum value, the path started with a sawtooth pattern, which was not expected. Due to too long calculations for FDL=0.05, the path finished before reaching the last iteration. It was not a case for FDL=0.10, which started to converge to 0 again after iteration number 270, so after the sawtooth pattern. On the contrary, the FIN path for FDL=0.50 reached 0 value at about iteration number 100

and remained at 0 until the end. The critical forms, after subtraction of displacement from the critical point (the last ULTI step), were presented in Fig. 5.43.

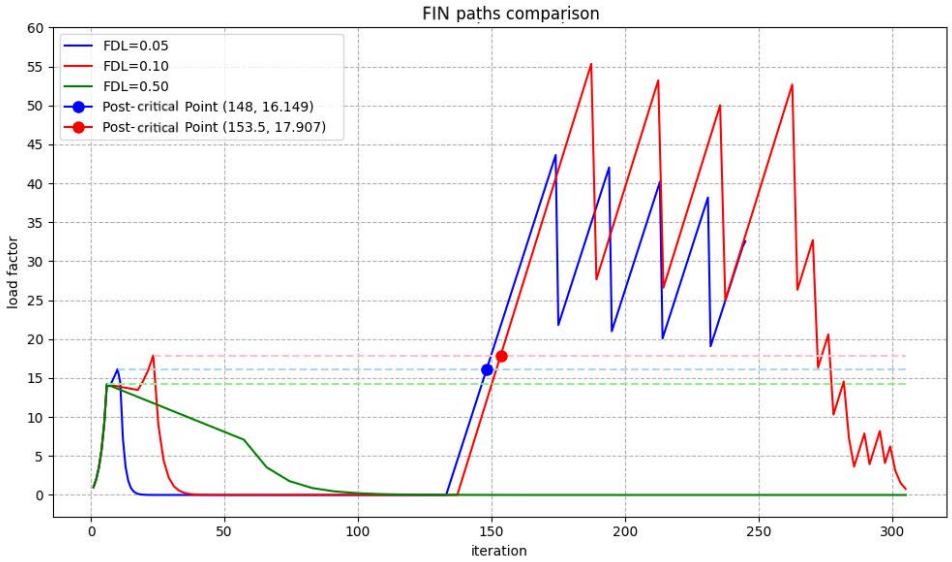

Figure 5.42 The comparison of the FIN paths for (blue) FDL=0.05, (red) FDL=0.10 and (green) FDL=0.50 with marked post-buckling points for FDL=0.05 and FDL=0.10.

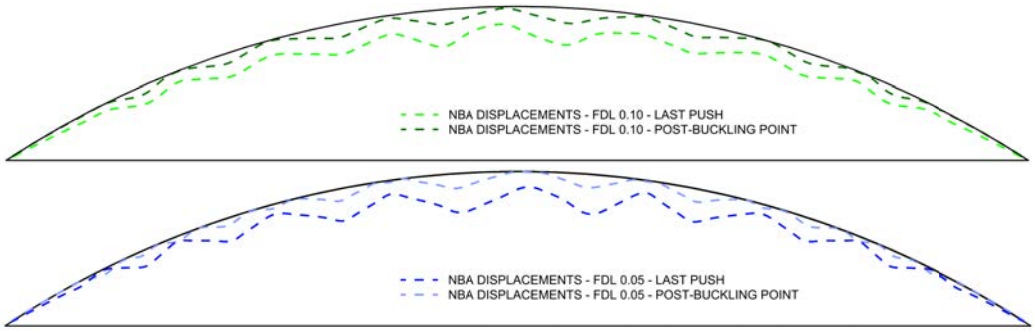

(a) The displacements comparison

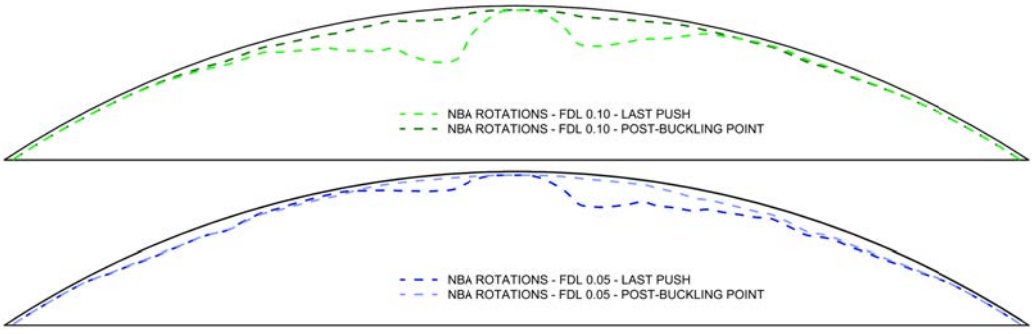

(b) The rotations comparison

Figure 5.43 The comparison of the (a) displacements and (b) rotations from the critical forms between the last PUSH iteration and the first results after the post-buckling point. The graphs scaling factor was the same for the last pushs and post-buckling point.

The displacements for both last PUSH and post-critical point, after subtraction of displacement from the critical point (the last ULTI step), kept the same wave shape, but the form for

the post-critical point had smaller bow-like imperfection than the last PUSH form, Fig. 5.43. The ratio of the maximum wave amplitude for the last PUSH iteration to the post-critical point was 1.72 for FDL=0.05 and 1.45 for FDL=0.10. At the same time, the maximum rotation ratio of the last push to the post-critical point was 5.75 for FDL=0.05 and 5.09 for FDL=0.10. This investigation showed that the increase of rotations was about 3 times smaller in relevance to the increase of displacements in plane of the arches, if the critical form after reaching post-critical point was considered instead the last calculated PUSH step.

The calculations required inspection of the FIN path and finding the post-critical point. If the post-critical point was not present, as for FDL=0.50 path, the calculations should be repeated for the smaller FDL value. The smaller the FDL value was, the more time was needed. The certainty regarding the presence of the post-critical point was unknown. If the post-critical point existed, the minimum number of iterations to obtain its value was unknown. Therefore, it could be a case, that even though this point existed for the considered FIN path, but would not be achieved due to too small number of iterations set in the calculations. **The number of iterations should then be high to reach certainty, which again would require more calculations time and put the search at risk of not finding the correct imperfection form**, since the hangers' arrangement could be irregular during the optimization process, not only well-known network or vertical arrangements. This made it hard to generalize and required more effort to solve.

For the offset geometry, the LBA critical load factor was 12.96 and for the NBA 7.96, Fig. 5.44. The form was oriented around the arch buckling near the skewbacks in both cases as expected. The difference in critical load factors' values was considered significant.

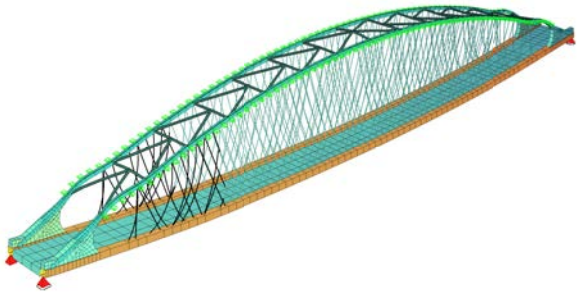

(a) The critical point deformation - scaled 5 times - load factor 7.96

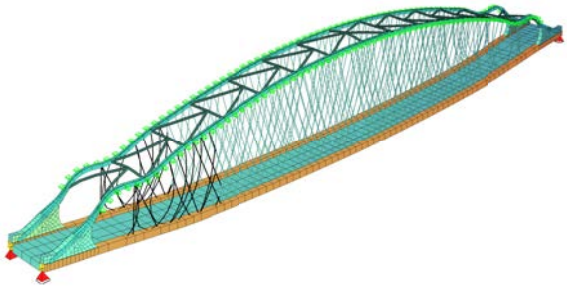

(b) The 20 post-critical pushes after the critical point deformation - scaled 5 times

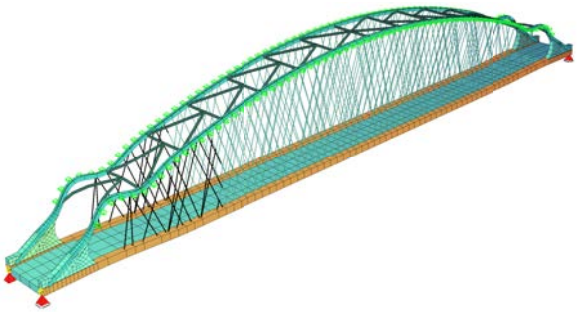

(c) The LBA form - load factor 12.96

Figure 5.44 The results of the geometrical nonlinear analysis and LBA of offset geometry with (a) critical point, (b) post-critical and (c) LBA deformations

The PUSH analysis did not finish for the desired number of 50 steps but finalized at 24 steps instead due to too high rotations, which was considered by SOFiSTiK as an error. The forms from 10, 20 and 24 PUSH steps were compared with the LBA form, Fig. 5.45. The further the PUSH step was, the greater the displacements near skewbacks were in relevance to the middle bow-like buckling form. The form was a combination of the local sinusoidal imperfection near skewbacks and global bow-like imperfection, similar to the observation from the Fig. 4.21 in

Sec. 4.3.1. The bow-like buckling form was greater than the bow-like displacement component from the LBA's form. The sinusoidal linear elastic bifurcation form near skewbacks was very similar to the nonlinear form, but the nonlinear buckling wave closer to the skewbacks had greater amplitude than the further wave. The LBA form was not symmetrical in relevance to the axis of the non-deformed arch. The right wave had a smaller amplitude compared to the left wave, while the nonlinear form was symmetrical.

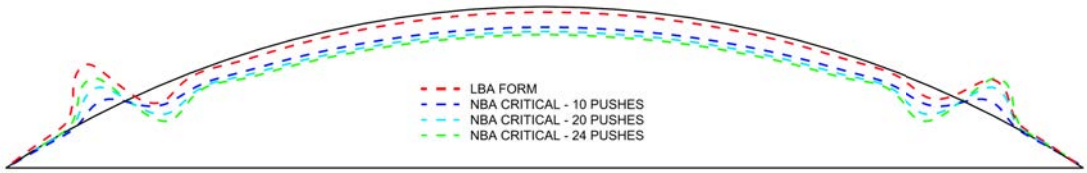

Figure 5.45 The buckling forms comparison of LBA with NBA with different number of PUSH steps

The nonlinear critical load factor was about 40% smaller than the linear critical load factor, which was similar to the greatest difference obtained in the accidental, single rapture test in Sec. 4.3.3. This phenomenon showed the importance of a need for nonlinear buckling analysis in case of any hangers' arrangement. The author agreed, that in certain cases, the Shanack's formula, Eq. (4.3), provided good approximation of the critical force of the arch in relevance to the nonlinear buckling analysis, Sec. 4.3.1, but in more generic case, more general method was recommended based on the considered geometry.

The PUSH procedure did not allow to start post-critical analysis if the convergence in the last ULTI step was not reached. This assumption was reasonable, but in this example, the last ULTI step did not converged enough even though the number of iteration steps was increased to 500. To obtain the post-critical results, it was decided to manually set the number of ULTI iterations to be second to last with the convergence problem. Unfortunately, **it required launching the ULTI procedure twice** to first check, if the PUSH procedure succeeded after the last ULTI step, and if not, repeat the calculations for the second to last step from the ULTI procedure. **These issues added extra complexity and time consumption to the optimization algorithm, as well as uncertainty of obtaining the right results.**

The analysis of the ULTI procedure lasted between 300 and 400 seconds. The PUSH procedure lasted between 1600 and 1900 seconds, which was much longer than the ULTI procedure. **With the twenty-one positions of the vehicle, which would result in between around 40k and 48k seconds, so between around 11 and 13.5 hours per one step without including the time needed for other processes in the optimization algorithm**. The same would be applicable for the GA optimization.

In the next step of Evolutionary Structural Optimization, the hangers' normal force was investigated for the non-offset geometry. The results were symmetrical as expected, Fig. 5.46. The total range of the normal forces was between 31.9 kN and 219.9 kN. All hangers were under tension despite the lack of a pretension force. The analysis of the tension force amplitude from all of the vehicle positions showed, that the greatest and the lowest force amplitude occur at the end of the bridge, Fig. 5.47. The closer to the center a hanger was, the closer the amplitude of tension force got to the amplitude's middle range value.

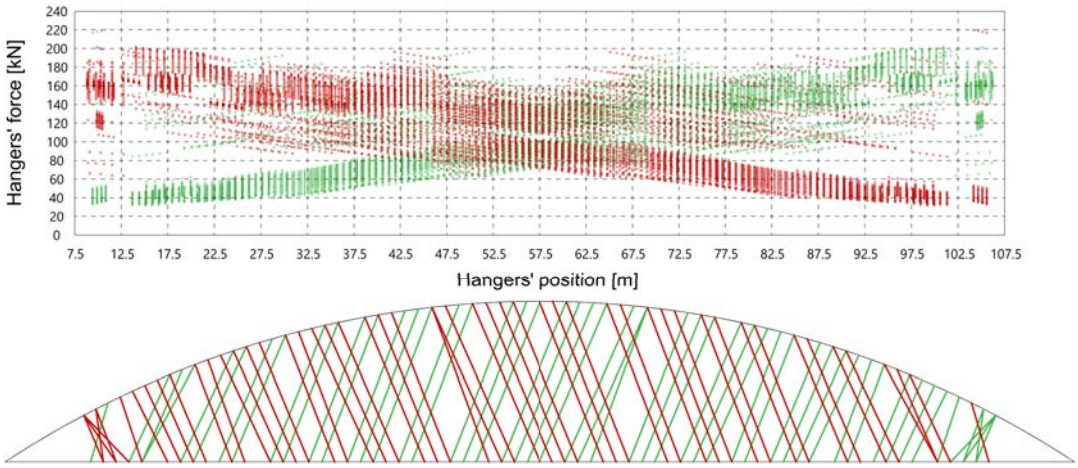

Figure 5.46 The hangers' normal forces diagram for every hanger and every vehicle position.

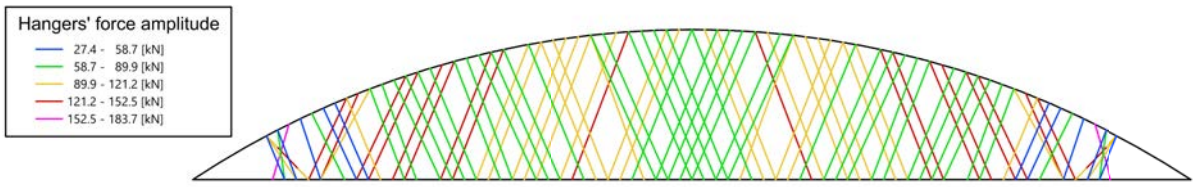

Figure 5.47 The hangers' normal forces amplitude diagram for every hanger and every vehicle position.

Hangers effective stiffness $K_{cable,eff}$ was also investigated. The minimum effective stiffness ratio k_{eff} values were presented in Fig. 5.48 according to Eq. (5.10).

$$K_{cable,eff} = k_{eff} \frac{EA_{cable}}{L_{cable}} \tag{5.10}$$

The greater the k_{eff} was, the less sagged the hanger was. **The greatest sagging effect was observed in about 1/4 span length distance from the supports**. The hangers pointed inwards in this region experienced more sagging than the pointed outwards. The hangers in the very ends and in the middle part experienced the least sagging effect. The minimum k_{eff} values in Fig. 5.48 corresponded with the greatest change of the k_{eff} values for all vehicle positions, Fig. 5.49. **The hangers in about 1/4 span length distance from the supports experienced the greatest sagging change, which made them vulnerable to the fatigue more than other hangers. This also corresponded with the greatest force amplitude diagram**, Fig. 5.47. The uneven hangers sagging could be fixed by the change of cross section area of these hangers, but the same cross section for all the hangers would be preferable from the practical point of view. More simple solution would include the pretension force. **To omit higher bending moments amplitude in the arch, the hangers should have smaller sagging. This check showed, that the middle and the end parts could potentially be constructed without pretension force. The pretension force applied on the hangers could be uneven.**

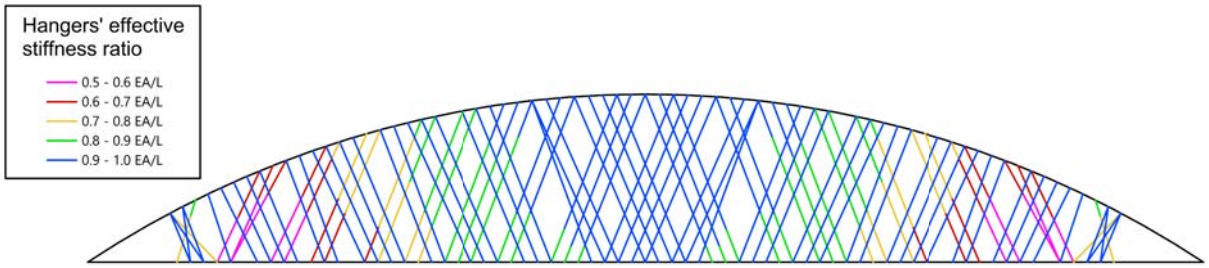

Figure 5.48 The hangers' minimum effective stiffness ratio values for every hanger and every vehicle position.

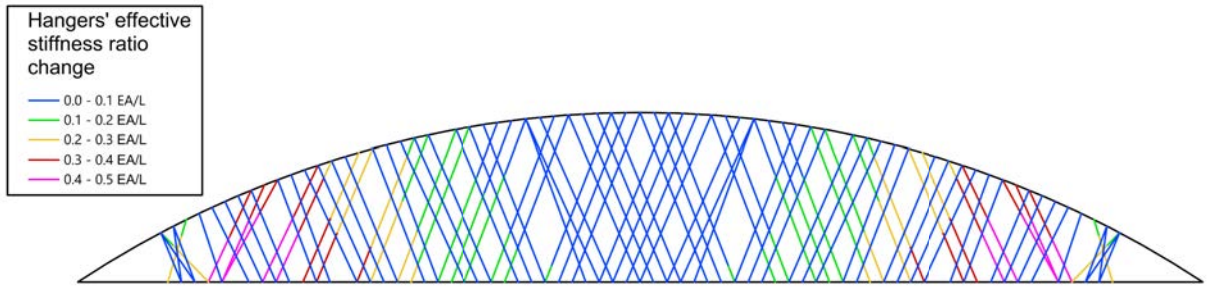

Figure 5.49 The hangers' effective stiffness ratio values change for every hanger and every vehicle position.

5.2.4 GA - stage 2

The results from the genetic algorithms were not achieved due to technical issues from the very beginning.

Galapagos was a great tool for small task optimization, but for greater and more time-consuming task, it started to be the bottleneck of the whole process. The first thing was, that the user had to run Galapagos after each step in the second stage in the optimization algorithm. That slowed the algorithm and required user to be present during the calculations, which was against the idea of automated optimization process, which was crucial when the simulation was planned to last days or even weeks. The problem would be even greater than in ESO phase 2 mentioned in Sec. 5.2.3, since GA required multiple individual geometries to be calculated during one iteration step, and the time needed would be proportional to the population number. In ESO, each step included one geometry to consider.

The second thing was too random selection of input data for the first generation. It caused many instabilities during the calculations in SOFiSTiK, which stopped the solver. This issue might have been solved by predetermining the first generation, but Galapagos allowed to make only one predefined data input and made all other randomly within the given parameters' domains. Nevertheless, even if the first generation did not imply any instabilities during the calculations in SOFiSTiK noticed in ESO investigation, the mutation caused significant change of hangers' topology, especially when two hangers were selected with a great distance from each other. The solution to this issue was to base the mutation on the point or multi-point mutation, but Galapagos did not allow to choose which option could be used.

The third, and the most important issue, was related to the way how Grasshopper worked. When Galapagos changed the value of the variable, it caused the change of geometry, loads and the code for exporting data. When it reached the import/export component, it exported the

code needed to export the data to the text file and the text file with the information, that the import/export component should be refreshed to import the data to the Grasshopper file. The problem was, that when the data were passed through this component, the goal function component related to the output of the import/export component was refreshed even if it did not change the results, because the internal force had not been still updated and calculations were done in meanwhile. When the import/export component was refreshed after the calculations, it triggered the goal function component for the second time. For Galapagos, the first value provided to the goal function component was considered as the one related to the current case, which meant, that the results were correlated not with the current but the previous geometry. The second issue was that, the cross section properties were taken from the data available in the Grasshopper file, which were also connected to the goal function component and triggered it before the new results from the import/export component had an impact on the goal function value. These two issues were supposed to be solved by the data dam component, which forced the wire signal to wait until the results from other component were updated, but the import/export component was triggered twice during one loop, so this method did not work. Then the import export component was divided into export and import components. The calculations were going in between these two components, but since the data were exported from SOFiSTiK's database, every time when the new line of data was added to the text file, the import component in Grasshopper refreshed its value, even though the export was not completed, which provided partially new and partially old result for goal function determination. This method was tested earlier on a simple task of freely support beam with I-shape cross section optimization, but the only data exported then was the bending moment, so one value and the problem was not noticed. The only solution left was to refer to the SOFiSTiK's database directly by API reference, but Grasshopper did not allow at that point to import libraries other than predefined, so SOFiSTiK's libraries were not implementable (Rhinoceros 7 and Grasshopper 1). Regardless of these problems, Grasshopper itself used to occasionally lag when the data were imported, which crashed it, closed the software and stopped the whole optimization process.

5.3 Conclusions

After the investigation made in the approach 1, the summary of the experienced and potential problems, that might occur but were not investigated, was presented in this section.

5.3.1 Stability

During the PUSH procedure, the buckling shape was supposed to have an in-plane arch-oriented form. Instead, **the arch experienced significant twist near skewbacks for high FDL value or twist near the middle of the arch for lower FDL values**. Despite the restricted movement of the arch in out-of-plane direction, the out-of-plane related internal forces occurred in the arches. Furthermore, **the first forms were bracing-oriented instead of desired arch-oriented**. The out-of-plane buckling phenomenon in case of restriction implementation could be fixed in LBA by added torsional restrictions along the tangent vector of the arch in each anchorage node. The author did not see this solution to work in NBA, since these restrictions should be applied from the very first iteration of the ULTI procedure, which would affect the internal force distribution in the arch and would make their values artificially changed. Another **solution to the torsional form would be the rectangular or circular hollow section implementation to the arch instead of the H-type section**, which would significantly increase the torsional stiffness of the section in relevance to its bending and axial stiffness. **The solution to**

the bracing buckling occurring before the arches' buckling and arches' unintended out-of-plane buckling could be solved by geometry definition in 2D instead of 3D. The degrees of freedom that would allow for the out-of-plane buckling would not be present and the bracings would not be modelled. That would not allow to determine χ_{op} value, but its value was mainly dependent [35, 4] on the properties related to the out-of-plane characteristics, including: (i) portal frame size and stiffness, (ii) bracing system stiffness, (iii) out-of-plane moment of inertia of the arch ribs, (iv) inclination of the arches, as well as (v) hangers' arrangement. Because of that, it was decided, that the characteristics (i)-(iv) would be responsible in the determination of χ_{op} and would be a separate optimization task independent from in-plane optimization. **Since the thesis was related to the hangers' arrangement, it was justified to focus on in-plane stability and do not include out-of-plane instability.**

5.3.2 General method

As one of the general method requirements, the imperfection in-plane should be applied for the sake of $\alpha_{ult,k,ip}$ value determination. As investigation showed, the nonlinear buckling analysis should be used over the LBA in case of any hangers' arrangement. For a well-defined network-type arrangement, the analytic equation was a good critical force estimation. Since any hangers' arrangement was intended to occur in the optimization process, the nonlinear analysis was preferred as more general. This approach required the post-critical analysis with PUSH procedure from SOFiSTiK. **The equilibrium path obtained from this method did not look as expected for the cases considered with time demand up to about 2 hours**. The more precise the calculations were, the more converged the solution got. In the everyday case, greater time demand of the calculations would be acceptable, but in this optimization case, where each calculation had to be repeated more than hundreds/thousands of times, the calculations of even 5 minutes was considered too long. Moreover, the PUSH procedure provided the equilibrium path, which exhibited the undesired sawtooth fluctuations after the post-critical point. **This phenomenon cast doubt on the credibility of the obtained results**. **The proposed solution was the 2D model instead of the 3D, which would decrease time demand and limit the potential instabilities probability. The general method could be used in the proposed simplified form, where instead of geometrically imperfect form, the in-plane buckling factor χ_{ip} could be used. That would remove the need of PUSH procedure and would remain much stable ULTI procedure with nonlinear critical load factor determination until reaching the critical point on the equilibrium path for the χ_{ip} coefficient determination purpose**. That would keep the influence of the geometrical nonlinear behaviour of hangers in the analysis and omit the problematic nonlinear imperfection form investigation. **Lack of imperfection form implementation would cut the time needed at least twice as well. The simplified approach with χ_{ip} coefficient would be conservative in comparison to the UGLI method implementation [67, 66]**, but time restriction was very crucial factor of the entire process. The χ_{op} would not be determined in the analysis for the reasons as presented in Sec. 5.3.1. **The load amplification factor $\alpha_{ult,p,k}$ without imperfection would be applicable and the in-plane imperfection would be substituted by the χ_{ip} coefficient.**

5.3.3 Hangers sagging

The investigation in the ESO from Sec. 5.2.3 showed, that **the sagging effect** of the hangers was mostly concentrated in the region located at one-quarter of the span length distance from the ends, and the minimum effective stiffness ratio was equal to 0.50, which was considered low. **That would cause a higher bending moment amplitude in the arch in this region,**

which was not preferable. To prevent that, the pretension force should be applied. Since the distribution of the minimum sagging effect was localized, the pretension force application should follow this distribution to compensate for smaller tension force and not add more where it was already tensioned enough from the sagging effect point of view. **Hangers cross section should be chosen with smaller cross section area if possible, since that would compensate the sagging effect as well.**

5.3.4 Too detailed traffic load application

The traffic load application was too detailed. As a practical approach, **the most important load cases were load applied on the full and half length of the span. That would limit the number of loadcases from twenty-one to only two.** It was true that the hangers would be less utilized in the 2 load cases scenario, since the localized effect of the movable load would not be considered, but it was acceptable as a part of the simplified approach. Load application on both full and half length of the span was more significant from the global point of view than applying uniform load at full width and moving loads locally. Also, the arches' steel mass was greater than the hangers' steel mass [75], which justified the global approach as well.

5.3.5 Galapagos limitation in Grasshopper

The main problems with Galapagos genetic optimization in Grasshopper were related to great time consumption, low control of the process, errors of the Grasshopper combined with incorrectly working import/export components and goal function information exchange, as well as the need of manual intervention in the optimization process. **These issues could be solved by orienting the GA optimization process in the external Python code**, using Grasshopper for only geometry generation, **simplifying the model to 2D and limiting number of load cases**. Moreover, **the own coded algorithm without any external libraries would have as much flexibility as needed for the optimization process and individual part of the optimization algorithm could be changed according to current needs and improvement possibilities**. This was not possible with predefined solver.

5.3.6 Concrete capacity determination

The design of the post-tensioned tie would add unnecessary complexity to the process. Tendon trajectory optimization could be a separate optimization task in its complexity and would be a topic for separate research on its own. If the hangers' positions changed, the change in bending moments in the tie would occur. The tendons trajectory should be then changed to compensate for the change of the bending moments and keep the concrete section always compressed. This process would be iterative since the structure was calculated nonlinearly, which would increase time consumption of the calculations at least twice if the process succeeded after first iteration. Otherwise, the capacity of the tie would be exceeded, and the optimization algorithm would consider the promising geometry as not worth investigating anymore and remove it from the system after next iterations. This would be waste of potential, since right tendon trajectory shaping would solve it without any effect to the hangers and arch force distribution if the concrete side beams would not require cross section dimensions change. **The solution to this problem would be steel tie.** In general, for road bridges up to 15 m in arches' spacing, the post-tensioned concrete slab was recommended [115], but for the sake of simplicity and time saving, the steel tie would be preferable. The bridges with steel-composite ties had been constructed, so this solution was not unusual, **but could be potentially more expensive**. The

concrete deck could be treated as non-structural component of the tie's cross section in longitudinal direction, which would allow to apply it as a load and exclude it from the design process assuming, that the capacity of reasonably assumed thickness of the deck was always fulfilled.

5.3.7 ESO limitations

The optimization responsibility split into elimination managed by ESO and geometry adoption managed by GA was considered reasonable, since it was better to focus on one optimization problem at the same time. This approach would end up in the local goal function value as presented conceptually in Fig. 5.12. However, **stage 1 would generate the same solution as an input to stage 2, so this stage could be run once**. The obtained hangers' angular principles matched the solutions from the literature for the CSM arrangement [75]. **A better approach would be to take the different initial arrangements from literature as a starting point, which would allow to omit stage 1, reduce the time consumption and allow more flexibility by the investigation of initial arrangements other than CSM type.**

Stage 1 limited the possibility to manually defined initial geometries. The GA managed by Galapagos did not allow to manually predefine the initial population except one geometry, since others were generated randomly. If the randomly generated geometry were better than the only predefined one from the ESO stage 1, then stage 1 could be omitted in the process.

The ESO was implemented into the optimization algorithm, since the reasonable mechanism, which would allow to change the number of hangers as an extension of GA. However, **it would be a better solution, if the number of hangers changed in the GA optimization process and was not limited to only one fixed number of hangers reduced earlier by ESO. If the procedure providing the possibility of hangers' number manipulation and mixture of hangers' arrangement with different number of hangers was implemented into GA, the ESO principles could be substituted by more sophisticated GA.**

5.3.8 Local extremum

Even if the GA data-updating issue was solved, the convergence of the algorithm remained unclear. The genetic algorithm was limited by the ESO due to deletion of hangers from the system. Because of restricted number of generations in GA, the chance of reaching optimization task's convergence was reduced. The GA might reach better results for fewer number of hangers not because it was the best possible one, but because the GA did not have enough generations in one of the higher hangers' quantity case. As a result, the advantage of GA was not fully used. **It was considered better to allow GA to optimize with greater number of individuals in the population and/or greater number of generations instead of repeating the optimization task for limited number of hangers by every ESO step. Adding possibility of manipulating with the number of hangers during GA process was considered as the solution to this problem.**

6 Optimization algorithm - 2nd attempt

6.1 Description

6.1.1 Software

As in approach 1, SOFiSTiK FEA software was used for obtaining internal forces and deflections from the prescribed FEA model. For the geometry and task generation, Rhinoceros supported with Grasshopper was used. Its purpose was geometry and analysis definition. The data was imported from the text files generated by external Python code. Grasshopper exported the geometry, loads and analysis principles coded in SOFiSTiK input language into text files. These files were executed in SOFiSTiK's WPS by the external Python code. Grasshopper and SOFiSTiK were considered as extensions for obtaining needed internal forces, displacements, and nonlinear critical load factors, which were imported by direct references to the SOFiSTiK database by Python API provided by the SOFiSTiK's provider. **The genetic optimization algorithm was an authored script without external optimization-oriented libraries. The code was improved based on the tests conducted to make the algorithm more efficient and provide greater cost minimization, check its performance and outputs, fix errors.** Not all the tests conducted were presented, but the ones with the greatest improvements to the algorithm.

6.1.2 Geometry

The first step in time reduction was defining the geometry in 2D not 3D. In consequence, the out-of-plane critical load factor was unable to be determined. Hangers impact on out-of-plane buckling was much less significant than the in-plane buckling, since hangers' change of length, and as a result the effective stiffness, had more impact for the deformations in-plane rather than out-of-plane. The bracings stiffness and spacing and arches' out-of-plane stiffness were the most driven factors in out-of-plane critical load factors value determination. The bracings were not optimized in this model and the arches' cross sections were chosen circular, which provided equal stiffness in both directions. Since the thesis was concentrated around hangers' topology optimization, that justified the change from 3D to 2D system and focus on arches, ties and hangers as the more price driven components. By default, the axial distance between arches was considered as 12.0 m and was used as a reference distance when applying non-structural and variable traffic loads.

The second step was change of tie cross section from post-tension concrete to steel. Both arch and tie had circular cross section. It simplified determination of utilization and optimization process, since only two variables were needed, the diameter and the thickness. Due to lack of post-tension force, less variables were needed in the optimization model, reducing complexity. The cross-section class of both tie and arch was checked in each iteration to not allow 4^{th} class to occur. Thin wall parts were not wanted in bridges due to increased vulnerability to fatigue. It would also complicate the solution for hangers' anchorage and other structural connections from a practical point of view. At least 3rd class was required in the optimization algorithm. The wall thickness was increased to the minimum fulfilling the 3rd class criterion achievement. The cross section along the arch's and tie's length was considered constant, which was both practical and reduced the number of variables if the sections were intended to change along the bridge. In the examined Cracow NAB the arch increased its cross section in the regions close to the skewback. That aspect was not considered to avoid additional variable in the process.

The next change was related to skewback. By default, there were no skewbacks implemented into the model. The exception from this rule was the test of the existing structures when

the skewbacks were present in the structure. Skewbacks provided more stiffness in the support region which had significant effect on the results of the hangers, which was not desirable when any configuration of hangers was possible during the optimization process.

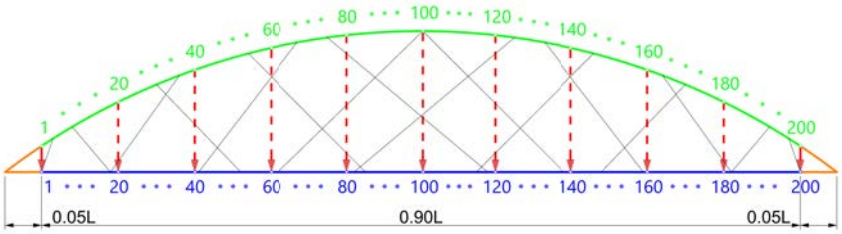

Figure 6.1 The numbering system for the structure.

6.1.3 Loads

Load were also simplified as well as the geometry. Since the tie was modelled as a circular hollow section, the concrete deck was considered as non-structural part and was applied as a line load along the tie. The deck thickness was assumed to be 0.60 m with all layers and cross beams supporting the deck. The total weight was then $0.60 \cdot 12.0/2 \cdot 25 = 90kN/m$. The self-weight of all structural elements was automatically calculated by the software.

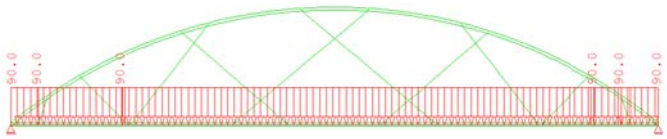

Figure 6.2 The permanent load case application on an example bridge.

The traffic load was simplified to two load cases, which are considered as the most unfavourable ones for NAB. The first was a uniformly distributed load along the tie and the second was a uniformly distributed load along the half of the tie's length. The first load case is supposed to cause the highest possible normal forces in the arch and tie. On the other hand, the second load case causes the highest bending moments in the arch and tie. Hangers used to be more stressed when the load is applied on the half of the tie. The traffic load was assumed as the highest possible uniform part of LM1 road traffic load according to Polish national Annex, which is $q_{UDL,max}$=12.0 kPa. Instead of tandem TS load, the maximum UDL load was considered at all lanes. The number of possible lanes was 4 with the width of 3.0 m each, which means that the traffic load was applied at the total axial distance between the arches. The resultant load was $12.0 \cdot 12.0/2 = 72kN/m$. The load was decided to be amplified by the combination factor of 1.35, resulting in 97.5 kN/m in approximation, since the Tandem component was not included.

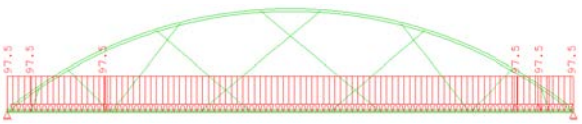

(a) Full span length load application

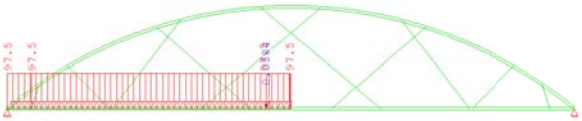

(b) Half span length load application

Figure 6.3 The traffic load application on (a) full span and (b) half span on an example bridge.

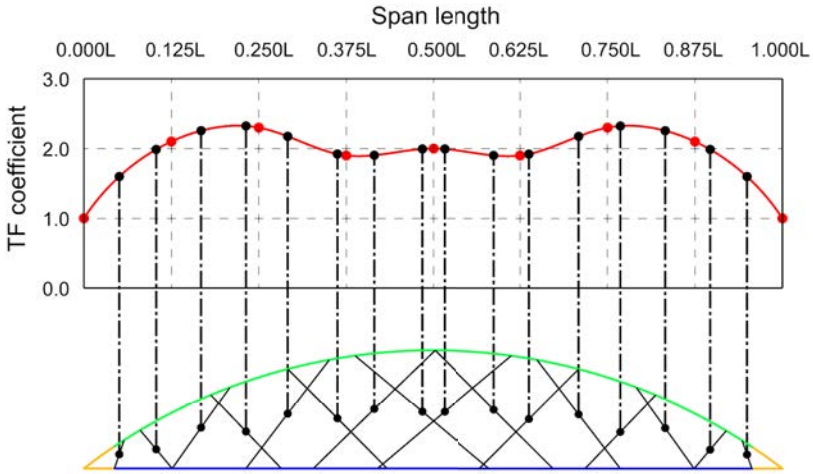

Figure 6.4 The pretension force coefficient graph example with 9 symmetrically distributed interpolation points and the hangers' center point projections on the interpolated function.

The pretension load for hangers was decided to be applied in this attempt compared to approach 1. The reason behind it has been already described in Sec. 5.3.3. To not add too much complexity to the optimization task and determine pretension force for every hanger individually, it was decided to define a 9-grade symmetrical polynomial as a weight function for pretension force in hangers, so called pretension force (TF) coefficient. The default pretension force was set to 300 kN for the shortest hangers and it increased proportionally to the length of the hanger. If the longest hanger was twice as long as the shortest hanger, the default pretension force for it was 600 kN. Then pretension force in every hanger was multiplied by the polynomial function value of TF coefficient, which ranged between 0 and 3, Fig. 6.4. The center point of the hangers was chosen as the representative coordinate when projecting it on the TF coefficient function.

6.1.4 Design and combinations

The ULS and SLS were checked. The ULS for the arch was based on the simplified general method expressed by Eq. (5.8), which was considered conservative [67, 66]. The argumentation behind utilizing χ_{ip} and not considering χ_{op} was also included in Sec. 5.3.2 and Sec. 5.3.1, the simplified formula was presented in Eq. (6.1).

$$\frac{\chi_{ip}\alpha_{ult,p,k}}{\gamma_{M1}} \geq 1.0 \tag{6.1}$$

To determine the value of the $\alpha_{ult,p,k}$, the resultant stresses were used in the perfect geometry with TH3 analysis in order to include hangers sagging. The value of γ_{M1} was set to 1.1 as for bridges in general version of code EN 1993-2 [134]. The buckling factor χ_{ip} was determined for the geometrically nonlinear analysis with ULTI procedure until reaching the critical point. When it came to the tie, in the ULS the resultant stresses were used and since the tie was always in tension, the buckling coefficient χ_{ip} was not applicable. Nevertheless, the safety factor γ_{M0} for the tie was set to 1.1 as for buckling state for simplification purposes. In ULS design for hangers, their characteristic capacity was divided by safety factor of 2, which was higher than the standard safety factor, but according to author's experience, that should cover the utilization

check in fatigue limit state. This reduced time consumption needed for considering another type of fatigue loads.

The SLS design was reduced to the check of deflections of the tie. It was justified by the fact of using the same load factors in ULS and SLS, so the check of stresses in SLS was fully fulfilled by ULS criterion. The deflection, however, was checked by reducing the deflections of tie from the half and fully loaded loadcases by the deflections of the self-weight loadcase. The maximum allowed deflections of L/600 were chosen as default. The deflection criterion changed according to the analysed bridge, but the L/600 was the default value during tests. The load amplifications were equal to 1.0 for both ULS and SLS for simplification.

6.1.5 Parameters

The variable parameters included the change of the cross sections' dimensions and materials, bridge geometry and pretension forces for hangers. Other aspects such as bridge span, width, type of arch's curvature, applied loads except hangers' pretension forces, type of conducted analysis and prices per steel grade and hangers' assembly per hanger were considered as constants for the analysed case. Parameters might change when comparing with the existing structures, especially the variable loads. The default constants and variables were summarized in Tab. 6.2 and Tab. 6.1. The price origin of structural steel was already described in Sec. 5.1.6.

Table 6.1 Variables in the optimization algorithm

	Variables	Range
Bridge	length-to-height ratio	5 - 7 every 0.2
Arch	steel grade	S235, S275, S320, S355, S420, S460
	cross section	hollow circular
	diameter	0.5 - 3.0 m every 0.1 m
	thickness	0.005 - 0.100 m every 0.005 m
Tie	steel grade	S235, S275, S320, S355, S420, S460
	cross section	hollow circular
	diameter	0.5 - 3.0 m every 0.1 m
	thickness	0.005 - 0.100 m every 0.005 m
Hangers	diameter	10,12,16,20,24,30,36,42 48,56,64,76,85,90,100 mm
	pretension force coefficient	0 - 3
	pretension force constant	300 kN
	steel grade	S235, S275, S320, S355, S420, S460
	quantity	8 - 50
	position on the arch	0.05 - 0.95 L
	position on the tie	0.05 - 0.95 L

Table 6.2 Constants in the optimization algorithm

	Constants	Range
Bridge	span length	60-200 m
	curvature type	circular
	width	12 m
Load	load case	half, full and self-weight
	class	road based
	traffic value	72 kN/m
	permanent value	90 kN/m
Design	criteria	ULS & SLS
	analysis	GNA
Cost	structural steel	S235 - 15,500 PLN/ton S355 - 18,000 PLN/ton S460 - 20,500 PLN/ton
	hangers assembly	5000 PLN/anchor/side

6.1.6 Goal function

Authors based the goal function in the second optimization approach on the solutions presented already in the description included in Sec. 5.1.7 from the first optimization approach. The formula from Eq. (5.7) was modified in order to adopt constant punishment factor *p* to the increasing span length *L*. The reference length was used from the Cracow NAB on which the first optimization approach was based, where the span span length was equal to 120 m. Since the static schema of the NAB is the freely supported beam, the punishment increasing component depended on the normalized influence of the span length was raised to the second power, as presented in Eq. (6.2).

$$\min_{v} GF(cv, v, \eta, p) = \begin{cases} C(cv, v) & \text{if } \eta \leq 1.0 \\ C(cv, v) + \left(\dfrac{L}{L_{ref}}\right)^2 \cdot \eta \cdot p & \text{if } \eta > 1.0 \end{cases} \tag{6.2}$$

where *C* was the total cost expressed in PLN, η was the maximum utilization, *cv* were the constant values from Tab. 6.2, *v* were the variable values from Tab. 6.1, *p* was a punishment component set to 10^8 PLN, *L* was the span length of a considered bridge, which was a part of the set of constant values *cv* and L_{ref} was the reference span length of Cracow NAB equal to 120 m.

Since bridges in the initial population had varying number of hangers and all the geometries had utilization below 100%, the goal function put in favour geometries with lower number of hangers, since they were cheaper due to lower number of hangers. In the initial tests, this issue was solved by assuming the same goal function value for all the individuals in the first population. This solution was not perfect, since elimination at the end of the first population was random. Therefore, new solutions were investigated and described with more details in Annex D, Sec. D.6 and concluded in Sec. 6.3.6 and Sec. 6.3.10.

6.2 Definition - general concept

6.2.1 Files structure

The principles presented in this chapter were the starting point for the tests conducted later, which modified and improved the algorithm. The tests were conducted before the final analysis. The algorithm was divided into 5 phases: initial population, selection, crossing, mutation and tournament. The optimization algorithm was defined in Python code in 4 dependent files. The main execution file was called *GA*, where the optimization algorithm was defined and the data inputs. The support files were called *GA_help*, *cdb_import* and *calc*. The functions defined in them were used in the main *GA* file via library references. The main structure of the files remained unchanged in the process. For the reader's convenience, the detailed description of each of these execution files was presented in the appendix C.

6.2.2 Initial

It was decided, that for the initial stage, the hangers' angle had been used from the final result from the optimization algorithm in the first attempt. This angle of hangers was about 67.2^o to the horizontal line. The results were not satisfying in comparison to any well-known hangers' arrangement. Due to that, the hangers' arrangement, which did not represent any known topology, was proposed. The reason behind it was not to initialize the calculations with the already known good solutions and add a kind of noise. The number of hangers were set from 10 to 40 every 2, so 16 unique geometries in total. The sample hangers' arrangements were presented in Fig. 6.5.

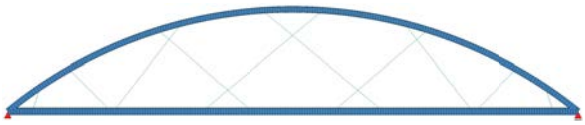

(a) Initial topology with 10 hangers

(b) Initial topology with 24 hangers

(c) Initial topology with 40 hangers

Figure 6.5 Three examples of hangers initial topology

The angle was not the same for every hanger, since the arch and tie were defined discretely and distribution of hangers anchorages in the arch and the tie were described by a function, Eq. (6.3)-(6.4).

$$P_a(n,i) = \max\left[\min\left[\frac{N-1}{n-1}\cdot i\cdot(a_1(n)+i/b_1(n))\cdot(-1)^i/c_1(n), N-1\right], 0\right] \tag{6.3}$$

$$P_t(n,i) = \max\left[\min\left[\frac{N-1}{n-1}\cdot i\cdot(a_2(n)+i/b_2(n))\cdot(-1)^{i+1}/c_2(n), N-1\right], 0\right] \tag{6.4}$$

where P_a was the position on the arch, P_t was the position on the tie, n was the considered number of hangers, i was the position of current hanger, N was number of nodes on the arch and remaining a_1, b_1, c_1, a_2, b_2, c_2 were the coefficients determined individually for all numbers

of hangers. Galapagos with genetic algorithm was used for the determination of these coefficients iteratively. It was obligated to minimize the sum of square differences between individual hanger's angle and the desired 60^o angle, which was chosen obligatory, by manipulating with that 6 parameters.

The idea behind these functions was to make a hangers' arrangement in the initial population, that was not defined as other well-known solution, in order to not include already optimal network arch principles from the literature, which might narrow the exploration of the optimization algorithm. The geometries used later in the simulation for the initial population were presented in Annex E and the number was reduced into range from 12 to 40 number of hangers with step size of 4 instead of 2, since the initial predefined population was considered too great.

The cross sections for the arch, tie and hangers were set the same for every geometry. The diameter of the arch was 1.3 m, thickness 0.05 m and steel S320. The diameter of the tie was 1.5 m, thickness 0.04 m and steel S320. The diameter of the hangers was 0.085 m and steel S460. Even though the structural steel S320 was less common than S235 or S355, its yield strength was in between these two steel grades, which justified this choice. The bridge height was 21.4 m with span length denominator of 5.6. Hangers' initial pretension function coefficients were set to 1, 2.1, 2.3, 1.9 and 1.5 respectively. The data about variables, pretension forces coefficients and permanent values were stored in vectors. The permanent vector was not changed during the optimization process.

When the number of parents was set greater than 16, for example 20, the remaining 4 geometries were chosen randomly with uniform PDF. The number of geometries should have always been even and that applied to the number of parents as well. The individuals were defined with the same permanent and pretension vectors, but the variable vector was different in just hangers' topology. After the definition, the cost function was utilized for each geometry including utilization, cost and GF value determination. The output results were assigned to the result vector.

The geometries and loadcases were calculated and data were imported by API. The results, including utilization of each finite element, utilized limited deflection, buckling coefficient, costs and goal function value were stored in the result vector.

Apart from that, all this information was exported to the text files to make tracing of the results easier in post-processing. Before exporting, a folder was created for each individual geometry. The main folder was called `GA_num`, where the `num` was the current generation's number starting from value 0 for the initial step. There was a folder structure inside the main folder with the name `ind_i`, where `i` was the number of the individual geometry, starting from value 0 for the first individual. When it was done, the Selection phase started.

6.2.3 Selection and Coupling

Since the number of individuals was mostly in range between 20 and 30, it was decided to isotropic selection, where almost all individuals were selected. The number of created pair was set in the `GA` function and used to be close to the maximum allowed. That implicated lack of local groups forming in comparison to biased selection. If the number of individuals were higher than 50, it would have been opted for biased selection, but due to long time consumption of the calculations, it was not considered.

The number of individuals in one pair was always two. The geometries were chosen randomly according to uniform PDF. All individuals' IDs were arranged in a list of pairs. The first ID in each pair was always smaller than the second ID in pair.

6.2.4 Coalescence

For greater diversity in descendants impacted by smaller number of individuals in the population, the blend coalescence was implemented. Both parents' genes were equally important.

The new variable, pretension and result vectors for descendants were defined. The permanent vector was not needed, since it was always the same for both parents and descendants.

Material, dimensions, pretension The determination of the material, cross section geometrical properties and pretension forces were chosen uniformly random between parents' gene values. First of all, a uniformly random real coalescence number between 0 and 1 was chosen individually for each pair. This number reflected the relatedness to the first parent in the pair. For the example of the arch diameter value, if the random number was 0.3 it meant, that the first descendant would take 0.7 diameter dimension from the first parent in the pair and 0.3 from the second parent. The second descendant would then be defined in the same way, but the relatedness was the opposite. That always created symmetrical descendants.

Hangers intermediate mixing This parameter was the most complicated among all variables. That required 6 versions to get the desired result.

The function responsible for mixing two hangers' topology was defined. Function created two geometries for a given coalescence number. It required to provide hangers position at the arch and the tie of both parental geometries in form of node number, coalescence coefficient for the first and the second generated geometries, bridge height from both parental geometries and the span length.

The function obtained the hangers angle at the first step based on the node numbers, bridge height, known division and the fact that the arch was described as a part of a circle. The second step was the hangers' center coordinates. The data hangers and the assigned angle were sorted in respect to hangers center position. Next the hangers' center positions were plotted on a graph as vertical assignment and normalized hanger ID number as horizontal axis. Since the data was discrete, the graph was turned into continuous polyline-shape function. The example was presented in Fig. 6.6 and Fig. 6.7.

(a) The first parental geometry (b) The second parental geometry

Figure 6.6 Example of parental geometries

The first parental geometry was a NAB type topology represented by a green graph, Fig. 6.7. The second was a Nielsen type topology showed as blue graph in the same figure. In network arch bridge, the distances between hangers' anchorages in the curved arch and the straight tie were the same, but because of unparalleled correlation between the arch and the tie, the center distances used not to be even which caused the zigzag pattern on the graph. On the contrary, in the presented Nielsen arch bridge the distances of the hangers' center point were set equal, which was presented as a straight-line graph. The NAB had 48 hangers, and Nielsen type arch bridge had 12 hangers. The coalescence ratios were set to 0.7 and 0.3 respectively, which resulted in 22 and 38 hangers' topology. The horizontal axis was then divided into the obtained number of hangers and values for these arguments were determined for both parental functions represented by the respective points. The final step was the linear interpolation for

both descendants relating to the coalescence ratio. The first ratio was 0.7, so the resultant points were further from the NAB topology. The opposite correlation was observed for the second 0.3 coalescence ratio.

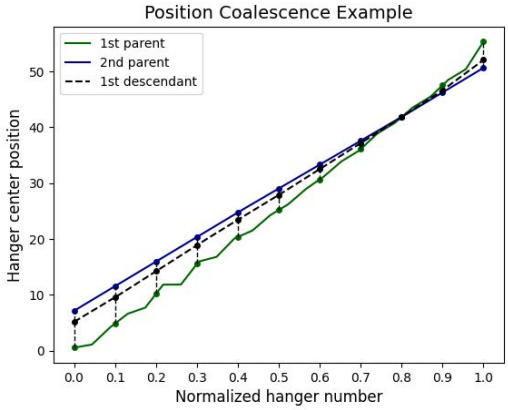

(a) Position for the first descendant with 70% coalescence ratio to the first and 30% to the second parent

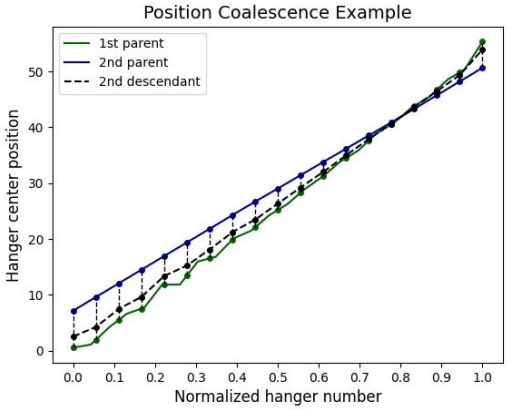

(b) Position for the second descendant with 30% coalescence ratio to the first and 70% to the second parent

Figure 6.7 Example of descendants' hanger center point determination for (a) the first and (b) the second descendant

After achieving hangers' center positions, the next needed data was the angle value. It was solved by choosing the closest hanger from both original hangers' topology to the considered hanger from the new geometries and assigning its angle to it. There was no linear interpolation of hangers' angles between both parental geometries. It was tried in earlier variant of this algorithm, but it was not succeeded in the desired way. After many generations, the hangers used to get more and more vertical when the coalescence ratio was applied to the hangers' angle, so it was abandoned. With the presented approach, the angle value was inherited from the parents in similar way to crossover coalescence. The randomness of this heritage was not specified by the PDF directly but by the deterministic definition of the hangers' distribution and its relation to the original parental topology with indirect dependence to the uniformly random choice of coalescence ratio. With both positions and angles, hangers' anchorages were found on the arch and the tie. The resultant descendants were presented in the Fig. 6.8.

(a) The first descendant geometry

(b) The second descendant geometry

Figure 6.8 Example of descendant geometries

The network topology trend was included in both descendants. The second descendant (b) kept the same angle in the most centered hangers as from the first parent. More triangular trend with different angles than in the center was observed for the regions closer to skewbacks, which was inherited from the second parental geometry. The angle in the middle was similar for both parental geometries, but it started to diverse in Nielsen topology in closer range to skewbacks, which explained keeping network trend in the middle and diverse in the skewbacks. On the other hand, the first descendant (a) was dominated by Nielsen topology in the middle but hangers were

doubled at the trace of Nielsen-like topology. For the ranges closer to skewback the topology evolved into topology similar to vertical but at the same time it was skewed into one direction, which looked similar to half of Nielsen hangers' arrangement. The reason behind the same angle was the mechanism of choosing the angle of the closest hanger, which coincidentally was skewed in the same direction. As expected, the first geometry was more similar to the second parental geometry, and the second descendant to the first one.

Ending procedure The generated variables were assigned to the variable and pretension vectors of descendants. Each descendant required determination of the GF value and the results were stored in the result vector of descendant. The data were exported to the `txt` files in the corresponding folders. Descendants' folder numbering continued after the last parent's folder number `ind_i` within the same generation folder `GA_num`. At the end, the vectors corresponding with descendants were added to the main vectors defined for the entire population, in the same order as their IDs in the folder structure. This expanded population was an input in the next process called mutation.

6.2.5 Mutation

The decision, if the individual should have been mutated, was proceeded uniformly random. It was allowed, that all or no individual were mutated. Both parents and descendants were considered. The mutation was applied to all individuals' variables except the number of hangers. The normal PDF was chosen when determining the change of variable value. It allowed to change the variable's value with the greatest probability around its non-modified value. The standard deviation was unique for variable and pretension vectors. Even though the PDF was continuous, the chosen values were rounded to the nearest integer value for variables, which represented the change of the position number in the predefined list of allowed variable values. For the pretension variables the values were not rounded to the nearest integer, but they were applicable directly to the original pretension vector values. The individual with the best GF value was not mutated, since it was not desired to lose the best geometry. This decision added a mechanism similar to a swarm algorithm. It was considered reasonable to keep the best geometry and allowed other to slowly follow the best solution with possibility of finding better solution in this process. The more diverse spectra of individuals, the less gradient-oriented algorithm.

The number of hangers was not changed, since the output was too unpredictable and the effect of changing number of hangers was greater than the change of other variables. To avoid favouring this variable over others without a significant change of deviation, it was decided to keep the number of hangers unaffected in the mutation process.

The change of ID value generated from the normal PDF was stored in the index mutation vector, where the change of pretension value was stored in the pretension value change mutation vector as float numbers directly applicable to the pretension vector. The information of which individual required mutation operation was stored in the selection mutation vector.

After that the mutation was proceeded. The values from the pretension value change mutation vector were directly added to the pretension vectors. For other variables, firstly the ID position was modified by adding the index mutation vector to the corresponding ID numbers from variable vectors. Secondly the new variable values were obtained based on the new ID numbers. In the next step, the new folders for the mutated individuals were created with additional prefix `_m` resulted in `ind_i_m` folder naming convention. Then the GF values were determined for all mutated individuals and the results were saved in the corresponding folders.

If the individual did not require mutation proceeding, the files from the corresponding folder without prefix _m were copied to the newly defined folder with _m prefix. It saved time of unnecessary proceeding of the already processed individual.

In the final step, the folders without prefix _m were deleted from the GA_num folder, since they were not needed anymore and the disk occupation was released.

6.2.6 Tournament

The tournament was the final step in the GA. The previous mechanisms were responsible for new individuals creation and modification of all of them. To prevent the whole population from expanding after each generation, the elimination process should have been applied. This was the opposition to the trend observed in nature, where the higher number of individuals, the greater chances for species survival, but this dangerous was not present in this algorithm. Thanks to that, the computation power and time consumption of the calculation of a single generation did not increase overtime and kept the time prediction consistent.

First of all, the list of the individuals to eliminate was defined. The selected number should have been double the value of the descendants created. Secondly, the pairs were selected with the uniform PDF. Each pair contained 2 individuals. Based on that, the vector containing the GF values was defined by taking data directly from the result vector. The individual with the better GF value was kept in the system, but the second individual was removed from the vector with pair numbers. It resulted in deletion of half of the selected individual for tournament phase, which was the exact number of descendants. The survived individuals' numbers were defined by excluding the deleted geometries' numbers.

The new variable, pretension and result vectors were created by selecting the geometries from the list of survived in the same order. After that, the new GA_num folder was made with the next generation number value. Inside it, the ind_i folders were done with the numeration starting from 0 and the data from the survived individuals were copied into these folders in the same order, as they were defined in the corresponding vectors for variables, pretension force and results. With that finished, all the steps in a single generation were proceeded and the process was repeated.

6.2.7 Next generations

The initial population determination was not needed in the next generations and its place was substituted by the after-tournament population arrangement from the previous generation. The output from the given generation was the input for the next one. The process contained selection, crossover, coalescence, mutation and tournament phases, as presented in the summary diagram, Fig. 6.9.

Since the freedom for the algorithm at the initial state was recommended to be greater than in the later stages, it was decided, that after specified number of generations, the parameters should have been more restricted. One of the greatest examples of this phenomenon was simulated annealing. The restricted parameters were standard deviation for variables and pretension vector in mutation, number of parental geometries and more restricted GF definition. Higher deviations, greater number of parental geometries and less restricted cost punishment in GF value would help in increasing diversity of the considered space of possible geometries. This would increase chances of finding global extreme GF value and help compensating the negative impact of limited number of individual in a single generation. However, the time needed to find the extreme GF value in a considered local extreme space would increase, if the freedom was limited at later stage by lowering the number of parents and deviations. The proposed solution

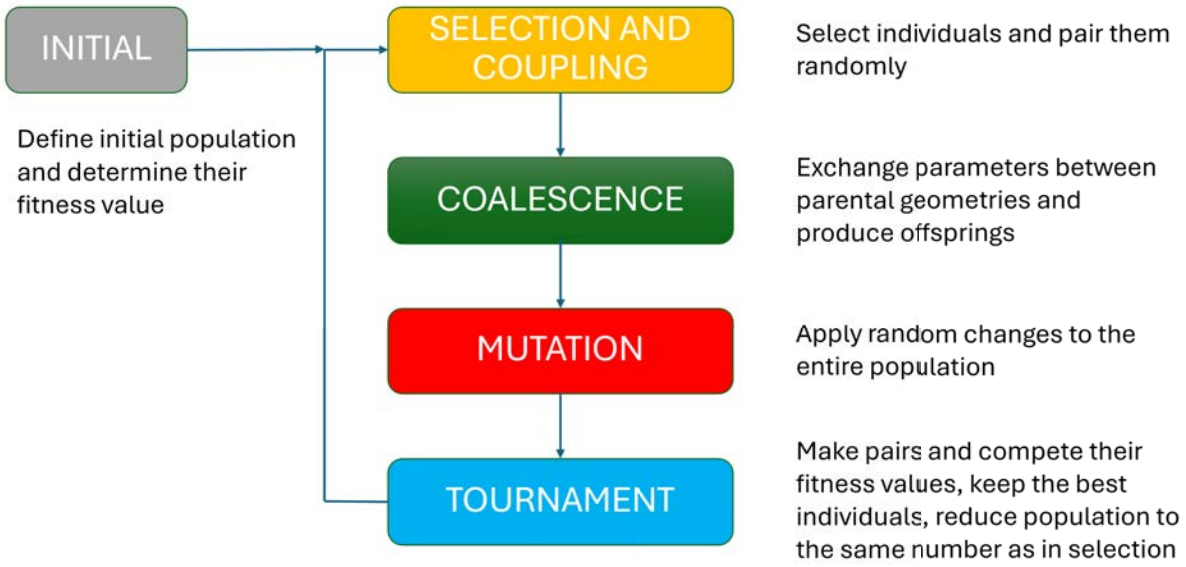

Figure 6.9 The summary diagram of the genetic algorithm

to this problem was keeping reduced but still relatively high freedom for the algorithm in the late stages and adding gradient based stage to the algorithm. The impact of this approach was presented in Sec. D.1 in Annex D and conclusions were presented in Sec. 6.3.1.

6.3 Algorithm tests and improvements

For the reason of algorithm adjustment in terms of time consumption and global extreme value searching process, it was decided to conduct several tests. The tests involved modifications to both the algorithm procedures and the geometry of the bridges.

For the convenient of the reader, the detailed explanations, results and detailed analysis were included in the Annex D. This section included detailed conclusions from each test and general conclusions from all the tests. These tests did not cover the entire possible improvement of the optimization algorithm and this investigation could be extended in the future researches.

6.3.1 Gradient

Gradient-based tests improved GF value three times out of four tested gradients gradations in comparison to the test without gradient descent approach. **It was decided to keep gradient-based algorithm in every future investigation with the gradient step size of 5 as the one with the best results**. Since there were still significant changes of GF values at the latest generations, it was decided to be worth investigating the impact of greater number of generations in a single optimization process. Furthermore, two tests had utilizations of 94.3% and 93.7%, which suggested that there was still potential for improvement. **It was decided worth investing the impact of multiplying the cost of the structure by its maximum utilization in order to gratitude the hidden potential in the structure over the structures with 100% utilization already**. It would encourage the algorithm to consider the geometries with theoretically better potential of cost reduction than the geometries which have already reached their capacities limits and did not have any space for improvement.

The most and the less optimal solutions comparison functioned as expected in terms of utilization distribution along the arch and the tie. The stresses distribution was shifted

into higher utilization compared to less optimized solutions. Bending diagram with smaller amplitudes did not always conclude into worse results, since the best solution had less even distribution than the worst one. Stresses were more reliable measurement criteria than bending moments.

Since the gradient step size of 10 had much smaller utilization than the best solution and it was decided to keep the test including both step size of 5 and 10 to investigate more in details, which approach was better on larger number of samples and with different approaches.

6.3.2 Goal Function modification

The investigation showed a potential for further improvement, since the modified GF value, Eq. (6.5), was smaller than the unmodified GF value even though the absolute costs were greater. The GF value improvement was not noticed at the end of the simulation, which happened for non-modified GF. Therefore, it was decided to conduct longer simulations. Furthermore, **to dispel doubts regarding possibly better solution achievement with modified GF formula, the new calculations should be proceeded, where the best geometry from GSSo5 with modified GF formula was used as an input in a case without any modification to the GF formula. This could be an alternative approach to longer simulations.**

6.3.3 Extended number of generations

The extended calculations for GSSo5 resulted in better cost values but worse GF values compared to short calculations. **Even though the calculations were twice as long, the theoretical, potentially lower costs were still greater than the ones with short tests.** The time needed for shorter simulations was about 2 days and about 6 days for longer tests. The longer GSSo10 tests resulted in better cost and GF values in comparison to the short GSSo10 tests but still, they were worse than the GSSo5 results. **The improvement of less than 2% was not worth spending almost 3 times more time to achieve from the practical, engineering point of view**. The need for longer calculations was concluded to be not worth implementing in further investigations. The GSSo10 was also not considered in further tests, since after multiple attempts it consistently provided worse results than for GSSo5. **The GSSo5 was used as default from this point**.

6.3.4 Initial population with known hangers' arrangements

The Nielsen arrangements got better than Network Arch arrangements after 3rd iteration. It was dictated by the faster optimization of the arch and tie costs than in the network arch in these first generations. The other factor was high utilization of the hangers in all cases, which put limitation to modification of hangers' arrangement. This could be solved by expanding the available steel grades by prestressed steel, which would provide greater capacity and more freedom in shaping hangers' topology. **Due to greater costs of the arch and the tie, it was preferable to not make hangers triggering the punishment component of the GF and allow further progress of structure shaping.**

Another conclusion was to omit mixing hangers' arrangements if there was a risk, that at the initial stages, the commonly considered worse arrangements in terms of costs minimization would take a lead reducing the chance of long-term perspective of improvement. It was considered worth investigation of randomly generated initial population instead of intentionally worse hangers' arrangements.

6.3.5 Prestressed steel for hangers

The manually added hangers' arrangements in the initial generation, which were commonly considered as worse solutions than network arrangements, provided again worse results than only network arrangements in the initial generation. **It was decided to not include intentionally well-arranged worse hangers' arrangements in the initial generation**. **The prestressed steel helped in reaching better results and omitting vertical and Nielsen arrangements in further generations. It was decided to keep prestressed steel as an alternative.**

6.3.6 Manual initiation after standard GF formula

The application of the previous best individual to the initial generation of the new test was a successful implementation. Both considered attempts, BIWNP and BIWAP, achieved lower GF values than the original analysis. The BIWAP, where all of the parameters from the previous best individual were implemented to the manually added geometry in the initial generation, made minor improvement in comparison to the original geometry. The hangers' topology remained almost the same and only material manipulation changed in other parameters. On the contrary, the BIWNP, where only hangers' topology of the previous best individual was implemented to the manually added geometry to the initial generation in the new test with keeping all other parameters as default, achieved major improvement in GF value reduction. The hangers' topology and the arch geometry were drastically changed and all elements got different steel grades than the original geometry. The application of only hangers' topology provided less restrictions in the way of population development compared to implementation of all aspects from the previous best individual.

The presented approach with goal function manipulation by utilization component for the first step of calculations solved partially the issue with goal function manipulation for the initial generations due to different numbers of hangers, mentioned in Sec. 6.1.6. The geometry with greater number hangers had greater price than the structure with lesser number of hangers, which resulted in deletion of the arrangements with greater number of hangers in the first generations. With the cost multiplied by the maximum utilization, the greater the number of hangers was, the probability of smaller bending moment amplitude in the arch and the tie was higher, and so the potential of lower utilization of the arch and the tie was greater. As a result, a greater number of hangers and so greater cost was compensated by lower utilization of the structure. This was true if the hangers were not the dominated utilized elements and if the hangers' arrangement was network-based.

6.3.7 Manual initiation after GF formula modification

Even though the manually added geometry was the best shaped from the previous optimization process, one of the initial hangers' arrangements provided better GF value in APA approach, even though all the initial arrangements were the same in both optimization processes. The only change was adjusting all properties other than hangers' arrangements to match the one from the manually inserted individual. This led to into conclusion, that **the algorithm focused on optimizing many variables at the same time, and the overall optimization process ended up with much better results than the initial set. However, implementation of these set to non-changed topology, resulted in lower cost with initial topology, which meant that the improvement was driven by the reduction of cross section costs rather than the hangers' arrangements.** Nevertheless, both were significant. On the contrary, **not applying all of the parameters to other individuals in NPA approach resulted in more gradual improvement**

over generations than in APA procedure, which might provide more possibilities in exploring for better solution than already restricted and suggestive solution from the very beginning, which was a case in APA, focused on exploitation.

6.3.8 Identical arrangement in the initial stage

Even though both GF value paths over generations were the same for reference and random tests, the distribution of the population was much different between them. **The random test had its populations more concentrated around to the best individual in comparison to the reference test.** The greater variety of geometries was a good sign in GA, since it might result in better investigation of the possibilities in the given domain of possible results. However, the variety described in this chapter was related to the results, not input. The more diverse the results got over iterations, the less divergence the optimization process was. **Despite greater deviation at the beginning, the random test presented better performance from the population distribution perspective than the reference set.** Nevertheless, the mean and median values were oscillating around the same constant value with visible improvement. This trend was expected due to the high complexity of the structure itself.

Application of the already well optimized solution to the system resulted in improvement caused by gradient descent part of the algorithm rather than taking full advantage of other genetic-based part of the optimization process. It was considered worth investigating the system with less utilized geometry, but with keeping random generated population in the initial generation.

6.3.9 Skewbacks impact

Even though both tests were conducted for two different sets of variable loads and assumptions regarding skewbacks, the magnitude of results' deviation was similar to the difference in load values from the statistical point of view. The hangers' arrangements and most of geometry properties were comparable to each other. Tests without skewbacks had still remaining capacity in terms of deflection, which was not a case in the test with skewbacks, where all the utilizations were above 90%. Skewbacks used to have a positive impact on reducing the bending moments at the end of the bridge.

However, in this test it showed that it might not act properly if the skewback's geometry was determined incorrectly. **The bending moments diagram for the test with skewbacks had distinguished peak at the end of tie comparing to other part of the structure, which was not desired**. On the contrary, this phenomenon did not occur for the test without skewbacks and bending moments were more evenly distributed. In future calculations, **the last part of the arch and the tie would not be considered in the design assuming that these regions were shaped and designed properly, which would imitate the advantages of skewbacks and neglect their drawbacks**. The skewbacks required proper shaping allowing for smooth transition of stiffness in order to avoid peaks. **This would add unnecessary complexity to the already complex optimization task, therefore the simplification of not considering internal forces from skewbacks regions were suggested.**

6.3.10 Summary

Author investigated the influence of, among others, (1) integrating gradient descent into the optimization algorithm, (2) modifying goal function, (3) conducting long calculations, (4) including Nielsen, vertical and network arrangements in the initial generation, (5) including

prestressed steel for hangers, (6) manipulation with the initial population by taking parameters of the best individual from the previous step, expressed by BIWNP, BIWAP, APA and NPA approaches, (7) random parameters in the initial population and (8) influence of the skewbacks.

The gradient descent method made calculations faster in reaching the optimal solution comparing to the method without its implementation, as presented in Sec. D.1. The most optimal gradient descent generation step was 5 and this setting was implemented to the algorithm in the next calculations.

Most of the improvements used to happen for the first 50 generations out of 100. Nevertheless, in some cases a non-negligible improvement happened during the last 20 generations. For these reasons, the 200 generations test was conducted in Sec. D.3 but the additional effort resulted in both greater time consumption and deterioration of GF value, so the assumed 100 generations was considered as satisfying for the given conditions.

Since there was a possibility of having two solutions with the same or very similar costs, but different utilization levels, it was decided to gratitude the individual with smaller utilization and expose its potential for further improvement over the ones with similar costs but greater utilizations. In Sec. D.2 the GF formula was modified by multiplying the cost by the maximum utilization reducing the GF value in the process, Eq. (6.5). Other parameters definitions were kept the same as described in Sec. 6.1.6. Thanks to that, the assumption of applying the same goal function value for all the bridges in the first population was not needed. The bridges with greater number of hangers had lower utilizations, and bridges with lower number of hangers but higher utilizations were equalized more in the goal function due to multiplying costs by utilization than earlier, when the reduction influence of the utilization to the costs was not implemented.

$$\min_{v} GF(cv, v, \eta, p) = \begin{cases} C(cv, v) \cdot \eta & \text{if } \eta \leq 1.0 \\ C(cv, v) \cdot \eta + \left(\dfrac{L}{L_{ref}}\right)^2 \cdot \eta \cdot p & \text{if } \eta > 1.0 \end{cases} \tag{6.5}$$

The best gradient step of 5 with modified GF formula resulted in greater costs than the solution without GF modification, but with smaller GF value than the unmodified one reflecting potentially smaller cost. Similar conclusions were obtained with gradient step size of 10, but improvement was less significant and absolute values were greater than for step size of 5.

The longer calculations of 200 iterations conducted in Sec. D.3 with the same assumption of modifying GF formula, Eq. (6.5), for 5 and 10 gradient step size did not provide the answer, if lower modified GF value could practically provide lower costs than the original unmodified formula. Longer calculations did not improve the solution compared to 100 iterations and therefore were not considered in the improved optimization algorithm.

To find the answer to the positive or negative impact of the GF formula modification, the tests were done of two step approach. Firstly, 100 iterations with modified or unmodified GF formula were conducted. In the second step, the best solution from the modified GF calculations was implemented as an additional individual to the initial geometry, but this time the GF formula was not modified. Two types of tests were conducted. In Sec. D.7 two variants were considered with so called APA and NPA procedures, where APA included modifications to the remaining individuals in the initial generation, but NPA did not. In the first step the modified GF formula was used. Both methods improved the reference GF value as expected. They achieved more optimal solutions than the theoretically predicted costs by modified GF formula from the first phase, which was promising. A similar test was conducted, but the GF formula was kept

unmodified in the first step, so called BIWNP and BIWAP, Sec. D.6. The other individuals in the population were unchanged. Both resulted in GF value improvement but not as much as the test based on the modified GF formula with APA and NPA. The first approach with implementation of result from the modified GF formula as an input to the new optimization process without GF formula interference provided better results than the solution based on non-modified GF formula in two steps. It was decided to implement APA/NPA to the existing optimization algorithm.

Next, the impact of inserting different and worse according to literature [115] topology into the initial generation was investigated in Sec. D.4. The results were worse than expected in comparison to the previous attempts, where network topologies were used in the initial generation. Nevertheless, this test highlighted the limitation in topology shaping with high utilization of hangers in the first generation and lack of prestressed steel grades. Therefore, addition of prestressed steel grade was investigated in Sec. D.5 for the same population. It helped in achieving a better solution, so it had a positive impact. Nevertheless, the results were still not satisfying and the usage of topology other than network-based was abandoned, but greater steel grades for hangers were implemented into the optimization algorithm.

The mix of various hangers' topologies was used as an initial population in other test in Sec. D.8, where the results of the predefined various hangers' arrangement were compared with the results from random parameters in the initial population except the hangers' arrangement applied to all individual from the reference geometry. Both scenarios had the same reference geometry included in the initial population. The most optimal results were the same, therefore the entire population's cost distribution was investigated. The average cost and deviations were lower with random generated parameters than for predefined population, which results diverged the greater the further the generation was. The considered suboptimal arrangements in the initial generations were proven again to provide less efficient solutions. The randomly generated parameters were worth considering in the optimization algorithm. The implemented geometry at the initial generation should not be so utilized in order to provide the algorithm more flexibility during the optimization process and prevent progression driven mainly by gradient-based method.

The last test checked the impact of skewbacks with implementation of random parameters based on the conclusions from the previous test. In Sec. D.9 skewbacks were removed from the system in comparison to the analysis in Sec. D.8. The deletion of skewbacks forced a reduction of variable loads in order to keep the existing reference bridge underutilization of 100% with previously assumed variable loads and skewbacks. Nevertheless, the resultant topology was similar for both skewbacks and no-skewbacks tests. The population distributions over generations were characterized by similar trends, which proved the consistency in smaller divergence of randomly generated population within taken assumptions. Author decided to exclude the results in the region of skewbacks in utilization determination, since peaks were observed both in cases with and without skewback, which additionally had an impact on the stiffness and hangers' distribution. This would allow to avoid bending moments peaks above supports and peak of stiffness. Since these regions were usually strengthened, it was decided to assume that in detail design these regions were strengthened properly in order to avoid peaks.
The conclusions after the tests resulted in the following algorithm modifications:

- Integration the **gradient descent** with the step size of 5,
- Added **prestressed steel** grades available for hangers,
- **Network-based hangers' arrangements in the initial generation**. The random geometries were also implemented by randomly selected predefined geometries and randomly

changing their parameters accept hangers' arrangement. The number of randomly generated geometries was the same as number of bridges in the predefined set. The predefined network-like arrangements were presented in Annex E. These arrangements were not based on the known arrangements in order to avoid intentional orientation of the optimal solutions on the well-defined solutions. The arrangements were modified manually in order to avoid similarities to predefined solutions,

- **Two steps optimization process including modified GF formula in the first phase and non-modified GF formula in the second phase with the implementation of the most optimal geometry from the first phase into the initial generation of the second phase**. The NPA method was used even though it provided worse results than the APA. The decision behind it was that the APA concentrated more on the manually added solution and its progress over time was negligible entering exploitation very quickly. The NPA progressed gradually over time, which gave an opportunity for greater exploration and exploitation would be covered by gradient-based algorithm. This also kept inter-phase elitism between modified and unmodified GF phases,
- The manually added geometry into the initial generation should not be highly utilized for higher flexibility of the optimization process. The utilization of about 85% was suggested as maximum,
- **Exclusion of internal forces in the arch and the tie from the support regions** in order to avoid peaks of the internal forces,
- Keeping 100 iterations per phase.

Additionally, the investigations showed, that if **the number of individuals at the beginning of the generation was 30 and the number of pairs 10**, resulting in generating 20 descendants, then the time demand of a single phase was two days, which was considered acceptable, since the calculations could be finished during weekend between two working days. Preferably, if the calculations were conducted within 16 hours between two working days, but this time was not achieved.

6.4 Comparison with real structures

In this section the optimization algorithm after tests was utilized on the real structures in order to investigate its effectiveness in reducing costs of the structure. During these comparisons to the existing NAB, author also tested new modifications to the optimization algorithm instead of conducing separate tests.

6.4.1 Brandanger

The first tested bridge was Brandanger bridge, Fig. 6.10, which was considered as the slenderest bridge [113]. The span length was 220 m, the axial height was 30.8 m. Due to division in the algorithm, the height was changed to 31.0 m. The total section width was 7.6 m. The arch was made of circular section 711 mm in diameter and wall thickness of 40 mm. The tie was a post-tensioned concrete slab with maximum thickness of 0.400 m and width of 7.6 m. The hangers' diameter was assumed 56 mm. According to author from [113], the hangers' arrangement was irregular near the supports comparing to well-defined arrangement. The hangers were there oriented more vertically comparing to the inclinations in the middle.

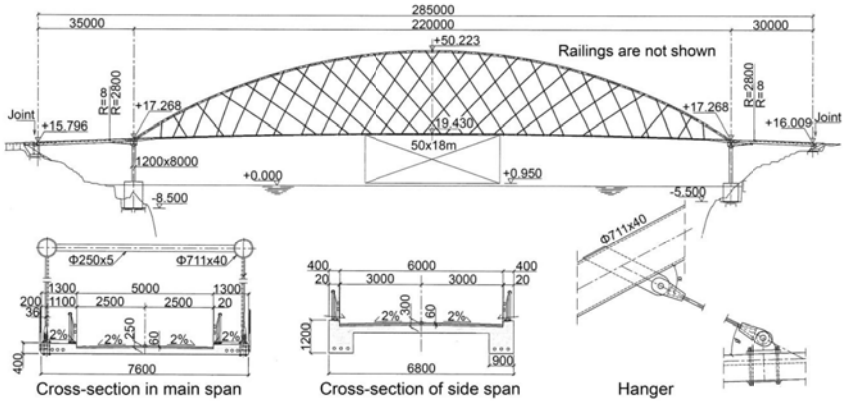

Figure 6.10 The detailed drawings of the Brandanger bridge [113]

Figure 6.11 The view of the Brandanger bridge model in SOFiSTiK

The arch cross section was modelled as 700 mm in diameter with wall thickness of 40 mm. The 711 mm diameter was not used, since the step of the arch's diameter was 100 mm in the algorithm. The tie was made of concrete, so it was replaced by steel section by keeping the same parameters of bending moment capacity and bending moment of inertia modified by the steel and concrete Young modulus ratio. The side beam with dimensions of 1.3 m by 0.4 m was considered as well as half of the deck plate with dimensions of 2.5 m by 0.25 m. It resulted in pipe with diameter of 400 mm and wall thickness of 60 mm.

The permanent load was equal to 26.4 kN/m. It included the weight of the concrete tie and bracings subtracted by the weight of the equivalent circular steel tie. The variable load was increased until reaching utilization of 90% of any structural part. The hangers' diameter was set to not be decisive utilized element. The obtained variable load was equal to 62.0 kN/m. In this iterative process, the tie diameter was increased by 100 mm to 500 mm to prevent tie to be a bottle neck in determining the variable load. Increase of 50 mm in diameter was not possible due to predefined diameter step size of 100 mm. The model of the bridge was presented in Fig. 6.11.

Two approaches were conducted in the analysis. The first kept the principles presented in Sec. 6.3, Eq. (6.5), where the cost was multiplied by the utilization in the first phase. The second modified this utilization component by raising its value to the power of 0.5 in order to reduce the positive impact of the utilization in improving GF value in the first phase, Eq. (6.6).

$$\min_{v} GF(cv, v, \eta, p) = \begin{cases} C(cv, v)\sqrt{\eta} & \text{if } \eta \leq 1.0 \\ C(cv, v)\sqrt{\eta} + \left(\dfrac{L}{L_{ref}}\right)^2 \cdot \eta \cdot p & \text{if } \eta > 1.0 \end{cases} \tag{6.6}$$

Author wanted to reduce the positive influence of the cost reduction caused by utilization in the first phase of the optimization algorithm. Any power between 0 and 1 could be applicable and chosen power of 0.5 was not special. Author was aware, that this power could be different than the chosen one in terms of achieving lower cost value and this investigation did not cover

all cases. Nevertheless, this investigation would be time consuming and defining the most optimal optimization algorithm was not intended. However, this research modification to the goal function definition was carried out with author's objective to test and improve the algorithm, if possible, due to time demanding calculations.

Table 6.3 Comparison between the Brandanger (Br) bridge and two the most optimized results, one with cost multiplied by square-rooted utilization (0.5) and one with cost multiplied by unmodified utilization (1)

	Br 0.5	Best 0.5	Br 1	Best 1
arch diameter [m]	0.7	0.7	0.7	0.7
arch thickness [m]	0.040	0.040	0.040	0.035
tie diameter [m]	0.5	0.5	0.5	0.5
tie thickness [m]	0.060	0.040	0.060	0.045
hanger diameter [m]	0.056	0.048	0.056	0.056
hanger number [-]	44	44	44	44
bridge height [m]	31.0	31.0	31.0	31.4
arch steel	S460	S460	S460	S460
tie steel	S460	S460	S460	S420
hanger steel	S460	S460	S460	S460
buckling factor [-]	0.880	0.883	0.880	0.868
utilization arch [%]	89.2	99.2	89.2	98.3
utilization tie [%]	74.3	99.5	74.3	95.1
utilization hanger [%]	70.2	95.0	70.2	92.6
utilization deflection [%]	56.2	85.1	56.2	80.4
utilization all [%]	89.2	99.5	89.2	98.3
cost [PLN]	6,958,039	5,936,413	6,958,039	5,829,132
goal function [PLN]	6,571,204	5,936,413	6,205,875	5,829,132

The Brandanger bridge was included in the initial populations. Its cost and GF values in *Br* column were presented in the Tab. 6.3 for the comparison with the most optimized results named *Best*. As presented in Sec. D.2, the optimization approaches were run in two phases. First phase was conducted with cost multiplied by the modified (0.5) or unmodified (1) utilization and second without costs multiplied by utilization. The GF values for Brandanger bridge were presented for the modified and unmodified utilization component multiplied by costs, in order to show the potential costs if the utilization was equal to 100%. The fact, that the GF value for *Best 0.5* and *Best 1* were equal to cost was that they presented the results from the second phase, where the cost was not multiplied by utilization, and they differentiated in the first phase, where cost was multiplied by modified and unmodified utilization, according to conclusions presented in Sec. 6.3. The results were presented in Tab. 6.3 and Fig. 6.12. The Brandanger bridge was not optimized *Br*, but used in the initial population in *Best* calculations.

In both cases, the best solutions were better than the potential cost of the original geometry, with dominance of the non-modified formula. The most change was done to the tie's thickness, which was reduced to 40 mm or 45 mm from 60 mm. The utilization of structural elements got equalized. The number of hangers remained as in the original geometry. The arrangement of hangers remained similar as well. The center part kept the network arrangement with sparser arrangement in the non-modified version. Two vertical hangers appeared near the ends in contrary to the original one with one hanger, if the two parallel in Fig. 6.12a were considered as one. Then the network arrangement continued with occasional, local irregularities.

a) The most optimal geometry from *Best 1* optimization after second phase - cost and GF values of 5,829,132 PLN

b) The most optimal geometry from *Best 0.5* optimization after second phase - cost and GF values of 5,936,413 PLN

Figure 6.12 The comparison of the most optimal solutions after the second phase with (a) no modification to the utilization component multiplied by cost value in the GF formula, Eq. (6.5), and (b) with the utilization raised to the power of 0.5 and multiplied by cost value in the GF formula, Eq. (6.6)

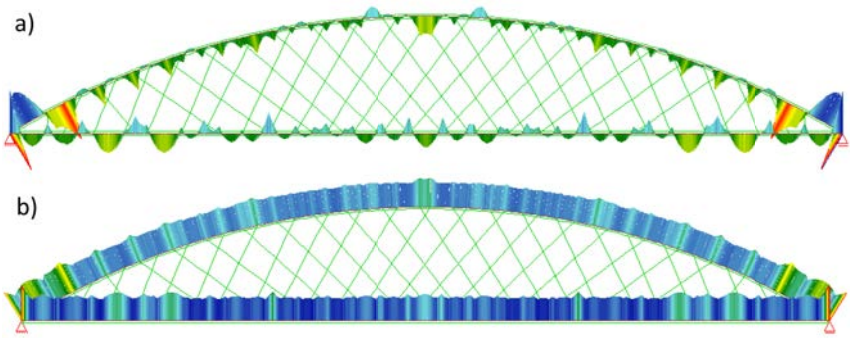

Figure 6.13 The (a) bending moments and (b) von Mises stress diagrams of the original geometry

The tendency of vertical hangers presents near the ends was noticed earlier in the conducted test with the most distinguished example in Fig. D.23a and Fig. D.23c. This was similar to the results from the literature [93, 94] for the sparse system, Tab. 3.5.

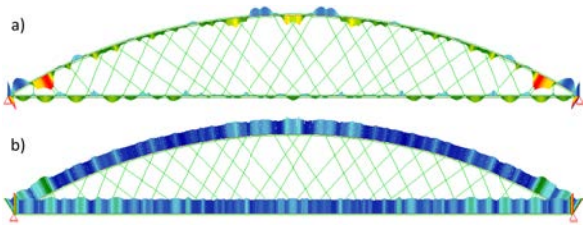

Figure 6.14 The (a) bending moments and (b) von Mises stress diagrams of the best solution with no modification to the GF formula

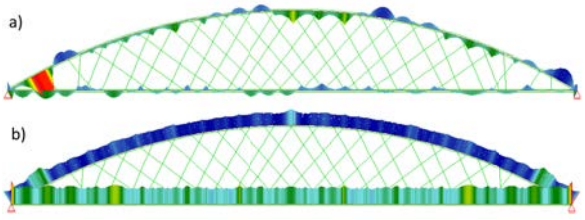

Figure 6.15 The (a) bending moments and (b) von Mises stress diagrams of the best solution with modification to the GF formula

The internal forces and von Mises stresses diagrams for the original geometry, best for non-modified formula and modified formula were presented in Fig. 6.13, Fig. 6.14 and Fig. 6.15

respectively. The last 5% of the arch and tie length were not considered in the optimization process. In the same order, the greatest bending moments were 1176 kNm, 1949 kNm and 2045 kNm, and stress 347 MPa, 383 MPa and 415 MPa respectively.

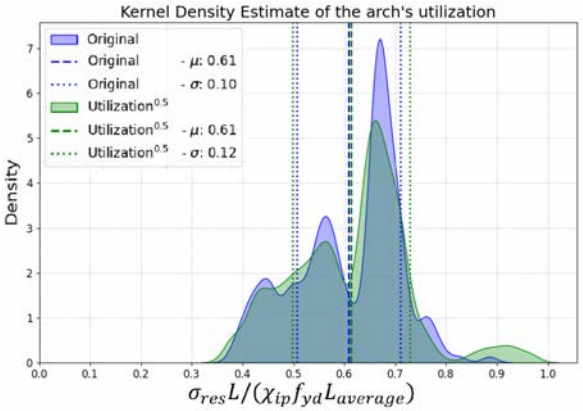

(a) KDE - arch - Best 0.5 (utilization$^{0.5}$)

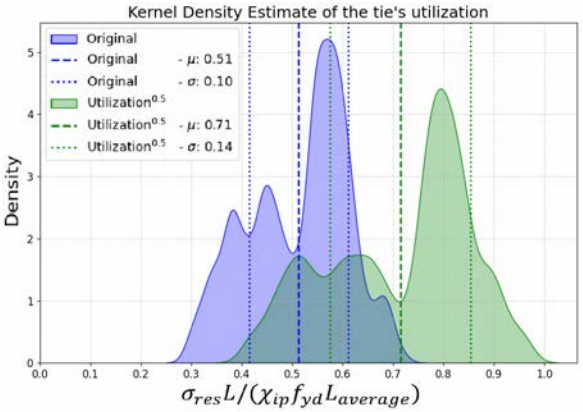

(b) KDE - tie - Best 0.5 (utilization$^{0.5}$)

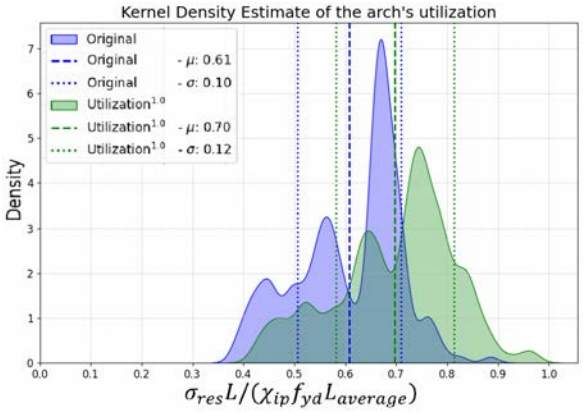

(c) KDE - arch - Best 1 (utilization$^{1.0}$)

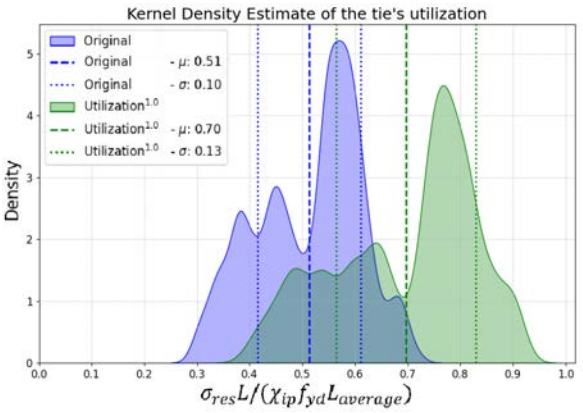

(d) KDE - tie - Best 1 (utilization$^{1.0}$)

Figure 6.16 Kernel Density Estimate of the arch and the tie utilization for modified (a, b) and non-modified (c, d) GF formula with comparison to the original geometry

The stresses comparison of the arch and the tie were presented in Fig. 6.16. The original geometry was characterized by distinguished peak at 0.66 utilization for the arch and 0.57 for the tie. The modified and non-modified results had peak values less extreme. The average and deviation values were similar for the arch in modified formula and the original geometry. The non-modified formula had average utilization increased by 9% in comparison to the original. The KDE diagram of the best solutions of the arch had local peak in 0.9-1.0 range, which was much less distinguished for the original geometry. This phenomenon corresponded with the local extreme von Mises value near the ends, Fig. 6.15b and Fig. 6.14b.

The tie was improved the most by reducing the wall thickness in comparison to the original geometry, which reflected in the increase of the mean stress by about 40%. The shape of the stress distribution remained similar but with greater spread of the stress corresponding with the deviation increase by also about 40%.

Author expected, that in more optimal geometry the utilization should be greater and with lower deviation. The results were repeated only for the loadcase with the greatest utilization, Fig. 6.17.

The concentration of stress was up to three times greater than for both loadcases. The tie remained comparable in stress distribution. The concentration of stresses near 100% for the arch

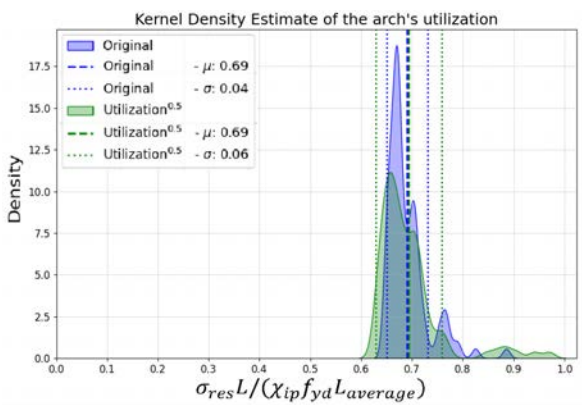

(a) KDE - arch - Best 0.5 (utilization$^{0.5}$) - max

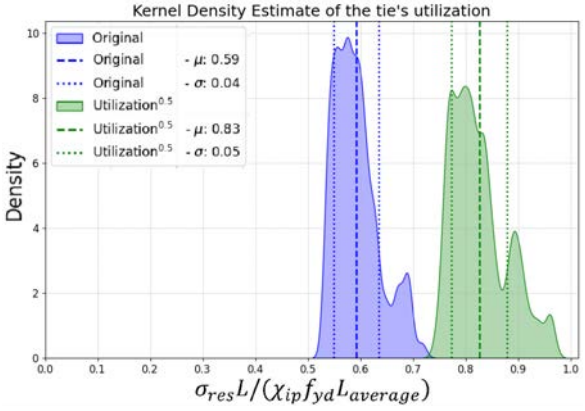

(b) KDE - tie - Best 0.5 (utilization$^{0.5}$) - max

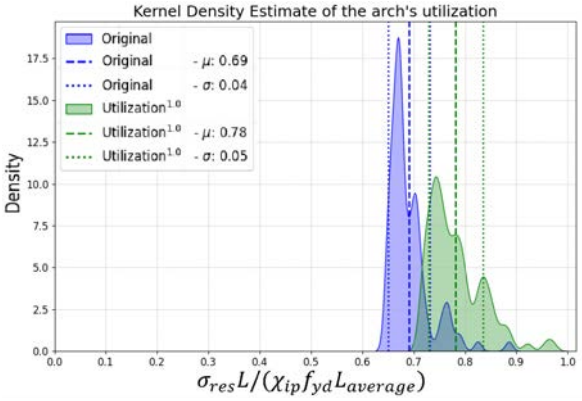

(c) KDE - arch - Best 1 (utilization$^{1.0}$) - max

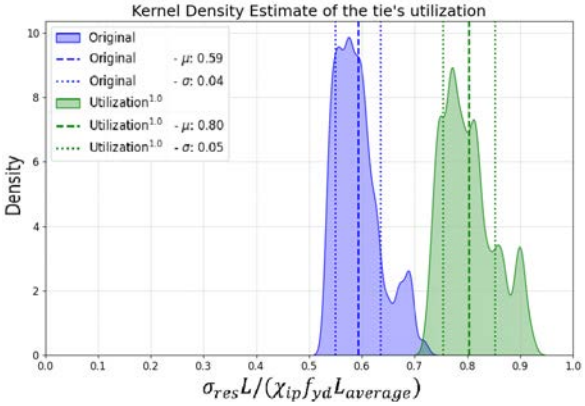

(d) KDE - tie - Best 1 (utilization$^{1.0}$) - max

Figure 6.17 Kernel Density Estimate of the arch and the tie utilization for modified (a, b) and non-modified (c, d) GF formula with comparison to the original geometry - only maximum loadcase

reflected again the greatest utilization near skewback and relatively constant for the remaining length. It was suspected, that if the section has remained capacity for bending in this case, the algorithm would take advantage of this and accept worse hangers' arrangement, which caused local peak value, unwanted in the manual design. Therefore, the gratification of lower and more even bending moments diagram could solve this issue. On the other hand, too much gratification could lead to the situation with very low material utilization and even bending moments with low amplitude but very high cost, which as a resultant goal function value could lead to favouring more costly solutions. This phenomenon was noticed in Sec. 6.4.2. **Nevertheless, the non-modified GF formula resulted in greater mean value and less divergence for the arch in case of both loadcases and single loadcase comparing to the modified formula. The tie experienced better outcomes for the modified formula, but the difference was about three times smaller than for the arch. The non-modified formula was considered better than the modified, which was also proved by lower costs for the best solution.**

6.4.2 Palma del Rio

The next tested bridge was Palma del Rio over Guadalquivir river, Fig. 6.18. This bridge was made of circular cross section for both the arch and the tie [64, 32] as it was assumed in the optimization algorithm. Both sections had 900 mm in diameter, arch had 50 mm of wall thickness and tie of 40 mm. The arches were included inwards, but in the simplified model it

was not inclined. The height was 25 m, the length 130 m.

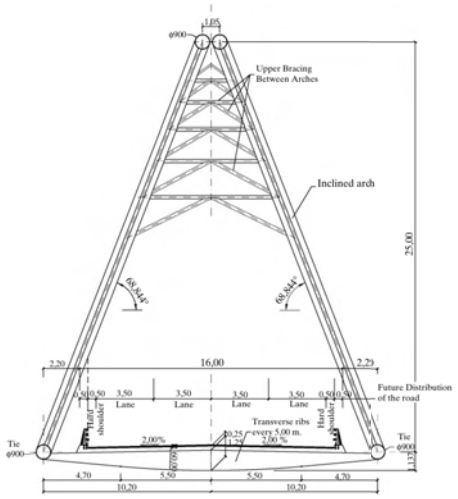

Figure 6.18 Cross section of the Palma del Rio bridge [64, 32]

Figure 6.19 The view of the Palma del Rio bridge [64, 32]

In the optimization, the weight of the steel cross beams, bracings and concrete deck were included in the self-weight. Their weight was equal to 164 kN/m per bridge, so 82 kN/m per side. The weight of the deck with asphalt was the main component of self-weight except the hangers, arch and tie and was equal to 160 kN/m. The weight of the cross beams included only the flanges, since no data about the web thickness was found and their weight was negligible in comparison to concrete deck weight. The steel grade was S355. The hangers' arrangement was achieved from the picture, Fig. 6.19. The hangers' diameter and steel grade were chosen as 64 mm and Y1770 in order to provide good margin of safety and not make hangers decisive in the process.

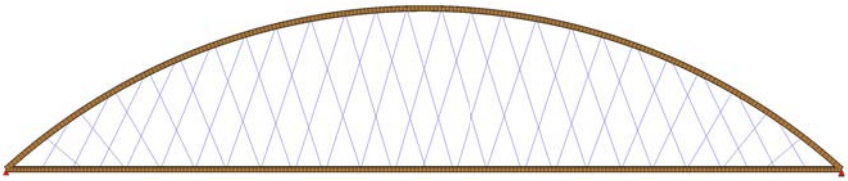

Figure 6.20 The view of the Palma del Rio bridge model in SOFiSTiK

Since the loads were not known and deflection design criterion, it was decided to apply the load until reaching similar utilization of all elements and deflection. In the process, the tie's wall thickness was reduced to 40 mm as it was designed for the arch, since the utilization of the tie was significantly lower and author wanted to equalize that in order to not put the results of his algorithm into favor. The applied variable load was 85 kN/m. The model was presented in Fig. 6.20.

The optimization was conducted with and without modification to the utilization value multiplied by costs in the GF formula in the first phase, as it was done in Sec. 6.4.1. The results were presented in Tab. 6.4, Fig. 6.21 and Fig. 6.22. Palma del Rio bridge was not optimized *PdR*, but the GF value for both 1 and 0.5 cases was presented in order to show potential cost reduction, if the utilization was equal to 100%, with respective utilization component modification. Palma del Rio bridge was used in the initial population for *Best* calculations.

Table 6.4 Comparison between the Palma del Rio (PdR) bridge and two the most optimized results, one with cost multiplied by square-rooted utilization (0.5) and one with cost multiplied by unmodified utilization (1).

	PdR 1	Best 1	PdR 0.5	Best 0.5
arch diameter [m]	0.9	1.4	0.9	0.9
arch thickness [m]	0.040	0.025	0.040	0.045
tie diameter [m]	0.9	0.9	0.9	0.9
tie thickness [m]	0.040	0.030	0.040	0.030
hanger diameter [m]	0.064	0.042	0.064	0.056
hanger number [-]	46	40	46	20
bridge height [m]	25.0	23.6	25.0	24.5
arch steel	S355	S320	S355	S355
tie steel	S355	S320	S355	S355
hanger steel	Y1770	Y2060	Y1770	Y1770
buckling factor [-]	0.970	0.948	0.970	0.902
utilization arch [%]	76.1	99.5	76.1	95.5
utilization tie [%]	80.6	99.7	80.6	95.7
utilization hanger [%]	21.1	74.6	21.1	50.5
utilization deflection [%]	96.2	88.5	96.2	52.1
utilization all [%]	96.2	99.7	96.2	95.7
cost [PLN]	5,675,961	4,329,496	5,675,961	4,532,563
goal function [PLN]	5,458,517	4,329,496	5,566,178	4,532,563

The best solution was achieved for the non-modified utilization in GF formula. The improvement in comparison to the original was 24% when referring to costs. The deflection utilization of the simulated Palma del Rio was much higher by 20% in relevance to material utilization, but even if deflection utilization was not included, the GF value would be 4,574,825 PLN, which would be still higher than both obtained optimal results.

The best results from the modified utilization in GF formula had 20 hangers in total, which was significantly smaller number than the other results which exceeded 40. Other parameters of geometry were not distinguished from others significantly. All buckling coefficients were greater than 0.90. The divergence between GF and cost was the highest observed in the 1^{st} phase. The amount of material used should have been so high, that the very low utilization compensated for high costs drawbacks in GF value. Since the approach with modified utilization in GF formula reduced the improving factor of the cost, the divergences between GF and cost values were lower than for the case with non-modified original approach, Fig. 6.21. After first phase, so after 100 generations, the non-modified approach provided in the end cheaper solution than modified one.

The best solution from non-modified utilization in GF formula resulted in subjectively chaotic hangers' arrangement comparing to the modified utilization results, Fig. 6.22. If the aesthetic criterion was included, the chaotic results would not win. Nevertheless, the algorithm achieved the goal of providing better results than the original geometry.

Since the arch and tie members of the Palma del Río Bridge were designed as circular hollow sections, consistent with the assumptions adopted in the optimization procedure, it was decided to retain the weight estimates of the bracing and cross beams from this bridge for use in subsequent optimization processes. These structural components were not explicitly modelled in the two-dimensional framework, but their mass values from the Palma del Río Bridge were considered representative because the geometry of these elements was similar to that used in the optimization study.

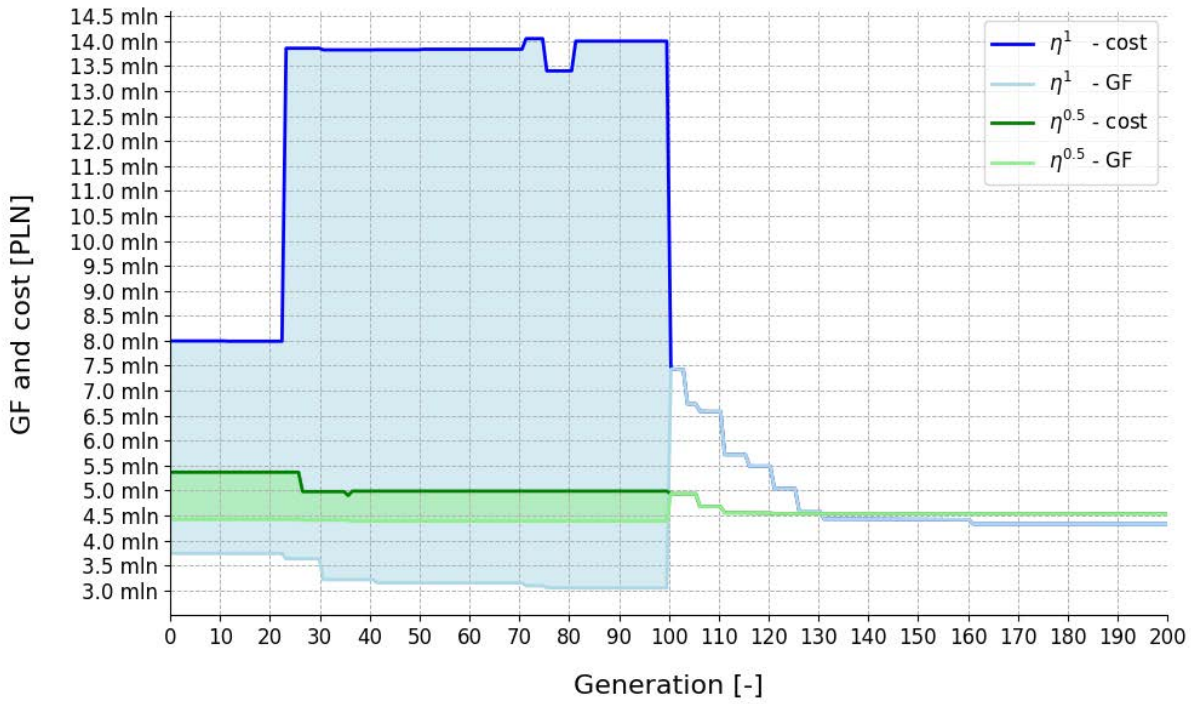

Figure 6.21 The goal function and cost progression for the utilization η raised to the first power (blue) and square-rooted (green)

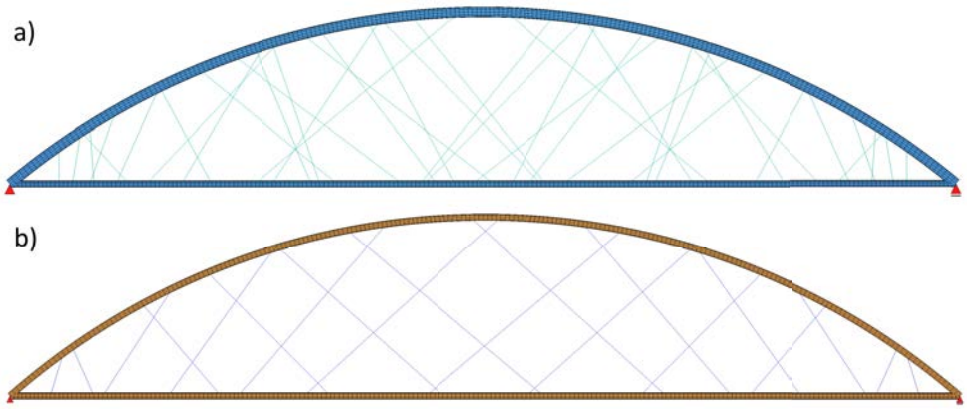

Figure 6.22 The comparison of the most optimal solutions after the second phase with (a) no modification to the utilization component multiplied by cost value in the GF formula, Eq. (6.5), and (b) with the utilization raised to the power of 0.5 and multiplied by cost value in the GF formula, Eq. (6.6)

6.4.3 Cracow NAB

The last test was conducted for the Cracow's network arch bridges [126, 45, 89]. The geometry used in Sec. 4.3 was utilized. The HD cross section of the arch and the concrete rectangular cross section of the tie were replaced by the equivalent circular cross section in the same way as in Sec. 6.4.1. The cross section area, bending moment of inertia and bending index were obligated to match. It resulted in arch's cross section made of 500 mm x 100 mm dimensions and 600 mm x 85 mm for the tie's cross section. The hangers were modelled with 85 mm in diameter. The span length was 116 m and elevation of 17.4 m, rounded to 17.6 m

due to predefined span division list. The skewbacks were modelled as in the original geometry. The self-weight was set to 36.2 kN/m and variable load resulted in 130 kN/m until reaching acceptable utilization of the structure. The steel for all components was chosen to be S235. This steel grade was used in order to make utilization of the arch and tie equal to the deflection criteria utilization and reduce the costs. The geometry was presented in Fig. 6.23.

Figure 6.23 The used model of the Network Arch Bridge in Cracow

The analysis included two tests. First was only the second phase where the GF did not include the cost reduced by utilization component. The second which included two phases as explained in Sec. 6.3. The Cracow network arch bridge geometry was included in the initial generation in the first test and in the first phase in the second test. The comparison was presented in Tab. 6.5. Both solutions had identical geometric properties, but not the buckling factor, which should only be influenced by hangers' arrangement, Fig. 6.24. The difference in price of them was negligible. **The overall improvement was about 21% in comparison to the original geometry.** Cracow bridge was not optimized *Cr*, but the GF value for both cases was presented in order to show potential cost that optimization algorithm should at least achieve with respective utilization component modification. Cracow bridge was used in the initial population for *Best* calculations.

a) The most optimal geometry from *Best p2* optimization after only the second phase - cost and GF values of 3,722,302 PLN

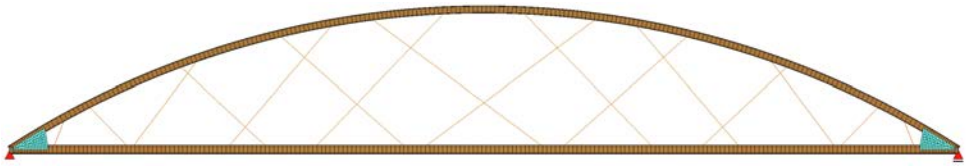

b) The most optimal geometry from *Best p1&2* optimization after the second phase - cost and GF values of 3,722,690 PLN

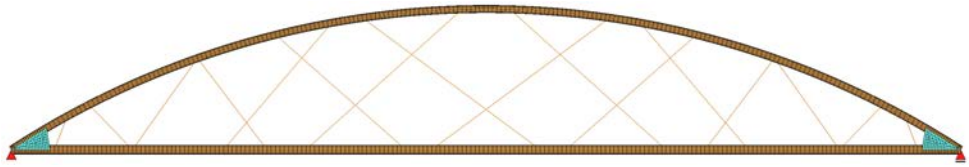

Figure 6.24 The comparison of the most optimal solutions after the second phase with (a) only the second phase characterized by no cost reduced by utilization in the GF formula, Eq. (6.2), and (b) with two phase optimization as described in Sec. 6.3 where in the first phase the cost was reduced by utilization in the GF formula, Eq. (6.5)

The difference in hangers' arrangement was minor. The maximum deviation in hangers' position was 4, applicable to the 4th hanger from both ends, which did not cross with the third hanger in the full simulation but did in the limited analysis. The second greatest difference

occurred for the hanger second to center, with more horizontal orientation in Fig. 6.24b than on Fig. 6.24a.

Table 6.5 Comparison between the Cracow (Cr) bridge and two optimized, one with only phase 2 (p2) and one with both phase 1 and 2 (p1&2)

	Cr p2	Best p2	Cr p1&2	Best p1&2
arch diameter [m]	0.5	0.9	0.5	0.9
arch thickness [m]	0.100	0.040	0.100	0.040
tie diameter [m]	0.6	1.1	0.6	1.1
tie thickness [m]	0.085	0.025	0.085	0.025
hanger diameter [m]	0.085	0.064	0.085	0.064
hanger number [-]	44	16	44	16
bridge height [m]	17.6	17.1	17.6	17.1
arch steel	S235	S355	S235	S355
tie steel	S235	S355	S235	S355
hanger steel	S235	Y1700	S235	Y1700
buckling factor [-]	0.952	0.930	0.952	0.919
utilization arch [%]	96.3	96.1	96.3	99.8
utilization tie [%]	90.4	99.8	90.4	91.4
utilization hanger [%]	58.3	44.8	58.3	50.4
utilization deflection [%]	96.2	58.9	96.2	61.1
utilization all [%]	96.3	99.8	96.3	99.8
cost [PLN]	4,750,260	3,722,302	4,750,260	3,722,690
goal function [PLN]	4,750,260	3,722,302	4,574,320	3,722,690

Compared to the original geometry, the arch and the tie's outer diameter increased almost twice. The arch section area decreased by 28% and tie by 46%. Even though the arch bending moment of inertia increased almost 3 times, the reduced from 44 to 16 number of hangers resulted in decrease of the buckling factor.

Since the differences between the best solutions were minor, it was decided to compare the behaviour of the first three best solutions in each generation. The results were presented in Fig. 6.25 and Fig. 6.26. The great diverges between cost and GF values were observed in the phase 1 as it was described in Sec. 6.4.2. After that, both paths acted similarly not exceeding 12.5 mln PLN cost value. The best individual experienced improvements at the beginning of the phase 2 in both cases, which correlated with the gradient step size of 5. The greatest improvement was achieved by gradient. Involvement of the genetic algorithm principles in cost improvement was negligible. In this case, phase 1 of the optimization process provided worse solution than the predefined initial population's set, which was the intended prevention rule of phase 2.

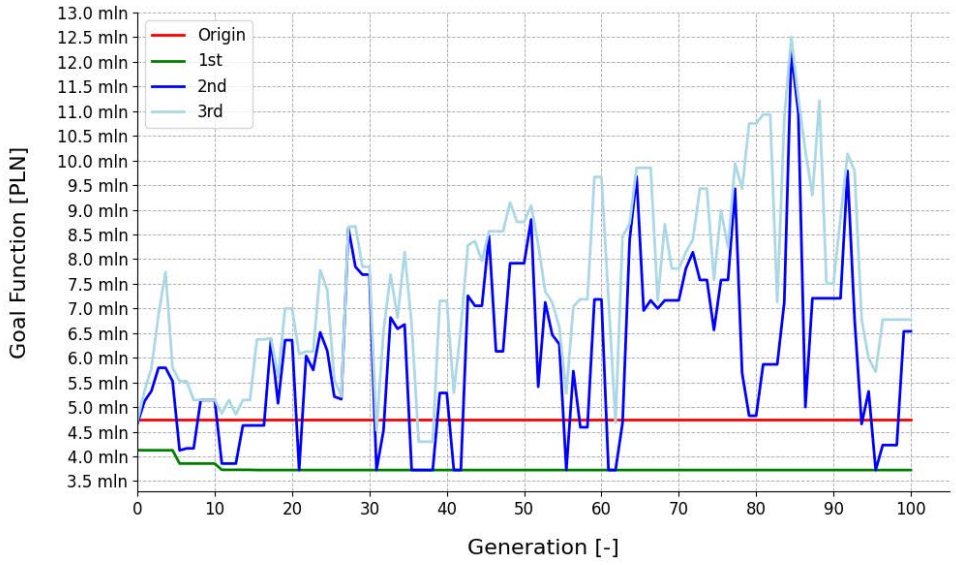

Figure 6.25 The goal function progression for the first three best costs values over generations with the reference starting value - only phase 2

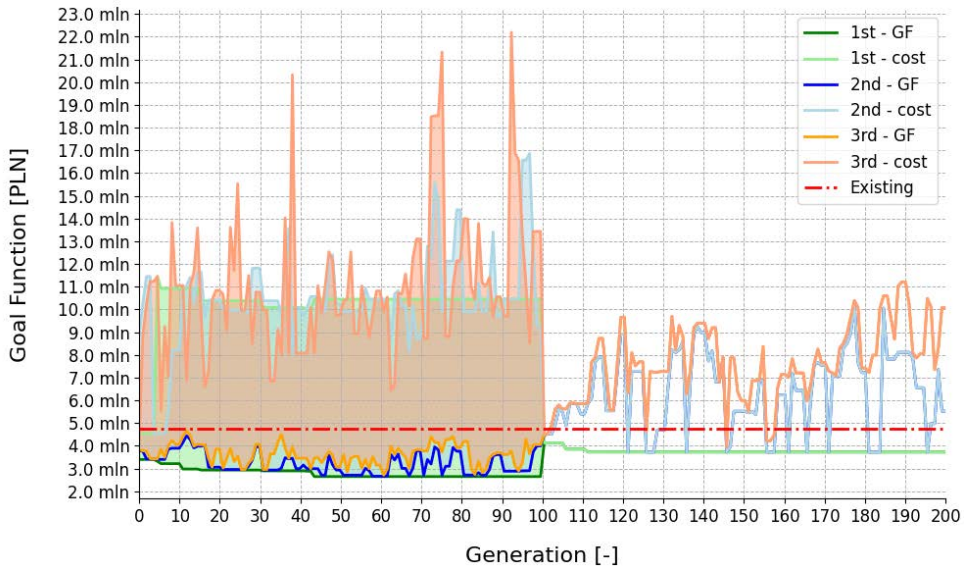

Figure 6.26 The goal function progression for the first three best costs values over generations with the reference starting value - phase 1 and 2

6.4.4 Conclusions

All tests on three bridges resulted in lower costs than the reference geometries. The improvement was up to 24%. Author was aware, that the optimized structures were simplified, loaded differently and designed in more detail than the presented. Nevertheless, their principal geometrical properties were reflected in the simplified models and they were loaded with equivalent loads until reaching their capacities. In these principles, the optimization algorithm managed to always provide cheaper solutions with two digits cost reduction. It was considered successful. The additional modifications implemented in these tests were not utilized in the final simulation presented in Sec. 6.5. The goal function definition form Sec. 6.3, Eq. (6.5), was applicable.

6.5 Simulations

6.5.1 Description

Calculations so far checked specific geometries and loads. The algorithm managed to improve the initial geometry in every situation. Therefore, it was decided to simulate geometries with various span lengths and deck widths in order to observe trends and rules in shaping optimal bridges by the algorithm depending on these parameters. The investigated span lengths were 100 m, 150 m, 200 m and 250 m, which covered the reasonable domain of most common network arch bridges. For each of these span lengths, the deck widths of 3.0 m, 6.0 m, 9.0 m and 12.0 m were considered. The deck width corresponded with 1, 2, 3 and 4 traffic lanes respectively.

All the calculations were conducted for the road traffic loads TS and ULD. They were based on the basic Eurocode 1991-2 [131] recommendations. The wider the deck was, the more lanes were included, and so the greater the applied load was. The point load *Q* was evenly distributed on the full length $q_{eq,full}$ or at the half of the span length $q_{eq,half}$. This distribution of the point load into uniform load effectively reduced the maximum bending moments. Therefore, it was decided to amplify *a* the magnitude of the point load in order to achieve the same maximum bending moment after load distribution $M_{max,udl}$ as for the maximum bending moments for caused by the point load $M_{max,point}$. Since the static schema was freely supported beam and two load situations were considered, the resultant load amplification for fully loaded deck and half loaded deck were calculated as in Eq. (6.7) and (6.8). The uniformly distributed load UDL was multiplied by the lane width. The total applied variable loads including TS and ULD were listed in the Tab. 6.6. The equivalent load got smaller over the span length increase, since the longer the bridge was, the longer the distribution length for the point load got. The effects of the environmental loads were not included and the same combination coefficient of 1.0 was used for ULS and SLS purposes.

$$\left(M_{max,point} = \frac{QL}{4}\right) = \left(M_{max,udl} = \frac{a \cdot QL}{8}\right) \Rightarrow \quad a = 2 \Rightarrow \quad q_{eq,full} = \frac{2Q}{L} \tag{6.7}$$

$$\left(M_{max,point} = \frac{3QL}{16}\right) = \left(M_{max,udl} = \frac{a \cdot 9QL}{64}\right) \Rightarrow \quad a = \frac{4}{3} \Rightarrow \quad q_{eq,half} = \frac{8Q}{3L} \tag{6.8}$$

Table 6.6 Variable loads for full and half loaded deck (full/half) [kN/m]

	width [m]			
span length [m]	3	6	9	12
100	39.0 / 43.0	54.5 / 61.2	62.0 / 68.7	73.5 / 81.5
150	35.0 / 37.7	47.8 / 52.3	55.3 / 59.8	65.5 / 70.8
200	33.0 / 35.0	44.5 / 47.8	52.0 / 55.3	61.5 / 65.5
250	31.8 / 33.4	42.5 / 45.2	50.0 / 52.7	59.1 / 62.3

Permanent loads were based on the approach from the Palma del Rio bridge, since it had the most similar geometry as simulated. The bracing, cross beams and deck weights were considered. The loads were presented in Tab. 6.7.

Table 6.7 Permanent loads [kN/m]

	width [m]			
span length [m]	3	6	9	12
100	31.3	62.1	92.9	123.7
150	31.3	62.1	92.9	123.7
200	31.3	62.1	92.9	123.7
250	31.3	62.1	92.9	123.7

The variable parameters got domain update according to the conducted test. The bridge span length denominator range for height determination was increased to 5-7.5 and step was reduced to 0.1. The steel range for the hangers was extended by the prestressed steel from Y1700 to Y2160.

All other aspects remained the same as in the tests conducted.

6.5.2 Results - price and weight

Firstly, the weights of all the components for the optimal results were analysed in comparison to the literature. The most representative graph from literature, which included the weight of bridge components separately, was already presented in Fig. 3.12b [75]. Since the graph covered the span length range between 60 m and 200 m, the graphs of each component were approximated with the maximum 3rd order polynomial and extrapolated to 250 m and 50 m in order to match the range of span length from the simulations. The weight of the arch, hangers, tie and total weight of the structural steel were compared. Since the estimations from the literature included the post-tensioned concrete tie, the reinforcement, prestressed steel and temporary chord were provided instead of structural steel weight of the chord. Therefore, it was decided to divide the tie comparison into two parts. The first included the temporary chord and reinforcement, which were compared with the tie's weight from the analyses. The second included temporary chord, reinforcement and all other provided components including prestressed steel, wind brackings, bearings, which were compared with the chord weight with brackings and cross beams. The reason why the prestressed steel's weight was not included in the first tie comparison was the fact that it was not separated from the weight costs in the literature. When comparing the total weights, the weight of bracing and cross beams from the calculations were also included as it was done in the second comparison of the tie. The results were presented in Fig. 6.27, Fig. 6.28, Fig. 6.29, Fig. 6.30 and Fig. 6.31.

The reference literature's weight was presented with the +-10% margin. The literature's estimated weight was prepared for the two lanes road and railway network arch bridges. Since the purpose of the analyses was to minimize the cost not weight, the impact of steel grade cost was not included in weight comparison. Starting from the total weight of the structure, Fig. 6.31, the simulated geometries resulted in parabolic trend, similarly as the reference curve. The results for the 1, 2 and 3 lanes were below the -10% deviation of the reference weight with very good margin. The results for the 4 lanes started to exceed the -10% zone at 170-175 m range, but they did not exceed the reference curve. In favour of literature, the total weight excluding the temporary chord weight was presented as gray curve. Even with this conservative assumption, all the results for 1, 2 and 3 lanes were below this curve with good margin, results for 4 lanes started to be above from span length of 130-135 m.

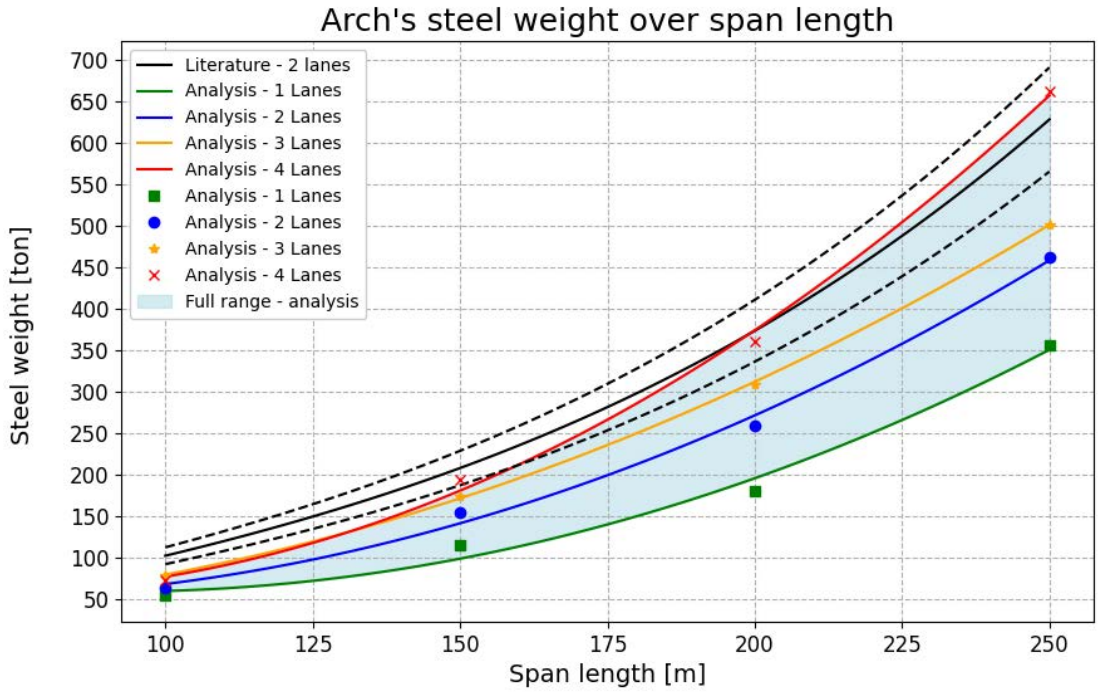

Figure 6.27 Arch's steel weight comparison with the literature results for all the deck widths - the dashed lines represented literature weight estimation with deviation of 10%

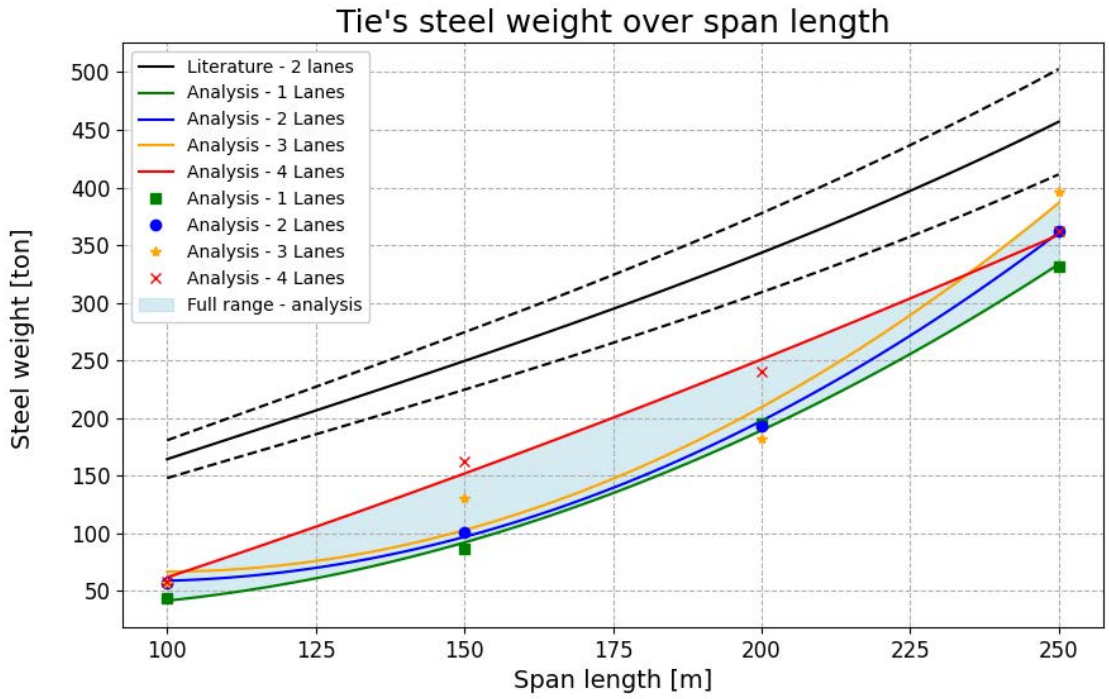

Figure 6.28 Tie's steel weight comparison with the literature results for all the deck widths, considered as reinforcement and temporary chord weights - the dashed lines represented literature weight estimation with deviation of 10%

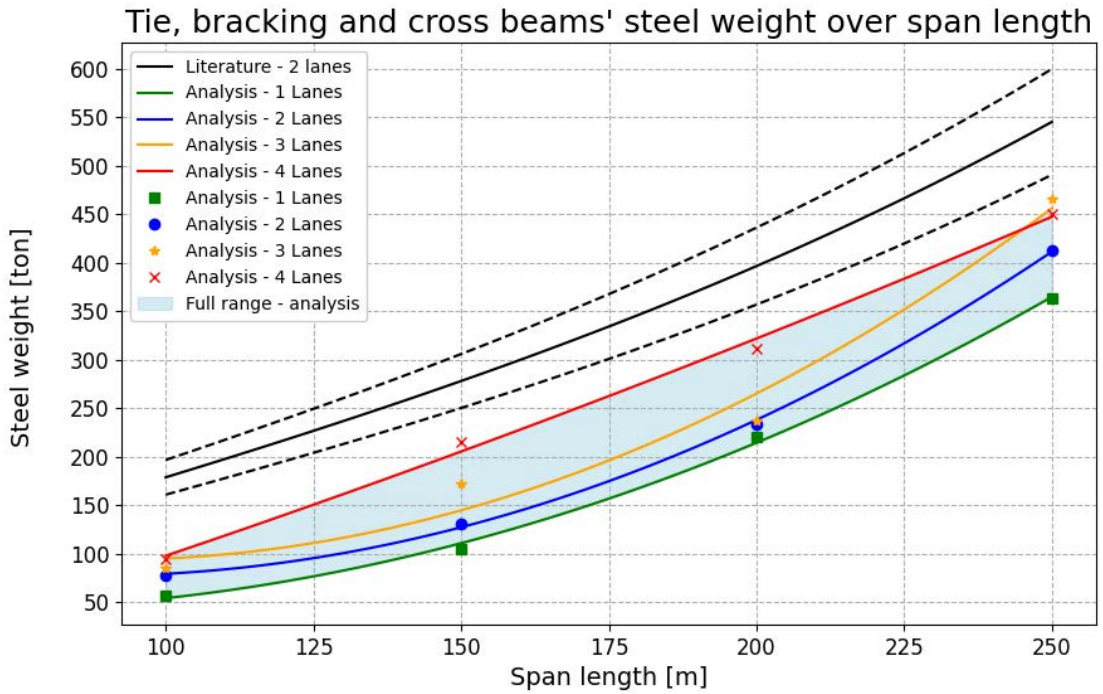

Figure 6.29 Tie, bracking and cross beams' steel weight comparison with the literature results for all the deck widths, considered as reinforcement, temporary chord weights and other remaining weight - the dashed lines represented literature weight estimation with deviation of 10%

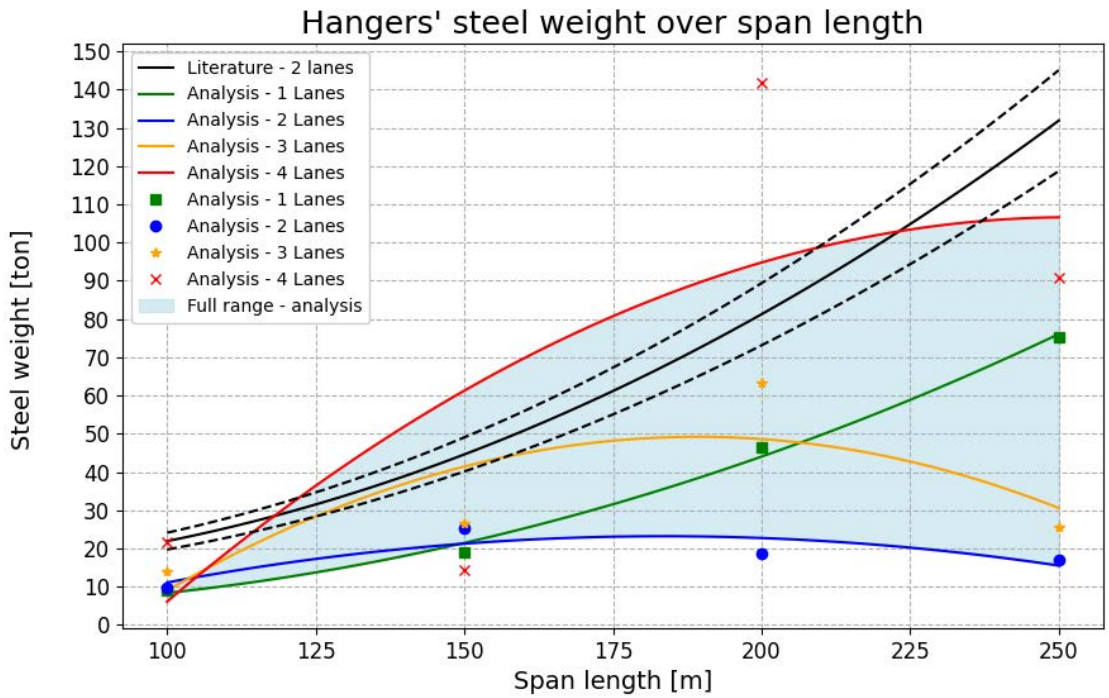

Figure 6.30 Hangers' steel weight comparison with the literature results for all the deck widths - the dashed lines represented literature weight estimation with deviation of 10%

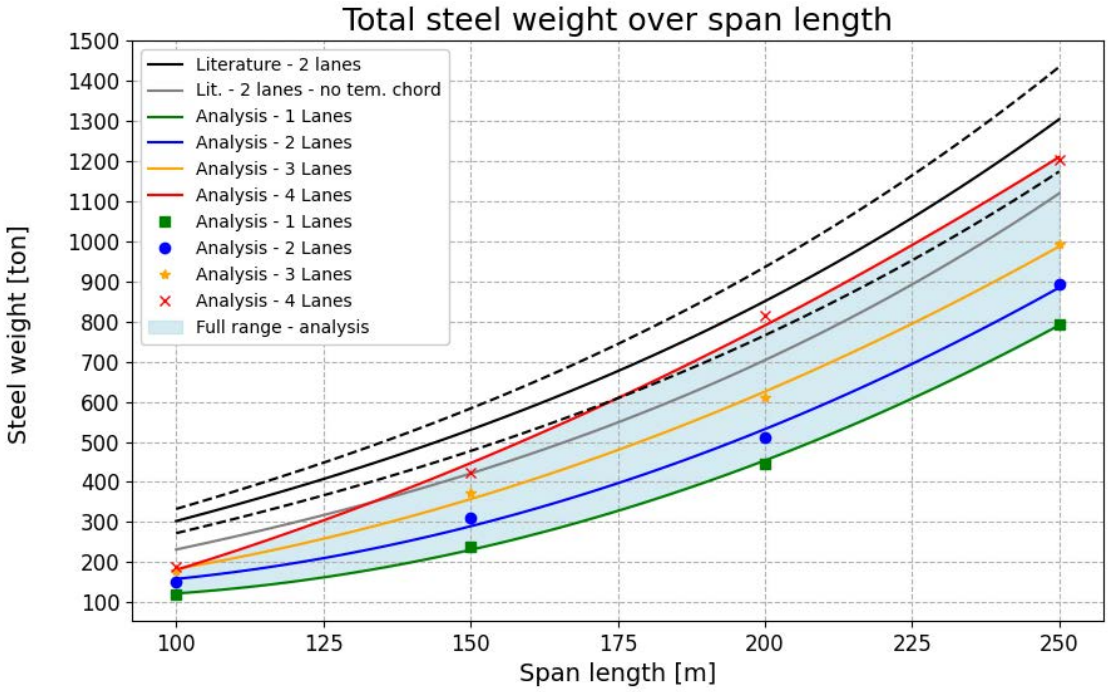

Figure 6.31 Total steel weight comparison with the literature results for all the deck widths - the dashed lines represented literature weight estimation with deviation of 10% - for investigation, the weight of the temporary chord was excluded from the literature's total steel weight

The total weight (TW) approximated functions expressed in kilograms were expressed in Eq. (6.9)-(6.12). They were determined using Python external libraries with the root mean square error (RMSE) principles were used.

$$TW(3m, L) = 22.88 \cdot L^2 - 3,544 \cdot L + 247,549 \tag{6.9}$$
$$TW(6m, L) = 22.19 \cdot L^2 - 2,918 \cdot L + 227,993 \tag{6.10}$$
$$TW(9m, L) = 18.82 \cdot L^2 - 1,221 \cdot L + 116,983 \tag{6.11}$$
$$TW(12m, L) = 15.40 \cdot L^2 + 1,481 \cdot L - 121,489 \tag{6.12}$$

The results of the arch, Fig. 6.27, followed the full weight trend. The results of the 1, 2 and 3 lanes were always below the -10% divergence from the expectations from the literature with great margin. The results of the 4 lanes exceeded the reference curve at 200 m of span length, but were still within +-10% range.

The 3 out of 4 curves for tie approximation were with parabolic trend, Fig. 6.28. Only the heaviest, 4 lanes option, had near linear trajectory. All the results were below -10% divergence with great margin until 225 m of span length. The greater the span length was, the lower the margin was. In average, all the simulated curves kept similar trajectory of steel weight increase as the reference. For the situation, where all the other components were included in the tie weight, Fig. 6.29, the trends were kept the same and the margins decreased. Nevertheless, all the curves resulted below the -10% divergence from the literature.

The results for hangers were not as consistent in trend as the results of other structural components, Fig. 6.30. Only the results for the 1 lane followed the previous parabolic-like trends. The results for the 2 and 3 lanes were pointed downwards after 175-220 m of span length. The results for the 4 lanes exceeded significantly the reference curve and had opposite parabolic upwards trend in the considered domain. Even though these trends might be considered chaotic, the weight influence of the hangers on the total weight was not greater than 10%.

The noticed unsustainable trends for the tie and hangers' components could be justified by the fact that the optimization was oriented around the cost of the structure, not weight. The weight could be greater, but the used material could be much cheaper resulting in cheaper solution in the end. The second analysed parameter was the price.

The results were presented in relevance to the deck width and span length, Fig. 6.32 and 6.33 respectively.

The results dependent on the deck width were expected to be linearly approximated. All the span length matched this expectation. The linear expectation was justified by linear increase of permanent loads and almost linear increase of the variable loads over the deck width. Comparing the price for the smallest deck width for all the span length, it was noticed, that the greater the span length was, the smaller the price ratio for 12 m and 3 m of deck width. For example, for the span length of 100 m, the price increased almost twice between 3 m and 12 m of deck width, but for 250 m this ratio was 1.7 instead. It was relatively better to increase the deck width for longer span lengths rather than shorter.

When it came to the price relevance to the span length, the trend was parabolic-like and also the parabolic approximation was used using Python external libraries. The root mean square error principles were used. The approximated curves were not evenly spaced. Potentially, if the results for 2 lanes (6 m) for 250 m were repeated, all the curves would be almost evenly spaced. **All the graphs were very consistent in following parabolic trend, as expected.** The approximated prices P for each deck width expressed in PLN were described in Eq. (6.13)-(6.16).

$$P(3m, L) = 272L^2 - 21,699L + 1.74 \cdot 10^6 \tag{6.13}$$
$$P(6m, L) = 375L^2 - 32,903L + 2.31 \cdot 10^6 \tag{6.14}$$
$$P(9m, L) = 408L^2 - 32,109L + 2.50 \cdot 10^6 \tag{6.15}$$
$$P(12m, L) = 433L^2 - 15,775L + 1.03 \cdot 10^6 \tag{6.16}$$

Since the cost function depended on the width, and the span length could be approximated by polynomials, the approximation in 3D, so the dependence from both of these variables at the same time, should be manageable to approximate with polynomials as well. The result was presented in Fig. 6.34, and the approximated polynomial was described in Eq. (6.17). The root mean square error was equal to 327,260 PLN and standard deviation equal to 337,993 PLN, which was considered reasonable for price range 2.0-24.0 mln PLN. The approximation was achieved in Python with external libraries.

$$P(W, L) = 372 \cdot L^2 + 4,391 \cdot W^2 + 6,638 \cdot WL - 604,116 \cdot L - 75,409 \cdot W + 6,130,779 \tag{6.17}$$

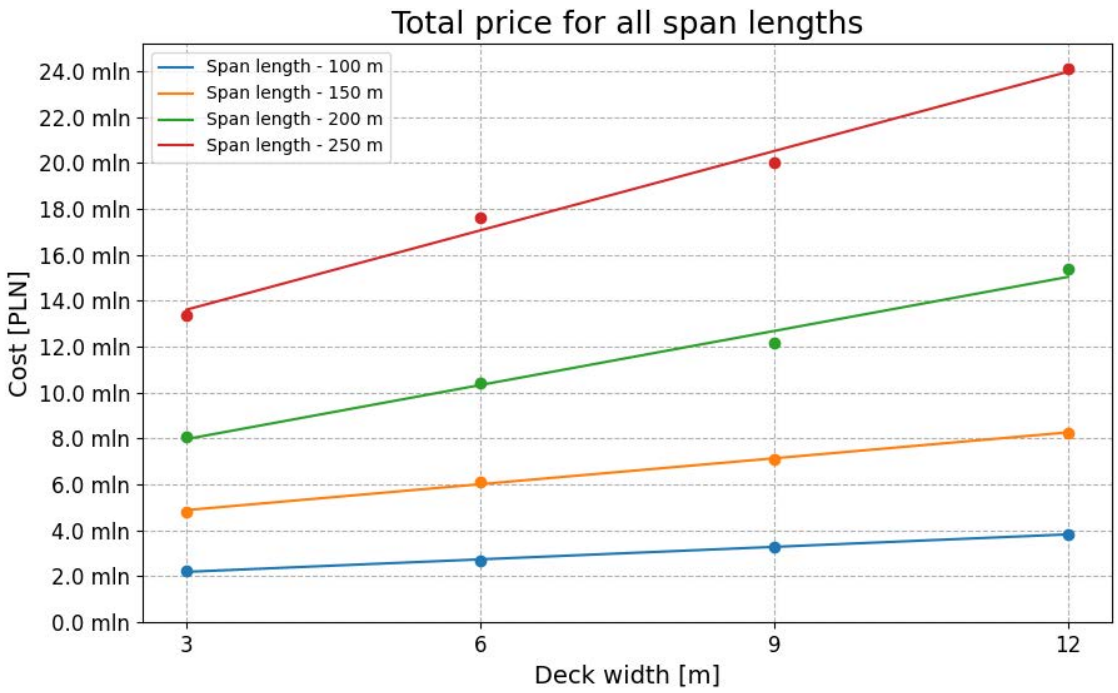

Figure 6.32 The cost depended on the deck width for all span lengths - cost per two sides

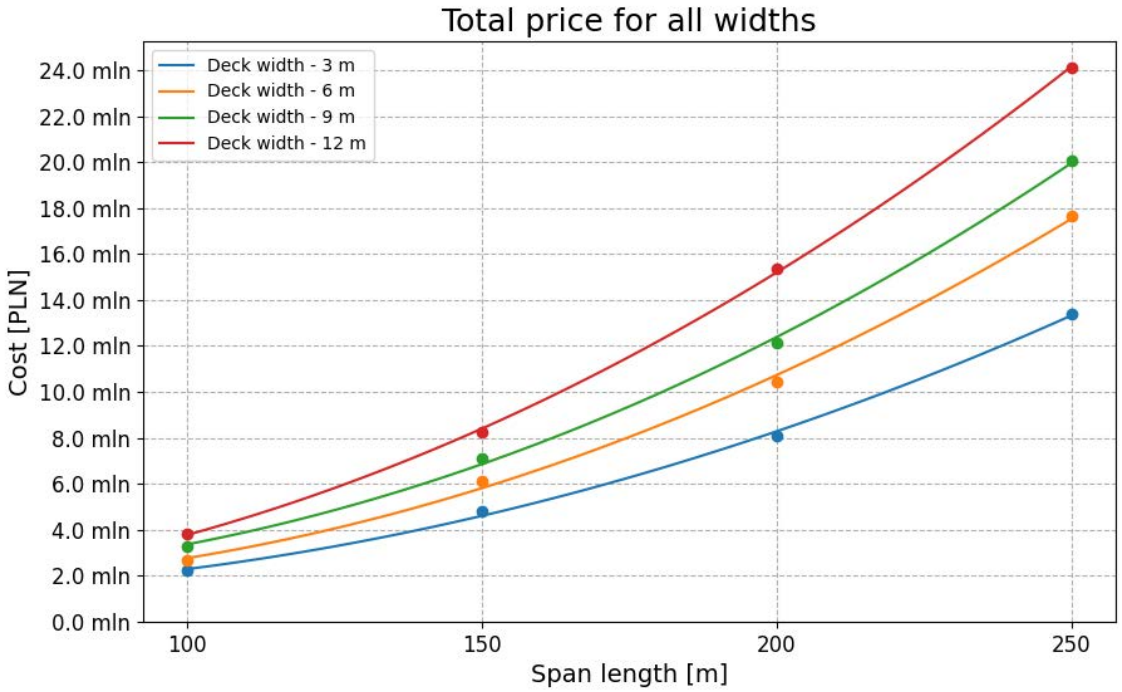

Figure 6.33 The cost depended on the span length for all deck widths - cost per two sides

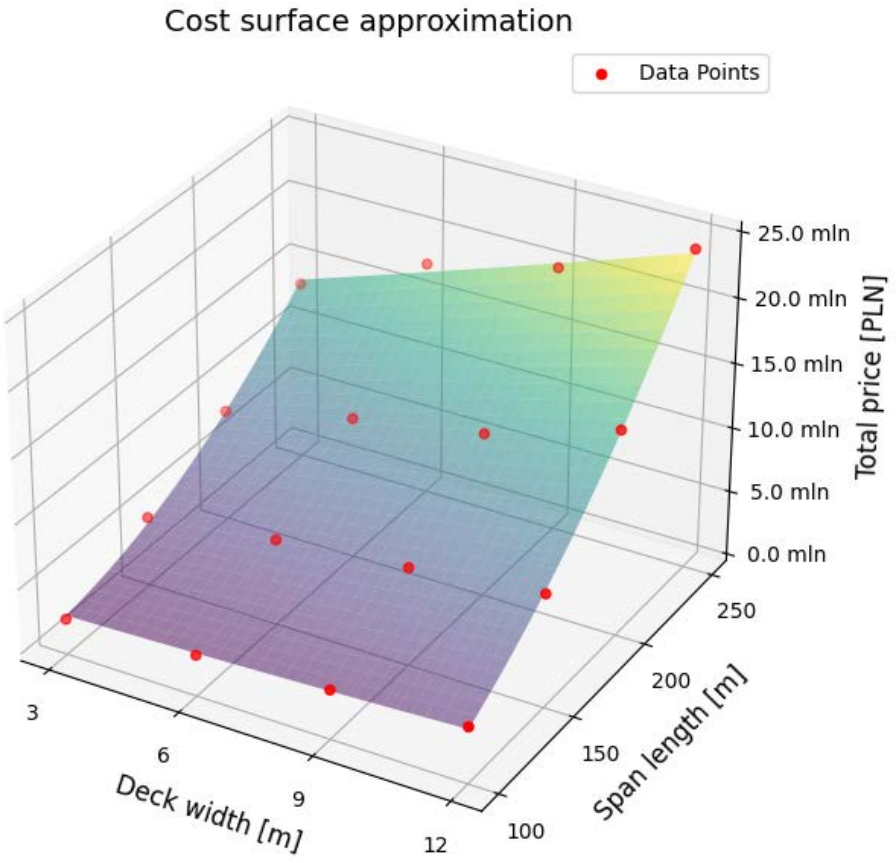

Figure 6.34 The cost approximation depended from both deck width and span length

Since the literature did not provide the estimated cost of the material, which was very reasonable considering the change of prices during the years 2019-2025 when the PhD had been prepared, it was decided to assume a reasonable range of steel grades for arch, tie and hangers and compare it with the obtained results. Since the reference steel weights were presented by Tveit in 2011 [75], it was decided to refer to the steel grades used in bridges at that time. As Schanack and Brunn presented in [86] from 2009, the used steel grades in their example were steel S355 and S460 for structural steel, B500 for reinforcement steel, and Y1080 and Y1500 for prestressed steel. It was decided to make the following assumptions regarding pricing based on Fig. 3.12b data: (a) the arch price range between S355 and S460 price tags, (b) position prestressed steel, bracings, bearings assumed half structural S355, half prestressed steel price tags, (c) hangers price range between S355 and prestressed steel price tags, (d) temporary chord price range between S355 and S460 price tags, (e) reinforcement assumed as S355 price tag. The description of the prices of each of presented steel grades were presented in Sec. 6.1.5 and Sec. D.5. The minimum and maximum options were calculated. The results were presented in Fig. 6.35, Fig. 6.36 and Fig. 6.37.

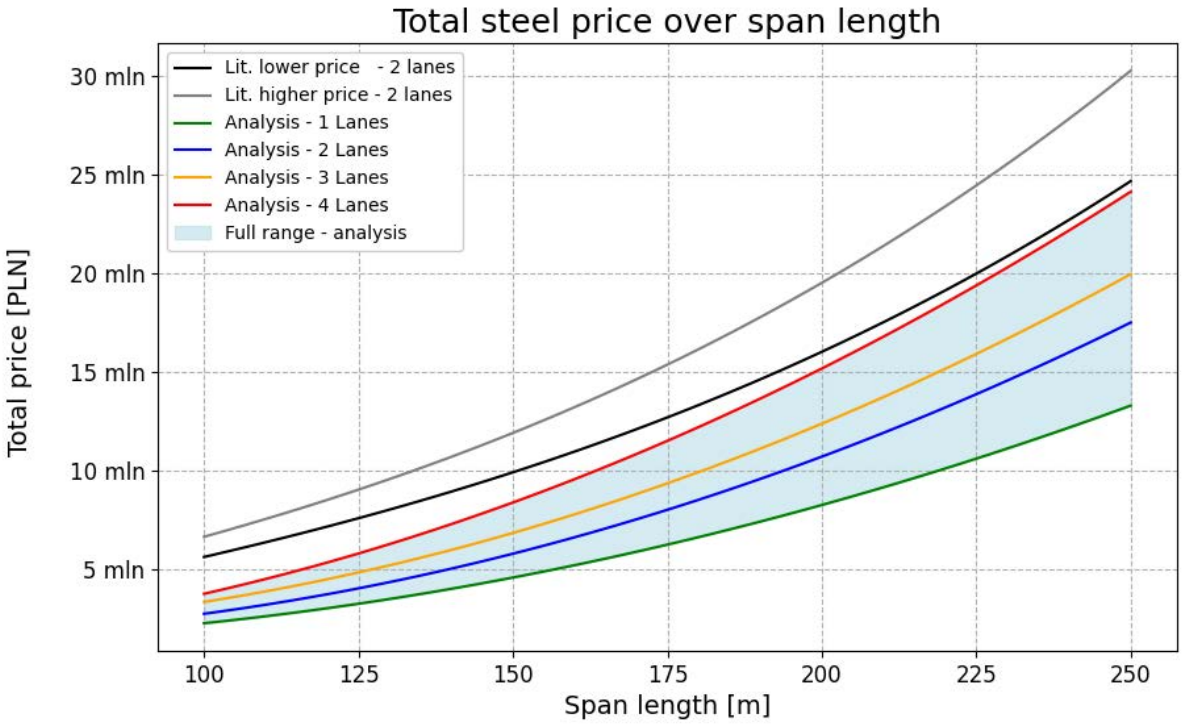

Figure 6.35 The cost depended on the span length for all deck widths and estimated prices from literature data - cost per two sides

The analysis showed, Fig. 6.35, that all the results were below the lower price estimation from literature and with great margin to the higher price estimation. Results for the 4 lanes almost reached the lower estimation from the literature. The most relevant results for 2 and 3 lanes in comparison to the literature were characterized with similar, almost parallel trajectory for greater span lengths. To visualize that, the ratio of the price of the obtained results to the literature estimations were done, Fig. 6.36 and Fig. 6.37. The obtained approximations had lower ratio value at lower span lengths reached asymptotically a constant value for greater span lengths. For the most reference 2-3 lanes ratios, the ratios started with 0.5-0.6 value for 100 m and reached 0.7-0.8 value for 250 m in case of lower price reference. In case of higher price reference, these values change to 0.4-0.5 and 0.58-0.67 respectively. The advantage at the lower span lengths was suspected to be caused by the sparse hangers' arrangement effect described in [93, 94]. In these literature positions, the number of hangers was equal to 12, and in the 2 and 3 lanes cases for 100 m of span length 12 and 14 respectively, Fig. F.1b and Fig. F.1c in Appendix F. Therefore, the well-defined hangers' arrangements started to be less competitive in comparison to custom and irregular hangers' arrangements. At the same time, the greater the span length was, the greater the influence of the loads on the structure was, so the network regular arrangement started to be more advantages and the number of hangers increased. In this case, the results for 2 and 3 lanes for 250 m of span length resulted in 16 and 24 hangers respectively, Fig. F.4b and Fig. F.4c. The results for 4 lanes reached very close to the lower estimations from literature at 250 m and seemed to converge to it. Compared to higher estimations, the ratio reached 0.8 level. The results for 1 lane started from a ratio value of 0.4 and stabilized at 0.55 for lower price estimate. For higher price estimate, the trajectory was the same with range 0.35 to 0.44.

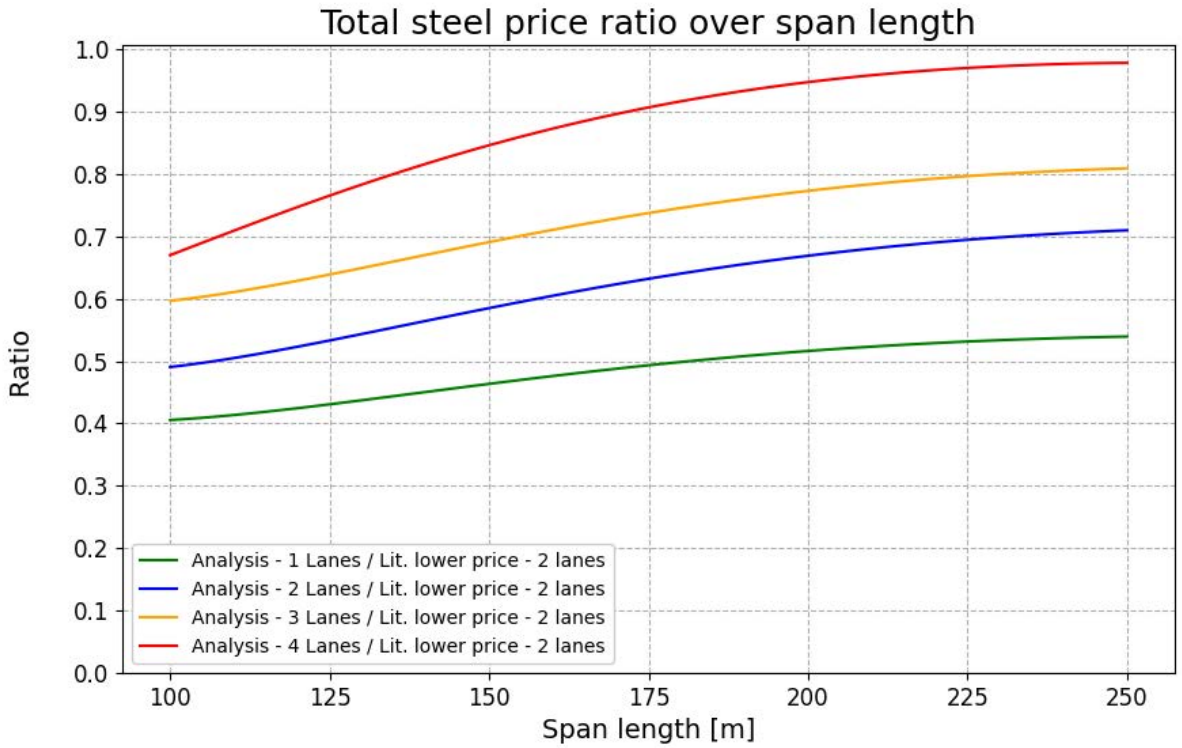

Figure 6.36 The cost ratio depended on the span length for all deck widths in relevance to the lower estimated prices from literature data - cost per two sides

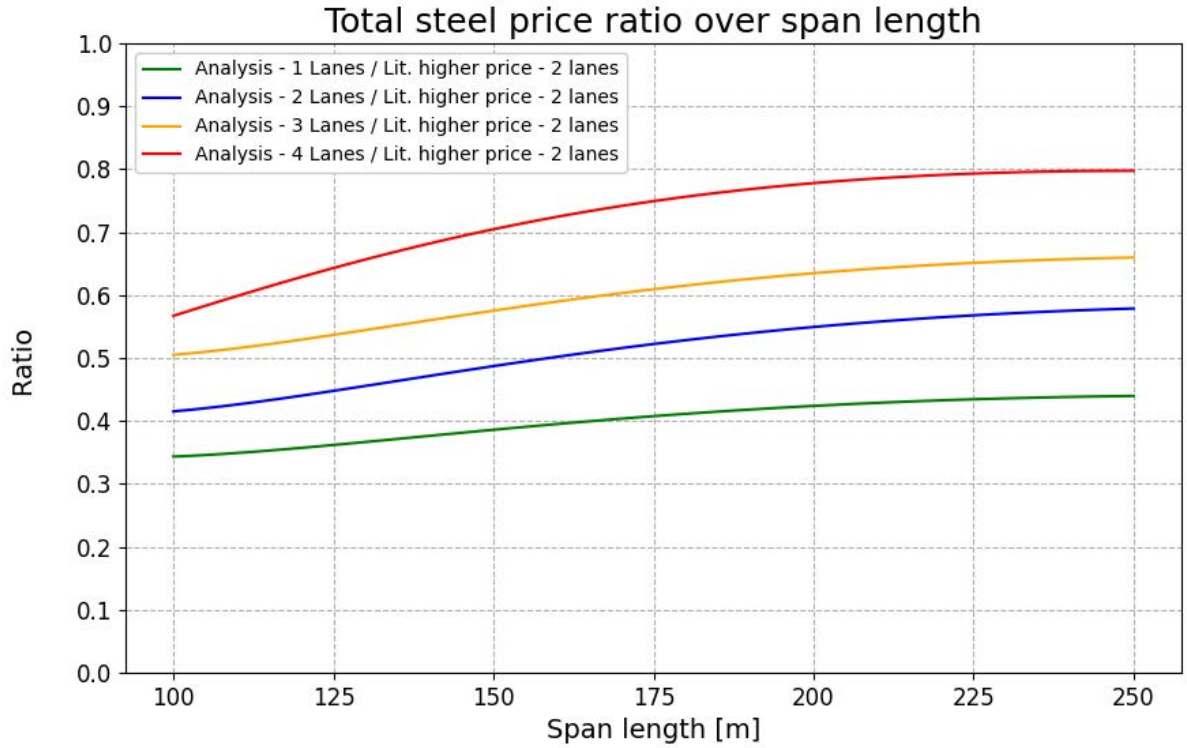

Figure 6.37 The cost ratio depended on the span length for all deck widths in relevance to the higher estimated prices from literature data - cost per two sides

The next comparison was made for the weight of steel per square area of the bridge. The reference presented in [117, 113] for Åkvik Sound network arch of 135 m was chosen. It included two lanes of road traffic of 3.5 m each and two set of pedestrian lanes with 2.7 m of width each, Fig. 6.38. The weights of the structural and reinforcement steel were divided by the area of the bridge and compared with other bridges with vertical hangers, Fig. 6.39. It showed the superiority of the network arch bridge over the classic vertical hangers' arrangements in terms of saving structural steel with comparable quantity of reinforced steel.

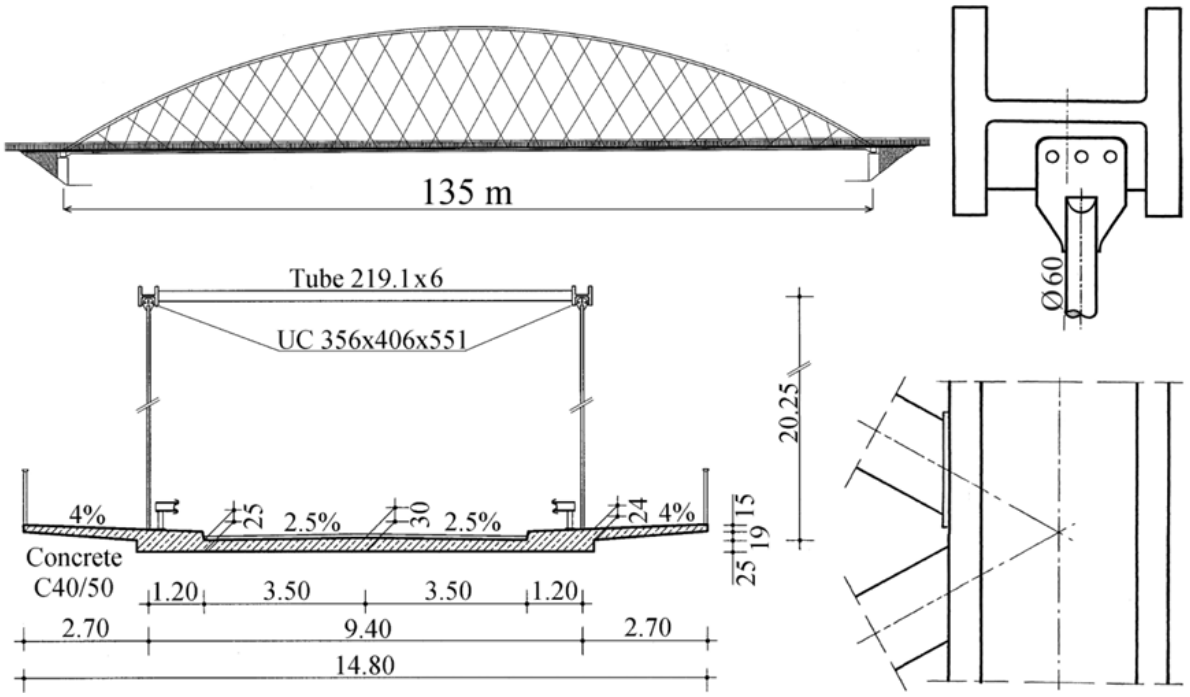

Figure 6.38 The detail technical pictures of Åkvik Sound network arch bridge [117, 113]

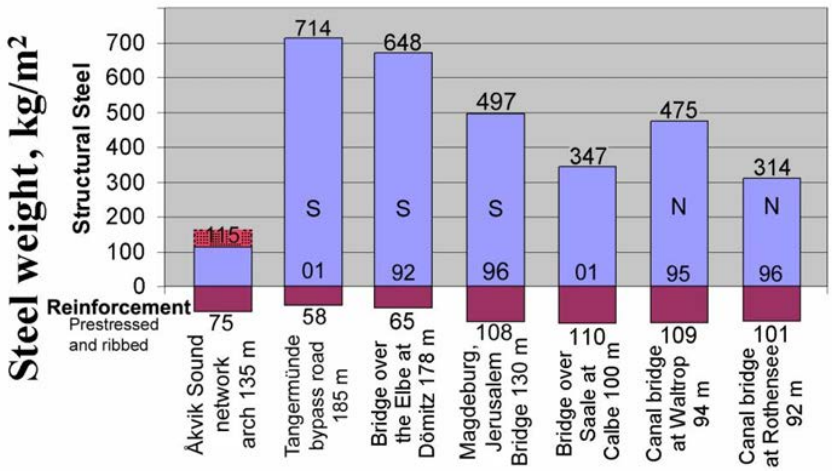

Figure 6.39 The comparison of steel weight in Åkvik Sound network arch bridge and other arch bridges with vertical hangers' arrangements [117, 113]

Since in the simulations, the reinforcement was not present, it was decided to consider both reinforcement and structural steel weight of the Åkvik Sound NAB as a reference, because reinforcement steel had the same rule as the structural steel in the simulated steel tie. Since the Åkvik bridge had pedestrian paths on both sides with lower pedestrian variable load comparing to the traffic variable loads and unloaded parts of 1.2 m on both sides, it was decided to modify the presented steel estimates in order to match the simulated results. The following assumptions were used when calculating the loads on Åkvik Sound bridge:

- UDL - 3.0 m of 9.0 kPa, 3.0 m of 2.5 kPa and 1.0 m of 2.5 kPa,
- TS - 600 kN and 400 kN,
- Pedestrians - 5.4 m of 3.0 kPa.

The 3.0 kPa for the pedestrian loads was used, even though the Norwegian national Annex required smaller 2.5 kPa. These loads summarized and divided by the length of the bridge resulted in 8182 kN / 135 m = 60.6 kN/m. Following the same principles presented in the Tab. 6.6 for 135 m, the closest deck width to the calculated variable load would be for 3 lanes, for which loads were 56.8 and 61.8 kN/m. Therefore, the width of 3 lanes, so 9.0 m, was used as a reference width for the Åkvik Sound bridge in order to match the same principles as in the simulation. Then the total steel weight in the reference bridge would be $(115 + 75) \cdot 14.8/9 = 312.4$ kg/m^2. Using the approximated formula for the total weight for 3 lane simulations, Eq. (6.11), the total weight was determined as 329,610 kg, so for the bridge of 135 m by 9.0 m that resulted in 271.3 kg/m^2. This meant, that the total saving was 13.1%, which was considered as a good outcome and showed, that the algorithm acted as expected. Author was aware, that the weight of bearing and connections was not included in the simulations, but the pedestrian load was considered conservative from the Norwegian Annexes perspective, so it was expected to be compensated by that. The steel weight approximation for 3 lanes was more divergent than approximations for other lanes. The algorithm's orientation around the price, not the weight, could also be a justifying factor for the divergence. Since the results for 1 and 2 lanes were very similar and well matched the parabolic approximation with low divergence, it was decided to simulate the results for 3 lanes assuming, that the weight between 1 and 2 lanes would be the same as between 2 and 3 lanes, since loads increased almost linearly in relevance to deck width. The weight for 1 lane would be 196,172 kg for 135 m of span length according to Eq. (6.9), and 276,320 kg for 2 lanes according to Eq. (6.10). Therefore, the extrapolated weight for 3 lanes should be 356,467 kg, which would result in 293.4 kg/m^2. This areal weight was greater than the previous calculations from the approximated curve, but was still lower by 6.0% than the literature estimations. **Even with these favourable estimations from the literature perspective, the lower weight was achieved than the literature suggested.**

All the provided comparisons from price and weight perspective led to better outcomes than the literature's recommendations. The algorithm was considered as operating as desired and managed to provide the optimal solutions in terms of cost reduction.

6.5.3 Results - geometrical properties

The χ_{ip} value varied between 0.70 and 0.96, Fig. 6.40 and Fig. 6.41, **but without results for the deck width of 9 m all the results would be narrowed to 0.80-0.96 range**. In general, the buckling coefficient roes over the increase of the span length. **Both full and half loaded deck had similar trajectory.** The buckling factor was in average smaller for half loaded deck up to 200 m of span length and after that the situation reversed.

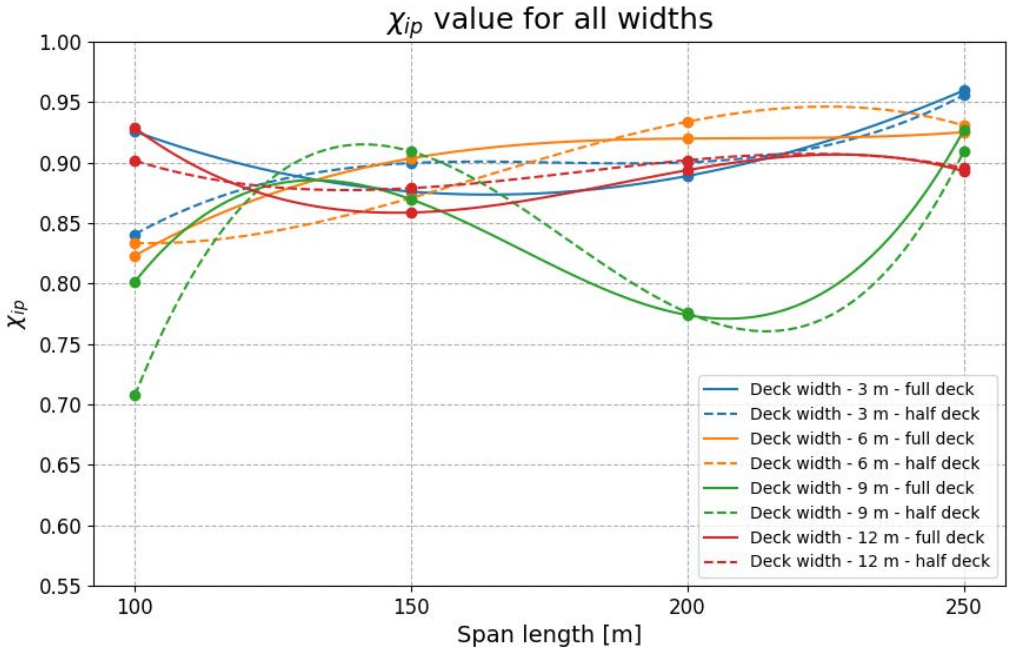

Figure 6.40 The comparison of the buckling coefficients for all the deck widths over span length including full (solid) and half (dashed) loaded deck

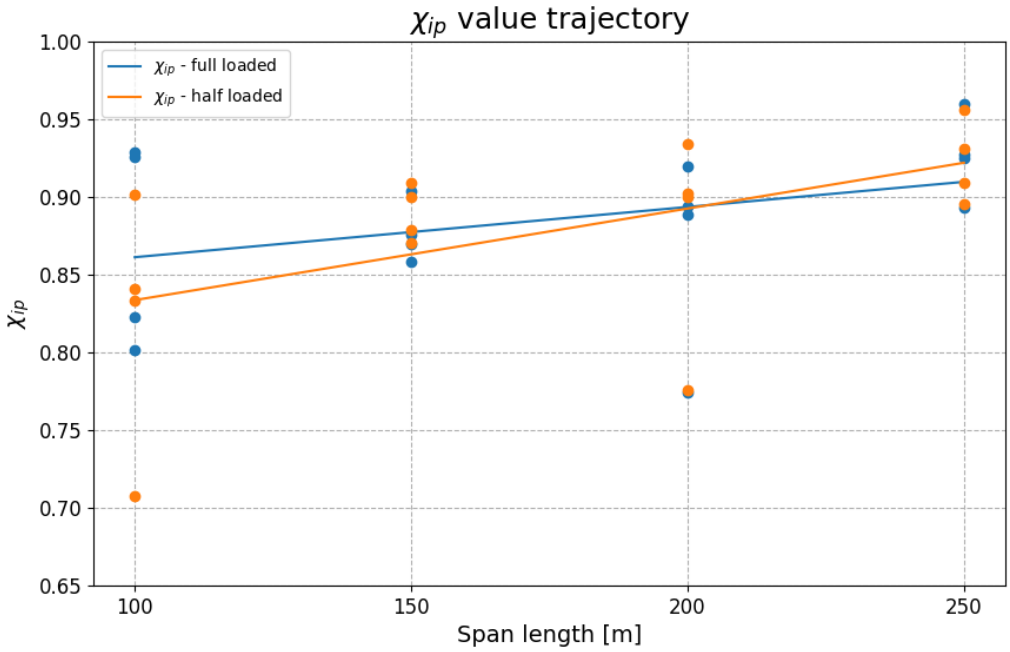

Figure 6.41 The trajectories of the χ_{ip} values for full and half loaded deck

The ratio of tie's and arch's bending moment of inertia occurred in wide range from 0.30 to 1.15, Fig. 6.42, without clear trend. The optimal results obtained in article [6] laid in range from 0.135 to 0.476, which was much lower than the obtained results. The value for both arch and tie laid within 0.002 m^4 to 0.010 m^4 except results for deck width of 12 m, which had much wider range between 0.012 m^4 to 0.055 m^4. **Mostly arch had greater I_y value.** According to literature, Fig. 3.7 [13], the optimal obtained value for the arch should be at magnitude of 0.02-0.03 m^4 and for the tie at magnitude of 0.03-0.04 m^4. **Most of the results for arch laid significantly below the suggested values** and only result for 250 m of span length

and 12 m of deck width exceeded the suggested values. **All the results for tie were at least twice lower than the suggested values**.

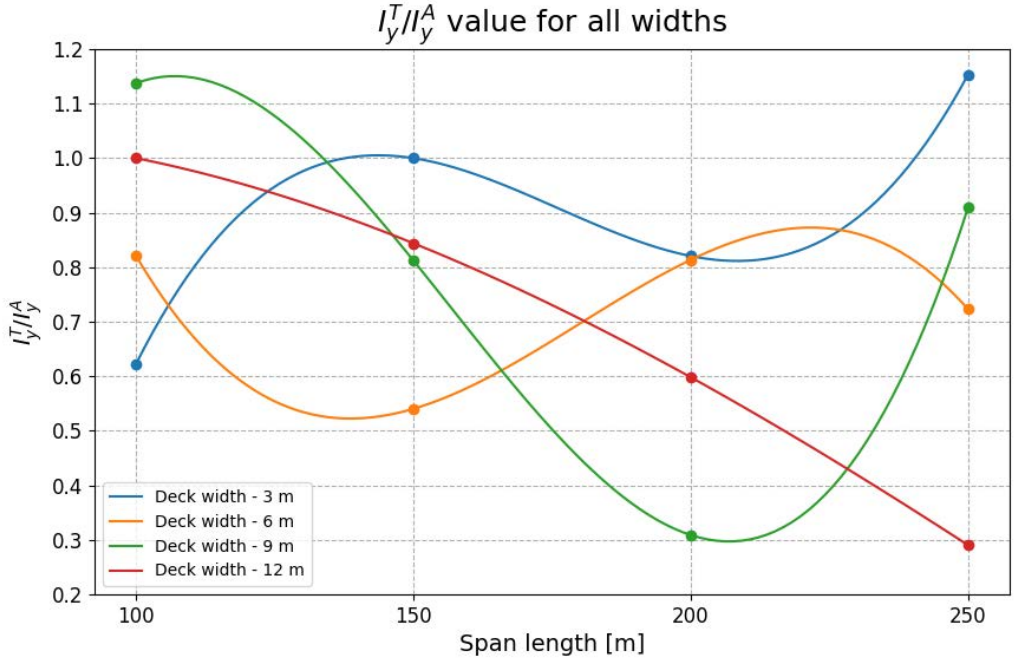

Figure 6.42 The bending moment of inertia ratio comparison of the tie (T) and the arch (A)

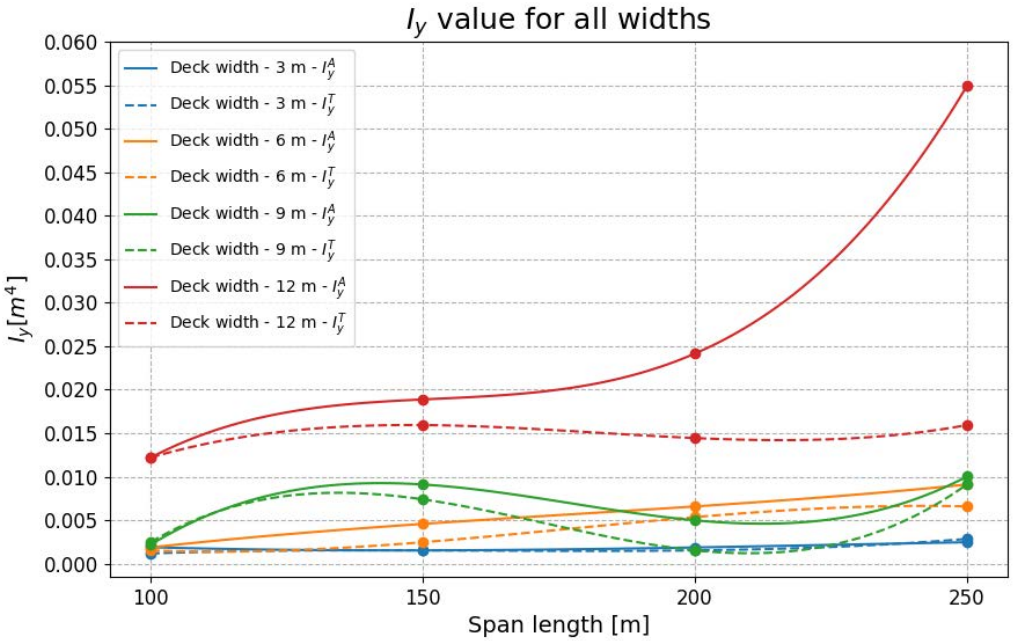

Figure 6.43 The bending moment of inertia value comparison of the tie (T - dashed) and the arch (A - solid)

The ratio of section area of the tie over arch had downwards trend over the span length, Fig. 6.44, within range from 0.8 to 1.16 for span length of 100 m and range from 0.58 to 0.90 for span length of 250 m. The absolute value of section areas had linear upwards trend, Fig. 6.45. The greater the deck width was, the greater the inclination of the linear approximation was. Arch's section area increased more than the tie's section area over the span length

and the greater the deck width was, the greater this difference got. According to literature, Fig. 3.7 [13], the optimal section area for the arch should be at magnitude of 0.25-0.30 m^2 and for the tie at magnitude of 0.08-0.09 m^2. **The section area of the arch from the analysis for the arch changed from 0.035 m^2 to maximum 0.16 m^2, which was about 2-6 times less than recommendation. The tie had section area from 0.03 m^2 to 0.10 m^2, which covered the recommended range, but was in majority smaller than that.**

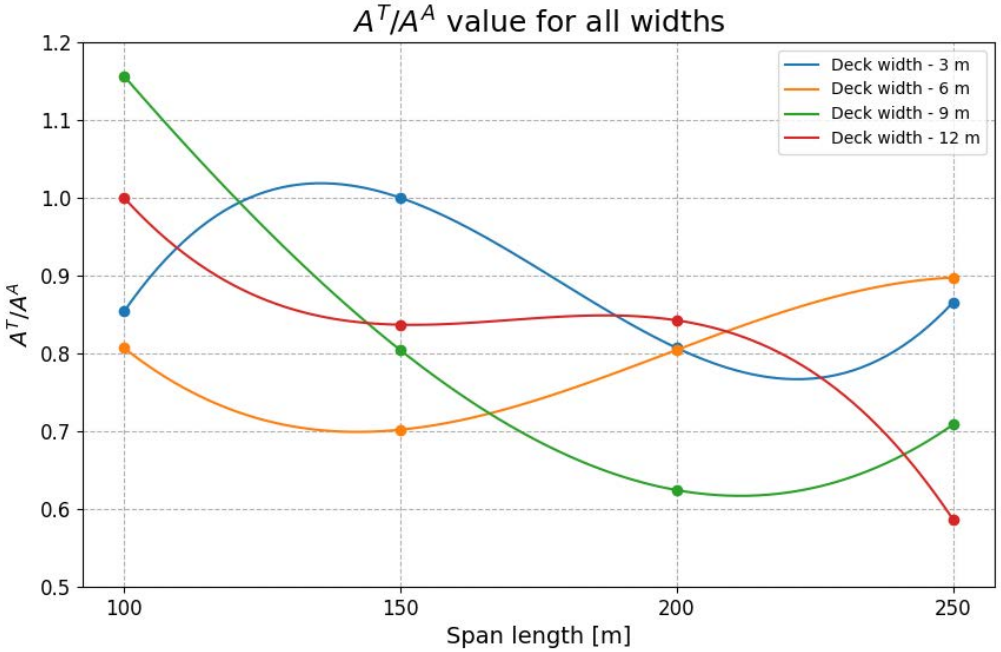

Figure 6.44 The section area ratio comparison of the tie (T) and the arch (A)

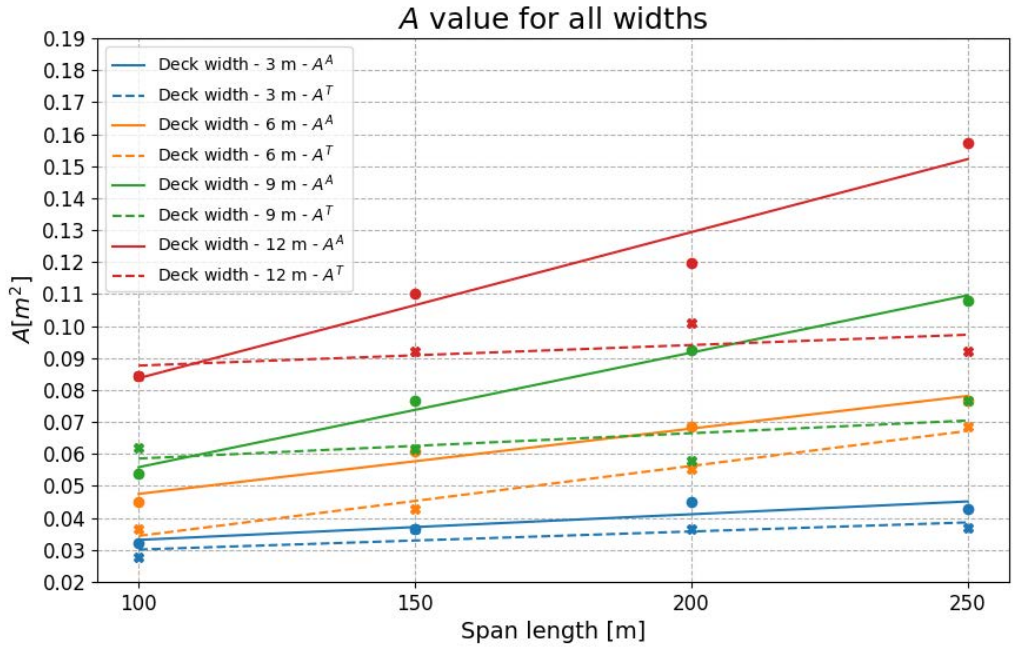

Figure 6.45 The section area value comparison of the tie (T - dashed) and the arch (A - solid)

The tie's over arch's diameter ratio was not characterized by any visible trend, Fig. 6.46. The total range was from 0.70 to 1.15 and the arch was smaller in size than the tie. The diameter

for 1, 2 and 3 lanes did not exceed 1.0 m, Fig. 6.47. Again, as in previous analysis, the results for 4 lanes were outstanding with range from 1.1 m to 1.7 m. No visible trend was noticed.

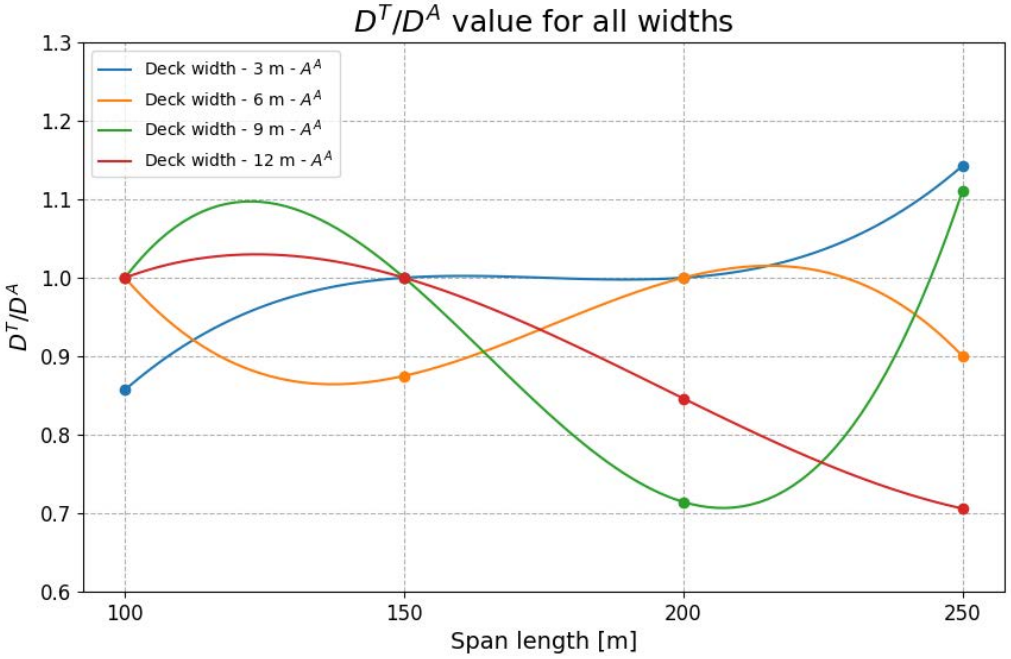

Figure 6.46 The section diameter ratio comparison of the tie (T) and the arch (A)

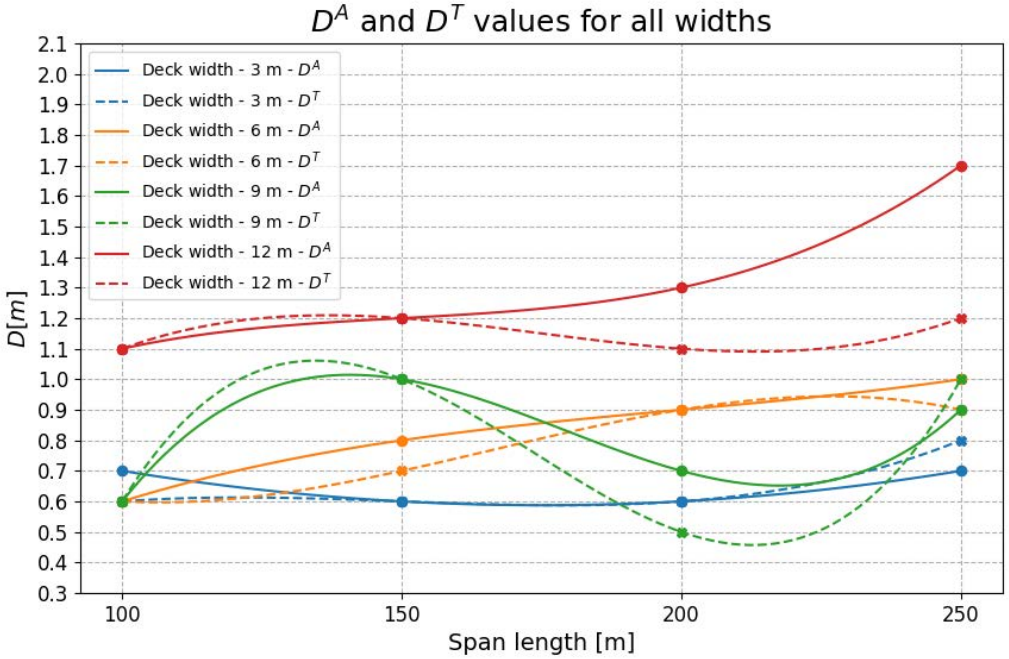

Figure 6.47 The section diameter value comparison of the tie (T - dashed) and the arch (A - solid)

The structural steel grade had rapid upwards trend over the span length, Fig. 6.48. The results for 100 m of span length covered the entire grade spectra, but after that vast majority of the results utilized the highest steel grade possible. It was applicable for both arch and tie. Similar trend was observed in hangers' steel grade, Fig. 6.49. There was great gap between steel S460 and Y1700, which had to be economically justified to overcome, since the price difference

was about 3 times. The majority of hangers kept structural steel rather than prestressed steel. The results for 12 m of deck width utilized prestressed steel 3 times and that was the most often case. All the results for 3 m of deck width were within structural steel range. The remaining 6 m and 9 m of deck width utilized prestressed steel once. **The grade limitation of the structural steel grade for the arch and the tie, as well as too significant gap between structural and prestresses steel grade for hangers were the fields for improvements in order to make algorithm less restrained.**

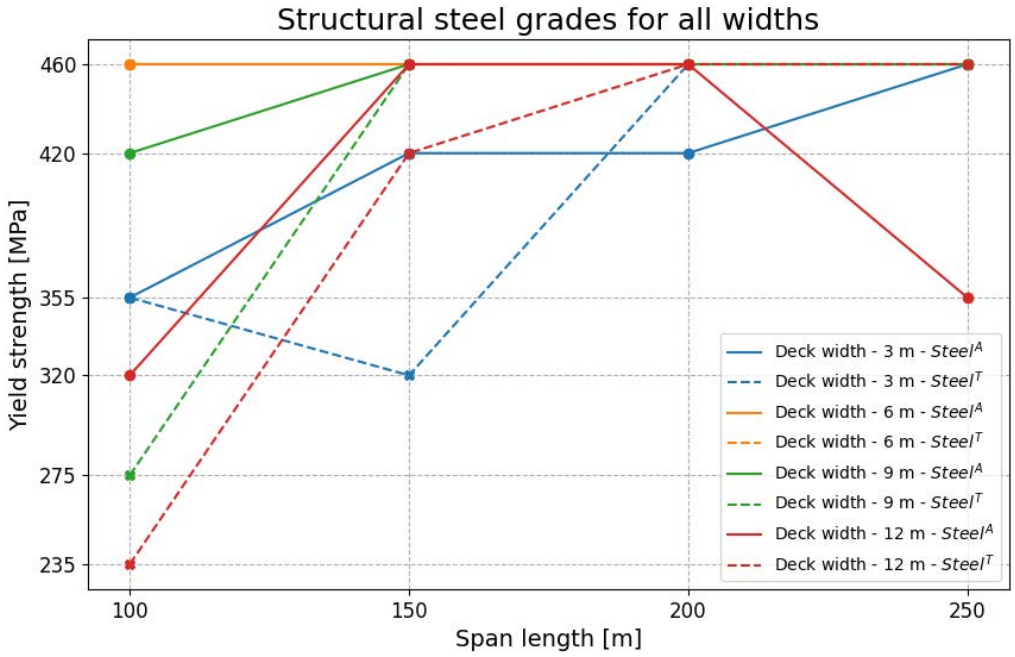

Figure 6.48 The structural steel grade of the tie (T - dashed) and the arch (A - solid)

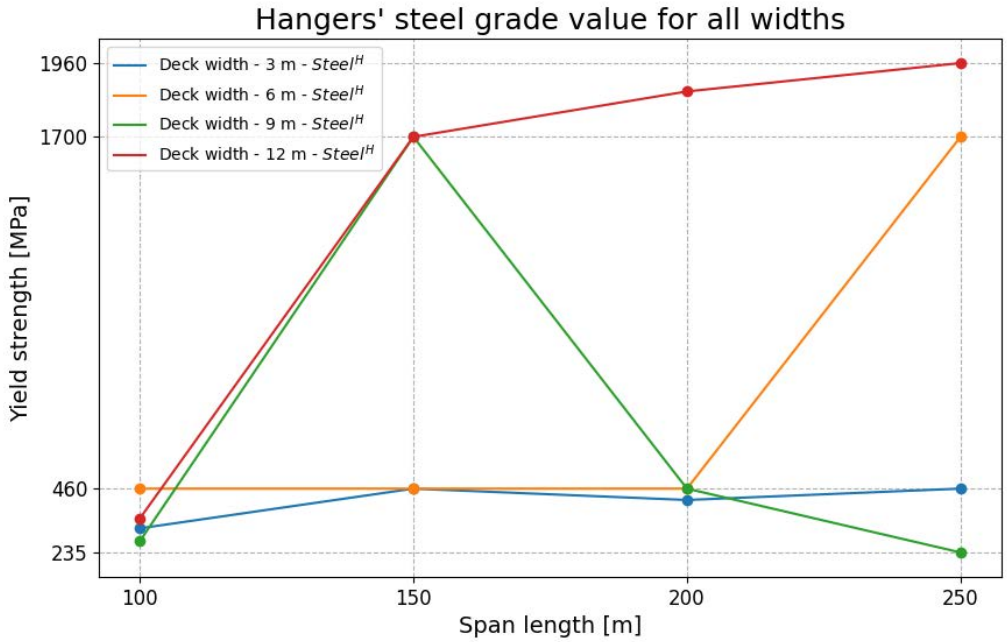

Figure 6.49 The structural steel grade of the hangers (H)

The height to span length ratio was in vast majority below 0.17, Fig. 6.49, with only two cases for 3 m of deck with and 150 m and 200 m of span length exceeded this value. **Except these two cases, the range was between 15.5% to 16.7%, which laid within the top part of the typical range from 14% to 17% of arch rise value in network arch bridge [86].**

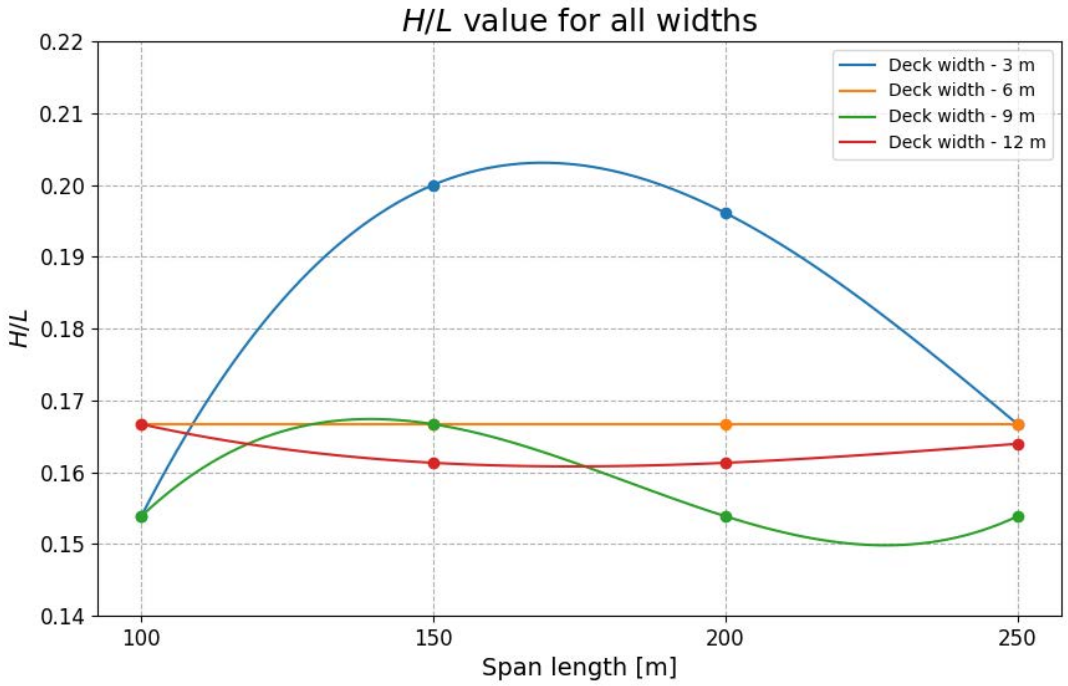

Figure 6.50 The height to length ratio

The number of hangers was mostly below 25 in all cases, Fig. 6.51. The smallest number of hangers was present with 1 and 2 lanes. The 4 lanes cases had in majority less hangers than for 3 lanes with the greatest difference of 16. In general, number of hangers was between 12 and 42. No clear trend was noticed. In next step, number of hangers was divided by the span length, Fig. 6.52. The total range laid between 7% to 38% of span length, but except two results for 3 and 4 lanes with 100 m of span length, the range would be between 7% to 20%. According to literature [97], the optimal number of hangers for 100 m should be 36-46% of span length value, and decrease to 17-20% for 250 m of span length. Similar trend was observed in the analysis, where the range was 16-38% for 100 m of span length, and reached 7-20% after that. The diversity was greater in the obtained results, but with focusing on greater loads, the initial results would be 32-38% for 100 m and 11-20% for further span lengths, so less diverse. The lower ratio values for 6 m deck width showed clear down trend, but the results for 3 m deck width were constant with average value of 11%. For 3 m, 9 m and 12 m of deck width results, the downward trend was not consistent but with sudden drop from 100 m to 150 m of span length and then varied with slight downwards, constant and upwards trends. **In general, more sparse systems were obtained than the ones suggested by the literature, which showed a potential of sparse system over the well described arrangements. Authors in [94, 93] also suggested, that custom made arrangement in sparse systems provided better performance than the well-known network and Nielsen arrangements, which matched author's conclusions.**

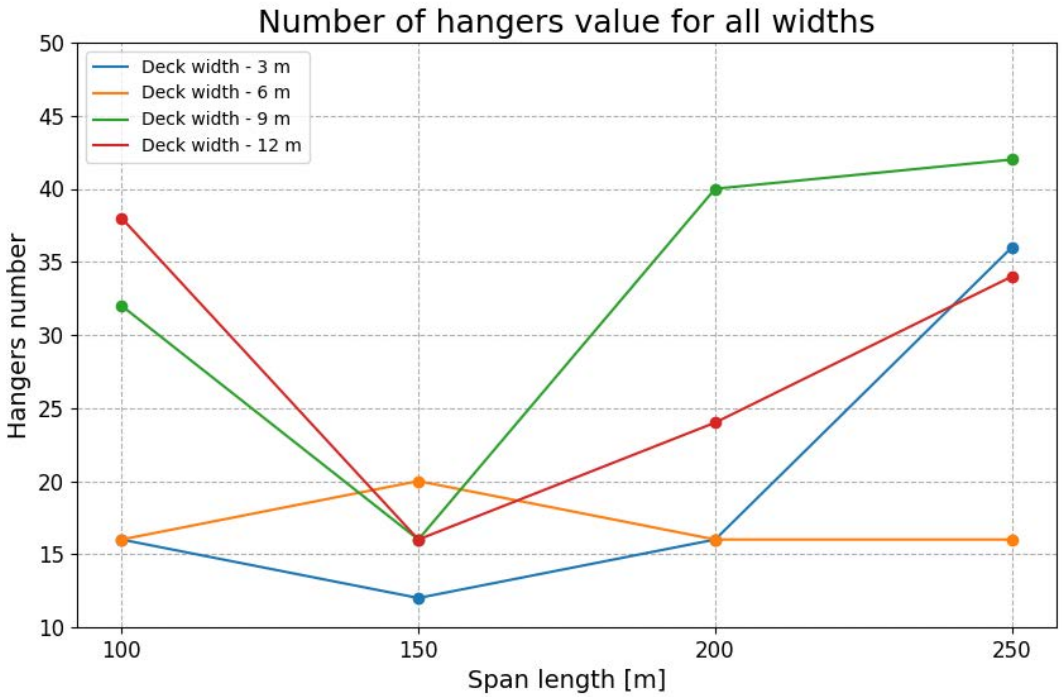

Figure 6.51 The hangers number

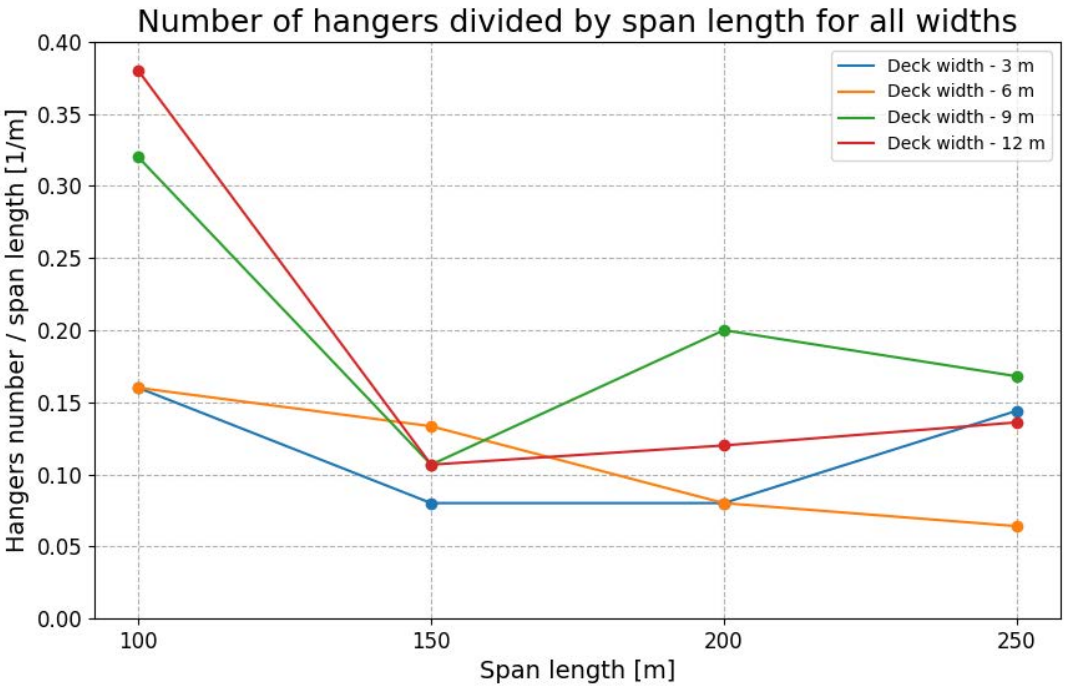

Figure 6.52 The hangers number to span length ratio

The majority of **hangers' diameter** was below 65 mm, Fig. 6.53. **No visible trend was noticed**. The average diameter for 100 m of span length was much smaller than for 250 m, but results in between did not provide predictable trajectory.

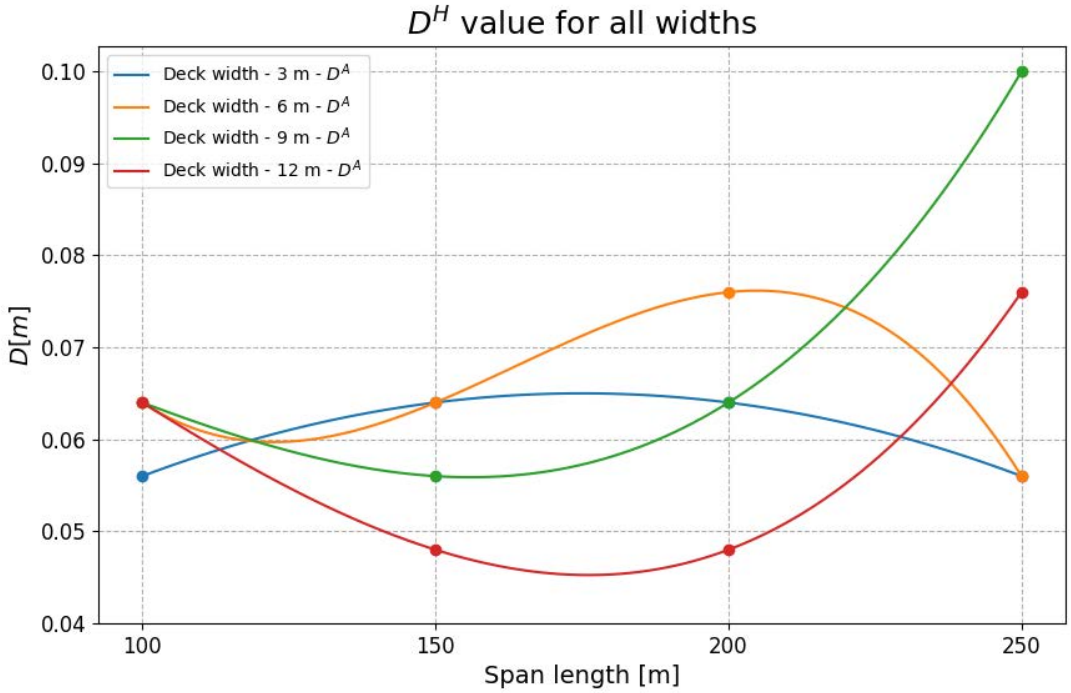

Figure 6.53 The section diameter value comparison of the hangers (H)

The hangers' inclination angles investigation showed, that in relation to relevant span length, all the results for each span length and each deck width kept the same parabolic trajectory, Fig. 6.54 and Fig. 6.55. The graphs presented the minimum inclination angle to the tie. **The lowest inclination angle occurred for the middle part with expected value of 45^o and increased the more the closer the hangers were to the ends of the bridge reaching the expected value of 67^o.** The total range of inclination angle was from 35^o to 90^o. The equation describing the parabola trajectory was determined with genetic algorithm included in Galapagos component in GH with self-coded RMSE minimization criterion and expressed in Eq. (6.18).

$$\alpha(x) = \frac{22}{(L'/2)^2}\left(x - L'/2\right)^2 + 45 \tag{6.18}$$

where L' was the distance of hangers' presence equal to 0.9 of total span length and x was a position from the beginning of hangers' possible presence.

The phenomenon of angle inclination increased towards the ends reminded the best results from the article [93, 94], where vertical hangers were presents close to the ends with network arrangement presented in the middle part with close to 45^o inclination. Also, the authors [87, 86, 83] mentioned, that the hangers near the ends should be adjusted iteratively in order to get even stress distribution. This meant, that **the well described arrangements required a modification near the ends which locally diverged the hangers' arrangement from being regular, which was reflected in these results.**

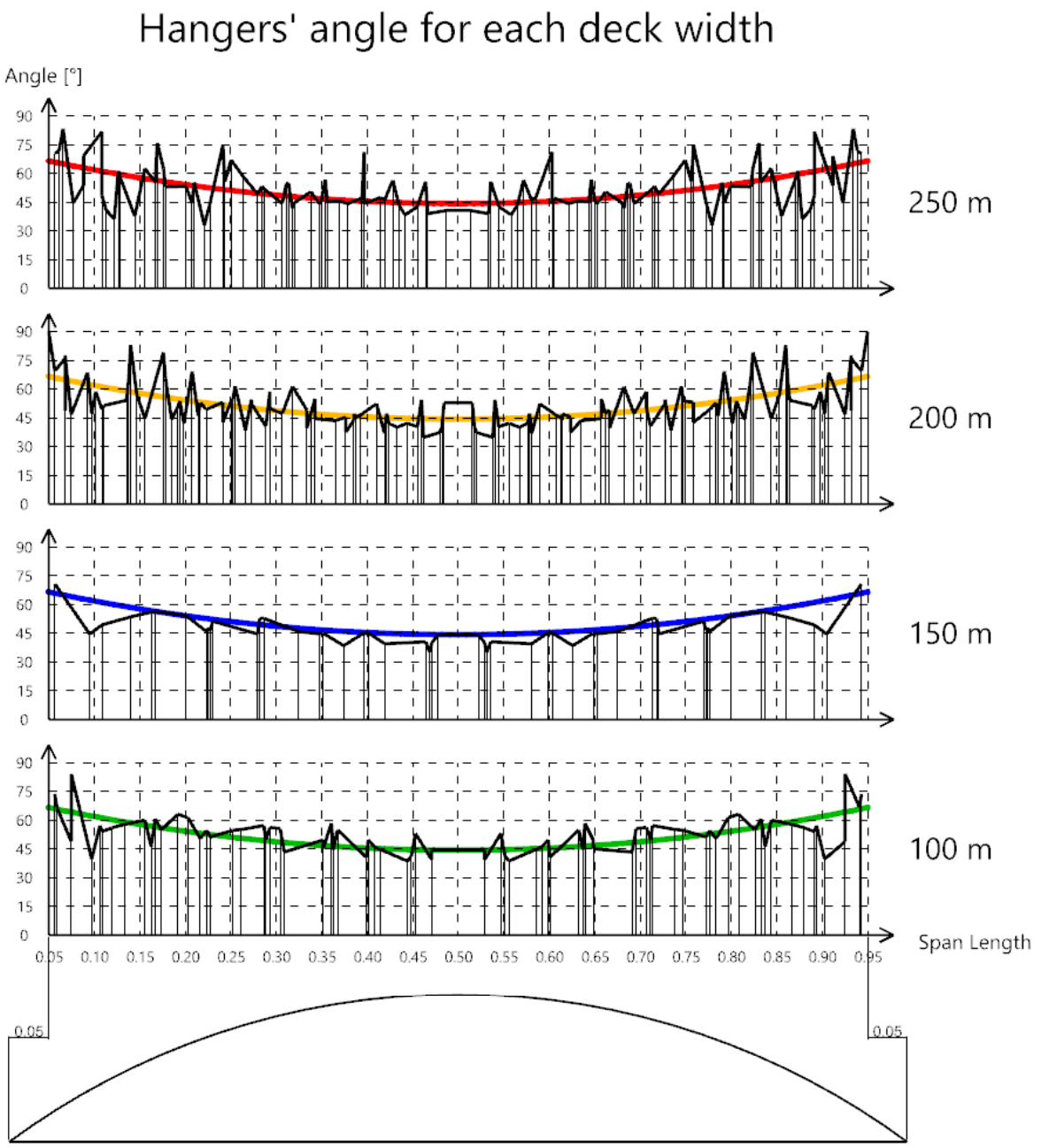

Figure 6.54 The hangers smaller inclination angle to the tie determined for the middle point of each hanger - results for each deck width. The middle point was chosen as a intermediate position between the arch and the tie, and was intended to reflect trend for both of them

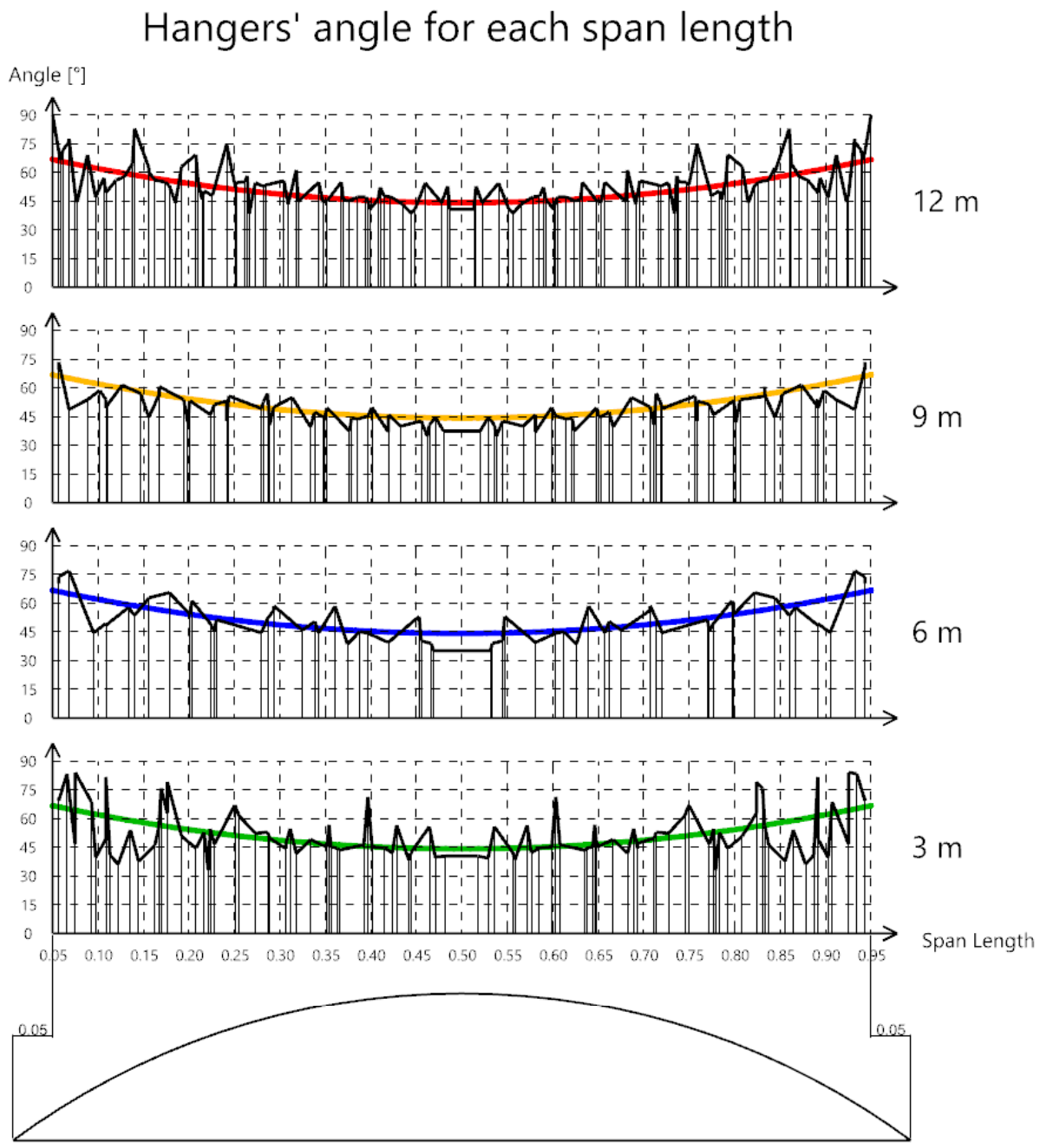

Figure 6.55 The hangers smaller inclination angle to the tie determined for the middle point of each hanger - results for each span length. The middle point was chosen as a intermediate position between the arch and the tie, and was intended to reflect trend for both of them

The next analysed aspect was the number of hangers' crossings and their positions, Fig. 6.56 and Fig. 6.57. **The results for 100 m, 150 m and 200 m of span length had the greatest number of crossings in the middle part**. In a distance of about 35% of span length from the ends, the number of crossings started to decline the more, the closer the hangers were to the ends. The results for 250 m were characterized by ascending number of hangers from the middle part perspective towards the ends and at about 25% of span length distance from the ends started to decline. Similar trends were present if the crossing points on the arch and tie were included and excluded. **Considering all cases at once, the downwards trend of hangers' crossing points from the middle part towards ends was observed, Fig. 6.58**.

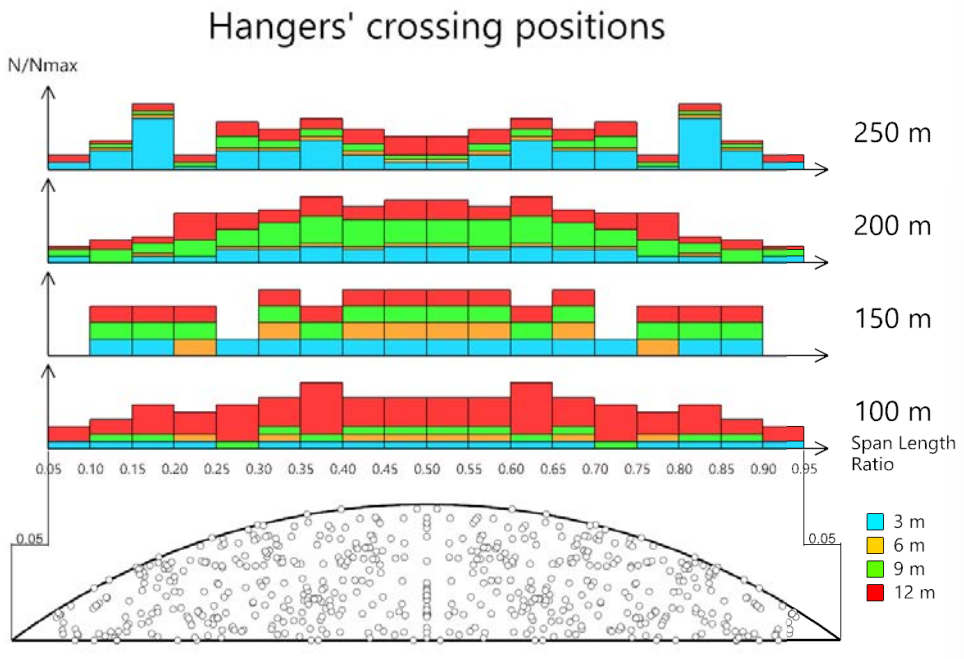

Figure 6.56 The hangers' cross positions histogram for each deck width and presentation of all hangers' crossing points - with points on the arch and tie - where N was the number of cross points per considered histogram bar and N_{max} was the maximum number of cross points among all the histogram bars

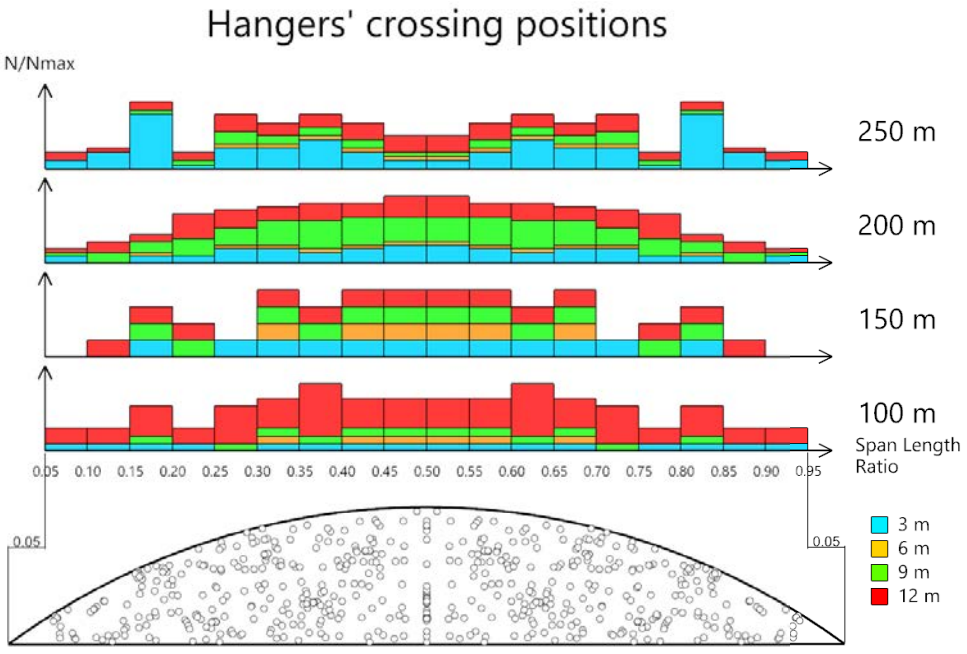

Figure 6.57 The hangers' cross positions histogram for each deck width and presentation of all hangers' crossing points - without points on the arch and tie - where N was the number of cross points per considered histogram bar and N_{max} was the maximum number of cross points among all the histogram bars

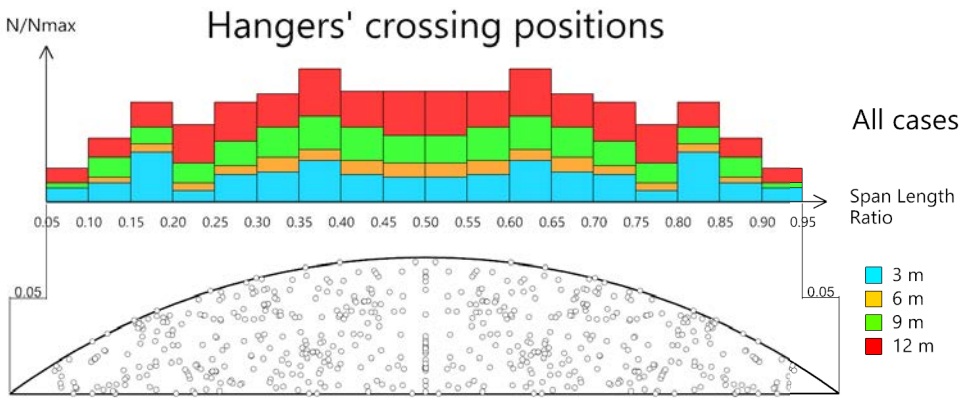

Figure 6.58 The hangers' cross positions histogram for all cases - with points on the arch and tie - where N was the number of cross points per considered histogram bar and N_{max} was the maximum number of cross points among all the histogram bars

The trends of hangers' arrangements were noticed when showing all the hangers from all the obtained best results, Fig. 6.59. Hangers' arranged along visible lanes were marked with red color. These lanes were more visible in the middle part and got weaker the more the closer the hangers got to the ends. These uncertain trajectory regions close to the ends were marked orange. In the middle part, a less dense regions were noticed, compared to the red-marked trajectories. These regions were marked blue. **These trends of having more crossings in the middle part corresponded with the trends of reduced number of crossings towards the ends in Fig. 6.58**.

The red lanes configured in a network arrangement. The angles of the crossing within the space between the arch and the tie resulted in a relatively regular configuration of 70.3^o, 75.5^o, 77.2^o, 84.4^o, 90.0^o and 97.5^o. These sequence was very similar to arithmetic-like sequence of 70^o, 77^o, 77^o, 84^o, 91^o and 98^o, where the space was 7^o between the angles, the starting value was 70^o and final 98^o with one exception of double of 77^o value. **The closer the hangers were to the ends, the smaller the angle got**.

Similar regular pattern was noticed for hangers' crossings outside the space between the arch and the tie. The angles there were 71.9^o, 82.8^o, 82.7^o, 92.0^o and 82.4^o, which could be simplified to 72^o, 82^o, 82^o, 92^o and 82^o. The sequence had space of 10^o, starting value of 72^o, maximum value of 92^o, but it was not an increase sequence.

This regular trend in angular divergences attracted author's attention and correlation between hangers' anchorage points on the arch and the tie were investigated.

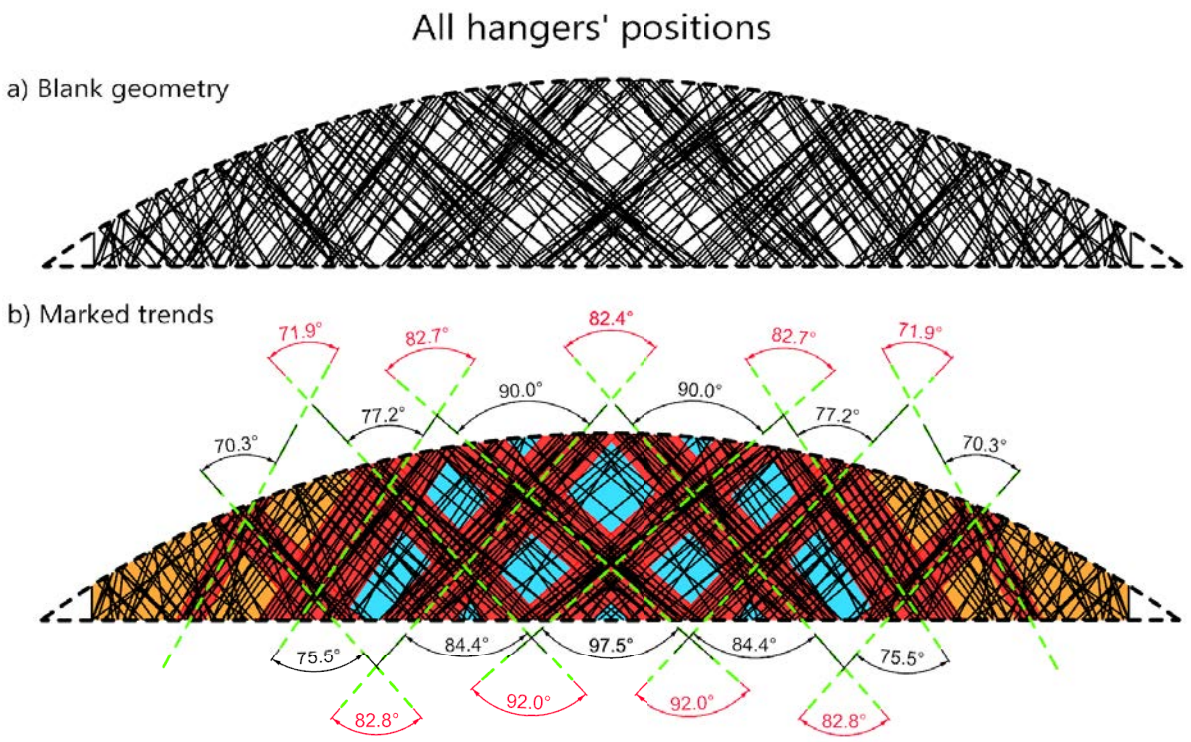

Figure 6.59 The hangers' arrangements for all span lengths and deck widths with (a) unmarked arrangements and (b) marked trends

First, the positions of the hangers on the arch and the tie were analysed, Fig. 6.60. The positions matched the obtained marked trajectories intersections with the arch and the tie from the Fig. 6.59. The graph did not answer the question, what was the correlation between hangers' anchorage on the arch and those on the tie.

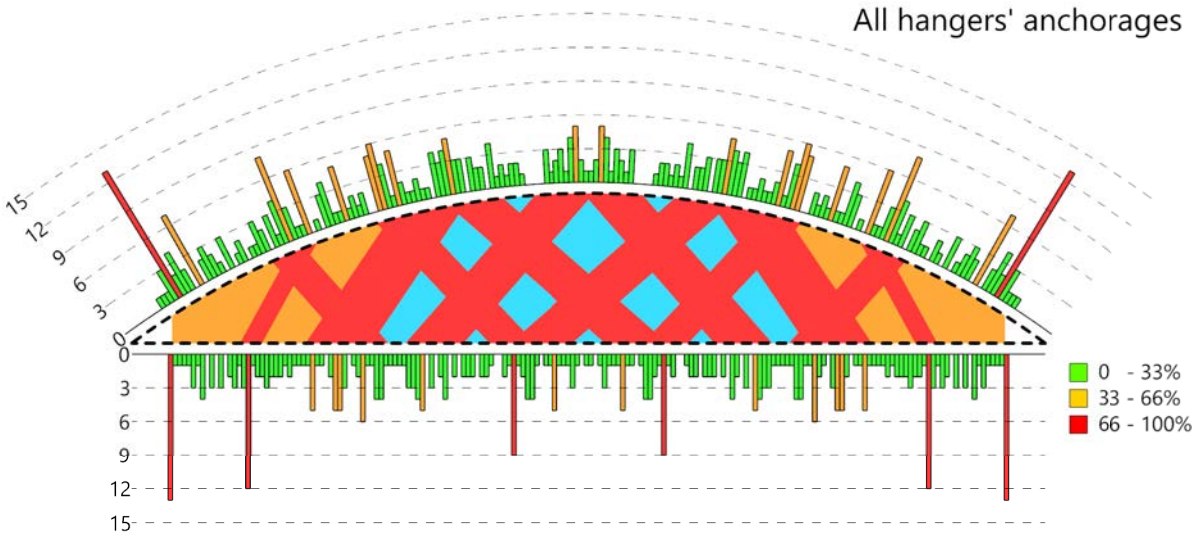

Figure 6.60 The hangers' anchorages positions on the arch and the tie with the histogram frequency of their presence in the selected graph ranges

In order to find expected hangers' trajectories from each section on the arch, the hangers for each section were sorted into two groups. The first included hangers which inclination was oriented leftwards to the radial line of considered section, the second group included hangers oriented rightwards from this line. Then the average leftwards and rightwards inclined hangers were determined for each section. Their position within each section was also averaged. **The results matched the already marked trends with 9 segments in total, Fig. 6.61**. The projected hangers' positions on the tie showed uneven distribution, but the number of segments was too low to conclude, therefore it was increased, Fig. 6.62. **The anchorages on the tie matched the marked trend as well, but except slightly denser presence of the anchorages near the end, no distinguished pattern was noticed**.

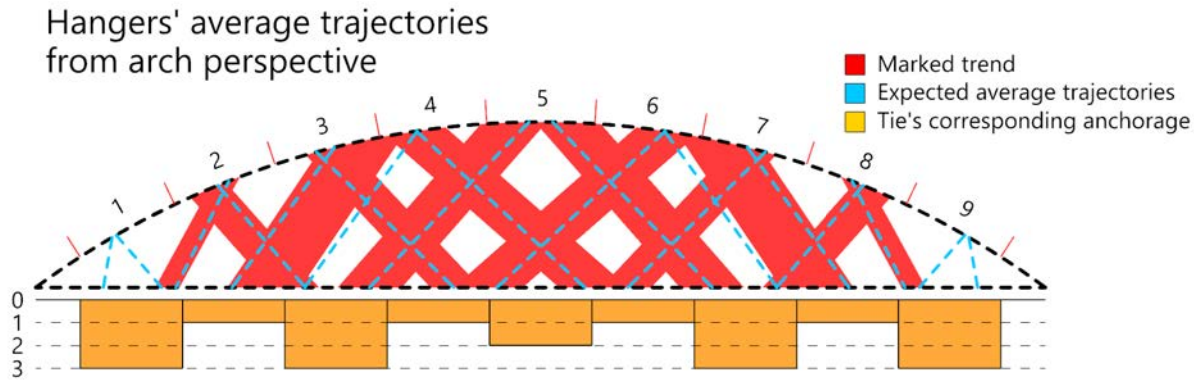

Figure 6.61 The hangers' trajectories from arch perspective and corresponding histogram distribution of corresponding expected hangers' anchorages on the tie

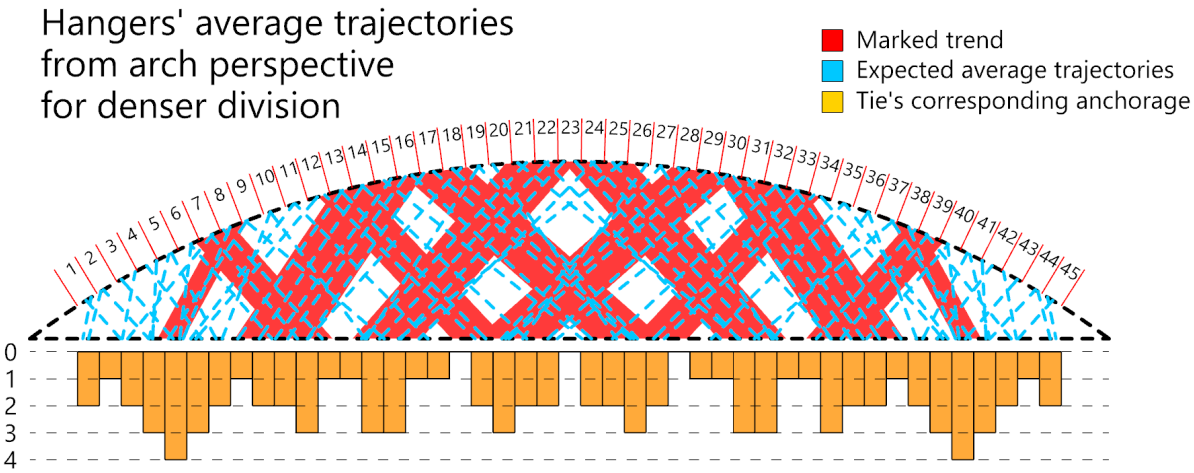

Figure 6.62 The hangers' trajectories from arch perspective and corresponding histogram distribution of corresponding expected hangers' anchorages on the tie - results for denser division

Since investigation of hangers' anchorages distribution on the tie did not provide meaningful information, it was decided to analyse the angular divergence of central lines of hangers' pairs from the radial lines, Fig. 6.63. The arch was divided into 24 segments and the same principles of determination of leftwards and rightwards expected hangers' inclinations were utilized. In the obtained arrangement, the center lines of each hangers' pairs were constructed and the corresponding radial line. The divergence between radial line and center line of each hangers' pair was measured. Left positioned center lines in relevance to the radial line

were assumed negative, and opposite oriented positive. The resultant divergence of these two lines and corresponding hangers' arrangement was marked red in Fig. 6.63.

For comparison, the optimal hangers' arrangements from literature [75, 97] were analysed for the divergence angle. Radial (CARSM) arrangement was always equal to 0 due to its principles. CSM arrangement provided the same outcome regardless of number of hangers and inclination. The most variant was V-CSM, which was mostly dependent on the angular value and number of hangers. The initial inclination angle had much lower impact. Due to provided ranges in [97], the results were marked as fillet plots with dashed alternatives mentioned by the author of this article.

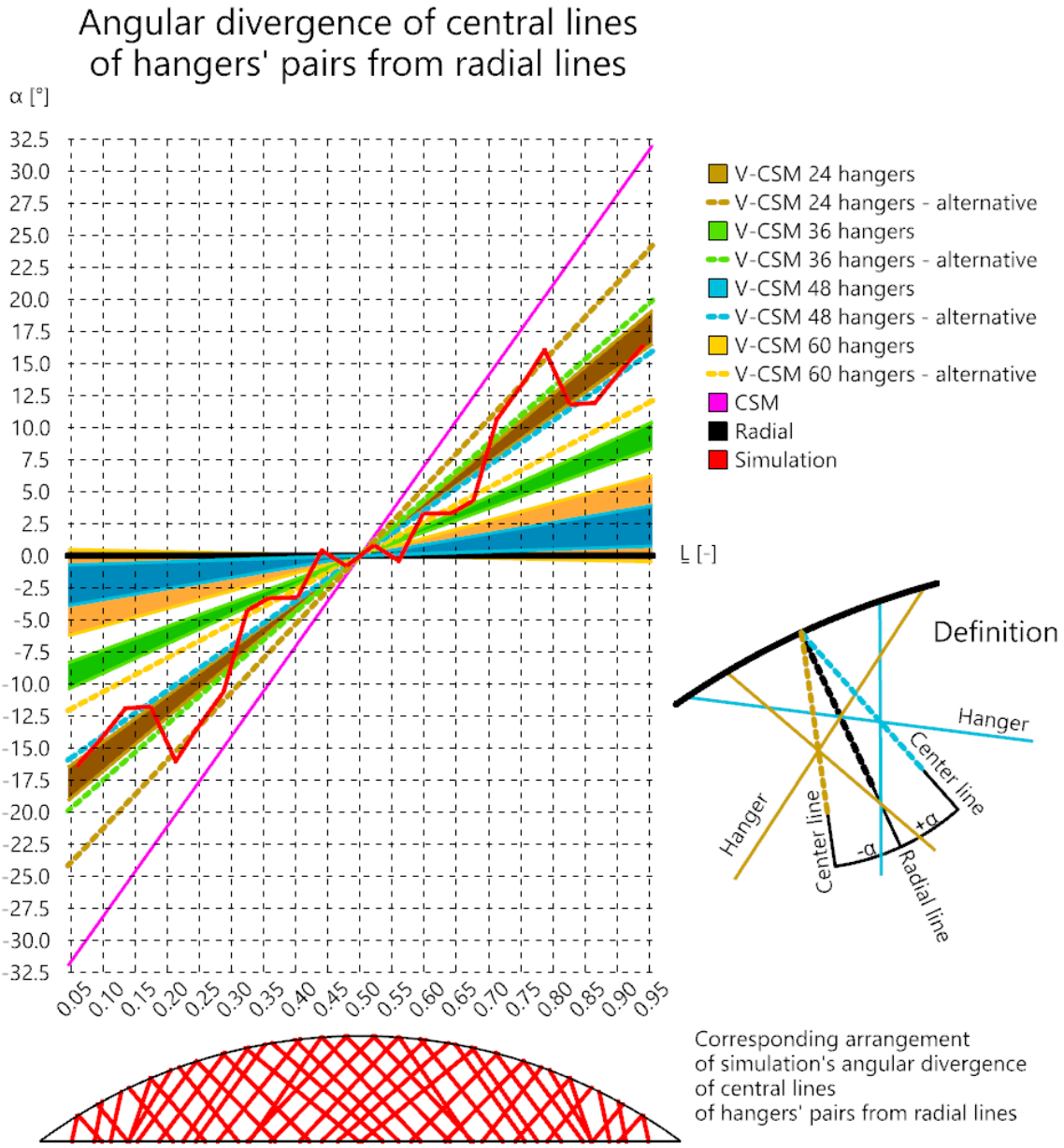

Figure 6.63 The hangers' pairs angular divergence from radial lines. The expected angular inclinations for the results from the simulation were compared with the best CSM, V-CSM and CARSM arrangements [75, 97]. The simulation included results from all the considered deck widths and lengths

The CSM and CARSM arrangements marked the boundaries in which other arrangements were defined. **The obtained path from the simulation was unique compared to the linear function for other arrangements**. The path was approximated by constant segments in both the central region and the end regions. Between them, the linear transition occurred, Fig. 6.64. Alternatively, the graph could be approximated by double sigmoid functions, Eq. (6.19). **The piecewise approximation was recommended**, Eq. (6.20), since it resulted in 40% lower average divergence. Both approximations were achieved with genetic algorithm included in Galapagos component in GH with self-coded RMSE minimization criterion.

$$\alpha_s(x) = 71.7 \left[\frac{1}{1 + e^{-32.6(x-0.687)}} - \frac{1}{1 + e^{+32.6(x-0.313)}} \right] \tag{6.19}$$

$$\alpha_p(x) = \begin{cases} -13.8, & x \in [0.00, 0.23) \\ -13.8 + 72.63 \cdot (x - 0.23), & x \in [0.23, 0.42) \\ 0, & x \in [0.42, 0.58] \\ 0.0 + 72.63 \cdot (x - 0.58), & x \in (0.58, 0.77] \\ 13.8, & x \in (0.77, 1.00] \end{cases} \tag{6.20}$$

where x was a fraction of span length.

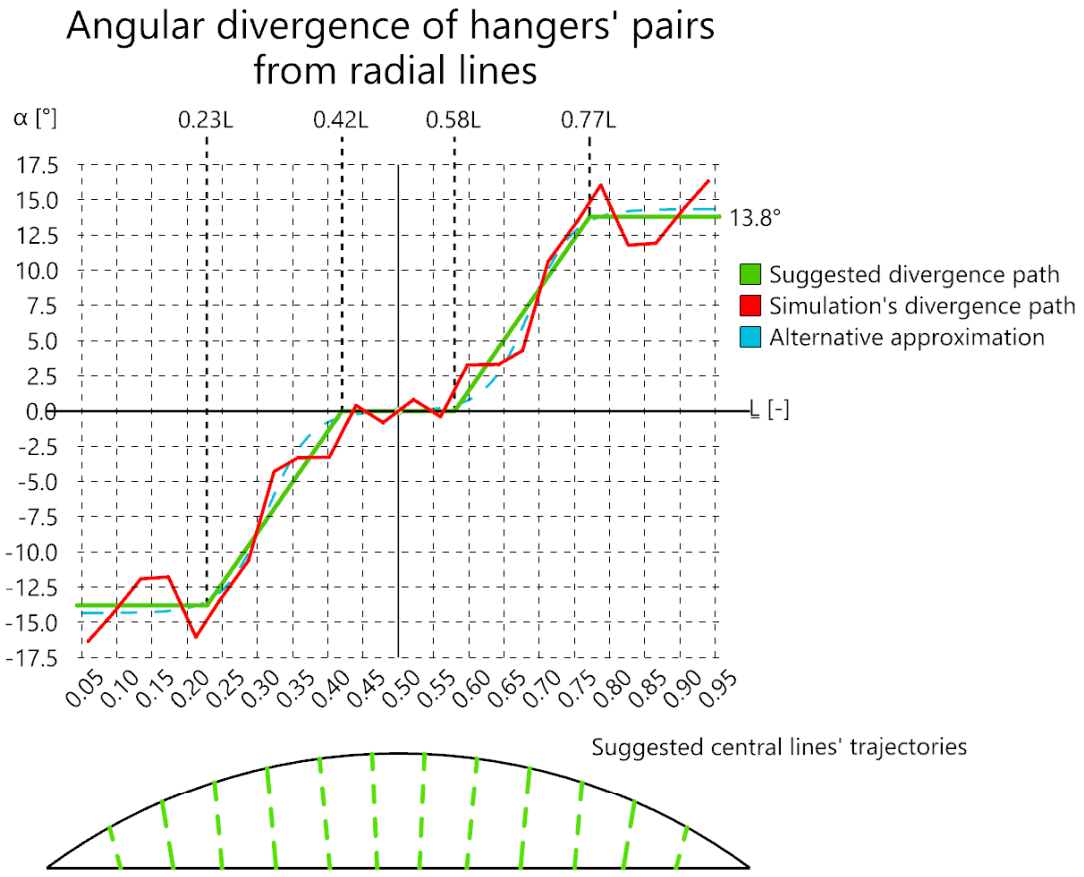

Figure 6.64 The suggested hangers' pairs angular divergence from radial lines (ADHR) based on the simulation's results with graphical representation of center lines. The simulation included results from all the considered deck widths and lengths

The angular divergence of hangers' pairs from radial lines (ADHR) analyses over the span length was not found in the known literature. Surprisingly to author, the well-described arrangements always had linear ADHR change over the span length. **The closest arrangements to the piecewise approximation were V-CSM for 24 hangers in the transition regions and radial for constant regions in the middle part, Fig. 6.63**. **The constant value near the end was not similar to any trend from known arrangements**. **Since the ADHR had extreme values at the ends, hangers' inclination should be more vertical at the ends, which matched the analyses of hangers' inclination from Fig. 6.54 and Fig. 6.55**. The transition part was concentrated in the middle part and covered almost 40% of a span length.

In the next step, the center lines determined from the simulation and presented in Fig. 6.63, were elongated in order to find their intersection points for a dense hangers' spacing for higher precision. The elongated trajectories of the center lines resulted in three focal points, Fig. 6.65. **The concept of having two focal points was mentioned in [72], but not three. Moreover, the transition region between these focal points occurred, which was not presented in the cited paper and considered as an original concept.** Center lines in the transition zone were parallel to the extreme center lines from the nearby focal points. Three focal points were not defined horizontally, but the middle focal point was always higher than the two remaining by height $h_f = 0.263H$, which was linearly depended from the arch elevation *H*. Focal points were approximated by a circle, but comparisons of its radius R_f to the main arch's radius R_a did not allow to determine reasonable correlation between these two parameters. The middle focal point was equal to the arch center point. The circular approximations of focal points for various height-to-span length ratio *H/L* were presented in Fig. 6.65 in the correct vertical distance to the bridge and scale. The left and right focal points positions could be approximated linearly. **The obtained three focal points principle was not observed in the initial population presented in Appendix E, which excluded the origin of this concept in the initial population.**

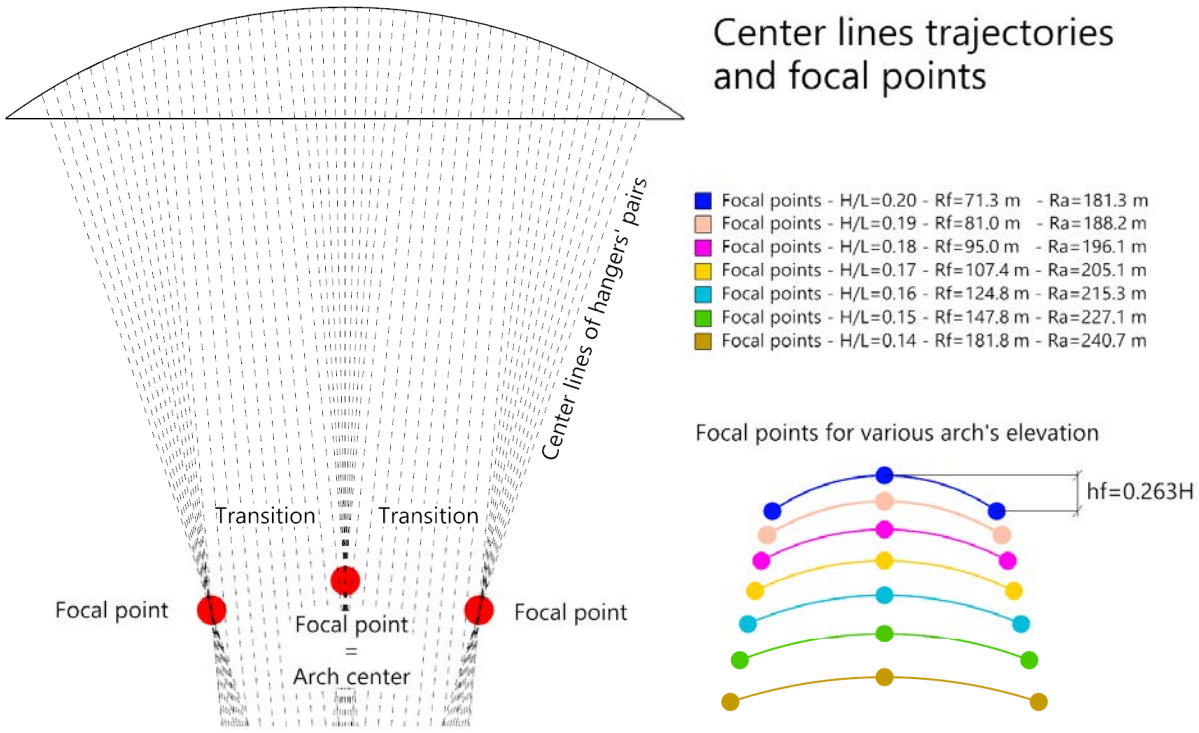

Figure 6.65 Center lines trajectories with focal points of various arch's inclinations

The next analysed parameter was angular divergence between hangers within pair, Fig. 6.66.

For comparison, the optimal hangers' arrangements from literature [75, 97] were analysed as earlier. Radial arrangement was defined between 66^o and 88^o. CSM arrangement provided the greatest range of values between 30^o to 90^o. Both CARSM and CSM had constant value of divergence angle. The V-CSM provided diverged range spreading from 50^o to 90^o. The trend was not constant, but parabolic with rising value towards ends.

The results from the simulation were approximated by cosine function with downwards trend towards ends using genetic algorithm included in Galapagos component with self-coded RMSE minimization criterion, Eq. (6.21). **The approximated results from the simulation were oriented with downwards trend towards ends, which was reversed comparing to V-CSM and not present in other hangers' arrangements**. The divergence angle covered range between 45^o and 90^o. **The range of covered divergence angle was much greater than for a single V-CSM case.**

$$\beta(x) = 54.1 \cos\left(3(x - 0.5)\right) + 34.3 \tag{6.21}$$

where x was a fraction of span length. The trend of decreasing total divergence angle matched the observation from Fig. 6.59, where the angle changed from 90^o in the middle to 70^o in about 1/5 of total span length. These values should be according to approximation 88.4^o and 67.9^o.

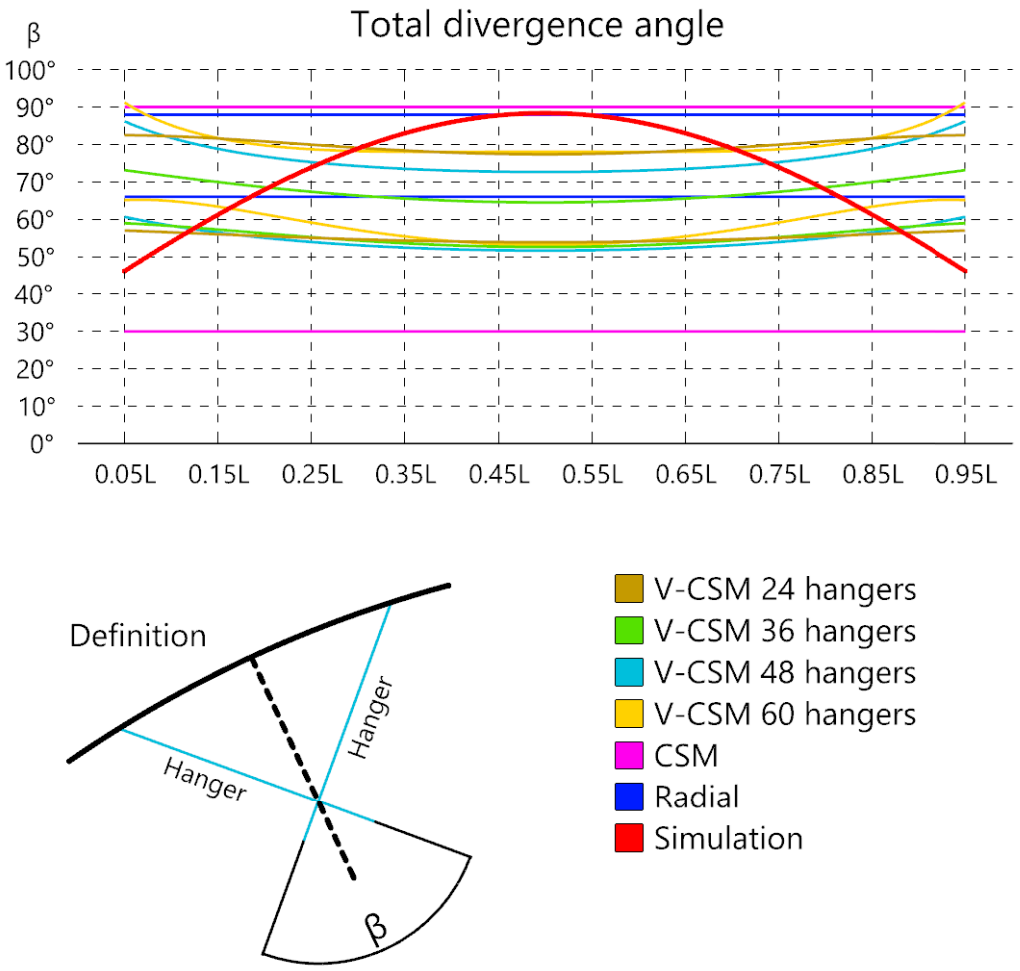

Figure 6.66 The angular divergence graph with approximation of the simulation results from all the considered deck widths and lengths

The example of hangers' arrangements including both information about ADHR and total divergence angle were presented in Fig. 6.67. The suggested **new arrangement of hangers** was called **Multi-Variant Angular Divergence Model (MVADM)** arrangement. The highest value of ADHR and the smallest total divergence angle value near the ends, Fig. 6.64 and Fig. 6.66, matched the trend, where hangers closer to the ends were inclined the most vertically among all hangers, Fig. 6.55.

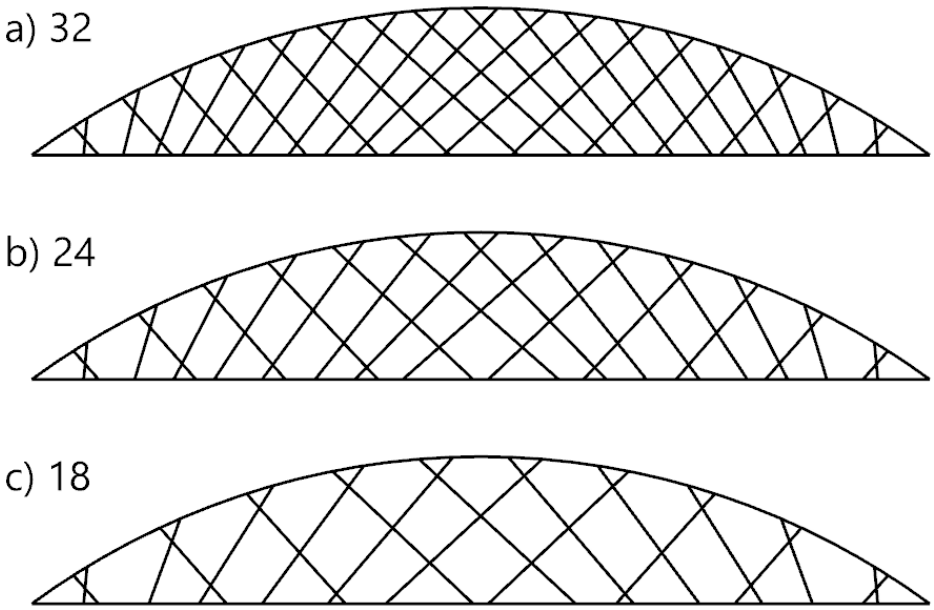

Figure 6.67 Examples of MVADM arrangements

It was worth to mention, that the obtained hangers' arrangements were the generalization of the results from the simulation, not predefined by author. The ADHR regular principles (i), existence of three focal points with transition regions (ii) and cosine change of total angular divergence (iii) were discovered from the optimization algorithm's results, not directly from author's assumed arrangement principles. **That would not be possible in algorithm restrained by known hangers' arrangements, if the new arrangement was not predefined in advance.**

At the same time, not all of the resultant hangers' arrangements followed the MVADM principles. Hangers were not supposed to follow any predefined arrangement principles, therefore each hanger was shaped by the algorithm independently, which was one of the reasons for obtaining lower costs comparing to literature [75]. **The MVADM arrangement missed information about optimal distribution of the hangers along the arch and distance of the first crossing point from the arch. The simulations with MVADM arrangement were not conducted, which would help in determining these two components.**

Nevertheless, author decided to compare the MVADM arrangement with the CARSM arrangement for span lengths of 100 m and 250 m, and deck widths of 3 m and 12 m. This would allow to cover the extreme span lengths and deck widths cases. The cross sections and arch elevation were set from the results presented in Fig. 6.44, Fig. 6.45, Fig. 6.46, Fig. 6.47, Fig. 6.50, Fig. 6.51, Fig. 6.52 and Fig. 6.53. The number of hangers was checked for the obtained number of hangers in the optimal results and for the sparse system of 10 hangers. The CARSM arrangement shaping was based on the results presented in Fig. 3.3 included in the [97]. The hangers spacing was planned to be equal along the arch if the number of hangers was enough.

Each hanger was planned to cross other hangers at least twice following network arrangement principles. The arrangement was set manually to minimize stresses in both arch and tie. For the MVADM arrangement, the distribution of hangers, their spacing and position of the first hangers' crossing point from the arch were set manually with minimizing stresses in both arch and tie. The manual manipulation did not guarantee reaching the lowest possible stress, but it presented an initial overview of what could be expected from the MVADM arrangement comparing to CARSM arrangement. The results were included in the Sec. G and presented in Fig. G.1-G.12. The results were compared in Tab. 6.8.

Table 6.8 Results comparison for CARSM and MVADM arrangements. L - span length, N - number of hangers, Q - deck width, σ_A - von Mises stress in an arch, σ_T - von Mises stress in a tie, u_L - deflection from variable loads

	σ_A [MPa]	σ_T [MPa]	u_L [mm]
L 100 - N 16 - Q 3 - CARSM	238	212	111
L 100 - N 16 - Q 3 - MVADM	232	277	137
L 100 - N 38 - Q 12 - CARSM	167	141	68
L 100 - N 38 - Q 12 - MVADM	171	149	72
L 100 - N 10 - Q 12 - CARSM	263	208	104
L 100 - N 10 - Q 12 - MVADM	244	227	113
L 250 - N 36 - Q 3 - CARSM	350	323	448
L 250 - N 36 - Q 3 - MVADM	387	354	485
L 250 - N 18 - Q 12 - CARSM	263	402	387
L 250 - N 18 - Q 12 - MVADM	279	434	407
L 250 - N 10 - Q 12 - CARSM	490	609	546
L 250 - N 10 - Q 12 - MVADM	421	598	664

The CARSM arrangement always resulted in lower deflection than in MVADM arrangement. Maximum difference was 20%, but most common was between 5% and 10%. In sparse system of 10 hangers the MVADM arrangements provided lower stress in the arch or in the arch and tie than CARSM arrangement even by 15%. In one more case of L100, N16 and Q3 the stresses in the arch were 2.5% smaller in MVADM than in the CARSM model. In other cases, the stresses were smaller in CARSM arrangement by 2-10% for the arch and by 5-24%, but mostly 5-10%.

In general, the CARSM arrangement worked better in cases with greater number of hangers. The greater load and the lower the number of hangers were, the more advantageous the MVADM arrangement was. The expected, preliminary analyses showed expected favour of one arrangement over another at 10%. Author believed, that more detailed simulation of hundred MVADM variations would help in improving these results for the new arrangement. At this moment, author considered both arrangements comparable and alternative.

Nevertheless, the MVADM arrangement showed, that it worked better in sparse systems and did not need manual change of hangers' arrangement near ends as CARSM arrangement. By its definition, it had more flexibility in shaping, which made it more complex, but provided more possibilities to explore. More research would be continued in order to determine the remaining parameters of hangers' distribution along the arch and distance of the hangers' first crossing point from the arch. That would help in improving the presented preliminary results.

6.6 Conclusions

After analyses of the results obtained from the optimization algorithm in the second attempt, author concluded the following:

- In the optimal solutions, hangers were in average more inclined in the middle section and more vertical in the regions near the ends. The transition was parabolic,
- The discovered MVADM arrangement from the simulation showed smooth transition from CARSM arrangement in the center to progressively more vertical network arrangement near ends. It was considered competitive to CARSM arrangement and require more investigation in order to improve its remaining shaping parameters and effectively compare it to the most optimal CARSM arrangements,
- The MVADM was more generally defined than arrangements from literature so far with 3 focal points and transition zones between them. Its comparable results to CARSM arrangements and the fact, that this arrangement was discovered from the set of optimal solutions from the simulation with low restraints, made it a good candidate for being an universally defined arrangement in both sparse and dense systems, but required more investigation,
- The possibility of having any hangers' arrangement with changing hangers' quantity, rise of the arch, cross section dimensions, material capacities and cost-oriented goal function provided cheaper solutions than the expectations from the literature for known regular arrangements,
- The arrangement of hangers in the optimal solutions obtained from the simulation were characterized by various hangers' arrangements. The discovered MVADM arrangement also reflected this phenomenon,
- In the MVADM arrangement, the smooth transition from the middle region into the end regions was observed,
- The GA with gradient descent and two-step approach was suitable for the optimization process. The obtained results of goal function value were well describable, smooth and well predictable across all analysed span lengths and deck widths,
- The comparisons to individual structures proved that algorithm provided cheaper solution. Also, implementation of existing structures into the initial population allowed cost reduction of them. The algorithm proved its effectiveness on the direct and indirect comparison to the existing structures,
- Simplification of the model and calculations allowed for significant time consumption reduction and helped avoiding numerical errors,
- The tests allowed to increase effectiveness and efficiency of the optimization algorithm.

7 General conclusions

The conclusions regarding in-plane geometrically nonlinear analysis were the following:

- (R3) The geometrically nonlinear critical form in network arch bridges matched the expected multi-periodic sinusoidal critical form with similar value of the maximum amplitude distributed along the entire length of the arch, Fig. 4.20c and Fig. 4.21, as the analytical formula suggested, Eq. (4.3)-(4.5) [85]. The geometrically nonlinear critical form included the bow imperfection component, which matched the expectations from EN 1993-2 [134], Tab. 4.1a, row 1,
- (R3) The geometrically nonlinear analysis revealed a substantial reduction in buckling resistance relative to the linear elastic bifurcation analysis. For a reasonable relative slenderness values between 0.4 and 0.6 and reasonable rolled I-sections corresponding with "c" buckling curve, the average reduction reached 4% in normal scenario and 9-14% in accidental, cable loss case. The maximum possible reduction within this relative slenderness range and "d" buckling curve was 6% in normal case and 20% in accidental case. The worst position of vehicle in about 30% of span length distance from the supports resulted in greater reduction than the middle vehicle position,
- (R3) The geometrically nonlinear buckling resistance for normal case matched the analytical solution with maximum deviation of 2% for high pretension force in hangers,
- The conducted geometrically nonlinear buckling analysis could be used with success as a more generalized method than the analytical solution in determination of geometrically nonlinear buckling resistance in network arch bridges expanding its possibilities to custom hangers' arrangement,
- The influence of arch elevation on the critical load factor reduction was negligible and was mainly driven by the geometrically nonlinear analysis itself,
- (R3) The investigation showed the importance of conducting geometrically nonlinear analysis for the purposes of arches capacity determination, as the linear elastic bifurcation results provided significant overestimation of arches capacity,
- (R3) The accurate capacity determination from the geometrical nonlinear analysis was considered crucial for the need of optimization algorithm, since the overestimated results from the linear elastic bifurcation analysis would lead to unrealistic solutions.

The first (O) authored optimization algorithm allowed for optimization of number of hangers, geometry, cross section, material capacity with possibility of any hangers' arrangement in the process. The goal function was cost based and included the costs of material its transport and assembly, as well as individual additional hangers' assembly cost. The hangers' number was not optimized simultaneously with other parameters since hangers' number was reduced with ESO and other parameters were modified by GA. The approach had various issues. The lessons learned from this investigation were taken and the approach was substituted by the improved second optimization algorithm. Nevertheless, author presented the following conclusions:

- (O) The optimization approach was defined with alternating GA and author-coded ESO methods controlled by external author-coded Python script, which was an unique optimization approach in network arch bridges, since ESO was not used so far in the optimization of network arch bridges according to author's best knowledge,
- (O) The optimization algorithm was divided into two stages, where the details and complexity of the calculations increased when the number of hangers decreased, which optimized the time consumption,

- (O) To avoid any dependence of the optimization algorithm on the predefined initial hangers' arrangement, the algorithm in stage 1 gradually reduced the number of hangers from very high number to manageable values and was not limited to only network arrangements, which was unique for the optimization of network arch bridges and allowed to explore more possibilities in hangers' arrangement shaping,
- Despite out-of-plane movement restriction, the arch experienced twist near skewbacks and the middle of the arch in the buckling analysis, which was not desired. The stability form was in some investigations bracing-oriented instead of desired arch-oriented,
- The post-critical analysis with PUSH procedure resulted in unstable solutions with sawtooth fluctuations, which was not desired. The time demand for reached 2 hours, which was unacceptable from the optimization algorithm point of view due to the number of vehicle positions and number of geometries to consider in the optimization process,
- In the obtained solutions, the hangers experienced sagging, which caused undesired internal forces increase in the arch and so demanded section capacity increase,
- From the global optimization point of view, the number of vehicles positions was too high and required great time demand,
- The predefined genetic algorithm implemented in Galapagos required manual actions from user during optimization process and was not adjustable enough for the process's needs,
- The post-tensioned concrete tie would add unnecessary complexity and time consumption to the optimization process. Theoretically, the most optimal in terms of cost minimization solution could have wrong tendons' trajectory in the tie, which would cause unnecessary greater internal forces in the system and require from algorithm to increase sections in order to remain within capacity range, even though the tendons' trajectory adoption would be solvable, but would require separate iteration for each case,
- ESO elimination purpose was considered reasonable, but the initial elimination of hangers in the first stage could be substituted by predefined hangers' arrangement, since the obtained arrangement was similar to CSM type, which would save time. Furthermore, the elimination in stage 2 was very simple, and could be incorporated into GA, reducing algorithm complexity,
- The GA would be launch for gradually reducing number of hangers, which would be a process that takes an unacceptable amount of time.

In order to solve the issues learned from the first optimization approach, the following modifications were implemented:

- (O) Hollow circular cross section of the arch and the tie, which helped in providing greater torsional stiffness for the in-plane buckling purposes and allowed to include the optimization of the tie during the optimization process,
- (O) The geometry was defined in 2D instead of 3D, which reduced the time consumption severely and allowed to avoid the out-of-plane critical form in in-plane buckling analysis, as well as the critical form was only arch-oriented. It eliminated the risk of bracing-oriented buckling forms before the arch-oriented form happened. The other out-of-plane-oriented properties, including portal frame size, out-of-plane moment of inertia of the arch ribs and inclination of the arches were also excluded,
- (O) The general method was simplified to in-plane case without out-of-plane bucking factor determination. The in-plane geometrically nonlinear effects with imperfections determined from UGLI method were substituted by in-plane buckling factor determined for the geometrically nonlinear critical load factor, which saved numerical issues in determination of post-critical form and reduced the calculations demand severely,

- (O) The pretension force was included in the optimization process and the diameter of hangers was decreased for sagging effects reduction,
- The vehicle loads were simplified to two cases with full and half loaded deck, since it was considered enough for global optimization purposes,
- (O) The entire optimization process was custom coded without any external and ready optimization solutions and libraries in order to allow for more flexibility in modifications and prevent future unknown issues requiring algorithm adoption,
- For complexity and time demand reduction, the tie was considered made of hollow circular section,
- (O) The ESO elimination principles were implemented into authored custom-made GA,
- (O) The authored custom-made GA allowed to have changing number of hangers during the optimization process as well as mixing various hangers' arrangements with various number of hangers in the coalescence eliminating the need of repeating the calculations for various number of hangers and saved time.

The second (O) authored optimization algorithm solved the issues mentioned in the first version. This time author managed to (R1) simultaneously optimize the number of hangers, geometry, cross section, material properties and allowing for any hangers' arrangement. The cost-oriented goal function was implemented (R1). The conclusions from the second optimization approach were the following:

- (O) The implementation of the solutions learned from the first optimization approach allowed to obtained results without any issues,
- (O) Gradient-based optimization implemented into GA resulted in lower costs and the optimal step size of gradient optimization was 5,
- (O) Goal function modification with gratification of lower utilization was successful. It allowed the structure with the same absolute costs as other individuals but with lower utilization, to be considered as more optimal by the goal function. Since all the initial geometries were always set to have utilization lower than 100% and the number of hangers was different for each of them, the modification solved the issue of perceiving geometries with greater number of hangers as less optimal by the goal function,
- (O) Second modification of the GF by raising utilization to the power of 0.5 in order to reduce the gratification effect resulted in higher costs and therefore the original modification of GF formula was implemented into the final simulation,
- (O) Longer calculations did not improve the results enough to compensate for the disproportionately increased time demand,
- (O) Two-step optimization, including modified and unmodified GF formula in the first and the second step respectively with implementation of the best solution from the first step into the initial population of the second step within NPA concept was a successful implementation that allowed to achieve lower costs,
- (O) The expansion of prestressed steel for hangers was a successful implementation allowing for cost reduction,
- (O) The network-based arrangement with randomly generated parameters except hangers' arrangement in the initial population were preferable over network-based arrangements with vertical and Nielsen arrangements. The random generation with network-based arrangement was more effective than implementation of arrangements considered as less optimal,
- (O) The skewbacks were not modelled, since they produced undesired peaks and rapid change of stiffness could cause potential issues. The regions near the supports were ex-

cluded from the design assuming, that these regions would be strengthened in the detailed design and were solvable,
- (R1) (R4) The optimization of three real network arch bridges resulted in successful cost reductions up to 24%, all the resultant arrangements were network-type,
- (R1) In simulation, the total steel weight was always lower than the steel weight suggested in literature. Only the results obtained for 4 lanes exceeded the steel weight from the literature conservative reduced by the weight of the temporary chord,
- (R1) The total steel cost for all considered span lengths and deck widths was always lower than the suggestions from the literature even for lower price estimation,
- (R1) The approximated formulas for the optimal steel weights and costs were compared with the literature with success of reaching lower values.

After cost and weight comparison with the literature, author compared the geometrical properties of the obtained results and found principles useful for optimal shaping of the network-like arch bridges. The optimal shaping conclusions were the following:

- (A) The in-plane geometrically nonlinear buckling coefficient had values mainly between 0.80 and 0.96 in the optimal solutions over the span length and deck widths with value increasing trend over the increasing span length,
- (A) Most of the arch's in-plane moment of inertia had significantly lower values than the suggested in literature. All the results for the tie's in-plane moment of inertia were at least twice smaller than the literature suggestions. The I_y was mostly constant for a considered deck width over the span length increase. The arch had mostly greater in-plane moment of inertia than the tie. The ration of tie-to-arch in-plane moment of inertia was about up to 2.5 times greater than the suggested in literature,
- (A) The cross section area of the arch was 2-6 times smaller than the recommendation from the literature for the optimal solutions. The cross section area of the tie covered the recommendation range of optimal value, but laid mostly in the lower part of this range,
- (A) The results for the arch and tie diameter were not characterized by any visible trend and they laid between 0.5 m and 1.7 m,
- (A) The steel grade was limiting the arch and the tie progression, since both were characterized by a rapid increase to the maximum steel grade S460 between 100 m and 150 m of span length and then remained mostly with S460 steel grade. Therefore, higher steel grades for the arch and the tie should be considered. There was too great gap between structural and prestress steel grade for hangers and intermediate grades should be considered,
- (A) Most of the height-to-span length ratio value was within 15.5-16.7% range, which matched with the recommendations from literature,
- (A) The number of hangers was mostly, regardless of the span length, below 25 and below 20% of the span length expressed in meters, which was a more sparse system than literature suggestions, which started for up to 40% for 100 m of span length and finish with up to 20% for the span length of 250 m, which was the closest to the achieved results,
- (A) The majority of the hangers' diameter was below 65 mm but with predictable trajectory over the span length,
- (R2) (A) The hangers' inclination was the lowest in the middle section and increased with a parabolic trend towards the ends. It trends and its value was independent from the span length and deck width results. The approximated function results in inclination angle between 45^o and 67^o,
- (R2) (A) The number of crossing points along the bridge was characterized by a downward trend towards the ends with a local peak at distance of about 35% of the span length

from the ends. The trend was downwards parabolic,
- (R2) (R4) (A) The obtained angular divergence of center lines of hangers' pairs from the radial lines was unique and not present in other known hangers' arrangements. It was characterized by piecewise approximation, where other arrangements were described by linear or constant trends. The approximated angular values laid within range between -13.8^o and 13.8^o,
- (R2) (R4) (A) The total divergence angle between hangers within their pair was characterised by cosine downwards trend towards the ends, where other arrangements were constant or pointed upwards but not as rapidly as obtained results from the simulations. The approximated angular values were defined within range of 45-90^o, which was greater than the range covered by V-CSM approximation,
- (R2) (R4) (A) The center lines of hangers' pairs crossed in 3 focal points and the transition between these points was smooth characterized by parallel center lines between each focal point regions. This arrangement definition was not present in the literature and was named Multi-Variant Angular Divergence Model. The new hangers' arrangement had network-type arrangement,
- (R1) (R4) The MVADM was more generally defined than arrangements so far with 3 focal points and transition zones between them. Its comparable results to CARSM arrangements and the fact, that this arrangement was discovered from the set of optimal solutions from the simulation with low restraints, made it a good candidate for being an universally defined arrangement in both sparse and dense systems, but require more investigation.

8 Further research plans

Based on the findings and prior research, the author aimed to pursue further investigation in:

- Include the concrete tie with tendons in the optimization process,
- Repeat the analysis in 3D and solve the problem of determination in-plane and out-of-plane buckling parameters taking into account geometric nonlinearity,
- Repeat the optimization process for higher structural steel grades, since it was considered limiting the arch and the tie from even further cost reduction progression. That should also include providing more options of steel grades between structural and prestressed steel for hangers in order to reduce the drastic change of capacity and price,
- Investigate MVADM arrangement in terms of determining missing optimal parameters of hangers first crossing point position distance to the arch and distribution of hangers' anchorage points along the arch. Compare the optimal results with optimal well-known arrangements as well as sparse systems,
- Determine the goal function formulation with exclusion of two step optimization approach with both modified and unmodified GF. That would save time consumption of the optimization algorithm,
- Determine the imperfection value for geometrically nonlinear in-plane buckling of network arch bridge in order to substitute the UGLI procedure with shape and imperfection value guidelines as included in EN 1993-2 [134].

Literature

[1] M. N. Ab Wahab, S. Nefti-Meziani, and A. Atyabi. “A Comprehensive Review of Swarm Optimization Algorithms”. In: *PLoS ONE* 10 (5 May 2015). ISSN: 19326203. DOI: 10.1371/journal.pone.0122827.

[2] R. Ahsan and N. Islam. “Optimization of Hanger Arrangement of Network Arch Bridges”. In: IABSE-JSCE Joint Conference on Advances in Bridge Engineering-II, Aug. 2010, pp. 107–119. ISBN: 978-984-33-1893-0. URL: www.iabse-bd.org.

[3] A. S. M. Al-Azzawi et al. “A Novel Semi-Analytical Approach for Predicting the Buckling and Postbuckling Behaviour of Glare Fibre Metal Laminates”. In: *Thin-Walled Structures* 181 (2022), p. 109987. ISSN: 0263-8231. DOI: https://doi.org/10.1016/j.tws.2022.109987. URL: https://www.sciencedirect.com/science/article/pii/S0263823122005912.

[4] D. Ammendolea et al. “Strategies to Improve the Structural Integrity of Tied-Arch Bridges Affected by Instability Phenomena”. In: *Procedia Structural Integrity*. Vol. 25. Elsevier B.V., 2020, pp. 454–464. DOI: 10.1016/j.prostr.2020.04.051.

[5] A. Auger and N. Hansen. “Linear Convergence on Positively Homogeneous Functions of a Comparison Based Step-Size Adaptive Randomized Search: the (1+1) ES with Generalized One-fifth Success Rule”. In: *hal-00877161v1* (2013). URL: https://inria.hal.science/hal-00877161v1/document.

[6] R. Belevičius, A. Juozapaitis, and D. Rusakevičius. “Parameter Study on Weight Minimization of Network Arch Bridges”. In: *Periodica Polytechnica Civil Engineering* 62 (1 2018), pp. 48–55. ISSN: 15873773. DOI: 10.3311/PPci.10036.

[7] R. Belevičius et al. “Optimal Schemes of Radial Network Arch Pedestrian Bridges: An Extensive Dataset of Solutions Under Different Conditions”. In: *Data in Brief* 36 (May 2021). ISSN: 2352-3409. DOI: 10.1016/j.engstruct.2021.112182. URL: https://www.sciencedirect.com/science/article/pii/S2352340921004339?via%3Dihub.

[8] R. Belevičius et al. “Parametric Study on Mass Minimization of Radial Network Arch Pedestrian Bridges”. In: *Engineering Structures* 237 (June 2021). ISSN: 18737323. DOI: 10.1016/j.engstruct.2021.112182.

[9] K. Bell and L. Wollebaek. “Large Glulam Arch Bridges”. In: (2004).

[10] D. P. Billington and P. N. Billington. *Arch Bridges*. 2024. URL: https://www.britannica.com/technology/arch-bridge.

[11] A. Blonka. “Optimization of Single-Span Simply Supported I-Beam Welded from Steel Sheets”. Master’s thesis. Wroclaw University of Science and Technology, 2019.

[12] A. Blonka and L. Skretkowicz. “Nonlinear Buckling Analysis of Network Arch Bridges”. In: *Studia Geotechnica et Mechanica* 44 (2 June 2022), pp. 123–137. ISSN: 2083831X. DOI: 10.2478/sgem-2022-0007.

[13] D. Bruno, P. Lonetti, and A. Pascuzzo. “An Optimization Model for the Design of Network Arch Bridges”. In: *Computers and Structures* 170 (July 2016), pp. 13–25. ISSN: 00457949. DOI: 10.1016/j.compstruc.2016.03.011.

[14] H. Cao et al. “Enhanced Particle Swarm Optimization for Size and Shape Optimization of Truss Structures”. In: *Engineering Optimization* 49 (11 Nov. 2017), pp. 1939–1956. ISSN: 10290273. DOI: 10.1080/0305215X.2016.1273912.

[15] S. C. Chapra and R. P. Canale. *Numerical Methods for Engineers*. McGraw-Hill Education, 2015, p. 970. ISBN: 9780073397924.

[16] J. Cheng. "An Artificial Neural Network Based Genetic Algorithm for Estimating the Reliability of Long Span Suspension Bridges". In: *Finite Elements in Analysis and Design* 46 (8 Aug. 2010), pp. 658–667. ISSN: 0168874X. DOI: 10.1016/j.finel.2010.03.005.

[17] M. Y. Cheng et al. "A Hybrid Harmony Search Algorithm for Discrete Sizing Optimization of Truss Structure". In: *Automation in Construction* 69 (Sept. 2016), pp. 21–33. ISSN: 09265805. DOI: 10.1016/j.autcon.2016.05.023.

[18] B. M. da Costa. "Design and Analysis of a Network Arch Bridge". PhD thesis. Tecnico Lisboa, Oct. 2013.

[19] A. D. Danciu et al. *A Review of the Network Arch Bridge*. Oct. 2023. DOI: 10.3390/app131910966.

[20] B. De Pauw et al. "Steel Tied Arch Bridges With Fan Hanger Arrangement". In: *ARCH ´04*. 2004, pp. 1–10. URL: http://awww.Ugent.be.

[21] D. Delahaye, S. Chaimatanan, and M. Mongeau. "Simulated Annealing: From Basics to Applications". In: 272 (2019), p. 978. DOI: 10.1007/978-3-319-91086-4_1Ãŕ. URL: https://enac.hal.science/hal-01887543v1.

[22] M. Dorigo. "Optimization, Learning and Natural Algorithms". PhD thesis. Politecnico di Milano, 1992.

[23] P. Díez. "A Note on the Convergence of the Secant Method for Simple and Multiple Roots". In: *Applied Mathematics Letters* 16.8 (2003), pp. 1211–1215. ISSN: 0893-9659. DOI: https://doi.org/10.1016/S0893-9659(03)90119-4. URL: https://www.sciencedirect.com/science/article/pii/S0893965903901194.

[24] *Equilibrium Equations of the von Mises Truss*. URL: https://paulino.princeton.edu/NLS/Analytical_vmt.pdf.

[25] B. Etim et al. *Machine Learning-Based Modeling for Structural Engineering: A Comprehensive Survey and Applications Overview*. Nov. 2024. DOI: 10.3390/buildings14113515.

[26] K. V. Fedin, A. Gritsenko, and P. Gromyko. "Diagnostics of the Stability State of the Bugrinsky Bridge by Acoustic Noise Method". In: (Jan. 2023), pp. 33–41. DOI: 10.1007/978-3-031-16575-7_4.

[27] C. Fisk et al. "Using Simulated Annealing to Investigate Sensitivity of SEM to External Model Misspecification". In: *Educational and Psychological Measurement* 83 (Jan. 2022), p. 001316442110731. DOI: 10.1177/00131644211073121.

[28] P. Fiziev and D. Staicova. "Two-Dimensional Generalization of the Muller Root-Finding Algorithm and Its Applications". In: *Computing Research Repository - CORR* (May 2010).

[29] P. Frantík. *Simulation of the Stability Loss of the von Mises Truss in an Unsymmetrical Stress State*. Tech. rep. 2007, pp. 155–161.

[30] N. Ganchovski and A. Traykov. "Modified Anderson-Bjork's Method for Solving Non-Linear Equations in Structural Mechanics". In: *IOP Conference Series: Materials Science and Engineering* 1276 (Feb. 2023), p. 012010. DOI: 10.1088/1757-899X/1276/1/012010.

[31] P. Gangl. “A Multi-Material Topology Optimization Algorithm Based on the Topological Derivative”. In: *Computer Methods in Applied Mechanics and Engineering* 366 (July 2020). ISSN: 00457825. DOI: 10.1016/j.cma.2020.113090.

[32] E. García-Macías et al. *Operational Modal Analysis and Detection of Non-Linear Structural Behavior of Bowstring Arch Bridge*. Tech. rep. 2016. URL: https://www.researchgate.net/publication/281462628.

[33] M. Georgioudakis and V. Plevris. “A Comparative Study of Differential Evolution Variants in Constrained Structural Optimization”. In: *Frontiers in Built Environment* Volume 6 - 2020 (2020). ISSN: 2297-3362. DOI: 10.3389/fbuil.2020.00102. URL: https://www.frontiersin.org/journals/built-environment/articles/10.3389/fbuil.2020.00102.

[34] K. Ghabraie. “The ESO Method Revisited”. In: *Structural and Multidisciplinary Optimization* 51 (6 Dec. 2015), pp. 1211–1222. ISSN: 16151488. DOI: 10.1007/s00158-014-1208-6.

[35] F. Greco, P. Lonetti, and A. Pascuzzo. “Structural Integrity of Tied Arch Bridges Affected by Instability Phenomena”. In: *Procedia Structural Integrity*. Vol. 18. Elsevier B.V., 2019, pp. 891–902. DOI: 10.1016/j.prostr.2019.08.240.

[36] H. Guan et al. “Bridge Topology Optimisation with Stress, Displacement and Frequency Constraints”. In: *Computers and Structures* 81 (3 2003), pp. 131–145. DOI: 10.1016/S0045-7949(02)00440-6. URL: www.elsevier.com/locate/compstruc.

[37] M. Herzog. “Stahlgewichte moderner Eisenbahn- und Straßenbrücken”. In: *Stahlbau* 9 (1975), pp. 280–282.

[38] A. F. Hobbacher. *IIW Collection Recommendations for Fatigue Design of Welded Joints and Components*. Second. Vol. 1. 2019. ISBN: 978-3-319-23757-2. DOI: 10.1007/978-3-319-23757-2. URL: http://www.springer.com/series/13906.

[39] J. H. Holland. “Adaptation in Natural and Artificial Systems”. In: *University of Michigan Press* (1975).

[40] N. Islam et al. “An Optimized Design of Network Arch Bridge Using Global Optimization Algorithm”. In: *Advances in Structural Engineering* 17 (2 2014).

[41] K. S. Jagadish and J. L. Pahwa. “The Vibration of Cantilever Bridges”. In: *Journal of Sound and Vibration* 7.3 (1968), pp. 449–459. ISSN: 0022-460X. DOI: https://doi.org/10.1016/0022-460X(68)90142-9. URL: https://www.sciencedirect.com/science/article/pii/0022460X68901429.

[42] V. Janata et al. *Construction of the Troja Bridge in Prague*. Tech. rep. 2012. URL: https://home.uia.no/pert/data/Troja_bridge.pdf.

[43] V. Janata et al. “New Troja Bridge in Prague - Structural solution of steel parts”. In: *Procedia Engineering*. Vol. 40. Elsevier Ltd, 2012, pp. 159–164. ISBN: 9781627486033. DOI: 10.1016/j.proeng.2012.07.073.

[44] X. Jia et al. *Finite Element Analysis of Buckling of Structures at Special Prebuckling States*. Tech. rep. 2012, pp. 785–796. URL: https://www.researchgate.net/publication/266282963.

[45] T. Kaczmarek et al. “Polish Experience With Network Arch Bridges Using Cold-Bent HD Sections”. In: *Steel Construction* 13 (4 Nov. 2020), pp. 271–279. ISSN: 18670539. DOI: 10.1002/stco.202000034.

[46] I. Kale et al. “Hybrid ACO-CI Algorithm for Beam Design Problems”. In: *SN Computer Science* 5 (Feb. 2024). DOI: 10.1007/s42979-024-02612-y.

[47] M. Kamal and M. Inel. “Optimum Design of Reinforced Concrete Continuous Foundation Using Differential Evolution Algorithm”. In: *ARABIAN JOURNAL FOR SCIENCE AND ENGINEERING* 44 (Oct. 2019), pp. 8401–8415. DOI: 10.1007/s13369-019-03889-5.

[48] A. Kaveh, B. Farahmand Azar, and S. Talatahari. “Ant Colony Optimization for Design of Space Trusses”. In: *International Journal of Space Structures* 23 (Sept. 2008), pp. 167–181. DOI: 10.1260/026635108786260956.

[49] J. Kennedy and R. Eberhart. “Particle swarm optimization”. In: *IEEE International Conference on Neural Networks*. 1995, pp. 1942–1948.

[50] E. Kerscher, K. H. Lang, and D. Löhe. “Increasing the Fatigue Limit of a High-Strength Bearing Steel by Thermomechanical Treatment”. In: *Materials Science and Engineering: A* 483-484 (1-2 C June 2008), pp. 415–417. ISSN: 09215093. DOI: 10.1016/j.msea.2006.09.170.

[51] S. Kirkpatrick, D. Gelatt, and M. P. Vecchi. *Optimization by Simulated Annealing*. Tech. rep. IBM Research Report RC 9355, 1982.

[52] K. Korus, M. Salamak, and M. Jasiński. “Optimization of Geometric Parameters of Arch Bridges Using Visual Programming FEM Components and Genetic Algorithm”. In: *Engineering Structures* 241 (Aug. 2021). ISSN: 18737323. DOI: 10.1016/j.engstruct.2021.112465.

[53] M. Koyama et al. “Bone-Like Crack Resistance in Hierarchical Metastable Nanolaminate Steels”. In: *Science* 355 (6329 Mar. 2017), pp. 1055–1057. ISSN: 10959203. DOI: 10.1126/science.aal2766.

[54] J. Kregting and R. C. White. “Adaptive Random Search”. In: *Group Measurement and Control* (1971). URL: https://pure.tue.nl/ws/portalfiles/portal/4368926/7202641.pdf.

[55] A. Kværnø. *Lecture Notes for TMA4125/4130/4135 Mathematics 4N/D Polynomial Interpolation: Lagrange Interpolation*. Jan. 2021. URL: https://www.math.ntnu.no.

[56] Y. Lai et al. “Conceptual Design of Long Span Steel-UHPC Composite Network Arch Bridge”. In: *Engineering Structures* 277 (Feb. 2023). ISSN: 18737323. DOI: 10.1016/j.engstruct.2022.115434.

[57] C. Li et al. “An Improved Analytical Algorithm on Main Cable System of Suspension Bridge”. In: *Applied Sciences (Switzerland)* 8 (8 Aug. 2018). ISSN: 20763417. DOI: 10.3390/app8081358.

[58] Y. Li and Y. M. Xie. “Evolutionary Topology Optimization for Structures Made of Multiple Materials with Different Properties in Tension and Compression”. In: *Composite Structures* 259 (Mar. 2021). ISSN: 02638223. DOI: 10.1016/j.compstruct.2020.113497.

[59] Y. Li and Y. M. Xie. “Evolutionary Topology Optimization of Spatial Steel-Concrete Structures”. In: *Journal of the International Association for Shell and Spatial Structures* 62 (2 June 2021), pp. 102–112. ISSN: 19969015. DOI: 10.20898/j.iass.2021.015.

[60] Y. Ma et al. “Efficient Design Optimization of Cable-Stayed Bridges: A Two-Layer Framework with Surrogate-Model-Assisted Prediction of Optimum Cable Forces”. In: *Applied Sciences (Switzerland)* 14 (5 Mar. 2024). ISSN: 20763417. DOI: 10.3390/app14052007.

[61] SOFiSTiK Manual. *ASE*. 2023.

[62] K. Mathias et al. “An Empirical Evaluation of Genetic Algorithms on Noisy Objective Functions”. In: *Genetic Algorithms for Pattern Recognition* (Aug. 2002).

[63] U. Meier, L. Haspel, and A. U. Winistörfer. “World’s First Large Bridge Fully Relying on Carbon Fiber Reinforced Polymer Hangers”. In: *SAMPE Europe Conference 2020*. Dec. 2020. URL: https://www.researchgate.net/publication/347239711.

[64] F. Millanes, M. Ortega, and A. Carnerero. “Palma del Río Arch Bridge, Córdoba, Spain”. In: Structural Engineering International, Mar. 2010. URL: https://gpreman-cp165.wordpresstemporal.com/wp-content/uploads/2017/03/Palma-del-Rio.pdf.

[65] M. C. Montoya et al. “Efficient Modal-Based Method for Analyzing Nonlinear Aerostatic Stability of Long-Span Bridges”. In: *Engineering Structures* 244 (2021), p. 112556. ISSN: 0141-0296. DOI: https://doi.org/10.1016/j.engstruct.2021.112556. URL: https://www.sciencedirect.com/science/article/pii/S0141029621007069.

[66] S. Nemer, J. Szalai, and F. Papp. “Out-of-plane Stability Design by GMNIA – Equivalent Imperfections and Strain Limits”. In: *The International Colloquium on Stability and Ductility of Steel Structures* (). DOI: https://doi.org/10.1002/cepa.wileyonlinelibrary.com/journal/cepa.1761. URL: https://d-nb.info/1268052760/34.

[67] S. Nemer, J. Szalai, and F. Papp. “The overall imperfection method for fire design situation”. In: *Engineering Structures* 283 (2023), p. 115884. ISSN: 0141-0296. DOI: https://doi.org/10.1016/j.engstruct.2023.115884. URL: https://www.sciencedirect.com/science/article/pii/S0141029623002985.

[68] O. F. Nielsen. “Foranderlige Systemer med Anvendelse på Buer med Skraatstillede Hængestenger, (Discontinuous Systems Used on Arches with Inclined Hangers)”. PhD thesis. Gad Copenhagen, 1930.

[69] A. Niklison. “Statical Analysis of Network Arch Bridges”. PhD thesis. Institute of Structural Mechanics Universität Stuttgart, Apr. 2010.

[70] D. Orlando et al. “Influence of the Mechanics of Escape on the Instability of Von Mises Truss and Its Control”. In: *Procedia Engineering*. Vol. 199. Elsevier Ltd, 2017, pp. 778–783. DOI: 10.1016/j.proeng.2017.09.048.

[71] G. Orlando and G. Taglialatela. “A Review on Implied Volatility Calculation”. In: *Journal of Computational and Applied Mathematics* 320 (2017), pp. 202–220. ISSN: 0377-0427. DOI: https://doi.org/10.1016/j.cam.2017.02.002. URL: https://www.sciencedirect.com/science/article/pii/S0377042717300602.

[72] A. W. Ostrycharczyk. “Network Arch Timber Bridges with Light Timber Deck on Transverse Crossbeams”. PhD thesis. NTNU, Nov. 2017. ISBN: 978-82-326-2705-9.

[73] Szymon Palkowski. “Buckling of parabolic arches with hangers and tie”. In: *Engineering Structures* 44 (2012), pp. 128–132. ISSN: 0141-0296. DOI: https://doi.org/10.1016/j.engstruct.2012.05.028. URL: https://www.sciencedirect.com/science/article/pii/S0141029612002714.

[74] G. Pierre. “Application of a Gradient-Based Algorithm to Structural Optimization”. PhD thesis. Massachusetts Institute of Technology, 2009. URL: http://hdl.handle.net/1721.1/47758.

[75] A. Pipinato. “Structural Optimization of Network Arch Bridges with Hollow Tubular Arches and Chords”. In: *Modern Applied Science* 12 (2 Jan. 2018), p. 36. ISSN: 1913-1844. DOI: 10.5539/mas.v12n2p36.

[76] K. Price and R. Storn. “Differential Evolution - A Simple and Efficient Heuristic for Global Optimization over Continuous Spaces”. In: *JournalofGlobalOptimization* (1997), pp. 341–359.

[77] J. Qin et al. *Newton Iteration Method for Analysis of Suspension Cable*. Tech. rep. 2015.

[78] O. M. Querin, G. P. Steven, and Y. M. Xie. “Evolutionary Structural Optimisation (ESO) Using a Bidirectional Algorithm”. In: *Engineering Computations* 15 (8 1998), pp. 1031–1048.

[79] S. Rana et al. “Application of Evolutionary Operation to the Minimum Cost Design of Continuous Prestressed Concrete Bridge Structure”. In: *Engineering Structures* 46 (Jan. 2013), pp. 38–48. ISSN: 01410296. DOI: 10.1016/j.engstruct.2012.07.017.

[80] L. A. Rastrigin. “The Convergence of the Random Search Method in the External Control of Many-Parameter System”. In: *Automation and Remote Control* 24 (1963), pp. 1337–1342.

[81] D. Renfrew. “Traffic Signal Control with Ant Colony Optimization”. PhD thesis. California Polytechnic State University, 2009.

[82] D. Rutten. *Galapagos Principles*. Sept. 2010. URL: https://ieatbugsforbreakfast.com/2011/03/04/epatps01/.

[83] M. Räck. “Entwurf einer kombinierten Straßen-Eisenbahn-Netzwerkbogenbrücke”. PhD thesis. TECHNISCHE UNIVERSITÄT DRESDEN, Aug. 2003. URL: https://home.uia.no/pert/backup/diplomarbeit/Diplom_Mathias_Raeck.pdf.

[84] D. Safari, M. Maheri, and A. Maheri. “Optimum Design of Steel Frames Using Different Variants of Differential Evolution Algorithm”. In: *Iranian Journal of Science and Technology, Transactions of Civil Engineering* 45 (July 2021). DOI: 10.1007/s40996-021-00711-x.

[85] F. Schanack. *In-Plane Arch Buckling of Network Arch Bridges*. Tech. rep. Nov. 2009. URL: https://www.researchgate.net/publication/301198072.

[86] F. Schanack and B. Brunn. “Analysis of the Structural Performance of Network Arch Bridges”. In: *Indian Concrete Journal* 83 (Jan. 2009), pp. 7–13.

[87] F. Schanack and B. Brunn. “Calculation of a Double Track Railway Network Arch Bridge Applying the European Standards”. PhD thesis. Dresden University of Technology, Aug. 2003. DOI: 10.13140/RG.2.1.2139.9445.

[88] M. A. Schumer and K. Steiglitz. “Adaptive Step Size Random Search”. In: *IEEE transactions on automatic control* 13 (June 1968). URL: https://www.cs.princeton.edu/~ken/adaptivestepsize68.pdf.

[89] R. Sek et al. “Bridge Over Vistula River in Cracow: The First Railway Network Arch Bridge Using Cold-Bent HD Sections and Composite Dowels”. In: Synergy of Culture, Civil Engineering – History, and Challenges, May 2020. URL: http://krakow-rudzice.pl/.

[90] P. Smarzewski. “Numerical Solution of Reinforced Concrete Beam Using Newton-Raphson Method With Adaptive Descent”. In: *Bulletin of the Military University of Technology* 64 (4 Dec. 2015), pp. 207–221. ISSN: 1234-5865. DOI: 10.5604/12345865.1186371.

[91] H. H. Snijder et al. *Buckling Curves for Heavy Wide Flange Steel Columns*. Tech. rep. 2010.

[92] D. Stankovic et al. “Fretting Fatigue Performance of Unidirectional, Laminated Carbon Fibre Reinforced Polymer Straps at Elevated Service Temperature”. In: *Polymers* 13 (19 Oct. 2021). ISSN: 20734360. DOI: 10.3390/polym13193437.

[93] Y. Tan and Y. Yao. “Optimization of Hanger Arrangement in Pedestrian Tied Arch Bridge With Sparse Hanger System”. In: *Advances in Structural Engineering* 22 (12 Sept. 2019), pp. 2594–2604. ISSN: 20484011. DOI: 10.1177/1369433219849842.

[94] Y. Tan and Y. Yao. *Optimization of Hanger Arrangement in Tied Arch Bridge Using Genetic Algorithm*. Tech. rep. 2018. URL: https://www.researchgate.net/publication/325545539.

[95] P. Tanskanen. *The Evolutionary Structural Optimization Method: Theoretical Aspects*. Tech. rep. 2002, pp. 5485–5498. URL: www.elsevier.com/locate/cma.

[96] S. Teich. “Beitrag zur Optimierung von Netzwerkbogenbrücken (Contribution to Optimizing Network Arch Bridges)”. PhD thesis. Technical University of Dresden, Feb. 2012.

[97] S. Teich. “Entwicklung allgemeiner Entwurfsgrundsätze für Hängernetze von Netzwerkbogenbrücken”. In: *Stahlbau* 80 (2 Feb. 2011), pp. 100–111. ISSN: 00389145. DOI: 10.1002/stab.201001395.

[98] S. Teich and S. Wendelin. “Vergleichsrechnung einer Netzwerkbogenbrücke unter Einsatz des Europäischen Normenkonzeptes”. PhD thesis. TECHNISCHE UNIVERSITÄT DRESDEN, Aug. 2001. URL: https://home.uia.no/pert/data/Masters%20theses/Diplomarbeit.pdf.

[99] M. J. Thoresson et al. “Efficient Optimisation of a Vehicle Suspension System, Using a Gradient-Based Approximation Method, Part 2: Optimisation Results”. In: *Mathematical and Computer Modelling* 50 (9-10 Nov. 2009), pp. 1437–1447. ISSN: 08957177. DOI: 10.1016/j.mcm.2009.07.012.

[100] P. Tveit. *About the Network Arch*. Tech. rep. Agder University, 2009. URL: https://home.uia.no/pert/backup/documents/About_the_network_arch.pdf.

[101] P. Tveit. *About the Network Arch*. Tech. rep. 2019. URL: http://thost-iabse-elearning.org/l20/data/downloads/tveit_handouts.pdf.

[102] P. Tveit. *An Introduction to the Optimal Network Arches*. Tech. rep. Agder University College, 2000. URL: http://pchome.grm.hia.no/~pert/.

[103] P. Tveit. “Bogebruer med Skrå Krysstilte Hengestenger, (Arch Bridges with Inclined Intersecting Hangers)”. PhD thesis. Technical University of Norway, 1959.

[104] P. Tveit. “Considerations for the Design of Network Arches”. In: *Journal of Structural Engineering* 1113 (1987), pp. 2189–2207. ISSN: 0733-9445/87/0010-21897.

[105] P. Tveit. “Design of Network Arches”. In: *Structural Engineering* (1966), pp. 247–259.

[106] P. Tveit. “Graduation Thesis on Arch Bridges with Inclined Hangers”. PhD thesis. Technical University of Norway, Sept. 1955.

[107] P. Tveit. “How to Design Economical Network Arches”. In: *IOP Conference Series: Materials Science and Engineering*. Vol. 471. Institute of Physics Publishing, Feb. 2019. DOI: 10.1088/1757-899X/471/5/052078.

[108] P. Tveit. “Nettverkbogar, ein ny brutype, (Network Arches, a New Type of Bridge)”. In: *Bygg* 12 (1964), pp. 105–113.

[109] P. Tveit. “Network Arches”. In: *11th IABSE Congress*. 1980, pp. 817–818.

[110] P. Tveit. *Network Arches for Railway Bridges*. Tech. rep. Danmarks Ingeniorakademi, Aug. 1973.

[111] P. Tveit. “Optimal Design of Network Arches”. In: *IABSE Symposium*. 2002. ISBN: 3-85748-107-2.

[112] P. Tveit. “Optimal Network Arches for Coastal Regions”. In: *International conference on bridges*. 2006, pp. 721–728. ISBN: 953-95428-0-4.

[113] P. Tveit. *The Network Arch*. Tech. rep. 2014, pp. 1–142. URL: http://home.uia.no/pert.

[114] P. Tveit. *The Network Arch - Bits of Manuscript in July 2016 after Lectures in 50+ Countries*. Tech. rep. 2016.

[115] P. Tveit. *The Network Arch. Bits of Manuscript in March 2014 after Lectures in 50 Countries*. Tech. rep. Mar. 2014. URL: http://home.uia.no/pert/.

[116] P. Tveit. “Visit to the Steinkjer Network Arch 44 Years Later”. In: *ARCH’07, 5th International Conference on Arch Bridges*. Sept. 2007. ISBN: 978-972-8692-31-5.

[117] P. Tveit et al. *Systematic Thesis on Network Arches*. Tech. rep. UiA, July 2014. URL: http://home.uia.no/pert/.

[118] G. Vantyghem et al. “3D Printing of a Post-Tensioned Concrete Girder Designed by Topology Optimization”. In: *Automation in Construction* 112 (Apr. 2020). ISSN: 09265805. DOI: 10.1016/j.autcon.2020.103084.

[119] F. Wang. “Research on Dynamic Detection Method of Bridge Vehicle Load Based on Optimization Algorithm”. In: (2023). ISSN: 2444-8656. DOI: 10.2478/10.2478/amns.2023.2.00028. URL: https://doi.org/10.2478/10.2478/amns.2023.2.00028.

[120] P. Wilson and H. Law. “Earthquake Ground Motions for Design of the Sixth Street Viaduct”. In: *Structures Congress 2015 - Proceedings of the 2015 Structures Congress*. American Society of Civil Engineers (ASCE), 2015, pp. 514–525. ISBN: 9780784479117. DOI: 10.1061/9780784479117.045.

[121] L. Xia et al. “Bi-directional Evolutionary Structural Optimization on Advanced Structures and Materials: A Comprehensive Review”. In: *Archives of Computational Methods in Engineering* 25 (2 Apr. 2018), pp. 437–478. ISSN: 18861784. DOI: 10.1007/s11831-016-9203-2.

[122] P. Yang, J. Deng, and A. Wang. “Multiobjective Optimization of Suspension Bridges via Coupled Modeling and Dual Population Multiobjective Particle Swarm Optimization”. In: (2025). DOI: https://doi.org/10.1038/s41598-025-06392-0.

[123] H. Yousefpour, T. A. Helwig, and O. Bayrak. “Construction Stresses in the World’s First Precast Network Arch Bridge”. In: (2014).

[124] Z. B. Zabinsky. *Random Search Algorithms*. Tech. rep. Department of Industrial and Systems Engineering, Apr. 2009. URL: https://courses.washington.edu/inde510/516/AdapRandomSearch4.05.2009.pdf.

[125] Q. Zaheer, T. Yonggang, and F. Qamar. *Literature Review of Bridge Structure's Optimization and Its Development Over Time*. 2022. DOI: 10.1051/smdo/2021039.

[126] R. Zanon et al. "Network Arch Bridges with Rolled Sections: Ideas for Economic and Durable Detailing". In: *ce/papers* 3 (5-6 Dec. 2019), pp. 106–116. ISSN: 2509-7075. DOI: 10.1002/cepa.1186.

[127] R. Zanon et al. *Tied-Arch Bridges with Jumbo Shapes as Arch Member—State of the Art and Developments*. Apr. 2020. URL: https://www.researchgate.net/publication/343189366_TIED-ARCH_BRIDGES_WITH_JUMBO_SHAPES_AS_ARCH_MEMBER_State_of_the_art_and_developments.

[128] M. Zhou and G. Rozvany. "On the Validity of ESO Type Methods in Topology Optimization". In: *Structural and Multidisciplinary Optimization* 21 (2001), pp. 80–83. DOI: 10.1007/s001580050170.

[129] B. Zwingmann, S. Marx, and F. Schanack. "Asymmetric Network Arch Bridges". In: *Structures and Architecture - Proceedings of the 1st International Conference on Structures and Architecture, ICSA 2010*. 2010, pp. 1240–1247. ISBN: 9780415492492. DOI: 10.1201/b10428-165.

Standards

[130] *EN 1990: Eurocode - Basis of Structural Design*. Tech. rep. CEN, 2002.

[131] *EN 1991-2: Eurocode 1: Actions on Structures - Part 2: Traffic Loads on Bridges*. Tech. rep. CEN, 2003.

[132] *EN 1993-1-1: Eurocode 3: Design of Steel Structures - Part 1-1: General Rules and Rules for Buildings*. Tech. rep. CEN, 2005.

[133] *EN 1993-1-9: Eurocode 3: Design of Steel Structures - Part 1-9: Fatigue*. Tech. rep. CEN, 2005.

[134] *EN 1993-2: Eurocode 3: Design of Steel Structures - Part 2: Steel Bridges*. Tech. rep. CEN, 2006.

[135] *Specification for Structural Steel Buildinds*. Tech. rep. Design of Members for Tension, 2005.

[136] *Standard Specifications for Highway Bridges*. Tech. rep. American Association of State Highway and Transportation Officials, 2002.

Websites

[137] ArcelorMittal. *Sections and Merchant Bars*. Tech. rep. 2025. URL: https://sections.arcelormittal.com/repository2/Sections/Sections_MB_ArcelorMittal_FR_EN_DE_V2023-5.pdf.

[138] *Arch Bridges*. 2017. URL: https://www.sciencedirect.com/topics/engineering/arch-bridges.

[139] L. As. *Hangar Bridge*. URL: https://leirvik.com/infrastructure/hangar-bridge/.

[140] A. Blonka. *Import data from SOFiSTiK to Grasshopper - workflow and examples*. URL: https://www.youtube.com/watch?v=Vdlnt3a-CZY&ab_channel=GrassSTiK.

[141] A. Blonka. *SOFiSTiK for Grasshopper - beam and cable components*. URL: https://www.youtube.com/watch?v=m0TXJZJwbHM&ab_channel=GrassSTiK.

[142] *Brandangersundet Bridge*. URL: https://bridgeinfo.net/bridge/index.php?ID=213.

[143] *Bugrinsky Bridge*. URL: https://depositphotos.com/photos/bugrinsky-bridge.html.

[144] *Ceny w Budownictwie*. URL: https://sekocenbud.pl/ceny-w-budownictwie/.

[145] *Introduction to Scientific Computing*. Tech. rep. Stanford University, 2020. URL: https://web.stanford.edu/class/math114/lecture_notes/intro_opt.pdf.

[146] *Network Arch Bridge in Cracow*. URL: https://www.railwaypro.com/wp/rail-bridges-in-krakow-completed/.

[147] *Newton's Method*. URL: https://www.britannica.com/science/Newtons-method.

[148] *Newton's Method*. Tech. rep. John Hopcroft Center of Computer Science. URL: https://jhc.sjtu.edu.cn/~kuanyang/teaching/MATH3806/notes/lec12.pdf.

[149] *Nielsen-Lohse Bridge*. URL: https://structurae.net/en/structures/bridges/nielsen-lohse-bridges.

[150] *Palma del Rio Network Arch Bridge*. URL: https://www.megusa.com/index.php/2-uncategorised/39-puente-palma-del-rio.

[151] *River Irwell Bridge*. URL: https://resource.midasuser.com/en/blog/bridge/casestudy/river-irwell-network-arch-bridge-modelling.

[152] F. Sellke. *Bruckenweb.de – Brucke Nr. 230, 230A GroBer Kolonnenweg*. URL: https://structurae.net/de/bauwerke/bruecke-grosser-kolonnenweg-1961.

[153] *Sixth Street Viaduct*. URL: https://www.sofistik.com/en/references/sixth-street-viaduct-replacement.

[154] *Steien bridge*. URL: https://www.mdpi.com/applsci/applsci-13-10966/article_deploy/html/images/applsci-13-10966-g016.png.

[155] *The Iron Bridge*. URL: https://en.wikipedia.org/wiki/The_Iron_Bridge.

[156] *Tied-Arch Bridge Facts, History and Examples*. URL: https://www.historyofbridges.com/facts-about-bridges/tied-arch-bridge/.

[157] *Troja Netowrk Arch Bridge*. URL: https://d34-a.sdn.cz/d_34/c_img_gV_3/m2vyLd.jpeg?fl=res,2200,2200,1.

[158] P. Tveit. *Network Arch Map*. URL: https://home.uia.no/pert/index.php/Map_of_Bridges.

[159] *Windsor Railway Bridge*. URL: https://www.nationaltransporttrust.org.uk/heritage-sites/heritage-detail/windsor-railway-bridge.

Appendices

A The review of optimization methods

This section includes the literature review of optimization algorithms used in civil engineering. Author started from historically the oldest optimization algorithms and finished with modern ones. This review was helpful in familiarizing with various optimization tools, getting more intuition and decide, which would be the most suitable for author's needs.

A.1 Root and solution searching

A.1.1 Bracketing methods

The braced method are characterized by operating within given finite interval and the searched solution will be limited to this region [15].

Graphical Graphical method is based on the plotting a graph of the investigating function or phenomenon and mostly search for the characteristics points on the graph, such as function's root, extreme values and numerical integration [15]. The method is very simple in implementation and does not require much computing power as other methods. The investigating phenomenon has to be described by the function and be visualized, which mostly is limited to the function of two variables. For larger and more complex descriptions, the graphical method is impossible to use [15]. Despite of minor impact in multi-variable functions, it is still a useful method for visual investigation of the phenomenon trends and acts as supportive tool for other methods [15]. The analysed function is only limited to its dimensionality, no continuity or differentiability, which is usually a request in other methods [15].

Bisection The bisection method is another simple method as graphical, but it requires iterative process in finding the function's root, which is the purpose of this method [15]. The mathematical description can be expressed by Eq. (A.1).

$$f(x_l)f(x_u) < 0 \tag{A.1}$$

Where:

- x_l - the lower interval axes value,
- x_u - the upper interval axes value,
- $f(x_l)$ - the lower interval function value,
- $f(x_u)$ - the upper interval function value.

The equation expresses, that in the given interval between x_l and x_u the function has to have at least one root, since the function has different sign at interval ends. In order to search for the more precised root determination, the iterative process is used. In the first step, the interval is divided into two parts exactly in the middle. Then the function value is determined for the middle point. The criteria described in Eq. (A.1) is applied to both subintervals. The subinterval, which fulfills the criteria is considered and the process starts again for the selected interval. It continues until reaching function value smaller than the assumed precision or when

the axes value difference between the current and the previous steps is smaller than the accepted accuracy. Coincidentally the root might be determined exactly during interval division, then the obtained value is precised and the process ends as well since there is no more space for improvement. In general, the two convergence criteria can be expressed by Eq. (A.2)-(A.3).

$$|x_n - x_{n-1}| < \epsilon \tag{A.2}$$
$$|f(s)| < \delta \tag{A.3}$$

where ϵ and δ are small tolerances for the interval and the function value, respectively. This criteria is applicable also for other iterative methods.

The method can be supported by the graphical method for determining the initial interval boundaries. Nevertheless, the analysed function has to be continuous but not differentiable. The method does not solve for all function's roots in the given interval and because of the definition of the method and iterative process, only one root is determined. The graphical method can be as well helpful in this situation. The example of bisection graphical representation is presented in Fig. A.1. In the given example the initial division provided the value of 1.6, the second 1.4 and the third 1.5. The actual root value in this interval is 1.414, which means that even though the second iteration was relatively close to the actual value, the third iteration step made this result worse. The method does not reduce the error after every step. In this case, it would require 4 more steps, so iteration 6, to match the error smaller than the error obtained in the second iteration step. The algorithms characterized by slow error reduction progression are called brute-force algorithms.

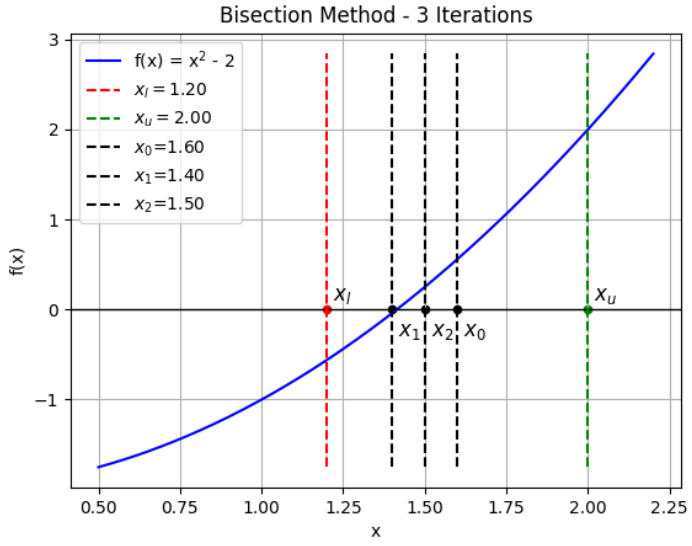

Figure A.1 Example of the bisection method convergence for function $f(x) = x^2 - 2$ with 3 iterations. The root value, accurate to three decimal places, is approximately 1.414

The bisection method is very common method in civil engineering, among others in solving for parameters in frequent equations for vibration modes [41], in shape-finding of cables in suspension bridges [122], finding instability bifurcation point [65].

False position False position method is similar to bisection method [15]. In bisection, the interval is divided into two equal length parts, even if the one of the interval ends is very close

to the root and the value of the function is much lower than the value of the function on the other end of the interval. It is faster, if the division acts closer to the interval end with lower function value, which should be then closer to the actual root position [15]. The division point is determined by connecting function value at the interval ends by a line and finding the crossing point of this line with the x-axis. This point is a root of the line not the analysed curve, which might be considered as a false-root or false position of the root. The false-position is determined from the Tales theory expressed in Eq. (A.4) [30].

$$\frac{f(x_l)}{x_i - x_l} = \frac{f(x_u)}{x_i - x_u} \Rightarrow x_i = \frac{f(x_l)x_u - f(x_u)x_l}{f(x_l) - f(x_u)} \tag{A.4}$$

Where:

x_l - the lower interval axes value,
x_u - the upper interval axes value,
$f(x_l)$ - the lower interval function value,
$f(x_u)$ - the upper interval function value,
x_i - the false-position axes value.

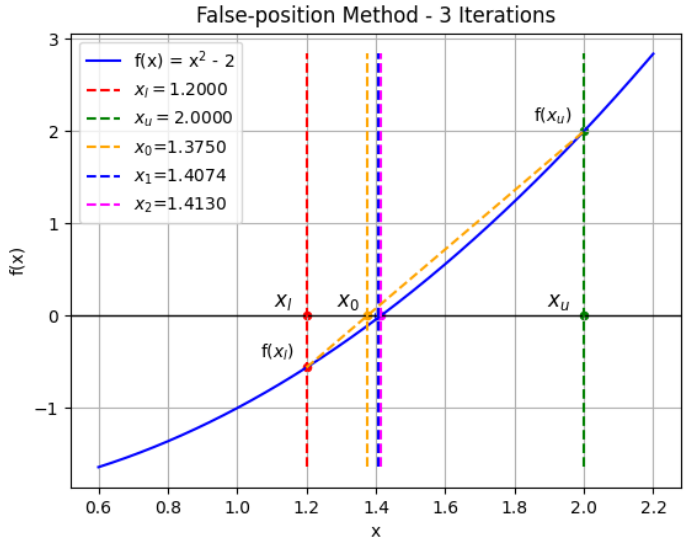

Figure A.2 Example of the false position method convergence for function $f(x) = x^2 - 2$ with 3 iterations. The root value is 1.414 with accuracy to three decimal places

The example of the false position method is presented in Fig. A.2 using the same example as for the bisection method. The first conclusion after these 3 iterations is, that the false position method converges faster than the bisection method and the error value decreases over time. In the analysed example, the first root approximation is 1.375, the second 1.4074 and the third 1.413, which has already error lesser than a permille from the precise root. For a comparison, the bisection and false position methods error are presented in Fig. A.4a. The false position method results in faster convergence than bisection method and the error decreases over iterations until reaching the allowed precision in Python script language of 10^{-16}, whereas bisection's lowest error value is at magnitude of 10^{-10} - 10^{-9}.

In this example, the false position is without any doubts faster than the bisection method, but there are cases, where the situation is opposite. A good example is function $x^{15} - 1$ with

starting interval between 0 and 1.2 as presented in Fig. A.3a and A.3b. At the first glance, the bisection method reaches the convergence much faster than the false position method. Even the first estimated root is closer to the solution than the 10th estimation from the second method. The error comparison is presented in Fig. A.4b. The bisection reaches the maximum allowed precision at 50th iteration much faster than the false position which achieved that at about 165th iteration. This example shows, that both methods are able to reach convergence but the number of iterations needed to achieve that depends on the type of function to analyse.

From the analytic point of view, the function should be continuous and is not required to be continuous from derivation perspective [15]. The false root method is used in similar fields, as the bisection or Newton-Raphson methods in among other solving nonlinear equations in structural mechanics [30].

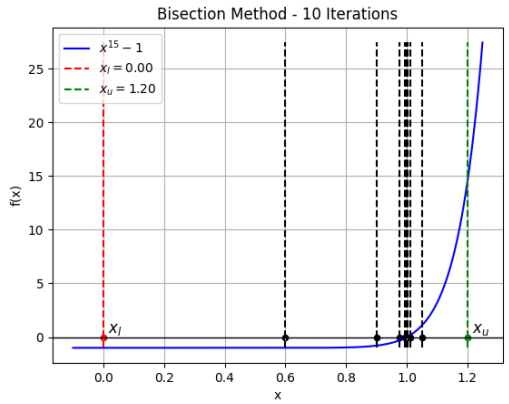

(a) Example of bisection method convergence for function $f(x) = x^{15} - 1$ with 10 iterations. The precise root value is 1.00

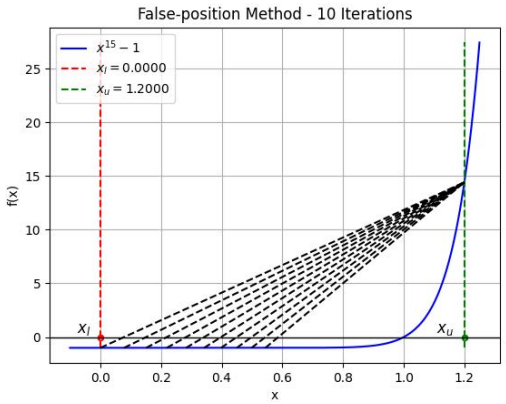

(b) Example of false position method convergence for function $f(x) = x^{15} - 1$ with 10 iterations. The precise root value is 1.00

Figure A.3 Example of the false position and bisection methods convergence for function $f(x) = x^{15} - 1$ with 10 iterations. The precise root value is 1.00

(a) The comparison of a difference between the estimated root value over 20 iterations for bisection and false position methods for function $x^2 - 2$

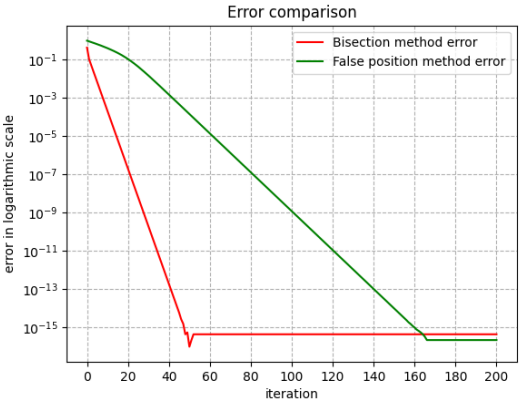

(b) The comparison of a difference between the estimated root value over 200 iterations for bisection and false position methods for function $x^{15} - 1$

Figure A.4 The comparison of a difference between the estimated root value and the actual root value for bisection and false position methods

A.1.2 Open methods

As a contrary to the braced methods, the open methods are not limited to any finite interval [15]. For their definition one or two points are needed as a starting points but the methods are not restricted by these points and can search in regions even far from them. The general trend is that if the open methods converge, they converge faster than the braced methods, but convergence is not guaranteed [15].

Fixed-Point The method search for a root of a given function. The considered function $f(x)$ is assumed to be described as in the Eq. (A.5) [15].

$$f(x) = x - g(x) \tag{A.5}$$

Since the goal is the determination of x to satisfy $f(x) = 0$, the task convert into finding the solution of $x = g(x)$ with function $f(x)$ described as in Eq. (A.5) [15]. The process is iterative and require providing the starting point in a way, that the process converge [15]. All points during the iterative process should satisfy the criterion expressed in Eq. (A.6) [15]. The function $f(x)$ has to be continuous and have continuous derivatives [15].

$$|g'(x)| < 1 \tag{A.6}$$

Let's consider the function $f(x) = x^2 - x - 2$. Searching for $f(x) = 0$, the equation transforms into $x^2 - x - 2 = 0$. With simple transformation into $x = 1 + 2/x$, the function $g(x)$ can be expressed as $g(x) = 1 + 2/x$ and its derivative is then $g'(x) = -2/x^2$. Since the absolute value of the first derivative of function $g(x)$ should be smaller than 1, the fixed point should satisfy this criteria. The range to satisfy this criteria is $\mathbb{R}\backslash[-\sqrt{2}, \sqrt{2}]$ and the fixed point is equal to 2 for function $f(x)$, which lays in the given domain for the chosen function $g(x)$. In this case, the method will converge to the root value of 2. To get another root of function $f(x)$, the transformation $x = 2/(x-1)$ was chosen. The function $g(x) = 2/(x-1)$ and its derivative $g'(x) = -2(x-1)^{-2}$ results in allowed range of $\mathbb{R}\backslash\left([1-\sqrt{2}, 1) \cup (1, 1+\sqrt{2}]\right)$ where the second function $f(x)$ root of -1 lays.

After defining the range for the starting point, the iterative process expressed by Eq. (A.7) should be applied.

$$x_{n+1} = x_n - g(x_n) \tag{A.7}$$

The iteration for $g(x) = 1 + 2/x$ with starting point $x_0 = 1$ and $g(x) = 2/(x-1)$ with starting point $x_0 = -0.5$ were presented in Fig. A.5.

The method provides more flexibility root searching, since the only restriction is the Eq. (A.6) in terms of choosing the initial points [15]. Nevertheless, it requires transformation of the function $f(x)$ in such way, that the obtained $g(x)$ has a convergence domain with the root that is searched for. The function $f(x)$ should be continuous and function $g(x)$ should be differentiable [15].

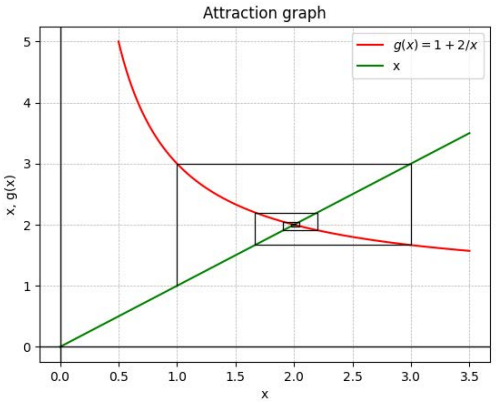

(a) The attraction convergence graph with 10 iterations

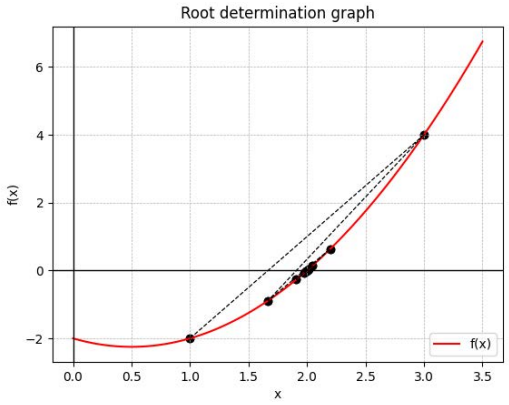

(b) The root convergence graph with 10 iterations

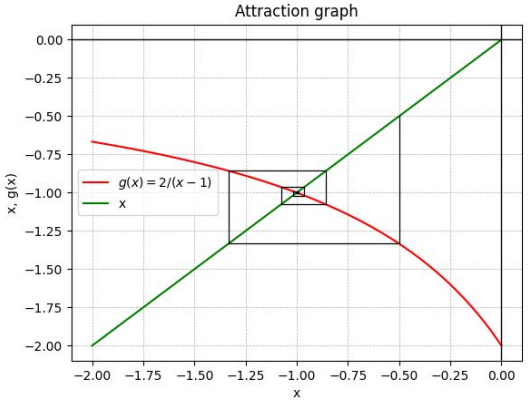

(c) The attraction convergence graph with 10 iterations

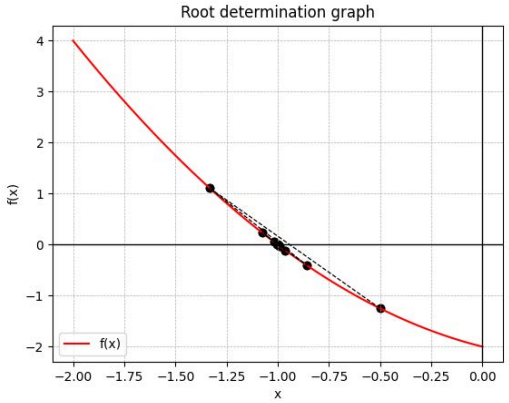

(d) The root convergence graph with 10 iterations

Figure A.5 The example of the fixed-point method attraction and root convergence graphs with 10 iterations. The root value is (a)-(b) 2.00 and (c)-(d) -1.00

Newton-Raphson The Newton-Raphson method is one of the oldest analytical method for finding solutions. It was established first by Isaac Newton in 1669 and developed by Joseph Raphson in 1690 [147]. It allows to iteratively find an argument for which function has value of zero. Due to its speed and simplicity, it has been greatly used in engineering and mathematics. The method is based on approximating the root of an equation by linear approximation and local derivative calculations [55]. The algorithm can be described by Eq. (A.8) [147].

$$x_{n+1} = x_n - \frac{f\left(x_n\right)}{f'\left(x_n\right)} \tag{A.8}$$

Where:

x_{n+1}	-	the next approximated root,
x_n	-	the current approximated root,
$f\left(x_n\right)$	-	the function value for x_n,
$f'\left(x_n\right)$	-	the value of the first derivative of function for x_n.

The method is based on the fixed-point method with $g(x) = f(x)/f'(x)$. The positive aspect in comparison to the general fixed-point method is no need for function transformation in order to obtain the functions $g(x)$ with domains including all possible roots of function $f(x)$, which simplifies the method by making it depended on the initial point x_0 value.

The method requires to have a determination of the function analytically and the function itself needs to be continuous as well as its first derivative [147, 15]. The initial value x_0 should be close to the searching root of the function, otherwise the method might not converge [147, 15]. Moreover, the derivative in close range of the function root should not be zero [15]. The method is characterized by quadratic convergence, which means that the error in each iteration decreases quickly [15]. The visual representation of the method was presented in Fig. A.6a. In this example, the approximated root after 3 iterations was 1.416 which was close enough to the exact solution of $\sqrt{2} \approx 1.414$. However with the choice of the x_0 value closer to the function derivative's root, the convergence will take longer as it is presented in Fig. A.6b or even not reach the function's root that was intended to achieved as presented in Fig. A.6c.

Newton-Raphson, similarly as the bisection method, is used for converging task in civil engineering, among others, in cables' form-finding in suspension bridges [77], in finding numerical solution of a reinforced concrete beam [90].

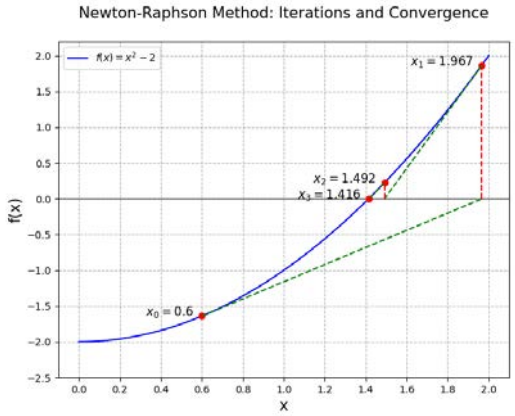

(a) Convergence for function $f(x) = x^2 - 2$ with 3 iterations. The convergence was fast achieved

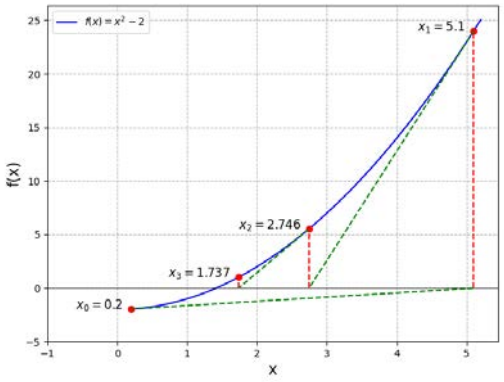

(b) Convergence for function $f(x) = x^2 - 2$ with 3 iterations. The convergence was slower due to starting point closer to the function derivative's root

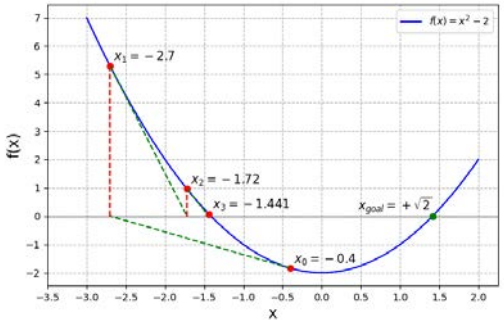

(c) Convergence for function $f(x) = x^2 - 2$ with 3 iterations. The convergence was fast but the desired positive root was not achieved

Figure A.6 Examples of the Newton-Raphson method convergence for function $f(x) = x^2 - 2$ with 3 iterations

Secant The secant method is another variation of fixed-point method with the iterative process expressed as follows.

$$x_n = x_{n-1} - f(x_{n-1})\frac{x_{n-1} - x_{n-2}}{f(x_{n-1}) - f(x_{n-2})} \tag{A.9}$$

Where:

x_{n-2}, x_{n-1}, x_n	-	the three consecutive approximated roots,
$f(x_n)$, $f(x_{n-1})$, $f(x_{n-2})$	-	the function values for x_n, x_{n-1} and x_{n-2} respectively.

The method is a hybrid solution between bracket methods, since two first values should be determined in close range of the searched root of the function, and open methods since the approximated root values may lay outside the predefined interval as a consequence of an iterative process. If the distance between two initial points is approaching 0, the method converge to Newton-Raphson method. In principles, the secant method is converging superlinearly with the power of the golden ratio $\varphi \approx 1.618$ [23], which is slower than Newton-Raphson method with quadratic convergence [71]. The example with starting points interval not including the root was presented in Fig. A.7a and Fig. A.7b. The case with including the root in the starting interval was presented in Fig. A.7c and Fig. A.7d. In both cases, the two starting points were the same, but their order was changed, which also affected the way the algorithm converged. The algorithm approached the root faster, when the interval included the root. The order of starting points did not matter that much as for the case without including the root between starting points.

The secant method is used in the iterative algorithms. One of the examples is cables iterative force determination process for hangers in suspension bridges [57].

An extension to the secant method, the **Müller** method was introduced by David E. Müller in 1956. While the secant method approximates the root using a linear function between two points, Müller's method uses a quadratic approximation based on three points [15]. This makes the method useful when dealing with functions that are nonlinear or when faster convergence is desired [28]. It does not require the derivative of the function, which is beneficial for cases where function equation is unknown [15].

The method begins with three initial points, x_0, x_1, and x_2, and uses a parabolic approximation to determine the estimated root of the function described by $y = ax^2 + bx + c$. The next root approximation is given by the solution to the quadratic equation as presented in Eq. (A.10) [15].

$$x_n = x_{n-1} - \frac{2c}{b \pm \sqrt{b^2 - 4ac}} \tag{A.10}$$

where the sign is chosen to minimize the denominator and avoid division by a small number.

Müller method converges faster than linear methods like secant but slower than Newton-Raphson method [28]. As in the iterative methods, the initial points have impact to the convergence of the method, especially if they are far from the desired root [28], as it was presented in Newton-Raphson method. Similarly as the false position method, the Müller method is applicable for solving non-linear equations in structural mechanics [28].

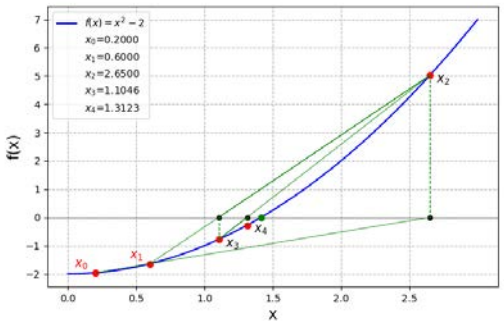

(a) Convergence for function $f(x) = x^2 - 2$ with 3 iterations. Close initial points

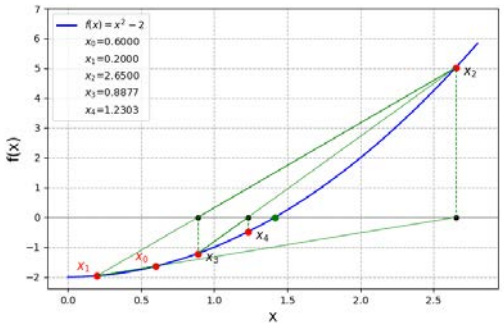

(b) Convergence for function $f(x) = x^2 - 2$ with 3 iterations. Close initial points but reversed order

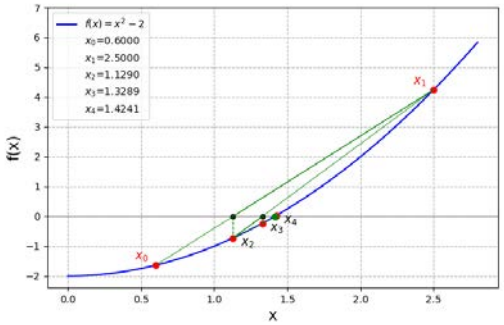

(c) Convergence for function $f(x) = x^2 - 2$ with 3 iterations. Root in between initial points

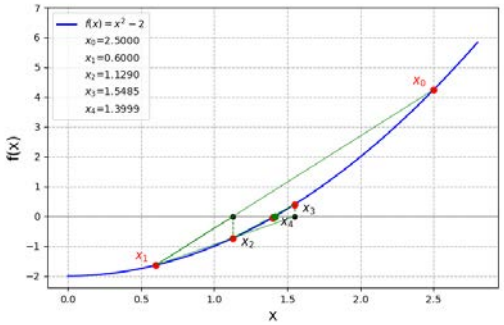

(d) Convergence for function $f(x) = x^2 - 2$ with 3 iterations. Root in between initial points, but reversed order

Figure A.7 Example of the secant method convergence for function $f(x) = x^2 - 2$ with 3 iterations

A.2 Minimum/maximum search

Minimum or maximum searching algorithms are an unique solution search algorithms. In root search, the solution of $f(x) = 0$ is obtained, but in more generalized formula $f(x) = a$ in solution search the specific value a is searched for. This criteria might be modified into $w(x) = f(x) - a = 0$ and be solved by the root search algorithms. The max/min search methods are similar in principles as root search algorithms described as $f(x) = \min f(x)$ or $f(x) = \max f(x)$, however the max/min value searched for is unknown [15]. That requires different solutions for this problem [15].

Gradient Descent/Ascent The gradient method has two variant of ascending when the maximum value is searched for, and descending when it is minimum value [15]. The process is iterative and is similar in principles to fixed-point method [15]. The adjustment of x_n value is based on the gradient, $\nabla f(x)$, which points in the direction of the steepest change of the function [15]. The gradient part can be modified by a step size learning rate λ as described by the Eq. (A.11) [145].

$$x_{n+1} = x_n - \lambda \nabla f(x_n) \tag{A.11}$$

The goal is to find x such that $f(x)$ is minimized or maximized, which corresponds to a point where the gradient is zero, $\nabla f(x) = 0$ [15]. The function $f(x)$ must be continuous and differentiable, as this ensures that the gradient $\nabla f(x)$ exists at each point in the domain [15]. The function can be multidimensional [15]. As the solution progress the function derivative values should converge to 0 and function values should be monotonic during the iterative process as described in Eq. (A.12) [15].

$$f(x_0) > f(x_1) > f(x_2) > \dots \tag{A.12}$$

Consider the function $f(x) = x^2 - x - 2$. The gradient of $f(x)$ is obtained as $\nabla f(x) = 2x - 1$. The function has global minimum value and no global maximum value if the considered domain is $x \in \mathbb{R}$. However, if the domain is restricted to the finite range, there is a possibility to find maximum value within this range, so called local maximum. Starting with the global minimum, the initial point can be any value and the $x_0 = -1.1$ and $x_0 = 1.70$ were selected. The learning coefficient $\lambda = 0.3$ was arbitrary chosen. The results were presented in Fig. A.8a and Fig. A.8b. The method pointed into the global minimum value regardless of the starting point in the local convex region of the global minimum value. If the method is supposed to be used in this case for searching the maximum value, the limits should be applied. The limits of -1.3 and 1.7 were applied. The results for the starting points $x_0 = 0.10$ and $x_0 = 0.70$ are presented in Fig. A.8c and Fig. A.8d respectively. In this case, the algorithm reached once the left limit maximum value and right limit maximum value. If the starting point is set left from this local minimum, it will not be able to reach maximum value on the right side of this local minimum. The opposite relation also applies. That means, the starting point position in relevant to the local extreme value determines into which direction the algorithm will search for the extreme value.

The method approach local extreme value fast and guarantee convergence, but is highly depended from the starting point and the quantity of the local convex regions [15]. The algorithm does not guarantee reaching the global extreme value, only local [15]. The example was presented in Fig. A.8e and Fig. A.8f. In general, multiple starting points are chosen being spread in the limited domain, which increases the probability of reaching global extreme value [15].

In civil engineering, the gradient method can be used in, among others, obtaining "the deflection influence line of the bridge dynamic test structure and the overall vibration frequency of the structure" [119], "optimising a vehicle's suspension characteristics for ride comfort" [99] and in the shape optimization of the structure [74].

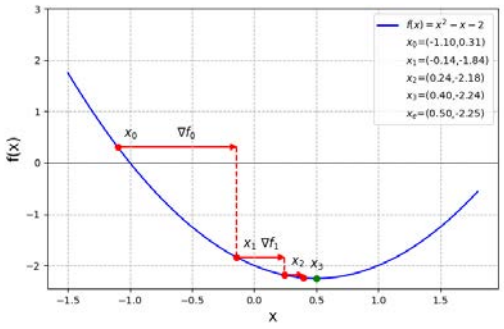

(a) Convergence to the minimum value for function $f(x) = x^2 - x - 2$ with 3 iterations

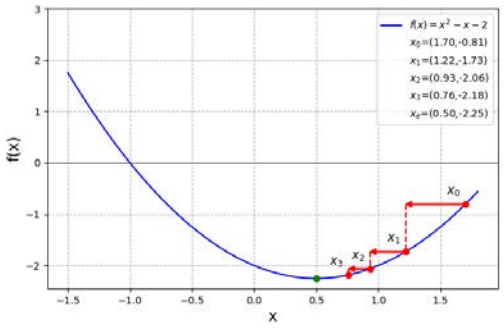

(b) Convergence to the minimum value for function $f(x) = x^2 - x - 2$ with 3 iterations

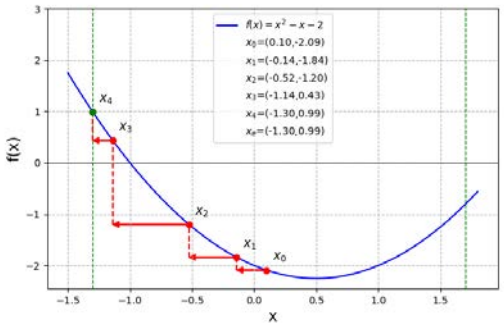

(c) Convergence to the maximum limit value for function $f(x) = x^2 - x - 2$ with 4 iterations

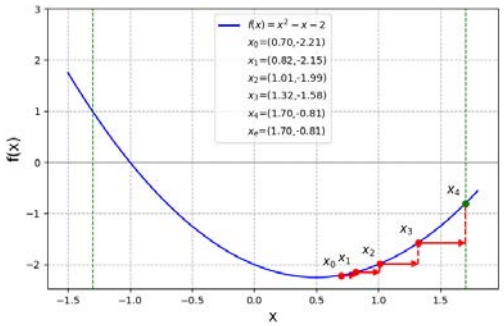

(d) Convergence to the maximum limit value for function $f(x) = x^2 - x - 2$ with 4 iterations

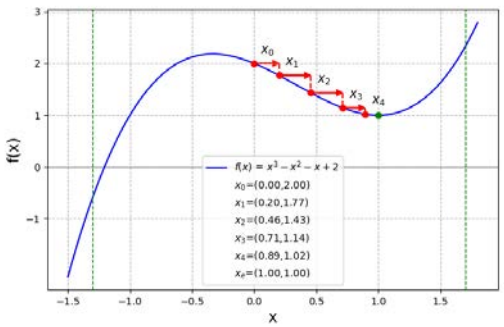

(e) Convergence to the minimum value for function $f(x) = x^3 - x^2 - x + 2$ with 4 iterations

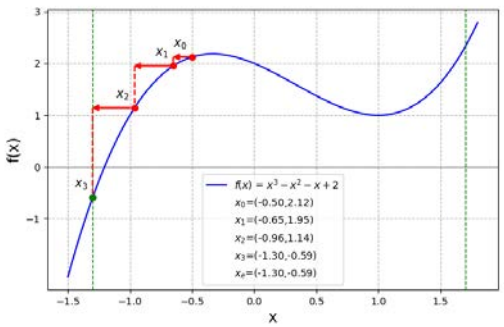

(f) Convergence to the minimum limit value for function $f(x) = x^3 - x^2 - x + 2$ with 3 iterations

Figure A.8 Examples of gradient descent method convergence to the minimum/maximum value

Newton method The Newton method for finding the maximum or minimum value of the function is very similar in principles to the root finding method [15]. The methods is based on the Taylor expansion of the function $f(x)$ expressed by Eq. (A.13) [15].

$$f(x+t) = f(x) + \sum_{n=1}^{\infty} f^{(n)}(x) \cdot t^n / n! \tag{A.13}$$

The value t is a change of value x. Since the local extreme values are characterized by $\nabla f = 0$ except the values of the function at its limited boundary, the first three terms of Taylor

expansion are considered result in approximation presented in Eq. (A.14) and their derivative is applied in Eq. (A.15) which result in t value equal to the one presented in Eq. (A.16) [148].

$$f(x+t) \approx f(x) + f'(x)t + 1/2 \cdot f''(x)t^2 \tag{A.14}$$

$$\nabla f(x+t) \approx \nabla \left[f(x) + f'(x)t + 1/2 \cdot f''(x)t^2 \right] = f'(x) + f''(x)t = 0 \tag{A.15}$$

$$t = -f'(x)/f''(x) \tag{A.16}$$

After obtaining the solution for x_n value change t, the iterative formula for the next x_{n+1} can be described as in Eq. (A.17), which is very similar to the Eq. (A.8) for searching for the function root.

$$x_{n+1} = x_n + t = x_n - \frac{f'(x_n)}{f''(x_n)} \tag{A.17}$$

The requirements are that function should be continuous as well as its first and second derivatives [15]. The method does not guarantee the convergence [15]. For greater dimension functions, the solution might converge to the saddle point [15]. Similarly as for the root search, the method converged quadratically fast. The examples for function $f(x) = x^3 - x^2 - x + 2$ were presented in Fig. A.9a - Fig. A.9d.

Since the second derivative can not be equal to 0, the closer the starting point is to this point the less accurate the next point will be. It is also a separation between two local convex with attraction points of -1/3 and +1. The value of the second derivative nullification is 1/3 and the points selected left from this point attract to the left attraction point and the points on the right side to the right attraction point.

Golden section search The golden section search is similar in principles to the bisection method but the division of the intervals is done not evenly but with golden ratio φ proportions [15]. The algorithm needs three points at the beginning [15]. These three points x_i should correspond with the function values f_i relation with local extreme value, $f_1 > f_2 < f_3$ for local minimum or $f_1 < f_2 > f_3$ for local maximum [15]. The greatest interval is divided by the golden ratio and function value is evaluated for the new position. If the function value is more extreme than the middle point, it becomes new middle point and the interval limitation point from the previous shorten interval on the other side of the previous middle point is removed [15]. The second option is when the new point is less extreme than the middle point. Then the previous middle point remained unchanged and the interval limitation point from the divided interval is replaced by the new determined point [15]. The process continues until the progression is small enough [15]. The example of searching for the maximum value was presented in Fig. A.10.

The algorithm has similar advantages as the bisection method as well as disadvantages [15]. It does not require continuous differentiation of the function and finding the local extreme value is guaranteed, since the methods is bracket based and deterministic [15]. It is comparable efficient as the bisection method, which could also be used for the extreme value search since it is a matter of goal function [15].

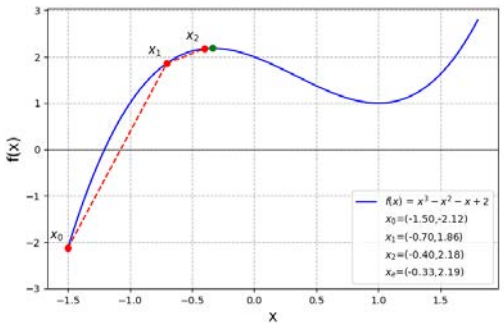

(a) Convergence to the minimum/maximum value for function $f(x) = x^3 - x^2 - x + 2$ with 2 iterations

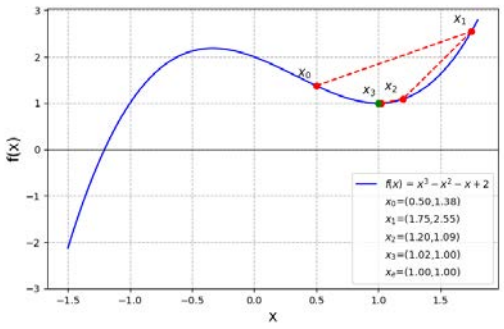

(b) Convergence to the minimum/maximum value for function $f(x) = x^3 - x^2 - x + 2$ with 3 iterations

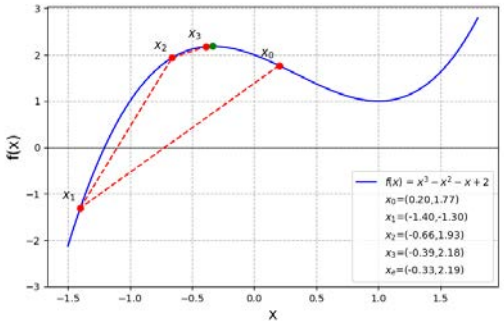

(c) Convergence to the minimum/maximum value for function $f(x) = x^3 - x^2 - x + 2$ with 3 iterations

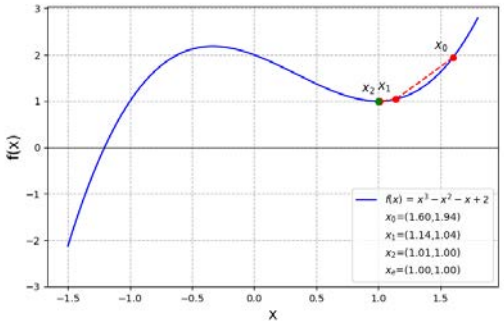

(d) Convergence to the minimum/maximum value for function $f(x) = x^3 - x^2 - x + 2$ with 2 iterations

Figure A.9 Example of Newton method convergence to the minimum/maximum value

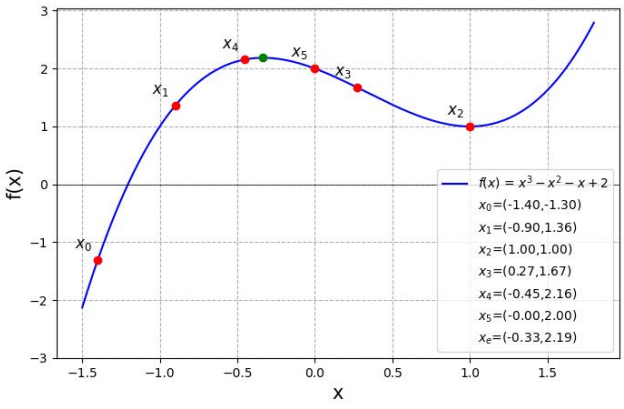

Figure A.10 Example of golden section method convergence to the minimum/maximum value for function $f(x) = x^3 - x^2 - x + 2$ with 3 iterations

A.3 Modern Optimization Algorithms

A.3.1 Random Search methods

Random Search Unlike deterministic algorithms, random search (RS) algorithm does not require description of the search pattern and it is very simple in application [15]. The foundation of RS was introduced in 1963 [80], aiming to offer a general-purpose optimization technique that does not require gradient information or a sophisticated understanding of the function being optimized [80]. The method started to be used in various disciplines including civil engineering [15].

The function does not have to be continuous or have any derivative continuous [15]. The determination of the derivative does not occur [15]. The domain can be multidimensional and even complex [15]. Unlike the deterministic methods, it does not stop in the local extreme value of the function [15]. It always find the global optimum if the search last for long enough [15]. Every next iteration is unrelated to the precious one [15]. The basic algorithm starts with determining the limited domain where the search of solution will be conducted. Aside that, the number of iterations should be specified as well as the optimization criteria. Then, in the iterative process, the points in the limited domain are randomly chosen according to a uniform probability density function.

Alternatively, the first point in the given domain is random and the next point is chosen also randomly in relevance to the previous point with specified in advance step size and the process continues, as determined in Eq. (A.18) [124].

$$x_{n+1} = x_n + s_n r_n \tag{A.18}$$

where x_n and x_{n+1} are previous and current selected point, s_n is a step amplitude or radius of searching region from the best individual and r_n is a random-oriented vector in the domain of all x.

The value for each point is determined and the results are stored and compared with the goals [15]. After precise number of iterations, the process stops and the best matching result is presented [15]. Since each point in the domain has the same probability to be chosen, the domain in a enough long iteration is uniformly investigated [15].

Despite all of the flexibility and simplicity, the main disadvantages of this method are low efficiency, which propagates as the task complexity increase, and random progression without guarantee of reaching neither global nor local extreme value in a reasonable time [15]. The right solution has the same probability to be investigated on the first any next iteration step, which is opposite to the deterministic algorithms, which used to progress in finding the solution as the algorithm simulation lasts [15]. To overcome some of the inherent limitations of the basic RS, several modifications have been developed to improve its efficiency and/or convergence speed [15].

Step-size Adaptive Random Search One of the RS variant is step-size adaptive random search (SARS), which adjust the search range dynamically as the algorithm progresses [88, 5, 54]. Algorithm first generate a point or a set of points in the given domain and determine the best candidate based on the goal function principles. The normalized vector with random direction is multiplied by a random number and added to the current best solution [5]. If the new points produces worse goal function value, it is not accepted and the process repeats [5].

The shape of the distribution is modified as the algorithm progresses. If the results are getting better in a given direction, the algorithm increases gradually the searching radius and

favour the search direction looking for a new points outside the near region of the current best solution [88, 5, 54]. The success of searching can be determined as a ratio of improved points over the total number of searched points [5]. The increasing radius prevents the algorithm from stopping progressing in local extreme value [54]. If the algorithm does not progress, then the opposite relation occurs and radius is getting smaller and smaller to increase search efficiency in the local region [54, 88]. The algorithm used to converge linearly towards local optima for a wide class of functions [5].

A.3.2 Simulated Annealing

The simulated annealing (SA) was introduced in early 1980s in combinatorial optimization [51]. Its name refers to the cooling process in metallurgy, where the metal crystals move faster when the temperature is high at the beginning of the annealing process and stabilize their position as the temperature decreases [21]. The method is used in search of global extreme value, however it does not guaranty finding the global extreme in a finite search process. SA has stochastic methods implemented, which is characteristic for metaheuristic methods [21]. The SA is very flexible and it does not require the function to be continuous and have any continuous derivative [21].

The process starts with definition of the initial points manually or randomly [27]. Secondly, the principles how the new point will be determined is defined [27]. For example, the new point can be defined with the gradient descent/ascent approach. Next, the initial temperature T of the system and the cooling parameter α are chosen. These parameters are needed for the definition of the acceptance principle P [27], Eq. (A.20).

$$P(t, s, T_i) = \begin{cases} 1 & \text{if } F(t) \leq F(s), \\ e^{(F(t)-F(s))/T_i} & \text{if } F(t) > F(s), \end{cases} \tag{A.19}$$

$$T_{i+1} = \alpha T_i \tag{A.20}$$

where F is the goal function value for a given candidate t from the neighbourhood of the present value s, and T_i is the temperature of the current step [27].

Too high temperature value will result in higher chance of worse outcome acceptance and provide higher free and chaotic search at the beginning, so called exploration. Too low temperature will result in more stagnation in searching increasing the chance of limiting the searched domain, so called exploitation. The cooling parameter controls the tempo of temperature decrease over iterations. This simulate the gradual cooling process of the metal structure [27]. The values are taken from 0 to 1. The greater the value is, the longer worse solutions will be accepted. The smaller cooling factor is, the faster algorithm will settle in the local region [27].

If the next candidate provided better results, it is always accepted and considered as the new best candidate. However, if the candidate is worse, then it is accepted with certain probability described in Eq. (A.19).

Since the exponential function expressed in this form is a decreasing function and for the $F(t) - F(s)$ difference equal to 0 the function is 1, which means, that the formula takes values between 0 and 1. The greater the difference in energy is, the lower chance of acceptance. Simultaneously, the lower the temperature is, the lower the chance of acceptance is. Both acceptance reduction of worse solution represents the gradual stabilization of the search process [27].

A.3.3 Evolutionary Structural Optimization methods

Evolutionary structural optimization (**ESO**) is based on the idea that inefficient element, determined by low stress or strain energy density, can be systematically removed [95]. This process follows basic structural mechanics principles and uses iterative algorithms to eliminate material that contributes least to the structural performance [95].

The primary criterion for material removal in ESO is based on the strain energy density presented in Eq. (A.21) [95].

$$W_e = \frac{1}{2}\mathbf{f}^\top \mathbf{u} = \frac{1}{2}\mathbf{u_i}^\top \mathbf{K_i u_i} = W_i \tag{A.21}$$

where W_e is the work done the the external load, W_i is elastic strain energy, $\mathbf{f}$ and $\mathbf{u}$ are external force and respective displacements, $\mathbf{K_i}$ and $\mathbf{u_i}$ are element stiffness and inner deformation.

In the iterative process, the elements are removed from the system permanently. This type of approach is called *hard-kill method* [34]. The deletion criteria might be based on the threshold coefficient or rejection ratio, which eliminates given number of elements after each iteration step which internal energy is smaller than a fragment of maximum elastic energy from the system [78, 34]. Other type of threshold is von Mises stress criteria instead of energy [78], which is easier to adopt in FEA software.

The most examined design case is minimization of compliance *c* [34]. It reflects the energy of applied load which has direct correlation with internal stored energy of the material, Eq. (A.21) and (A.22) [34]. The compliance is expressed by a Taylor series and since it converges, the precision of the algorithm can be set by the right *M* parts of Taylor series. Each Taylor series component number m of compliance is written as $\delta^m c$ except the first component called the mean compliance c_0, Eq. (A.23) [34]. The more series elements, the more accurate the compliance value is [34].

$$c = \mathbf{f}^\top \mathbf{u} \tag{A.22}$$

$$c = c_0 + \sum_{m=1}^{M} \delta^m c \tag{A.23}$$

All of these approaches does not consider neither local buckling phenomenon nor material capacity. For a simple cases, the method is useful in determining potentially the best shape and can be used in the preliminary study [34, 78]. The methods does not guarantee reaching the best solution and due to irreversible deletion of the elements from the system, which might be crucial for the optimal solution despite their low compliance, the structure can significantly be worsen [34]. One of the test used for the ESO validation is described in [128].

The additive evolutionary structural optimization (**AESO**) is a variation of the ESO method. Instead of permanent elements deletion, the method adds them [121]. This additive approach mimics organic growth seen in biological systems, where structures adapt to external forces by reinforcing areas under excessive stress.

Bidirectional evolutionary structural optimization (**BESO**) is a method which combines the principles from both ESO and AESO [121]. It allows both deletion and addition of the elements in the limited space [121]. The low contributing elements are deleted and more stressed regions are strengthened by new elements [121]. With these principles, the BESO algorithm is able to remove low contributing elements from the core in the same example of cantilever beam, Fig. A.11.

More advanced version of BESO implements so called soft-kill mechanism [121]. In hard-kill method, the normalized stiffness or density of each elements have only binary value [121]. This have a consequences in forming chequerboard patterns, presented in Fig. A.12 [121]. This problem is solved by changing the normalized stiffness or density domain from natural to real numbers allowing for intermediate contributions of the elements [121]. The increase of contribution or rejection is controlled additionally by the filter radius [121]. Its value can not be neither too small to avoid hard-kill local concentration nor too great to prevent smoky pattern, Fig. A.13 [121].

The one material ESO approach, and its variations AESO and BESO, are utilized in civil engineering in the global optimization of structures. In [36] authors optimized bridges with stress, displacement and frequency constraints. In [118] authors presented a real made post-tensioned concrete girder optimized with structural optimization approach, which was also 3D printed.

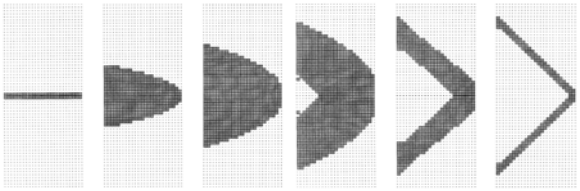

Figure A.11 Evolution of cantilever beam loaded with vertical point load oriented downwards with hard-kill BESO algorithm [121]

Figure A.12 Example of checkerboard pattern formation in hard-kill mechanism and fixed solution with soft-kill mechanism [121]

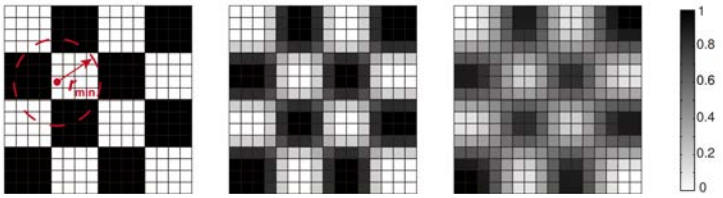

Figure A.13 Example of softening radius impact on surrounding elements contribution [121]

Figure A.14 Example of 3D printed post-tensioned concrete girder [118]

Multi-material bidirectional evolutionary structural optimization (**MBESO**) is an extension of BESO but more than one material is allowed [58, 59]. In the presented approach with 2D [58] and 3D [59] elements, the method assumed, that the two used materials are distinguished in tension and compression strength. The materials are isotropic and the volume elements are allowed. In order to distinguish if the element should be considered compressed or tension, the sum of the main stresses criteria is used. The interface between compressed and tension elements is considered to bear any load. The third material is void, which is incapable of bearing

loads. In other aspects, the method has the same principles as the BESO methods [58, 59]. The examples of cantilever and bridge structures are presented in Fig. A.15 [59] and Fig. A.16 [58] respectively.

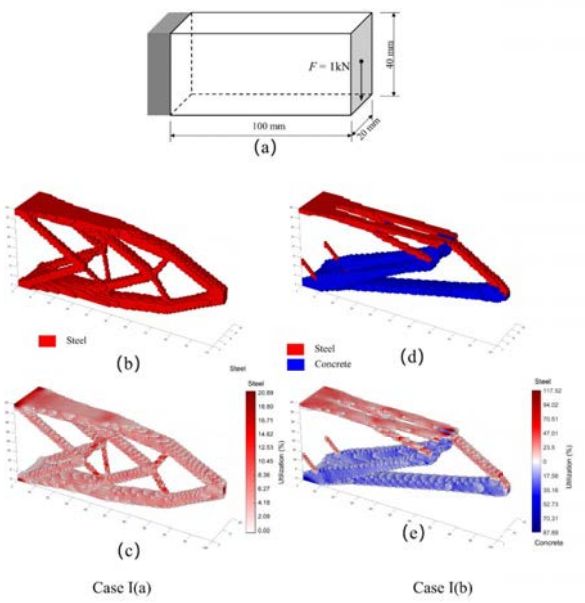

Figure A.15 Example of MBESO algorithm with (a) task definition, (b) the steel only solution, (c) the utilization of the steel solution, (d) the steel and concrete composite solution, (e) the utilization of the steel and concrete composite solution [59]

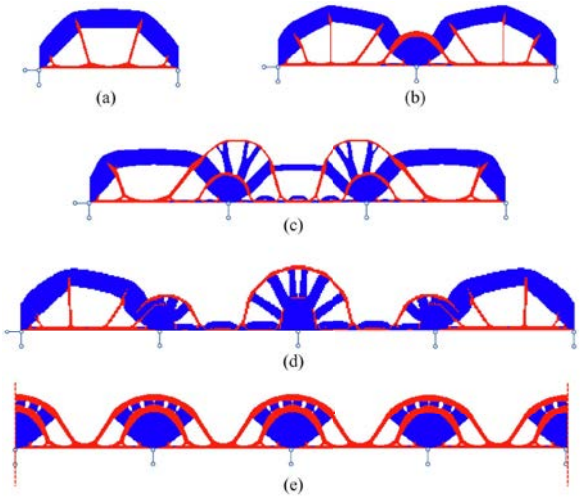

Figure A.16 Example of MBESO algorithm with single and multi-span bridges of (a) 1, (b) 2, (c) 3, (d) 4 and (e) infinity number of spans [58]

A.3.4 Particle Swarm Optimization

Particle swarm optimization (PSO) is an optimization algorithm inspired by the behaviour of swarm-like colonies [1]. It has been developed in 1995 [49]. There are three major behaviours describing this model. Separation represents the tendency of avoiding the surrounding flockmates by taking velocity opposite to their positions [1]. Alignment is the ability to move the same as the surrounding towards the same directory [1]. The last is cohesion, which represents moving towards the center of the surrounding individual [1]. Graphic in Fig. A.17 represent these three mechanisms [1].

The individuals are represented by their position and velocity. The adjustment of these two parameters occurs every iteration and is described as in Eq. (A.24) and (A.25) [1].

$$v_{id}^{t+1} = v_{id}^{t} + c_1 r \left(p_{id}^{t} - x_{id}^{t}\right) + c_2 r \left(p_{gd}^{t} - x_{id}^{t}\right) \tag{A.24}$$

$$x_{id}^{t+1} = x_{id}^{t} + v_{id}^{t+1} \tag{A.25}$$

where v_{id}^{t} and x_{id}^{t} are the *i*-th individual velocity and position respectively for the *t*-th iteration, all in *d*-th dimension. Coefficients c_1 and c_2 are a weight coefficient regulating the magnitude of speed. The symbol p_{id}^{t} denotes the best position attained by the i-th particle up to iteration t, whereas p_{gd}^{t} indicates the best position identified by the surrounding particles of the same

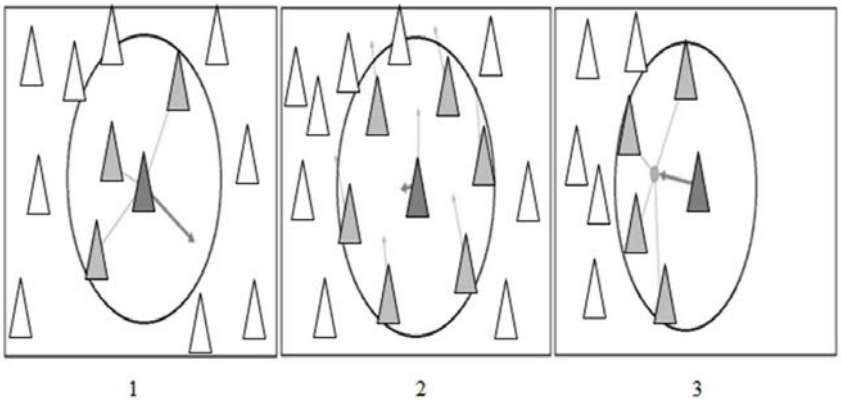

Figure A.17 The three mechanisms in PSO: (1) separation, (2) alignment and (3) cohesion [1]

i-th particle. The symbol *r* represents a random real number between 0 and 1. The algorithm explores the domain, if the difference between current position and the best position of both the given individual and its surrounding is great, and it stagnates, if the differences are small [1].

The algorithm is efficient in aspect of searching through high dimensional space [1]. Since it is based on stochastic and does not require analyses of the multidimensional function of the given problem, it does not require the function to be continues and differentiable, which makes it more useful than deterministic algorithms [1]. The first step is to specify the domain and allocate individuals in it manually, preferably sparser than locally-oriented [1]. Then the fitness function of each individual, as well as their velocity and the best individuals for each particle surrounding are determined [1]. Then all of the steps expect the first are repeated. In the first iterations, the swarm used to have more exploration behaviour due to high distance between individuals and turn into exploitation over time making the precision of the best results greater [1]. There are two major factor improving the algorithm. First is the number of individuals, the greater the better the exploration is but the time needed also increases [1]. The second approach is finding the balance between exploration and exploitation [1]. The most common improvement is the modification of the v_{id}^t in Eq. (A.24) by weight coefficient *w*, as presented in Eq. (A.26) [1]. If its value is high, the greater the exploration is, and if it is lower, the greater the exploitation is [1]. Its value can vary over iterations and be greater at the beginning to increase the chance of avoiding local extreme value, and smaller at the end, to increase the precision at the exploitation phase [1].

$$v_{id}^{t+1} = w v_{id}^t + c_1 r \left(p_{id}^t - x_{id}^t\right) + c_2 r \left(p_{gd}^t - x_{id}^t\right) \tag{A.26}$$

Another, but similar method is to multiply the entire definition of velocity in Eq. (A.24) by constriction factor *K*, as presented in Eq. (A.27) [1].

$$v_{id}^{t+1} = K \left[v_{id}^t + c_1 r \left(p_{id}^t - x_{id}^t\right) + c_2 r \left(p_{gd}^t - x_{id}^t\right)\right] \tag{A.27}$$

The research shows, that the constriction factor allows for better performance than weight coefficient [1]. There is no universal number of particles for given *d*-dimensional problem [1]. Each optimization task requires individual approach of determining the PSO parameters [1]. In the optimization of network arch bridges, one of the methods used is the PSO algorithm [125], but also as a hybrid method, including harmony search algorithm with PSO [17], gradient-based algorithm with PSO [14].

A.3.5 Ant Colony Optimization

The ant colony optimization (ACO) has its origin in 1992 [22]. The method takes inspiration from ant behaviour [1]. It is driven by number of ants, pheromones, daemon action and decentralized control [1]. In nature ants produce pheromones on their way from nest to the source of food. Ants want to achieve the goal by taking the shortest, or so called the most optimal path, so they will leave more pheromones on the path they considered as better. The greater the intensity of the pheromones on the path, the more likely is that the next ants will follow this path strengthening its intensity. At the same time, the pheromones evaporate over time, so the unused paths are less and less likely to be chosen again by ants. Each ant can not gather information about other ants' behaviour. In order to gather all of this information and manage the process, the decentralized control with daemon action is implemented [1]. In such system, ants are treated as exploration identities, so called agents in artificial intelligence systems [1]. The decentralized system helps in making algorithm robust and flexible according to system development [1].

At the beginning, the ants explore randomly the space close to set initial solution [1]. This solution can be determined manually or achieved by other optimization algorithm. Node is an instance from which at least two paths are available [1]. For example, in a grid system in 2D, there are 3 paths to choose from each node except the path that agents came from, since going two times on the same path is forbidden [1]. The probability of choosing path in a node is expressed in Eq. (A.28) [1].

$$p_{ij}^{k}(t) = \frac{\left[\tau_{ij}(t)\right]^{\alpha}\left[\eta_{ij}\right]^{\beta}}{\sum_{k\in J_k}\left[\tau_{ij}(t)\right]^{\alpha}\left[\eta_{ij}\right]^{\beta}} \tag{A.28}$$

where p_{ij} is the probability of choosing path from node *i* to *j*, *k* represent a specific ant, J_k is a set of possible locations of the nodes that ant *k* is allowed to travel, *t* represents time or iteration, τ_{ij} represent the amount of unevaporated pheromone between nodes *i* and *j*, η_{ij} determines the visibility parameter between nodes *i* and *j*, coefficients α and β manipulate with the importance of pheromones strength and visibility. The greater the α is in relevant to β, the more important the pheromones intensity is over visibility [1]. Visibility corresponds with the distance from the original point. The greater the distance, the lower η value is [1].

After each agent visit to the path, its pheromones strength is increased the a certain amount expressed in Eq. (A.29) [1].

$$\Delta\tau_{ij}^{k}(t) = \frac{Q}{L_k}(t) \tag{A.29}$$

where *Q* is a predefined constant and *L* is the cost of the ant's tour represents by the length of the generated path. For the non-selected paths, their added deposit of pheromones is 0 instead. If the pheromones value on the certain path were only increased, other paths would not have any chance to be chosen and the solution would fast become elitist. In order to not favour only the best solutions, the evaporation mechanism described by Eq. (A.30) [1].

$$\tau_{ij}(t+1) = (1-p)\tau_{ij}(t) + \sum_{k=1}^{m}\Delta\tau_{ij}^{k}(t) \tag{A.30}$$

where m is the total number of agents in the system and p is the pheromones evaporation rate. If the path started to be less used, the evaporation part would decrease more than the pheromones addition part over time. The greater the pheromone value and greater the evaporation rate, the harder it is to keep high pheromones value. The strength of the path increase faster at the beginning and decrease faster when the value is high [1].

The ACO algorithms have advantage in providing independent calculations for agents and fast searching the close space around the initial solution [1]. Nevertheless, the convergence is slow in complex, multidimensional tasks and due to lack of centralization the time consumption in decision making is high [1]. Overtime many modifications to the method were implemented such as ant colony system (**ACS**) [1]. It used centralized system in terms of pheromones update and concentrating the search mechanism over the paths closer to the current best solution [1]. Another type is max-min ant system (**MMAS**) [1], where the pheromones value is limited to a domain between the predefined minimum and maximum values, which prevent the paths to be negligible or in favour [1]. At the beginning each path has the maximum pheromones value, which increase the searching. Only one ant is allowed to add pheromones, which helps in exploring the best path. The latest version is so called multi-objective ant colony system (**MOACO**) algorithm [1], which integrates the multi-criteria decision making mechanism, turning various objections into a single scalar [1].

The ACO is utilized in traffic flows management [81], but also in the structural optimization. For instance, among others, optimization of truss structures [48] and optimization of beam elements [46].

A.3.6 Genetic Algorithm and Differential Evolution

The genetic algorithm (**GA**) is algorithm inspired by nature, where the best individuals from the population used to have the highest chances of survival and passing their genes to the next generation, so called "survival of the fittest" [1]. The individuals are represented by w set of numbers, which used to be called chromosome or genotype [1]. This numbers are used to determine the value of the fitness of goal function, which reflects the adoption to the provided goal function [1]. The better the goal function value is, the more valuable/adopted the individual in the population is. The algorithm is offspring-oriented optimization algorithm and contains selection, crossover, mutation. First, the individuals are determined in a given domain and each of them is represented by a individual chromosome. Then the fitness function is determined based on the goal function to answer the question, how good each member of the population is. Thereafter pairs containing two or more individuals are chosen based on their fitness function value [1]. Depending on the version of GA, the parents can be selected from the best part of the population judged by their goal function value, but it can be random as well [1]. The chromosomes of the parents are mixed by taking randomly genes or interpolating values of genes between parents in order to establish a new individual/offspring with mixed and potentially more adopted chromosome [1]. After offspring's chromosomes are established, their goal function is determined. The next step is a mutation, which makes a random change to a random genes in a random number of individuals in the population. The random change prevents the population from reaching exploitation too early and allows to explore part of the domain unavailable from crossover operation [1]. Crossover explores the regions within the space occupied by individuals, while mutation allows to explore beyond this range. At the end, the worse individuals can be removed from the system in order to keep the same quantity in population in every iteration [1]. It can be achieved by removing the weakest individuals in the same number as the added offspring, or by selecting pairs and removing the weaker individual from

each pair [1]. This makes the algorithm less greedy and allows less fit individuals to survive, which promotes greater exploration at the beginning [1]. Other way is to keep only offspring and the best individual from the previous generation in order to not loose the best solution so far, called elitism [1]. The process is repeated until reaching satisfied convergence [1].

The GA is useful in case of complex tasks and does not require the function to be known or differentiable, which makes it flexible [1]. The drawback is slower convergence comparing to other deterministic approaches as gradient descent, because of the crossover and mutation are random [1]. Some of the improvement includes N-point cross over where multiple genes are selected [1]. Another is adaptive GA, where the probability of mutation and crossover change over iterations depending on the progress [1]. If there is no progress in convergence, the mutation and probability of crossover are increases in order to boost the exploration. However, if convergence is progressing, these values are gradually decreasing [1].

Another, but similar, type of evolutionary-based algorithm is differential evolution (**DE**) developed in 1997 [76]. When the GA is more crossover-oriented optimization algorithm, the DE is more mutation-oriented algorithm [1]. It is described by target, mutation and trial vectors [1]. The target vector is the solution vector, the mutation vector includes mutation of the target vector, and the trail vector is a crossover product of the target and mutation vectors [1]. The mutation vector is determined by taking a random reference gene and adding a randomly scaled difference with range (0,1) between two other randomly selected genes [1]. After establishing the mutation vector, the trial vector is defined by choosing step by step a gene from target or mutation vector depending on the randomly obtained value in range (0,1) [1]. If it is greater than crossover rate, also defined between 0 and 1, then the gene is inherited from the target vector, but if smaller, then from mutation vector [1].

The main difference between DE and GA is the fact, that the fitness value is not considered in the selection of parental individuals [1]. The evaluation of the trail vector occurs after mutation and crossover, which makes the progression more random than in GA [1]. The DE method is suitable more for a local search [1]. Some of the improvements in this method are the following: increase of the population size and scaling factor of mutation, introduce of elitism in order to not loose the best solution so far [1].

In civil engineering, the DE method is used in global optimization. In [47] authors optimized reinforced concrete continuous foundation, whereas in [84] the steel frame was optimized by DE and compared with other optimization methods as GA, ACO and PSO and showed comparable efficiency. The lattice structures of various kinds were optimized in [33] with 5 different variations of DE algorithm.

A.3.7 Meta-heuristic methods comparison

In the article [1], the multiple modern optimization algorithms were compared. The tested algorithms were: genetic algorithms (GA), ant colony optimization (ACO), differential evolution (DE), particular swarm optimization (PSO), artificial bee colony (ABC), glowworm swarm optimization (GSO) and cuckoo search algorithm (CSA) [1]. The 30 attempts were made and the average was considered [1]. The authors used 30 different test functions with various characteristics [1].

The method, that achieved the optimization goal the fastest, was DE, then PSO and GA [1]. The DE and PSO methods were checked for different variations of them and the best results were presented, which was not done for the GA, where one version was considered [1]. This favours DE and PSO methods over the remaining considered optimization algorithms. However, GA outperformed DE when the objective function exhibited a high rate of change for

small variations in the input parameters. The examples of these functions are Schaffer Function N2, Schaffer Function N4, Schwefel Function and Eggholder Function, all presented in Fig. A.18. This property is considered as valuable in environment, when the small change of value has great implication on the function value change. In Network Arch Bridges, which are vulnerable to the bending moments in the arch, a small difference in hangers' arrangement might have disproportional effect on the bending moments diagram, especially in the arch and so the utilization and cause a need for strengthening, which increasing costs.

At the same time GA was the best performing in smooth functions with low value change, such as Colville function, as well as in the smooth function with added noise, such as Rastrigin function, Fig. A.18.

At the same time, the article [1] was not testing structural optimization, but idealized functions. In the article [84] authors showed, that the DE can achieve similar performance as GA, ACO and PSO methods in global optimization of the frame structure. In [7] authors optimized network arch bridges using GA and PSO and obtained similar efficiency. By author's opinion, more important is the suitability of the method to the given structural optimization problem than the time compilation form idealized tests. The FEA calculations require much more time than the optimization algorithm compiles. Nevertheless, the better adoption of GA in more unstable [62] and smooth environment, makes it a good candidate in the structural optimization.

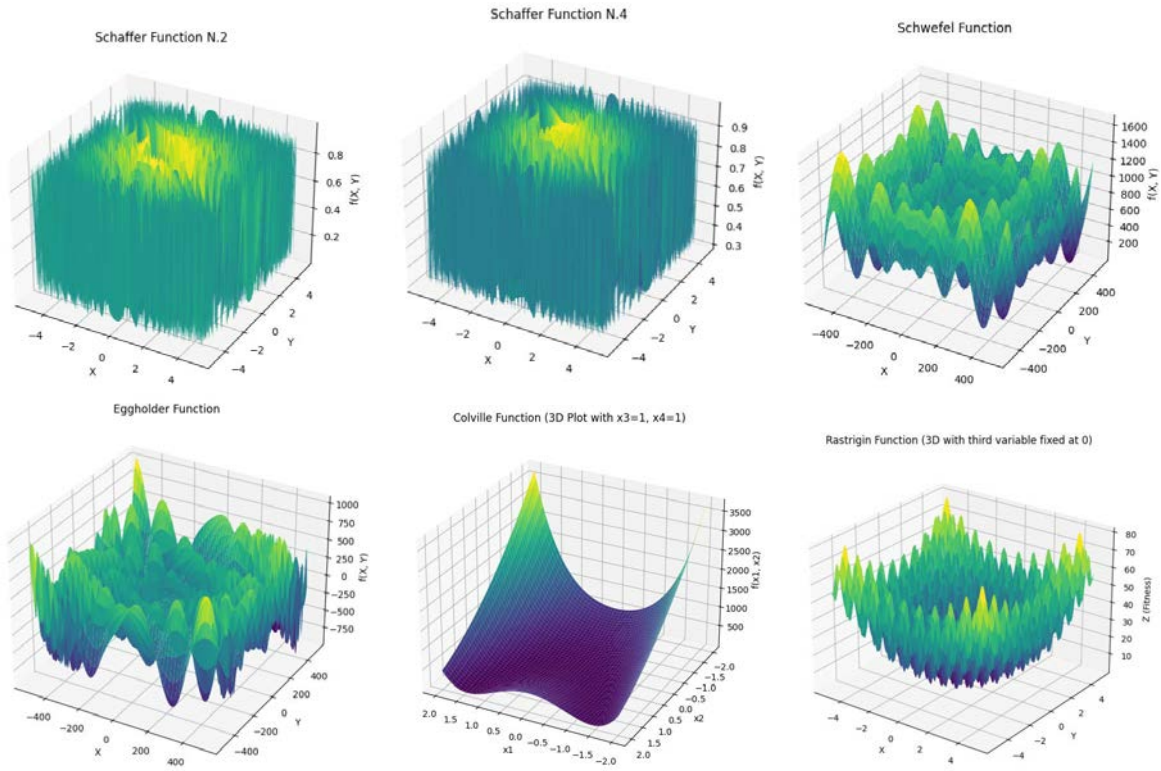

Figure A.18 Examples of Schaffer 2, Schaffer 4, Schwefel, Eggholder, Colville and Rastrigin functions

B The extension to the approach 1 of the optimization algorithm

This section includes the extension to the description presented in the first optimization algorithm, which are: loads definition, description of authored import/export component and Galapagos shortened principles.

B.1 Loads

a) The LM1 uniformly distributed load combined with equipment load

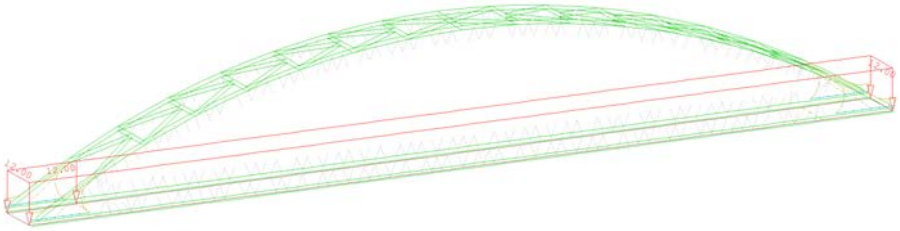

b) The LM1 equivalent tandem load at the beginning of the bridge

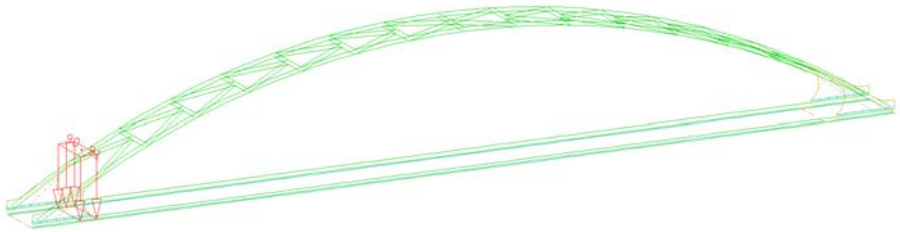

c) The LM1 equivalent tandem load in the middle of the bridge

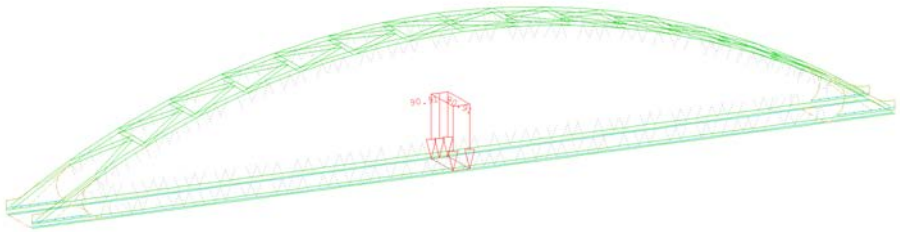

d) The LM1 equivalent tandem load at the end of the bridge

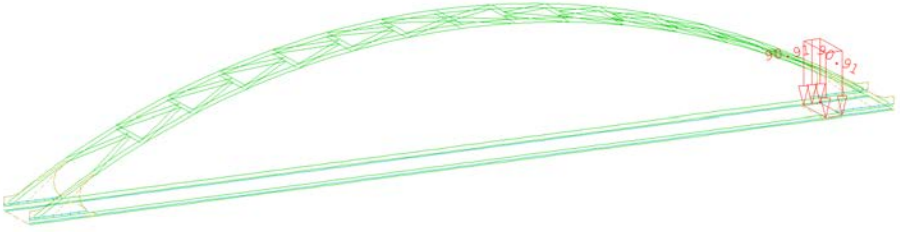

Figure B.1 The (a) uniformly distributed traffic load (UDL) with other permanent load and (b, c, d) equivalent tandem traffic load (TS) based on LM1 model

B.2 Data exchange components

Figure B.2 Import/export/visualization components for cable, beam and shell elements

Beam and cable components. The beam and cable components were defined in an analogous way with the following input arguments:

- + before apply - determined if the component should be included in the SOFiSTiK txt input code,
- text at the beginning/ending - added custom text to the code,
- import - determined the need of importing the results,
- show result - presented the visualization of the chosen results,
- refresh - recompiled the component,
- SLN - provided number of beam or cable structural elements which will be analysed,
- single element - provided information about the division of structural lines,
- ID - identification number for the exported results,
- project path - the path to the project,
- type of results - determined which results should be imported from the CDB,
- local coordinate - determined the need of visualizing local coordinate axis imported from CDB,
- LC to import – load case numbers to consider,
- LC to visualize - determined the load case number to present,

- Rhino model unit - determined the project units in Rhino,
- only extreme - visualized only the most extreme value tags,
- precision - determined the precision of the presented results,
- flip text - determined the flip of the text in value tags,
- text size - determined the size of the text in the value tags,
- show edge - changed contrast of the visualized graph,
- local scale - determined the scale of the graph,
- displacement curve color - set the color of the displacement curve interpolation graph,
- displacement arrow color - set the color of the displacements' vector representation.

After execution, the beam and cable components provided the following output arguments:

- apply text - SOFiSTiK CDB language code,
- startlend point - start and end points graphical representation of beam/cable elements from the structural line elements,
- N ... MB startlend - text representation of all internal forces of start and end points of the beam/cable elements from the structural line elements,
- UX ... UR startlend - text representation of all displacements and rotations of start and end points of the beam/cable elements from the structural line elements,
- dis/rot points - result points graphical representation,
- dis/rot curve - results curve graphical representation,
- local x,y,z - local vectors definition.

Quad component. The quad component was defined with the following input arguments:

- trigger - refresh the component - it was useful with the loop component to import the exported results,
- Sar - provided number of area structural elements which will be analysed,
- Mesh Options - includes the information, if the structural area was meshed or made of a single element,
- ID - identification number for the exported results,
- Loadcase to import – load case numbers to consider,
- Project folder - the path to the project folder,
- Loadcase to present - the number of load case to present,
- Results Type - determined if the results should be internal forces, stress, displacements or reinforcement area,
- QUAD results - determined which results should be imported from the CDB,
- Result precision - determined the precision of the imported results,

- Text size - determined the text size of the presented results,
- Text color - determined the color of the text,
- Text offset - determined the offset of the text from the graph's result value point,
- Flip text in plane - flipped the plane in which the text is defined,
- Flip text out of plane - flipped the plane in perpendicular plane to the view vector,
- Plot scale - determined the scale of the presented results,
- Only extreme values - determined, if only the extreme values should be presented,
- Reinforcement LC - the load case of the reinforcement results to export,
- LCR to present - the reinforcement load case to present,
- QUAD reinforcement - determined which reinforcement results should be imported from the CDB,
- Reinforcement - determined if the reinforcement results or other results should be presented.

After execution, the quad component provided the following output arguments:

- txt - provided the results text definition of the export rules in SOFiSTiK CDB language,
- txt rein - provided the reinforcement text definition of the export rules in SOFiSTiK CDB language,
- Base shell - provided the shell elements as they were in SOFiSTiK,
- shell points - provided the corner points of the shell elements from SOFiSTiK,
- Results data - provided all the exported results,
- Selected results - provided the results according to the selected load cases and type of the results,
- Result rein data - provided all the exported reinforcement results,
- Selected rein results - provided the reinforcement results according to the selected load cases and type of the results,
- Local x, y, z vector - provided the shell local X, Y and Z vector in global coordinate system,
- mxx, myy, ..., nxy - text representation of all internal forces of the shell results in their internal point,
- ux, uy, ..., urz - text representation of all translations and rotations of the shell results in their internal point.

B.3 Galapagos

B.3.1 Selection

Galapagos uses three types of selection: isotropic, exclusive and biased [82]. Users can specify which one to use. In the first one, the Isotropic Selection, all individuals possess an equal opportunity to reproduce, regardless of their position on the fitness spectrum [82]. Isotropic Selection serves to limit the pace at which a population ascends toward an optimal state, acting as a buffer against premature convergence towards potentially suboptimal solutions [82].

The second one, the Exclusive Selection, permits only the top N% of the population to reproduce [82]. Individuals in this select method produce multiple offspring [82].

The third one, the Biased Selection, is yet another common pattern observed in nature, where pair matching opportunities increase with an individual's fitness level [82]. While every individual theoretically has the capacity to find a partner, those possessing superior characteristics over others tend to engage in more frequent reproductive activity, thereby augmenting their likelihood of becoming genetic progenitors in subsequent generations [82]. Biased Selection can be fine-tuned using power functions, which modulate the distribution curve to either flatten or accentuate it, thereby influencing the intensity of selection pressure [82].

B.3.2 Coupling

Coupling, the initial step in genetic algorithms, involves the selection of individuals once a genome has been designated for reproduction by the active selection algorithm [82]. Galapagos uses selection by genomic distance [82]. The individuals are selected in a given range forming a kind of ring [82]. The in-breeding and out-breeding can be specified within the component [82]. It prevents population from collapsing if the individuals were chosen from the nearest distance for the considered coupled individual and prevents the population from segregating into local groups [82].

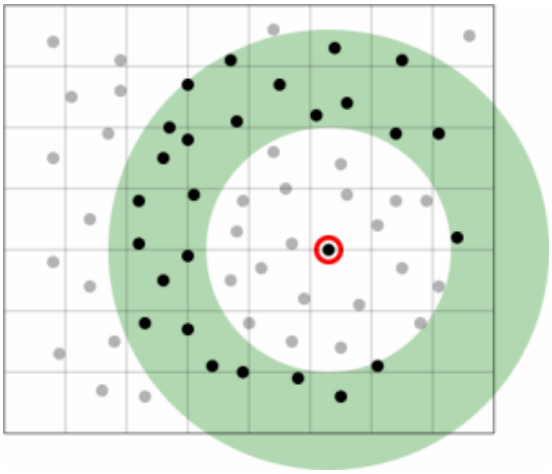

Figure B.3 Graphical representation of coupling method in Galapagos [82]

B.3.3 Coalescence

Similarly, as in selection, Galapagos provides three methods of coalescence: crossover, blend and preference-blend [82]. Users can choose which method should be used. [82]

In the crossover coalescence, the gene values of the descendants are selected from parental genes' values [82]. The values themselves are not changed, but the gene inherits unchanged values partially from two parents' genes [82]. New values within genes are not created [82]. Usually, one of the parents is more prominent over the second parent [82].

In the blend coalescence, the descendant's gene values are interpolated between each parental gene value [82]. It creates new values within genes [82].

The last preference-blend coalescence contains similarities to both aforementioned methods [82]. The gene values are interpolated between the genes' values of the two parents, but interpolation is mostly oriented on one of the parents [82].

B.3.4 Mutation

The mutation in Galapagos allows two manipulations of the population's genes values [82]. The first one, so called point mutation, shifts one gene's value by a single step, Fig. B.4a [82]. The second one, so called inversion mutation, allows to switch places between two nearest gene's values [82]. This change is more drastic than point mutation, Fig. B.4b [82].

a) Point Mutation

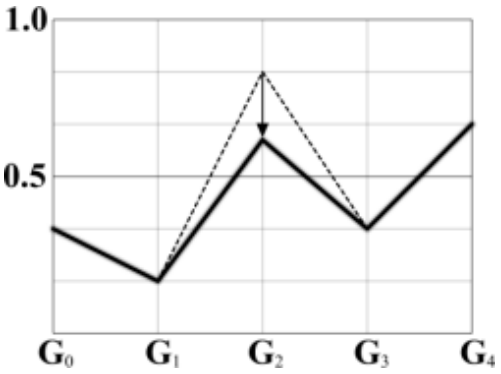

b) Inversion mutation

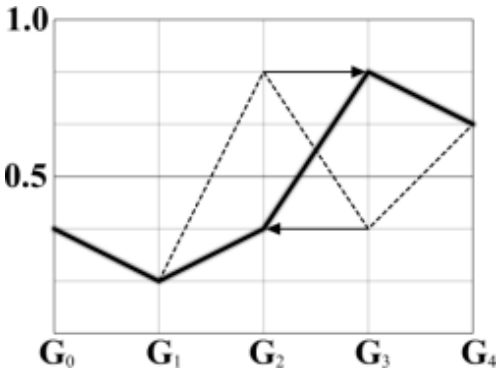

Figure B.4 Graphical representation of two mutation methods in Galapagos [82]

Galapagos, however, does not allow to add or remove genes from the population [82]. These methods are called respectively additive and deletion mutations [82]. Both methods might cause significant changes to the genome distribution, Fig. B.5 [82].

a) Deletion

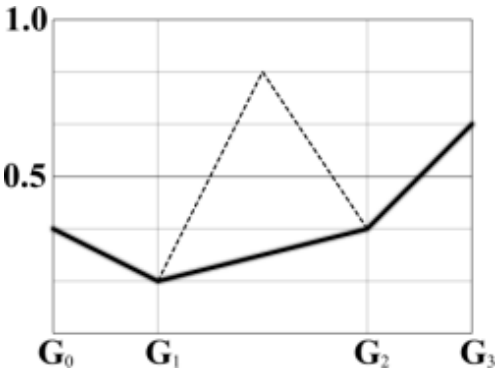

b) Addition

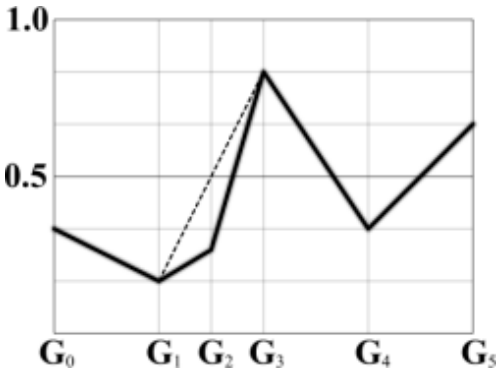

Figure B.5 Graphical representation of the mutation method not allowed in Galapagos [82]

C The execution files

This section includes the detailed description of the most important self-coded functions in Python involved in the second optimization algorithm.

CDB_import file The file was responsible for importing results from the arch, tie and hangers and provided stresses according to resultant stresses equation. SOFiSTiK's API was used in this process. Furthermore it imported load factor from the ULTI procedures, which was the needed nonlinear critical load factor.

CALC file The file was responsible for providing tools needed during the calculations in GA file and they were related to:

- price of steel function,
- cost of the whole structure including utilization,
- utilization function,
- goal function,
- saving data to files - separate function for each exported data, 12 in total,
- running process of the geometry calculations by SOFiSTiK,
- running process of the load calculations by SOFiSTiK,
- determining buckling parameters and slenderness,
- design of all elements including avoiding 4th class,
- mass calculations,
- running SOFiSTiK as an sub-process,
- finding the closest value of the chosen material and cross section dimension according to predefined lists of possible values.

The function responsible for cost of the whole structure was one of the most important one, since its output was used for the GF value determination. The function was responsible for:

- variables adjustment to predefined lists,
- arch and tie thickness modification according to 4th class requirement,
- geometry calculation run as a sub-process,
- loads and GNA calculation run as a sub-process,
- increase arch and tie dimensions if the calculations of GNA took longer than 2 minutes. The cross section of the arch had been increased, if the area of the arch was smaller than tie's area. The same comes to the opposite relation. The process was repeated until reaching convergence. Diameter had been increased, if the thickness had higher ID position in the predefined list than the diameter's ID position. The 4th class criteria was checked after each increment,

- geometry data export to `txt` files,
- results import by SOFiSTiK API,
- utilization check of full and half loaded cases including nonlinear buckling phenomenon,
- cost calculation of each individual element as an envelope from full and half loaded states,
- summary cost calculation of the whole structure,
- GF value calculation,
- cost and utilization export to `txt` file,
- all calculated data assign as the function output.

The utilities of this function were defined in previously defined functions.

GA_help file The file was responsible for defining tools needed for the optimization algorithm perspective, which included:

- definition of possible values for each variable according to the lists,
- limitation of the chosen value to the predefined range,
- hangers initial positions according to the results from the first attempt of optimization,
- hangers initial positions according to the custom list of geometries,
- probability density function with normal distribution,
- mixture of two hangers' topology with different distribution and number,
- hangers sorting function,
- function finding hangers' angle,
- copying files and folders,
- function checking if the variable was in the given range,
- selection of geometries for the procreation,
- flattening graphs,
- graphing lists,
- hangers allowed position range,
- import costs,
- folder deletion,
- SOFiSTiK CDB deletion,
- import all variables, stressing and results,
- definition of local desecrate gradient.

GA file The last file was responsible for the optimization process and used all of the functions defined in the previous files. It contained just one function utilizing the whole optimization

process. It helped to run multiple calculations at the same time. The input data for this function, also named by **GA**, were:

- vector of permanent data,
- vector of initial variable data,
- vector of initial stressing force data,
- number of parents,
- initial copulation number reflected number of pairs,
- copulation number reflected number of pairs,
- calculation of initial geometry - helpful when the initial geometries were the same comparing to the previous run, so the geometry was already defined,
- calculation of initial design process - helpful when the initial geometries were the same comparing to the previous run, so the results were already obtained,
- importing of initial results - helpful when the initial geometries were the same comparing to the previous run, so the results were already exported.

Other parameters were predefined in the algorithm itself and were adopted according to the analysed case in test and comparison sections.

GA function The initial data input for the GA function had to be defined first. The dimensions of the arch, tie and hangers were big enough to guarantee that all the geometries at the start were utilized under 100%. The **permanent data** vector included:

- load case number for variable loads applied at the full span length,
- load case number for variable loads applied at the half span length,
- initial number for GNA of fully loaded tie,
- initial number for GNA of half loaded tie,
- load case number of self-weight,
- group number of the arch elements,
- group number of the tie elements,
- initial group number of the hanger elements,
- type of cross section manufacture - warm or cold formed,
- allowed deflection,
- span length,
- all allowed steel grades for the arch,
- all allowed steel grades for the tie,
- all allowed steel grades for the hangers,

- all allowed diameters of the arch,
- all allowed thickness of the arch,
- all allowed diameter of the tie,
- all allowed thickness of the tie,
- all allowed diameter of the hangers,
- all allowed denominator of the span length needed to determine the bridge height.

The **initial variable data** vector included:

- arch diameter,
- arch diameter ID in the predefined list,
- arch thickness,
- arch thickness ID in the predefined list,
- tie diameter,
- tie diameter ID in the predefined list,
- tie thickness,
- tie thickness ID in the predefined list,
- bridge height,
- bridge span length denominator ID in the predefined list,
- hanger diameter,
- hanger diameter ID in the predefined list,
- hanger number,
- hangers' point number in the arch,
- hangers' point number in the tie,
- arch steel grade ID,
- tie steel grade ID,
- hangers steel grade id.

The last vector was **initial stressing data** vector, which consisted 5 numbers from 0 to 3, since pretension force coefficient TF was defined as symmetrical 9-grade polynomial.

D The tests and improvements in the approach 2 of the optimization algorithm

This section includes the detailed descriptions of the conducted tests in the second optimization algorithm in order to improve its efficiency and effectiveness. These are not all the conducted tests, but the most important.

D.1 Gradient

Gradient solution was implemented to shorten the time consumption needed in approaching the extreme goal function value in a local space of influence of this value. It was described in the Fig. D.1. There were 4 points representing the GF value for a sample variables. Two local minimum values can be found with their space of influence. The right space has lower local extreme value than the left one. The edge between these two spaces was determined by the local top value (black line). The lower the goal function value, the better the point was. Three of the points were located in the left space on influence, and one in the right. The average variable value for this population was positioned left to the local top value (red line), which meant, that the expected descendants would have variables' values defined more on the left space of influence rather than on the right. Since the best individual variables did not mutate, it would not move closer to the local extreme value. Gradient descent would help in this process. When the local gradient vector was defined, the best individual variable was changed by adding the gradient vector projection on the variable axis to the original variable value and the new goal function value was determined (green point). With that change, the average variables' value was change to the right of the local top value (green line), and more individuals would be defined in better space of influence.

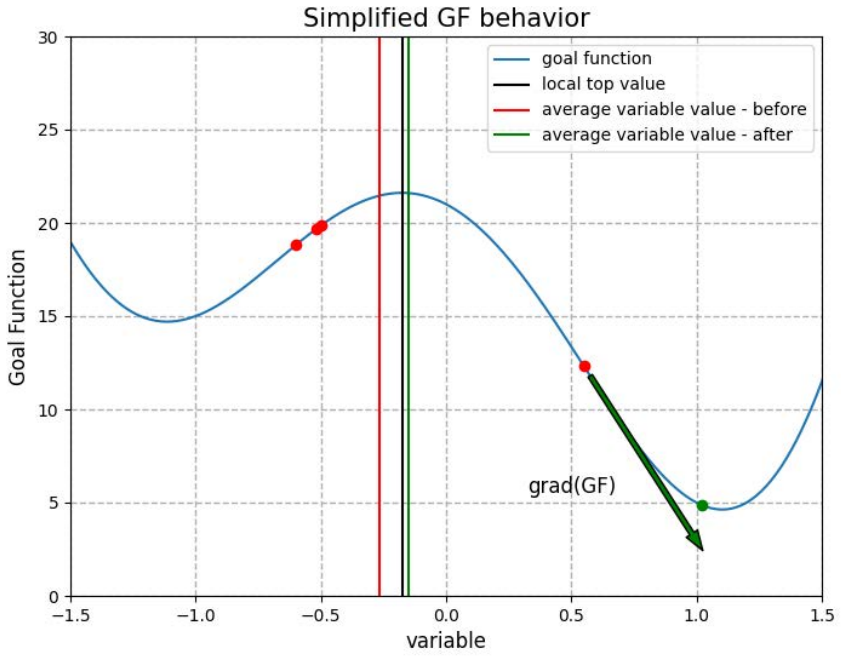

Figure D.1 Example of gradient impact on average position change

The same mechanism was applied in the genetic algorithm. The gradient function searched

for the best individual first. Then, since the variables were listed, the discrete multidimensional gradient was chosen. For the pretension vector, the values were not listed, and the change of 0.1 was used instead of list's position. The values lower and greater than the variable values of the best individual were determined. If the variable's ID in the list was already extreme, the lower or greater value exceeding the list's range was substituted by the original variable's ID. The gradient vector was determined from the best individual's values to the values obtained from the lower and higher variable values. The same procedure was done for every variable.

For example, the number of variable inputs excluding the hangers' anchorages was always 15, 10 from variable vector and 5 from pretension vector. Therefore, considering both the lower and upper positions in the variable list, the 30 geometries should have been calculated. Then considering total number of hangers in range between 10 and 40, the total number of additional cases to considered would have been between 10 and 40 since the topology was always symmetrical. That resulted in 40 to 70 geometries to consider and obtain their goal function values. If the list of specific variable contained 20 positions and the reference ID was 5, the new geometries for 4th and 6th positions were calculated. When the ID was already 0, the geometry with 1st ID was checked and one gradient vector instead of two was obtained.

The gradient' directory, providing the greatest improvement in the goal function value, determined the geometry, which replaced the previous best individual. All the results were stored in the folder with `_g` prefix. The best individual was substituted in the `vec_var`, `vec_pre` and `vec_res` and the procedure moved to the next generation.

Since the gradient-based might neglect the positive aspects of the genetic algorithms metaheuristic nature, the optimal frequency of gradient descent method usage was tested. The gradient method was used every 1st, 3rd, 5th and 10th generation. The initial population definition and boundary conditions were always the same. The number of generations was 100, twice per each generation step. The initial geometry was based on the topology generations presented in Sec. 6.2.2. The best results were presented in Fig. D.2 and Tab. D.1.

Table D.1 Iterations best results

	no grad	1st	3rd	5th	10th
arch diameter [m]	1.1	1.2	1.3	1.3	1.1
arch thickness [m]	0.025	0.025	0.030	0.025	0.030
tie diameter [m]	0.8	1.3	1.4	1.1	1.4
tie thickness [m]	0.035	0.025	0.020	0.025	0.025
hanger diameter [m]	0.100	0.085	0.085	0.100	0.085
number of hangers [-]	26	26	24	14	22
bridge height [m]	17.6	18.75	19.35	20.69	21.40
arch steel	S460	S420	S275	S355	S420
tie steel	S460	S355	S320	S355	S355
hangers steel	S275	S355	S355	S460	S460
buckling factor [-]	0.97	0.92	0.98	0.96	0.96
arch utilization [%]	94.3	98.1	99.4	99.6	93.7
tie utilization [%]	86.6	98.7	97.3	94.8	83.7
hangers utilization [%]	92.9	100	100	80.2	61.5
deflection utilization [%]	68.1	61.3	41.0	48.0	30.9
max utilization [%]	94.3	100	100	99.6	93.7
cost [PLN]	4,109,903	4,037,725	3,921,010	3,716,154	4,267,728
goal function [PLN]	4,109,903	4,037,725	3,921,010	3,716,154	4,267,728

a) No gradient - GF = 4,109,903 PLN, utilization = 94.3%

b) Every generation - GF = 4,037,724 PLN, utilization = 100%

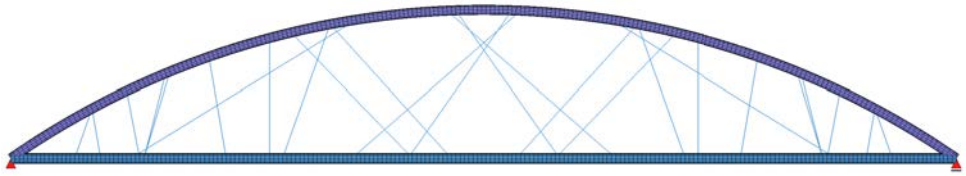

c) Every 3rd generation - GF = 3,921,010 PLN, utilization = 100%

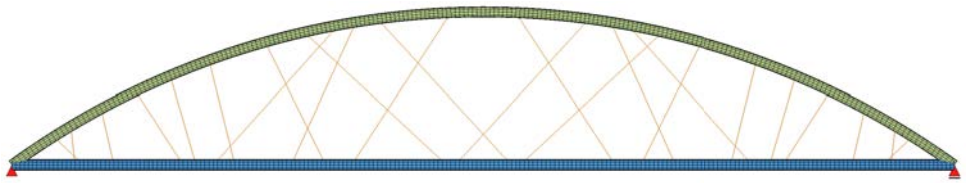

d) Every 5th generation - GF = 3,716,154 PLN, utilization = 99.6%

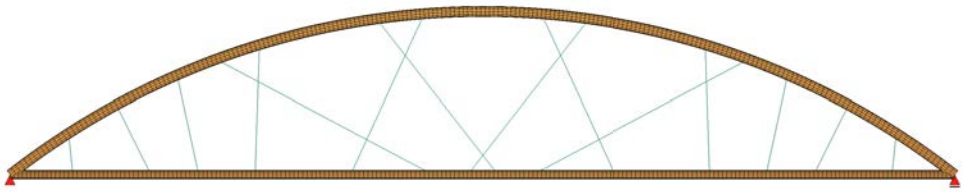

e) Every 10th generation - GF = 4,267,728 PLN, utilization = 93,6%

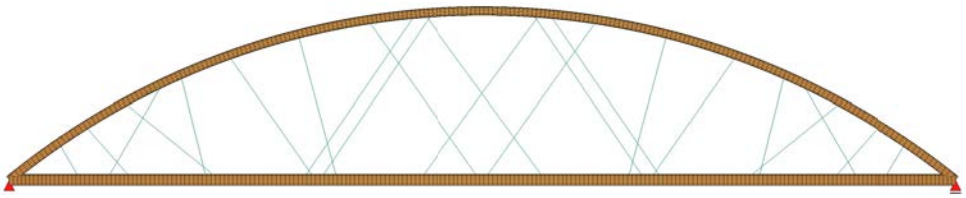

Figure D.2 Tested gradient descends for various generations' steps number

The best results were obtained for every 5th generation. The topology for this solution was also the less random-like comparing to the remaining iterations. The hangers in the middle were concentrated down radially. The network-like topology was present in the middle on about 60% of the total span length. For the remaining length close to skewbacks the hangers' topology was vertical-like shape with slight skewness. Even though the remaining tests resulted in worse solutions, the tendency of network-like topology in the middle and skewed vertical topology nearby skewback was observed. The every 10th generation solution was the worst and the vertical topology occurred in about 1/4 span length distance from the ends, but apart from this region the topology was mixed network-Nielsen type. The reference case without any gradient algorithm, had topology similar to the gradient step size of 1 and 3. There were network-like arrangement in the middle of the span and then mix topology in transition to vertical-like topology close to the ends. The GF value was also similar to these with gradient step size of 1 and 3.

Most of the geometry data for the results presented in Tab. D.1 was very similar for all the iterations. The biggest difference were tie diameter and thickness, number of hangers and bridge height. The diameter of the tie for the best iteration was 1.1 m and the remaining were 1.3 m, twice 1.4 m and 0.8 m for the reference case which was significantly smaller than for the remaining cases. This resulted in the highest tie thickness of 0.035 m for the reference case and 0.020 m and 0.025 m for the remaining cases. The number of hangers was the most significant with 14 hangers for the best solution and 22, 24 and 26 for the remaining iterations. The last was the bridge height of 20.69 m for the best test and 17.6 m, 18.75 m, 19.35 m and 21.40 m for others. The every 5th solution was oriented from the optimization point of view on minimizing number of hangers, which demanded the biggest diameter of hangers and the highest possible steel grade. The steel grade for the arch and tie was S355 and that was the only solution with the same steel grade for both arch and tie for cases with gradient implementation. The second best test was every 3rd generation iteration with the strategy of minimizing cost by implementing lower and cheaper steel grade of S275 for the arch, S320 for the tie and S355 for hangers. The utilization for every iteration was close to 100%, but the best solution still had slight capacity left comparing to the 2nd and 3rd the best solutions. The lowest utilization occurred in two the worst iterations, so there were still possibilities for improvement. On the other hand, if the optimization process lasted longer, the solutions with lower utilization would have higher chances of improvement than the solutions with almost 100%. As a simplification, it might be assumed that the case without gradient implementation would theoretically reach the cost of 0.943*4,109,903=3,875,639 PLN if the remaining capacity was utilized. That would place this case on the second best place instead of the second worst. The same came to the gradient step size of 10, which might be reduced to the cost of 3,998,861 PLN assuming theoretical 100% utilization and place it not as the worst case anymore. Nevertheless, even with these assumptions, the best solution would still remain its position.

The GF values over generations for 4 gradient steps were presented in the Fig. D.3. The greatest changes for all of unique steps occurred at the very beginning and ending of the total generation range. The range of the smallest changes was observed between about 30th and 80th generation. The possible reason behind significant cost reduction at the very beginning was increased randomness in mutation for the first generations and the fact that more individuals were selected for coupling. Then populations reached the zone close to local extreme value or a zone of relatively small changes of goal function value, so called flat region. For this regions, gradient-based algorithm helped in reaching local extreme value or moved faster the best individual in the flat regions. This phenomenon was observed for all gradient step sizes. It occurred between 60th and 100th generation for step size of 1, between 24th and 100th

generation for step size of 3, between 20th and 85th generation for step size of 5 and between 40th and 80th generation for step size of 10. The significance of these changes was sometimes so small, that the GF values' changes was not visible on the graph. On the contrary, the non gradient case changed up to 40th generation and stopped improving GF value up to the end.

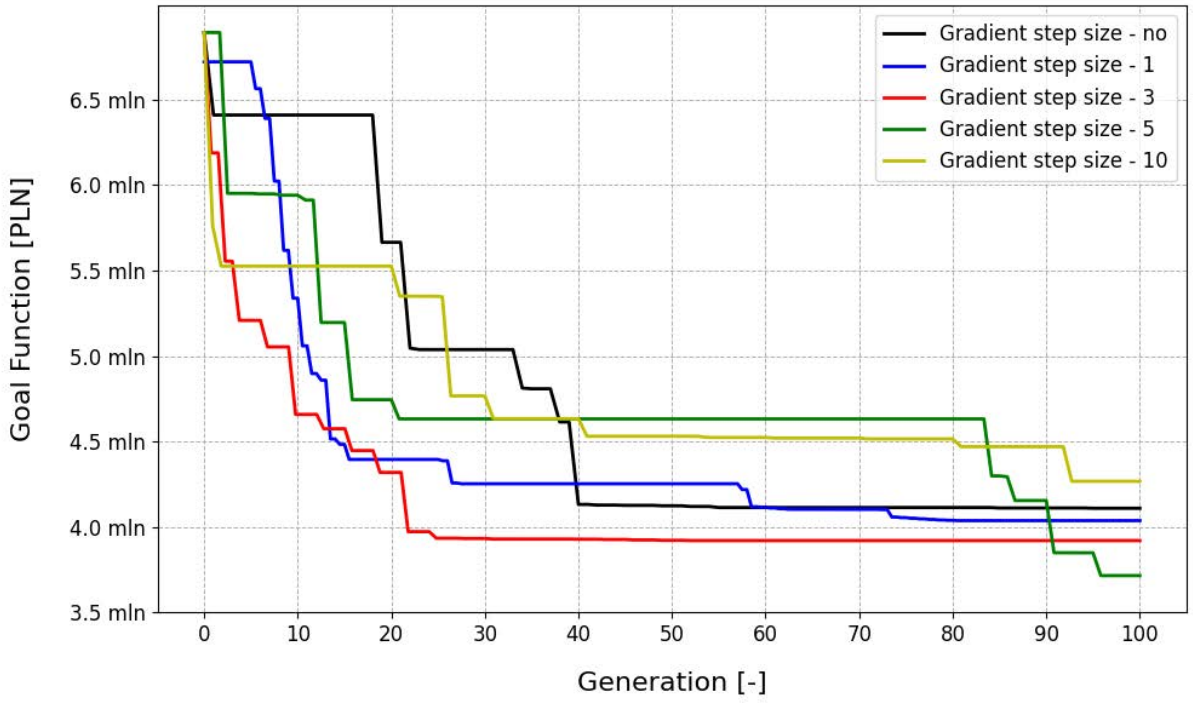

Figure D.3 Goal function values over generations for 4 gradient steps

The bending moments, normal forces and von Mises stresses for the best and the worst runs, step size of 10 and 5 respectively, were presented in Fig. D.4-D.6. It was expected, that a better solution would produce a more uniform bending moments distribution along the arch, which was typical for NAB considered as the most cost-efficient solutions. Even though both cases had network-like topology, worse of them had more even bending moments diagram in the arch than better solution. On the contrary, the tie for better solution had actually more even bending moments diagram than worse solution. Since the bridge height was lower for better solution, the normal forces were greater than in worse solution, as expected. Because cross section dimensions were different for both cases, the resultant stresses diagram was more suitable for comparing the results in terms of impact of internal forces onto utilization. Since the stresses distributions looked similar in both cases, it was decided to perform statistic analysis.

a) Every 5th generation - extreme values in the arch 4747 kNm, and in the tie 3092 kNm

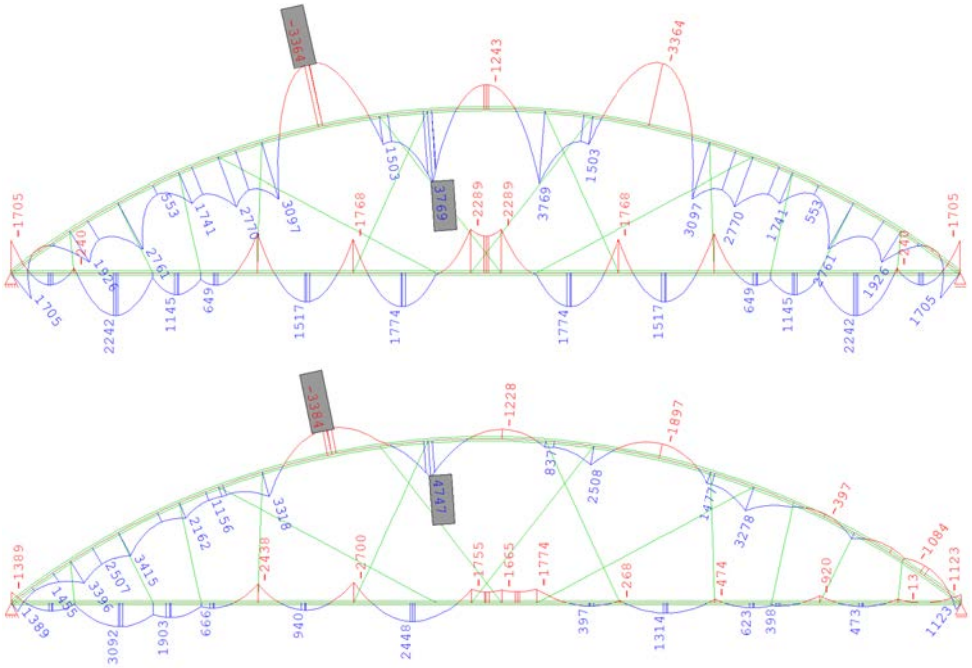

b) Every 10th generation - extreme values in the arch 3841 kNm, and in the tie 4407 kNm

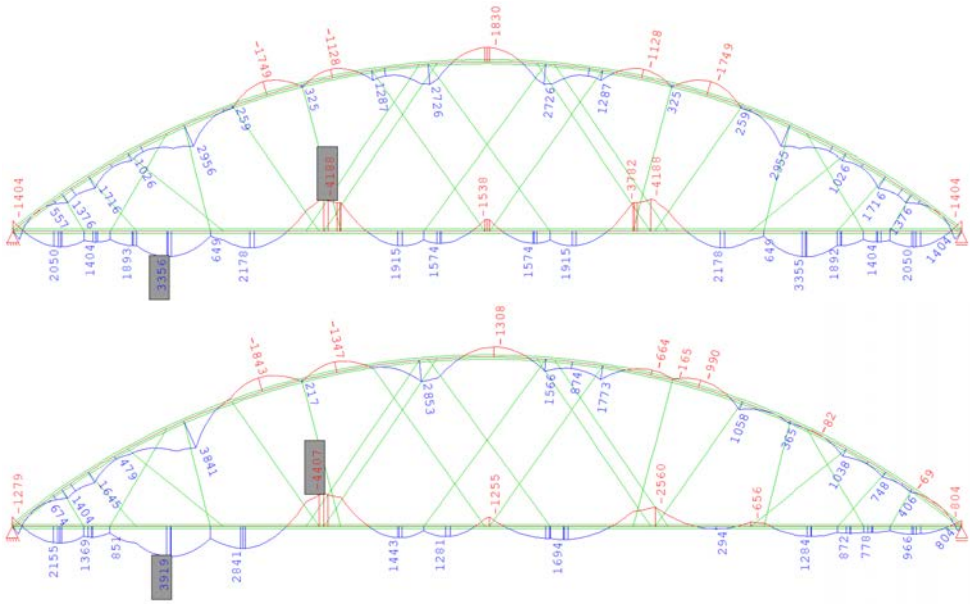

Figure D.4 Bending moment diagrams M_y [kNm] for full and half loaded deck

a) Every 5th generation - extreme values in the arch 19402 kN, and in the tie 17098 kN

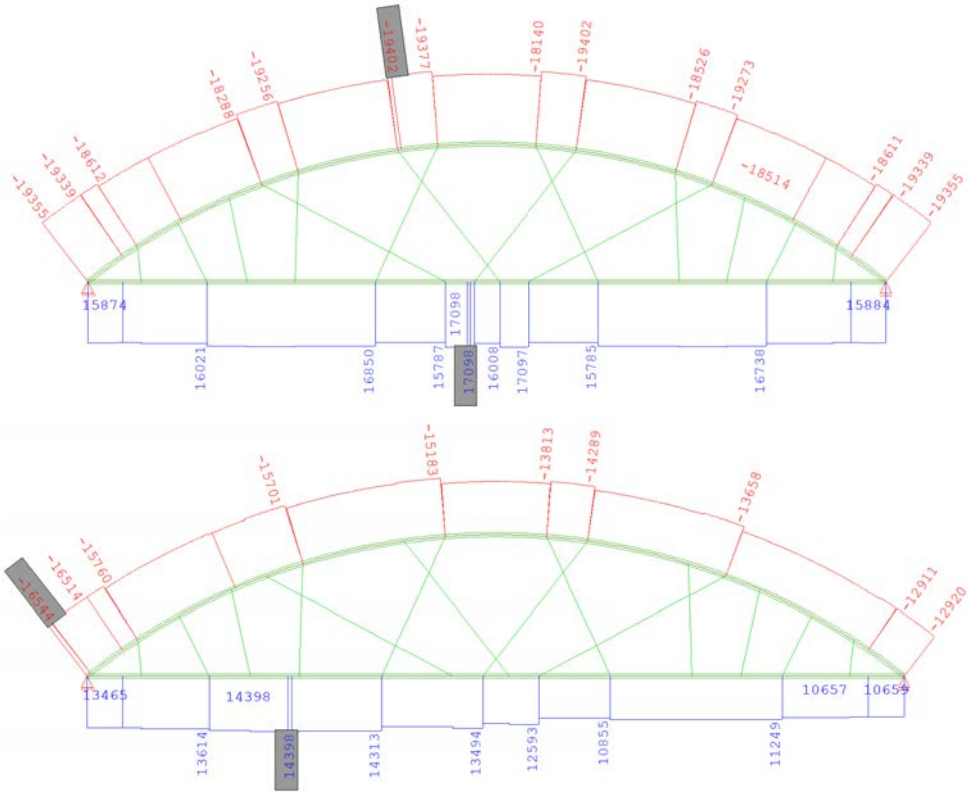

b) Every 10th generation - extreme values in the arch 18925 kN, and in the tie 16845 kN

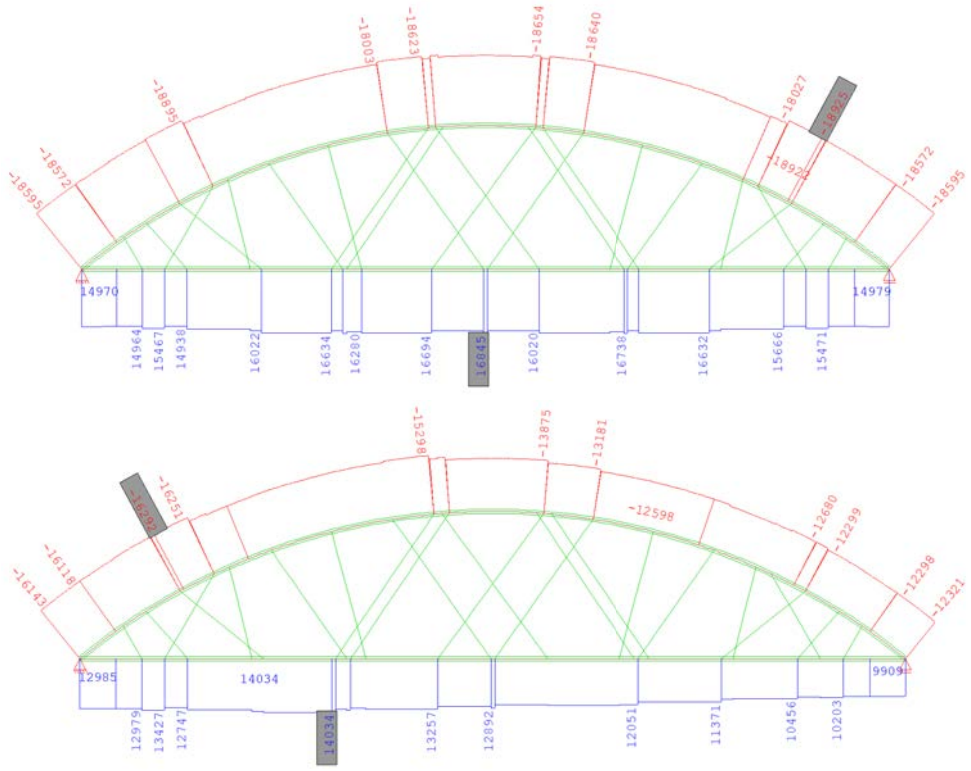

Figure D.5 Normal force diagrams N [kN] for full and half loaded deck

a) Every 5th generation - extreme values in the arch 314 MPa, and in the tie 306 MPa

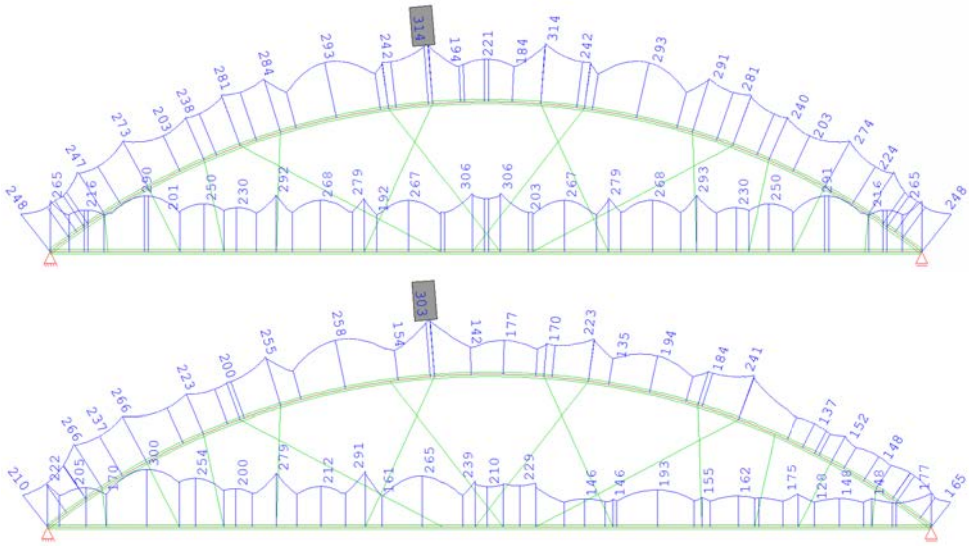

b) Every 10th generation - extreme values in the arch 296 MPa, and in the tie 267 MPa

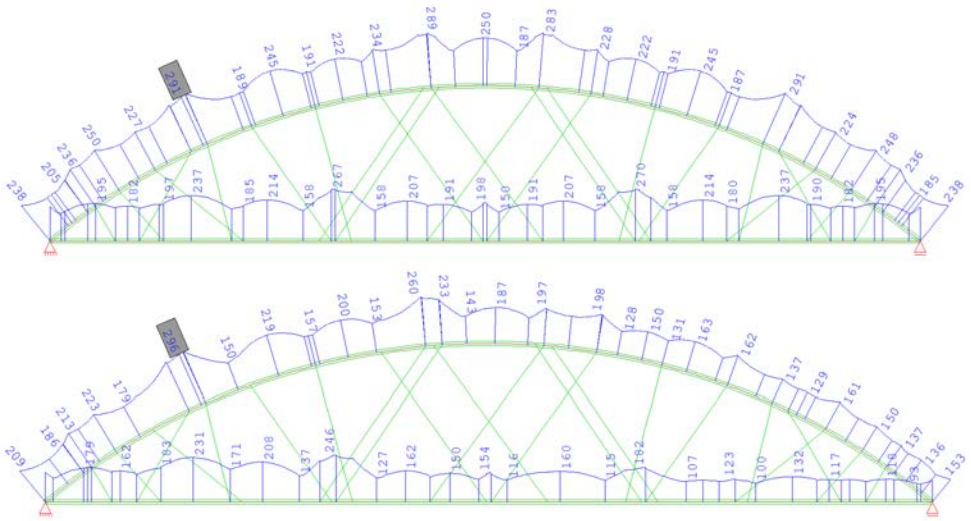

Figure D.6 Von Mises stress diagrams σ_{vM} [MPa] for full and half loaded deck

First of all, the stresses were divided by buckling coefficient and the designed steel yield strength to get the utilization. Secondly, the results were multiplied by the length of the element where they occurred, which reflected the importance of these results in the whole set of stresses along the arch and the tie. The final results were divided by the average length of all relevant arch or tie elements. The results for the arch and the tie were presented in Fig. D.7a-D.7b.

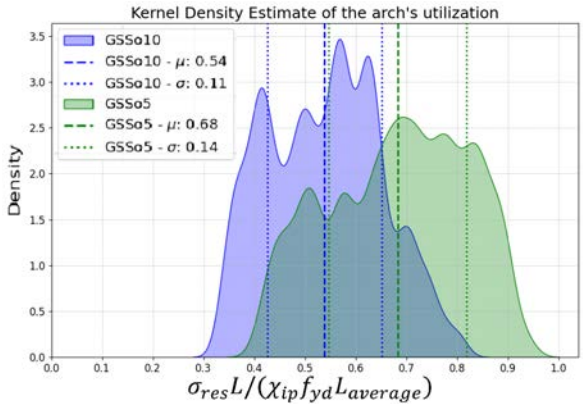

(a) Kernel density estimate of the arch utilization for gradient step size (GSS) of 5 and 10

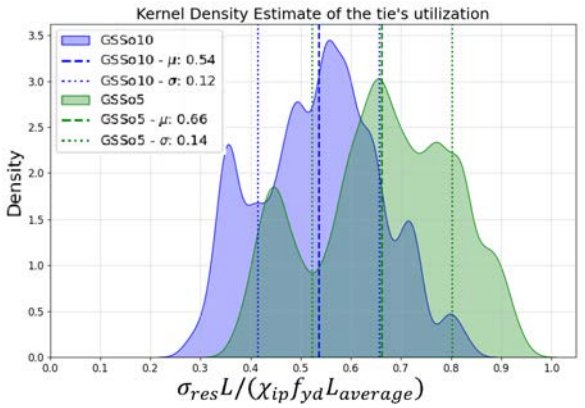

(b) Kernel density estimate of the tie utilization for gradient step size (GSS) of 5 and 10

Figure D.7 Kernel density estimate of the arch and tie utilization for gradient step size (GSS) of 5 and 10

The kernel density estimate was used to smooth the probability density function of utilization distribution in the arch and the tie. It was considered as better method to present this distribution than histogram due to its continuity. On the both figures the results for GSSo5 were more shifted to higher utilization than the results for GSSo10. The mean value in GSSo5 for the arch and the tie were 0.68 and 0.66 with standard deviation of 0.14 and 0.14 respectively. On the contrary, the mean value in GSSo10 for the arch and the tie were 0.54 and 0.54 with standard deviation of 0.11 and 0.12 respectively. It acted as expected, since more optimal solution used to have the average utilization value as high as possible to utilize all elements as maximum as possible. Since the utilization of the arch was characterized by the highest utilized element in the arch, the utilization of all elements should be shifted toward greater values in order to have entire arch optimal shape in the final optimal result. If the average utilization of the arch was low, there would be still a possibility for further improvement caused by remaining capacity margin. The same principles were applicable to the tie.

D.2 Goal Function modification

As it was mentioned in conclusions in Sec. D.1, the modification to GF formula for the utilization lower than 100% was decided to be investigated. The formula in Eq. (6.2) was modified by multiplying the cost value by the utilization η but without floor operation, Eq. (6.5).

With this modification, the calculations were repeated for the GSS of 5 and 10 as the best and the worst solutions in Sec. D.1. There were conducted two runs for each GSS. The best results from these two runs were considered. The results were presented in Tab. D.2 with comparison to the results without GF formula modification. The topology were also compared in Fig. D.8.

The GSSo10 improved its GF value comparing to the non modified case. Nevertheless, the total cost was higher as well as the utilization, which theoretically reduced the possibility of further cost reduction. From GSSo10 perspective, the modification to GF formula made things worse. On the contrary, the GSSo5 improved by 5% the GF value, but the cost was 4.2% higher than the non modified case. The most important change was in the level of utilization, which was reduced from 99.6% to 91.1%, providing more theoretical chance of further improvement of cost up to corresponding GF value.

The topology for the modified cases looked much more random than the corresponding non modified. All new topologies were network-like without clear visible distinctions in forms. The

Table D.2 Parameters comparison between old, Eq. 6.2, and new, Eq. 6.5, GF formula

	5th old	5th new	10th old	10th new
arch diameter [m]	1.3	1.0	1.1	1.0
arch thickness [m]	0.025	0.025	0.030	0.025
tie diameter [m]	1.1	1.0	1.4	0.9
tie thickness [m]	0.025	0.020	0.025	0.050
hanger diameter [m]	0.100	0.090	0.085	0.076
hanger number [-]	14	34	22	28
bridge height [m]	20.69	22.22	21.40	20.00
arch steel	S355	S460	S420	S460
tie steel	S355	S460	S355	S275
hanger steel	S460	S460	S460	S420
buckling factor [-]	0.96	0.97	0.96	0.96
utilization arch [%]	99.6	88.7	93.7	98.1
utilization tie [%]	94.8	91.1	83.7	94.0
utilization hanger [%]	80.2	78.5	61.5	91.9
utilization deflection [%]	48.0	31.3	30.9	25.4
utilization all [%]	99.6	91.1	93.7	98.1
cost [PLN]	3,716,154	3,872,683	4,267,728	4,322,971
goal function [PLN]	3,716,154	3,528,351	4,267,728	4,239,208

(a) GSSo5 no modification - cost = 3,716,154 PLN, GF = 3,716,154 PLN, utilization = 99.6%

(b) GSSo5 with modification - cost = 3,872,683 PLN, GF = 3,528,351 PLN, utilization = 91.1%

(c) GSSo10 no modification - cost = 4,267,728 PLN, GF = 4,267,728 PLN, utilization = 93.6%

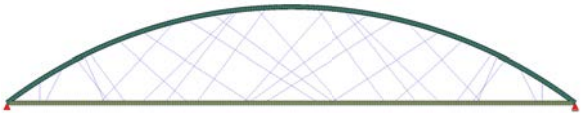

(d) GSSo10 with modification - cost = 4,322,971 PLN, GF = 4,239,208 PLN, utilization = 98.1%

Figure D.8 Tested modified GF formula with comparison to the cases without modification

number of hangers was significantly higher than earlier, with the highest difference for GSSo5 increasing from 14 to 34 hangers.

The GF and cost changes over generations for modified and not modified GF formulas were presented in Fig. D.9. The filling between GF and cost values was used for better pairing of graphs. The filling at the beginning was very big stretching from 3.5 mln PLN to 7.5 mln PLN, which meant that the utilization was about 50%. This difference was reduced severely after 10th generation. The dynamic of change for these paths was similar both for modified and non-modified GF formulas. The modified samples established their best solutions between 40th and 60th generation and then did not change, which was in contrary to the non-modified samples with further reduction even at the last generations. The divergence between GF and cost

values enlarged after the 15th generation for GSSo5. For the GSSo10 they increased after 20th generation until the 30th generation and then decreased again. The GSSo10 after modification was closer to the non-modified solution than the GSSo5, even though it reached better GF value.

For more detailed analysis, the kernel density estimate was used for the utilization distribution. The results were presented in Fig. D.10-D.11.

First of all the KDE was conducted for the utilization level as previously in Sec. D.1 for both GSSo5 and 10. In Fig. D.10a and Fig. D.10b the results of the arch's and tie's utilization KDE were compared for modified and non-modified GF formula. The modified cases had the mean utilization of 0.60 and 0.58 for the arch and the tie respectively, which were significantly less than the non-modified samples with 0.69 and 0.66 respectively. The utilization results were more concentrated around the mean value for modified samples with standard deviation of 0.11 in comparison to 0.14 for non-modified cases. Additionally, the impact of theoretical improvement was investigated by increasing the utilization by the ratio of actual costs and GF value, Fig. D.10 (c) and (d). It helped increasing the mean value for the arch and the tie to 0.66 and 0.64 respectively, which was still lower than the mean values for non-modified samples. This output suggested, that theoretically better solution did not have to have utilization distribution diagram shifted more to the higher values, which was counter intuitive to the principle of keeping all elements as much utilized as possible to ensure more cost-efficient solution achievement.

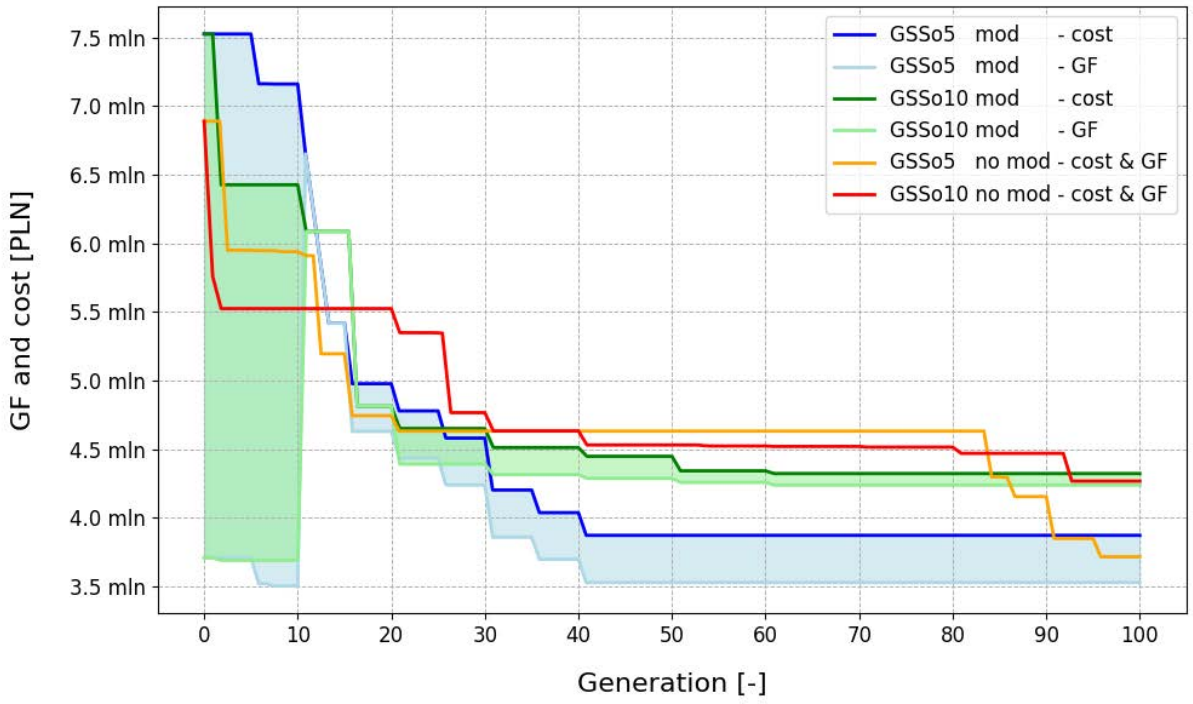

Figure D.9 Goal function values over generations for GSSo5 and GSSo10 with and without modification

On the contrary, the results for GSSo10 with modified formula were better in both cases situations with and without utilization definition change. In Fig. D.11a and Fig. D.11b the modified cases had the mean utilization of 0.68 and 0.56 for the arch and the tie respectively, which were significantly higher than the non-modified samples with 0.54 and 0.54 respectively. The utilization results were more concentrated around the mean value for non-modified samples with standard deviation of 0.11 and 0.12 in comparison to 0.12 and 0.14 for modified cases. As before, the impact of theoretical improvement was investigated by increasing the utilization by

the ratio of actual costs and GF value, Fig. D.11c and Fig. D.11d. It helped increasing the mean value for the arch and the tie to 0.69 and 0.57 respectively, which was even higher than earlier. This output suggested, that theoretically better solution should have utilization distribution diagram shifted more to the higher values, which was in opposition to the conclusion in GSSo5 analysis. On the other side, the GSSo10 provided worse GF value in general in comparison to GSSo5, which should be a reference point in concluding. Since the solution from GSSo5 with modified GF formula provided theoretical chance of reaching lower costs but at the same time resulted in utilization diagram values shifted more to the lower value, the analysis with taking the output from GSSo5 with modified GF formula as an input for the calculations, where no modification was used, should be conducted to dispel doubts regarding the conclusions and conjecture.

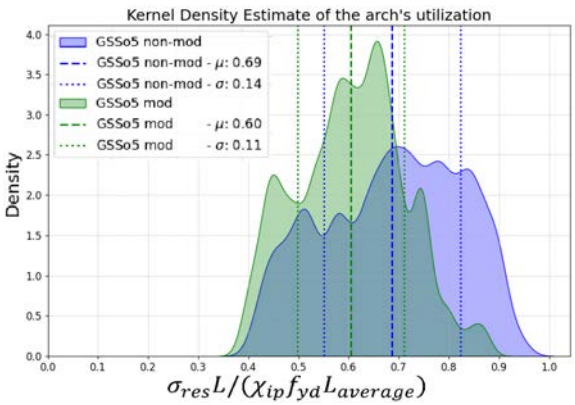

(a) KDE - arch - GSSo5

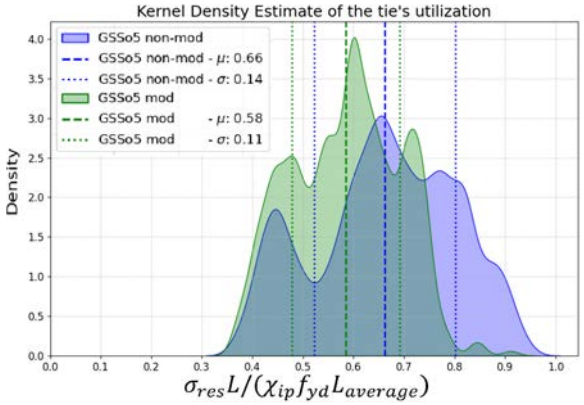

(b) KDE - tie - GSSo5

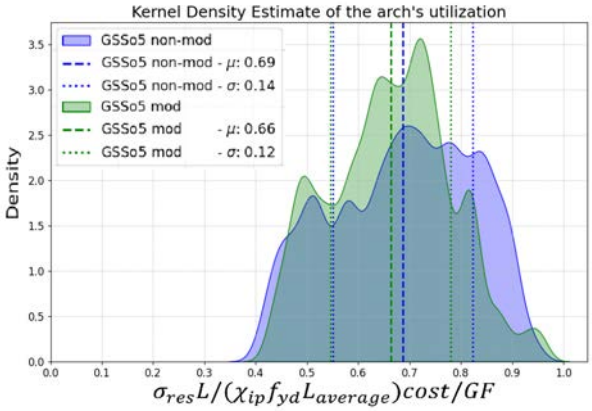

(c) KDE - arch - GSSo5 with theoretical improvement

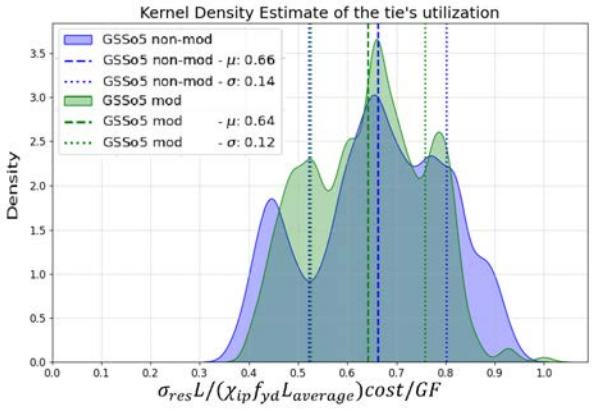

(d) KDE - tie - GSSo5 with theoretical improvement

Figure D.10 Kernel density estimate of the arch and tie utilization for GSSo5

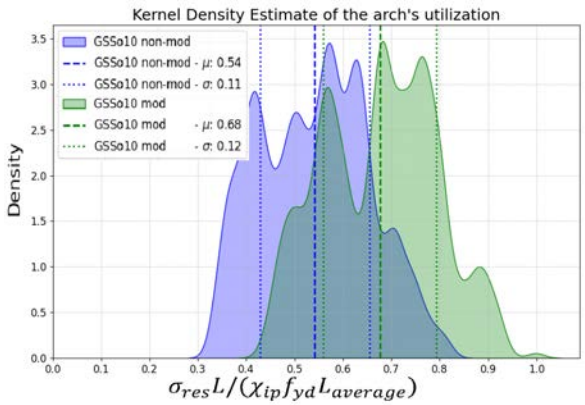

(a) KDE - arch - GSSo10

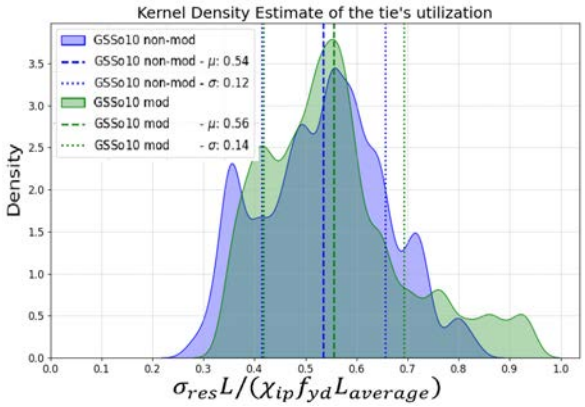

(b) KDE - tie - GSSo10

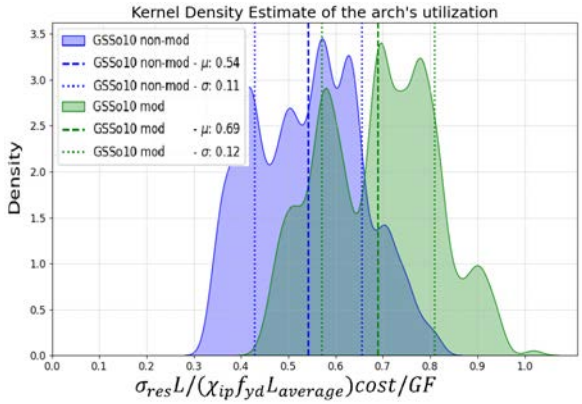

(c) KDE - arch - GSSo10 with theoretical improvement

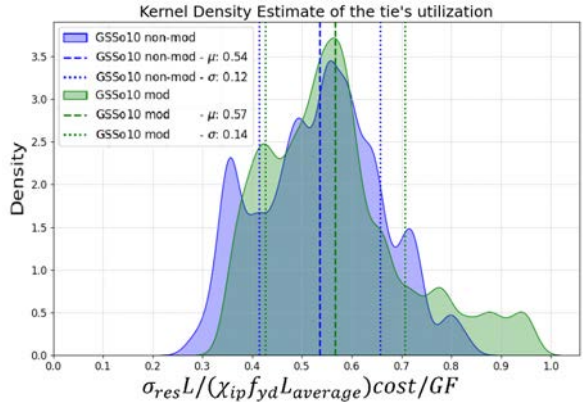

(d) KDE - tie - GSSo10 with theoretical improvement

Figure D.11 Kernel density estimate of the arch and tie utilization for gradient step size GSSo10

D.3 Extended number of generations

Since there were still a positive trend of GF value reduction at the end of the analysed cases in Sec. D.1, it was decided to investigate the impact of generations number increase. The settings were the same as before and both the worse and the best cases were investigated, so with gradient step size of 5 and 10 respectively. Especially the best case was the most important due to its the highest change of GF value at the end of optimization process. The number of generations was increased to 200. The modified GF formula from Sec. D.2 was implemented, since it was concluded as worth to investigate. The results were presented in Tab. D.3 with comparison to shorten calculations from Sec. D.2.

The utilization in longer samples were higher in general comparing to the shorter tests. Both longer cases provided better results in terms of cost values in relation to the shorter tests. Even though longer GSSo5 had worse GF value, it achieved lower cost. Otherwise, longer GSSo10 had GF value lower than that obtained in shorter test. The improvement of cost and GF values for GSSo10 were about 2% and 1% respectively. In contrary, the cost value for GSSo5 improved by 3.5% and GF value worsen by 4.5%. In general, the costs for both GSSo5 and GSSo10 were comparable or worse than the shorter sampler without GF formula modification.

From the geometrical perspective, all the topology were much random but with network-like arrangement, Fig. D.12. The span length to height ratio was mostly 6 but for longer GSSo10 it was the lowest allowed 5. It looked visually much higher than the remaining geometries. The

Table D.3 Parameters comparison between 100 and 200 generations iterations with modified GF formula

	5th short	5th long	10th short	10th long
arch diameter [m]	1.0	1.0	1.0	1.7
arch thickness [m]	0.025	0.025	0.025	0.025
tie diameter [m]	1.0	1.0	0.9	0.9
tie thickness [m]	0.020	0.025	0.050	0.030
hanger diameter [m]	0.090	0.076	0.076	0.090
hanger number [-]	34	30	28	28
bridge height [m]	22.22	20.69	20.00	24.00
arch steel	S460	S460	S460	S235
tie steel	S460	S420	S275	S320
hanger steel	S460	S420	S420	S320
buckling factor [-]	0.97	0.96	0.96	0.98
utilization arch [%]	88.7	96.7	98.1	97.3
utilization tie [%]	91.1	98.7	94.0	99.0
utilization hanger [%]	78.5	88.1	91.9	94.1
utilization deflection [%]	31.3	48.3	25.4	36.0
utilization all [%]	91.1	98.7	98.1	99.0
cost [PLN]	3,872,683	3,739,822	4,322,971	4,242,740
goal function [PLN]	3,528,351	3,692,629	4,239,208	4,200,313

second noticeable characteristic was much greater diameter of the arch comparing to the others geometries, which was 70% greater than the tie for the same sample. The massive arch was one of features of vertical arch bridges and the considered geometry had the less crossings and the most vertical oriented hangers from other results.

(a) GSSo5 with 100 generations - cost = 3,872,683 PLN, GF = 3,528,351 PLN, η = 91.1%

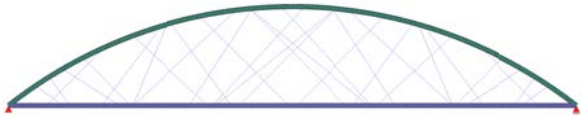

(b) GSSo5 with 200 generations - cost = 3,739,822 PLN, GF = 3,692,629 PLN, η = 98.7%

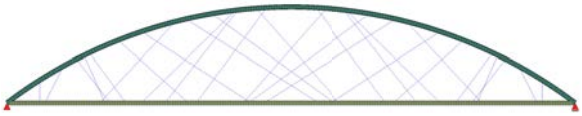

(c) GSSo10 with 100 generations - cost = 4,322,971 PLN, GF = 4,239,208 PLN, η = 98.1%

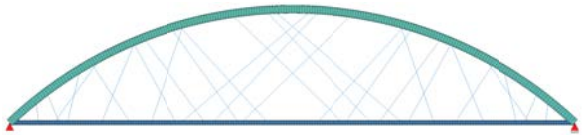

(d) GSSo10 with 200 generations - cost = 4,242,740 PLN, GF = 4,200,313 PLN, η = 99.0%

Figure D.12 Tested modified GF formula comparison with 100 and 200 generations

The cost and GF values for both longer and shorten generation samples were presented in Fig. D.13. At the very beginning up to 10th generation, the divergence between cost and GF values were very high covering the range between 3.5 mln PLN and 7.5 mln PLN. That was partially cast by not well optimized structures in the initial step and high allowed standard deviation in mutation process. All the samples reached their almost constant value at about 50th generation. After that, the shorter tests barely improved. The longer GSSo5 started to reduce cost and GF values after 110th and until 130th generation. In contrary, the longer GSSo10

insignificantly reduced its value by 5% at 170th generation. The divergence between cost and GF values were noticeably smaller for longer than for shorter samples.

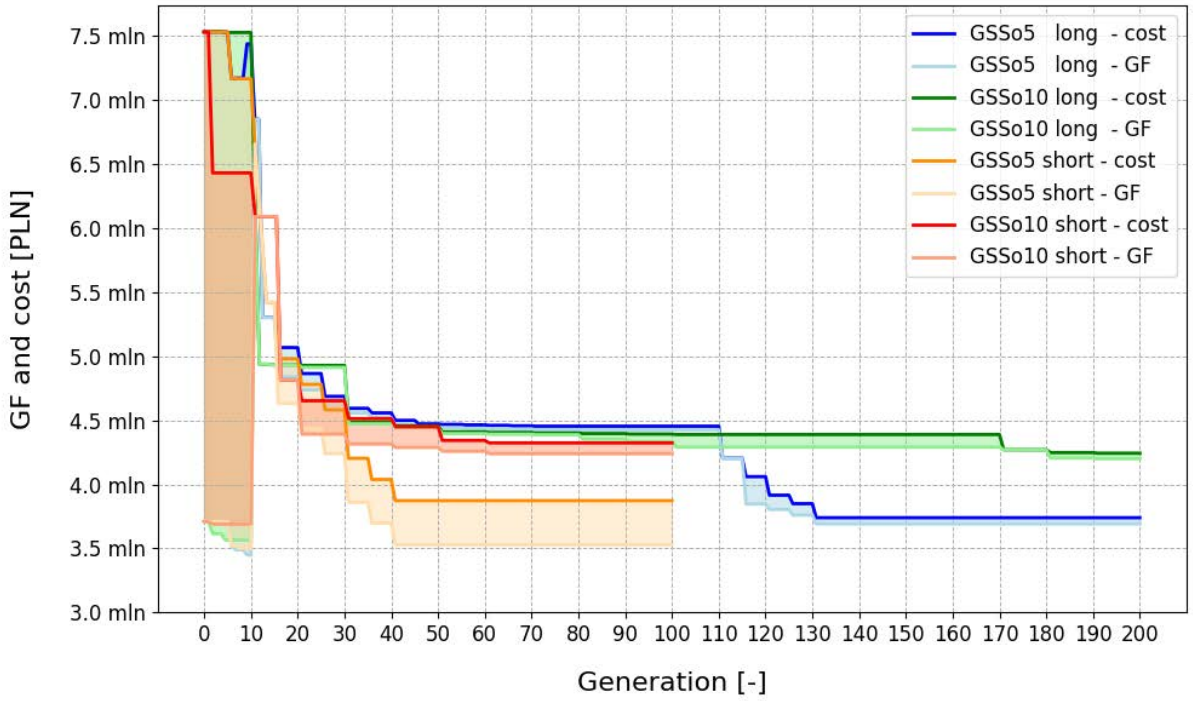

Figure D.13 Goal and cost function values for GSSo5 and GSSo10 with modification over 100 and 200 generations

The stresses distribution for GSSo5 with short and long run were presented in Fig. D.14. The mean utilization in arch was 0.60 with 0.11 of standard deviation for short test and 0.66 with 0.13 for longer. The longer calculations resulted in greater average utilization of the arch, than for the shorten version with an advantage of 0.06. Smaller improvement was also visible for the tie, where the shorter average run resulted in average utilization of 0.58 and 0.62 for the longer. The standard deviation for longer runs was in both cases greater than for the shorten tests. The updated results for theoretical improvement were not far from the actual, since the divergence between GF and costs values was relatively negligible. That resulted in small improvement to 0.63 of average utilization for the tie. The results in arch remained the same. Since the shorten test had greater divergence between GF and cost values, the progression was far greater for both arch and tie. The average utilization for both short and long tests were almost the same with small advantage for shorten calculation over longer for the tie. That corresponded with lower cost value for longer run than shorten, but worse GF value than for shorten test, which meant that shorten calculation could potentially resulted with element greater utilization than the longer run.

Adequate differences were identified for GSSo10, as presented in Fig. D.15. The average utilization in shorten test in the arch was 0.66 and 0.68 for longer. The theoretical improvement increased the shorten utilization to 0.67 and longer to 0.69. Similarly, for the tie the average utilization for the shorten test was 0.56 and 0.62 for longer. The theoretical improvement changed the shorten average utilization to 0.57 and longer to 0.63.

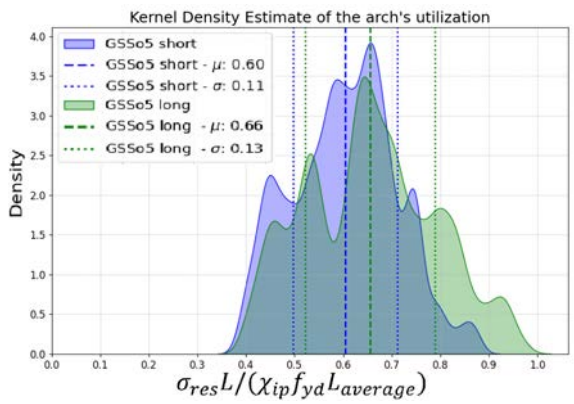

(a) KDE - arch - GSSo5

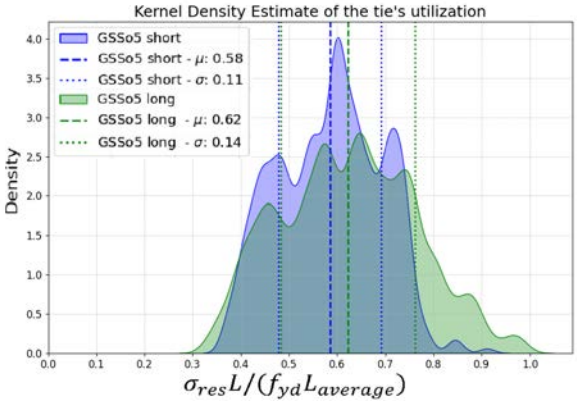

(b) KDE - tie - GSSo5

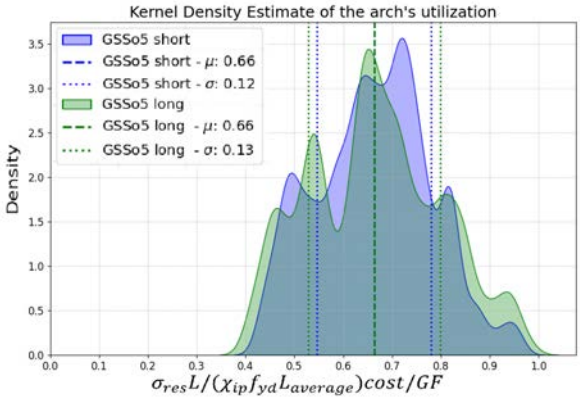

(c) KDE - arch - GSSo5 with theoretical improvement

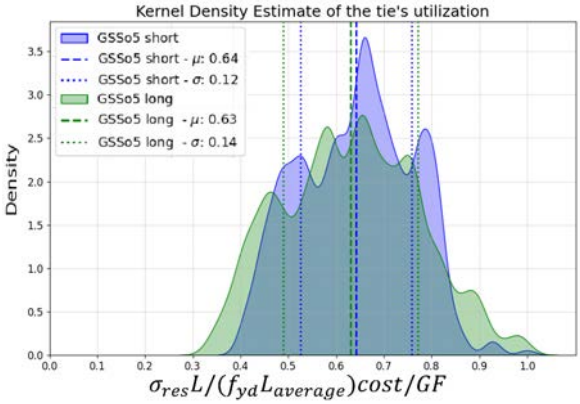

(d) KDE - tie - GSSo5 with theoretical improvement

Figure D.14 Kernel density estimate of the arch and tie utilization for GSSo5

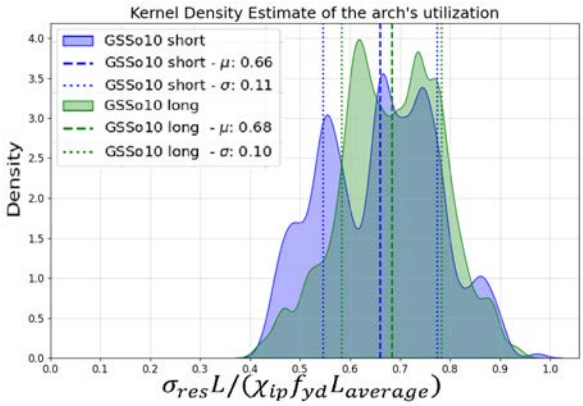

(a) KDE - arch - GSSo10

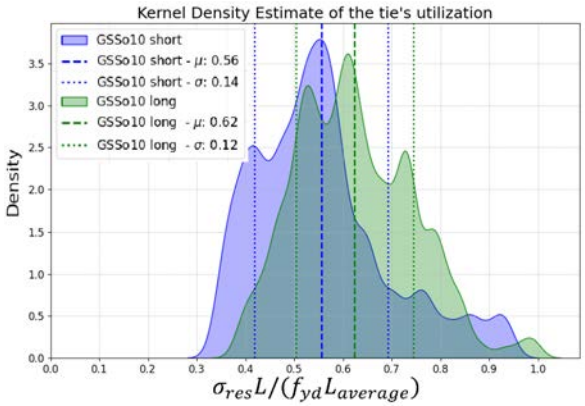

(b) KDE - tie - GSSo10

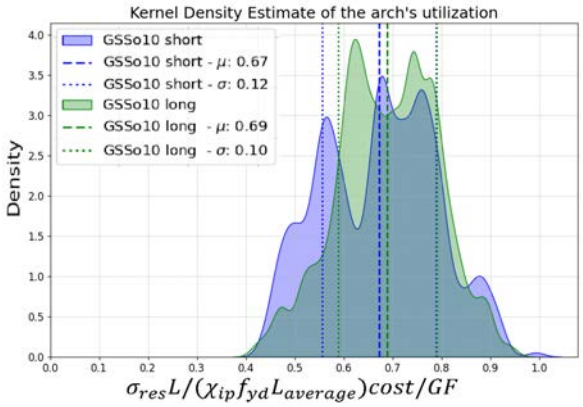

(c) KDE - arch - GSSo10 with theoretical improvement

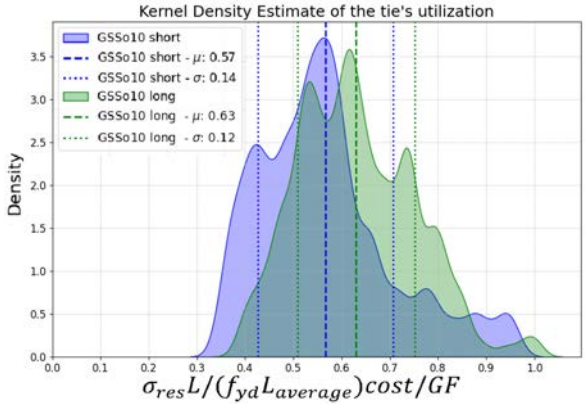

(d) KDE - tie - GSSo10 with theoretical improvement

Figure D.15 Kernel density estimate of the arch and tie utilization for GSSo10

D.4 Initial population with known hangers' arrangements

Until now, the starting topology for all initial geometries was network type. In order to not favour one topology type, it was decided to use both vertical and Nielsen type topology in the initial set together with NA. The samples were presented in Fig. D.16.

In analysis, the GSSo5 and gradient descent were used. No GF value modification was implemented. The total number of individuals at the start was 30, so 10 geometries per each type of topology. The GF value path was presented in Fig. D.19.

The GF value path had similarities to the previous analyses. The biggest improvement was at the beginning and after stabilization at about 20th generation, the path had further progress after about 78th generation. The price dropped to 4,611,878 PLN, which was significantly worse than the results from the previous tests, where results finalized at about 3.6 mln PLN. The most optimized geometry was presented in Fig. D.17.

The topology was similar to Nielsen and vertical hangers' topology. These types were known to not be the most economical solutions, which was also reflected in the resultant price after optimization process. During the first 3 generations, the NA topology was the favourite, Fig. D.18a. That was the expected result, but at the 4th generation the Nielsen topology took the first place, Fig. D.18b.

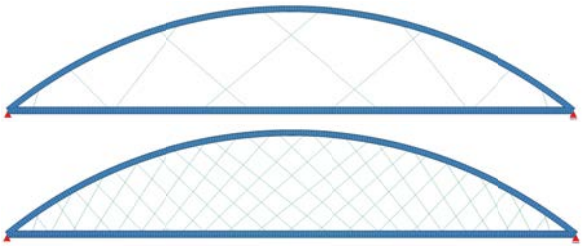

(a) Network topology

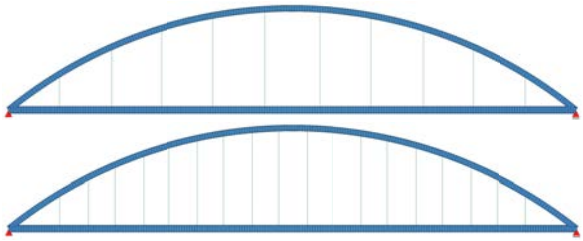

(b) Vertical topology

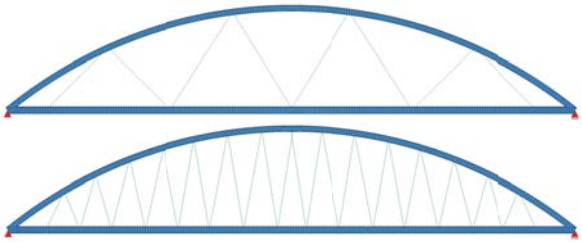

(c) Nielsen topology

Figure D.16 Three types of used topology with examples of the minimum and maximum number of hangers

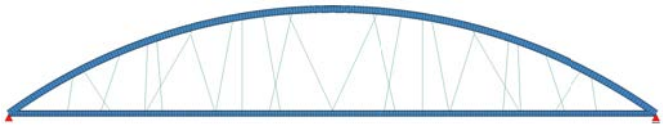

Figure D.17 The most optimized geometry for mix topology approach

(a) Topology after 3 generations

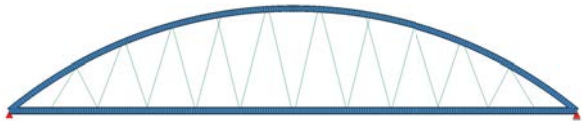

(b) Topology at 4th generation

Figure D.18 The topology hanger for (a) the first 3 and (b) for the 4th generations

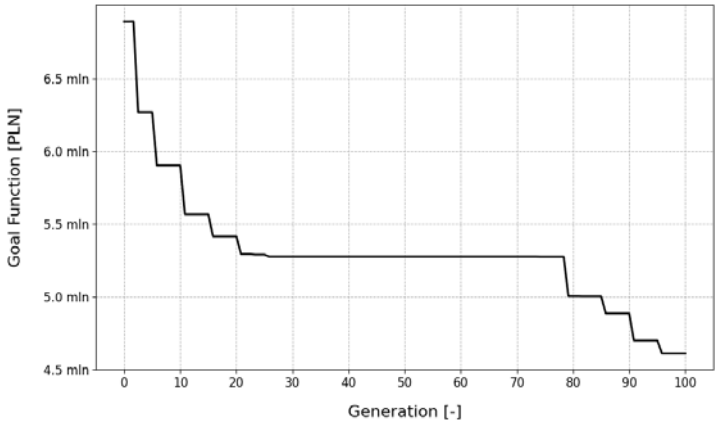

Figure D.19 Goal function values for GSSo5 with mix of topologies

As it was presented in Tab. D.4, the arch and the tie got optimized for 4th generation even if the topology itself was known to be more expensive, if the utilization of all elements were the same. Algorithms did not have this experience implemented, so it went into improving solution in this direction. Unfortunately, the remaining NA geometries did not get cheaper than the Nielsen topology, and were deleted in further stages from the system, with mainly Nielsen-like

Table D.4 Data comparison for 3rd and 4th geometry

	3rd gen	4th gen
arch diameter [m]	1.3	1.3
arch thickness [m]	0.050	0.045
tie diameter [m]	1.5	1.5
tie thickness [m]	0.040	0.035
hanger diameter [m]	0.090	0.090
hanger number [-]	16	20
utilization arch [%]	55.8	78.6
utilization tie [%]	52.3	72.5
utilization hanger [%]	94.8	92.0
utilization deflection [%]	27.2	86.1
utilization all [%]	94.8	92.0
cost arch [PLN]	3,459,329	3,125,225
cost tie [PLN]	2,984,736	2,620,588
cost hangers [PLN]	287,643	322,719
cost hangers anchorage [PLN]	160,000	200,000
cost [PLN]	6,891,708	6,268,532
goal function [PLN]	6,891,708	6,268,532

topology. At the same time, the hangers got very utilized from the very beginning at above 90% rate, which was much higher than for the arch and the tie with above 50% utilization. To be more precise, the maximum hangers utilization was 176% with mean and standard deviation values of 91.2% and 31.4% respectively. In total, 13 initial geometries were not considered due to exceeding hangers capacity. The other geometries, which optimized their hangers' topology, might have experienced much improvement in the arch and the tie cost reduction, but due to exceeding hangers capacity in the process, the geometry was punished in GF value and the change was abandoned.

D.5 Prestressed steel for hangers

As mentioned in Sec. D.4, the hangers' steel grade was updated to prestressed for higher yield strength needs. The cost of the prestressed steel was assumed as 45,000 PLN/ton, being more than twice as expensive as steel S460, and was the same for all considered prestressed steel grades: Y1700, Y1770, Y1860, Y1960, Y2060 and Y2160. Doubling the price in comparison to steel S460 was chosen in order to make a great difference in price and observe, if increased capacity of hangers was great enough gratitude for the algorithm to choose much more expensive steel. The starting population was the same as in Sec. D.4 with the different arrangements mixture. The resultant path was presented in Fig. D.20.

This time, the GF with prestressed steel for hangers (green) reached lower value faster than the GF for hangers with structural steel (red). The first arrangements were more network-based, Fig. D.21. The result for 4th generation (c) was similar to the best geometry in Fig. D.2e in Sec. D.1. Examples of the first generations were presented in Fig. D.21. The 3rd generation was the most Nilsen type similar among all earliest generations, but the algorithm did not maintained it in longer perspective, which was a problem described in Sec. D.4 with structural steel for hangers. The maximum utilization for hangers this time was 43.4% with mean and standard

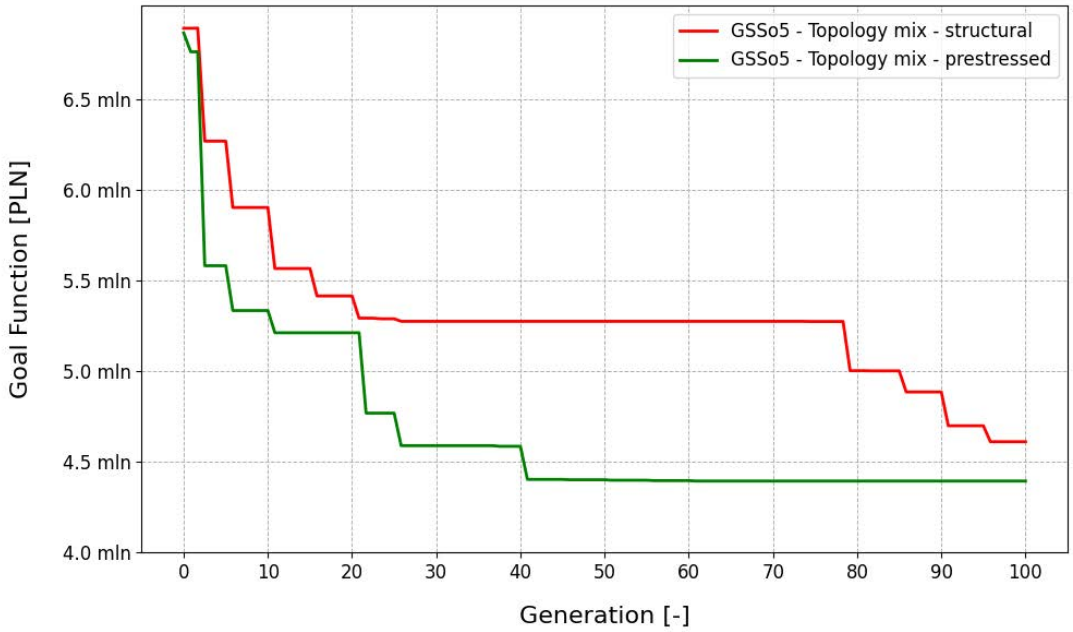

Figure D.20 Goal function values comparison of mix topology with hangers made of structural and prestressed steel

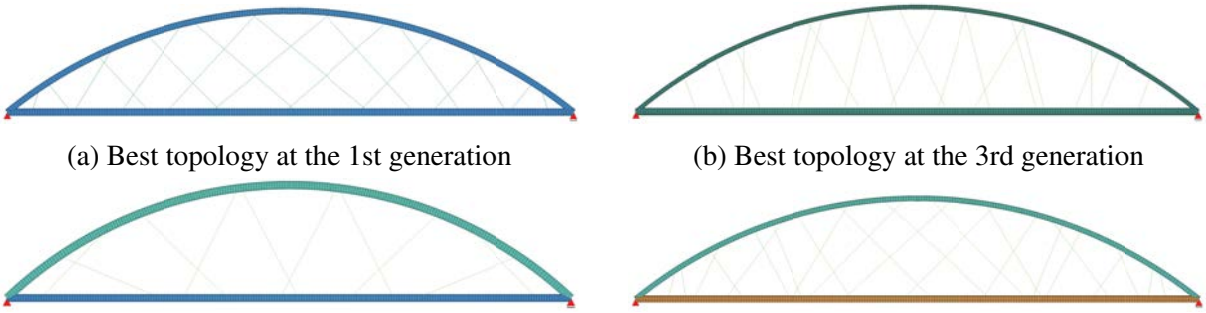

(a) Best topology at the 1st generation

(b) Best topology at the 3rd generation

(c) Best topology at the 4th generation

(d) Best topology at the 10th generation

Figure D.21 The topology hanger for the (a) 1st, (b) 3rd, (c) 4th and (d) 10th generation

deviation values of 22.5% and 8%. These values were much lower compared with the results for structural steel, where 13 of initial geometries were not considered due to hangers capacity exceed. The hangers utilization stopped to be major process limitation after considering prestressed steel in the allowed domain of possible solutions.

The information of the most optimized structures in mix topology approach with structural and prestressed steel were compared in Tab. D.5. The arch's diameter got significantly slender reaching 0.7 m in value comparing to 1.3 m for structural variant. The thickness had to be compensated with the value of 0.055 m instead of 0.030 m. The ties dimensions were comparable. Since the hangers got much higher allowed steel yield strength, the diameter could have got lower with the value of 0.048 m instead of 0.090 m. Steel grades got higher as well for the arch and the tie with the value of S420 and S460 respectively in comparison to S355 and S320 for structural steel solution. Since the steel arch obtained lower bending stiffness, the buckling factor got lower value as expected reaching 0.94 comparing to 0.97 for structural steel solution. The maximum utilization was almost 100% for both cases, but the prestressed steel solution had hangers and deflection utilization significantly lower than the variant with structural steel.

Nevertheless, the overall cost was reduced by around 4.5%.

The topology of hangers for the best solution with prestressed steel was presented in Fig. D.22. Hangers were arranged in network type structure in the middle part, and vertical-nielsen type structure in ranges close to skewbacks. The hangers in at the ends were skewed almost perpendicularly to the arch. Then the topology started to match the network type, but it was more random arranged than in known solutions. In the middle, the network became less dense arranged and relatively big rhombus-shape hole occurred in the very center of the span.

Table D.5 Parameters comparison between structural and prestressed steel for hangers in mix topology at the initial generation

	structural	prestressed
arch diameter [m]	1.3	0.7
arch thickness [m]	0.030	0.055
tie diameter [m]	1.1	1.0
tie thickness [m]	0.035	0.025
hanger diameter [m]	0.090	0.048
hanger number [-]	24	32
bridge height [m]	19.4	21.4
arch steel	S355	S420
tie steel	S320	S460
hanger steel	S420	Y2060
buckling factor [-]	0.97	0.94
utilization arch [%]	99.9	99.98
utilization tie [%]	96.6	94.4
utilization hanger [%]	93.7	56.4
utilization deflection [%]	93.3	73.6
utilization all [%]	99.9	99.98
cost [PLN]	4,611,878	4,395,128
goal function [PLN]	4,611,878	4,395,128

Nevertheless, the topology looked better than the one with structural steel for hangers, the overall costs of 4.4 mln PLN were much greater than the GSSo5 approach presented in Sec. D.2 with 3.7 mln PLN. However, the results remain competitive, as demonstrated by GSSo10, which achieved comparable outcomes with a total cost of 4.3 mln PLN. That drives into conclusion, that a mixture of different topology for used number of individuals and generations was less optimized approach than just network type topology. The idea behind this solution, was greater diversity in descendants and possible faster progression, but it did not behaved as expected.

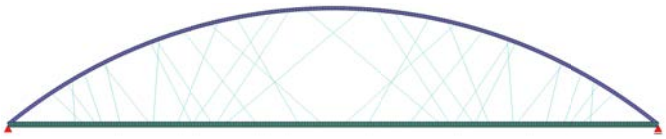

Figure D.22 The most optimized geometry for mix topology approach with prestressed steel for hangers

D.6 Manual initiation after standard GF formula

In this chapter, the impact was considered of adding the best individual from the previous calculations with non-modified GF value to the new calculation's initial generation also with non-modified GF value. The investigation was divided into two parts. The first one added individual with the topology hangers the same, as the previous best one with keeping its parameters the same as in the remaining geometries in the initial generation, so the default setting (BIWNP). The second one took all the parameters from the best individual and applied them to the one manually added into the initial generation, but the remaining geometries in the generation kept their initial, default parameters (BIWAP). The initial geometry set was the same as in the mix topology calculations presented in Sec. D.4 but with additional manual individual. The results were presented in Tab. D.6 and Fig. D.23.

Table D.6 Parameters comparison between reference calculations, BIWNP and BIWAP

	original	BIWNP	BIWAP
arch diameter [m]	1.3	0.9	1.3
arch thickness [m]	0.025	0.025	0.025
tie diameter [m]	1.1	1.0	1.1
tie thickness [m]	0.025	0.025	0.025
hanger diameter [m]	0.100	0.085	0.100
hanger number [-]	14	28	14
bridge height [m]	20.69	23.08	20.69
arch steel	S355	S460	S355
tie steel	S355	S320	S355
hanger steel	S460	S420	S420
buckling factor [-]	0.96	0.96	0.96
utilization arch [%]	99.6	99.96	99.99
utilization tie [%]	94.8	95.2	97.3
utilization hanger [%]	80.2	90.0	92.1
utilization deflection [%]	48.0	30.4	41.3
utilization all [%]	99.6	99.96	99.99
cost [PLN]	3,716,154	3,501,324	3,698,874
goal function [PLN]	3,716,154	3,501,324	3,698,874

The BIWAP resulted in almost the same geometry and materials as the original manually added geometry. The hangers got lower steel grade from S460 to S420. That had the major impact on the utilization of the hangers, which increased from 80.2% to 92.1%, but still lower than the arch and the tie's utilization, which were the dominant. When considering the hangers' topology, the 1st and the 3rd closest hangers to the ends were re-positioned as well as the two closest to the span center point, Fig. D.23c. All of those changes caused minor improvement to the original model, so the cost reduction by less than 0.5% followed this trend.

On the contrary, the BIWNP managed to significantly reduce the cost in comparison to the original test. The first major difference started from the arch's diameter, which was smaller by 0.40 m comparing to the original analysis with keeping the same dimension of thickness. That would result in much higher utilization than the capacity of the arch's cross section, since the original utilization was already above 99%, so algorithm compensated it with greater inclination of 23.08 m comparing to the 20.69 m in the original geometry and higher steel grade of S460 comparing to S355 in the original case. The tie geometry remained unchanged, but its steel grade decreased from S355 to S320. Hangers diameter was reduced to 0.085 m from

(a) GSSo5 no modification - cost = 3,716,154 PLN, GF = 3,716,154 PLN, utilization = 99.6%

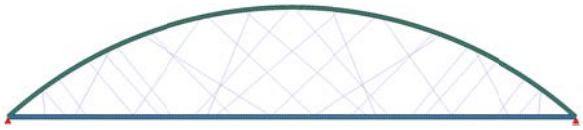

(b) GSSo5 with BIWNP - cost = 3,501,324 PLN, GF = 3,501,324 PLN, utilization = 99.96%

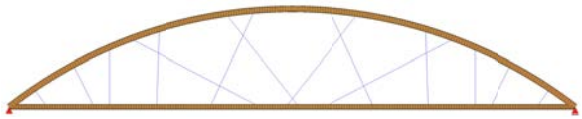

(c) GSSo5 with BIWAP - cost = 3,698,874 PLN, GF = 3,698,874 PLN, utilization = 99.99%

Figure D.23 Comparison of the best individuals from the (a) original calculations, (b) manually added best individual with hangers' topology but without the original remaining parameters (BIWNP) and (c) manually added best individual with all remained parameters (BIWAP)

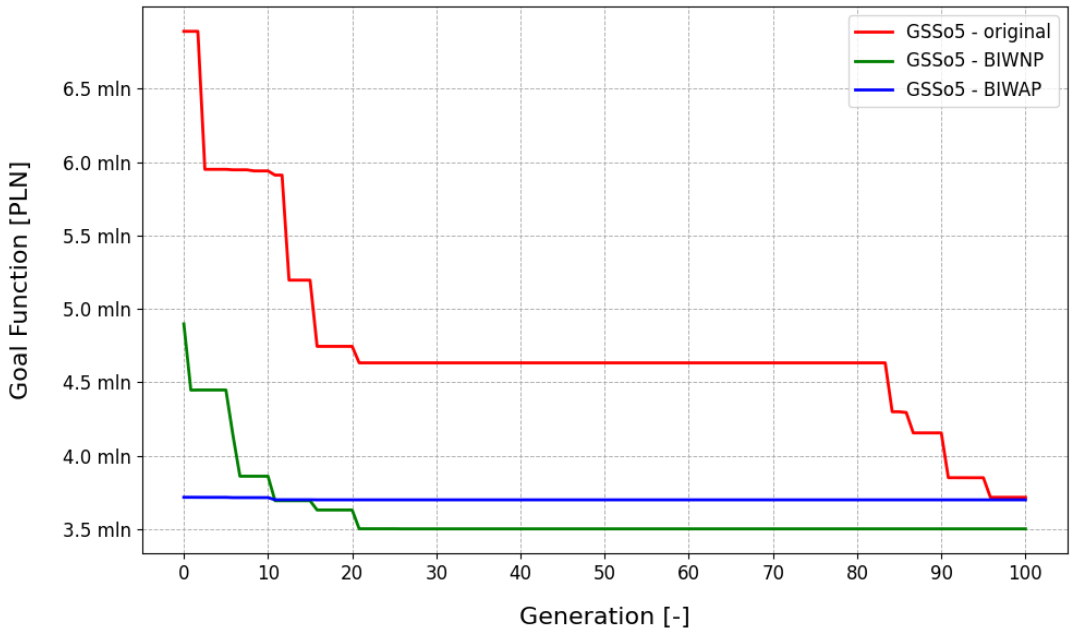

Figure D.24 Goal function values progression comparison of the impact of final geometry application from the previous optimization cycle as one of the initial geometries in the first generation

0.100 m and their number doubled from 14 to 28, which helped in reducing the bending moments in the tie justifying its steel grade reduction. The hangers steel grade also decreased due to that from S460 to S420. The resultant hangers' topology was much different from the original test, Fig. D.23b. The middle section was regular network arch topology with parallel hangers. The remaining part were more chaotic arranged but with more hangers pointed perpendicularly to the arch, which reminded the tendency from the original test, but with denser hangers' arrangement.

When it came to the GF value progression, the BIWNP progressed faster than BIWAP at the very beginning and finalized in lower value than the first one at the 10th generation, Fig. D.24. After 20th generation, no progression was observed in both GF paths. Finally, both paths achieved lower GF value than the reference test.

D.7 Manual initiation after GF formula modification

The best geometry from the GSSo5 with modified GF value was used as one of the geometries in the initial generation of the continued analysis without modified GF formula in order to investigate the impact of implementing the geometry with lower GF value than cost. The research expected achievement of lower cost than the results with non-modified GF value from Sec. D.2. Two approaches were investigated. The first with keeping the same arch, tie and hangers parameters of the implemented geometry for all geometries in the initial generation, but remaining their hanger topology, so called APA (all parameters applied). The second kept the default parameters for the remaining geometries and with no changes to the added individual, so called NPA (no parameters applied), which followed principles of BIWAP from Sec. D.6. The initial population was the same as in Sec. D.2, so different variant of NAB topology. The results were compared in Tab. D.7 and Fig. D.25.

Table D.7 Parameters comparison between original, APA and NPA procedures

	original	APA	NPA
arch diameter [m]	1.0	0.9	1.1
arch thickness [m]	0.025	0.025	0.025
tie diameter [m]	1.0	1.0	0.9
tie thickness [m]	0.020	0.020	0.020
hanger diameter [m]	0.090	0.090	0.090
hanger number [-]	34	22	34
bridge height [m]	22.22	22.22	22.22
arch steel	S460	S460	S355
tie steel	S460	S420	S460
hanger steel	S460	S460	S235
buckling factor [-]	0.97	0.96	0.97
utilization arch [%]	88.7	99.9	95.4
utilization tie [%]	91.1	91.7	98.5
utilization hanger [%]	78.5	77.6	99.9
utilization deflection [%]	31.3	50.8	55.6
utilization all [%]	91.1	99.9	99.9
cost [PLN]	3,872,683	3,268,112	3,436,907
goal function [PLN]	3,528,351	3,268,112	3,436,907

Both results obtained from APA and NPA procedures had similar geometry properties as the original result, Tab. D.7. The most difference was in hanger number in APA, which was 22 comparing to 34 in both original and NPA results. Arch was smaller by 0.1 m from APA procedure and NPA was greater by 0.1 m in comparison to original geometry. APA resulted in similar steel grade as original, but NPA used grades from S235 for hangers, through S355 for the arch and S460 for the tie. Buckling factor was as usual around 0.96 - 0.98 range. Utilization for both APA and NPA were almost 100%, when in the original test 91.1%. The highest utilization in APA was related with arch and tie, but for NPA all elements were highly utilized. The deflection criterion was not determinant. Even though the NPA resulted in higher utilization than APA, the NPA provided 5% greater cost than APA. Both APA and NPA obtained much better GF and cost values than original test. Comparing to original GF value, NPA and APA got 2.6% and 7.4% of improvement respectively, which was higher than anticipated in Sec. D.2.

(a) Reference modified GF - cost = 3,872,683 PLN, GF = 3,528,351 PLN, utilization = 91.1%

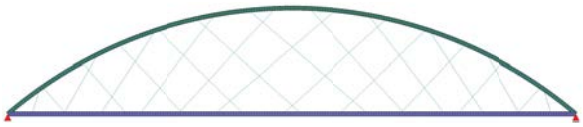

(b) GSSo5 with APA - cost = 3,268,112 PLN, GF = 3,268,112 PLN, utilization = 99.9%

(c) GSSo5 with NPA - cost = 3,436,907 PLN, GF = 3,436,907 PLN, utilization = 99.9%

Figure D.25 GF value improvement over generations for (a) reference geometry, (b) implemented reference geometry with APA procedure and (c) implemented reference geometry with NPA procedure

When it comes to the topology, the results were much different, Fig. D.25. Since NPA made favourite the geometry from the original calculations, the topology itself had similarities to the original solution. The more empty region in the middle part remained in the NPA solution, but changed its shape. Even if the two solutions had the same number of hangers, the NPA solution looked less chaotic, since hangers were not crossing that often with each other. The maximum crossing of a single hanger in the original test was 6 and in NPA 4. The topology changed from network-like arrangement in the middle to vertical in the area close to ends.

On the contrary, the topology from APA was very different from the original, but it was almost unchanged from one of the default set of topology in the initial generation. It turned out, that by implementing the geometry properties except the hangers' topology from the best individual in reference test to all of the initial geometries, one of the default network topology provided better GF value than the reference geometry. It might have driven into conclusion, that the optimization of both sectional properties and hangers' topology may improve sectional properties and make topology worse for the respective properties, which was not an unexpected behaviour. The resultant solution achieve the lowest GF value among three tests and was the most organized.

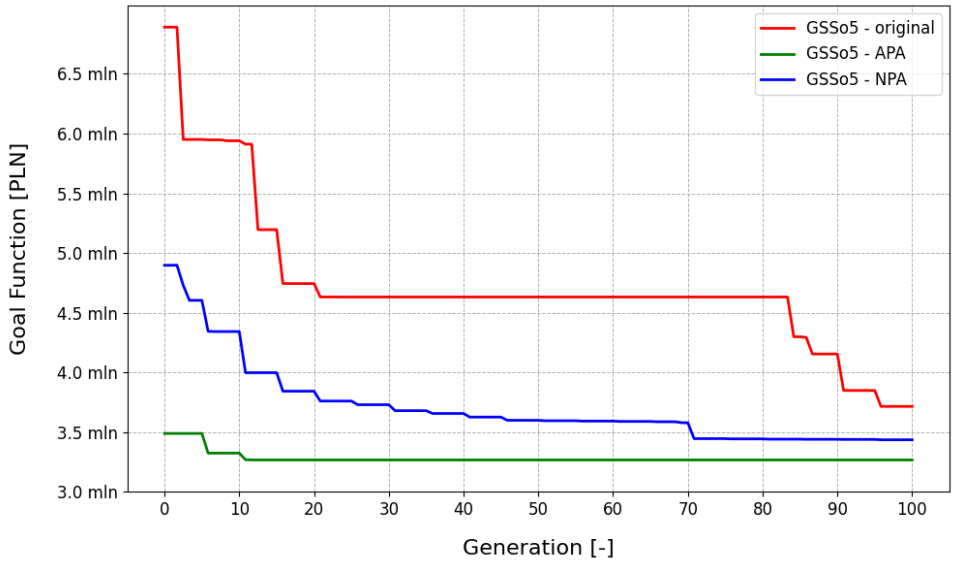

Figure D.26 Goal function values progression comparison of the impact of final geometry application from the previous optimization cycle as one of the initial geometries in the first generation

The GF paths of the reference geometry and NPA had similar trend with the greatest improvement at the beginning, then minor or lack of improvement in the middle part and another improvement at the end of the test, Fig. D.26. The APA's GF path had the improvement at the very beginning and remained unchanged after 10th generation. The starting point was lower than the endpoint from the reference path.

D.8 Identical arrangement in the initial stage

In this test, the topology of the existing bridge was used as an example. This topology was manually added to the initial generation. In the reference test, the geometry of the arch, tie and hangers including steel grades was similar to the original bridge, but the remaining geometries were default with different types of topology as in Sec. D.4. The second test kept the topology of hangers as in the reference example, but all other dimensions and parameters were chosen randomly without predefined set of geometries. The impact of random population was investigated.

The choice was a bridge located in Åkvik Sound in northern Norway and designed by Tveit in 1999 but redesigned by Teich and Wendelin in 2001 [117, 113], called Åkvik Sound network arch, Fig. D.27. The span length was 135 m, the height 20.25 m and arches' axial spacing of 7.55 m. The arch was made of profile UC 356x406x467 and steel grade S460. The tie was a concrete post-tension slab. The main parts in the arches' plane had dimensions of 500 mm x 827.5 mm. The slab in between was two-sided inclined from 240 mm to 280 mm in the middle. Additional one-sided pavement was 2050 mm width and thick from 180 mm to 140 mm. The concrete class was C35/45. Hangers were 55 mm in diameter and steel grade was assumed as S460.

a) Topology of hangers

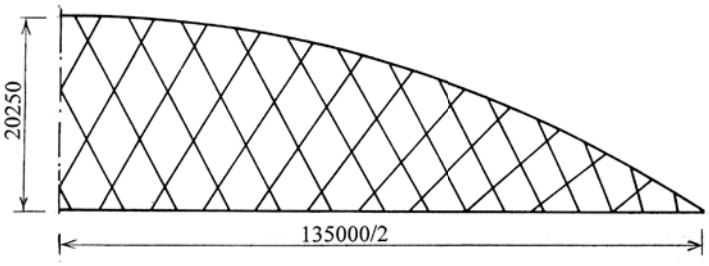

b) Deck and arch geometry

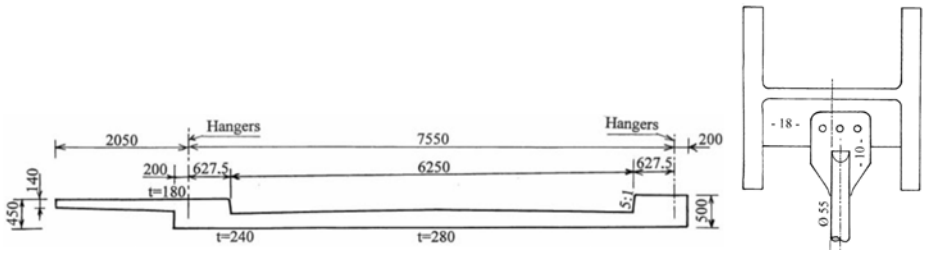

Figure D.27 Topology of hangers, deck and arch geometry in Åkvik Sound NAB [117, 113]

Since the model was not prepared for concrete slab, the cross section area and bending moment of inertia were determined for each of the main longitudinal edge beams made of concrete C35/45. This two properties were considered as the most important from the mechanical

properties of the bridge perspective, since NAB used to act mainly axially and lateral stiffness determined the load distribution between arch and tie through hangers. Similar procedure was used when determining parameters of the circular arch from UC profile. The remaining part of the slab plus additional layers for road and pedestrians and symmetrical pedestrian path distribution were treated as self-weight load resulted in 56.5 kN/m per side. hangers' topology was determined based on the photos from the literature and preparing 2D drawings following lines from the pictures.

Additionally skewback were added at the end of the bridge. The impact of those was investigated in Sec. D.9. Skewbacks were intended to be as stiff as possible and 1.0 m of thickness was decided to be enough for this reasons. Their length was 4% of span length and C35/45 of concrete class. They were not designed and were intended to increase stiffness at the ends of the bridge decreasing bending moments in these regions.

a) Topology of hangers and bridge geometry

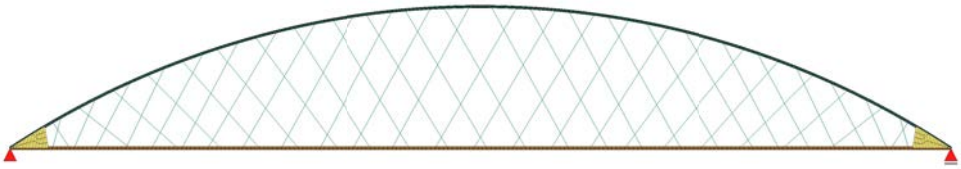

b) Deck and arch geometry - thickness 60 mm and 75 mm - diameter 375 mm and 500 mm

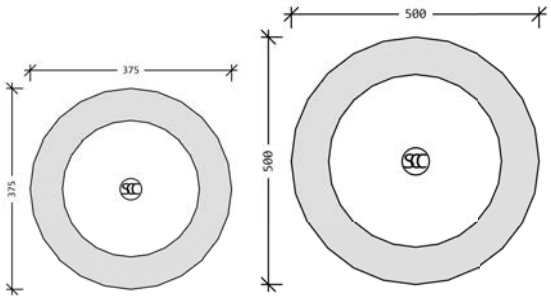

Figure D.28 Topology of hangers, deck and arch geometry in SOFiSTiK model

After the first calculations, the utilization was too high for the default variable loads. It was decided to gradually decrease applied load and increase arch and tie cross sections. Until reaching enough capacity to carry loads. As a result, the arch had diameter 375 mm and 60 mm of thickness, the tie was 500 mm in diameter with the thickness of 75 mm and hangers with 64 mm in diameter. All steel elements had S460 grade. The applied variable load was changed to 78 kN/m. The geometry was presented in Fig. D.28.

The presented geometry was manually added to the both tests. The remaining part of the population in the reference test had the same geometries as in Sec. D.4. The second test had random geometries except hangers' topology, which was same as the reference geometry. Several examples were presented in Fig. D.29.

The presented geometries were significantly more massive or a mixture of massive and light parts. This diversity was desired. All of the geometries were adjusted each time to keep their utilization below 100%. For this reason, the cross sections dimensions were gradually increased until fulfilling this criteria. The results were presented in Tab. D.8 and Fig. D.30.

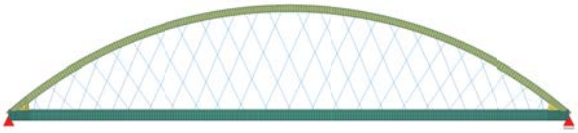

(a) Example 1

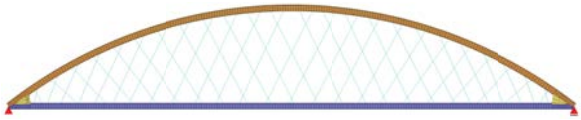

(b) Example 2

(c) Example 3

Figure D.29 Several examples of geometries in the initial generation for the random geometry test

(a) Existing geometry

(b) Reference test result

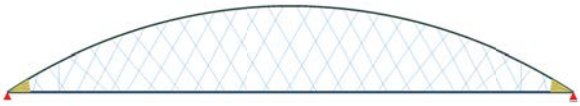

(c) Random test result

Figure D.30 Geometry comparison of the existing one with the reference and random tests

Table D.8 Comparison between the existing geometry, results from reference and random tests

	existing	reference	random
arch diameter [m]	0.375	0.375	0.375
arch thickness [m]	0.060	0.060	0.060
tie diameter [m]	0.500	0.500	0.500
tie thickness [m]	0.075	0.065	0.065
hanger diameter [m]	0.064	0.056	0.056
hanger number [-]	48	48	48
bridge height [m]	20.25	20.45	20.45
arch steel	S460	S460	S460
tie steel	S460	S320	S320
hanger steel	S460	S320	S320
buckling factor [-]	0.93	0.91	0.91
utilization arch [%]	98.34	99.99	99.99
utilization tie [%]	83.97	99.34	99.34
utilization hanger [%]	49.56	92.81	92.81
utilization deflection [%]	81.46	95.38	95.38
utilization all [%]	98.34	99.99	99.99
cost [PLN]	4,177,481	3,743,785	3,743,785
goal function [PLN]	4,177,481	3,743,785	3,743,785

The most noticeable results was the same resultant geometry for both reference and random tests. It meant, that the best individual was improved by gradual gradient descent method every 5th generation and the remaining geometries did not managed to reach better result than that. From the parameters point of view, the cost reduction was done by decreases of the tie thickness from 0.075 m to 0.065 m, hangers diameter reduction from 0.064 m to 0.056 m, bridge height increase from 20.25 m to 20.45 m and steel grade reduction for tie and hangers from S460 to

S320. From the topology perspective, the hangers remained the same in the middle part of the bridge, but changed in the regions close to skewbacks, where 3 hangers where rotated to more vertical position, Fig. D.30a and b.

The buckling factor was reduced in this process from 0.93 to 0.91. The utilization was improved for each element and even deflection utilization was above 90%, but at the same time the span length was much greater than in the previous analysis, so it was harder to compare this aspect directly. All elements utilization was above 92% for both reference and random tests. The GF value was improved by 10.3%.

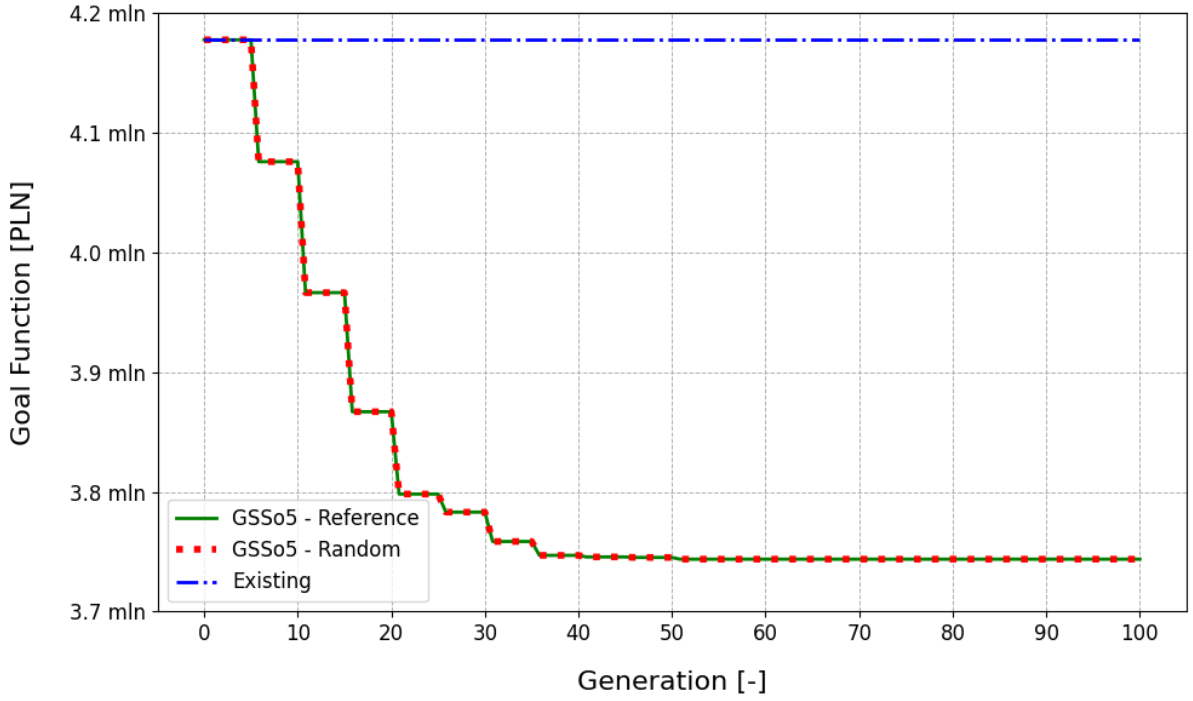

Figure D.31 Goal function values progression comparison of between reference and random tests with marking the existing geometry as constant

The GF value progression was presented in Fig. D.31. As expected, the reference and random paths covered each other and gradient determined it, since each of the steps occurred every 5 steps as it should happen in GSSo5 procedure. The major improvement was caused by steel grade reduction for tie and then for the hangers up to 35th generation. Then there were 4 more steps correlated with hangers position change between 40th and 55th generation, but with much smaller magnitude. After that, no progression occurred.

In order to compare the two tests, it was decided to analyze GF value progression over generations for geometries other than the best in the given generation. For these reasons, the graphs presenting the GF value of top 10 individuals from each generation were presented in Fig. D.32 and Fig. D.33. That gave the general overview of the best cases. In both graphs, the buffer zone could be observed between the GF value level of the best individual equal about 4 mln PLN and about 6-7 mln PLN range for reference test or about 5 mln PLN for random test. In this zone, the individuals closer to the best solution used to almost point-wise reach the best individual and then, after mutations and crossings, returned back to the top level of the buffer zone. For the reference test, the point-wise attempts were more often and distributed more evenly along all of the generations in comparison to random test with more concentration at the first half of simulation. The first top ten results in random test were more

compacted in terms of GF value range than reference test. In the random test, this range was mostly between 5 mln PLN and 8 mln PLN, when in the reference test between 6 mln PLN and 13 mln PLN. That might have concluded in more consistency in random test over predefined reference test and resulted in providing better GF value. In order to investigate this phenomenon, the statistic analysis of the whole population was conducted and example graphs were presented in Fig. D.34-D.35.

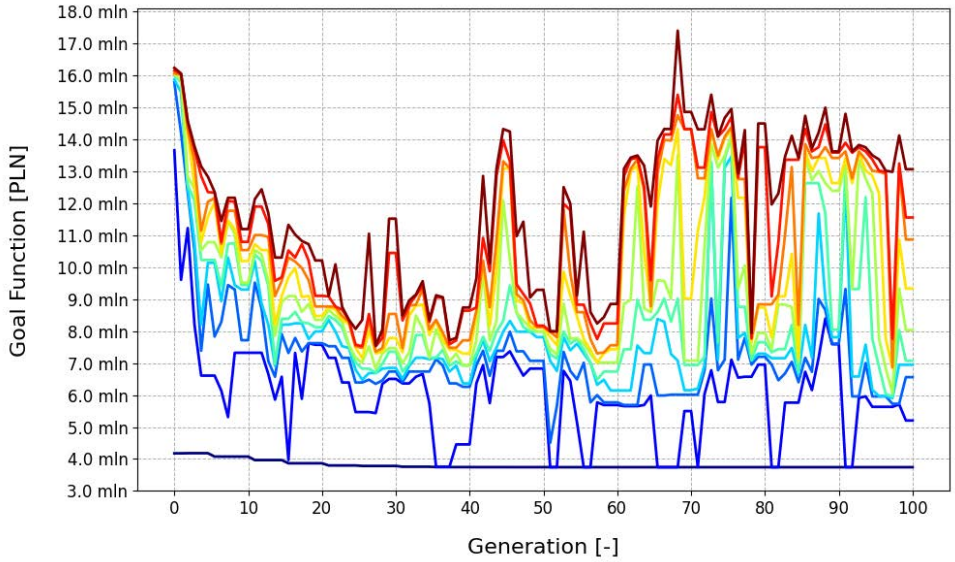

Figure D.32 Goal function values distribution for the best 10 results from reference test

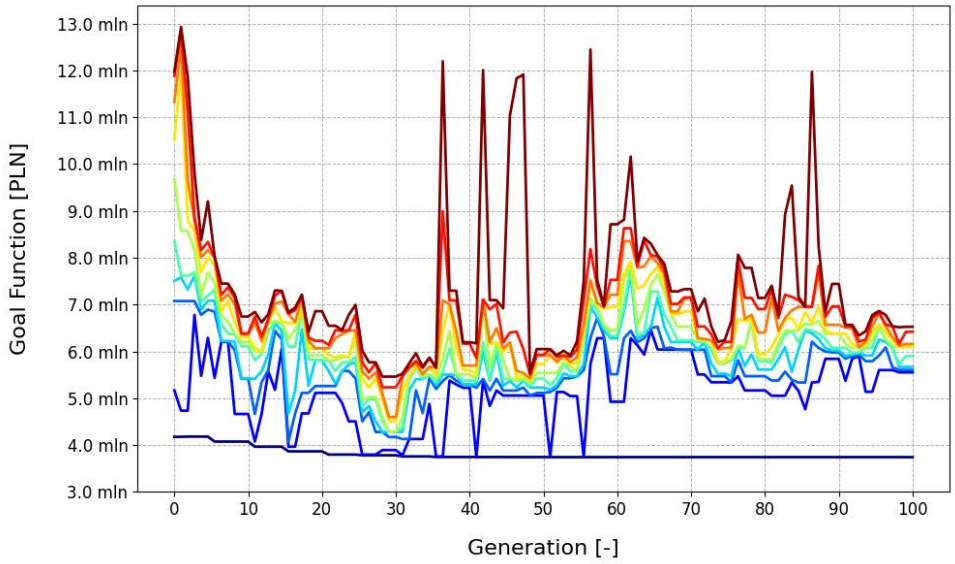

Figure D.33 Goal function values distribution for the best 10 results from random test

The graphs in Fig. D.34 and Fig. D.35 presented the histograms and continues PDF of GF value for the initial and the last generation. In the first step, the histogram was plotted and the higher concentration of GF value was present closer to the lower GF value as it was presented in Fig. D.32 and Fig. D.33. At the same time, there where significantly fewer number of individuals with much higher GF value. The histogram distribution was similar to Log-Normal PDF distribution and was approximated in this way. The top sub-graph was analyzed,

but since the Log-Normal tail was relatively long, it disturbed the analysis by a significant increase of standard deviation and mean value and resulted in negative values after subtracting standard deviation from the mean value, which were marked as purple and yellow vertical lines respectively. In order to limit their influence, the last 20% of the population was deleted from the system, which was marked with the green vertical line and red histogram bars, and the best 80% was analyzed again with the same approach. The mean value, standard deviation, median and mode values were investigated. The median value used to be less affected by the population reduction mechanism than the remaining parameters, which was expected from the definition of them. This method was repeated for all generations and for both tests. The results were presented in Fig. D.36-D.37.

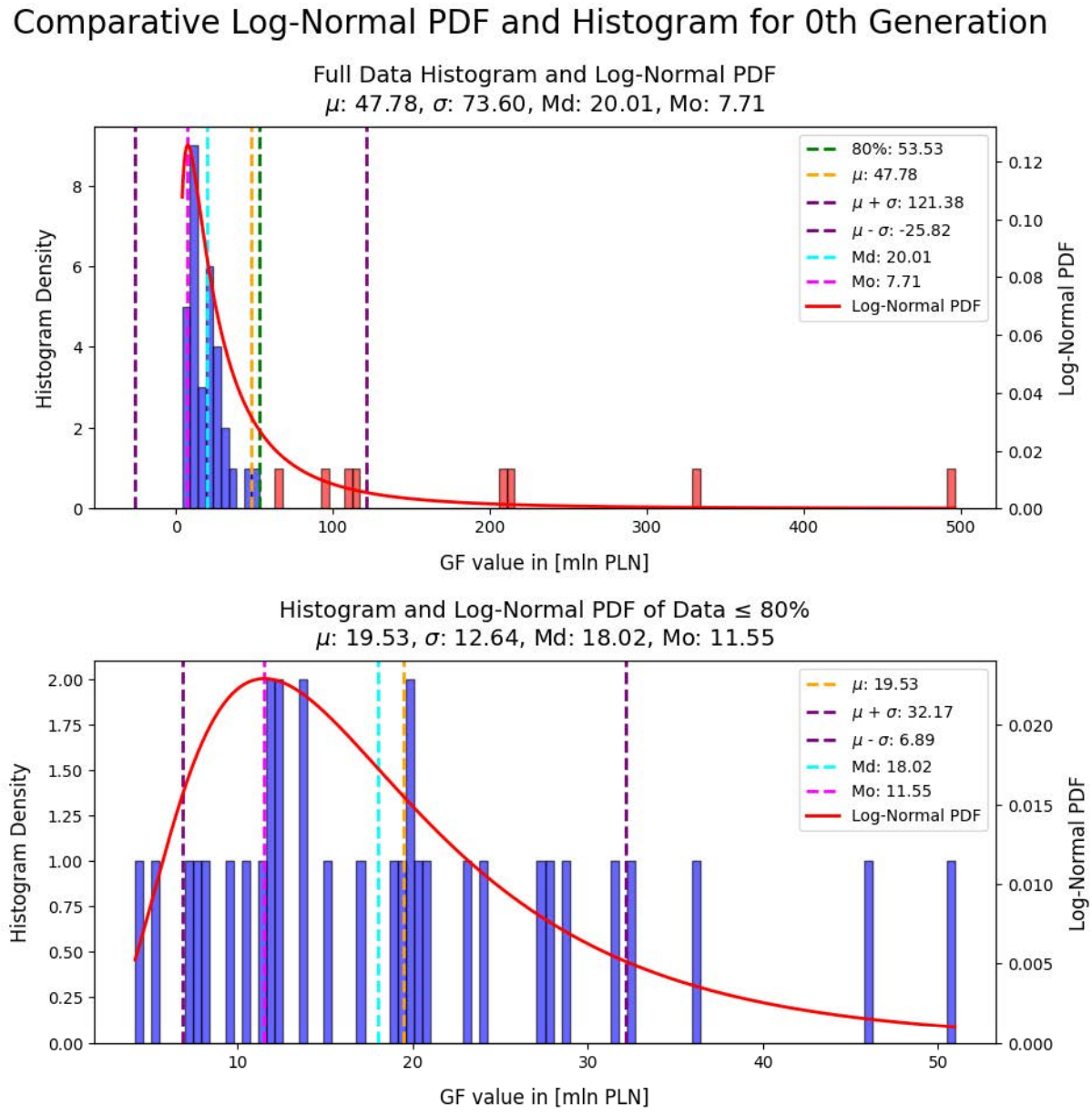

Figure D.34 Comparative log-normal PDF and histogram for 0th Generation in random test

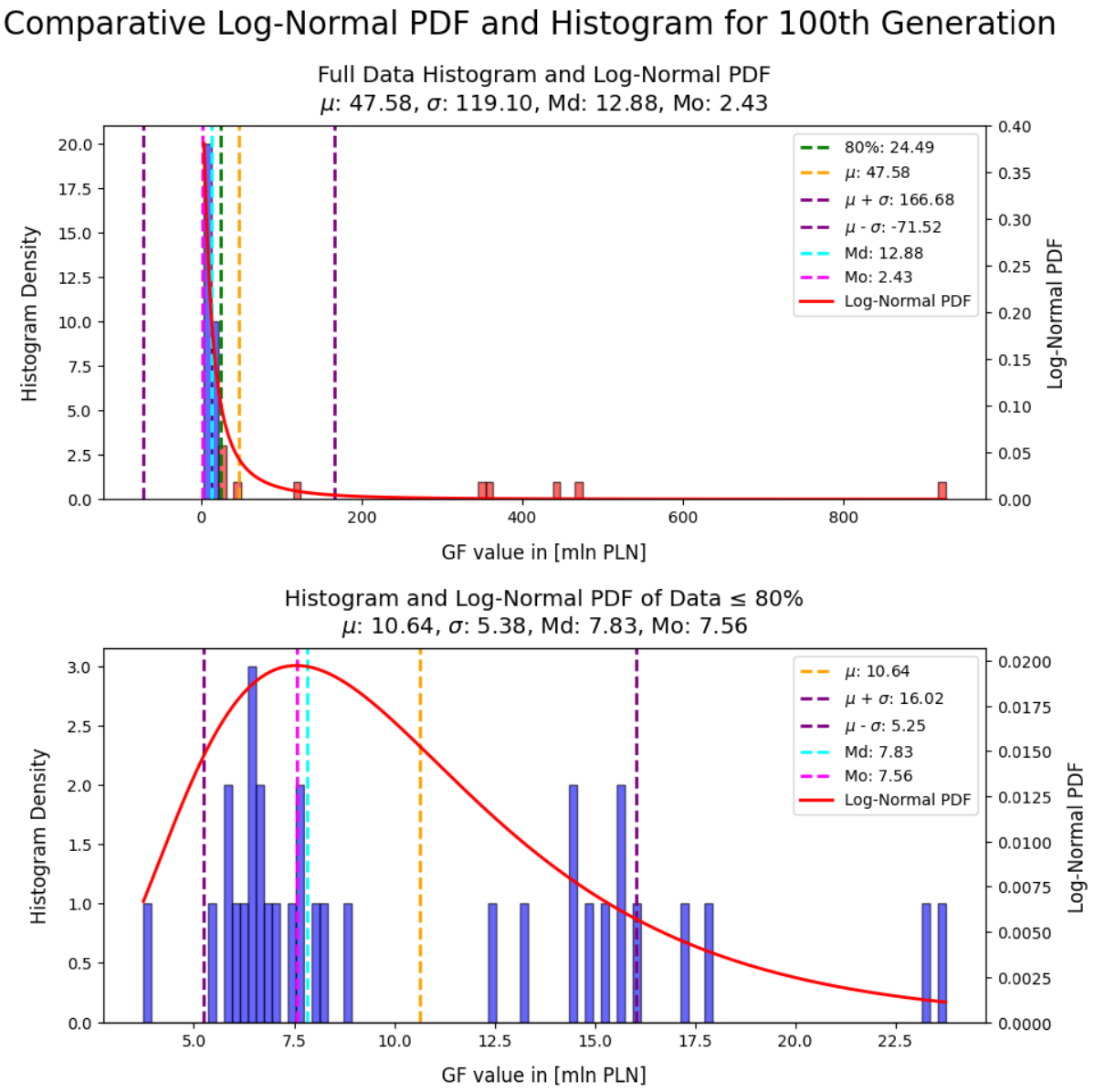

Figure D.35 Comparative log-normal PDF and histogram for 100th Generation in random test

The results in random test were significantly better in almost any aspect. The mean value was similar at the very beginning of the simulation until 60th generation, but standard deviation and median values were noticeably lower in random test. The values started to deviate after the 60th generation in the reference test. The mean value peaked at 70 mln PLN and almost 190 mln PLN including standard deviation. In the contrary, random test maximum mean value at 22 mln PLN level and 44 mln PLN including standard deviation. Median was less affected by the divergence of results, and kept in 10-26 mln PLN range in the reference test and 6-16 mln PLN after excluding the first few generations.

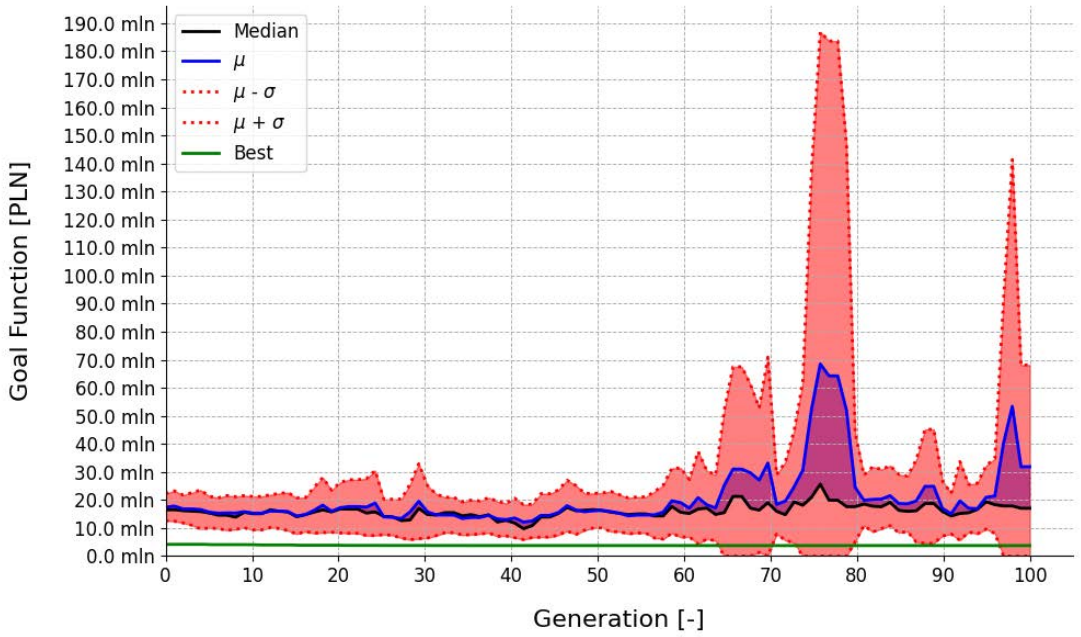

Figure D.36 GF value progression of the first 80% of each population over generations including median and mean values with deviation. Results for reference test

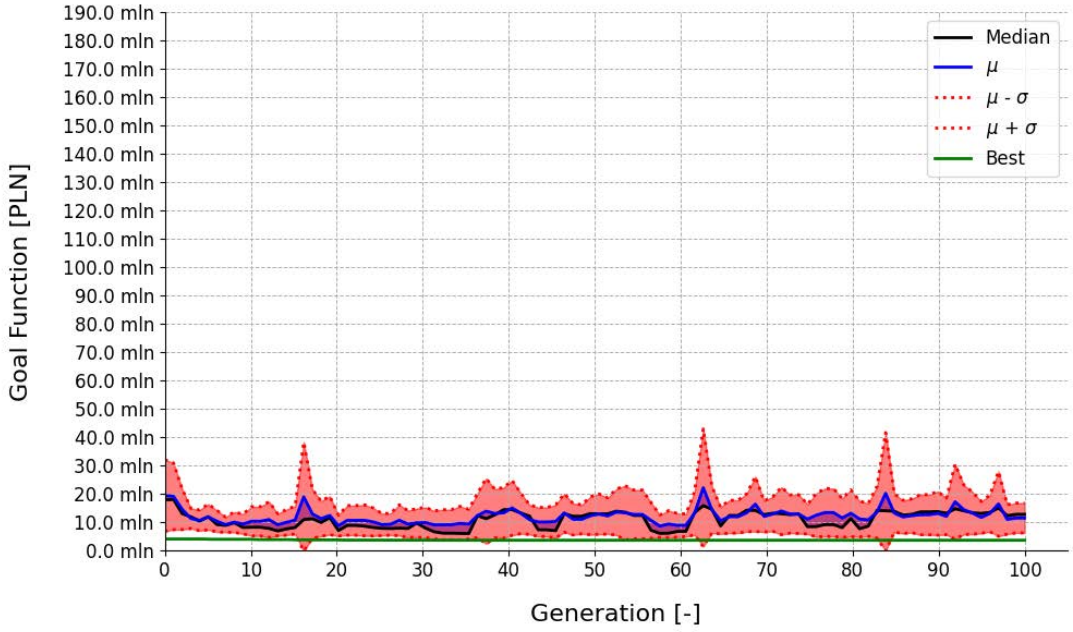

Figure D.37 GF value progression of the first 80% of each population over generations including median and mean values with deviation. Results for random test

D.9 Skewbacks impact

The impact of skewbacks addition was investigated. For this reasons, the two test were conducted. The first test contained skewbacks and the second did not. Since the random test was conducted once, it was decided to use random populations. The topology of hangers from the reference Åkvik Sound bridge was implemented the same for all of the geometries as it was done in Sec. D.8. The remaining parameters were random except one manually added reference bridge. The applied variable load was reduced from 78 kN/m to 48 kN/m due to the increase of the utilization in the endings regions of the bridge, where higher bending moments occurred. That implicated lack of possibility to directly compare the best results over generations with previous tests from Sec. D.8. The results were presented in Tab. D.9, Fig. D.39 and Fig. D.38.

Table D.9 Comparison between the existing geometry of Åkvik Sound bridge, results from the tests with skewbacks and random population (SK) and without skewbacks and random population (NSK)

	Åkvik	SK	NSK
arch diameter [m]	0.375	0.375	0.375
arch thickness [m]	0.060	0.060	0.060
tie diameter [m]	0.500	0.500	0.400
tie thickness [m]	0.075	0.065	0.060
hanger diameter [m]	0.064	0.056	0.042
hanger number [-]	48	48	48
bridge height [m]	20.25	20.45	20.45
arch steel	S460	S460	S460
tie steel	S460	S320	S355
hanger steel	S460	S320	S460
buckling factor [-]	0.93	0.91	0.88
utilization arch [%]	98.34	99.99	99.98
utilization tie [%]	83.97	99.34	97.92
utilization hanger [%]	49.56	92.81	91.74
utilization deflection [%]	81.46	95.38	40.31
utilization all [%]	98.34	99.99	99.98
cost [PLN]	4,177,481	3,743,785	3,249,656
goal function [PLN]	4,177,481	3,743,785	3,249,656

As mentioned, the resultant GF value should not be compared, since the variable load was different. Nevertheless, the algorithm optimized the structure not mainly in the material grade reduction, as it was executed in Sec. D.8, but reduced significantly the diameter of the hangers and cross section area of the tie. The utilization were above 90% except deflection, which was just above 40%. The cost was significantly reduced by another 13% despite reducing the total weight including variable loads from 21.1 MN to 15.9 MN, so 24.6% reduction. The topology of hangers changed more than previously, Fig. D.39, but not significant. The hangers remained network-type along the whole bridge, even in close distance to the ends, which was usually directed into vertical topology. The middle part got less dense with hangers, as well as endings. There was also position change of the hangers in a distance of approximately 1/4th of the span length from the endings.

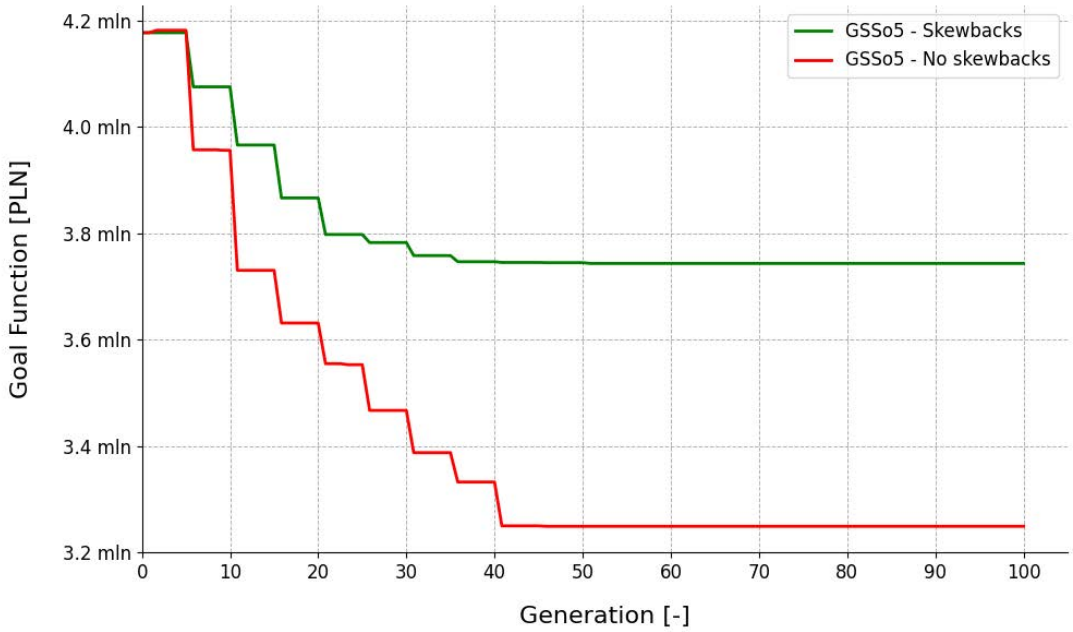

Figure D.38 Goal function values progression comparison of between random skewback and no skewbacks tests

The GF value progression over generations was presented in Fig. D.38. The trend was similar in both case with all of the progression happened in the first half of the simulation, but since test without skewbacks had greater margin of safety in capacity, the progression was faster.

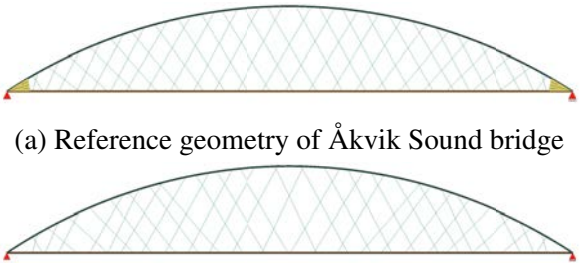

(a) Reference geometry of Åkvik Sound bridge

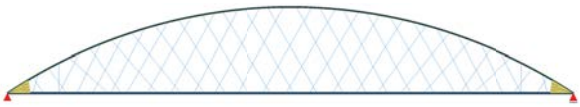

(b) Random test result with skewbacks

(c) Random test result without skewbacks

Figure D.39 Geometry comparison of the existing one with the random tests with skewbacks and without them

In Fig. D.40 and Fig. D.41 the GF value distribution over generations for the first 10 the best result sets were presented. Both tests resulted in similar scale of deviation with the greater distribution in the first 5 generations. After that, the paths had several peaks into greater GF values but stabilized rapidly after that in a matter of couple generations. The test without skewbacks had greater number of point-like contacts to the best GF path than the second test. Moreover, these approaches were evenly distributed across generations, where in the second test it was limited to the first half. From these approaches, three managed to improve the best path at 61st, 81st and 96th generations. The example of the best individual before and after 61st generation was presented in Fig. D.42. Even though both of them had the same GF values, the algorithm chose the best geometry with the lowest ID number which reached the same GF value as the best individual in he current generation. Usually the best individual had ID number 0 the longer it had remained the leading geometry, so the new best individual usually should have better GF value to become new leading geometry. Their hangers' topology had minor differences at about 1/4th of bridge span length. In the previous leading geometry, the left skewed single zone of

greater spacing was present, but in the new leading individual it was right skewed from the left side perspective. The second difference was for the lest two hangers, where they were crossed in the previous leading and converged at the arch in the alternative leading geometry. No more differences were observed. Similar conclusions could be made for the 81st and 96th generation presented in Fig. D.43 and Fig. D.44. The alternatives were literately the same, which showed algorithm's consistency in searching for the best alternatives and that no much possibilities were left for the best geometry looking at the 99.98% utilization of the arch.

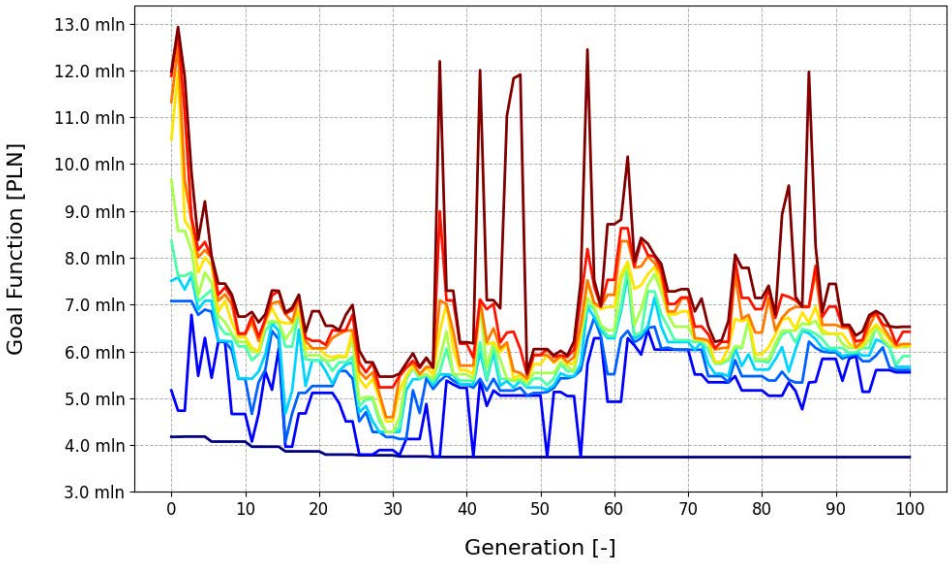

Figure D.40 Goal function values distribution for the best 10 results from random test with skewbacks

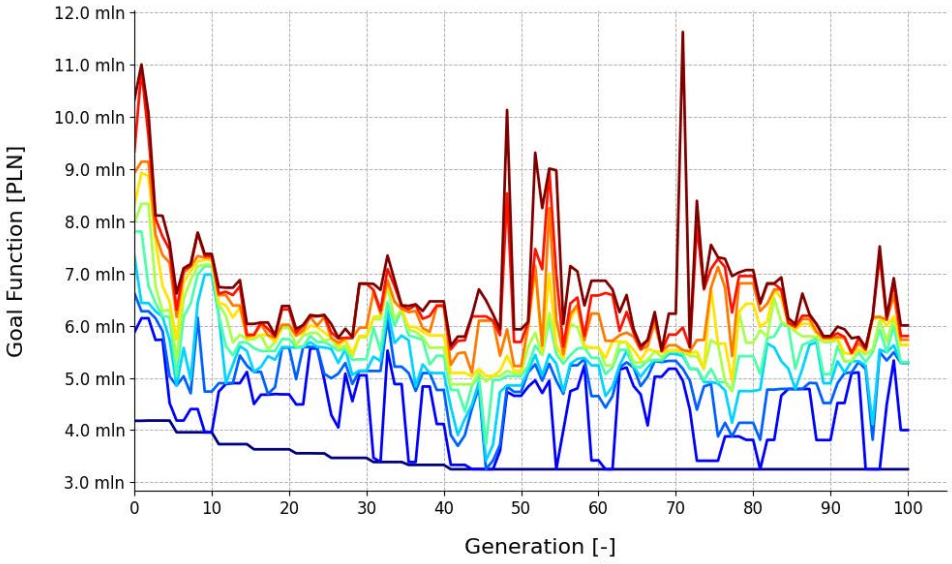

Figure D.41 Goal function values distribution for the best 10 results from random test without skewbacks

(a) Best geometry before the 61st generation - GF value of 3,249,656 PLN

(b) Alternative best geometry at the 61st generation - GF value of 3,249,656 PLN

Figure D.42 Geometry comparison of the best individual (a) before the 61st generation and (b) alternative best at the 61st generation

(a) Best geometry before the 81st generation - GF value of 3,249,656 PLN

(b) Alternative best geometry at the 81st generation - GF value of 3,249,656 PLN

Figure D.43 Geometry comparison of the best individual (a) before the 81st generation and (b) alternative best at the 81st generation

(a) Best geometry before the 96th generation - GF value of 3,249,656 PLN

(b) Alternative best geometry at the 96th generation - GF value of 3,249,656 PLN

Figure D.44 Geometry comparison of the best individual (a) before the 96th generation and (b) alternative best at the 96th generation

Similarly as in Sec. D.8, the log-normal distribution was used in order to represent analytically the probability distribution of the each generation. The examples were presented in Fig. D.45 and Fig. D.46 for the 1st and the 100th generation distributions. The first 80% was chosen from the whole population, since some of the individuals were significantly worse than the most of the population. This significance meant sometimes two order of magnitude difference. After this reduction, the reduced histogram with its log-normal PDF was defined again. The mean, deviation and median were determined to statistically analyze the population over generations. The results were presented in Fig. D.47 and Fig. D.48.

Since both test had different variable loads, the range of variety might be different. The mean and median values oscillated between 7.5 mln PLN and 20 mln PLN for the test with skewbacks and between 6 mln PLN and 17.5 mln PLN for the test without skewbacks. The peak value including deviations were 43 mln PLN for skewback test and 35 mln PLN for no skewback test. These differences laid in the range between 13% of load reduction and 24.6% of weight reduction. In both cases the deviation was high for the first generations and then stabilized. The most noticeable peaks occurred 3 times for the skewback test and 2 times for no skewback test, but this difference was too minor to make any distinguished conclusion. The median and mean values seemed to be in an increasing trend over generations for the skewbacks test and increasing-deceasing trend for the no skewbacks test.

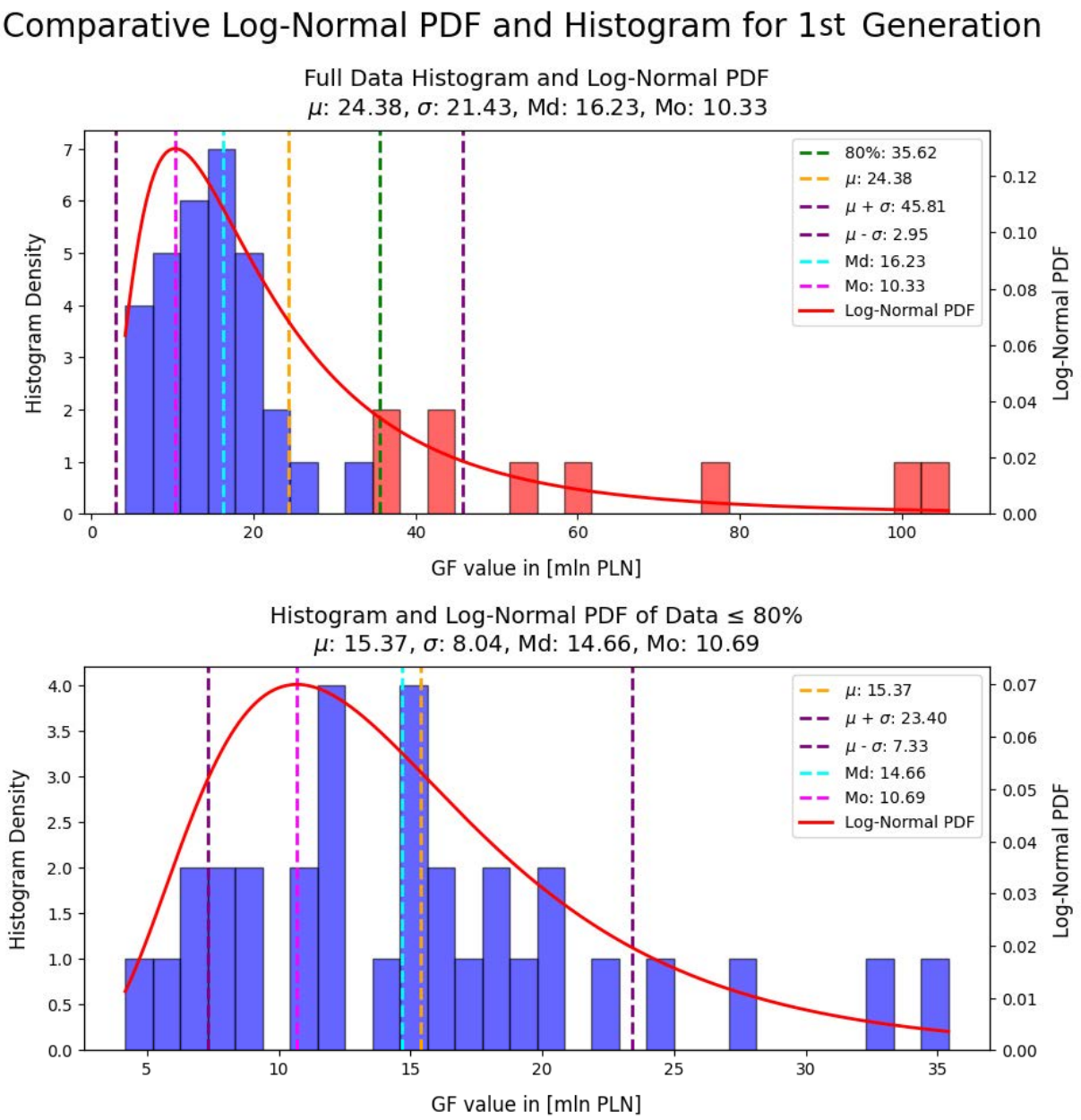

Figure D.45 Comparative log-normal PDF and histogram for 1st Generation in random test without skewbacks

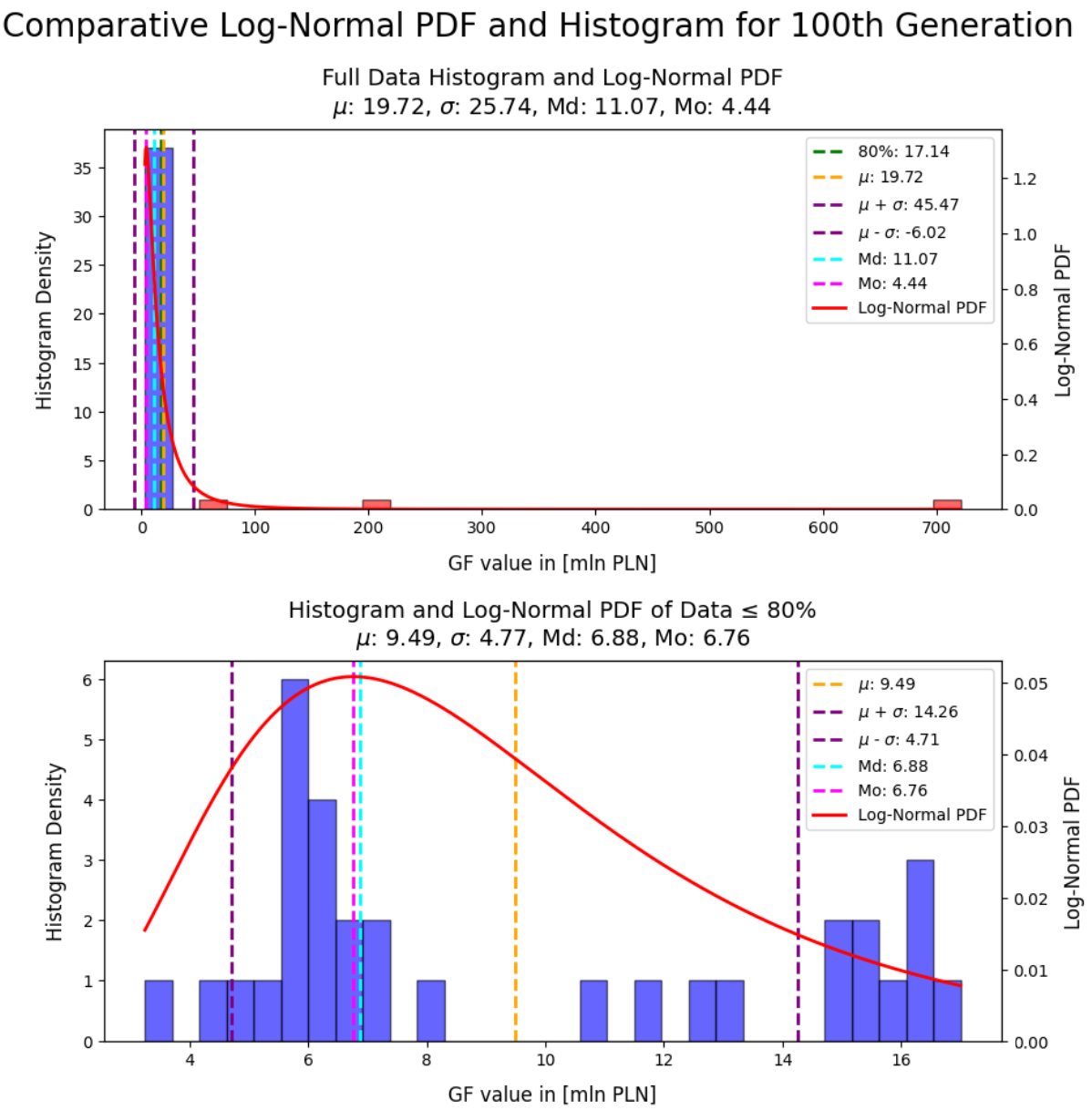

Figure D.46 Comparative log-normal PDF and histogram for 100th Generation in random test without skewbacks

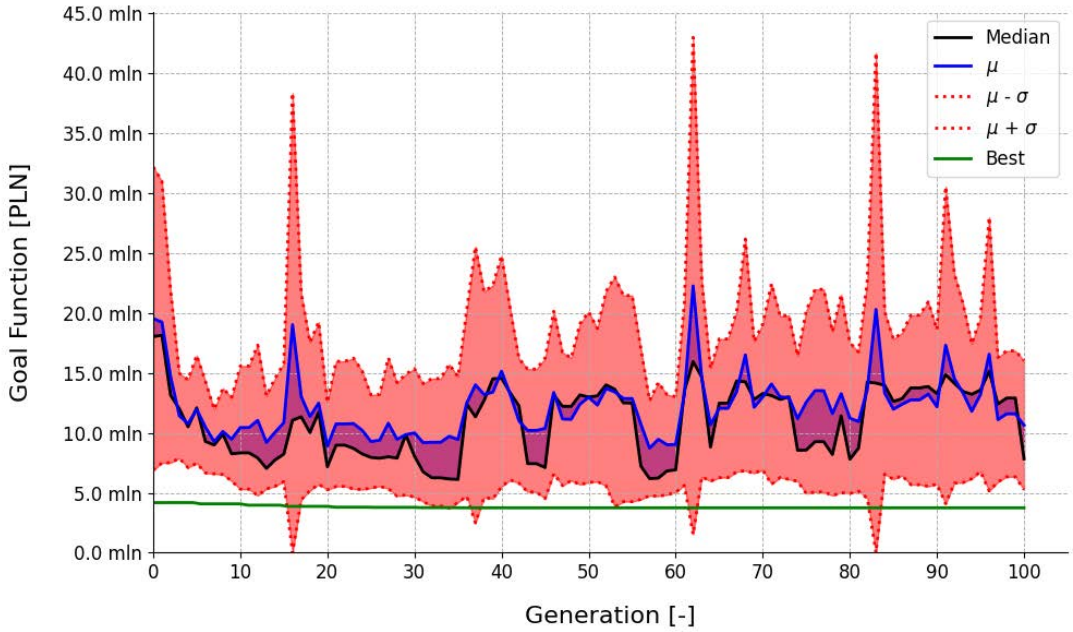

Figure D.47 GF value progression of the first 80% of each population over generations including median and mean values with deviation. Results for random test with skewbacks

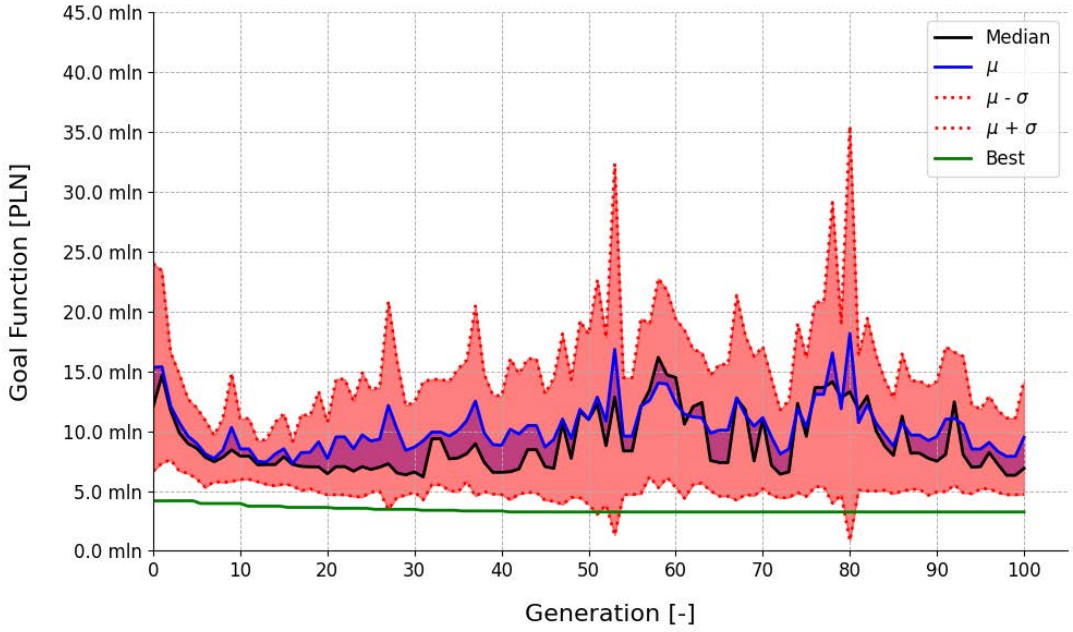

Figure D.48 GF value progression of the first 80% of each population over generations including median and mean values with deviation. Results for random test without skewbacks

a) Full load

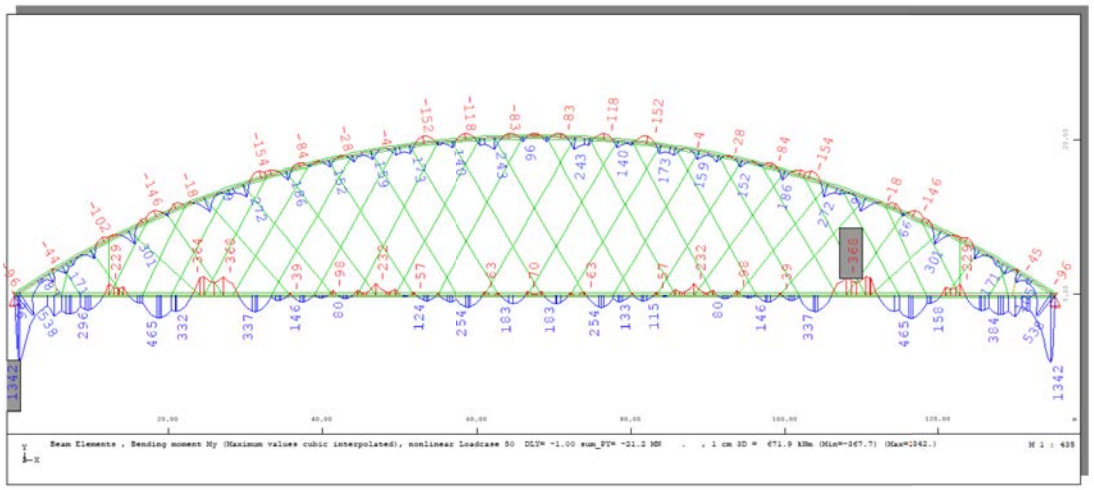

b) Half load

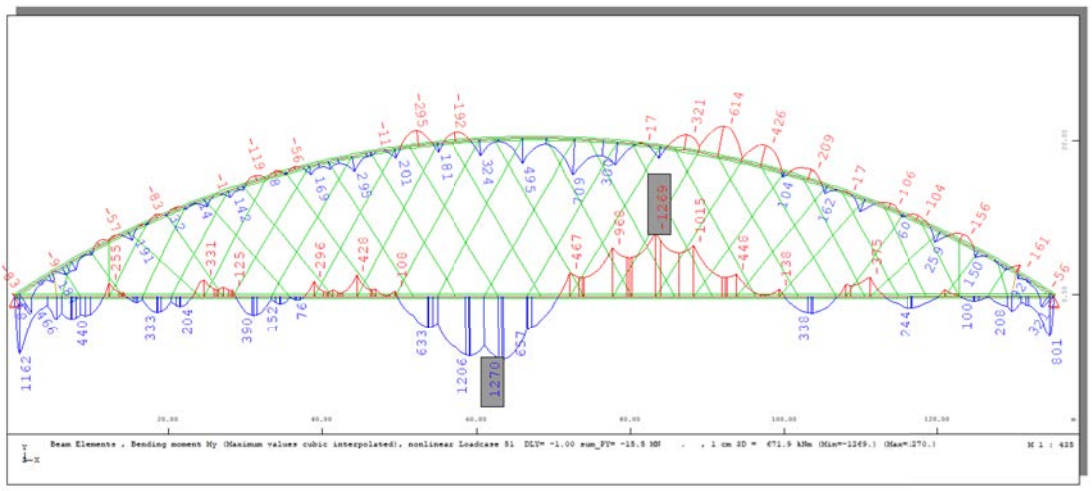

Figure D.49 Bending moments for the best individual with skewbacks

The main advantage of skewbacks should have been reduction of bending moments in the endings of the arch and tie. However in this case the greater bending moments occurred for the skewback test comparing to no skewback test, Fig. D.49 and Fig. D.50 respectively. This result was disturbed by applying different variable loads, as mentioned at the beginning of this section. If the variable loads were the same, the bending moments for no skewbacks case would have been greater than for the case with skewbacks and that was the reason of variable load reduction. Otherwise the reference bridge with the greater variable load exceeded capacity. The skewbacks made the bending moments in the middle of the tie almost matching the bending moment near the supports, Fig. D.49. The arch had maximum bending moments around the middle of the span length. In case of no skewbacks, the maximum bending moments occurred for both the arch and the tie above the supports, Fig. D.50, including half and full loaded deck.

a) Full load

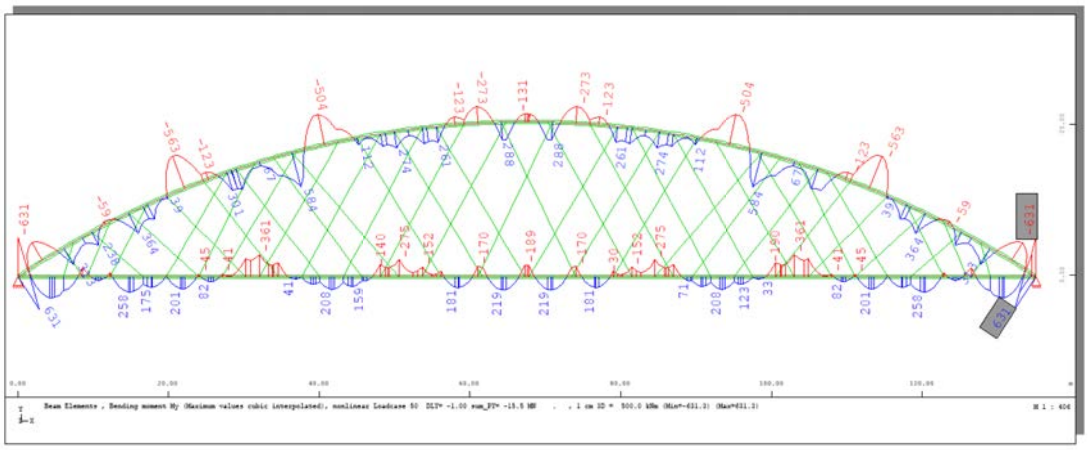

b) Half load

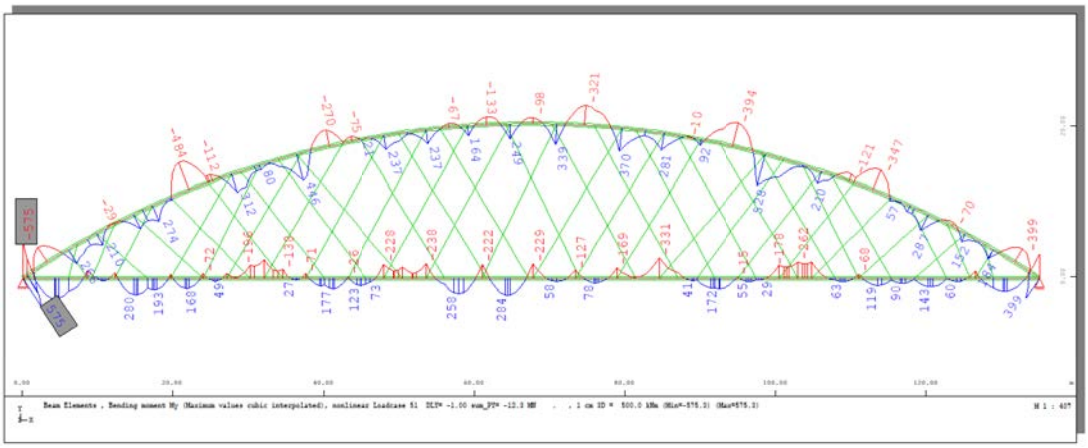

Figure D.50 Bending moments for the best individual without skewbacks

E The simulations' permanent arrangements in the initial population

This section includes the hangers' arrangements included in the initial population in the second optimization algorithm, as well as the extended center lines of hangers' pairs in order to present, that 3-focal-points concept, present in the MVADM arrangement, is no included in the initial population.

a) 20 pairs - 40 hangers

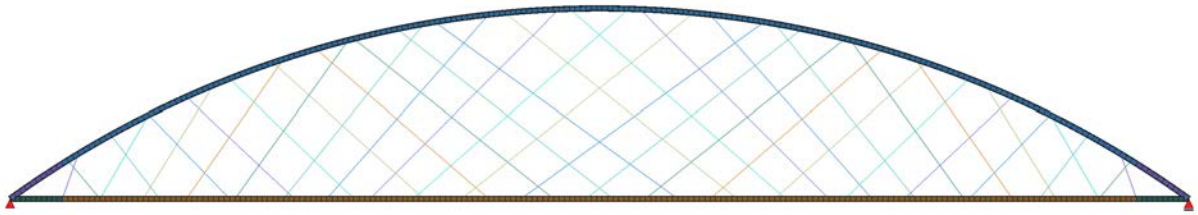

b) 18 pairs - 36 hangers

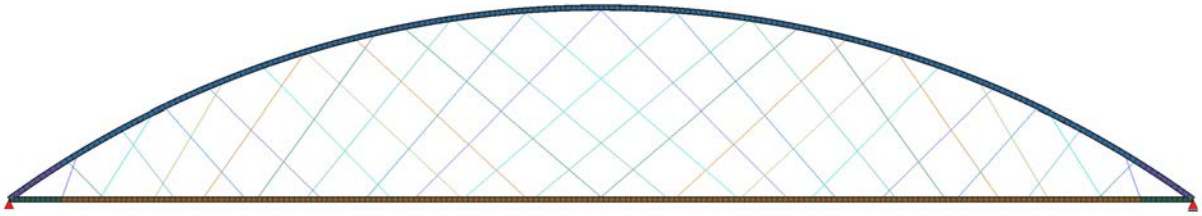

c) 16 pairs - 32 hangers

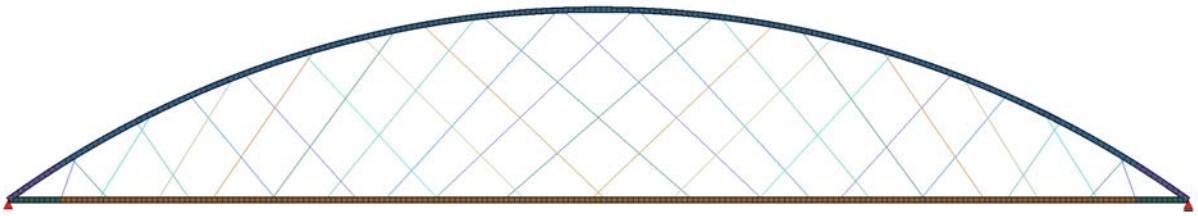

d) 14 pairs - 28 hangers

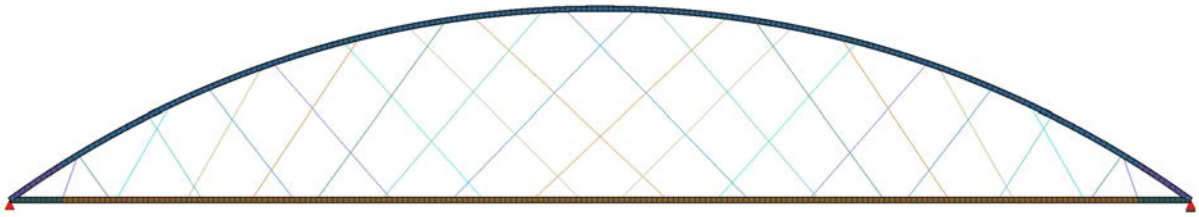

Figure E.1 The samples of the permanent arrangements present in the initial population in the simulations

e) 12 pairs - 24 hangers

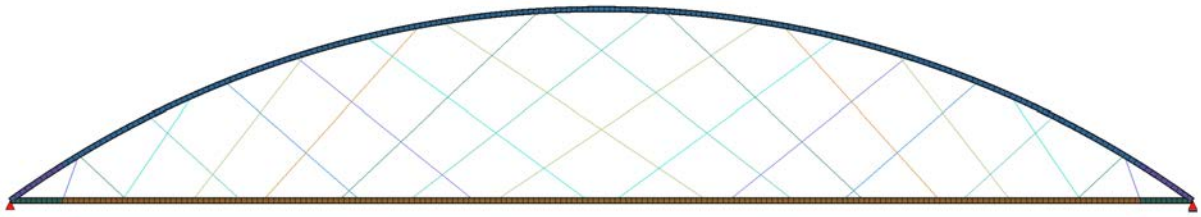

f) 10 pairs - 20 hangers

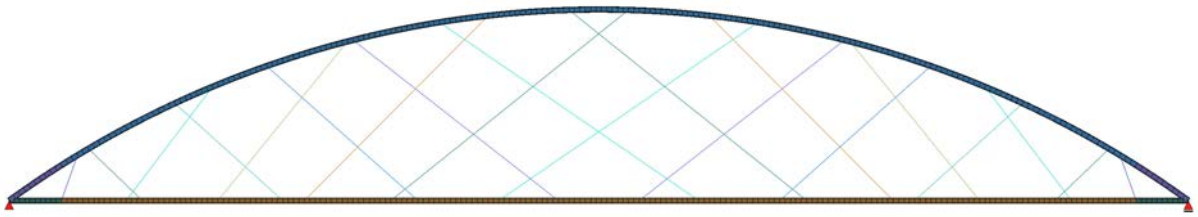

g) 8 pairs - 16 hangers

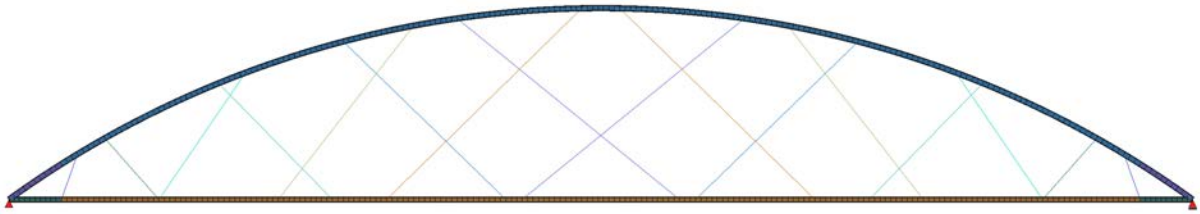

h) 6 pairs - 12 hangers

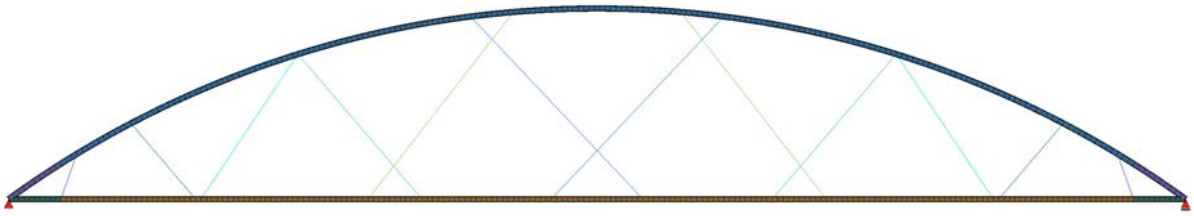

Figure E.2 The samples of the permanent arrangements present in the initial population in the simulations

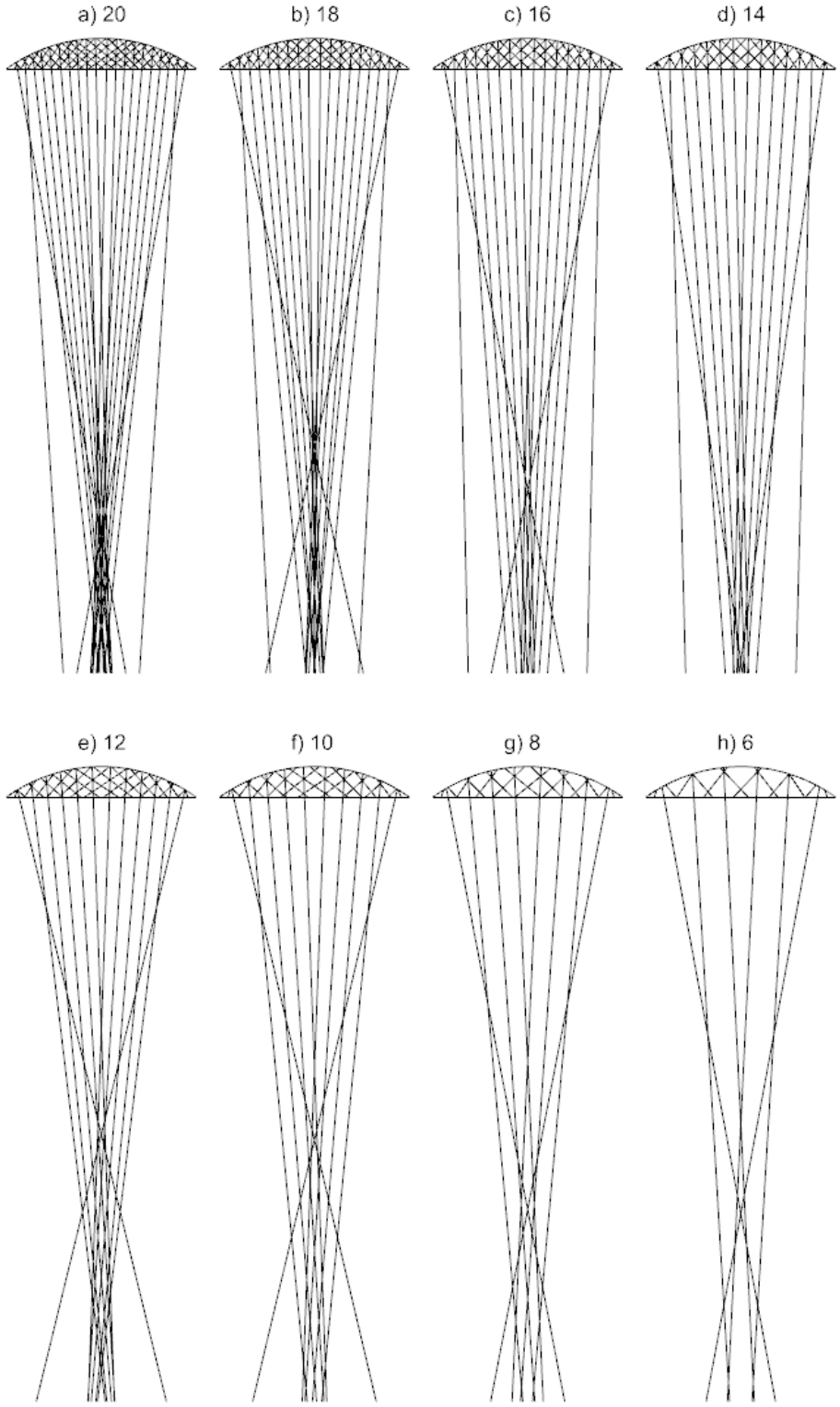

Figure E.3 The center lines from all the samples of the permanent arrangements present in the initial population in the simulations - described by number of number of hangers pairs

F The best results from the simulations

This section includes the best geometries from the simulation for each considered pair of span length and deck width.

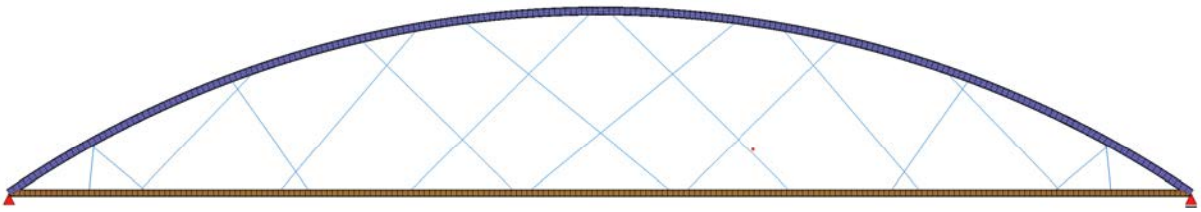

(a) Span length 100 m - deck width 3 m

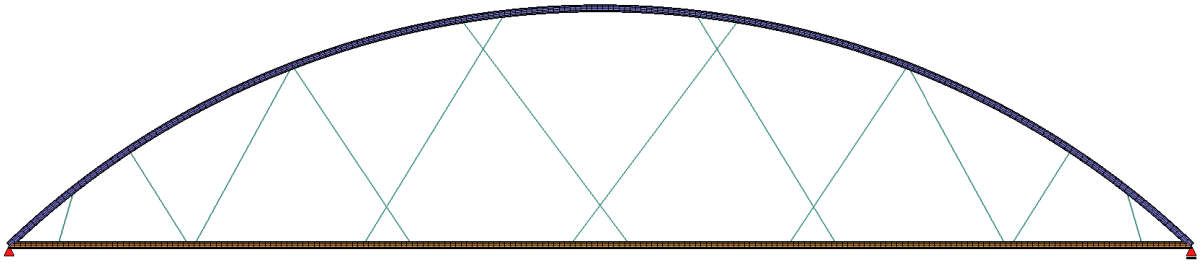

(b) Span length 100 m - deck width 6 m

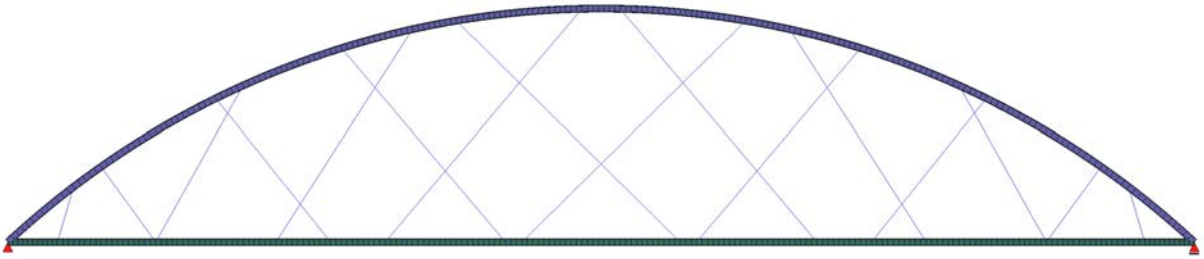

(c) Span length 100 m - deck width 9 m

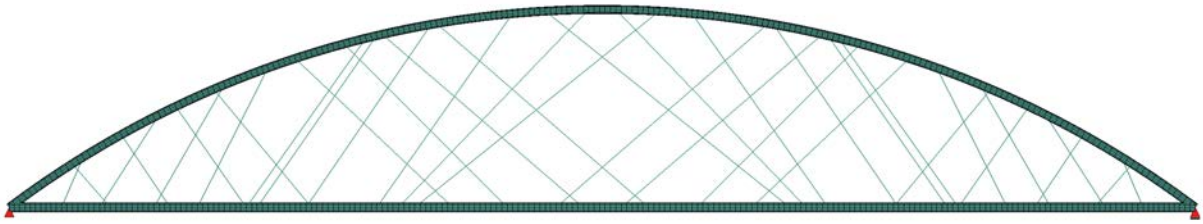

(d) Span length 100 m - deck width 12 m

Figure F.1 The best geometries for span length of 100 m with deck width of 3 m, 6 m, 9 m and 12 m respectively

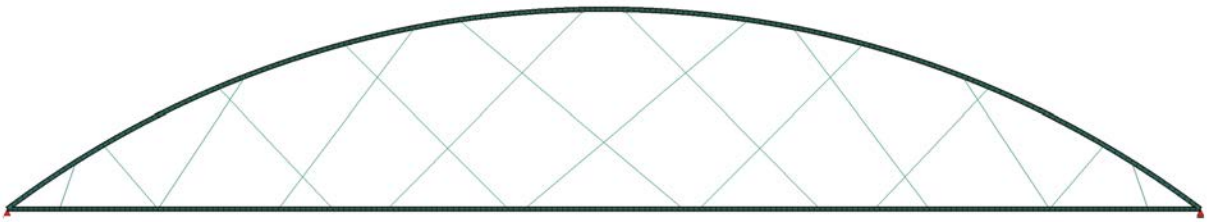

(a) Span length 150 m - deck width 3 m

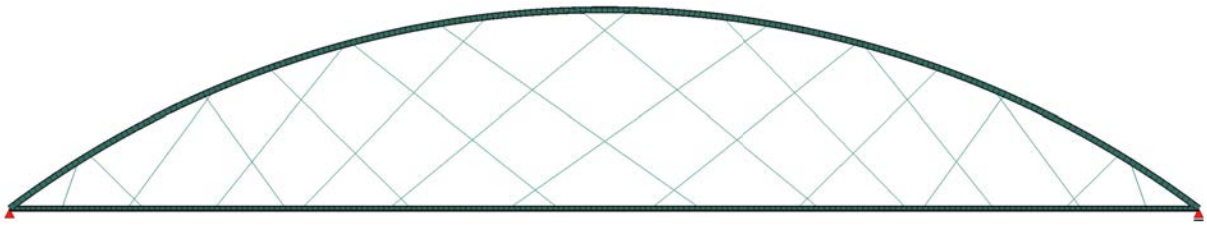

(b) Span length 150 m - deck width 6 m

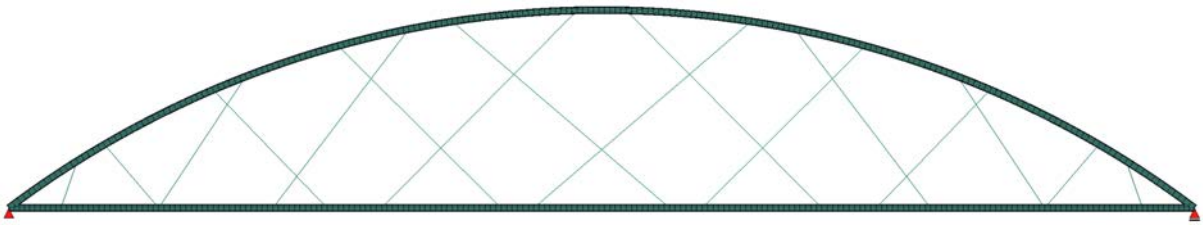

(c) Span length 150 m - deck width 9 m

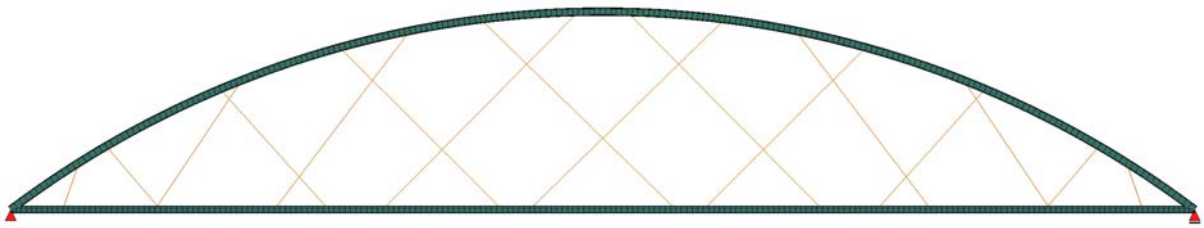

(d) Span length 150 m - deck width 12 m

Figure F.2 The best geometries for span length of 150 m with deck width of 3 m, 6 m, 9 m and 12 m respectively

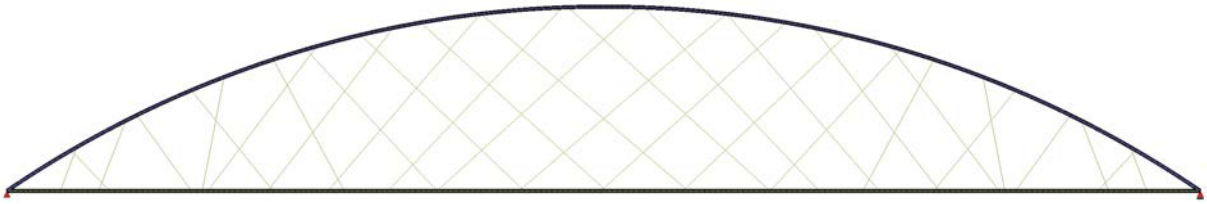

(a) Span length 200 m - deck width 3 m

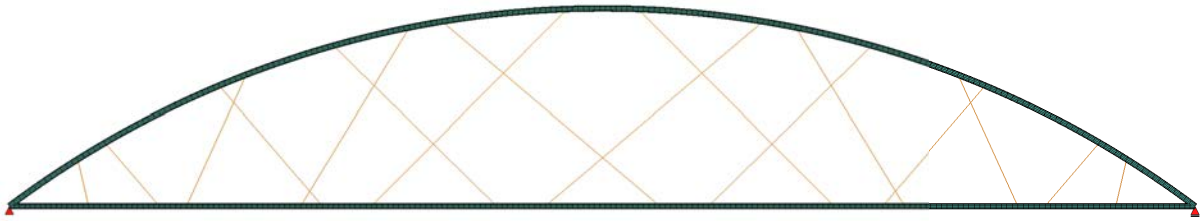

(b) Span length 200 m - deck width 6 m

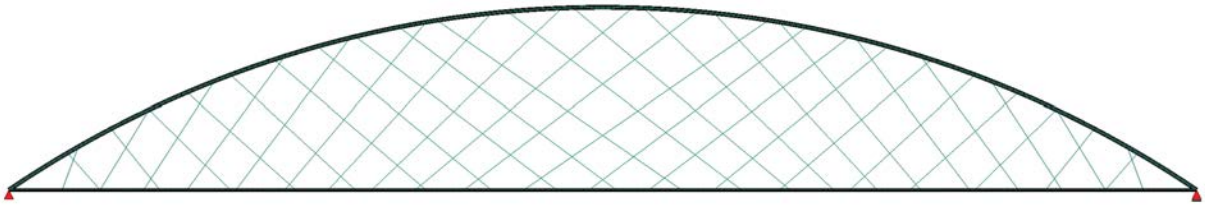

(c) Span length 200 m - deck width 9 m

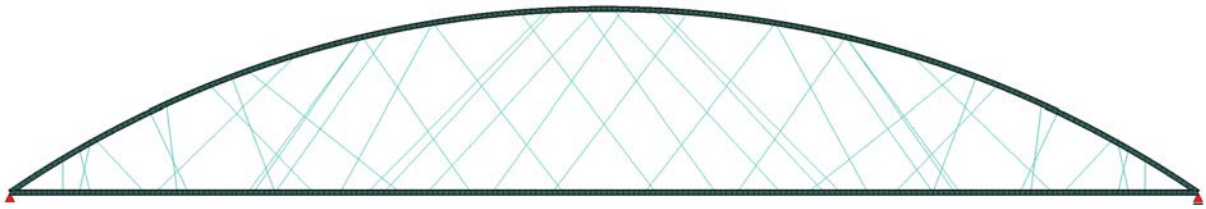

(d) Span length 200 m - deck width 12 m

Figure F.3 The best geometries for span length of 200 m with deck width of 3 m, 6 m, 9 m and 12 m respectively

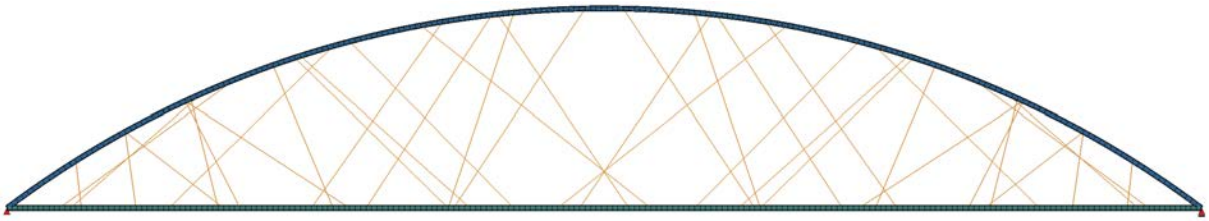

(a) Span length 250 m - deck width 3 m

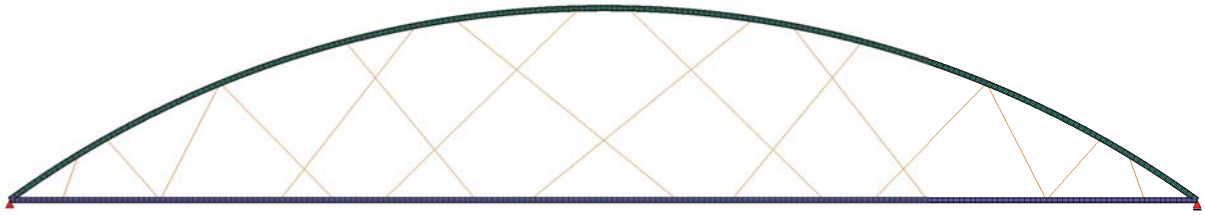

(b) Span length 250 m - deck width 6 m

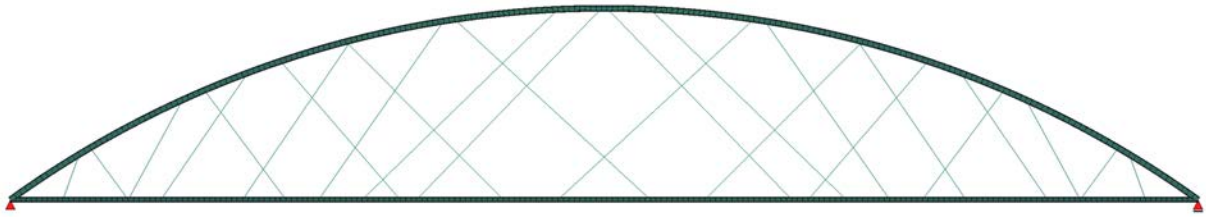

(c) Span length 250 m - deck width 9 m

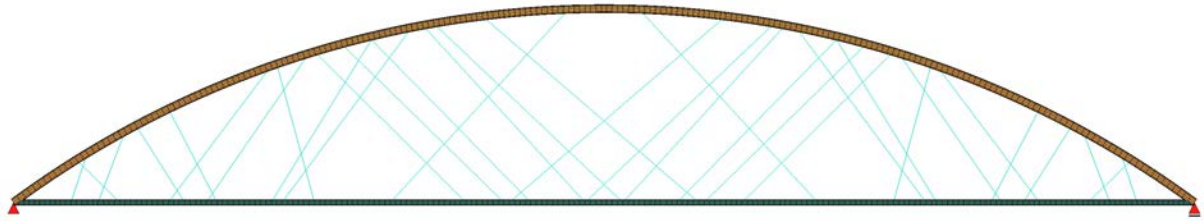

(d) Span length 250 m - deck width 12 m

Figure F.4 The best geometries for span length of 250 m with deck width of 3 m, 6 m, 9 m and 12 m respectively

G CARSM and MVADM arrangements results

This section includes the geometry, von Mises stresses and displacements for the geometries used in the performance comparison between CARSM and MVADM arrangements.

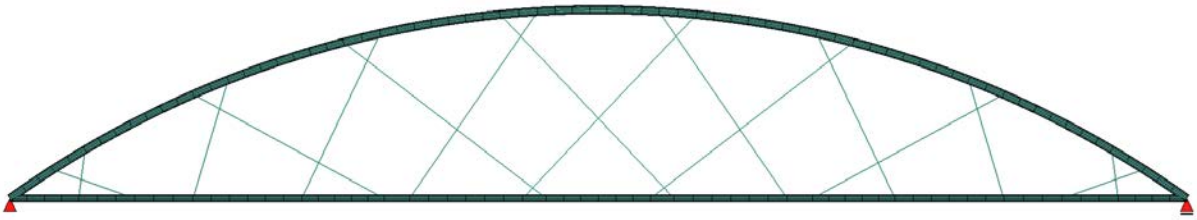

(a) Visual representation

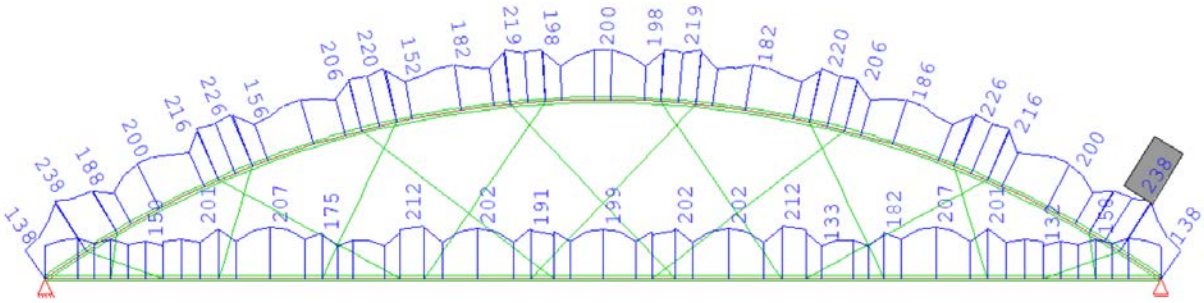

(b) Von Mises stress [MPa]

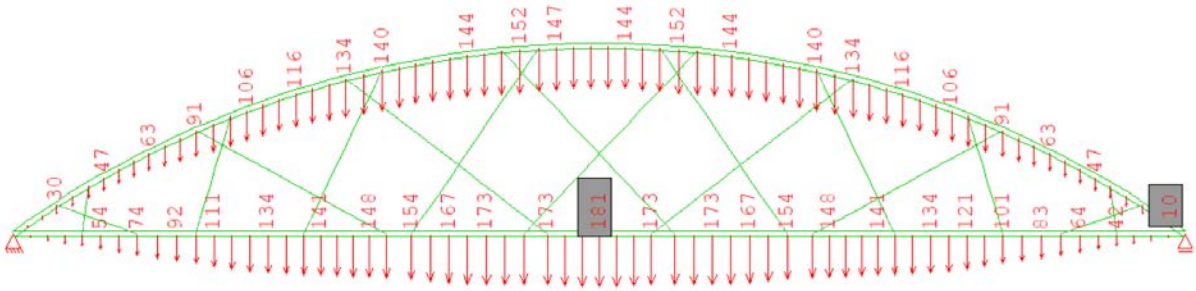

(c) Deflection from permanent and variable loads applied on the entire span length

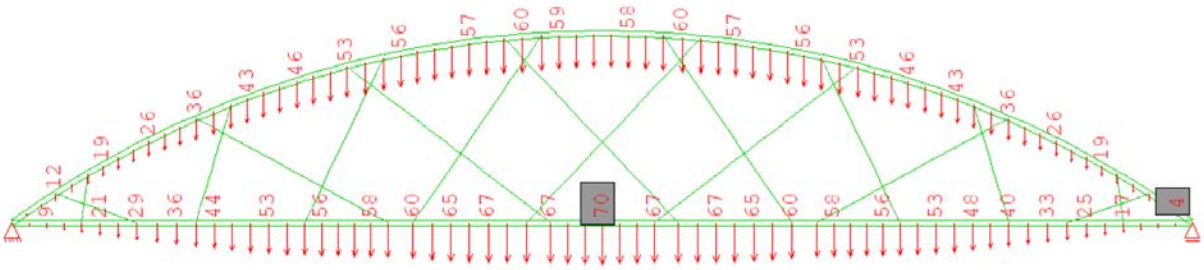

(d) Deflection from permanent load

Figure G.1 The results for CARSM arrangement - span length (L) 100 m, number of hangers (N) 16, deck width (q) 3 m

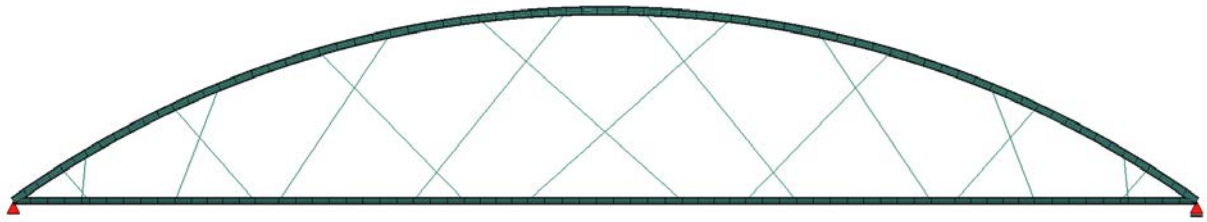

(a) Visual representation

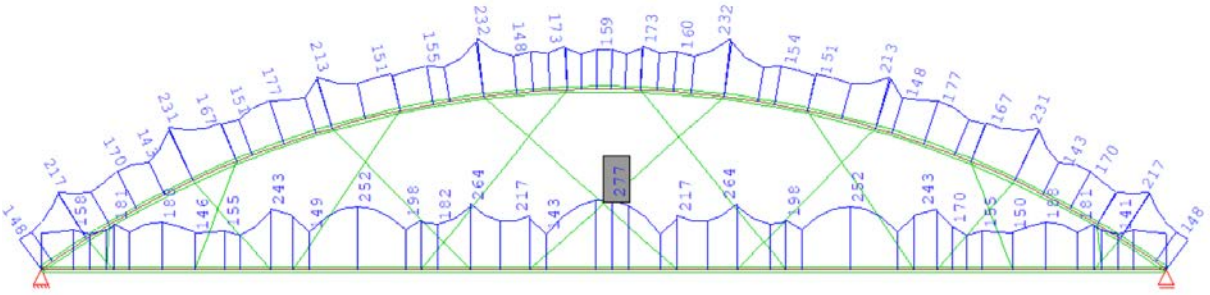

(b) Von Mises stress [MPa]

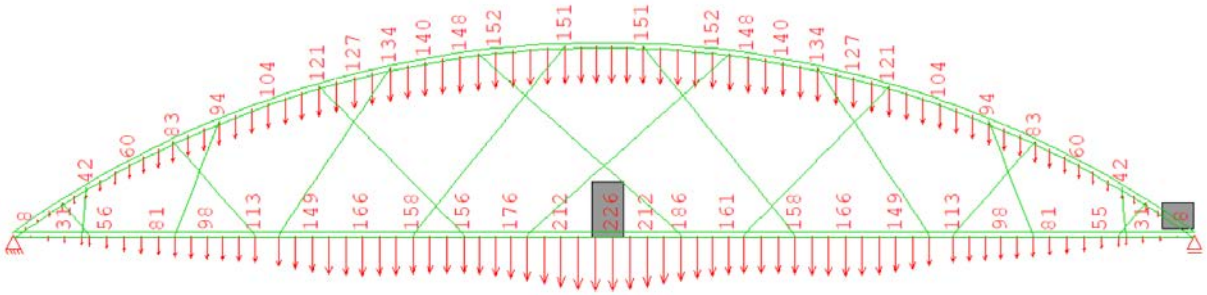

(c) Deflection from permanent and variable loads applied on the entire span length

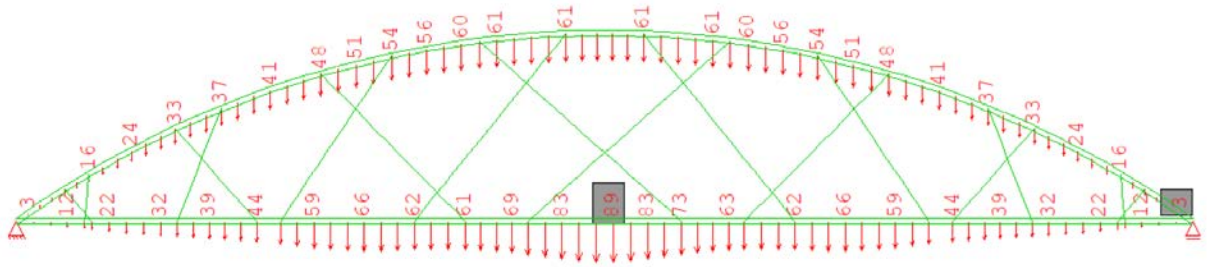

(d) Deflection from permanent load

Figure G.2 The results for the MVADM arrangement - span length (L) 100 m, number of hangers (N) 16, deck width (q) 3 m

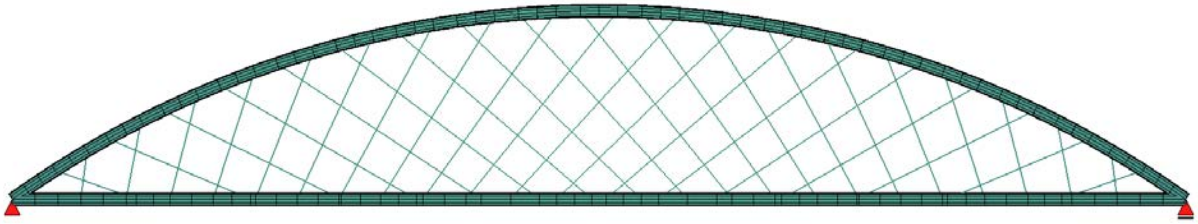

(a) Visual representation

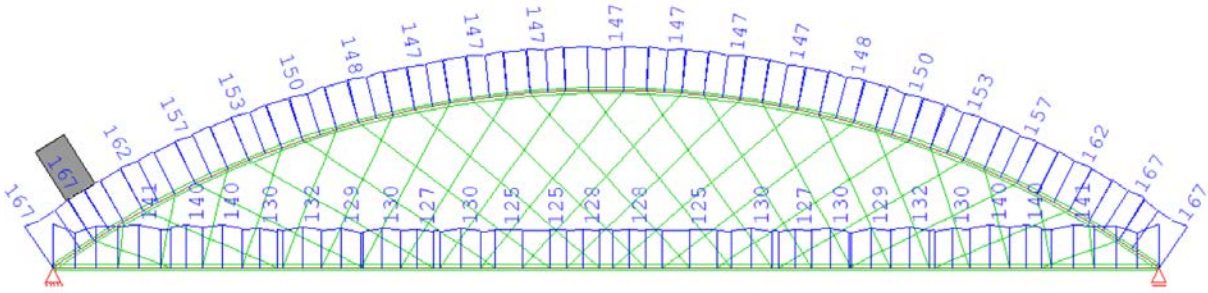

(b) Von Mises stress [MPa]

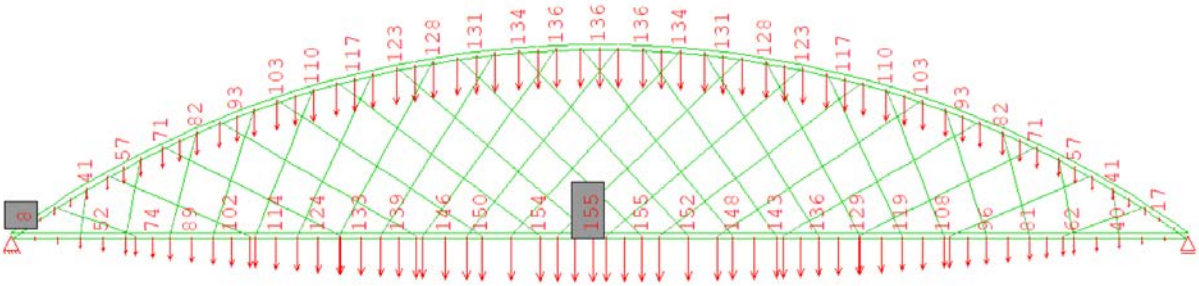

(c) Deflection from permanent and variable loads applied on the entire span length

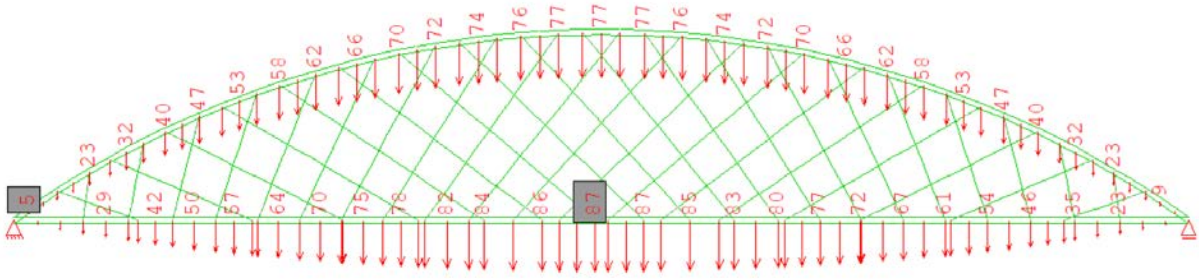

(d) Deflection from permanent load

Figure G.3 The results for CARSM arrangement - span length (L) 100 m, number of hangers (N) 38, deck width (q) 12 m

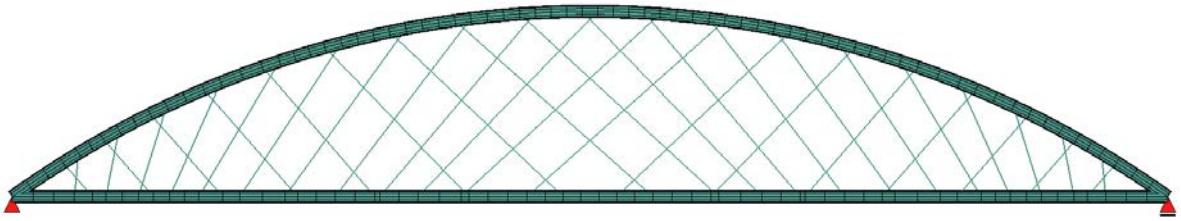

(a) Visual representation

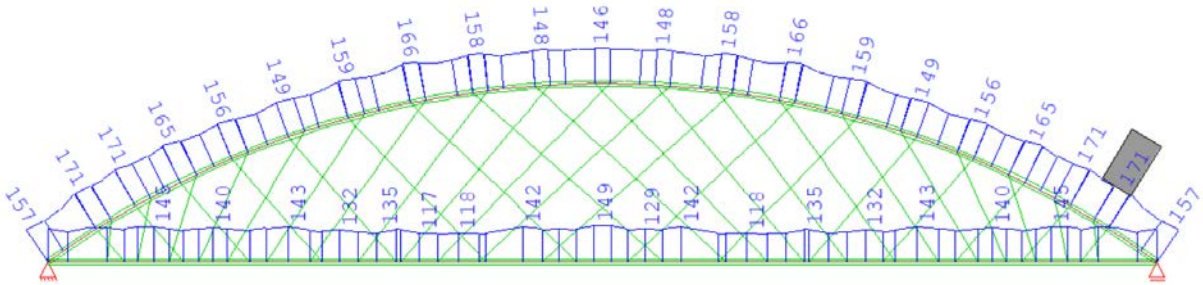

(b) Von Mises stress [MPa]

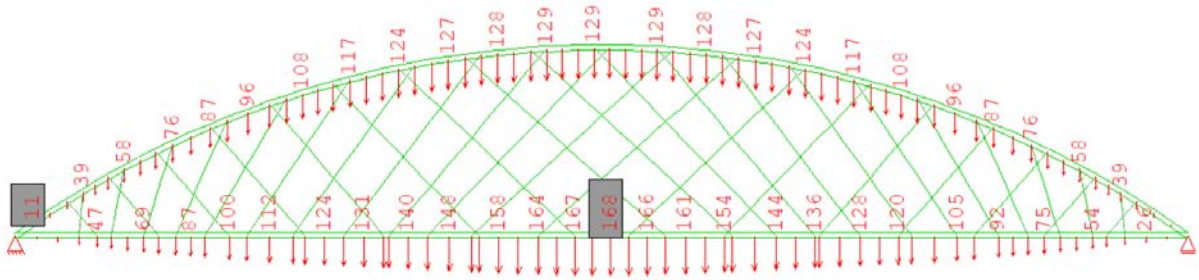

(c) Deflection from permanent and variable loads applied on the entire span length

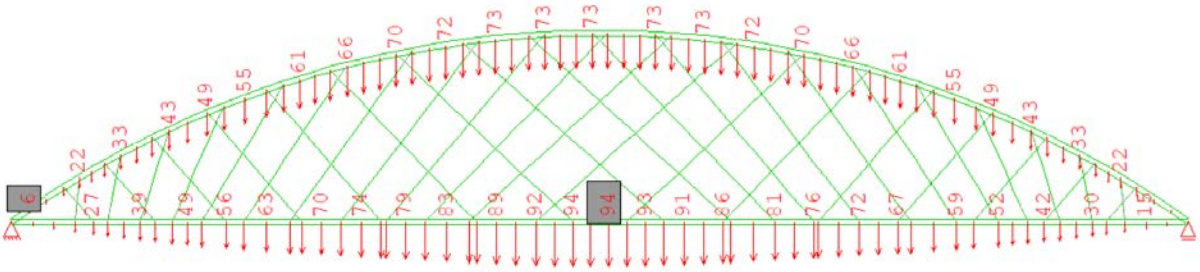

(d) Deflection from permanent load

Figure G.4 The results for the MVADM arrangement - span length (L) 100 m, number of hangers (N) 38, deck width (q) 12 m

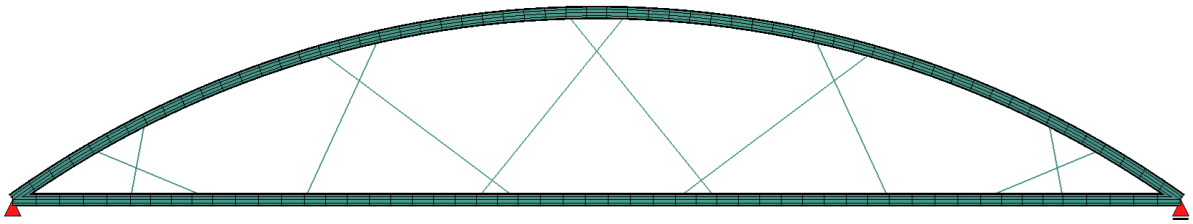

(a) Visual representation

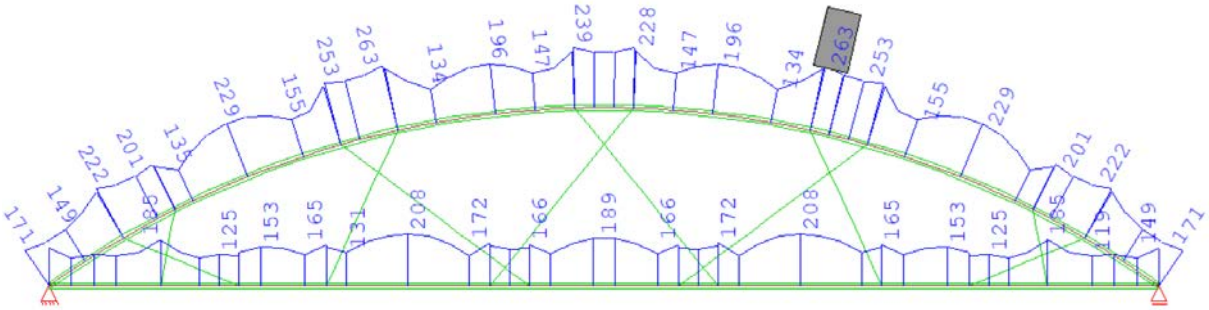

(b) Von Mises stress [MPa]

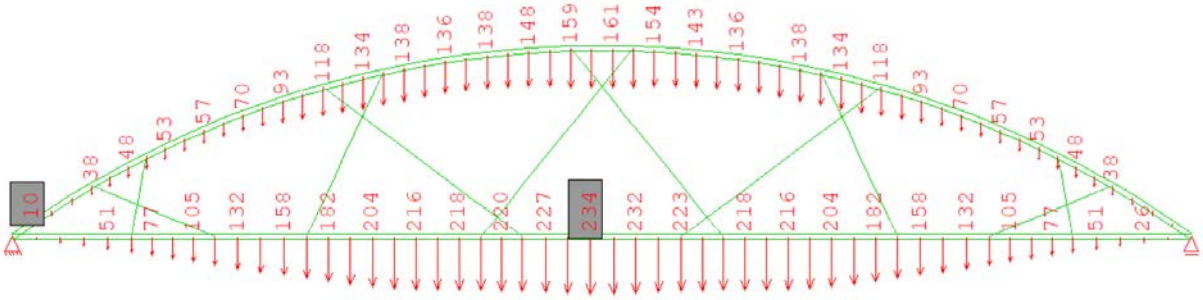

(c) Deflection from permanent and variable loads applied on the entire span length

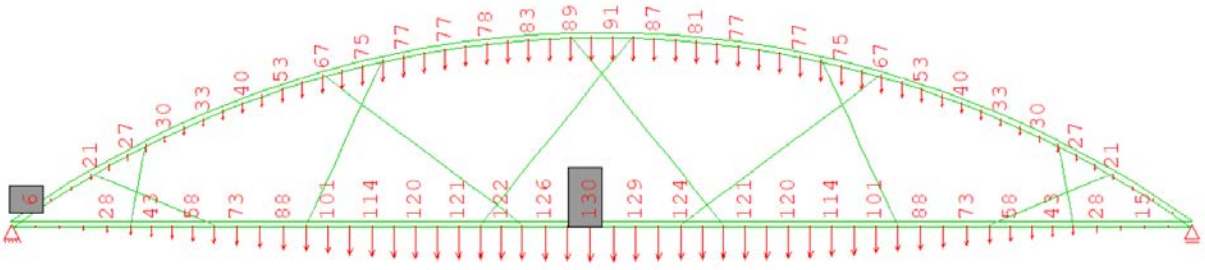

(d) Deflection from permanent load

Figure G.5 The results for CARSM arrangement - span length (L) 100 m, number of hangers (N) 10, deck width (q) 12 m

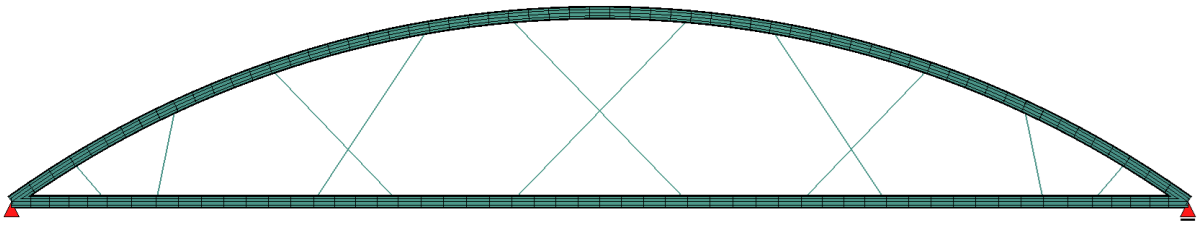

(a) Visual representation

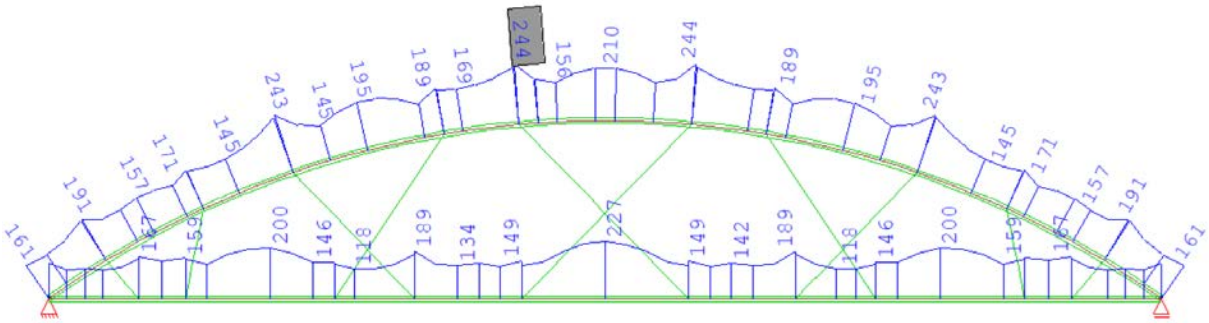

(b) Von Mises stress [MPa]

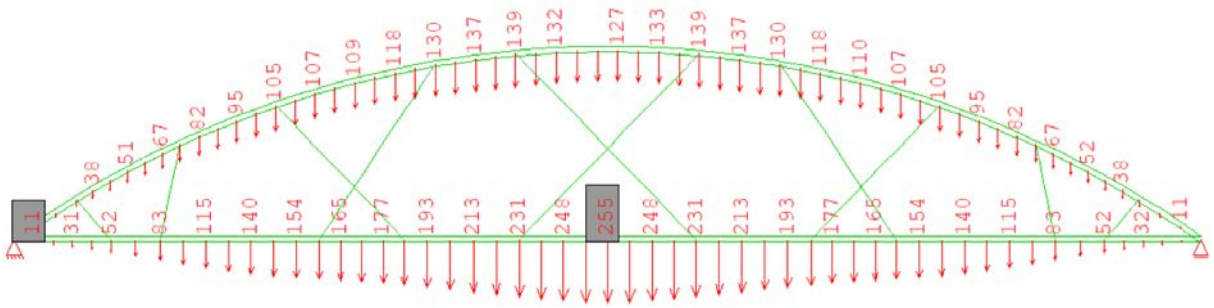

(c) Deflection from permanent and variable loads applied on the entire span length

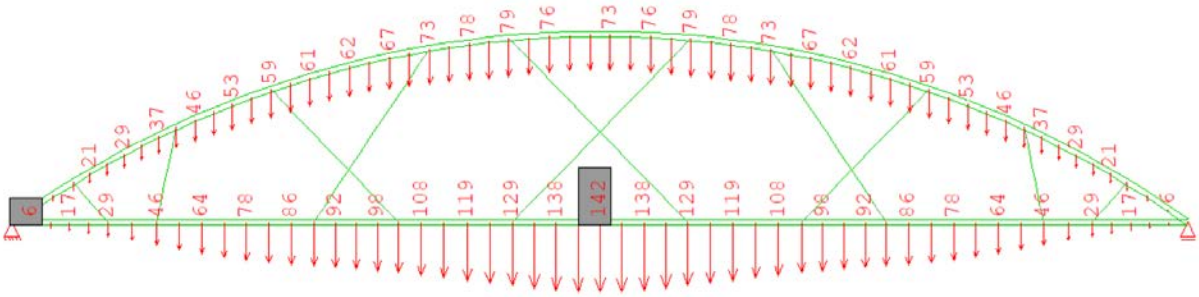

(d) Deflection from permanent load

Figure G.6 The results for the MVADM arrangement - span length (L) 100 m, number of hangers (N) 10, deck width (q) 12 m

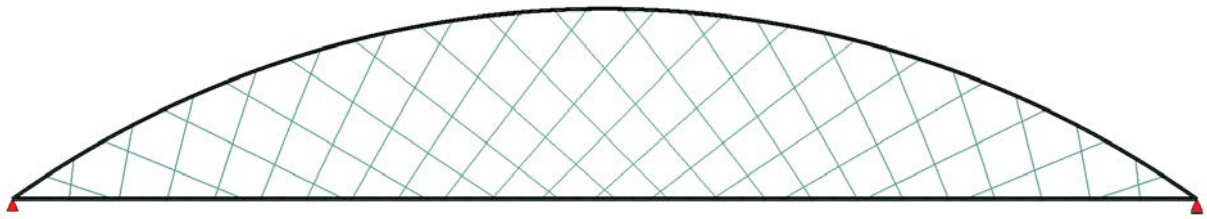

(a) Visual representation

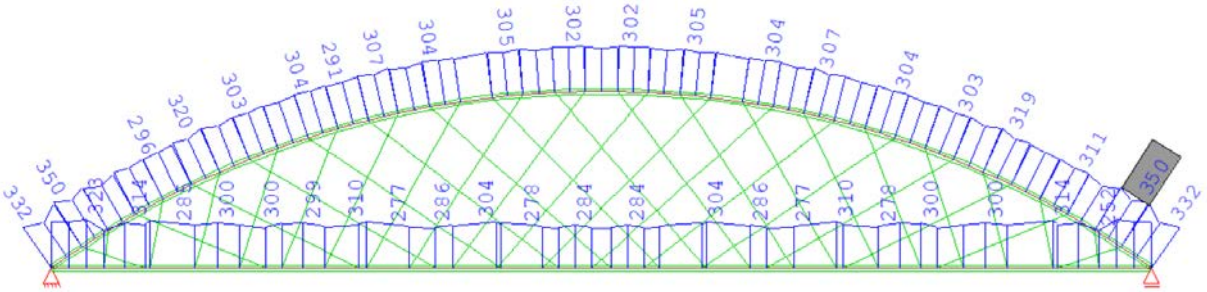

(b) Von Mises stress [MPa]

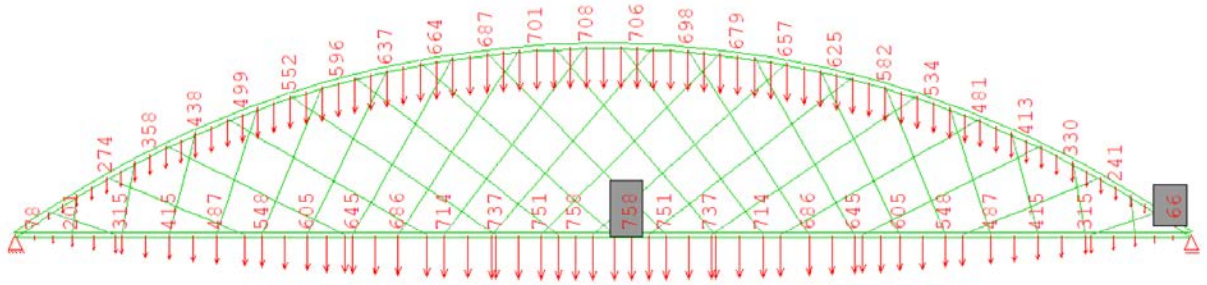

(c) Deflection from permanent and variable loads applied on the entire span length

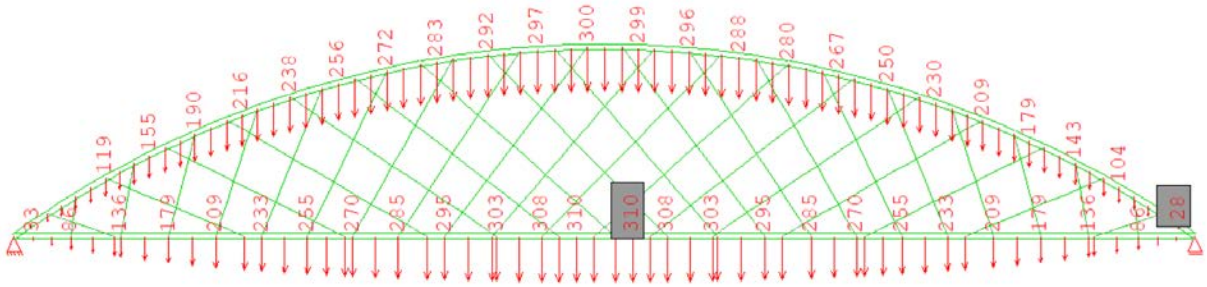

(d) Deflection from permanent load

Figure G.7 The results for CARSM arrangement - span length (L) 250 m, number of hangers (N) 36, deck width (q) 3 m

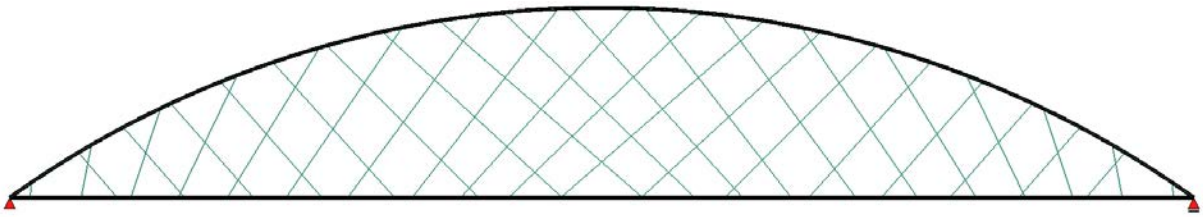

(a) Visual representation

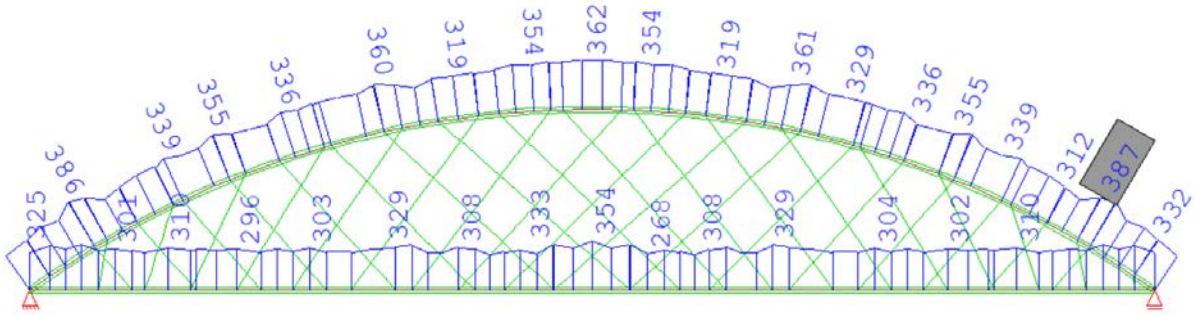

(b) Von Mises stress [MPa]

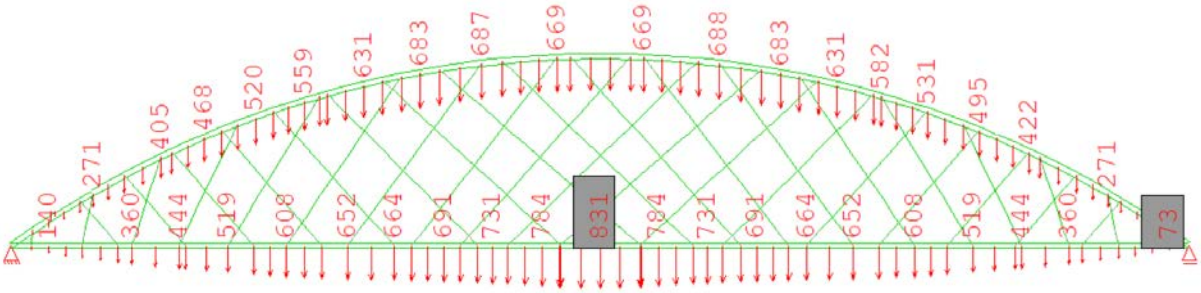

(c) Deflection from permanent and variable loads applied on the entire span length

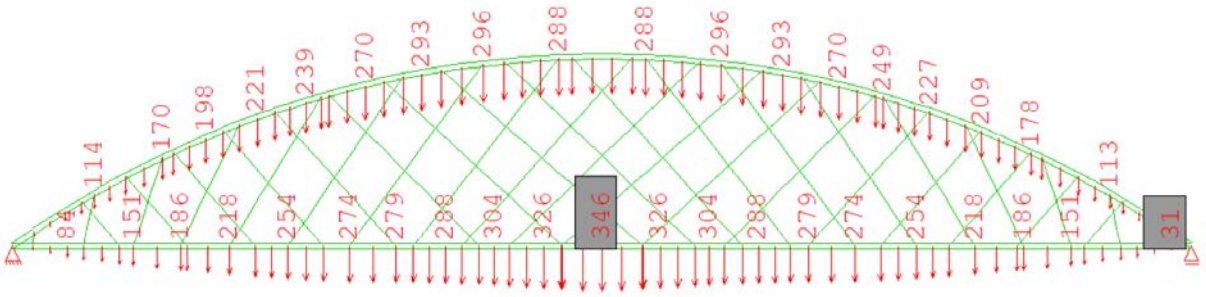

(d) Deflection from permanent load

Figure G.8 The results for the MVADM arrangement - span length (L) 250 m, number of hangers (N) 36, deck width (q) 3 m

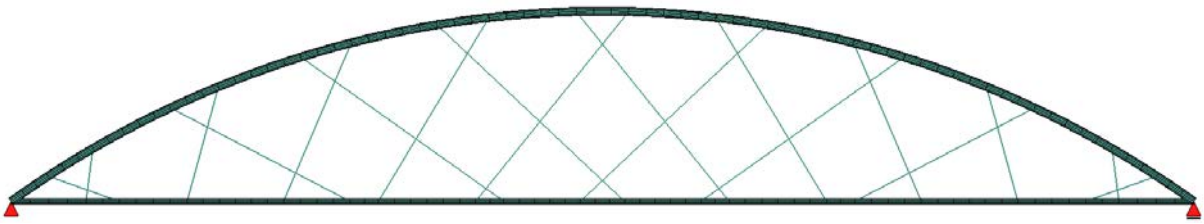

(a) Visual representation

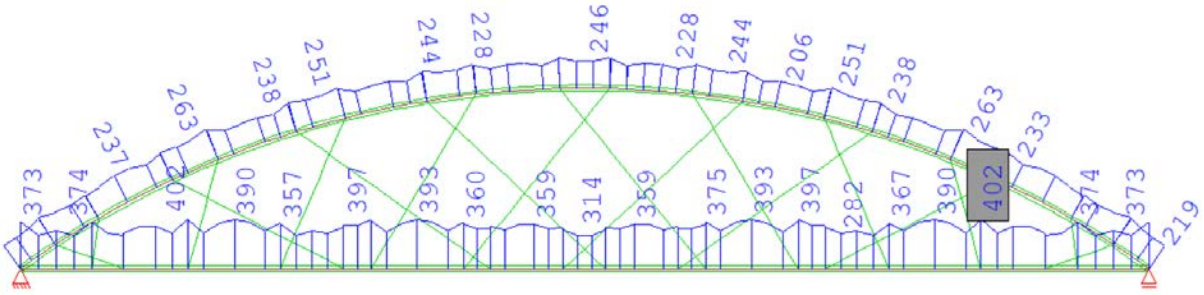

(b) Von Mises stress [MPa]

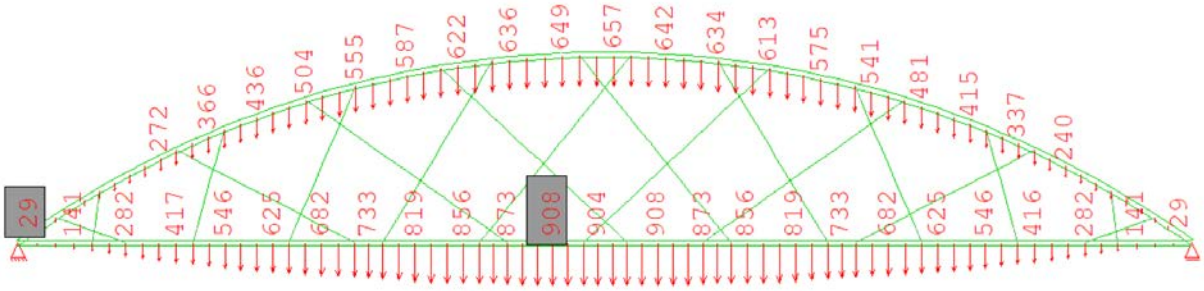

(c) Deflection from permanent and variable loads applied on the entire span length

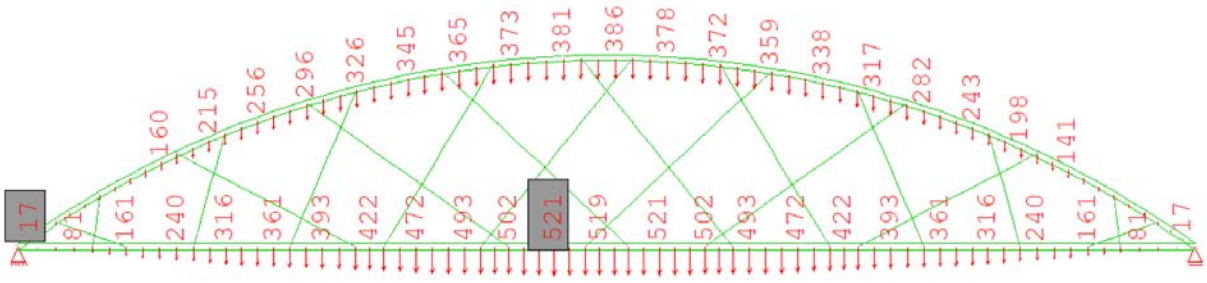

(d) Deflection from permanent load

Figure G.9 The results for CARSM arrangement - span length (L) 250 m, number of hangers (N) 18, deck width (q) 12 m

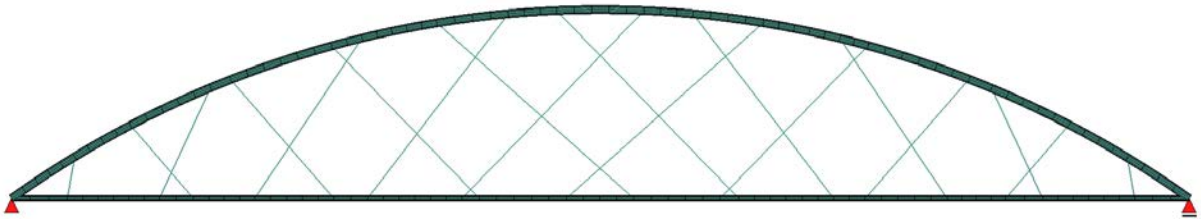

(a) Visual representation

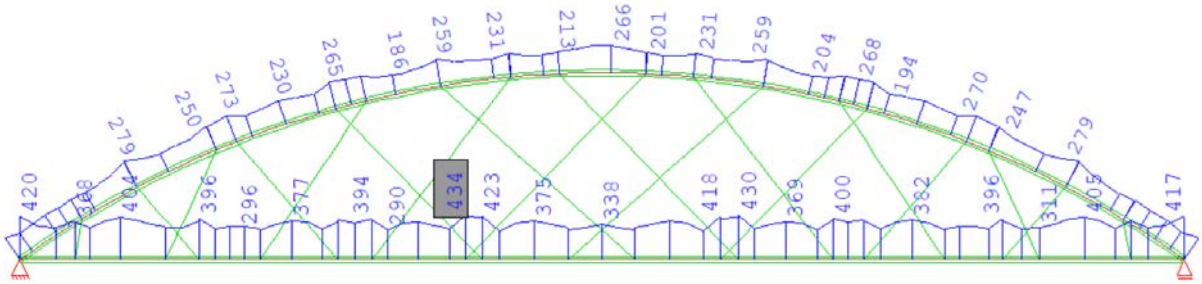

(b) Von Mises stress [MPa]

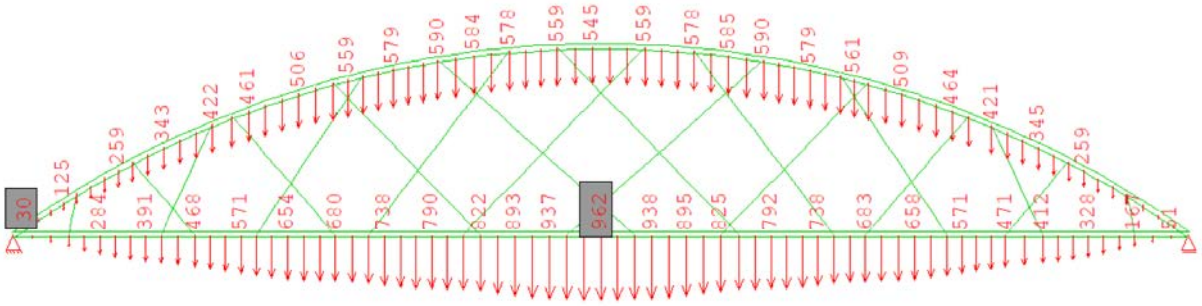

(c) Deflection from permanent and variable loads applied on the entire span length

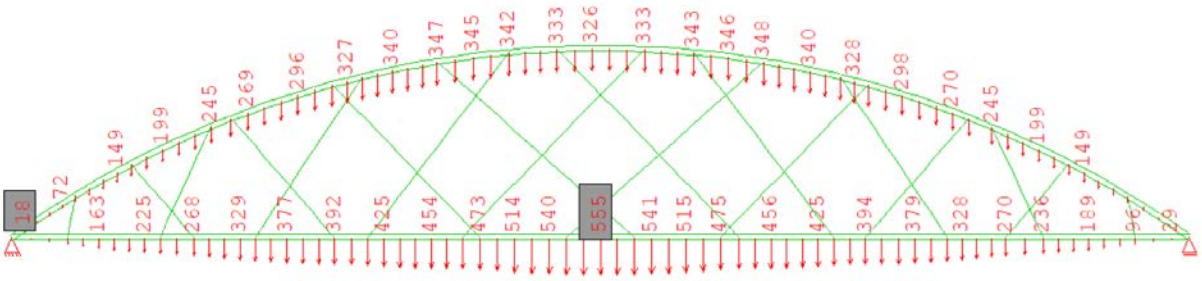

(d) Deflection from permanent load

Figure G.10 The results for the MVADM arrangement - span length (L) 250 m, number of hangers (N) 18, deck width (q) 12 m

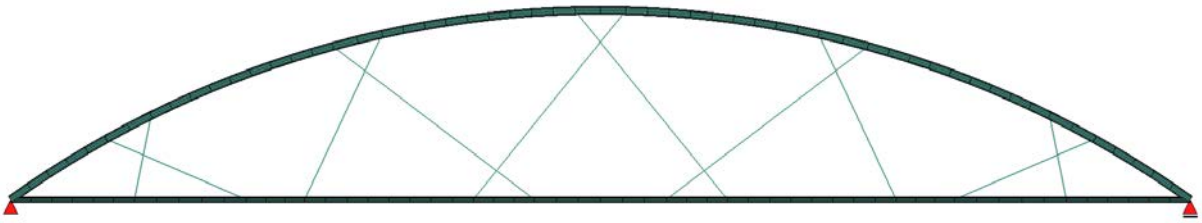

(a) Visual representation

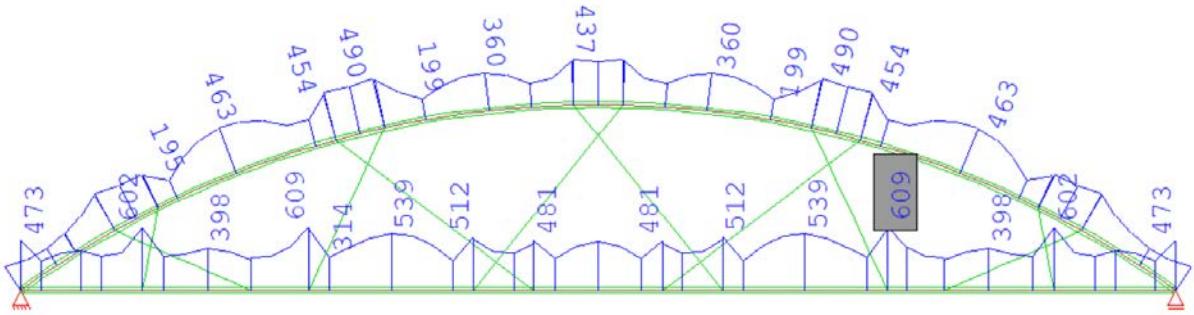

(b) Von Mises stress [MPa]

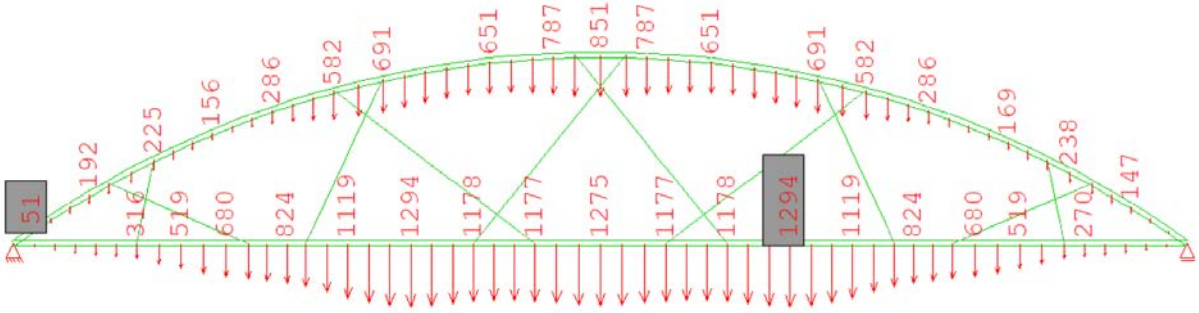

(c) Deflection from permanent and variable loads applied on the entire span length

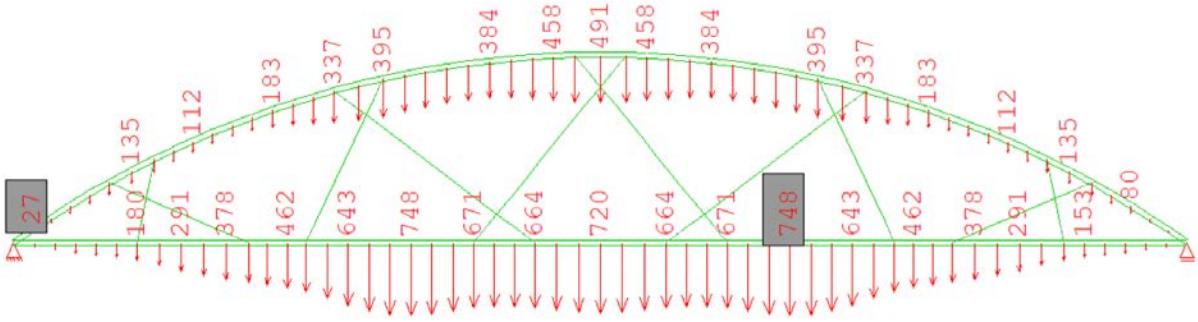

(d) Deflection from permanent load

Figure G.11 The results for CARSM arrangement - span length (L) 250 m, number of hangers (N) 10, deck width (q) 12 m

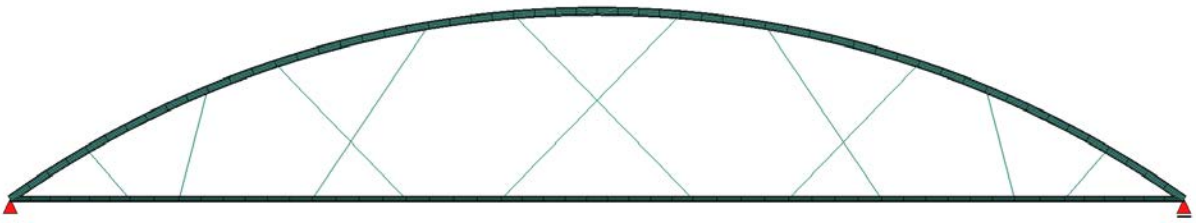

(a) Visual representation

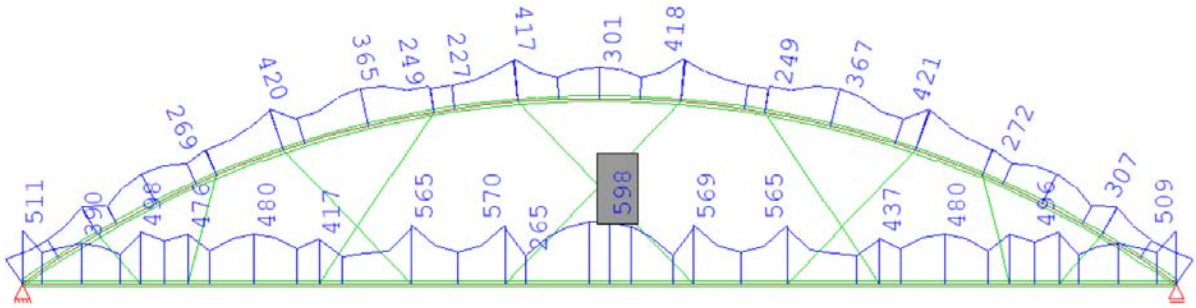

(b) Von Mises stress [MPa]

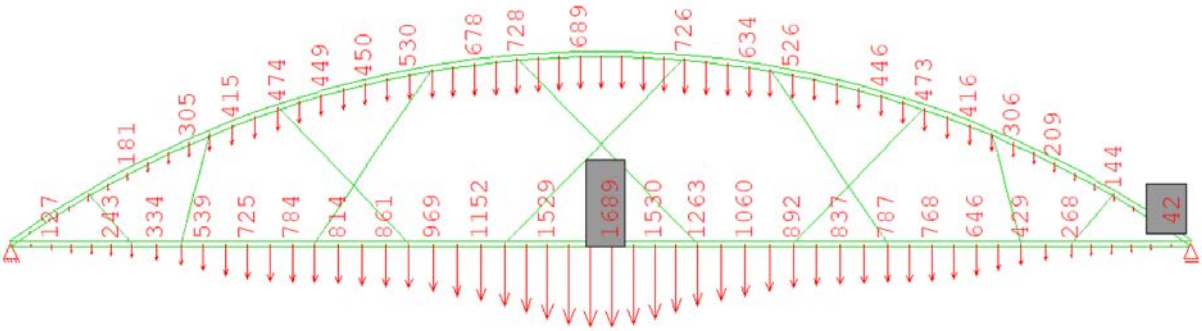

(c) Deflection from permanent and variable loads applied on the entire span length

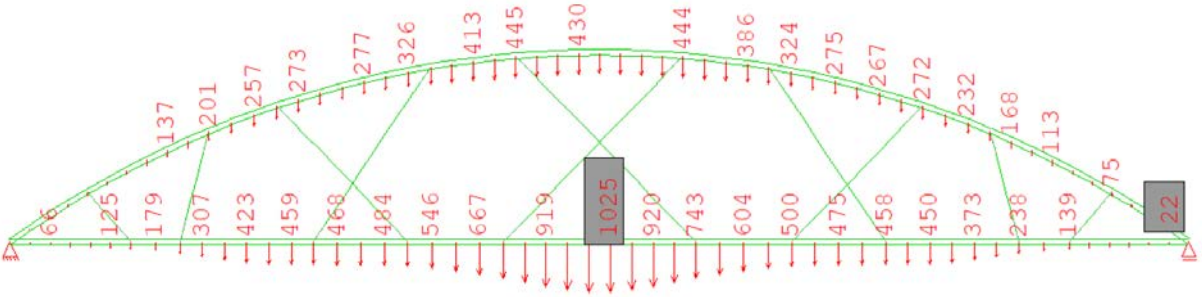

(d) Deflection from permanent load

Figure G.12 The results for the MVADM arrangement - span length (L) 250 m, number of hangers (N) 10, deck width (q) 12 m

Abstract

The network arch bridges are arch bridges with network-type hangers' arrangement developed by Per Tveit since the 1960s. In principle, the hangers cross each other at least twice providing great mechanical performance over the vertical and Nielsen arrangements, which makes them more cost-efficient. Various types of network arrangements were developed in literature and optimization investigations helped determining the suitable arrangement type and other parameters in terms of structural performance or weight minimization. However, the analyses were not generalized and considered either known arrangements or custom arrangements but with limitations. The literatures did not include in-plane geometrically nonlinear buckling of the arch, which reduced resistance and impacted the optimized results in comparison with linear elastic bifurcation. The generalized optimization algorithm with implemented more accurate in-plane buckling resistance determination was investigated in this dissertation.

The in-plane geometrically nonlinear buckling analysis resulted in non-negligible lower buckling resistance compared to linear elastic bifurcation analysis. The multi-periodic sinusoidal imperfection form was achieved in geometrically nonlinear post-critical analysis matching expectation from literature, but the approach was generalized comparing to the literature solution.

Two authored optimization algorithm combined genetic algorithm with evolutionary structural optimization and genetic algorithm with gradient-based algorithm. The new approach of cost-oriented goal function implementation into optimization of network-type arch bridges was presented. The possibility of having any hangers' arrangement at the same time with geometry, cross section, material capacity modification and any number of hangers in the optimization process defined with cost-oriented objective function allowed to obtain more cost-efficient solutions than the known and well-defined optimal network arch arrangement suggested in literature. The new hangers' arrangement was discovered and named Multi-Variant Angular Divergence Model. The guidelines for optimal shaping in terms of cost minimization of network-type arch bridges were presented.

Abstrakt

Siatkowe mosty łukowe należą do grupy mostów łukowych z układem wieszaków o charakterze siatkowym, rozwijanym od lat 60. XX wieku przez Pera Tveita. Zasadniczą cechą tego rozwiązania jest co najmniej dwukrotne krzyżowanie się wieszaków, co zapewnia bardzo korzystne właściwości mechaniczne w porównaniu z układami pionowymi i typu Nielsena, a tym samym podnosi efektywność ekonomiczną konstrukcji. W literaturze opracowano różne warianty układów siatkowych, a badania optymalizacyjne umożliwiły określenie odpowiedniego typu układu oraz innych parametrów z punktu widzenia nośności i minimalizacji masy własnej. Analizy te nie miały jednak charakteru uogólnionego i obejmowały jedynie znane układy lub dowolne konfiguracje, lecz obarczone ograniczeniami. Dotychczasowe badania nie uwzględniały geometrycznie nieliniowego wyboczenia łuku w płaszczyźnie, które prowadzi do obniżenia nośności i wpływa na wyniki optymalizacji w porównaniu z wyboczeniem bifurkacyjnym. W niniejszej rozprawie zaproponowano uogólniony algorytm optymalizacyjny z implementacją dokładniejszego wyznaczania nośności przy wyboczeniu geometrycznie nieliniowym w płaszczyźnie.

Geometrycznie nieliniowa analiza wyboczeniowa w płaszczyźnie łuku wykazała niepomijalnie niższą nośność wyboczeniową w porównaniu z analizą bifurkacyjną. W analizie geometrycznie nieliniowej w stanie pokrytycznym uzyskano wielookresową formę imperfekcji o charakterze sinusoidalnym, zgodną z oczekiwaniami znanymi z literatury, lecz podejście zostało uogólnione w porównaniu do rozwiązania z literatury.

Dwa autorskie algorytmy optymalizacyjne łączyły algorytm genetyczny z ewolucyjną optymalizacją strukturalną oraz algorytm genetyczny z algorytmem gradientowym. Zaprezentowano nowe podejście do implementacji kosztowo zorientowanej funkcji celu w procesie optymalizacji mostów łukowych typu siatkowego. Możliwość uwzględnienia dowolnego układu wieszaków jednocześnie z modyfikacjami geometrii, przekrojów oraz nośności materiałowej, a także dowolnej liczby wieszaków w procesie optymalizacji zdefiniowanym poprzez kosztowo zorientowaną funkcję celu pozwoliła uzyskać rozwiązania bardziej efektywne kosztowo niż znane i dobrze zdefiniowane układy siatkowe mostów łukowych sugerowane w literaturze. Odkryto nowy układ wieszaków, nazwany Modelem Wielowariantowej Dywergencji Kątowej (Multi-Variant Angular Divergence Model). Przedstawiono również wytyczne dotyczące optymalnego kształtowania mostów łukowych typu siatkowego pod kątem minimalizacji kosztów.